PALACKÝ UNIVERSITY IN OLOMOUC
FACULTY OF SCIENCE
Laboratory of Growth Regulators

Ivan Petřík

Determination of the bioactive compounds using modern LC-MS methods

P1527 Biology
1501V019 Experimental Biology

Ph.D. Thesis

Supervisor: Prof. Mgr. Ondřej Novák, Ph.D.
Consultant: Prof. Karin Ljung, Ph.D.

Olomouc
2024

Bibliografická identifikace

Jméno a příjmení	Ivan Petřík
Název práce	Stanovení bioaktivních látek pomocí moderních metod LC/MS
Typ práce	Ph.D.
Pracoviště	Laboratoř růstových regulátorů
Vedoucí práce	prof. Mgr. Ondřej Novák, Ph.D.
Rok obhajoby	2024
Abstrakt	V posledním desetiletí se fyziologie rostlin vyvinula v multidisciplinární obor zahrnující proteomiku, transkriptomiku, genetiku, fenomiku, a co je důležité, i rostlinnou hormonomiku. Výzkumné metody v dnešní době kladou důraz na miniaturizaci a vysokou propustnost, protože se zaměřují na stále menší části rostlinného organismu. Cílem této práce bylo vyvinout nové miniaturizované a vysoce propustné metody pro stanovení bioaktivních rostlinných hormonů, jejich metabolitů a prekurzorů. S využitím nejmodernějších přístupů kapalinové chromatografie s tandemovou hmotnostní detekcí byla ve spolupráci s dalšími obory rostlinné fyziologie objasněna role rostlinných hormonů při růstu rostlin a obraně proti stresovým podmínkám. Nově vyvinutý přístup přípravy vzorků založený na disperzní extrakci na pevné fázi a analytický přístup využívající superkritickou fluidní chromatografii v kombinaci s tandemovou hmotnostní detekcí rozšířily stávající portfolio metod rostlinné hormonomiky.
Klíčová slova	rostlinný hormon, kvantifikace, chromatografie, UHPLC, SFC, hmotnostní spektrometrie, MS/MS, návrh experimentu
Počet stran	70
Počet příloh	8
Jazyk	Anglický

Bibliographical identification

Author's name	Ivan Petřík
Thesis title	Determination of the bioactive compounds using modern LC-MS methods
Thesis type	Ph.D.
Department	Laboratory of Growth Regulators
Supervisor	Prof. Mgr. Ondřej Novák, Ph.D.
Presentation year	2024
Abstract	In the past decade, plant physiology has evolved into a multidisciplinary field encompassing proteomics, transcriptomics, genetics, phenomics, and notably, plant hormonomics. Research methods nowadays emphasize miniaturization and high throughput, as the focus is on increasingly smaller components of the plant organism. The aim of this thesis was to develop new miniaturized and high-throughput methods for the determination of bioactive plant hormones, their metabolites, and precursors. Utilizing state-of-the-art liquid chromatography with tandem mass detection, in collaboration with other branches of plant physiology, the role of plant hormones during plant growth and defence against stress conditions was elucidated. The newly developed sample preparation approach based on dispersive solid-phase extraction, and analytical approach employing supercritical fluid chromatography combined with tandem mass detection, has expanded the existing portfolio of plant hormonomics methods.
Keywords	plant hormone, quantification, chromatography, UHPLC, SFC, mass spectrometry, MS/MS, design of experiment
Number of pages	70
Number of supplements	8
Language	English

Acknowledgement

This work was carried out with the financial support of the Internal Grant Agency of Palacký University (IGA_PrF_2024_013) and the Czech Science Foundation (GAČR) (22-17435S). I would like to express my gratitude to my supervisor, Prof. Ondřej Novák, who has been an excellent mentor throughout my Ph.D. studies. This work would not have been possible without the contribution of Prof. Karin Ljung, who allowed me to gain invaluable experience at the Umeå Plant Science Centre in Sweden. Special thanks go to Hans Stenlund, Ph.D. from the Swedish Metabolomics Centre for introducing me to the world of biostatistics, chemometrics and data science, thus helping me shape my further research direction. I am also grateful to my colleagues Jitka Široká, Ph.D. and Michal Kaleta, Ph.D. for the critical reading of the thesis and their valuable feedback. I also thank the entire team at the Laboratory of Growth Regulators and the Umeå Plant Science Centre for their continuous support and assistance throughout this endeavour.

Declaration

I hereby declare that this work was produced using original results obtained during my Ph.D. studies and utilizing the literary sources listed below.

In Olomouc, ……

Ivan Petřík

Content

List of papers

This Ph.D. thesis represents a summary of the individual research publications presented as a *Supplement I-VIII*. The supplementary papers are enlisted here:

I. **Petřík I**, Hladík P, Zhang C, Pěnčík A, Novák O. [Submitted after revisions]. Spatio-temporal plant hormonomics: From tissue to subcellular resolution. J Exp B

II. **Petřík I**, Valníčková A, Stýskala J, Strnad M, Ljung K, Novák O. [In preparation]. DisperSpin solid phase micro-extraction: next generation micro-purification method for UHPLC-MS/MS determination of naturally occurring phytohormones.

III. **Petřík I**, Pěnčík A, Stýskala J, Tranová L, Amakorová P, Strnad M, Novák O. 2024. Rapid profiling of cytokinins using supercritical fluid chromatography coupled with tandem mass spectrometry. Anal Chim Acta 1285, 342010.

IV. Tan S, Abas M, Verstraeten I, Glanc M, Molnár G, Hajný J, Lasák P, **Petřík I**, Russinova E, Petrášek J, Novák O, Pospíšil J, Friml J. 2020. Salicylic acid targets protein phosphatase 2A to attenuate growth in plants. Curr Biol 30(3), 381–395.

V. Poitout A, Crabos A, **Petřík I**, Novák O, Krouk G, Lacombe B, Ruffel S. 2018. Responses to systemic nitrogen signaling in arabidopsis roots involve trans-zeatin in shoots. Plant Cell 30(6), 1243–1257.

VI. Kocáb O, Jakšová J, Novák O, **Petřík I**, Lenobel R, Chamrád I, Pavlovič A. 2020. Jasmonate-independent regulation of digestive enzyme activity in the carnivorous butterwort Pinguicula × Tina. J Exp Bot 71(12), 3749–3758.

VII. Jakšová J, Adamec L, **Petřík I**, Novák O, Šebela M, Pavlovič A. 2021. Contrasting effect of prey capture on jasmonate accumulation in two genera of aquatic carnivorous plants (Aldrovanda, Utricularia). Plant Physiol Biochem 166, 459–465.

VIII. Waidmann S, Ruiz Rosquete M, Schöller M, Sarkel E, Lindner H, LaRue T, **Petřík I**, Dünser K, Martopawiro S, Sasidharan R, Novak O, Wabnik K, Dinneny JR, Kleine-Vehn J. 2019. Cytokinin functions as an asymmetric and anti-gravitropic signal in lateral roots. Nat Commun 10(1), 3540.

Contribution report

The author of this Ph.D. thesis contributed on the supplementary papers as follows:

I. As the first author designed and performed comprehensive meta-study, visualized results and wrote the original draft.

II. As the first author designed and performed the experiments, analysed and evaluated data, visualized results, and wrote the original draft.

III. As the first author designed and performed the experiments, analysed and evaluated data, visualized results, and wrote the original draft.

IV. As the co-author contributed on the LC-MS/MS analysis and data processing of salicylic acid in the roots of Arabidopsis mutant lines.

V. As the co-author contributed on the LC-MS/MS analysis and data processing of cytokinins in the roots and shoots of Arabidopsis seedlings.

VI. As the co-author contributed on the LC-MS/MS analysis and data processing of stress related compounds in the terrestrial carnivorous plants.

VII. As the co-author contributed on the LC-MS/MS analysis and data processing of stress related compounds in the aquatic carnivorous plants.

VIII. As the co-author contributed on the LC-MS/MS analysis and data processing of cytokinins in the roots of Arabidopsis mutant lines.

Abbreviations

2-PIC	2-picolylamine stationary phase
7G	cytokinin *N*7-glucoside
9G	cytokinin *N*9-glucoside
ABA	abscisic acid
ABCG	ATP-binding cassette transporter G
AHPs	authentic histidine phosphotransfer proteins
ATPase	sodium-potassium adenosine triphosphatase pump
AZG	azaguanine purine transporter
C18	octadecyl
CE	capillary electrophoresis
cis-OPDA	*cis*-(+)-12-oxo-phytodienoic acid
CKs	cytokinins
CKX	CYTOKININ OXIDASE/DEHYDROGENASE
COI1	CORONATINE INSENSITIVE 1
*c*Z	*cis*-zeatin
*c*ZR	*cis*-zeatin riboside
DAO1	DIOXYGENASE FOR AUXIN OXIDATION 1
DHBA	dihydroxybenzoic acid
DHZ	dihydrozeatin
dnOPDA	dinor-(+)-12-oxo-phytodienoic acid
DoE	design of experiment
GC	gas chromatography
GH3	GRETCHEN HAGEN 3
EI	electron impact
ENT	equilibrative nucleoside transporters
ER	endoplasmic reticulum
ESI	electrospray ionization
FDA	Food and Drug Administration
FW	fresh weight
HKs	histidine kinases
HPLC	high performance liquid chromatography
HRMS	high resolution mass spectrometry
IAA	indole-3-acetic acid
IAM	indole-3-acetamide
IAN	indole-3-acetonitrile
IAOx	indole-3-acetaldoxime
IC	isochorismate
iP	isopentenyl adenine
IPyA	indole-3-pyruvic acid
IPT	ISOPENTENYL TRANSFERASE
IS	internal standard
JA	(+)-7-*iso*-jasmonic acid
JA-Ile	(+)-7-*iso*-jasmonoyl-L-isoleucine
JAs	jasmonates
LC	liquid chromatography
LLE	liquid-liquid extraction
LOG	“Lonely Guy” enzyme family
MRM/SRM	multiple/selective reaction monitoring
MS	mass spectrometry
MS/MS	tandem mass spectrometry
*m*T	*meta*-topolin
OFAT	One-Factor-At-A-Time experiment
OG	cytokinin *O*-glucoside
OPC-8	3-oxo-2-(2-pentenyl)-cyclopentane-1-octanoic acid
OPC-6	3-oxo-2-(2-pentenyl)-cyclopentane-1-hexanoic acid
oxIAA	2-oxoindole-3-acetic acid
*o*T	*ortho*-topolin

PALME	parallel artificial liquid membrane extraction
PIN	PIN-FORMED auxin transporters
PM	plasma membrane
PP	polypropylene
PRM	parallel reaction monitoring
PUP	purine permease
PVDF	polyvinylidene fluoride
RPLC	reversed-phase liquid chromatography
Q	quadrupole mass spectrometer
Q-LIT	quadrupole-linear ion trap mass spectrometer
QuEChERS	Quick, Easy, Cheap, Effective, Rugged, and Safe extraction
QqQ	triple quadrupole mass spectrometer
RP	reversed phase
RR	response regulator
S/N	signal to noise ratio
SA	salicylic acid
$scCO_2$	supercritical carbon dioxide
SFC	supercritical fluid chromatography
SP	sample preparation
SPE	solid phase extraction
tRNA	transfer ribonucleic acid
TRA	tryptamine
TRP	L-tryptophan
*t*Z	*trans*-zeatin
*t*ZRMP	*trans*-zeatin riboside monophosphate
UGT	URIDINE 5'-DIPHOSPHO-GLUCOSYLTRANSFERASE
UHPLC	ultra-high performance liquid chromatography

1 Introduction

It has been nearly a century since the elucidation of evidence for plant growth regulation. Auxin, one of the most extensively studied phytohormones to date, was identified as the first substance responsible for proliferation in meristematic tissues in grain crops (Went, 1926). Subsequent and continuous research efforts have led to the discovery of numerous signalling molecules with diverse chemical structures, natural occurrences, and biological activities. Despite their chemical and functional variability, three common features have been attributed to all of them: (i) low concentration in plant tissues, (ii) engagement in specific signalling pathways within cells, and (iii) a shared nomenclature - plant hormone or phytohormone.

The revolution in plant hormone research was catalysed by advances in technologies during the 20th century. First, the application of antibodies in immunoassays, such as radioimmunoassay or enzyme-linked immunosorbent assay, enabled the determination and quantification of naturally occurring plant hormones (Pengelly and Meins, 1976; Hofman et al., 1986; Geier et al., 1990). This breakthrough provided new insights into plant physiology in the 1970s and 1980s. Second, the development of liquid chromatography (LC) coupled with mass spectrometry (MS) systems toward the end of the millennium introduced new tools with improved separation performance and reduced detection limits. State-of-the-art ultra-high performance liquid chromatography (UHPLC) coupled with tandem mass spectrometry (MS/MS) systems with attomolar sensitivity and high scan speed, has facilitated the monitoring of multiple plant hormones at trace amounts (Tarkowská et al., 2014). Over the past decade, various methods for determining plant hormones in plant tissues based on UHPLC-MS/MS have emerged. These methods span a spectrum from deeply focused approaches targeting single or multiple compounds to targeted metabolomics of plant hormones. Most of these methods involve sample preparation procedures that aim to reduce sample complexity and simplify analysis. Modern analytical methods for plant hormones tend to emphasize miniaturization and high-throughput, utilizing minute amounts of plant samples to facilitate studies at the tissue, cellular or subcellular levels (Novák et al., 2017). Plant hormonomics, in conjunction with reversed genetics and complementary omics approaches such as genomics, transcriptomics, proteomics or phenomics, has become an integral part of modern plant physiology research.

2 Aims and scopes

The aim of this doctoral thesis was to develop innovative methods for determining plant hormones, aligning with the current trend toward miniaturization and high-throughput. The thesis encompasses an exploration of the physiological roles, biosynthesis, metabolism and homeostasis of selected groups of plant hormones together with the methodologies employed for their determination in biological samples. This comprehensive approach promises valuable insights into plant hormone dynamics and their impact on plant physiology.

The main objectives of the doctoral thesis were outlined as follows:

1. Conduct an extensive literature review covering the physiology, biosynthesis and metabolism of cytokinins (CKs) and acidic phytohormones. Next, review methodologies utilizing UHPLC-MS/MS to quantify these hormones in plants.
2. Develop a pioneering method for preparing CK samples employing Parallel Artificial Liquid Membrane Extraction (PALME).
3. Innovate the isolation method of CKs, auxins, and abscisic acid (ABA) using miniaturized dispersive solid-phase extraction (dSPE).
4. Introduce a ground-breaking analytical technique based on supercritical fluid chromatography (SFC) coupled with MS/MS.
5. Utilize advanced methodologies based on UHPLC-MS/MS to explore the roles of CKs, salicylic acid (SA), and jasmonates (JAs) in regulating plant growth, development and stress responses.

3 Literature review

Plant hormones, also known as phytohormones, are naturally occurring low molecular weight chemical compounds. In contrast to other bioactive molecules, plant hormones elicit their effects through specific signalling pathways and are present in low abundance within plants, typically ranging from 10^{-12} to 10^{-15} mol per gram of fresh weight. This characteristic renders the biological responses they mediate highly sensitive to fluctuations in their concentrations. Unlike animal hormones, which are typically synthesized in specific tissues or organs for specific functions, plant hormones exhibit greater heterogeneity. Their functions and biosynthesis are temporally and spatially dependent (Wong et al., 2023).

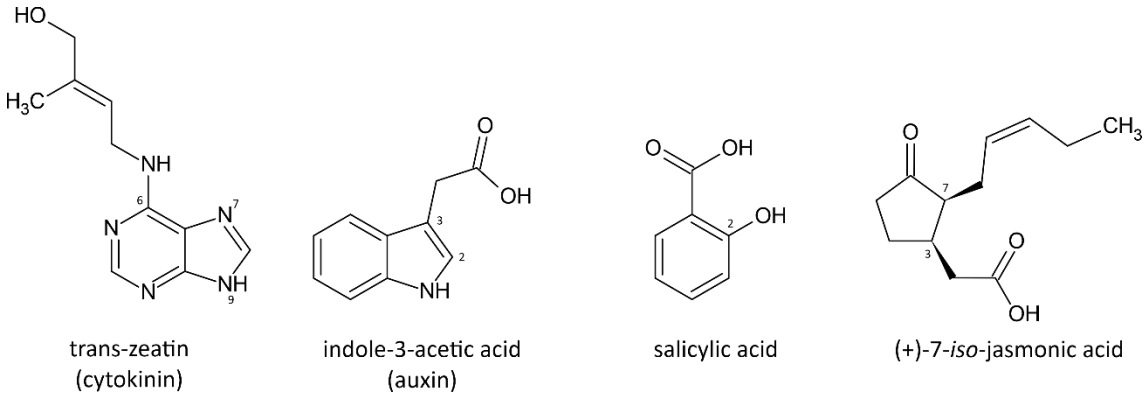

Fig. 1. Chemical structures of the plant hormone representatives studied within the scope of this Ph.D. thesis.

According to recent literature focused on the physiological roles of plant hormones, these bioactive compounds are classified into ten distinct groups. Specifically, these groups include CKs, auxins, JAs, ABA, SA, gibberellins, brassinosteroids, ethylene, polyamines and strigolactones (Novák et al., 2017). Among these groups, CKs are categorized as basic plant hormones, while auxins, JAs and SA are classified as acidic phytohormones (Fig. 1). The subsequent chapters of this thesis aim to provide a comprehensive theoretical overview by addressing the current understanding of the physiology, biosynthesis, metabolism, and methodologies relevant for the determination of selected phytohormone groups in plants.

3.1 Cytokinins

CKs stand as one of the most extensively studied and well-described phytohormones. The first CK, kinetin, was discovered in the mid-20th century (Miller et al., 1955). Although not originally isolated from a plant, but rather artificially obtained by autoclaving DNA, kinetin has demonstrated evident activity in promoting cell division (also known as cytokinesis). Subsequently, a similar activity was confirmed for zeatin, isolated from *Zea mays* corn kernels (Letham, 1963). The ability of CKs to promote cell division underlies their regulatory role in various physiological functions (Argueso and Kieber, 2024). In conjunction with another phytohormone, auxin, CKs orchestrate root and shoot development in plants. CKs regulate an embryo development during seed germination in the early stage of the plant's life. Later in the young seedling, they promote shoot apical meristem cell proliferation whereas inhibiting root apical meristem proliferation, promoting vascular formation, lateral root formation, chloroplast development, and stomata development. Simultaneously, CKs inhibit leaf senescence in adult plants and contribute to responses to biotic and abiotic stress conditions. They aid in nutrient uptake in the roots, initiate drought tolerance and regulate the formation of tumours, galls and knots in the presence of pathogens. Importantly, CKs play a role in the root nodulation process, where a symbiotic interaction with rhizobium bacteria enables aerial nitrogen fixation.

From the chemical point of view, CKs are N^6-substituted derivatives of adenine. The N^6-side chain moiety can be either isoprenoid or aromatic, thereby determining the CK types. Isopentenyladenine (iP) and its hydroxylated forms, *trans*-zeatin (*t*Z), *cis*-zeatin (*c*Z), and dihydrozeatin (DHZ), represent isoprenoid CK types. On the other hand, kinetin, benzyladenine, and its hydroxy derivatives *ortho*-topolin (*o*T), *meta*-topolin (*m*T), and *para*-topolin belong to aromatic CK types (Zürcher et al., 2016). The role of aromatic CKs in nature remains unclear, as their occurrence has only been confirmed in a few species related to the *Populus* genus (Strnad, 1997). Despite their rare natural presence, aromatic CKs such as *o*T and *m*T are extensively used as growth regulators in plant micropropagation (Holub, 1998; Baroja-Fernandez et al., 2002). Recent research has suggested that naturally occurring *o*T contributes to the circadian rhythm and daily growth in *Populus* trees (Edwards et al., 2018). It is believed that the metabolism of aromatic CKs is similar to that of isoprenoid CKs, although further clarification is still needed (Zürcher et al., 2016).

3.1.1 Biosynthesis

CK biosynthesis occurs in both roots and shoots, with the transfer ribonucleic acid (tRNA) being one of the traditional sources of *de novo* CKs. In most organisms, the cell cytosol is rich in ubiquitous tRNA containing adenine modified to *c*Z. Upon cleavage of tRNA by a nuclease, *c*ZR monophosphate is released. The subsequent action of phosphatases produces *cis*-zeatin riboside monophosphate, which is further converted to *c*ZR and *c*Z. Plant species such as rice, maize, pea, or potato utilize *c*Z as an active CK and tRNA as its significant source. However, recent research has revealed that *c*Z is evolutionarily older and less active compared to *t*Z in many plants, such as Brassicales (Gajdošová et al., 2011). These specific plant species prefer *t*Z or iP over *c*Z. Nevertheless, the conversion of *c*Z to *t*Z or iP has not yet been elucidated in any plant species. Therefore, it is hypothesized that these species cannot utilize tRNA as a source of CK biosynthesis. Instead, they rely on a tRNA-independent pathway initiated by ISOPENTENYL TRANSFERASE (IPT), which catalyses the linkage of an isoprene moiety from dimethylallyl pyrophosphate to the N^6 position of adenosine (Kakimoto 2001).

Several isoforms of IPT have been identified in the Arabidopsis genome, exhibiting variation in substrate preference (adenosine mono-/di-/tri-phosphate) and cellular compartmentalization (cytosol, mitochondria, plastids; Miyawaki et al., 2004). This reaction yields isopentenyladenosine monophosphate (iPRMP), which can be further hydroxylated by cytochrome P450 monooxygenase to form *trans*-zeatin riboside monophosphate (*t*ZRMP; Takei et al., 2004). The conversion of iPRMP and/or *t*ZRMP to their bioactive counterparts is catalysed by a crucial family of enzymes known as "Lonely Guy" (LOG). Recent studies have demonstrated that mutations in Arabidopsis LOG genes result in morphological defects in the shoot apical meristem (Kurakawa et al., 2007, Tokunaga et al., 2012). It is speculated that LOG genes are evolutionarily old and conserved, as they have been identified in the genomes of several lower plants, such as green algae, moss, and liverworts (Chen et al., 2022). Finally, DHZ types represent a quantitatively minor type of CKs (Kiba et al., 2023). It is proposed that DHZ types are converted from *t*Z types through the action of zeatin reductase (Martin et al., 1989; Spíchal et al., 2012).

3.1.2 Metabolism

The free CK bases serve as bioactive compounds, but plants possess enzymatic machinery responsible for CK metabolism to regulate endogenous concentrations crucial for CK signalling regulation. Isoprenoid CK metabolism primarily relies on glucosylation catalysed by URIDINE 5'-DIPHOSPHO-GLUCOSYLTRANSFERASES (UGT). In Arabidopsis, two UGT isoforms, UGT76C1 and UGT76C2, have been identified to glucosylate the *N*7 and *N*9 positions of the adenine moiety. The resulting CK *N*7-glucosides (7G) and *N*9-glucosides (9G) undergo a reaction catalysed by CYTOKININ OXIDASE/DEHYDROGENASE (CKX), responsible for final CK degradation (Spíchal et al., 2012). It was previously believed that *N*-glucosylation is an irreversible reaction determining the fate of glucosylated CK molecules. However, recent findings have challenged this notion, as *t*Z7G and *t*Z9G have been observed to convert back to the bioactive *t*Z in Arabidopsis seedlings (Hošek et al., 2020).

An alternative substitution at the *N*9 position is ribosylation, yielding *N*9-ribosides (R) involved in transport. Conversely, *O*-glucosylation catalysed by UTG85A1 in Arabidopsis is recognized as a temporary deactivation process. Unlike *N*-glucosylation, *O*-glucosylation links the glucosyl moiety to the oxygen on the isoprenoid side chain. Consequently, the resulting storage CK *O*-glucosides (OG) serve as substrates for a β-glucosidase, which converts them back to the bioactive CK bases (Brzobohatý, 1993).

3.1.3 Transport

Given that CKs are synthesized in various locations within plants, there is a need for their transport from the site of synthesis to the target organ, tissue or cell. Phloem and xylem are pivotal in facilitating both short and long-distance distribution of CKs. iP- and *c*Z-types, synthesized primarily in shoots, are transported via the phloem to the roots. Conversely, *t*Z types, predominantly synthesized in the roots, are distributed via the xylem to the shoots (Sakakibara, 2006).

As mentioned earlier in the metabolism section (3.1.2), CKs are often transported as *N*9-ribosides. Despite the lower activity of CK *N*9-ribosides compared to CK bases (Holub et al., 1998), their structure is proposed to serve as a substrate for CK transporters (Sakakibara, 2006; Lomin et al., 2015). A number of transporters involved in long-distance CK translocation have been identified (Argueso and Kieber, 2024).

EQUILIBRATIVE NUCLEOSIDE TRANSPORTERS (ENT) are proteins located in the plasma membrane (PM). While their group is relatively broad and non-specific, some ENTs are capable of transporting CKs downstream of concentration gradients in the phloem (Hyde et al., 2001; Hirose et al., 2005). Studies in Arabidopsis and rice *ent* mutants have revealed defects in exogenous CK uptake (Sun et al., 2005; Hirose et al., 2008). Another transporter protein, ATP-BINDING CASSETTE TRANSPORTER G (ABCG), is also localized in the PM. Several ABCG isoforms expressed in roots are responsible for the root-to-shoot translocation of *t*Z- and DHZ-types (Ko et al., 2014; Zhang et al., 2014). Conversely, ABCG isoforms expressed in shoots facilitate the transport of CKs through the apoplastic pathway (Zhao et al., 2021).

Concurrently, certain members of the purine permease (PUP) family localized in the PM near the apoplast are believed to pump CKs from the apoplast into the cell, regulating their apoplastic concentration and attenuating the signal at PM- localized CK receptors (Zürcher et al., 2016). Another hypothesis suggests the co-localization of PUPs and CK receptors on the endoplasmic reticulum (ER) in rice (Xiao et al., 2019), or alternatively, PUPs facilitate transport between the apoplast and ER-localized CK receptors (Romanov et al., 2018).

Recent studies have introduced newly discovered CK transporters. First, azaguanine (AZG) purine transporter AZG2 facilitates the translocation of CKs from the cytosol into the ER lumen, where the binding domain of CK receptors is oriented. Another azaguanine purine transporter, AZG1, has been suggested as a CK transporter potentially interacting with the PIN-FORMED (PIN) auxin transporters PIN1 responsible for auxin efflux (Tessi et al., 2021; Tessi et al., 2023). Second, SWEET (Sugars Will Eventually Be Exporter Transporters) have been identified as transporters in the phloem, contributing to simultaneous sugar and CK translocation (Radchuk et al., 2023).

3.1.4 Signalling

A longstanding theory posits that CK signalling is initiated by histidine kinases (HKs). This family of HKs comprises transmembrane proteins with a CK sensing domain exposed on one side of the membrane and a response domain localized on the opposite side. The first HK was identified in the Arabidopsis genome, thereby associating the canonical CK signalling pathway with Arabidopsis HKs (Kakimoto, 1996). The initial step involves autophosphorylation of HK upon binding of CK ligand to the HK receptor.

Subsequently, phosphate translocation occurs onto authentic histidine phosphotransfer proteins (AHPs), which shuttle between the cytosol and the nucleus (Hutchinson et al., 2006). AHPs have been identified across various plant species from lower plants to angiosperms, indicating their conserved evolution nature (Rashotte, 2021). In Arabidopsis, AHPs transmit the phosphoryl group to response regulator proteins (RR) within the nucleus. Two types of RR proteins have been distinguished in Arabidopsis – RR A and RR B (Punwani et al., 2010). RR B acts as a transcription factor, initiating the expression of target genes. Conversely, RR A lacks DNA-binding ability and competes with RR B for phosphate from AHPs. Consequently, RR A is posited to be a component of the negative feedback loop (To et al., 2007; Argyros et al., 2008; Hill et al., 2013).

Interestingly, subcellular localisation of HKs was initially proven in the PM (Kim et al., 2006). However, the later studies suggested their occurrence on the ER with the CK sensing domain oriented into the ER lumen (Wulfetange et al., 2011; Romanov et al., 2018). Recently, the evidence of the CK receptors on the PM has been supported by the study utilizing the CKs immobilized on the beads unable to penetrate into the cytosol (Antoniadi et al., 2020). The CK response was activated by the HKs localized on the PM. Another research group proved the dual occurrence of the CK receptors via fluorescently labelled CK probe and HK fused green fluorescent protein reporter (Kubiasová et al., 2020).

3.2 Acidic phytohormones

3.2.1 Auxins

Auxins, together with CKs, belong to the long-term studied phytohormonal classes (Went, 1937). They are best known for the regulation of the botanical motions reacting on the environmental stimuli. This acting has been named as tropism, which has been evolutionary developed in the plants as a strategy to reach favourable environmental conditions by change of the growth direction. Through the auxin, the plant drives self-motion towards the sunlight (phototropism; Kutchera and Briggs, 2016), regulates an organ development in reaction to touch (thigmotropism; Jaffe et al., 2002), or modulates the root growth vertically to penetrate deeper into the soil (gravitropism; Rosquete et al., 2013). The auxin stimulates the root tip to search for water (hydrotropism; Takahashi et al., 2009) and to avoid the salinized soil (halotropism; Galvan-Ampudia et al., 2013).

These tropic responses are driven by the previously described phenomenon, so called acid growth (Rayle and Cleland, 1992). Auxin signalling induces the expression of auxin-responsive genes, several of which are associated with sodium-potassium adenosine triphosphatase (ATPase) pump localized in the PM. This ATPase facilitates the translocation of H^+ ions out of the cell, resulting in a decrease of extracellular pH. Consequently, pH-dependent protein family of expansins loosen the cell wall, leading to increased cell volume and elongation, thereby facilitating macroscopic plant cell motion (Majda and Robert, 2018).

Currently, indole-3-acetic acid (IAA), 4-chloroindole-3-acetic acid, indole-3-butyric acid, and phenylacetic acid have been identified as naturally occurring auxins, with IAA being the most active and extensively studied compound (Simon and Petrášek, 2011). Signal transduction occurs within the nucleus following the binding of IAA to the TIR1 receptor employed in the canonical signalling pathway. Addition to IAA signalling, the biological response is intricately linked to transport of IAA into and out of the cell. Extracellular IAA is transported passively into the cell via diffusion. This process is facilitated by the fact that IAA, as a weak acid, remains uncharged in the acidic extracellular environment. However, upon entry into the neutral cytosol through the PM, the carboxyl group of IAA dissociates, resulting in the formation of a charged species that prevents its re-enter into the PM (Rubery and Sheldrake, 1974). Conversely, the efflux of IAA from the cytosol through the PM is a dynamic process. This process is facilitated by PIN transporters, which are dynamically localized in the PM, ER, or diffused within the cytosol. Family of PIN proteins, activated by phosphorylation, mediate the efflux of IAA. The transport of IAA via PIN proteins represents one of the strategies employed to regulate its intracellular concentration and maintain homeostasis (Friml et al., 2002). Another strategy involves the metabolism of bioactive IAA into non-active forms. Current knowledge about IAA metabolism delineates three mechanisms for deactivation.

First, IAA undergoes conjugation with amino acid, primarily with aspartic acid and glutamic acid, by the GRETCHEN HAGEN 3 (GH3). Subsequent IAA amino conjugates can be oxidated through the action of the DIOXYGENASE FOR AUXIN OXIDATION 1 (DAO1; Porco et al., 2016; Zhang et al., 2016; Hayashi et al., 2021). The product, amino acid conjugates of 2-oxoindole-3-acetic acid (oxIAA), can be hydrolysed further by amidohydrolase IAA-LEUCINE RESISTANT 1 (LeClere et al., 2002) to oxIAA, which is considered as the final inactive metabolite in Arabidopsis. The recent

update on auxin metabolism proposed the model delineating IAA amino conjugates as the preferred substrate for DAO1 (Hayashi et al., 2021). Therefore, it is believed that majority of oxIAA comes from IAA amino conjugates instead of free IAA.

Furthermore, the family of UGT catalyses the esterification of IAA to IAA-glucosyl ester by UGT84B1 (Jackson et al., 2001), and oxIAA to oxIAA-glucosyl ester by UGT74D1 (Tanaka et al., 2014). In contrast to metabolism, *de novo* IAA is synthesized via four pathways (reviewed by Ljung, 2013; Casanova-Sáez R and Voß, 2019). Briefly, in the indole-3-pyruvic acid (IPyA) pathway, tryptophan aminotransferases TAA1, TAR1, and TAR2 catalyse the production of IPyA from L-tryptophan (TRP). Subsequently, IPyA is converted to IAA by the YUCCA enzyme. This pathway is considered the primary biosynthetic route in higher plants (Stepanova et al., 2005; Mashigushi et al., 2011). Second, TRP is converted to indole-3-acetamide (IAM), and IAM hydrolases catalyse the conversion of IAM to IAA. Although originally described in bacteria, the presence of IAM has also been demonstrated in higher plants such as Arabidopsis (Sugawara et al., 2009; Novák et al., 2012). Third, tryptamine (TRA) is a metabolite of TRP catalysed by TRP decarboxylases and is considered an independent intermediate of IAA. However, its low concentration in plant tissues suggests that the TRA pathway plays a minor role in IAA biosynthesis (Novák et al., 2012). Fourth, the indole-3-acetaldoxime (IAOx) pathway involves the conversion of TRP to IAOx, which serves as the precursor of indole-3-acetonitrile (IAN). Finally, IAN can be converted to IAA by nitrilases. This pathway has been identified specifically in the *Brassica* genus (Normanly et al., 1997; Park et al., 2003).

3.2.2 Salicylic acid

Among the naturally occurring low molecular weight substances abundantly found in plant tissues are phenolic compounds, also referred as secondary metabolites. The term "secondary" originates from the historical belief that phenolic compounds do not play a fundamental role in plants (Vlot et al., 2009). However, for several decades, it has been known that phenolic compounds significantly contribute to lignin biosynthesis and thus cell wall formation, as well as to responses to the environmental condition changes. One of these compounds is SA. Although the role of SA in plants has only recently been discovered, its existence and medicinal uses have been known for over 200 years (Ding and Ding, 2020). In the 19th century, SA was isolated for its anti-inflammatory and

antipyretic effects. In plants, SA plays a similar role, as it is involved in resistance to phytopathogens and temperature regulation.

Studies on the *Sauromatum guttatum* have demonstrated that SA is involved in the process of thermogenesis, where the plant's temperature is increased compared to its close environment. The primary source of heat is the inhibition of the electron transport chain in mitochondria during respiration, releasing accumulated energy in the form of heat (Norman et al., 2004). SA induces this effect through the expression of alternative oxidases.

In case of pathogen infection, SA participates in local and systemic defence responses, which are most visibly manifested by the formation of lesions at the infection site due to accumulated reactive oxygen species (Dempsey et al., 1999). SA is also involved in the flowering process (Jin et al., 2008). The starting substrate for SA biosynthesis is chorismic acid derived from the shikimate pathway, which is converted to SA either through the isochorismate (IC) pathway (Wildermuth et al., 2001; Strawn et al., 2007), or via phenylalanine and cinnamic acid through the phenylalanine ammonia-lyase pathway (Raes et al., 2003; Rohde et al., 2004). Currently, it is believed that the IC pathway is dominant in Arabidopsis, accounting for 90% of SA biosynthesis (Ding and Ding, 2020).

Plants are equipped with a range of mechanisms responsible for maintaining homeostasis, particularly in the metabolism of SA. Essentially, these mechanisms are similar to those described in the metabolism of auxins. In Arabidopsis, uridine diphosphate glucosyltransferases UGT74F1 and UGT74F2 catalyse glucosylation at either the carboxyl or hydroxyl group, converting SA to salicylate glucosyl ester or SA 2-*O*-β-D-Glucoside. These two compounds are then transported into a vacuole, where they serve as storage forms, which can be converted back to bioactive SA by β-glucosidase (Dean and Delaney, 2008; George Thompson et al., 2017; Vaca et al., 2017). Similarly, methylation is another strategy for reversible SA biotransformation, catalysed by SA carboxyl methyltransferase. Methyl SA can be converted back to SA by methylesterases (Park et al., 2007). Also sulfonation is expected but the SA sulfonates has never been identified in plants yet (Ding and Ding, 2020). Additionally, similar to auxins, SA activity is regulated by the GH3 family of enzymes, which convert SA to inactive amino acid conjugates, primarily SA-L-aspartate (Bourne et al., 1991; Zhang et al., 2007). Finally, SA can undergo hydroxylation to form two isomers of

dihydroxybenzoic acid (2,3-DHBA and 2,5-DHBA; Maskos et al., 1990; Zhang et al., 2017).

3.2.3 Jasmonates

The stationary lifestyle represents a significant energy-saving strategy for plants, eliminating the need to invest energy in physically demanding locomotion. Unlike animals, plants are unable to move from their habitats when faced with adverse changes in their environment. Consequently, they have evolved mechanisms to defend themselves against immediate dangers while remaining in place. Besides pathogen infection, against which plants defend themselves via SA, they must confront a variety of other biotic and abiotic stress factors, including drought or mechanical damage. Biologically active compounds from the JAs group have been described as signalling molecules that mediate this defence (Wasternack and Hause, 2013). The response to the JAs signal involves not only gene expression but also influences various developmental processes such as senescence, root growth, or generative organ development (Smyth et al., 1990; Mandaokar et al., 2006).

From a chemical standpoint, (+)-7-*iso*-jasmonic acid (JA) belongs to the group of oxygenated fatty acids (oxylipins). Their biosynthesis is based on the gradual shortening of the carbon chain of the initial fatty acid, which can be either α-linolenic (18:3) or hexadecatrienoic (16:3) acid, also known as roughanic acid, both localized in the chloroplast membrane. These two independent substrates lead to the formation of JA through two independent metabolic pathways. Both pathways start with the action of three common enzymes: lipoxygenase, allene oxide synthase, and allene oxide cyclase. α-linolenic acid yields *cis*-(+)-12-oxo-phytodienoic acid (*cis*-OPDA), while roughanic acid produces dinor-(+)-12-oxo-phytodienoic acid (dn-OPDA; Weber et al., 1997; Schaller and Stintzi, 2009). These two intermediates are then transported to the peroxisome membrane, where they undergo peroxisomal activity of OPDA reductase OPR3. *cis*-OPDA is converted to 3-oxo-2-(2-pentenyl)-cyclopentane-1-octanoic acid (OPC-8), and dnOPDA is converted to 3-oxo-2-(2-pentenyl)-cyclopentane-1-hexanoic acid (OPC-6). Both intermediates are further transformed into JA through beta-oxidation (Vick and Zimmerman, 1984; Schaller et al., 1998; Stintzi and Browse, 2000).

In the signalling pathway of JAs, the CORONATINE INSENSITIVE 1 (COI1) receptor holds a pivotal position. Surprisingly, while IAA and SA exhibit biologically

active properties, JA itself demonstrates weak activity and binds only weakly to this receptor (Fonseca et al., 2009). Instead, the ligand for COI1 in vascular plants is (+)-7-*iso*-jasmonoyl-L-isoleucine (JA-Ile), which is formed by adenylation and subsequent conjugation with the amino acid isoleucine. This reaction is catalysed by the enzyme acyl acid-amido synthetase JAR1 from the gene family of GH3 (Staswick and Tiryaki, 2004). In addition to the well-described biological activity of JA-Ile, the idea has been recently introduced that the conjugation of *cis*-OPDA with isoleucine leads to a direct and specific gene response (Arnold et al., 2016; Floková et al., 2016). However, the perception of this signal remains largely unexplained.

To maintain balance in JAs signalling, plants are equipped with a wide array of enzymatic and non-enzymatic transformations, many of which are still not fully understood. Hydroxylation of JA leads to the formation of the inactive metabolite 12-hydroxy-JA, also known as tuberonic acid (Bruckhoff et al., 2016), which can subsequently undergo sulfonation via the sulfotransferase AtST2a derived from Arabidopsis (Hirschmann et al., 2014). Similarly, methylation catalysed by JA methyl transferase converts JA to its inactive methyl ester (Sheard et al., 2010). In contrast, glucosyl ester and 12-*O*-glucoside of JA exhibit partial biological activity (Andolfi et al., 2014), as does the product of decarboxylation, *cis*-jasmone (Mathes et al., 2010). A separate aspect of jasmonate metabolism involves conjugation with amino acids. In addition to conjugation with isoleucine, conjugation with alanine, valine, leucine, or methionine has been described (Yan et al., 2016). Biologically active conjugates can further undergo hydroxylation, carboxylation, methylation, glucosylation, or be converted back to JA by amidohydrolases IAR3 and ILL6 (Heitz et al., 2016).

3.3 Targeted analysis of plant hormones in the plant tissues

The following chapter represent a comprehensive study of representative papers on phytohormone analysis retrieved on Web of Science (Fig. 2). The examination of plant hormones requires the use of MS instrumentation for its exceptional selectivity and sensitivity. However, using standalone MS systems is not a practical approach. Some researchers focusing on plant hormones have combined MS with capillary electrophoresis (Contreras-Gutierrez et al., 2013). Nevertheless, the prevailing strategy in targeted applications involves the integration of MS with chromatography (Fig. 2A). This combination enables the robust separation of targeted compounds, both from each other

and from chemically similar compounds within the intricate plant matrix. Ongoing advancements in chromatographic systems have led to the development of various methodologies.

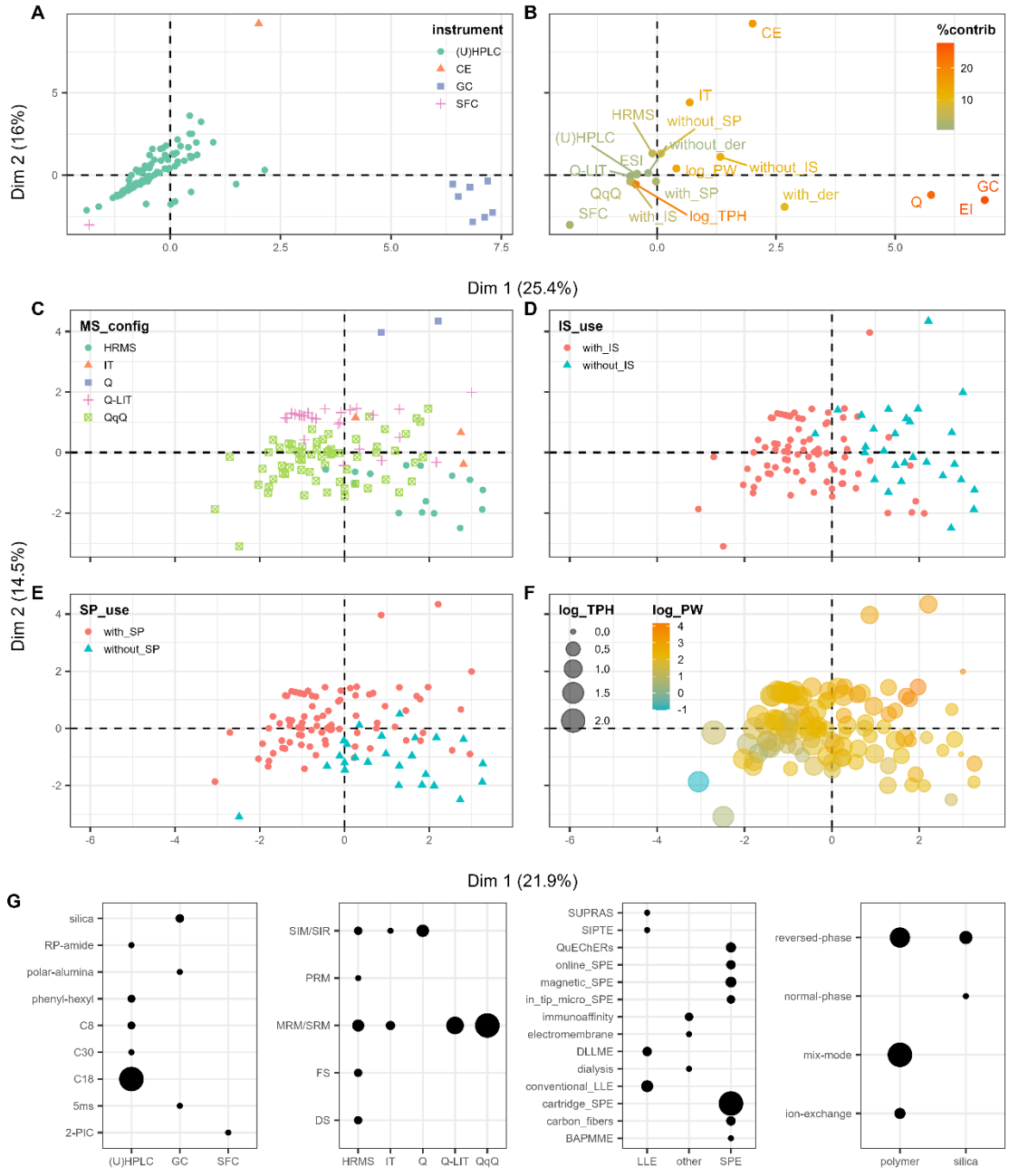

Fig. 2. Multivariate visualization of recent publications dealing with targeted plant hormone analysis retrieved from Web of Science. (**A**) The score factor map shows 113 publications analysing phytohormones with (U)HPLC-MS, 7 publications with GC-MS, 1 publication with CE-MS, and 1 publication with SFC-MS. The position of each publication in the score factor map is given by (**B**) the contribution (%) of the analytical features in the loading factor map. The axes in both factor maps represent first and second principal component calculated by factor analysis of mixed data. The (U)HPLC-MS publications are shown in individual score factor maps C-F coloured based on (**C**) mass spectrometry configuration, (**D**) internal standard use, (**E**) sample preparation use, and (**F**) sample plant weight used sized based on total number of plant hormones analysed. (**G**) The bubble plots show the proportion of publications using (from the left) types of chromatographic column, data acquisition mode, sample purification method and type of solid phase extraction sorbent. **Abbreviations:** (5%-phenyl)-methylpolysiloxane (5ms), octyl (C8), octadecyl (C18), triacontyl (C30),

capillary electrophoresis (CE), derivatization (der), dispersive liquid-liquid microextraction (DLLME), product ion scan (daughter scan; DS), electron impact (EI), electrospray ionization (ESI), full scan (FS), gas chromatography (GC), high resolution mass spectrometry (HRMS), internal standard (IS), ion trap mass spectrometer (IT), liquid-liquid extraction (LLE), multiple/selective reaction monitoring (MRM/SRM), parallel reaction monitoring (PRM), plant weight in milligram of fresh weight (PW), quadrupole mass spectrometer (Q), quadrupole-linear ion trap (Q-LIT), triple quadrupole mass spectrometer (QqQ), Quick, Easy, Cheap, Effective, Rugged, and Safe extraction (QuEChERS), reversed phase (RP), single ion monitoring/reaction (SIM/SIR), Sequential Solvent-Induced Phase Transition Extraction (SIPTE), sample preparation (SP), solid phase extraction (SPE), supramolecular solvents (SUPRAS), number of total plant hormones analysed (TPH), (ultra)high-performance liquid chromatography ((U)HPLC).

3.3.1 Gas chromatography–mass spectrometry

Among these methods, gas chromatography (GC) remains the oldest yet enduringly employed technique in plant hormone research. Notably, GC-MS has emerged as a suitable approach for volatile compound analysis, with recent investigations focused on ethylene (Rawlinson et al., 2015; Pereira et al., 2017). Furthermore, GC-MS, in conjunction with derivatization, has been utilized for the quantification of acidic plant hormones such as auxins, JA, ABA, SA, and gibberellins (Yang et al., 2013; Luo et al., 2013; Porfirio et al., 2016; Zou et al., 2019; Kebert et al., 2022). These applications have consistently employed silica-based chromatographic columns, electron impact ionization (EI), and single quadrupole detection (Q). It is important to note that EI is acknowledged as a hard ionization technique, resulting in the production of numerous in-source fragments. Consequently, the targeted determination of plant hormones by GC-MS relies on spectral analysis or single ion monitoring facilitated by the single quadrupole detector (Fig. 2B).

3.3.2 Liquid chromatography–mass spectrometry

Nevertheless, data retrieved from the Web of Science indicates a noticeable shift towards the increased prominence of high-performance liquid chromatography (HPLC) coupled with Mass Spectrometry (MS). Recently, HPLC-MS, and its ultra-high performance variant, UHPLC-MS, stand as the predominant technologies in the plant hormone research (Fig. 2A-B). This trend is not surprising, given that the majority of plant hormones and their metabolites are non-volatile and soluble in a liquid mobile phase. Moreover, the (U)HPLC mobile phase can be easily manipulated to facilitate the separation of polar compounds (such as auxins and CKs), semi-polar compounds (including JAs, abscisates, and gibberellins), or relatively non-polar compounds (such as strigolactones and brassinosteroids) without the necessity of chemical derivatization. As depicted in Fig. 2G, (U)HPLC-MS applications commonly employ reversed-phase (RP)

columns, comprising octadecyl, phenyl-hexyl (Trapp et al., 2014; Oklešťková et al., 2017), or amid in RP mode (Dziurka et al., 2019). In contrast to targeted analysis of plant hormones by GC-MS using exclusively EI sources, recent studies with (U)HPLC-MS employed electrospray ionization (ESI) (Fig. 2B). This trend is obvious, because the ESI belongs to the soft ionization techniques providing much less in-source fragmentation compared to EI. This facilitates the interpretation of MS spectra and the selection of the targeted molecular ions.

3.3.3 Supercritical fluid chromatography–mass spectrometry

A remarkable trend in the development of chromatographic instruments over the past decade has been the technological advancement of SFC (Desfontaine et al., 2015). SFC instruments are designed to maintain constant pressure and temperature within the chromatographic system. Thus, the gas introduced into the system can be converted into a supercritical state, where it serves as the mobile phase. Considering safety and physicochemical properties, carbon dioxide has proven to be a suitable type of gas for SFC, prevailing in the vast majority of applications. However, the high non-polarity of carbon dioxide limits applicability of separation to exclusively non-polar compounds. Nevertheless, modern SFC systems with significantly improved robustness allow for the addition of an organic modifier, such as methanol, ethanol, or acetonitrile, to the supercritical carbon dioxide ($scCO_2$; West, 2018). This modification increases the polarity and elution strength of the mobile phase, expanding the applicability of SFC to semi-polar and polar compounds. Additionally, contemporary SFC systems are equipped with an isocratic pump that adds supplementary organic solvent, also known as make-up solvent, between the chromatographic column and detector. This prevents sample precipitation, facilitates ionization, and enables the coupling of SFC with MS detection. Consequently, SFC-MS has gained popularity in various applications, ranging from pharmaceutical analysis to pesticide detection in food, and analysis of bioactive compounds (Gazárková et al., 2022). Despite its apparent advantages, SFC-MS instrumentation has not been utilized for the analysis of plant hormones until recently. As indicated in Fig. 2A, this was changed very recently when a study focusing on the analysis of CKs using SFC-MS/MS was published (Petřík et al., 2024).

3.3.4 Mass spectrometry configurations

The prevailing approach in recent plant hormone research involves the coupling of (U)HPLC with MS/MS (Fig. 2C). This strategic choice enhances the annotation of targeted compounds by introducing an additional identifier. In addition to the specific retention time and mass-to-charge ratio (*m/z*) value of the targeted ion, tandem mass spectrometry MS/MS facilitates identification through post-source fragmentation in a collision cell or an ion trap. The resultant fragment ions are either comprehensively analysed as whole spectra (Wu et al., 2014) or, more commonly, as a selected fragment ion resulting in higher sensitivity by multiple/selective reaction monitoring (MRM/SRM), which has gained widespread popularity (Fig. 2G).

One of the prevalent methodologies in MS/MS for targeted analysis of plant hormones involves the utilization of a triple quadrupole spectrometer (QqQ) (Fig. 2C). The primary advantage of the QqQ resides in its rapid switching between MRM/SRM transitions, enabling the simultaneous detection of numerous targeted compounds with adequate sensitivity and fast data acquisition. A comparable and widely adopted alternative is the employment of quadrupole-linear ion trap mass spectrometers (Q-LIT) (Cai et al., 2013; Záveská Drábková et al., 2015; Zemanová et al., 2019; Fresno et al., 2023). However, both solutions are constrained by low mass resolution (current QqQ and Q-LIT spectrometers operate close to unit resolution), leading to an increased likelihood of misannotated targeted compounds (Douglas & Konenkov, 2014; Geib et al., 2016). Consequently, some researchers have opted for high-resolution tandem mass spectrometers (HRMS), such as quadrupole-time-of-flight or quadrupole-Orbitrap (Q-Orbitrap), to enhance the selectivity of detected ions (Seto et al., 2014; Ordaz-Ortiz et al., 2015; Hashiguchi et al., 2023; Kijidani et al., 2023). However, the selectivity of HRMS depends on application, instrumentation and settings. Consequently, the selection of the appropriate MS configuration is kind of a trade-off between sensitivity and selectivity.

Recently, a novel approach to data acquisition known as parallel reaction monitoring (PRM) has been introduced in HRMS (Kisiala et al., 2019). The authors employed a Q-Orbitrap instrument operating in PRM to monitor multiple CKs. In comparison to MRM/SRM, PRM demonstrated a significant enhancement in sensitivity, reaching levels comparable to QqQ instruments. Despite this promising improvement in HRMS, the preceding decade has witnessed the continued prevalence of low-resolution instruments, and their inherent lack of selectivity has been addressed through other

strategies such as the utilization of internal standards (IS) or sample preparation procedures (Vrobel and Tarkowski, 2023).

3.3.5 Internal standards and their replacements for an accurate quantification

The complex composition of plant matrices introduces significant biases in the identification and quantification of plant hormones. The extent of this matrix effect varies depending on the chemical composition of the plant material, leading to changes in ionization yield causing signal suppression or enhancement (Tang and Kebarle, 1993; Cappiello et al., 2008). Moreover, components within the plant matrix may resemble the targeted compounds, resulting in false-positive outcomes due to similar *m/z* values and retention times. Additionally, factors such as random or systematic sensitivity fluctuations can alter the MS signal, introducing biases in quantification.

To address these challenges, a prevalent approach in recent years has been the integration of IS to mitigate matrix-induced alterations and improve signal annotation reliability. Stable isotope-labelled IS are being particularly favoured due to their physico-chemical resemblance to the targeted compounds, enabling accurate quantification through the isotope dilution method (Rittenberg & Foster, 1940). However, the synthesis of these IS is complex, leading to higher cost of analysis. Some of them are not commercially available. As an alternative, quantification utilizing structural analogues such as triphenyl phosphate has been employed (Martinez et al., 2020; Yao et al., 2022).

Current research has explored the analysis of plant hormones in biological materials even in the absence of IS using the non-labelled standard addition method (Yonny et al., 2020; Hashiguchi et al., 2021). This method involves preparing matrix-matched calibrations for individual samples to enable precise quantification. However, in large-scale studies, the standard addition method may prove impractical due to the generation of numerous samples. Some researchers have utilized matrix-matching to evaluate matrix effects and quantify phytohormones based on non-normalized signal intensities (Kasote et al., 2016; Cao et al., 2016; Mogal et al., 2022). Although straightforward, this approach is highly sensitive to variations in matrix composition or losses during analytical procedures, necessitating a specialized quality control system to address analytical anomalies.

Importantly, the utilization of IS combined with a sample preparation procedure has become the mostly adopted approach in mitigating the matrix effect for plant hormonomics (Fig. 2D-E).

3.3.6 Sample preparation

As illustrated in the Fig. 2G, the current landscape of plant hormone sample preparation is characterized by two well-established approaches: liquid-liquid extraction (LLE) and SPE. The traditional LLE method using ethyl acetate, hexane or diethyl ether stands as the oldest yet evolving technique (Xiao et al., 2018; Sugahara et al., 2020; Kojima et al., 2021). However, ongoing advancements in LLE have led to various modifications. The Dispersive Liquid-Liquid Microextraction technique has been employed for extracting acidic plant hormones such as auxins, ABA, or SA (Luo et al., 2013; Lu et al., 2015; Porfirio et al., 2016). A recently introduced method, Sequential Solvent-Induced Phase Transition Extraction, enables the purification of both alkaline and acidic phytohormones (Cai et al., 2015). Additionally, the use of supramolecular solvents has been proposed as a potential purification technique for quantifying stress-related phytohormones (Yonny et al., 2020).

Parallel artificial liquid membrane extraction (PALME) represents a miniaturized LLE method not yet implemented in plant hormonomics (Gjelstad et al., 2013). However, several works dealing with the analysis of pharmaceutically important compounds have been conducted recently suggesting the potential use of PALME for plant hormones purification (Pilařová et al., 2017; Bouchouareb et al., 2022; Ahmed et al., 2024). PALME employs the three-component system comprising two aqueous phases separated by an immiscible organic phase, immobilized within a polymeric membrane (Fig. 4A). The original study introduced PALME in a 96-well plate format (Gjelstad et al., 2013). The crude aqueous sample, also known as a donor phase, is pipetted into a well in the plate. Subsequently, a thin membrane, moistened with a minute amount of organic solvent, is positioned on the top of the well to cover the donor phase. Importantly, the upper surface of the liquid membrane is covered by the acceptor aqueous phase. Donor and acceptor phases differ in pH, which is crucial for the extraction process. Neutral analytes migrate from the donor into the liquid membrane and subsequently into the acceptor phase (Fig. 4B). This sandwich-like experimental design ensures that the analytes in the acceptor phase acquire a charge due to pH alterations, thus preventing them to return back into the

organic phase. Unlike the classical well-established protocols utilizing the conventional SPE, the PALME benefits from the production of the extract, which has not to be evaporated after the procedure. It is because the PALME extract is preconcentrated in aqueous solvent and can be directly injected into UHPLC-MS/MS system saving the analytical time and avoiding the losses during the evaporation (Gjelstad et al., 2013).

Among the SPE techniques, the current plant hormonomics relies on traditional extraction cartridges playing a pivotal role (Fig. 2G). Notably, RP polymeric sorbents have emerged as favoured choices within this context. Moreover, there is considerable rise in popularity of mixed-mode polymer sorbents that combine ion exchange and RP (Gong et al., 2017; Matsuura et al., 2019; Lopez-Guerrero et al., 2022). Both polymeric materials currently dominate over the previously favoured silica-based sorbents (Fig. 2G). Despite the widespread use of extraction cartridges, the research landscape increasingly emphasizes miniaturization within SPE. Adopted or innovative methodologies have been employed for the preparation and purification of phytohormone samples in the last decade. Boronate affinity polymer monolith microextraction has been applied to prepare endogenous brassinosteroid samples (Ding et al., 2013). In another instance, ionic liquid-functionalized carbon fibres microextraction has been proven effective for the purification of acidic, alkaline, and neutral phytohormones (Jon et al., 2020). The adoption of the Quick, Easy, Cheap, Effective, Rugged, and Safe (QuEChERS) dispersive SPE method has been notable in several procedures targeting CKs, auxins, gibberellins, and SA (Xie et al., 2014; Martinez et al., 2020; Mandal et al., 2021; Mogal et al., 2022). Additionally, advanced methods utilizing magnetic SPE particles for scavenging multiple phytohormones, including gibberellins, auxins, and stress-related compounds, have been implemented (Liu et al., 2014; Cai et al., 2015; Luo et al., 2021; Zhang et al., 2023). The same authors combined magnetic SPE with in-situ derivatization to increase the ionization yield of targeted compounds and enhance the MS response (Cai et al., 2019). Additionally, magnetic nanoparticles coated by immunosorbent were implemented for the selective purification of multiple CKs (Plačková et al., 2017). Methods based on in-tip SPE were successfully developed for the purification of auxins and JAs (Svačinová et al., 2012; Pěnčík et al., 2018; Široká et al., 2022).

These advancements underscore the ongoing efforts to minimize the consumption of consumables and the amount of input biological material, which allows the downscale in research on cellular or subcellular levels. As illustrated in Fig. 2F, the researchers

dealing with the broad studies of many plant hormones and metabolites worked with a minute amount of the sample more frequently than researchers aiming on one or several analytes (Fig. 2F). There can be several reasons for that observation. For example, the authors utilizing HRMS for targeted analysis of plant hormones (bottom right quadrant in Fig. 2C) were forced to employ a higher amount of plant material (bottom right quadrant in Fig. 2F) to achieve the detection limits.

In summary, the plant hormonomics benefits from the downscaling since lower amount of plant sample renders lower matrix effect. Consequently, the downscaling complements the internal standard, sample purification and UHPLC-MS/MS instrumentation in development of successful plant hormonomics workflow.

3.3.7 Method development and experimental design

The development of a bioanalytical method based on UHPLC-MS/MS is a long-term multistep process including sample preparation, purification, chromatography separation, detection, data normalization, calibration and validation (Nováková, 2013). Each step is a potential source of the systematic or random error, which may be critical for an accurate determination of the analyte in the sample. Therefore, it is essential to optimize the entire analytical process to ensure effective sample preparation, efficient chromatographic separation, sensitive and selective detection, and linear calibration, ultimately leading to accurate results.

The primary objective of optimization is to identify critical method parameters and determine their optimal setpoint. The traditional approach, known as One-Factor-At-A-Time (OFAT), involves optimizing parameters one at a time (Fig. 3A). In OFAT, the process is performed with one factor varied while keeping all other factors fixed. The value of the factor that yields the best result is selected for the next step. While this approach is straightforward and does not require specialized software, it has limitations. By optimizing factors individually, OFAT fails to detect interactions between factors, which can lead to the risk of achieving a false optimum (Czitrom, 1999).

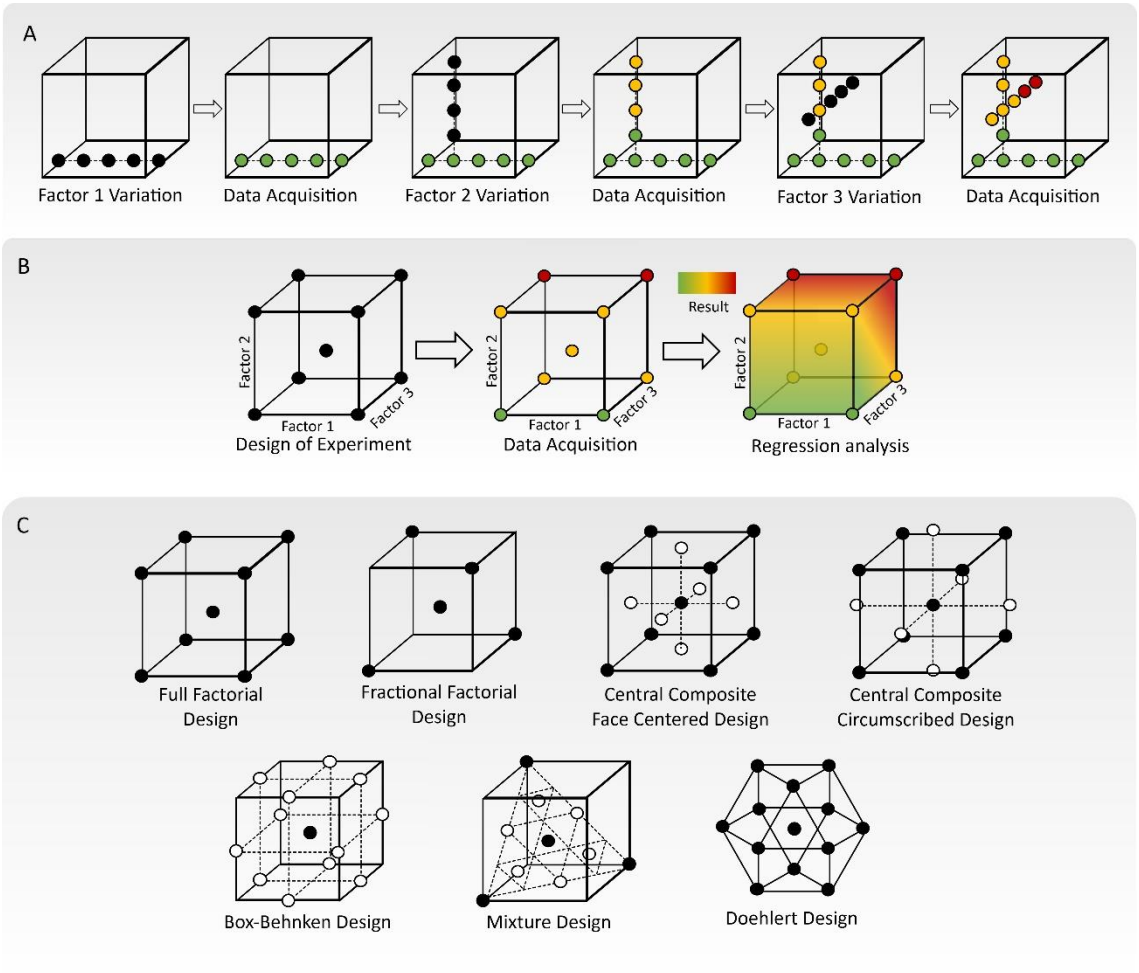

Fig. 3. Experimental designs for method development. (**A**) One-Factor-At-Time (OFAT) approach develops a method step-by-step. The cube represents three parameters (factors) of the developed method (one parameter corresponds to one edge of the cube). The circles inside represent samples prepared based on combinations of these parameters. In each step, one factor is varied while the others are fixed. The colour of the circles corresponds to the measured result. Optimal conditions are reached by selecting factor values that yield the best results at each step. (**B**) Design of Experiment (DoE) approach develops the method statistically. The positions of the samples are represented by the shape of a regular object, typically a cube, in the experimental space. Unlike OFAT, all factors in DoE are varied simultaneously to determine the direction of the optimum. The optimal setpoint is determined through regression analysis. (**C**) Examples of various DoE plans commonly recommended in chemometrics. Full Factorial Design and Fractional Factorial Design are particularly used for the screening phase of method development, while the other designs are employed for the optimization phase.

Recently, the statistically based Design of Experiment (DoE) have been adopted for the method development in the pharmaceutical research (Politis et al. 2017). Unlike OFAT approach, DoE optimizes all factors simultaneously, with results predicted through regression analysis (Fig. 3B). The concept of DoE can be visualized as an experimental space, where each factor represents a dimension bounded by low and high values set by the experimenter. This range between limits forms the edges of a regular object, typically a cube, with its corners representing individual samples. In other words, samples in DoE are defined by specific balanced combinations of low and high values for optimized

factors. During experimentation and data acquisition, results are assigned to particular positions within the cube, and values between corners are estimated mathematically through multiple linear regression. This aspect of DoE allows for investigation of factor interactions, enhancing the likelihood of finding the global optimum of the method.

Two main approaches of DoE are established in practice: screening and optimization (Fig. 3C). In the screening phase, the experimenter selects candidate factors suspected to have an effect, often when little is known about the process. In contrast, the optimization mode focuses solely on the most effective factors to attain an optimal setpoint, typically employing response surface methodology (Ferreira et al., 2017; Bezerra et al., 2008; Novaes et al., 2016).

Table 1. Number of publications found on Web of Science based on the search of "Design of Experiment" and specific application.

Specific application	No. of publications
Industry	1747
Pharmaceutics	173
Chemometrics	49
Metabolomics	27
Bioanalysis	8
Proteomics	8
Genomics	7
Transcriptomics	3
Genetics	2

The concept of DoE was initially introduced at the beginning of the 20th century by Sir Ronald Fisher, a statistician at Rothamsted Research, during the planning of field experiments (Fisher, 1926). Subsequently, several mathematical algorithms were developed to construct experimental designs, leading to their widespread adoption and establishment in various industries (Box and Hunter, 1957; Box and Hunter, 1961). One of the main advantages of DoE is its ability to provide maximum statistical information from a minimal number of samples, thus saving both time and financial resources. Importantly, DoE has been integrated as a chapter of chemometrics (Brereton, 2003), and various generic designs have been introduced in analytical method development (Fig. 3C; Ferreira et al., 2004; Ferreira et al., 2007; Bezerra et al., 2020). Nowadays, DoE is considered as a more efficient tool for method development compared to OFAT (Czitrom, 1999; Politis et al. 2017). On the other hand, it requires statistical software, expertise, and computational resources. Based on the search on the Web of Science from 4 April 2024, most applications utilizing DoE have been observed in the industry and pharmaceutical sectors, likely due to its benefits in saving time and financial resources (Table 1). Nevertheless, applications of DoE in other fields remain limited. Occasionally, the use of

DoE in plant-related methods has been reported, such as in the production of bacterial culture or the regeneration of transgenic plants (Clicquet et al., 1994; Chu et al., 2019). However, the application of DoE in plant hormone research has yet to be explored.

3.3.8 Method validation

Even the thoroughly developed and optimized quantitative bioanalytical method yield results with a certain degree of uncertainty. The reliability of the estimation is determined by method accuracy and precision, which are described as the magnitude of systematic error and random error, respectively. Both parameters may depend on recovery of the extraction procedure, matrix effect, detection limits or calibration linearity (Nováková, 2013). Their values are measured in the process called method validation and their acceptable limits depend on the rules given by the application field and/or requirements of the local authority, such as Food and Drug Administration (FDA; Matuszewski et al., 2003), European Medicines Agency (Kaza et al., 2019) or The International Council for Harmonisation of Technical Requirements for Pharmaceuticals for Human Use (Plachká et al., 2020; Mula et al., 2023). Unlike the pharmaceutics or diagnostics, the plant hormonomics is not regulated by any authority. However, the method validation should follow optionally one of the recommended guidelines (Šimura et al., 2018).

4 Material and methods

The following section provides a concise overview of the material and methods used to achieve the results discussed below. A detailed description of specific methods and equipment is available in *Supplements II-VIII*.

4.1 Chemicals

The plant hormone chemical standards and their stable isotope labelled analogues were obtained from Olchemim Ltd. or Palacký University in Olomouc, Faculty of Science (both Olomouc, Czech Republic). Stable isotope labelled standards of CK *N*7- and *N*9-glucosides were synthetized at Department of Organic Chemistry, Faculty of Science, Palacký University in Olomouc (Czech Republic). The organic solvents methanol, acetonitrile and 2-propanol, all in LC-MS purity, were purchased from Merck (Darmstadt, Germany). Ammonia hydroxide solution 25% (v/v) and formic acid 99% (v/v) both for LC-MS were obtained from Honeywell Fluka™ (Bucharest, Romania). Ultrapure deionized water was produced in-house using Millipore Direct-Q® 3 UV system (Millipore, Bedford, MA, USA).

4.2 Plant material

Arabidopsis thaliana (ecotype *Col-0*) seeds were planted on half Murashige & Skoog medium. The whole seedlings, grown under long-day conditions, were harvested 10 or 21 days after germination. Hybrid aspen clone T89 (*Populus tremula* × *tremuloides*) was obtained from the transformation facility at the Umeå Plant Science Centre (Umeå, Sweden). The leaves of 3-month-old treelings, cultivated under long-day conditions, were harvested 3 hours after dawn. *Triticum aestivum* (winter type, variety Turandot) was grown in the Laboratory of Growth Regulators in vermiculite irrigated with Hoagland's nutrient solution (Arnon and Hoagland, 1940), and 7-day-old leaves were harvested. The treelings of Norway spruce (*Pinea abies*) were obtained from the Umeå Plant Science Centre (Umeå, Sweden). Spruce cotyledons were harvested 14 days after sowing and growing under long-day conditions (Brunoni et al., 2020). The harvested samples of *Arabidopsis*, poplar, wheat and spruce were homogenized into fine powder using liquid nitrogen and stored in -70 °C for subsequent weighing of fresh weight (FW). The liverwort *Merchantia polymorpha* strain Tak1 were obtained from the Centre for

Research in Agricultural Genomics (Barcelona, Spain). Gametophytes of this liverwort were harvested from 3-week-old individuals planted on half Gamborg's B5 media under long-day conditions. The cyanobacterium *Nostoc sp.* CCAP 1453/38 was obtained from the Institute of Microbiology, Czech Academy of Sciences (Třeboň, Czech Republic) and grown according to previously described protocol (Chmelík et al., 2019). The samples of *Merchantia* and *Nostoc* were lyophilized and used subsequently as a dry weight. The detailed growing conditions are described in *Supplement II*.

4.3 Instrumentation

UHPLC-MS/MS experiments were performed with an Acquity UPLC® I-Class (Waters, Milford, USA) coupled to a Xevo TQ-XS triple quadrupole equipped with an ESI source (Waters, Manchester, UK). All CK profiles were determined by the previously described methodology in Svačinová et al. (2012). Auxin analysis followed the method published in Pěnčík et al. (2018). Stress related compounds were analysed according to Floková et al. (2014). The full phytohormone profiles were obtained by plant hormonomics method (Šimura et al., 2018). All methods worked with RP chromatography acquiring data in MRM mode. Data were processed using MassLynx v4.2 (Waters, Manchester, UK). Concentrations of the targeted compounds were calculated by the isotope dilution method (Rittenberg and Foster, 1940).

The SFC-MS/MS method was developed using an Agilent 1260 Infinity II LC/SFC hybrid system coupled with an Agilent 6495B Triple Quadrupole equipped with Jet Stream and Dual Ion Funnel systems. During the development, four different chromatographic columns were tested: Zorbax Eclipse Plus C18 3×50 mm, 1.8 µm (Agilent Technologies, Santa Clara, CA USA); Torus DIOL 3×100 mm, 1.7 µm (Waters, Milford, CT, USA); Zorbax RX-SIL 4.6×150 mm, 5.0 µm (Agilent Technologies, Santa Clara, CA USA); Torus 2-PIC 3×100 mm, 1.7 µm (Waters, Milford, CT, USA). For further details on the specific chromatographic conditions, MS tuning and optimal MRM transitions are described in *Supplement III*.

4.4 Sample preparation

4.4.1 Extraction of CKs and acidic plant hormones

10 mg FW of homogenized plant material was weighed into 2 ml microtube and extracted with 1 ml 5% formic acid in 10% methanol (both v/v). Stable isotope-labelled IS were added to the sample as follows: 0.2 pmol for CK bases, CK ribosides and *N*-glucosides, 0.5 pmol for CK nucleotides and *O*-glucosides, 5 pmol for ABA, IAA, oxIAA, IAA amino acid conjugates and glucosyl esters. The specific compounds are listed in *Supplement II*. Three zirconium oxide 2.0 mm extraction beads (Next Advance, Troy, NY, USA) were added and the sample was crushed using a Retsch MM400 bead mill (Retsch, Haan, Germany) at 27 Hz for 5 min. The extract was sonicated for 3 min, incubated in a refrigerator for 30 min with mild shaking and then centrifuged for 15 min at 20,000 rpm and 4 °C (Allegra 64R benchtop centrifuge, Beckman Coulter, USA). The resulting supernatant was collected.

4.4.2 Purification of CKs and acidic plant hormones with cartridge SPE

The crude plant extract was purified by the mix-mode Oasis® MCX 30 mg/1 cc extraction cartridge (Waters, Milford, CT, USA) according to the previously published protocols (Dobrev and Kamínek, 2002; Hoyerová et al., 2006). Briefly, cartridge was activated and equilibrated using methanol and 1 M aqueous solution of formic acid. The crude extract was then loaded onto the activated cartridge and washed with 1 M formic acid. The auxins and ABA were selectively eluted by application of 2 ml 80% methanol (v/v). CK nucleotides and *O*-glucosides were eluted using 1 ml of 0.35 M aqueous solution of ammonia and CK base fraction was eluted by 2 ml of 0.35 M solution of ammonia in 60% methanol (v/v). The auxin and CK fractions were evaporated in a SpeedVac (RC1010 Centrivap Jouan, ThermoFisher, USA), reconstituted in 40 µl of 10% methanol (v/v) and carefully transferred into an LC vial equipped with a glass insert (Chromservis Ltd., Czech Republic).

4.4.3 Purification of phytohormones with SPE in QuEChERs-like dispersive mode

Bulk Oasis® MCX sorbent 30 µm (Waters, Milford, CT, USA) was weighed (2-10 mg) into a 2 ml microtube. The sorbent was moistened with 1 ml methanol, vortexed and centrifuged at 10,000 rpm for 2 min (Allegra 64R benchtop centrifuge, Beckman Coulter,

USA). The supernatant was removed by pipetting, exchanged with 1 ml 1 M formic acid and then the suspension was vortexed and centrifuged. After the removal of supernatant, the crude plant extract was loaded onto the sorbent, vortexed and centrifuged. The following solvents were applied in the same way: 1 ml 1 M formic acid for washing, 1 ml 80% methanol (v/v) for ABA and auxin elution, 1 ml 0.35 M aqueous ammonia for polar CKs elution and 1 ml 0.35 M ammonia in 60% methanol (v/v) for semi-polar CKs elution. The eluates were then evaporated (RC1010 Centrivap Jouan, ThermoFisher, USA), reconstituted in 40 µl of 10% methanol (v/v) and transferred into a glass insert placed in a LC vial.

4.4.4 Purification of phytohormones with dispersive SPE on micro-spin filter (DisperSpin SPE)

The beginning of the protocol was similar to QuEChERs-like dispersive SPE protocol. Briefly, 100 mg of bulk Oasis® MCX sorbent 30 µm (Waters, Milford, CT, USA) was weighed into a 2 ml microtube. The sorbent was moistened with 1 ml methanol, vortexed and centrifuged at 10,000 rpm for 2 min (Allegra 64R benchtop centrifuge, Beckman Coulter, USA). The supernatant was removed by pipetting and exchanged with 1 ml 1 M formic acid. Unlike the QuEChERs-like protocol, the suspension of bulk sorbent was mixed thoroughly and 20-300 µl (2-30 mg) of suspension was pipetted onto a MicroSpin centrifuge nylon filter with 0.2 µm pores (Chromservis Ltd., Czech Republic). The crude plant extract was loaded onto the sorbent aliquot on the filter and centrifuged at 2000 rpm for 5 min. The filtrate was discarded, sorbent on the filter was washed with 0.4 ml 1 M formic acid and centrifuged. The following solvents were applied in the same way: 0.4 ml 80% methanol (v/v) for ABA and auxin elution, 0.4 ml 0.35 M aqueous ammonia for polar CKs elution and 0.4 ml 0.35 M ammonia in 60% methanol (v/v) for semi-polar CKs elution. Similar to QuEChERs-like dispersive SPE protocol, the eluates were evaporated, dissolved in 40 µl of 10% methanol (v/v) and transferred into an LC vial equipped with a glass insert.

4.4.5 Extraction of CK standards with PALME procedure

The PALME procedure was performed as depicted in Fig. 4A. A CK mixture of non-labelled standards (at a concentration of 1 pmol) was diluted into 250 µl of sodium phosphate buffer pH 7.5 and then transferred into a 96-well plate. The membrane

container, either polypropylene (PP) or polyvinylidene fluoride (PVDF), was activated using one of the following organic solvents: 1-hexanol, 1-octanol, 2-octanone, 2-nonanone, dihexyl ether, dodecyl acetate, dihexyl ether modified with 15% bis(2-ethylhexyl)phosphinic acid (DEHP) and dodecyl acetate modified with 15% DEHP.

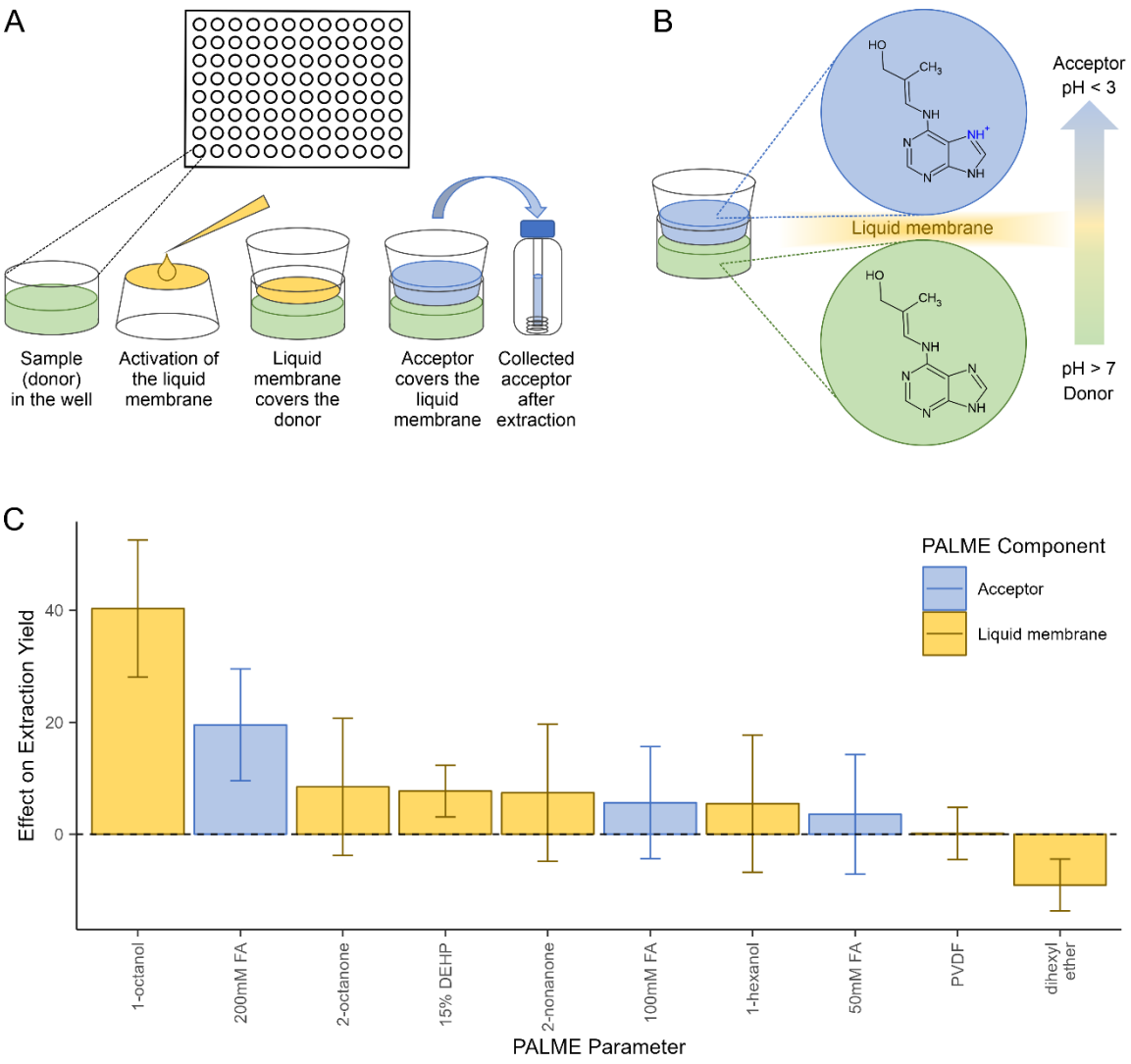

Fig. 4. Parallel Artificial Liquid Membrane Extraction (PALME) of cytokinin (CK) bases. (**A**) Scheme of extraction and workflow in a 96-well plate. (**B**) Principle of extraction. Uncharged CK trespass the liquid membrane into the acceptor, where the molecule is charged due to the acidic pH. The charged CK is not soluble in the liquid membrane and is collected in the acceptor. (**C**) Effect of PALME parameters on extraction yield of CK bases compared to default experimental conditions (liquid membrane consisting of polypropylene moistened in dodecyl acetate, acceptor consisting of 10 mM formic acid and donor consisting of 50 mM sodium phosphate buffer pH 7.5). The bars are coefficients of the statistical model calculated by multiple linear regression. Error bars represent 95% confidence intervals. If the confidence interval covers zero (black dashed line), the parameter is robust, rendering no significant difference compared to default conditions. The bars above the zero represent a positive effect on extraction yield, whereas negative bars indicate a negative effect. Abbreviations: formic acid (FA), bis(2-ethylhexyl)phosphinic acid (DEHP), polyvinylidene fluoride (PVDF).

The container with the activated liquid membrane was inserted onto the sample in the well and covered with 40 µl of acceptor containing an aqueous solution of formic acid at different concentrations (0.01, 0.05, 0.1 or 0.2 mol/l). The plate was covered with a lid and shaken on VWR® Standard 3500 Orbital Shaker (VWR, USA) operated at 900 rpm for 30 min. The acceptor solution was transferred into a LC vial equipped with a glass insert.

4.4.6 Extraction and purification of JAs and SA from plant material

The protocol followed the previously published procedure in Floková et al., 2014. Briefly, 10 mg FW of homogenized plant material was weighed into 2 ml microtube, 1 ml of 10% methanol and three zirconium extraction beads were added. Stable isotope-labelled IS containing 2.5 pmol [$^2H_4$]-SA, [$^2H_6$]-JA, [$^2H_5$]-cisOPDA, and 0.25 pmol [$^2H_2$]-JA-Ile were pipetted into the extract. Similar to *Extraction of CKs, auxins and ABA*, sample was extracted in bead mill at 27 Hz for 5 min, sonicated for 3 min and incubated for 30 min in a refrigerator. The sample was finally centrifuged at 20,000 rpm and 4 °C for 15 min, and supernatant was collected. The supernatant was purified using the RP SPE extraction cartridge Oasis® HLB 30 mg/1 cc (Waters, Milford, CT, USA) as follows: the cartridge was activated by 1 ml methanol and 1 ml water, the sample was loaded, and the cartridge was then washed with 1 ml 10% methanol (v/v). The targeted stress-related compounds were eluted from the sorbent using 3 ml 80% methanol, collected and evaporated using SpeedVac concentrator (RC1010 Centrivap Jouan, ThermoFisher, USA). The sample was reconstituted in 15% acetonitrile (v/v).

4.5 Multivariate data analysis and statistics

4.5.1 Estimation of PALME parameters effect on the extraction efficiency

PALME related data were processed using R studio (Posit Team, 2023) running on R base (R Core Team, 2023) and using the packages: readxl (Wickham and Bryan, 2023), ggplot2 (Wickham, 2016) and caret (Kuhn, 2008). The percentage yields of the total CK bases were calculated as a ratio of the molar amount determined in the acceptor and the theoretical molar amount added into the donor. All missing values were replaced by ⅔ of the mean detection limit. Data were fitted by a linear model predicting the percentage yield based on the membrane type, organic solvent type, concentration of DEHP and

concentration of formic acid in the acceptor. The model was cross-validated using leave-one-out training method (Kuhn, 2008) to assess goodness of fit ($R^2 = 0.72$) and goodness of prediction ($Q^2 = 0.57$), both suggesting moderate correlation. The model coefficients were visualized in a bar chart with error bars represented the 95% confidence interval of the estimated effect (Fig. 4C).

4.5.2 Estimation of DisperSpin SPE parameters effect on the extraction efficiency

For the initial screening, four parameters of DisperSpin SPE were selected to assess their effect on percentage extraction yield. This study was conducted using a full factorial design of experiment (Fig. 3C) for four factors (Box and Hunter, 1957). As shown in Table 1, 16 samples of CK, auxin and ABA standards (0.5 pmol), each representing one corner of a cube in the 4-dimensional experimental space and 3 samples representing the centre of this cube, were treated with DisperSpin SPE (Table 2). The percentage yield of each individual compound was calculated as a ratio between the molar amount determined in the purified extract and the molar amount added before the extraction. Data were analysed using Simca® 17 software (Sartorius Stedim Data Analytics AB, Umeå, Sweden).

Table 2. Full factorial DoE for screening of four candidate factors of DisperSpin SPE (number of elution cycles, elution volume, incubation time, sorbent amount) to investigate their effect on process efficiency. The design consists of 16 corners of a cube in 4-dimensional experimental space (samples 1-16) with a replicated centre point (samples 17-19).

# Sample	No. of elution cycles	Elution volume (ml)	Incubation time (min)	Sorbent amount (mg)
1	1	0.1	5	2
2	1	0.1	5	30
3	1	0.1	25	2
4	1	0.1	25	30
5	1	0.4	5	2
6	1	0.4	5	30
7	1	0.4	25	2
8	1	0.4	25	30
9	3	0.1	5	2
10	3	0.1	5	30
11	3	0.1	25	2
12	3	0.1	25	30
13	3	0.4	5	2
14	3	0.4	5	30
15	3	0.4	25	2
16	3	0.4	25	30
17	2	0.25	15	16
18	2	0.25	15	16
19	2	0.25	15	16

First, principal component analysis was performed to assess the data structure and detect potential outliers. The data were then fitted by partial least square regression (PLS) calculating the covariance between method parameters and extraction yield (Wold et al.,

2001). The resultant loadings of the two most important principal components were plotted against each other to visualize the relative effects of the factors on compound yield (Fig. 2A in *Supplement II*). The resultant model was cross-validated using leave-one-out method to assess its predictability.

Three representatives of phytohormones were selected (*t*ZRMP, iPR and oxIAA) based on the covariance calculated by PLS model (one from each quadrant of the PLS loading plot). An interaction model predicting the extraction yield based on the DisperSpin SPE parameters was calculated using Modde® 11 software (Sartorius Stedim Data Analytics AB, Umeå, Sweden). The predicted yield was visualized in the contour plots (Fig. 2B in *Supplement II*).

4.5.3 Optimization of DisperSpin SPE parameters

The amount of Oasis® MCX bulk sorbent (2-30 mg) and the amount of Arabidopsis seedlings or poplar leaves (2-20 mg FW) were selected to find the optimal setpoint determining an MS response of endogenous concentration of plant hormones. The optimization was performed using response surface methodology and D-Optimal design of experiment, both calculated by Modde® 11 software (Sartorius Stedim Data Analytics AB, Umeå, Sweden). The signal-to-noise ratio (S/N) was determined by a peak-to-peak algorithm in MassLynx v4.2 software (Waters, Manchester, UK). Data were fitted by multiple regression including interaction and quadratic terms. The estimation of S/N values was visualized as the contour plots (Fig. 3 in *Supplement II*).

5 Survey of results

First, the current trends and major challenges related to downscaling plant hormone metabolomics are summarized in *Supplement I*. Methods facilitating the spatio-temporal determination of plant hormones at a wide range of resolution from the tissue to the subcellular level using targeted and untargeted MS-based approaches were discussed. A comprehensive data-driven meta-study was conducted from recent publications on the Web of Science. Relevant publications were systematically collected and key plant hormone analytical features were processed by statistical methods including multivariate data analysis to describe recent progress.

Second, the main effort in this Ph.D. thesis was dedicated to the method development and application of sample preparation and detection of plant hormones. Two miniaturized methods have been validated: (i) PALME and (ii) dispersive SPE (*Supplement II*). Sample preparation methods were further complemented by the development of a novel high-throughput analytical method based on SFC coupled with ESI-MS/MS (*Supplement III*). Furthermore, the existing state-of-the-art analytical approaches based on UHPLC-MS/MS were utilized to elucidate several questions of plant physiology. The role of SA in crosstalk with IAA while defending Arabidopsis plants against a pathogen has been elucidated (*Supplement IV*). The role of *tZ* in root-to-shoot long-distance signalling in response to nitrate heterogeneity in soil has been deciphered (*Supplement V*). It has been shown that several species of carnivorous plants do not rely on JA signalling to initialize the digestion, whereas another do (*Supplements VI* and *VII*). Furthermore, the role of CK degradation in development of lateral roots was elucidated (*Supplement VIII*).

Supplement I: **Petřík I**, Hladík P, Zhang C, Pěnčík A, Novák O. [Submitted after revisions]. Spatio-temporal plant hormonomics: From tissue to subcellular resolution. J Exp B

5.1 Results and discussion

5.1.1 Method development of CKs purification based on PALME

The findings presented herein were previously introduced in the bachelor thesis by Anna Krnáčová, under the supervision of the author of this Ph.D. thesis (Krnáčová, 2021). As outlined in the theoretical introduction, the sample preparation plays a crucial role in the MS analysis of bioactive compounds. Particularly in plant hormonomics, the removal of

interfering compounds from the complex plant matrix is essential for enhancing analytical outcomes. Generally, two primary classes of sample preparation have been established: SPE and LLE. While LLE has relatively minor prevalence in applications, several purification protocols based on this method, such as PALME, have been developed for pharmaceutically significant compounds in human plasma or urine (Pilařová et al., 2017; Bouchouareb et al., 2022; Ahmed et al., 2024). However, no prior studies utilizing PALME for plant hormone extraction have been reported. Therefore, the objective of this Ph.D. thesis was to implement PALME as a novel plant hormone purification method.

The development of the PALME method began with the selection of the candidate phytohormonal group. Since the pH gradient of the liquid phases involved in PALME is critical for successful extraction, basic and acidic phytohormones cannot be extracted in a one-step procedure (Gjelstad et al., 2013). This limitation affects the implementation of PALME in plant hormonomics. However, CKs represent a large family of weak bases ranging from polar to semi-polar compounds, making them processable in a single PALME step. Moreover, as extracted into the acidic solution, CKs can be directly injected into UHPLC-MS/MS system (Svačinová et al., 2012). Therefore, CKs were chosen for further investigation.

The initial batch of experiments aimed to examine the extraction yield using pure CK chemical standards. The standards, diluted in a weak alkaline sodium-phosphate buffer as a donor solvent, were extracted through the liquid membrane consisting of PP moistened in dodecyl acetate into a solution of formic acid as an acceptor. Surprisingly, this experimental setup facilitated the extraction of only CK bases and CK ribosides. Other metabolites, including CK glucosides and CK nucleotides, were not detected. Moreover, the extraction efficiency of CK bases and ribosides was low, accounting for an average of 0.5% for CK ribosides and 16.8% for CK bases. Consequently, dodecyl acetate was replaced with less hydrophobic water-immiscible solvents, such as 1-hexanol, 1-octanol, 2-octanone, and 2-nonanone. However, liquid membranes consisting of these solvents suffered from poor reproducibility. Depending on the boiling point and partial miscibility with water, the thin layer of these organic solvents was corrupted during the PALME procedure, resulting in the loss of the acceptor. This effect was observed particularly for all organic solvents, except dodecyl acetate and dihexyl ether. Consequently, the poor stability of liquid membrane contributed to the high variability in the extraction yield. As illustrated in Fig. 4C, due to the tremendous variability in the

result, 1-hexanol, 2-octanone, and 2-nonanone did not changed significantly the extraction efficiency compared to dodecyl acetate. Surprisingly, despite the difficulties with a membrane stability, 1-octanol increased the extraction efficiency significantly, accounting for a 50% yield.

A previous study focused on the UHPLC-MS/MS analysis of the pharmaceutically significant compound hydralazine in human plasma employed PALME for sample preparation (Pilařová et al., 2017). Similar to CKs, hydralazine is a heterocyclic nitrogen-rich low molecular compound. In that study, the mean recovery of hydralazine was 16% with dodecyl acetate, dihexyl ether, or 2-nonanone, and 76% with 1-octanol. This finding was consistent with our observations regarding the impact of the liquid membrane on the extraction of CK bases. However, it is important to note certain limitations in making this comparison. Firstly, in the case of hydralazine, all organic solvents were modified with 15% DEHP. Second, although the poor stability of the liquid membrane was not reported, a high variability in recovery was observed instead.

To solve problems related to unstable liquid membrane and high variability in yield, the relatively efficient 1-octanol was excluded from the study. Instead, it was replaced with dodecyl acetate modified with 15% DEHP, a compound previously shown to facilitate the transfer of analytes through the liquid membrane (Pilařová et al., 2017). This modification resulted in an increase in the mean yield to 3.8% for CK ribosides and 22.6% for CK bases in our study.

Subsequently, our attention turned to optimizing the acceptor phase. Previous studies have highlighted the significance of acceptor phase composition in affecting the extraction yield (Lorenzo-Parodi et al., 2023; Ahmed et al., 2024). Consequently, we varied the concentration of formic acid in the acceptor phase to identify the optimal conditions. Interestingly, while concentrations of 10 mmol/l, 50 mmol/l, and 100 mmol/l yielded comparable extraction efficiencies, a concentration of 200 mmol/l resulted in a significant increase in yield (Fig. 4C).

The optimal concentration of formic acid, as reported in a study focusing on the extraction of repaglinide, a medication for diabetic patients, was found to be the same as in our investigation (Ahmed et al., 2024). Interestingly, the optimal concentration of formic acid for hydralazine extraction was five times higher (Pilařová et al., 2017). Recent studies have recommended the use of PP membrane instead of commercially available

PVDF to prevent nonspecific binding with basic analytes (Lorenzo-Parodi et al., 2023; Ahmed et al., 2024). Surprisingly, PVDF in our study exhibited similar behaviour to PP, showing no significant change in the extraction yield of weakly basic CKs (Fig. 4C). Nevertheless, PP membranes were preferred due to their in-house production. Despite the improvements in the PALME protocol described in this Ph.D. thesis, the extraction efficiency remained far from those achieved in SPE-based sample purification protocols (Dobrev and Kamínek, 2002; Svačinová et al., 2012).

Thus, we further examined the extraction capacity of dodecyl acetate modified with 15% DEHP by comparing it with ethyl acetate in a traditional LLE setup. Ethyl acetate, recognized as the most polar organic water-immiscible solvent, was previously utilized for LLE of CKs (Hahn, 1975). Our test results indicated that modified dodecyl acetate in the LLE setting provided similar extraction efficiency as ethyl acetate for most of the compounds, resulting in significantly higher yields (up to 70% on average) compared to PALME (Krnáčová, 2021). However, compare to dodecyl acetate, extraction with ethyl acetate was effective only for CK bases and CK ribosides. No enhancement was observed for CK nucleotides and CK glucosides, which were found below the detection limit. Consequently, it was concluded that PALME has limited applicability and does not allow for the determination of the entire CK profile compared to SPE. Hence, further efforts have been directed towards the development of a purification method derived from SPE, which promises better extraction efficiency and applicability for a wider range of analyte polarities (Dobrev and Kamínek, 2002; Svačinová et al., 2012).

5.1.2 Method development of phytohormones purification based on DisperSpin SPE

Current methods for plant hormone sample preparation rely mostly on SPE in extraction cartridges using polymer RP or mix-mode sorbents (Dobrev and Kamínek, 2002). This approach has obvious benefits. The extraction cartridges are commercially available, robust and easy-to-use with a wide range of applications. However, dispersive SPE also known as QuEChERs was adopted for plant hormones purification (Xie et al., 2014; Martinez et al., 2020; Mandal et al., 2021; Mogal et al., 2022). Unlike the cartridge setup, dispersive SPE facilitates the contact of solvents with large sorbent surface area potentially suggesting higher extraction efficiency. Despite the easy-to-use, QuEChERs protocol requires relatively large amount of sample (grams of fresh weight) in relatively large volume of solvents. This Ph.D. thesis was aimed on the development of miniaturized

dispersive SPE method based on commercially available sorbents typically used in cartridge SPE, such as Oasis® MCX 30 μm (Waters, Milford, CT, USA).

The pilot experiments testing the extraction efficiency of CKs, auxins and ABA in QuEChERs like setup was introduced previously in bachelor work by Anna Valníčková, which was co-supervised by the author of this Ph.D. thesis (Valníčková, 2019). Importantly, the classical QuEChERs produces a several millilitres of extract from which only a small aliquot is analysed by LC-MS. However, low abundant plant hormone analysis requires the preconcentration of whole extract to reach the quantification limits within LC-MS (Svačinová et al., 2012; Šimura et al., 2018; Cai et al., 2019). It was shown this prerequisite is a limiting factor for adoption of QuEChERs protocol as uncontrolled losses of sorbent during the process happened. Therefore, the method had to be modified to protect the sorbent from losses by filtration. As shown in *Supplement II*, the experimental setup was designed employing MicroSpin centrifuge nylon filters with 0.2 μm pores (Chromservis Ltd., Czech Republic), from which the name "DisperSpin SPE" was derived. This modification resulted in improved reproducibility and extraction efficiency comparable to the cartridge SPE (Dobrev and Kamínek, 2002; Svačinová et al., 2012).

The final method was optimized using the factorial design of experiment, while data were evaluated by the multivariate mathematical modelling, particularly multiple linear regression (*Supplement II*). It has been shown that balance between the sorbent amount and the elution volume determines the extraction efficiency. CK nucleotides and CK *O*-glucosides benefited from the high amount of sorbent used (30 mg), whereas CK bases, CK ribosides and IAA achieved higher efficiency at low amount of sorbent (2 mg). Importantly, ABA, oxIAA and IAA amino acid conjugates were sensitive to changes in parameters related to elution (number of elution cycles and elution volume). All of them benefited from high number of cycles and/or high volume. This means that one elution cycle with 0.4 ml elution solvent provided sufficient extraction yields for all compounds. The optimal amount of plant tissue corresponded to the capacity of SPE sorbent. The optimal setpoint was calculated for the combination of 10 mg FW of plant extract with 10 mg of Oasis® MCX bulk sorbent. The optimized method was validated based on FDA guidelines (Matuszewski et al., 2003). The method reported 9% mean accuracy, 7% mean precision, 47% mean extraction efficiency and 21% mean relative matrix effect, all indicating good reliability of the proposed method. Finally, the validated method was

applied for profiling of CKs, auxins and ABA in various types of plant material – *Arabidopsis thaliana* seedlings, *Populus sp.* leaves (both representatives of dicots), *Triticum aestivum* leaves (monocots), *Picea abies* seedlings (conifer), *Marchantia polymorpha* thallus (liverwort) and *Nostoc* colony (algae).

In summary, the presented DisperSpin SPE method offers a reliable tool for purification of selected CKs, auxins and ABA. The extraction efficiency and related MS response mostly depends on the capacity of Oasis® MCX bulk sorbent. The users particularly focussing mainly on CK bases, CK ribosides and IAA should use a small amount of sorbent (2 mg), whereas researchers aiming on CK nucleotides and CK *O*-glucosides should increase the sorbent amount to 30 mg to achieve the optimal MS response. However, the DisperSpin SPE has not been applied yet for the purification of other classes of plant hormones, such as JAs, SA or brassinosteroids. Since these classes of compounds are weak acids or relatively non-polar compounds, the utilization of RP or anion exchange bulk sorbents are proposed to explore the further possibilities of DisperSpin SPE (Dobrev et al., 2005). More details are available in *Supplement II*.

Supplement II: **Petřík I**, Valníčková A, Stýskala J, Strnad M, Ljung K, Novák O. [In preparation]. DisperSpin solid phase micro-extraction: next generation micro-purification method for UHPLC-MS/MS determination of naturally occurring phytohormones.

5.1.3 Method development of CKs analysis based on SFC-MS/MS

As introduced earlier, the purified plant hormone sample (for instance by DisperSpin SPE) is supposed to be analysed by highly sensitive MS/MS system for accurate detection and quantification of targeted plant hormones. The conventional approach relies on UHPLC-MS/MS instrumentation. However, the significant improvements in SFC have been reported in the past decade. The manufacturers of the chromatographic systems introduced the robust SFC instruments combining the advantages of LC (high separation efficiency) and GC (low solvent viscosity) resulting in breakthrough of chromatographic performance. SFC-MS/MS has been implemented in the various application fields, such as pharmaceutical, doping agent, environmental, or pesticide residues analysis etc. (Gazárková et al., 2022). However, despite the obvious benefits, no application of SFC-MS/MS in plant hormone research has been reported yet. Therefore, the next goal of the Ph.D. thesis was the development of an analytical method for the CKs quantification based on SFC-MS/MS. Importantly, SFC utilizes carbon dioxide in supercritical conditions as the major component of the mobile phase and a miscible organic solvent,

such as methanol, as a modifier. The addition of a modifier to the mobile phase enables the control of the physico-chemical properties of the mobile phase and consequently allows the elution of relatively polar compounds. However, unlike LC, the modification of SFC mobile phase is limited with emphasis on restricted use of water. Therefore, the separation of polar and semi-polar CK isomers was the most challenging part of the work. Four types of stationary phases (C18, bare silica, DIOL and 2-PIC) were tested for the separation of CK isomers.

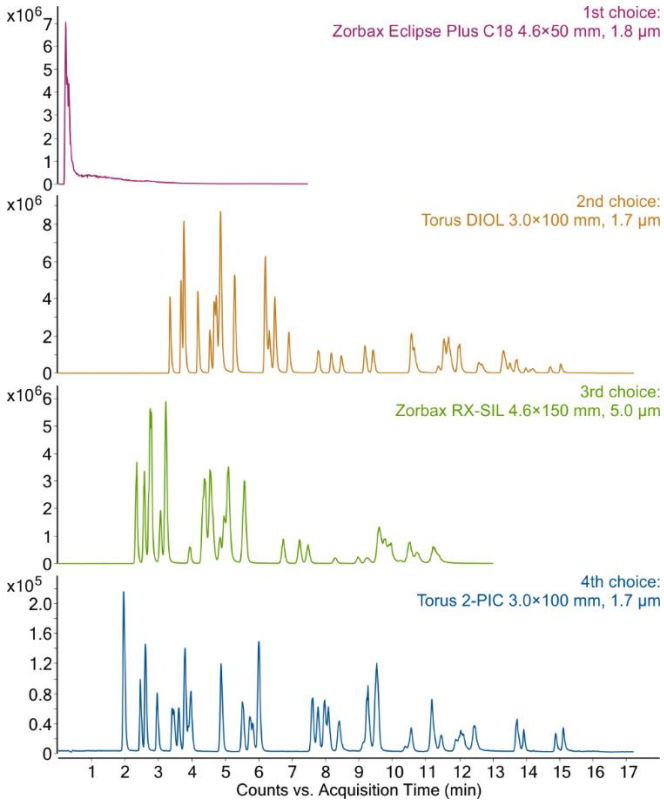

Fig. 5. Elution profiles of CKs with four tested chromatographic columns used in development of SFC-MS/MS method for analysis of CKs. 2 µl of 10^{-7} mol/l CK standards in methanol were injected into (**i**) Zorbax Eclipse Plus C18 (4.6×50 mm, 1.8 µm; Agilent Technologies, Santa Clara, CA, USA), linear gradient elution with $scCO_2$ (A) and 5% water (v/v) in methanol (B) starting at 5% B and ending at 40% B in 15 min. The flow rate 1.5 mL min^{-1}, column temperature 30 °C, back pressure 200 bar. (**ii**) Torus DIOL (3.0×100 mm, 1.7 µm; Waters, Milford, CT, USA), mobile phase $scCO_2$ (A) and 15 mmol/l ammonium formate in 5% water and 95% methanol (v/v) (B). A linear gradient from 0% to 40% B in 15 min at 1.5 ml min^{-1}, column temperature 40 °C, back pressure 160 bar. Mobile phase B was prepared as follows: an aqueous solution 300 mmol/l formic acid was prepared and adjusted with 25% ammonium hydroxide (v/v) to concentration 0.10, 0.41, 0.59, 0.68 and 1.02 mol/l. Each solution was then diluted 20-fold in methanol. (**iii**) Zorbax RX-SIL (4.6×150 mm, 5.0 µm; Agilent Technologies, Santa Clara, CA USA), linear gradient elution of $scCO_2$ (A) and methanol (B) raising 15–45% B in 12 min at a constant flow rate of 2.5 mL min^{-1}. The column temperature 30 °C, back pressure 200 bar. (**iv**) Torus 2-PIC (3.0×100 mm, 1.7 µm; Waters, Milford, CT USA), mobile phase $scCO_2$ (A) and 5% water in methanol (v/v) (B), elution with 0–40% B in 15 min, flow rate 1.5 ml min^{-1}, 50 °C, 160 bar.

C18 columns belong to the most popular columns in reversed-phase liquid chromatography (RPLC) and are generally considered the stationary phase of first-choice (Grumbach et al., 2004) They have been well-established in RPLC-MS/MS analysis of

plant hormones (Hradecká et al., 2007; Svačinová et al., 2012; Šimura et al., 2018). For this reason, C18 was the first column investigated in the development of the SFC-MS/MS method for CK analysis. In a pilot experiment, a 15-min generic gradient consisted of $scCO_2$ and methanol. In this configuration, the MS signal was observed at the very beginning of the gradient elution, indicating poor or no retention of CK metabolites (Fig. 5). It has been previously reported that polar/semi-polar basic compounds such as CKs are retained on RP by hydrogen bonding on residual silanol groups (Lesellier, 2020). As noted in Data Sheet, Zorbax Eclipse Plus C18 3×50 mm, 1.8 μm chromatographic column (Agilent Technologies, Santa Clara, USA) used in this experiment is doubly endcapped, thereby preventing the functionality of the silanols. Therefore, the retention of polar/semi-polar basic CKs was barely possible. However, even a non-endcapped C18 might not provide sufficient retention due to steric access to residual silanols requiring hydration (West and Lesellier, 2012; Khater et al., 2013). It is clear that hydration of silanol groups in $scCO_2$/methanolic mobile phase is limited. Therefore, the subsequent selection of a suitable stationary phase was restricted to polar columns only.

The sufficient retention of CKs was achieved with Torus DIOL column (Waters, Milford, CT, USA) (Fig. 2). Importantly, zeatin glucoside has been shown to consist of six isomers, namely *t*ZOG, *c*ZOG, *t*Z7G, *c*Z7G, *t*Z9G and *c*Z9G, and was the most critical group of compounds to separate. The mobile phase consisted of $scCO_2$ modified by methanol with the addition of ammonium formate, which was prepared by titration of ammonia into formic acid. The ratio between ammonia and formic acid determined the separation of CK *O*- and *N*9-glucosides, whereas column temperature affected the selectivity of *N*7- and *N*9-glucosides. Interestingly, the baseline separation was not achieved with any combination ammonium formate and column temperature. While *c*ZOG and *c*Z9G were separated at low concentration of ammonia (5 mmol/l), *t*ZOG and *t*Z9G coeluted in one chromatographic peak. Conversely, at a high concentration of ammonia (50 mmol/l), the satisfactory separation was observed for *t*ZOG and *t*Z9G but not for *cis*- isoforms. The reason and the consequences of this effect are discussed in *Supplement III*.

Another effort was dedicated to the separation of zeatin glucosides with Zorbax RX-SIL column (Agilent Technologies, Santa Clara, CA USA), which possess similar retention mechanisms like DIOL column. A gradient elution of $scCO_2$ modified by pure methanol was used to elute CKs from RX-SIL column (Fig. 2). As shown in Results and

Discussion section of *Supplement III*, column temperature and back pressure regulation has a significant effect on density of mobile phase, which was critical for the selectivity of zeatin glucoside isomers. The baseline separation was achieved by a combination of high temperature (60 °C) and high back pressure regulation (300 bar). However, the combination of silica-based column and $scCO_2$/methanol mobile phase resulted in poor interday repeatability of the method manifest by peak broadening and retention time instability. This effect may be related with absence of the water in the mobile phase leading to the methylation of silanol groups on stationary phase and the loss of its retention properties (Plachká et al., 2021). The addition of 5% water into the modifier led to a significant change of the selectivity and baseline separation of zeatin glucosides. Nonetheless, the presence of water also resulted in the loss of the selectivity of DHZ glucosides. Therefore, silica-based chromatographic column was discarded from the study and replaced with Torus 2-PIC column (Waters, Milford, CT, USA), which showed the sufficient selectivity and chromatographic resolution for all targeted CK metabolites. The final SFC-MS/MS method used linear gradient elution with $scCO_2$ modified with 5 mmol/l ammonia in methanol starting at 5% and ending at 40% in 7 min with a constant flow rate of 1.5 ml/min (Fig. 2). Furthermore, methanol was employed as a make-up solvent to improve the ionization efficiency of subsequent MS-based detection. The optimized MS/MS conditions are described in Material and Methods and Table A.2 of *Supplement III*. The new SFC-MS/MS method was validated based on the guidelines recommended by the FDA (Matuszewski et al., 2003) and used to determine CK profile in *Arabidopsis thaliana* seedlings. It was shown that both the novel SFC-MS/MS and previously published UHPLC-MS/MS method provided similar results emphasising the major representation of *N*-glucosides in the CK profile of *Arabidopsis* seedling. For more details see *Supplement III*.

Supplement III: **Petřík I**, Pěnčík A, Stýskala J, Tranová L, Amakorová P, Strnad M, Novák O. 2024. Rapid profiling of cytokinins using supercritical fluid chromatography coupled with tandem mass spectrometry. Anal Chim Acta, 1285, 342010.

5.1.4 Application of modern UHPLC-MS/MS methods for determination of phytohormones in plants

Determination of free SA in Arabidopsis roots to reveal its role in pathogen infection

The concentration levels of free SA were quantified in the roots of Arabidopsis seedlings in two developmental stages (5 and 10 days after germination). Three genotypes of

Arabidopsis were involved in the study. The mutant *sid2* was deficient in SA biosynthesis, the mutant *crp6* was altered to overproduce the SA, and *Col-0* was a standard line with no alteration. The research question was whether the concentration of free SA depends on genotype and/or developmental stage. The samples were prepared according to the previously described protocol (Floková et al., 2014). Whereas the mutant line *sid2* showed no significant change compared to *Col-0*, *crp6* reported twice higher concentration. This effect was observed in both developmental stages. Combined with the results from morphology analysis of lateral roots, protein immunoblotting, phosphorylation assays and gene expression the following conclusion of the study was conducted. When plant is infected by a pathogen, the cross-talk between SA and auxin is recruited to induce the defence response. A high concentration of SA in the cytosol blocks the enzymatic activity of phosphatase 2A responsible thefor dephosphorylation of auxin transporter PIN2. This leads to hyperphosphorylation of PIN2 and efflux of auxin from the nucleus. Hence, the auxin response is attenuated and root development is inhibited. Full results and discussion are available in *Supplement IV*.

Supplement IV: Tan S, Abas M, Verstraeten I, Glanc M, Molnár G, Hajný J, Lasák P, **Petřík I**, Russinova E, Petrášek J, Novák O, Pospíšil J, Friml J. 2020. Salicylic acid targets protein phosphatase 2A to attenuate growth in plants. Curr Biol 30(3), 381–395.

Quantification of CKs in Arabidopsis roots to reveal the nitrogen signalling response

This study addressed the question of what is the role of CKs in long-distance root-to-shoot signalling in response to nitrate heterogeneity. The study was performed with hydroponically grown Arabidopsis seedlings. Nitrogen heterogeneity was simulated by splitting the root system. Half of the root system was grown in a potassium nitrate solution simulating a nitrogen-rich environment, and the second half in a potassium chloride solution with no nitrogen source. The plants growing only in potassium nitrate and potassium chloride were involved into the study as controls. The samples of roots and shoots were prepared by extraction into modified Bieleski buffer followed by purification using mix-mode SPE. Finally, CK content was determined using UHPLC-MS/MS as described previously (Svačinová et al., 2012). Two mutant lines were employed in the study to elucidate the CK role in nitrogen heterogeneity. Triple mutant *ipt3,5,7* was deficient in CK biosynthesis and *abcg14* mutant line was altered in CK transport. Depending on mutant line and growth conditions, the total CK content varied from 50 to 300 pmol/g FW. The concentration of *t*Z in roots was shown to be significantly decreased in the *ipt3,5,7* mutant, whereas both mutants *ipt3,5,7* and *abcg14* reported significant

concentration drop in shoots. In conclusion, biosynthesis of CK *t*Z-types in the root depends on the availability of exogenous nitrogen. The translocation of *t*Z into the shoot induces short- and long-term responses by regulating of nitrogen-responsive genes, and regulating nitrate transport and root development. It has also been suggested that nitrogen distribution is mediated by glutamate and glutamine metabolism, which is putatively regulated by *t*Z signalling after root-to-shoot translocation. For more results and discussion see *Supplement V*.

Supplement V: Poitout A, Crabos A, **Petřík I**, Novák O, Krouk G, Lacombe B, Ruffel S. 2018. Responses to systemic nitrogen signaling in Arabidopsis roots involve trans-zeatin in shoots. Plant Cell 30(6), 1243–1257.

Determination of JAs in Pinguicula carnivorous plant

Carnivorous plants represent a special group within the plant kingdom that have developed evolutionarily alternative strategies for nutrient uptake. These strategies reacted on nutrient deficiency in the soil by the transformation of leaves into traps for capturing a prey. Several orders of carnivorous plants with different trapping mechanisms have been described (Albert et al., 1992). One of them is Lamiales order involving *Pinguicula sp.*, also known as butterwort, which is typical by its flowering and rosette of oval shaped leaves. The leaves are covered by the glands producing the sticky and digestive fluids to capture and digest the prey. The aim of this study was to answer the question whether the butterwort utilizes stress-related compounds in the signalling pathway inducing enzyme activity in response to prey capture similarly to Venus flytrap (*Dionaea muscipula*) from Caryophyllales order (Pavlovič et al., 2017). Leaves of the horticultural hybrid of *Pinguicula* × *Tina* were wounded mechanically or fed by *Drosophyla melanogaster* prey and collected in time-points 0 h, 2 h and 24 h after feeding/wounding. The wounding experiment was performed to obtain information about positive stress response. The samples were processed for determination of stress-related compounds using SPE sample clean-up and UHPLC-MS/MS analysis by Floková et al. (2014). Upregulation of JA, its biosynthetic precursor *cis*-OPDA and bioactive JA-Ile were shown to be triggered only in response for wounding but not for feeding. In combination with the results of membrane potential measurement of wounded/fed leaves and proteomics analysis of digestive fluid composition, the following conclusion was made: while both *Pinguicula* and *Dionaea* have similar composition of digestive enzymes, *Pinguicula*, unlike *Dionaea*, do not co-opt JAs in response to prey capture.

Hence, the *Dionaea* digestion signalling remains elusive. For more results see *Supplement VI*.

Supplement VI: Kocáb O, Jakšová J, Novák O, **Petřík I**, Lenobel R, Chamrád I, Pavlovič A. 2020. Jasmonate-independent regulation of digestive enzyme activity in the carnivorous butterwort Pinguicula × Tina. J Exp Bot 71(12), 3749–3758.

Elucidation of JAs role in prey digestion of aquatic carnivorous plants

As already indicated in the previous paragraph, several carnivorous plants, such as *Dionaea muscipula* from Caryophyllales order, have co-opted the JA signalling in the digestion of the captured prey. However, this strategy was not observed in the carnivorous plant *Pinguicula* from Lamiales order, whose digestion signalling is not yet fully explained (*Supplement VI*). In this study, two aquatic carnivorous plant species, *Aldrovanda vesiculosa* from Caryophyllales and *Utricularia reflexa* from Lamiales, were investigated in terms of JA accumulation after feeding. Interestingly, the traps of *Aldrovanda* utilize a similar mechanism of capture like terrestrial *Dionea*, as both are based on an electric action potential. On the other hand, the traps of *Utricularia* are passive flexible hollow bladders with the sealing. The plant continuously pumps the water out of the trap, maintaining a negative pressure inside the trap and driving the prey to be captured. This mechanistical difference raised the question of how the JA signalling defence pathway is incorporated in prey digestion in aquatic carnivorous plants. The traps of *Aldrovanda* and *Utricularia* containing prey were collected 2 h and 24 h after feeding and lyophilised, resulting in 2.5 mg of dry weight per sample. Dry trap samples were processed according to the protocol published by Floková et al. (2014) based on extraction in 10% methanol, subsequent purification using Oasis HLB cartridges and then UHPLC-MS/MS analysis. Results from plant hormone profiling were integrated with proteomics analysis of digestive enzymes and data from induced trap closing time span. Interestingly, feeding of *Aldrovanda* induced the accumulation of JA, JA-Ile, *cis*-OPDA, SA and IAA, but *Utricularia* fed traps showed no significant change compared to empty traps. Whereas both species used the same digestion enzymes, the mechanism of trapping/digesting action is closely related to the order. Representatives of Caryophyllales, *Aldrovanda* and *Dionaea* have reported co-optation of JA signalling from plant defence, suggesting that both species are derived from a common terrestrial ancestor. On the other hand, *Utricularia* and *Pinguicula* (studied in *Supplement VI*) both co-opted a different signalling mechanism that is not yet fully understood (Pavlovič et al., 2024). A more detailed discussion and explanations are available in *Supplement VII*.

Supplement VII: Jakšová J, Adamec L, **Petřík I**, Novák O, Šebela M, Pavlovič A. 2021. Contrasting effect of prey capture on jasmonate accumulation in two genera of aquatic carnivorous plants (Aldrovanda, Utricularia). Plant Physiol Biochem 166, 459–465.

Elucidation of anti-gravitropic mechanism mediated by CKs

The gravitropism is the main force of the root growth mediated by auxin signalling. However, as revealed in this work, CKs play a crucial role in Arabidopsis lateral root development. The CK content was determined in the roots of the standard genotype Col-0 and the double mutant *ckx2-1*, which is deficient in CK metabolism by knock-out of the CKX isoforms. The method used for CK determination was adopted from Svačinová et al. (2012). Results from CK profiling showed an increased level of iP-types in *ckx2-1* mutant line. This is consistent with previous findings that iP-types are preferred substrate for CKX degradation (Galuszka et al., 2007). On the other hand, other CK types were downregulated in *ckx2-1* mutant line, suggesting a compensation mechanism. Taken together with a genome-wide association study, the data showed that the naturally varied angular growth of lateral root is regulated by CK response factors. Enzymatic activity of CKX2 has a significant impact of lateral root development. The CK activity is tightly connected to cellular elongation and cell division in lateral roots determining its angular growth. All results and findings are discussed in detail in *Supplement VIII*.

Supplement VIII: Waidmann S, Ruiz Rosquete M, Schöller M, Sarkel E, Lindner H, LaRue T, **Petřík I**, Dünser K, Martopawiro S, Sasidharan R, Novak O, Wabnik K, Dinneny JR, Kleine-Vehn J. 2019. Cytokinin functions as an asymmetric and anti-gravitropic signal in lateral roots. Nature Communications 10(1), 3540.

6 Conclusions and future perspectives

Plant physiology research has evolved into an interdisciplinary field, encompassing proteomics, genomics, transcriptomics, genetics, phenomics, and notably, plant hormonomics. Integrating data from these diverse fields drives modern plant science forward. As interest in plant physiology narrows from organs to organelles, there is a need for novel tools capable of detecting plant hormones in minute samples. This Ph.D. thesis focuses on developing methods to address current analytical limitations, particularly in downscaling, enhancing throughput and ensuring robustness. Key findings are outlined below:

- A novel analytical method based on SFC-MS/MS was successfully developed and validated for the determination of CKs in plants. This method introduced an innovative chromatographic approach for plant hormone analysis.
- The PALME method was effective for sample preparation of less polar CKs. However, its applicability for broader phytohormonal profiling has been limited.
- A new method for the purification of CKs, auxins and ABA using DisperSpin SPE has demonstrated the protocol robustness and the extraction efficiency. Due to its practicality and easy-to-use, it has become firmly established as a routine procedure in the Laboratory of Growth Regulators.
- State-of-the-art analytical methods based on UHPLC-MS/MS have contributed to the elucidation of the role of CK in nutrient signalling and lateral root development, the involvement of SA in plant defense mechanisms, and the function of JA in botanical carnivory.

The findings highlight the increasing complexity of plant hormonomic data, especially when integrated with other omics fields. To navigate through large datasets effectively, researchers require advanced multivariate statistical approaches that can convert vast amounts of data into understandable results. While DoE represents a well-established advanced statistical method in industry, its application in integrated plant sciences remains limited. Plants as living organisms are inherently more complex compared to industrial processes, exhibiting higher random variability and non-linear dependencies that must be addressed. Therefore, adopting DoE in plant hormone research is quite a challenging task. However, its successful implementation can significantly help

to answer the questions of plant physiology research in a much shorter time with much less financial resources than so far.

7 References

Ahmed SA, Abdallah NA, Almaghrabi M, Alahmadi YM. 2024. Parallel artificial liquid membrane extraction coupled with UPLC-ESI-MS/MS method for high-throughput quantitation of repaglinide in diabetic patients. Talanta 269, 125498.

Albert VA, Williams SE, Chase MW. 1992. Carnivorous plants: phylogeny and structural evolution. Science 257, 1491–1495.

Andolfi A, Maddau L, Cimmino A, Linaldeddu BT, Basso S, Deidda A, Serra S, Evidente A. 2014. Lasiojasmonates A–C, three jasmonic acid esters produced by Lasiodiplodia sp., a grapevine pathogen. Phytochemistry 103, 145–153.

Antoniadi I, Novák O, Gelová Z, Johnson A, Plíhal O, Simerský R, Mik V, Vain T, Mateo-Bonmatí E, Karady M, Pernisová M, Plačková L, Opassathian K, Hejátko J, Robert S, Friml J, Doležal K, Ljung K, Turnbull C. 2020. Cell-surface receptors enable perception of extracellular cytokinins. Nat Commun 11(1), 4284.

Argueso CT, Kieber JJ. 2024. Cytokinin: From autoclaved DNA to two-component signaling. Plant Cell [Early access].

Argyros RD, Mathews DE, Chiang YH, Palmer CM, Thibault DM, Etheridge N, Argyros DA, Mason MG, Kieber JJ, Schaller GE. 2008. Type B response regulators of Arabidopsis play key roles in cytokinin signaling and plant development. Plant Cell 20(8), 2102–2116.

Arnon DI, Hoagland DR. 1940. Crop production in artificial culture solutions and in soils with special reference to factors influencing yields and absorption of inorganic nutrients. Soil Science 50, 463–485.

Baroja-Fernandez E, Aguirreolea J, Martinková H, Hanuš J, Strnad M. 2002. Aromatic cytokinins in micropropagated potato plants, Plant Physiol Biochem 40, 217–224.

Bezerra MA, Santelli RE, Oliveira EP, Villar LS, Escaleira LA. 2008. Response surface methodology (RSM) as a tool for optimization in analytical chemistry. Talanta 76(5), 965–977.

Bezzera MA, Lemos VA, Novaes CG, de Jesus RM, Filho HR, Araújo SA, Alves JP. 2020. Application of mixture design in analytical chemistry. Microchem J 152, 104336.

Bouchouareb K, Combes A, Pichon V. 2022. Determination of nerve agent biomarkers in human urine by a natural hydrophobic deep eutectic solvent-parallel artificial liquid membrane extraction technique. Talanta 249, 123704

Bourne DJ, Barrow KD, Milborrow BV. 1991. Salicyloylaspartate as an endogenous component in the leaves of Phaseolus vulgaris. Phytochem 30(12), 4041–4044.

Bruckhoff V, Haroth S, Feussner K, König S, Brodhun F, Feussner I. 2016. Functional characterization of CYP94-genes and identification of a novel jasmonate catabolite in flowers. PLoS One 11, e0159875.

Brereton RG. 2003. Chemometrics: Data Analysis for the Laboratory and Chemical Plant. John Wiley & Sons, Ltd. Chichester.

Brzobohatý B, Moore I, Kristoffersen P, Bako L, Campos N, Schell J, Palme K. 1993. Release of active cytokinin by a b-glucosidase localized to the maize root meristem. Science 262(5136), 1051–1054.

Brunoni F, Collani S, Casanova-Sáez R, Šimura J, Karady M, Schmid M, Ljung K, Bellini C. 2020. Conifers exhibit a characteristic inactivation of auxin to maintain tissue homeostasis. New Phytol 226(6), 1753–1765.

Cai BD, Zhu JX, Shi ZG, Yuan BF, Feng YQ. 2013. A simple sample preparation approach based on hydrophilic solid-phase extraction coupled with liquid chromatography-tandem mass spectrometry for determination of endogenous cytokinins. J Chromatogr B (942), 31–36.

Cai BD, Yin J, Hao YH, Li YN, Yuan BF, Feng YQ. 2015. Profiling of phytohormones in rice under elevated cadmium concentration levels by magnetic solid-phase extraction coupled with liquid chromatography tandem mass spectrometry. J Chromatogr A 1406, 78–86.

Cai WJ, Yu L, Wang W, Sun MX, Feng YQ. 2019. Simultaneous determination of multiclass phytohormones in submilligram plant samples by one-pot multifunctional derivatization-assisted liquid chromatography-tandem mass spectrometry. Anal Chem 91(5), 3492–3499.

Cao ZY, Sun LH, Mou RX, Zhang LP, Lin XY, Zhu ZW, Chen MX. 2016. Profiling of phytohormones and their major metabolites in rice using binary solid-phase extraction and liquid chromatography-triple quadrupole mass spectrometry. J Chromatogr A 1451, 67–74.

Cappiello A, Famiglini G, Palma P, Pierini E, Termopoli V, Trufelli H. 2008. Overcoming matrix effects in liquid chromatography−mass spectrometry. Anal Chem 80(23), 9343–9348.

Casanova-Sáez R, Voß U. 2019. Auxin Metabolism Controls Developmental Decisions in Land Plants. Trends Plant Sci 24(8), 741–754.

Chen L, Jameson GB, Guo Y, Song J, Jameson PE. 2022. The LONELY GUY gene family: from mosses to wheat, the key to the formation of active cytokinins in plants. Plant Biotechnol J 20(4), 625–645.

Chmelík D, Hrouzek P, Fedorko J, Vu DL, Urajová P, Mareš J, Červený J. 2019. Accumulation of cyanobacterial oxadiazine nocuolin A is enhanced by temperature shift during cultivation and is promoted by bacterial co-habitants in the culture. Algal Research 44, 101673.

Chu UC, Adelberg J, Lowe K, Jones TJ. 2018. Use of DoE methodology to optimize the regeneration of high-quality, single-copy transgenic Zea mays L. (maize) plants. In Vitro Cell Dev Biol Plant 55, 678–694.

Clicquet S, Durier C, Kobilinski A. 1994. Principle of a fractional factorial design for qualitative and quantitative factors: application to the production of Bradyrhizobium japonicum in culture and inoculation media. Agronomie 14, 569–587.

Contreras-Gutierrez PK, Hurtado-Fernández E, Gómez-Romero M, Hormaza JI, Carrasco-Pancorbo A, Fernández-Gutiérrez A. 2013. Determination of changes in the metabolic profile of avocado fruits (Persea americana) by two CE-MS approaches (targeted and non-targeted). Electrophoresis 34(19), 2928–2942.

Czitrom V. 1999. One-Factor-at-a-Time versus Designed Experiments. Am Stat 53(2), 126–131.

Dean JV, Delaney SP. 2008. Metabolism of salicylic acid in wild-type, ugt74f1 and ugt74f2 glucosyltransferase mutants of Arabidopsis thaliana. Physiol Plant 132(4), 417–425.

Dempsey DA, Shah J, Klessig DF. 1999. Salicylic Acid and Disease Resistance in Plants. Crit Rev Plant Sci 18, 547–575.

Desfontaine V, Guillarme D, Francotte E, Nováková L. 2015. Supercritical fluid chromatography in pharmaceutical analysis. J Pharm Biomed Anal 113, 56–71.

Ding J, Mao LJ, Wang ST, Yuan BF, Feng YQ. 2013. Determination of endogenous brassinosteroids in plant tissues using solid-phase extraction with double layered cartridge followed by High-performance liquid chromatography-tandem mass spectrometry. Phytochem Anal 24(4), 386–394.

Ding P, Ding Y. 2020. Stories of Salicylic Acid: A Plant Defense Hormone. Trends Plant Sci 25(6), 549–565.

Dobrev PI, Kamínek M. 2002. Fast and efficient separation of cytokinins from auxin and abscisic acid and their purification using mixed-mode solid-phase extraction. J Chromatogr A 950, 21–29.

Dobrev PI, Havlíček L, Vágner M, Malbeck J, Kamínek M. 2005. Purification and determination of plant hormones auxin and abscisic acid using solid phase extraction and two-dimensional high performance liquid chromatography. J Chromatogr A 1075, 159–166.

Douglas DJ, Konenkov NV. 2014. Mass resolution of linear quadrupole ion traps with round rods. Rapid Commun Mass Spectrom 28(21), 2252–2258.

Dziurka K, Dziurka M, Warchol M, Czyczylo-Mysza I, Marcinska I, Noga A, Kaploniak K, Skrzypek E. 2019. Endogenous phytohormone profile during oat (Avena sativa L.) haploid embryo development. In Vitro Cell Dev Biol - Plant 55(2), 221–229.

Edwards KD, Takata N, Johannson M, Jurca M, Novák O, Hényková E, Liverani S, Kozarewa I, Strnad M, Millar A, Ljung K, Eriksson ME. 2018. Circadian clock components control daily growth activities by modulating cytokinin levels and cell division-associated gene expression in Populus trees. Plant Cell Environ 41, 1468–1482.

Ferreira SL, dos Santos WN, Quintella CM, Neto BB, Bosque-Sendra JM. 2004. Doehlert matrix: a chemometric tool for analytical chemistry—review. Talanta 63, 1061–1067.

Ferreira SL, Bruns RE, Ferreira HS, Matos GD, David JM, Brandão GC, da Silva EG, Portugal LA, dos Reis PS, Souza AS, dos Santos WN. 2007. Box-Behnken design: an alternative for the optimization of analytical methods. Anal Chim Acta 597(2), 179–86.

Ferreira SL, Caires AO, da Borges TS, Lima AM, Silva LO, dos Santos WN. 2017. Robustness evaluation in analytical methods optimized using experimental designs. Microchem J 131, 163–169.

Fisher RA. 1926. The arrangement of field experiments. Journal of the Ministry of Agriculture 33, 503–515.

Fresno DH, Munne-Bosch S. 2023. Organ-specific responses during acclimation of mycorrhizal and non-mycorrhizal tomato plants to a mild water stress reveal differential local and systemic hormonal and nutritional adjustments. Planta 258(2), 32.

Floková K, Tarkowská D, Miersch O, Strnad M, Wasternack C, Novák O. 2014. UHPLC-MS/MS based target profiling of stress-induced phytohormones. Phytochemistry 105, 147–57.

Fonseca S, Chini A, Hamberg M, Adie B, Porzel A, Kramell R, Miersch O, Wasternack C, Solano R. 2009. (+)-7-iso-Jasmonoyl-L-isoleucine is the endogenous bioactive jasmonate. Nat Chem Biol 5, 344–350.

Friml J, Wiśniewska J, Benková E, Mendgen K, Palme K. 2002. Lateral relocation of auxin efflux regulator PIN3 mediates tropism in Arabidopsis. Nature 415(6873), 806–809.

Gajdošová S, Spíchal L, Kamínek M, Hoyerová K, Novák O, Dobrev PI, Galuszka P, Klíma P, Gaudinová A, Žižková E, Hanuš J, Dančák M, Trávníček B, Pešek B, Krupička M, Vaňková R, Strnad M, Motyka V. 2011. Distribution, biological activities, metabolism, and the conceivable function of cis-zeatin-type cytokinins in plants. J Exp Bot 62(8), 2827–2840.

Galuszka P, Popelková H, Werner T, Frébortová J, Pospíšilová H, Mik V, Köllmer I, Schmülling T, Frébort I. 2007. Biochemical characterization of cytokinin oxidases/dehydrogenases from Arabidopsis thaliana expressed in Nicotiana tabacum L. J Plant Growth Regul 26, 255–267.

Galvan-Ampudia CS, Julkowska MM, Darwish E, Gandullo J, Korver RA, Brunoud G, Haring MA, Munnik T, Vernoux T, Testerink C. 2013. Halotropism is a response of plant roots to avoid a saline environment. Curr Biol 23(20), 2044–2050.

Gazárková T, Plachká K, Švec F, Nováková L. 2022. Current state of supercritical fluid chromatography-mass spectrometry. Trends Anal Chem 149, 116544.

Geib T, Sleno L, Hall RA, Stokes CS, Volmer DA. 2016. Triple quadrupole versus high resolution quadrupole-time-of-flight mass spectrometry for quantitative LC-MS/MS analysis of 25-Hydroxyvitamin D in human serum. J Am Soc Mass Spectrom 27(8), 1404–1410.

Geier U, Werner O, Bopp M. 1990. Indole-3-acetic acid uptake in isolated protoplasts of the moss Funaria hygrometrica. Physiol Plant. 80(4), 584–592.

George Thompson AM, Iancu CV, Neet KE, Dean JV, Choe JY. 2017. Differences in salicylic acid glucose conjugations by UGT74F1 and UGT74F2 from Arabidopsis thaliana. Sci Rep 7, 46629.

Gjelstad A, Rasmussen KE, Parmer MP, Pedersen-Bjergaard S. 2013. Parallel artificial liquid membrane extraction: micro-scale liquid-liquid-liquid extraction in the 96-well format. Bioanalysis 5(11), 1377–1385.

Gong MX, Luo HL, Wang AQ, Zhou YY, Huang WJ, Zhu PC, He LF. 2017. Phytohormone profiling during tuber development of Chinese yam by Ultra-high performance liquid chromatography-triple quadrupole tandem mass spectrometry. J Plant Grow Regul 36(2), 362–373.

Grumbach ES, Wagrowski-Diehl DM, Mazzeo JR, Alden B, Iraneta PC. 2004. Hydrophilic Interaction Chromatography Using Silica Columns for the Retention of Polar Analytes and Enhanced ESI-MS Sensitivity. LCGC North America 22, 1010.

Hahn H. 1975. Cytokinins: A Rapid Extraction and Purification Method. Physiol Plant 34, 204–207.

Hashiguchi T, Hashiguchi M, Tanaka H, Fukushima K, Gondo T, Akashi R. 2021. Quantitative analysis of seven plant hormones in Lotus japonicus using standard addition method. PLoS One 16(2), e0247276.

Heitz T, Smirnova E, Widemann E, Aubert Y, Pinot F, Ménard R. 2016. The rise and fall of jasmonate biological activities. In: Nakamura Y, Li-Beisson Y, eds. Lipids in plant and algae development. Cham: Springer International Publishing, 405–426.

Hill K, Mathews DE, Kim HJ, Street IH, Wildes SL, Chiang YH, Mason MG, Alonso JM, Ecker JR, Kieber JJ, Schaller GE. 2013. Functional characterization of type-B response regulators in the Arabidopsis cytokinin response. Plant Physiol 162(1), 212–224.

Hirschmann F, Krause F, Papenbrock J. 2014. The multi-protein family of sulfotransferases in plants: composition, occurrence, substrate specificity, and functions. Frontiers in Plant Science 5, 556.

Hirose N, Takei K, Kuroha T, Kamada-Nobusada T, Hayashi H, Sakakibara H. 2008. Regulation of cytokinin biosynthesis, compartmentalization and translocation. J Exp Bot 59(1), 75–83.

Hofman PJ, Featonby-Smith BC, VanStaden J. 1986. The Development of ELISA and IRA for Cytokinin Estimation and their Application to a Study of Lunar Periodicity in Ecklonia maxima (Osbeck) Papenf. J Plant Phys 122(5), 455–466.

Holub J, Hanuš J, Hanke DE, Strnad M. 1998. Biological activity of cytokinins derived from Ortho- and Meta-Hydroxybenzyladenine. Plant Growth Regul 26, 109–115.

Hošek P, Hoyerová K, Kiran NS, Dobrev PI, Zahajská L, Filepová R, Motyka V, Müller K, Kamínek M. 2020. Distinct metabolism of N-glucosides of isopentenyladenine and trans-zeatin determines cytokinin metabolic spectrum in Arabidopsis. New Phytol 225(6), 2423–2438.

Hoyerová K, Gaudinová A, Malbeck J, Dobrev PI, Kocábek T, Solcová B, Trávnícková A, Kamínek M. 2006. Efficiency of different methods of extraction and purification of cytokinins. Phytochemistry 67(11), 1151–1159.

Hradecká V, Novák O, Havlíček L, Strnad M. 2007. Immunoaffinity chromatography of abscisic acid combined with electrospray liquid chromatography–mass spectrometry J Chromatogr B 847, 162–173.

Hutchison CE, Li J, Argueso C, Gonzalez M, Lee E, Lewis MW, Maxwell BB, Perdue TD, Schaller GE, Alonso JM, Ecker JR, Kieber JJ. 2006. The Arabidopsis histidine phosphotransfer proteins are redundant positive regulators of cytokinin signaling. Plant Cell 18(11), 3073–3087.

Hyde RJ, Cass CE, Young JD, Baldwin SA. 2001. The ENT family of eukaryote nucleoside and nucleobase transporters: recent advances in the investigation of structure/function relationships and the identification of novel isoforms. Mol Membr Biol 18(1), 53–63.

Jackson RG, Lim EK, Li Y, Kowalczyk M, Sandberg G, Hoggett J, Ashford DA, Bowles DJ. 2001. Identification and biochemical characterization of an Arabidopsis indole-3-acetic acid glucosyltransferase. J Biol Chem 276, 4350–4356.

Jaffe MJ, Leopold AC, Staples RC. 2002. Thigmo responses in plants and fungi. Am J Bot 89(3), 375–382.

Jin JB, Jin YH, Lee J, Miura K, Yoo CY, Kim WY, Van Oosten M, Hyun Y, Somers DE, Lee I, Yun DJ, Bressan RA, Hasegawa PM. 2008. The SUMO E3 ligase, AtSIZ1, regulates flowering by controlling a salicylic acid-mediated floral promotion pathway and through affects on FLC chromatin structure. Plant J 53(3), 530–540.

Jon, CS; Zou, YL; Zhao, JH; Ri, HC; Wang, LY; Kaw, HY; Meng, LY; Shang, HB; Li, DH. 2020. Simultaneous determination of multiple phytohormones in tomato by ionic liquid-functionalized carbon fibers-based solid-phase microextraction coupled with liquid chromatography-mass spectrometry. Anal Chim Acta 1137, 143–155.

Kakimoto T. 1996. CKI1, a histidine kinase homolog implicated in cytokinin signal transduction. Science 274(5289), 982–985.

Kakimoto T. 2001. Identification of plant cytokinin biosynthetic enzymes as dimethylallyl diphosphate: ATP/ADP isopentenyltransferases. Plant Cell Physiol 42(7), 677–685.

Kasote DM, Ghosh R, Chung JY, Kim J, Bae I, Bae H. 2016. Multiple reaction monitoring mode based liquid chromatography-mass spectrometry method for simultaneous quantification of brassinolide and other plant hormones involved in abiotic stresses. Int J Anal Chem, 7214087.

Kaza M, Karaźniewicz-Łada M, Kosicka K, Siemiątkowska A, Rudzki PJ. 2019. Bioanalytical method validation: new FDA guidance vs. EMA guideline. Better or worse? J Pharm Biomed Anal 165, 381–385.

Kebert M, Kostic S, Vuksanovic V, Markic AG, Kiprovski B, Zoric M, Orlovic S. 2022. Metal- and organ-specific response to heavy metal-induced stress mediated by antioxidant enzymes' activities, polyamines, and plant hormones levels in Populus deltoides. Plants 11(23), 3246.

Khater S, West C, Lesellier E. 2013. Characterization of five chemistries and three particle sizes of stationary phases used in supercritical fluid chromatography. J Chromatogr A 1319, 148–159.

Kiba T, Mizutani K, Nakahara A, Takebayashi Y, Kojima M, Hobo T, Osakabe K, Sakakibara H. 2023. The trans-zeatin-type side-chain modification of cytokinins controls rice growth. Plant Physiol 192, 2457–2474.

Kijidani Y, Tsuyama T, Tokumoto Y. 2023. Distribution of plant hormones and their precursors in cambial region tissues of Quercus myrsinifolia and Castanopsis cuspidata var.sieboldii after bending stems or applying ethylene precursor. Forests 14(4), 313.

Kisiala A, Kambhampati S, Stock NL, Aoki M, Emery RJN. 2019. Quantification of cytokinins using high-resolution accurate-mass orbitrap mass spectrometry and parallel reaction monitoring (PRM). Anal Chem 91(23), 15049–15056.

Ko D, Kang J, Kiba T, Park J, Kojima M, Do J, Kim KY, Kwon M, Endler A, Song W-Y, Martinoia E, Sakakibara H, Lee Y. 2014. Arabidopsis ABCG14 is essential for the root-to-shoot translocation of cytokinin. Proc Natl Acad Sci USA 111(19), 7150–7155.

Kojima K, Andou D, Ito M. 2021. Plant hormone changes in growing small watermelon fruit. Hortic J 90(2), 202–208.

Krnáčová A. 2021. Izolace fytohormonů s využitím paralelní extrakce pomocí umělých kapalných membrán. Bakalářská práce. Olomouc: Univerzita Palackého v Olomouci, Přírodovědecká fakulta.

Kubiasová K, Montesinos JC, Šamajová O, Nisler J, Mik V, Semerádová H, Plíhalová L, Novák O, Marhavý P, Cavallari N, Zalabák D, Berka K, Doležal K, Galuszka P, Šamaj J, Strnad M, Benková E, Plíhal O, Spíchal L. 2020. Cytokinin fluoroprobe reveals multiple sites of cytokinin perception at plasma membrane and endoplasmic reticulum. Nat Commun 11(1), 4285.

Kutschera U, Briggs WR. 2016. Phototropic solar tracking in sunflower plants: An integrative perspective. Ann Bot 117, 1–8.

Kuhn M. 2008. Building Predictive Models in R Using the caret Package. Journal of Statistical Software 28(5), 1–26.

Kurakawa T, Ueda N, Maekawa M, Kobayashi K, Kojima M, Nagato Y, Sakakibara H, Kyozuka J. 2007. Direct control of shoot meristem activity by a cytokinin-activating enzyme. Nature 445(7128), 652–655.

Lesellier E. 2020. Usual, unusual and unbelievable retention behavior in achiral supercritical fluid chromatography: Review and discussion. J Chromatogr A 1614, 460582.

Letham DS. Zeatin, a factor inducing cell division isolated from Zea mays. Life Sci. 1963:8, 569–573.

Liu JF, Ding J, Yuan BF, Feng YQ. 2014. Magnetic solid phase extraction coupled with in situ derivatization for the highly sensitive determination of acidic phytohormones in rice leaves by UPLC-MS/MS. Analyst 139(21), 5605–5613.

Ljung K. 2013. Auxin metabolism and homeostasis during plant development. Development 140(5), 943–950.

Lomin SN, Krivosheev DM, Steklov MY, Arkhipov DV, Osolodkin DI, Schmülling T, Romanov GA. Plant membrane assays with cytokinin receptors underpin the unique role of free cytokinin bases as biologically active ligands. J Exp Bot. 2015:66(7), 1851–1863.

Lopez-Guerrero MG, Wang P, Phares F, Schachtman DP, Alvarez S, van Dijk K. 2022. A glass bead semi-hydroponic system for intact maize root exudate analysis and phenotyping. Plant Methods 18, 25.

Lorenzo-Parodi N, Kaziur-Cegla W, Gjelstad A, Schmidt TC. 2023. Liquid-phase microextraction of aromatic amines: hollow fiber–liquid-phase microextraction and parallel artificial liquid membrane extraction comparison, Anal Bioanal Chem 415, 1765–1776.

Lu QM, Zhang WM, Gao J, Lu MH, Zhang L, Li JR. 2015. Simultaneous determination of plant hormones in peach based on dispersive liquid-liquid microextraction coupled with liquid chromatography-ion trap mass spectrometry. J Chromatogr B 992, 8–13.

Luo SS, Lin L, Wang XW, Zou SC, Luan TG. 2013. Determination of phytohormones in plant extracts using in-matrix ethyl chloroformate derivatization and DLLME-GC-MS. LCGC Europe 26(6), 310.

Luo ZF, Xu MW, Wang RZ, Liu XB, Huang YK, Xiao LT. 2021. Magnetic Ti3C2 MXene functionalized with beta-cyclodextrin as magnetic solid-phase extraction and in situ derivatization for determining 12 phytohormones in oilseeds by ultra-performance liquid chromatography-tandem mass spectrometry. Phytochemistry 183, 112611.

Majda M, Robert S. 2018. The Role of Auxin in Cell Wall Expansion. Int J Mol Sci 19(4), 951.

Mandal S, Poi R, Banerjee K, Ansary I, Bhattacharyya S, Hazra DK, Ghosh R, Karmakar R. 2021. Bioefficacy, residue dynamics and dietary risk assessment of gibberellic acid in improving the potential yield of tomato (Solanum lycopersicum L.). Environ Monit Assess 193(10).

Mandaokar A, Thines B, Shin B, Lange BM, Choi G, Koo YJ, Yoo YJ, Choi YD, Choi G, Browse J. 2006. Transcriptional regulators of stamen development in Arabidopsis identified by transcriptional profiling. Plant J 46, 984–1008.

Mano Y, Nemoto K. 2012. The pathway of auxin biosynthesis in plants. J Exp Bot 63(8), 2853–2872.

Martin RC, Mock MC, Shaw G, Mok DWS. An enzyme mediating the conversion of zeatin to dihydrozeatin in Phaseolus embryos. Plant Physiol. 1989:90(4), 1630–1635.

Martinez AG, Liebanas FJA, Valverde RS, Torres MEH, Casinello JR, Frenich AG. 2020. Multifamily determination of phytohormones and acidic herbicides in fruits and vegetables by liquid chromatography-tandem mass spectrometry under accredited conditions. Foods 9(7), 906.

Maskos Z, Rush JD, Koppenol WH. 1990. The hydroxylation of the salicylate anion by a fenton reaction and Γ-radiolysis: A consideration of the respective mechanisms. Free Radic Biol Med 8(2), 153–162.

Mashiguchi K, Tanaka K, Sakai T, Sugawara S, Kawaide H, Natsume M, Hanada A, Yaeno T, Shirasu K, Yao H, McSteen P, Zhao Y, Hayashi K, Kamiya Y, Kasahara H. 2011. The main auxin biosynthesis pathway in Arabidopsis. Proc Natl Acad Sci U S A 108(45), 18512–18517.

Matthes MC, Bruce TJ, Ton J, Verrier PJ, Pickett JA, Napier JA. 2010. The transcriptome of cis-jasmone-induced resistance in Arabidopsis thaliana and its role in indirect defence. Planta 232, 1163–1180.

Matsuura T, Mori IC, Himi E, Hirayama T. 2019. Plant hormone profiling in developing seeds of common wheat (Triticum aestivum L.). Breed Sci 69(4), 601–610.

Matuszewski BK, Constanzer ML, Chavez-Eng CM. 2003. Strategies for the assessment of matrix effect in quantitative bioanalytical methods based on HPLC-MS/MS. Anal Chem 75, 3019–3030.

Miller CO, Skoog F, Von Saltza MH, Strong F. Kinetin, a cell division factor from deoxyribonucleic acid. J Am Chem Soc. 1955:77(5), 1392.

Miyawaki K, Matsumoto-Kitano M, Kakimoto T. Expression of cytokinin biosynthetic isopentyltransferase genes in Arabidopsis: tissue specificity and regulation by auxin, cytokinin, and nitrate. Plant J. 2004:37(1), 128–138.

Mogal CS, Solanki VH, Kansara RV, Jha S, Singh S, Parekh VB, Rajkumar BK. 2022. UHPLC-MS/MS and QRT-PCR profiling of PGP agents and Rhizobium spp. of induced phytohormones for growth promotion in mungbean (var. Co4). Heliyon 8(5), e09532.

Mula J, Chiara F, Manca A, Palermiti A, Maiese D, Cusato J, Simiele M, De Rosa FG, Di Perri G, De Nicolò A, D'Avolio A. 2023. Analytical validation of a novel UHPLC-MS/MS method for 19 antibiotics quantification in plasma: Implementation in a LC-MS/MS Kit. Biomed Pharmacother 163, 114790.

Norman C, Howell KA, Millar AH, Whelan JM, Day DA. 2004. Salicylic acid is an uncoupler and inhibitor of mitochondrial electron transport. Plant Physiol 134, 492–501.

Normanly J, Grisafi P, Fink GR, Bartel B. 1997. Arabidopsis mutants resistant to the auxin effects of indole-3-acetonitrile are defective in the nitrilase encoded by the NIT1 gene. Plant Cell 9(10), 1781–1790.

Novaes CG, Bezerra MA, da Silva EG, dos Santos AM, Romão IL, Neto JH. 2016. A review of multivariate designs applied to the optimization of methods based on inductively coupled plasma optical emission spectrometry (ICP OES). Microchem J 128, 331–346.

Novák O, Hényková E, Sairanen I, Kowalczyk M, Pospíšil T, Ljung K. 2012. Tissue-specific profiling of the Arabidopsis thaliana auxin metabolome. Plant J 72(3), 523–36.

Novák O, Napier R, Ljung K. 2017. Zooming In on Plant Hormone Analysis: Tissue- and Cell-Specific Approaches. Annu Rev Plant Biol 68, 323–348.

Nováková L. 2013. Challenges in the development of bioanalytical liquid chromatography-mass spectrometry method with emphasis on fast analysis. J Chromatogr A 1292, 25–37.

Oklešťková J, Tarkowská D, Eyer L, Elbert T, Marek A, Smržová Z, Novák O, Franěk M, Zhabinskii VN, Strnad M. 2017. Immunoaffinity chromatography combined with tandem mass spectrometry: A new tool for the selective capture and analysis of brassinosteroid plant hormones. Talanta 170, 432–440.

Ordaz-Ortiz JJ, Foukaraki S, Terry LA. 2015. Assessing temporal flux of plant hormones in stored processing potatoes using high definition accurate mass spectrometry. Hortic Res 2, 15002.

Park WJ, Kriechbaumer V, Möller A, Piotrowski M, Meeley RB, Gierl A, Glawischnig E. 2003. The Nitrilase ZmNIT2 converts indole-3-acetonitrile to indole-3-acetic acid. Plant Physiol 133(2), 794–802.

Park SW, Kaimoyo E, Kumar D, Mosher S, Klessig DF. 2007. Methyl salicylate is a critical mobile signal for plant systemic acquired resistance. Science 318(5847), 113–116.

Pavlovič A, Jakšová J, Novák O. 2017. Triggering a false alarm: wounding mimics prey capture in the carnivorous Venus flytrap (Dionaea muscipula). New Phytologist 216, 927–938.

Pavlovič A, Koller J, Vrobel O, Chamrád I, Lenobel R, Tarkowski P. 2024. Is the co-option of jasmonate signalling for botanical carnivory a universal trait for all carnivorous plants? J Exp Bot 75, 334–349.

Pengelly W, Meins F. 1976. Radioimmunoassay for indole-3-acetic acid. Plant Physiol 57(5), 30–30.

Pereira L, Pujol M, Garcia-Mas J, Phillips MA. 2017. Non-invasive quantification of ethylene in attached fruit headspace at 1p.p.b. by gas chromatography-mass spectrometry. Plant J 91(1), 172–183.

Pěnčík A, Casanova-Sáez R, Pilařová V, Žukauskaite A, Pinto R, Micol JL, Ljung K, Novák O. 2018. Ultra-rapid auxin metabolite profiling for high-throughput mutant screening in Arabidopsis. J Exp Bot 69(10), 2569–2579.

Petřík I, Pěnčík A, Stýskala J, Tranová L, Amakorová P, Strnad M, Novák O. 2024. Rapid profiling of cytokinins using supercritical fluid chromatography coupled with tandem mass spectrometry. Anal Chim Acta 1285, 342010.

Pilařová V, Sultani M, Ask KS, Nováková L, Pedersen-Bjergaard S, Gjelstad A. 2017. One-step extraction of polar drugs from plasma by parallel artificial liquid membrane extraction. J Chromatogr B 1043, 25–32.

Plachká K, Khalikova M, Babičová B, Němcová Z, Roubíčková L, Svec F, Nováková L. 2020. Ultra-high performance supercritical fluid chromatography in impurity control II: Method validation. Anal Chim Acta 1117, 48–59.

Plachká K, Střítecký J, Švec F, Nováková L. 2021. The effect of column history in supercritical fluid chromatography: Practical implications. J Chromatogr A 1651, 462272.

Plačková L, Oklestkova J, Pospíšková K, Poláková K, Buček J, Stýskala J, Zatloukal M, Šafařík I, Zbořil R, Strnad M, Doležal K, Novák O. 2017. Microscale magnetic microparticle-based immunopurification of cytokinins from Arabidopsis root apex. Plant J 89(5), 1065–1075.

Politis SN, Colombo P, Colombo G, Rekkas M. 2017. Design of experiments (DoE) in pharmaceutical development. Drug Dev Ind Pharm 43(6), 889–901.

Porfirio S, Sonon R, da Silva MDRG, Peixe A, Cabrita MJ, Azadi P. 2016. Quantification of free auxins in semi-hardwood plant cuttings and microshoots by dispersive liquid-liquid microextraction/microwave derivatization and GC/MS alysis. Anal Methods 8(31), 6089–6098.

Posit team. 2023. RStudio: Integrated development environment for R. posit software, PBC, Boston, MA.

Punwani JA, Hutchison CE, Schaller GE, Kieber JJ. 2010. The subcellular distribution of the Arabidopsis histidine phosphotransfer proteins is independent of cytokinin signaling. Plant J 62(3), 473–482.

R Core Team. 2023. R: A language and environment for etatistical computing. R Foundation for Statistical Computing, Vienna, Austria.

Radchuk V, Belew ZM, Gündel A, Mayer S, Hilo A, Hensel G, Sharma R, Neumann K, Ortleb S, Wagner S, Maszynska A, Crocoll C, Xu D, Hoffie I, Kumlehn J, Fuchs J, Peleke FF, Szymanski JJ, Rolletschek H, Nour-Eldin HH, Borisjuk L. 2023. SWEET11b transports both sugar and cytokinin in developing barley grains. Plant Cell 35(6), 2186–2207.

Rashotte AM. 2021. The evolution of cytokinin signaling and its role in development before angiosperms. Semin Cell Dev Biol 109, 31–38.

Rawlinson C, Kamphuis LG, Gummer JPA, Singh KB, Trengove RD. 2015. A rapid method for profiling of volatile and semi-volatile phytohormones using methyl chloroformate derivatisation and GC-MS. Metabolomics 11(6), 1922–1933.

Rayle DL, Cleland RE. 1992. The Acid Growth Theory of auxin-induced cell elongation is alive and well. Plant Physiol 99(4), 1271–1274.

Rittenberg D, Foster GL. 1940. A new procedure for quantitative analysis by isotope dilution, with application to the determination of amino acids and fatty acids. J Biol Chem 133, 727–744.

Raes J, Rohde A, Christensen JH, Van de Peer Y, Boerjan W. 2003. Genome-wide characterization of the lignification toolbox in Arabidopsis. Plant Physiol1 133(3), 1051–1071.

Rohde A, Morreel K, Ralph J, Goeminne G, Hostyn V, De Rycke R, Kushnir S, Van Doorsselaere J, Joseleau JP, Vuylsteke M, Van Driessche G, Van Beeumen J, Messens E, Boerjan W. 2004. Molecular phenotyping of the pal1 and pal2 mutants of Arabidopsis thaliana reveals far-reaching consequences on phenylpropanoid, amino acid, and carbohydrate metabolism. Plant Cell 16(10), 2749–2771.

Romanov GA, Lomin SN, Schmülling T. 2018. Cytokinin signaling: from the ER or from the PM? That is the question! New Phytol 218(1), 41–53.

Rosquete MR, von Wangenheim D, Marhavý P, Barbez E, Stelzer EH, Benková E, Maizel A, Kleine-Vehn J. 2013. An auxin transport mechanism restricts positive orthogravitropism in lateral roots. Curr Biol 23(9), 817–22.

Rubery PH, Sheldrake AR. 1974. Carrier-mediated auxin transport. Planta 118, 101–121.

Sakakibara H. 2006. Cytokinins: activity, biosynthesis, and translocation. Annu Rev Plant Biol 57(1), 431–449.

Schaller F, Hennig P, Weiler EW. 1998. 12-Oxophytodienoate-10,11-Reductase: Occurrence of Two Isoenzymes of Different Specificity against Stereoisomers of 12-Oxophytodienoic Acid. Plant Physiol 188, 1345–1351.

Schaller A, Stintzi A. 2009. Enzymes in jasmonate biosynthesis – structure, function, regulation. Phytochemistry 70, 1532–1538.

Sheard LB, Tan X, Mao H, Withers J, Ben-Nissan G, Hinds TR, Kobayashi Y, Hsu FF, Sharon M, Browse J, He SY, Rizo J, Howe GA, Zheng N. 2010. Jasmonate perception by inositol-phosphate-potentiated COI1-JAZ co-receptor. Nature 7322, 400–405.

Seto Y, Sado A, Asami K, Hanada A, Umehara M, Akiyama K, Yamaguchi S. 2014. Carlactone is an endogenous biosynthetic precursor for strigolactones. Proc Natl Acad Sci USA 111(4), 1640–1645.

Simon S, Petrášek J. 2011. Why plants need more than one type of auxin. Plant Sci 180(3), 454–460.

Šimura J, Antoniadi I, Široká J, Tarkowská D, Strnad M, Ljung K, Novák O. 2018. Plant Hormonomics: Multiple Phytohormone Profiling by Targeted Metabolomics. Plant Physiol 177, 476–489.

Široká J, Brunoni F, Pěnčík A, Mik V, Žukauskaite A, Strnad M, Novák O, Floková K. 2022. High-throughput interspecies profiling of acidic plant hormones using miniaturised sample processing. Plant Methods 18, 122.

Smyth DR, Bowman JL, Meyerowitz EM. 1990. Early flower development in Arabidopsis. Plant Cell 2, 755–767.

Spíchal L. 2012. Cytokinins – recent news and views of evolutionally old molecules. Funct Plant Biol 39, 267–284.

Staswick PE, Tiryaki I. 2004. The oxylipin signal jasmonic acid is activated by an enzyme that conjugates it to isoleucine in Arabidopsis. Plant Cell 16(8), 2117-2127.

Stepanova AN, Hoyt JM, Hamilton AA, Alonso JM. 2005. A link between ethylene and auxin uncovered by the characterization of two root-specific ethylene-insensitive mutants in Arabidopsis. Plant Cell 17, 2230–2242.

Stintzi A, Browse J. 2000. The Arabidopsis male-sterile mutant, opr3, lacks the 12-oxophytodienoic acid reductase required for jasmonate synthesis. Proc Natl Acad Sci USA 97(19), 10625–10630.

Strawn MA, Marr SK, Inoue K, Inada N, Zubieta C, Wildermuth MC. 2007. Arabidopsis isochorismate synthase functional in pathogen-induced salicylate biosynthesis exhibits properties consistent with a role in diverse stress responses. J Biol Chem 282(8), 5919–5933.

Strnad M. 1997. The aromatic cytokinins. Physiol Plant 101(4), 674–688.

Sugahara K, Kitao K, Yamagaki T, Koyama T. 2020. Practical optimization of liquid chromatography/mass spectrometry conditions and pretreatment methods toward the sensitive quantification of auxin in plants. Rapid Commun Mass Spectrom 34(7), e8625.

Sugawara S, Hishiyama S, Jikumaru Y, Hanada A, Nishimura T, Koshiba T, Zhao Y, Kamiya Y, Kasahara H. 2009. Biochemical analyses of indole-3-acetaldoxime-dependent auxin biosynthesis in Arabidopsis. Proc Natl Acad Sci U S A 106(13), 5430–5435.

Sun J, Hirose N, Wang X, Wen P, Xue L, Sakakibara H, Zuo J. 2005. Arabidopsis SOI33/AtENT8 gene encodes a putative equilibrative nucleoside transporter that is involved in cytokinin transport in planta. J Integr Plant Biol 47(5), 588–603.

Svačinová J, Novák O, Plačková L, Lenobel R, Holík J, Strnad M, Doležal K. 2021. A new approach for cytokinin isolation from Arabidopsis tissues using miniaturized purification: pipette tip solid-phase extraction. Plant Methods 8(1), 17.

Takahashi H, Miyazawa Y, Fujii N. 2009. Hormonal interactions during root tropic growth: hydrotropism versus gravitropism. Plant Mol Biol 69(4), 489–502.

Takei K, Yamaya T, Sakakibara H. 2004. Arabidopsis CYP735A1 and CYP735A2 encode cytokinin hydroxylases that catalyze the biosynthesis of trans-zeatin. J Biol Chem 279(40), 41866–41872.

Tanaka K, Hayashi K, Natsume M, Kamiya Y, Sakakibara H, Kawaide H, Kasahara H. 2014. UGT74D1 catalyzes the glucosylation of 2-oxindole-3-acetic acid in the auxin metabolic pathway in Arabidopsis. Plant Cell Physiol. 55, 218–228.

Tang L, Kebarle P. 1993. Dependence of ion intensity in electrospray mass spectrometry on the concentration of the analytes in the electrosprayed solution. Anal Chem 65(24), 3654–3668.

Tarkowská D, Novák O, Floková K, Tarkowski P, Turečková V, Grúz J, Rolčík J, Strnad M. 2014. Quo vadis plant hormone analysis? Planta 240, 55–76.

Tessi TM, Brumm S, Winklbauer E, Schumacher B, Pettinari G, Lescano I, González CA, Wanke D, Maurino VG, Harter K, Desimone M. 2021. Arabidopsis AZG2 transports cytokinins in vivo and regulates lateral root emergence. New Phytol 229(2), 979–993.

Tessi TM, Maurino VG, Shahriari M, Meissner E, Novak O, Pasternak T, Schumacher BS, Ditengou F, Li Z, Duerr J, Flubacher NS. Nautscher M, Williams A, Kizimierczak Z, Strnad M, Thumfart JO, Palme K, Desimone M, Taele WD. 2023. AZG1 is a cytokinin transporter that interacts with auxin transporter PIN1 and regulates the root stress response. New Phytol 238(5), 1924–1941.

To JP, Deruère J, Maxwell BB, Morris VF, Hutchison CE, Schaller GE, Kieber JJ. 2007. Cytokinin regulates type-A Arabidopsis response regulator activity and protein stability via two-component phosphorelay. Plant Cell 19(12), 3901–3914.

Tokunaga H, Kojima M, Kuroha T, Ishida T, Sugimoto K, Kiba T, Sakakibara H. 2012. Arabidopsis lonely guy (LOG) multiple mutants reveal a central role of the LOG-dependent pathway in cytokinin activation. Plant J 69(2), 355–365.

Trapp MA, De Souza GD, Rodrigues E, Boland W, Mithofer A. 2014. Validated method for phytohormone quantification in plants. Front Plant Sci 5, 417.

Vaca E, Behrens C, Theccanat T, Choe JY, Dean JV. 2017. Mechanistic differences in the uptake of salicylic acid glucose conjugates by vacuolar membrane-enriched vesicles isolated from Arabidopsis thaliana. Physiol Plant 161(3), 322–338.

Valníčková A. 2019. Optimalizace extrakčního a purifikačního protokolu vybraných rostlinných hormonů. Bakalářská práce. Olomouc: Univerzita Palackého v Olomouci, Přírodovědecká fakulta.

Vick BA, Zimmerman DC. 1984. Biosynthesis of Jasmonic Acid by Several Plant Species. Plant Physiol 75, 458–461.

Vlot AC, Dempsey DA, Klessig DF. 2009. Salicylic Acid, a multifaceted hormone to combat disease. Annu Rev Phytopathol 47, 177–206.

Vrobel, O; Tarkowski, P. 2023. Can plant hormonomics be built on simple analysis? A review. Plant Methods 19, 107.

Wasternack C. 2007. Jasmonates: an update on biosynthesis, signal transductionand action in plant stress response, growth and development. Ann Bot 100, 681–697.

Wasternack C, Hause B. 2013. Jasmonates: biosynthesis, perception, signal transduction and action in plant stress response, growth and development. An update to the 2007 review in annals of botany. Ann Bot 111, 1021–1058.

Weber H, Vick BA, Farmer EE. 1997. Dinor-oxo-phytodienoic acid: a new hexadecanoid signal in the jasmonate family. Proc Natl Acad Sci USA 94, 10473–10478.

Went FW. 1926. On Growth-Accelerating Substances in the Coleoptile of Avena sativa. Proceedings of the Section of Sciences, Koninklijke Akademie van Wetenschappen te Amsterdam 30, 10-19.

Went FW. 1937. Salt accumulation and polar transport of plant hormones. Science 86, 127–128.

West C. 2018. Current trends in supercritical fluid chromatography. Anal Bioanal Chem 410, 6441–6457.

West C, Lesellier E. 2012. Chemometric methods to classify stationary phases for achiral packed column supercritical fluid chromatography. J Chemom 26, 52–65.

Wickham H, Bryan J. 2023. readxl: Read Excel Files. R package version 1.4.3.

Wickham H. 2016. ggplot2: Elegant Graphics for Data Analysis. Springer-Verlag New York.

Wildermuth MC, Dewdney J, Wu G, Ausubel FM. 2001. Isochorismate synthase is required to synthesize salicylic acid for plant defence. Nature 414(6863), 562–565.

Wold S, Sjostrom M, Eriksson L. 2001. PLS-regression: a basic tool of chemometrics. Chemom Intell Lab Syst 58, 109–130.

Wong C, Alabadí D, Blázquez MA. 2023. Spatial regulation of plant hormone action. J Exp Bot 74(19), 6089–6103.

Wu TB, Liang Y, Zhu XC, Zhao MP, Liu HW. 2014. Separation and quantification of four isomers of indole-3-acetyl-myo-inositol in plant tissues using high-performance liquid chromatography coupled with quadrupole time-of-flight tandem mass spectrometry. Anal Bioanal Chem 406(13), 3239–3247.

Wulfetange K, Lomin SN, Romanov GA, Stolz A, Heyl A, Schmülling T. 2011. The cytokinin receptors of Arabidopsis are located mainly to the endoplasmic reticulum. Plant Physiol 156(4), 1808–1818.

Xiao HM, Cai WJ, Ye TT, Ding J, Feng YQ. 2018. Spatio-temporal profiling of abscisic acid, indoleacetic acid and jasmonic acid in single rice seed during seed germination. Anal Chim Acta 1031, 119–127.

Xiao Y, Liu D, Zhang G, Gao S, Liu L, Xu F, Che R, Wang Y, Tong H, Chu C. 2019. Big grain3, encoding a purine permease, regulates grain size via modulating cytokinin transport in rice. J Integr Plant Biol 61(5), 581–597.

Xie HB, Zhou MY, Zhao HF, Wang YG, Jiang WF, Zhao S. 2014. Determination of three exogenous plant hormone residues in bean sprout by high performance liquid chromatography-quadrupole-time of flight mass spectrometry. Chin J Chromatogr 32(5), 493–498.

Yan Y, Stolz S, Chételat A, Reymond P, Pagni M, Dubugnon L, Farmer EE. 2007. A downstream mediator in the growth repression limb of the jasmonate pathway. The Plant Cell 19, 2470–2483.

Yang XH, Brown SK, Davies PJ. 2013. The content and in vivo metabolism of gibberellin in apple vegetative tissues. J Am Soc Hortic Sci 138(3), 173–183.

Yao XC, Xia NY, Meng X, Duan CQ, Pan QH. 2022. A one-step polyphenol removal approach for detection of multiple phytohormones from grape berry. Horticulturae 8(6), 548.

Yonny ME, Ballesteros-Gomez A, Adamo MLT, Torresi AR, Nazareno MA, Rubio S. 2020. Supramolecular solvent-based high-throughput sample treatment for monitoring phytohormones in plant tissues. Talanta 219, 121249.

Záveská Drábková L, Dobrev PI, Motyka V. 2015. Phytohormone profiling across the Bryophytes. PLoS One 10(5), e0125411.

Zemanová V, Pavlíková D, Dobrev PI, Motyka V, Pavlík M. 2019. Endogenous phytohormone profiles in Pteris fern species differing in arsenic accumulating ability. Environ Exp Bot 166, 103822.

Zhang Z, Li Q, Li Z, Staswick PE, Wang M, Zhu Y, He Z. 2007. Dual regulation role of GH3.5 in salicylic acid and auxin signaling during Arabidopsis-Pseudomonas syringae interaction. Plant Physiol 145(2), 450–464.

Zhang K, Novak O, Wei Z, Gou M, Zhang X, Yu Y, Yang H, Cai Y, Strnad M, Liu CJ. 2014. Arabidopsis ABCG14 protein controls the acropetal translocation of root-synthesized cytokinins. Nat Commun 5(1), 3274.

Zhang Y, Zhao L, Zhao J, Li Y, Wang J, Guo R, Gan S, Liu CJ, Zhang K. 2017. S5H/DMR6 Encodes a Salicylic Acid 5-Hydroxylase That Fine-Tunes Salicylic Acid Homeostasis. Plant Physiol 175(3), 1082–1093.

Zhang QC, Chen Y, Yang YQ, Liu YL, Wen M, Wang XY. 2023. Fabrication of magnetic ordered mesoporous carbon for quantitative analysis of acidic phytohormones in mushroom samples prior to their determination by ultra-high-performance liquid chromatography-tandem mass spectrometry. Acta Chromatogr 35(1), 60–69.

Zhao J, Ding B, Zhu E, Deng X, Zhang M, Zhang P, Wang L, Dai Y, Xiao S, Zhang C, Liu C, Zhang K. 2021. Phloem unloading via the apoplastic pathway is essential for shoot distribution of root-synthesized cytokinins. Plant Physiol 186(4), 2111–2123.

Zou YL, Meng LY, Cui MY, Zhao JH, He M, Kim J, Quinto M, Shang HB, Li DH. 2019. Fast on-fiber derivatization and GC/MS analysis of phytohormones in wheat based on pencil-type coated carbon fibers. Food Chem 274, 254–260.

Zürcher E, Liu J, di Donato M, Geisler M, Müller B. 2016. Plant development regulated by cytokinin sinks. Science 353(6303), 1027–1030.

8 List of Supplements

SUPPLEMENT I

Petřík I, Hladík P, Zhang C, Pěnčík A, Novák O. [Submitted after revisions]. Spatio-temporal plant hormonomics: From tissue to subcellular resolution. J Exp B

SUPPLEMENT II

Petřík I, Valníčková A, Stýskala J, Strnad M, Ljung K, Novák O. [In preparation]. DisperSpin solid phase micro-extraction: next generation micro-purification method for UHPLC-MS/MS determination of naturally occurring phytohormones.

SUPPLEMENT III

Petřík I, Pěnčík A, Stýskala J, Tranová L, Amakorová P, Strnad M, Novák O. 2024. Rapid profiling of cytokinins using supercritical fluid chromatography coupled with tandem mass spectrometry. Anal Chim Acta 1285, 342010.

SUPPLEMENT IV

Tan S, Abas M, Verstraeten I, Glanc M, Molnár G, Hajný J, Lasák P, **Petřík I**, Russinova E, Petrášek J, Novák O, Pospíšil J, Friml J. 2020. Salicylic acid targets protein phosphatase 2A to attenuate growth in plants. Curr Biol 30(3), 381–395.

SUPPLEMENT V

Poitout A, Crabos A, **Petřík I**, Novák O, Krouk G, Lacombe B, Ruffel S. 2018. Responses to systemic nitrogen signaling in arabidopsis roots involve trans-zeatin in shoots. Plant Cell 30(6), 1243–1257.

SUPPLEMENT VI

Kocáb O, Jakšová J, Novák O, **Petřík I**, Lenobel R, Chamrád I, Pavlovič A. 2020. Jasmonate-independent regulation of digestive enzyme activity in the carnivorous butterwort Pinguicula × Tina. J Exp Bot 71(12), 3749–3758.

SUPPLEMENT VII

Jakšová J, Adamec L, **Petřík I**, Novák O, Šebela M, Pavlovič A. 2021. Contrasting effect of prey capture on jasmonate accumulation in two genera of aquatic carnivorous plants (Aldrovanda, Utricularia). Plant Physiol Biochem 166, 459–465.

SUPPLEMENT VIII

Waidmann S, Ruiz Rosquete M, Schöller M, Sarkel E, Lindner H, LaRue T, **Petřík I**, Dünser K, Martopawiro S, Sasidharan R, Novak O, Wabnik K, Dinneny JR, Kleine-Vehn J. 2019. Cytokinin functions as an asymmetric and anti-gravitropic signal in lateral roots. Nat Commun 10(1), 3540.

Supplement I

Supplement II

Supplement III

Supplement IV

Supplement V

Supplement VI

Supplement VII

Supplement VIII

Petřík I, Hladík P, Zhang C, Pěnčík A, Novák O. [Submitted after revisions]. Spatio-temporal plant hormonomics: From tissue to subcellular resolution. J Exp B.

Spatio-temporal plant hormonomics: From tissue to subcellular resolution

Running Title: The current trends in plant hormone analysis

Ivan Petřík, Pavel Hladík, Chao Zhang, Aleš Pěnčík, Ondřej Novák*

Laboratory of Growth Regulators, Faculty of Science, Palacký University & Institute of Experimental Botany, The Czech Academy of Sciences, Šlechtitelů 27, CZ-78371, Olomouc, Czech Republic

E-mail addresses:

Ivan Petřík: ivan.petrik@upol.cz; ORCID 0000-0001-5320-7599

Pavel Hladík: pavel.hladik@upol.cz; ORCID 0000-0002-9817-2630

Chao Zhang: chao.zhang@upol.cz; ORCID 0000-0002-4173-2107

Aleš Pěnčík: ales.pencik@upol.cz; ORCID 0000-0002-1314-2249

Ondřej Novák: ondrej.novak@upol.cz; ORCID 0000-0003-3452-0154

The date of submission: January 17, 2024

The word count: 6,480

The number of tables and figures: 2 tables and 4 figures

Repository Files:

1. Statistical methods
2. Raw data from Web of Science for targeted plant hormone analysis
3. Raw data from Web of Science for untargeted plant hormone analysis

Highlight: A comprehensive meta-study was conducted to reveal research trends in plant hormone determination using targeted and untargeted metabolomic approaches published in the last decade.

Abstract

Due to technological advances in mass spectrometry, significant progress has been achieved recently in plant hormone research. Nowadays, plant hormonomics is well established as a fully integrated scientific field focused on the analysis of phytohormones, mainly on their isolation, identification and spatiotemporal quantification in plants. This review represents a comprehensive meta-study of the advances in the phytohormone analysis by mass spectrometry over the past decade. To address current trends and future perspectives, Web of Science data were systematically collected and key features such as mass spectrometry-based analyses were evaluated using multivariate data analysis methods. Our findings showed that plant hormonomics is currently divided into targeted and untargeted approaches. Both aim to miniaturize the sample, allowing high-resolution quantification to be covered in plant organs as well as subcellular compartments. Therefore, we can study plant hormone biosynthesis, metabolism and signalling at a spatio-temporal resolution. Moreover, this trend has recently been accelerated by technological advances such as fluorescence-activated cell sorting or mass spectrometry imaging.

Keywords: plant hormones, phytohormones, metabolomics, liquid chromatography, mass spectrometry, sample preparation, recent advances

Abbreviations:

µSPE	micro solid phase extraction
ABA	abscisic acid
ACC	1-aminocyclopropane-1-carboxylicacid
BRs	brassinosteroids
CE	capillary electrophoresis
CKs	cytokinins
DDA	data-dependent analysis
DESI	desorption electrospray ionization
DI	direct infusion
DIA	data independent analysis
DLLME	dispersive liquid-liquid micro extraction
DS	product ion scan (daughter scan)
EI	electron impact

59	ELISA	enzyme-linked immunosorbent assay
60	ER	endoplasmic reticulum
61	ESI	electrospray ionization
62	FS	full scan
63	GAs	gibberellins
64	GC	gas chromatography
65	GFP	green fluorescent protein
66	HESI	heated electrospray ionization
67	HRMS	high-resolution mass spectrometry
68	IAA	indole-3-acetic acid
69	IM	ion mobility
70	IT	ion trap mass spectrometry
71	JA	jasmonic acid
72	JA-Ile	jasmonyl-isoleucine
73	LC	liquid chromatography
74	LIT	linear ion trap mass spectrometry
75	LLE	liquid-liquid chromatography
76	m/z	mass-to-charge ratio
77	MALDI	matrix-assisted laser desorption/ionization
78	MRM	multiple reaction monitoring
79	MS	mass spectrometry
80	MS/MS	tandem mass spectrometry
81	MS^E	see DIA
82	MSI	mass spectrometry imaging
83	NMR	nuclear magnetic resonance
84	OH-JA	hydroxyjasmonic acid
85	OPDA	12-oxo-phytodienoic acid
86	oxIAA	2-oxoindole-3-acetic acid
87	PRM	parallel reaction monitoring
88	Q	single quadrupole mass spectrometry
89	Q-FT-ICR	quadrupole-Fourier transform ion cyclotron resonance mass spectrometry
90	Q-LIT	quadrupole-linear ion trap mass spectrometry
91	QqQ	triple quadrupole mass spectrometry
92	Q-TOF	quadrupole-time of flight mass spectrometry
93	QuEChERS	Quick, Easy, Cheap, Effective, Rugged, and Safe dispersive solid phase extraction

94	RIA	radioimmunoassay
95	SA	salicylic acid
96	SFC	supercritical fluid chromatography
97	SIM	single-ion monitoring
98	SIPTE	sequential solvent-induced phase transition extraction
99	SPE	solid phase extraction
100	SUPRAS	supramolecular solvents
101	TOF	time-of-flight mass spectrometry
102	(U)HPLC	(ultra)-high performance liquid chromatography

103

104 **Introduction**

105 Plant hormones play an irreplaceable role in the life cycle of all world-wide plant species. From ocean-wide
106 seaweeds to sky-climbing trees, all plants regulate their growth, development, and response to the
107 environment through a complex network of plant hormone chemical signals. Knowledge about the
108 biosynthesis, metabolism and signalling of plant hormones has been constantly increasing since the
109 beginning of the last century (Went, 1926). But notable breakthroughs have usually been associated with
110 some kind of technology advance. The discovery of the DNA chemical structure in the early 1950s led to the
111 elucidation of physiological mechanisms at the genomic level (Watson & Crick, 1953). Similarly, research on
112 plant hormones was facilitated primarily by two remarkable inventions. First, the utilization of the antibodies
113 in the 1970s and 1980s enabled the identification and quantification of naturally occurring phytohormones.
114 The radioimmunoassay (RIA) and the enzyme-linked immunosorbent assay (ELISA) have become very popular
115 methods that are still used recently (Fig. 1). However, the main boom in the plant hormone analysis began
116 at the end of the last millennium with the advent of mass spectrometry (MS) using soft ionization techniques.
117 This trend is well documented on the Web of Science (Fig. 1). Until the end of the 1980s, only a few research
118 articles aimed at the determination of plant hormones were published annually. However, publishing activity
119 increased dramatically a few years later. In particular, the articles utilizing MS have increased ten-fold
120 compared to the previous period. This analytical technique thus occupies a leading position in the
121 phytohormonal analysis due to its exceptional selectivity and sensitivity. Moreover, the popularity of MS in
122 the plant hormone research has been skyrocketing in the last decade. While 15 years ago there were
123 approximately 50 publications per year, today more than 150 articles are published. This remarkable rise
124 opens up an opportunity to examine what has happened in the plant hormone field in the past decade, what
125 the current trend is and whether future perspectives can be estimated. To properly answer these challenging
126 questions, we retrieved data from the Web of Science and analysed them with statistical methods including
127 multivariate data analysis (Repository File 1).

Recent developments in MS technology, together with reverse genetics, have contributed to our understanding of phytohormone patterns, biosynthesis, metabolism, and regulatory networks in plants (Arnold et al., 2016; Hayashi et al., 2021; Tang et al., 2022). Innovations in sample preparation methods, such as microscale solid-phase extraction (μSPE), enable the analysis of sub-milligram samples and organ-specific studies. The combination of ultra-sensitive MS analysis with other advanced technologies, such as flow cytometry-based cell or organelle sorting, offers a cutting-edge approach to obtain spatial patterns of phytohormones within plant tissues and cells. Another technique with high spatial resolution is mass spectrometry imaging (MSI), which allows us to map the distribution of phytohormones within plant tissues, similar to the more popular biosensors. In vivo visualization will give us a deeper insight into the localized effects of hormones in specific cells or structures.

Targeted Metabolomics of Plant Hormones

In general, plant hormone metabolomics, also known as plant hormonomics, is currently divided into two approaches. In targeted hormonomics, researchers focus on pre-selected plant metabolites and monitor them with sensitive and accurate quantification. Conversely, an untargeted approach is suitable in the studies aimed at characterizing the structures of unknown phytohormones. In this chapter, we present a comprehensive meta-study focused on the targeted plant hormonomics conducted through a systematic search of 122 relevant publications on the Web of Science since 2013 (Repository File 2). We performed a statistical analysis of the publication set to describe current trends in plant-targeted hormonomics.

Liquid chromatography-mass spectrometry as a leading hyphenated technique

The most remarkable observation in our meta-study is associated with the instrumentation coupled with MS (Fig. 2A). These hyphenated techniques involving electromigration or chromatographic procedures are an essential part of the analytical workflow due to their separation capability. Direct infusion of the complex plant sample into the MS without prior separation leads to difficult interpretation of the analytical outcome. While capillary electrophoresis (CE) and supercritical fluid chromatography (SFC) were each represented by one research article (Contreras-Gutierrez et al., 2013; Petřík et al. 2024), gas chromatography (GC) emerged in seven recent works (Fig. 2A). Notably, GC-MS has proven to be a suitable approach for the analysis of the volatile compounds, with the recent investigations focusing on ethylene (Rawlinson et al., 2015; Pereira et al., 2017). However, majority of plant hormones are non-volatile, polar and water-soluble molecules. Therefore, their analysis using GC-MS is barely possible without chemical derivatization. Coupling GC-MS with a derivatization step has facilitated the examination of acidic plant hormones such as auxins, jasmonates (JAs), abscisic acid (ABA), salicylic acid (SA) and gibberellins (GAs) (Yang et al., 2013; Luo et al., 2013; Porfirio et al., 2016; Zou et al., 2019; Kebert et al., 2022). Nonetheless, this step is time-consuming and potentially hazardous. The issue of analysing polar compounds by MS was finally solved with the advent of electrospray

ionization (ESI) (Fenn et al., 1989). This revolutionary technology is based on the infusion of a liquid sample in the form of an aerosol into the MS source. ESI enables direct coupling with liquid chromatography (LC) and leads to sensitive detection of compounds without a derivatization step. In addition, LC techniques have also made remarkable technological progress in recent decades. Continuous improvements in separation efficiency led to the advent of (ultra)high-performance liquid chromatography ((U)HPLC). It is therefore not surprising that an overwhelming 93% of the applications in our meta-study employed (U)HPLC-ESI-MS (Fig. 2A).

An essential part of the chromatographic system is the stationary phase enclosed in the chromatographic column. Various types of chromatographic columns are currently available on the market. Importantly, their selection depends on the physicochemical properties of the targeted compounds. Current plant hormonomics relies exclusively on the reversed phase columns (Fig. 2B). For example, an amide-modified stationary phase has recently been used for the analysis of several cytokinins and stress-related compounds (Dziurka et al., 2019). Another application recruited phenyl-hexyl sorbent for the separation of brassinosteroids or jasmonates (Oklešťková et al., 2017; Trapp et al., 2014). However, an overwhelming 103 out of 109 applications utilized an octadecyl column (C18), making it the most popular stationary phase in (U)HPLC-MS over the past decade (Fig. 2B). The C18 sorbent is robust and easy-to-maintain, and its chemical composition allows the separation of polar and non-polar compounds (Šimura et al., 2018). Despite the versatility of C18, some particular separations of plant hormones remain quite difficult. For example, specifically targeted methods require the separation of jasmonate-isoleucine (JA-Ile) isomers or 11- and 12-hydroxy-jasmonic acid (11-OH-JA/12-OH-JA) (Glauser et al., 2008; Fonseca et al., 2009). The recently introduced SFC technique represents an improved chromatographic performance by combining the advantages of GC and LC, thus opening an undiscovered path to new analytical procedures for the determination of phytohormones. The first pioneering publication recently introduced the SFC-MS method for the determination of cytokinin metabolites (CKs) including their isomers (Petřík et al., 2024). However, the chromatographic behaviour of other plant hormones in the SFC mode has not yet been sufficiently investigated.

Triple-quadrupoles running in multiple reaction monitoring dominate among MS configurations

As mentioned above, mass spectrometry is the preferred detection technique in plant hormonomics. Briefly, MS involves ionizing the analysed molecule, separating the ions based on their mass-to-charge ratio (*m/z*), and detecting their abundance in the sample. Various types of MS instruments are currently available on the market. They differ in the technical construction determining their sensitivity and selectivity. The most straightforward solution of MS detection is employment of single analysers (Lu et al., 2015; Kojima et al., 2021; Rogach et al., 2021), which detect ions based only on their *m/z*. On the other hand, tandem mass analysers (MS/MS) involve fragmentation of selected ions, which increases the specificity and selectivity of

MS instrument. The suitability of MS/MS mode for complex plant hormonomics is shown by 98% of recent applications that used triple-quadrupoles (QqQ) and quadrupole-linear ion traps (Q-LIT; Fig. 2C). Both techniques are characterised by high sensitivity, robustness and good price-performance ratio, which makes them suitable for routine analysis (Cai et al., 2013; Záveská Drábková et al., 2015; Zemanová et al., 2019; Fresno et al., 2023). However, they are low-resolution MS systems (LRMS) with relatively low selectivity. Therefore, high-resolution MS (HRMS) systems have been introduced to plant hormonomics in the last decade (Wu et al., 2014; Perin et al., 2018; Leng et al., 2018). Due to high resolving power, these MS systems are favourable for structural elucidation and identification of new plant metabolites. Ideally, plant hormonomics requires an MS system combining high resolution and superior sensitivity. Unfortunately, researchers often have to choose a compromise between LRMS or HRMS and the associated sensitivity or resolution, respectively.

The choice of data acquisition mode significantly influences the intensity of the MS/MS signal. Low-resolution MS/MS systems operate predominantly in multiple reaction monitoring (MRM) modes, utilizing their fast scan speed for the simultaneous detection of multiple targeted compounds (Fig. 2D). Recently, a novel data acquisition approach known as parallel reaction monitoring (PRM) has emerged for HRMS. The Q-Orbitrap instrument operating in PRM mode was used to monitor multiple CK metabolites, demonstrating a substantial enhancement in sensitivity comparable to QqQ instruments (Kisiala et al., 2019). The concept of PRM was adopted from proteomic applications aimed at the quantitative analysis of targeted peptides (Bourmaud et al., 2016, Kaufmann, 2018). Unlike MRM, in PRM mode all fragment ions produced in the collision cell are acquired simultaneously. Depending on the fill time, an MS instrument operating in PRM can achieve sensitivity close to 50 amol, which is comparable to QqQ. On the other hand, in PRM mode, only one or a few compounds can be monitored simultaneously, therefore complex hormonomic studies still rely on MRM.

Internal standards and their replacement

Typically, a targeted plant hormonomics faces several serious problems. First, the plant hormones are numerous and often occur as isobaric compounds (indistinguishable by MS). Second, plant hormones occur naturally in very low concentrations, and third, the plant matrix is usually very complex, leading to signal alteration or/and miss-annotation of detected plant hormones (reviewed by Tarkowská et al., 2014; Vrobel & Tarkowski, 2023). This matrix effect (ME) is highly dependent on the chemical composition of the specific plant material, resulting in alterations typically at the ionization level (Tang & Kebarle, 1993; Cappiello et al., 2008). Random or systematic drops in MS sensitivity can modify the MS signal and introduce quantification bias. Consequently, the predominant approach in applications over the past decade has involved incorporating internal standards to mitigate these alterations and enhance the reliability of the signal annotation. Stable isotope-labelled internal standards have proven to be the most commonly used, due to

their physicochemical similarity to the targeted compounds, facilitating accurate quantification by the isotope dilution method (Rittenberg & Foster, 1940). However, the synthesis of these standards is intricate, resulting in increased analysis costs, limited commercial availability and occasional reliance on in-house solutions (Tranová et al., 2019). As illustrated in Fig. 2E, the majority of authors (75%) have preferred the use of internal standards to overcome the above-discussed difficulties.

As a viable alternative, semi-quantification employing structural analogues such as triphenyl phosphate has been implemented (Martinez et al., 2020; Yao et al., 2022). Recent investigations have explored the analysis of plant hormones in biological materials even in the absence of internal standards using the unlabelled standard addition method (Yonny et al., 2020; Hashiguchi et al., 2021). This approach involves the preparation of matrix-matched calibrations for individual samples, facilitating accurate quantification. However, in large-scale studies, the unlabelled standard addition method may prove inefficient due to the generation of an excessive number of samples. Some researchers have applied matrix-matching to quantify phytohormones based on non-normalized signal intensities and evaluate matrix effects (Kasote et al., 2016; Cao et al., 2016; Mogal et al., 2022). While straightforward, this approach is highly sensitive to variations in matrix composition or unavoidable losses during analytical procedures, requiring a specialized quality control system to address analytical abnormalities.

Sample preparation enhances the analytical outcome

In targeted plant hormonomics, sample cleanup is a critical step in the analytical workflow. This process removes interfering compounds from the sample, reduces matrix effects and improves analytical results. Moreover, the purification step helps protect the LC-MS instrument from contamination and extends its lifespan. Current methods for purifying plant hormone samples primarily rely on two well-established approaches (i) liquid-liquid extraction (LLE) and (ii) solid-phase extraction (SPE).

Conventional LLE involves partitioning analytes between two immiscible liquid phases, which typically requires larger volumes of hazardous organic solvents such as ethyl acetate, hexane, or diethyl ether (Xiao et al., 2018; Sugahara et al., 2020; Kojima et al., 2021). However, advances in LLE have led to various modifications, including dispersive liquid-liquid microextraction, sequential solvent-induced phase transition extraction, and the use of supramolecular solvents. Although these methods have found applications in plant hormone analysis (Fig. 2F), they are less commonly represented compared to SPE, which utilizes a solid sorbent to retain targeted compounds from a liquid sample. It also offers improved selectivity, requires relatively low solvent volumes, and enables high-throughput and automated sample processing. Several SPE protocols have been in targeted plant hormonomics, differing in experimental setup, sorbent material, and interaction mode with analytes.

Conventional SPE using extraction cartridges remains popular due to ease of use, reproducibility, and commercial availability (Fig. 2F). However, there is a trend to replace the previously common silica-based

sorbents with different polymeric sorbents (Fig. 2G). Polymer-based SPE cartridges offer greater robustness and the ability to combine various types of interactions in a single sorbent, typically reversed phase and ion-exchange (Gong et al., 2017; Matsuura et al., 2019; Lopez-Guerrero et al., 2022). A significant trend of the last decade is the modifications of SPE protocols, including mainly miniaturization setups such as dispersive SPE methods (Xie et al., 2014; Martinez et al., 2020; Mandal et al., 2021; Mogal et al., 2022), magnetic SPE (Liu et al., 2014; Cai et al., 2015; Cai et al, 2019; Luo et al., 2021; Zhang et al., 2023) or in-tip micro SPE (Pěnčík et al., 2018; Široká et al., 2022). The miniaturization of SPE goes hand in hand with the reduction of the input amount of plant material as described in the chapter below (see *From organs to organelles*).

Importantly, most authors still use some kind of sample preparation to improve their analytical results (Fig. 2E). 61% of the authors relied on a combination of sample preparation and internal standard, 17% utilized sample preparation without internal standard, 14% added internal standard without sample preparation and only 8% analysed the plant hormones in crude plant extracts without normalization to an internal standard.

Complex plant hormonomics benefits from reduced sample weight

Interestingly, in our meta-study, we observed a negative correlation between the number of determined plant hormones and the weight of extracted samples (Fig. 2H). Studies focused on multiple phytohormone profiling more often used relatively small amounts of plant material (up to 100 mg FW) compared to applications targeting a narrow spectrum of analysed compounds (1-10 g FW). This result highlights the preference for sample weight reduction in complex plant hormone metabolomics. In our experience, reducing sample amount results in lower matrix effect, which can be further diminished by employing miniaturized SPE protocols. In combination with an ultra-sensitive detection method such as state-of-the-art QqQ or Q-LIT instruments, this approach leads to successful plant hormonomic analysis.

However, accurate quantification in trace analysis depends on sample size, and continuous weight reduction has obvious practical limitations. Since sub-milligram sample amounts are challenging to accurately measure, alternative characteristics of the sample such as the number of organs, cells or total protein content, have been employed (Zhang et al., 2010; Antoniadi et al., 2015; Skalický et al., 2021; Skalický et al., 2023).

Untargeted metabolomics of plant hormones

In recent years, there has been a significant increase in a different approach applied to phytohormone analysis (Fig. 3A). Untargeted methodologies indirectly search for phytohormones in a complex metabolomic pattern. However, the plant metabolome comprises the entire complement of small molecules involving tens of thousands of different compounds within a single organism (Fernie & Tohge, 2017). Analysing the whole metabolome is a formidable challenge due to the broad spectrum of metabolite polarity and concentrations.

This diverse array includes polar entities like sugars and amino acids alongside nonpolar lipids, as well as numerous secondary metabolism products responsible for growth, defence, and signalling (Brunetti et al., 2013; Viant et al., 2017). Furthermore, even after proper extraction and measurement procedures, the utilization of advanced software remains imperative for data processing and the essential annotation of metabolites.

Although biggest disadvantage of untargeted approaches is the ability to perform only qualitative or semi-quantitative analyses, they offer other significant advantages. They enable the comparison of metabolomes between species or organs, or the reactions of whole plants, microbes, or cells to various biotic or abiotic stresses (Roberts et al., 2012). Moreover, they facilitate the identification of novel unknown metabolites and signalling pathways (Fig. 3B). To discover the current trends in untargeted hormonomics, broad search keywords were used to search the Web of Science database. Each generated publication was manually processed and detailed notes were compiled concerning instrumentation, methodologies, and the specific phytohormone analysis. Ultimately, a subset of 58 publications from the past decade was selected as relevant due to their explicit annotation of at least one phytohormone via the untargeted analysis (Repository file 3).

Liquid-chromatography-mass spectrometry offers the best solution for the phytohormonal untargeted analysis

Various analytical methods have previously been used for plant metabolome studies, including ^{1}H NMR spectroscopy (Kim et al., 2011), LC-MS (Perez de Souza et al., 2021), GC-MS (Misra, 2021) or direct infusion MS (DI-MS) (Majchrzak et al., 2020). In plant hormonomics, LC-MS emerges as the most dominant method in both targeted (Fig. 2A) and untargeted analyses, in which online combination of (U)HPLC with mass spectrometer is extensively utilized (Fig. 3A). This dominant trend can be explained by the better sensitivity of MS-based detection combined with one-step sample preparation. For example, no derivatization is needed for acidic phytohormones. Several researchers have also applied GC-MS (Jia et al., 2020; Landi et al., 2020) and DI-MS instrumentation without any sample separation (Pétriacq et al., 2016; Lin et al., 2023). To our knowledge, no ^{1}H NMR spectroscopy was employed for the untargeted phytohormone analysis, likely due to its limited sensitivity and limited ability to detect less abundant metabolites (Perez de Souza et al., 2021).

As shown in Fig. 3E, the prevailing setup was a combination of (U)HPLC separation with ESI or heated electrospray ionization (HESI) followed by HRMS analysers required to accurately determine the elemental composition. Our findings correspond with trends in targeted analysis, showing ESI ionization as excellent tool coupling with LC without in-source analyte fragmentation. Several other ionization techniques have also been used, such as electron ionization (EI) (Jia et al., 2020; Landi et al., 2020), matrix-assisted laser desorption/ionization (MALDI) (Pétriacq et al., 2016), or flow infusion electrospray (Skalska et al., 2021; Kattupalli et al., 2021). Importantly, there are only minor differences between the two-leading tandem HRMS

techniques. The quadrupole-orbitrap (Q-orbitrap) analyser provides better resolution, while the quadrupole-time of flight (Q-TOF) operates with higher acquisition speed and a larger dynamic range (Perez de Souza et al., 2021). Furthermore, only two applications employed Fourier transform ion cyclotron resonance mass spectrometry (Q-FT-ICR), which is a very expensive technique (Fiore et al., 2015; Lin et al., 2023).

In the untargeted analysis, several MS approaches are used mainly based on HRMS. The first method is FS, wherein a selected *m/z* range is directly analysed by a HRMS detector, allowing the identification of compounds with a similar molecular weight. However, it may present problems with the detection of isobaric compounds (Kauffman, 2018). Another approach is the data-dependent analysis (DDA), where precursor ions are selected from a FS mode and subjected to further fragmentation. This method leads to better structural elucidation of analytes, but relies on their intensity for fragmentation selection, thus potentially neglecting low-abundance metabolites (Guo & Huan, 2020). Additionally, the data-independent analysis (DIA or MS^E) involves simultaneous fragmentations of precursor ions within a moderate mass window (around 20–25 Da) and analyses all resulting product ions. The disadvantage of this approach is losing the link between precursor and fragment ions, and the necessity to use complex informatics to deconvolute the MS^E spectra (Tsugawa et al., 2015). Surprisingly, all three approaches – FS, DDA and DIA – are extensively used in plant hormonomics and are suitable for the detection of trace amounts of phytohormones (Fig. 3C). Due to their low concentration, phytohormones cannot be easily detected using FS and DDA approaches. These two methods offer easier data interpretation compared to DIA, which requires operating complicated software and searching for compound fragmentation patterns in databases. However, DIA provides a valuable tool for the isolation of isobaric compounds and, with advances in machine learning algorithms, is likely to become a leading approach in untargeted metabolomics (Perez de Souza et al., 2021).

Sample preparation is a crucial step of the analysis

As mentioned above, the critical steps in metabolomic studies are the sample harvesting and preparation process. To prevent the analysis of metabolites from other unwanted sources, it is necessary to minimize any impurities, avoid microbial contamination and work in clean conditions (Brunetti et al., 2013). Even more than in the targeted analysis, it is essential to take multiple biological replicates for the statistical analysis to accurately identify metabolites, as the metabolome of each individual may vary over time (Roberts et al., 2012). Determining the appropriate sample quantity for hormonomics analysis is also a crucial consideration. In recent years, targeted phytohormonal profiling has shown a trend towards miniaturization (Fig. 2H). However, achieving this sample size reduction in untargeted analyses presents a formidable challenge. Here, method sensitivity is markedly lower due to the presence of numerous metabolites at higher concentrations than phytohormones, resulting in considerably lower overall detection limits. The analysis of publications with untargeted hormonomics revealed no trend towards miniaturization. Instead, it was observed that sample amounts ranging from 50 to 1000 milligrams of fresh weight or dry weight have been commonly used

across studies over the past decade. The smallest reported amount required for phytohormone detection was 50 mg FW from filbert shoot culture (Erland et al., 2020).

The selection of a universally effective method for the extraction of a wide range of metabolites poses a significant difficulty. Solvents situated in the middle range of polarity, such as methanol, ethanol, or acetonitrile, are typically favoured. In selected studies, the primary solvent for extraction was methanol, often acidified with formic or acetic acid and ranging from 75% to 100% concentration (Table 1). Other, less used extraction solvents are summarized in Table 1. Following extraction, samples are typically either directly injected into the LC-MS system or filtered through < 1 µm filters to protect the instrument from impurities (Fig. 3D).

Incorporating a purification step is also possible in untargeted hormonomics, however, it may result in the loss of some metabolites during the purification process. An important question then remains the purpose of MS-based analysis. While screening a wide range of metabolites requires minimal purification, experiments looking for similar groups of compounds can apply a purification step to improve the method sensitivity. As seen in various studies, SPE methods selectively retain analytes with similar chemical properties and offer efficient removal of the complex plant matrix (Xin et al., 2016; Aoki et al., 2019; Tadić et al., 2022). Another technique applied was solid-liquid extraction (SLE), where the sample was extracted with methanol/ultrapure water/formic acid solution (75:20:5) and subsequently purified by an additional step with a 30 kDa Amicon® Ultra centrifugal filter unit (Van Meulebroek et al., 2015). In specific analyses, such as BRs, LLE serves as a method to remove hydrophilic impurities. In this protocol, samples were initially extracted in acetonitrile, followed by centrifugation, evaporation to dryness, and then LLE with ethyl acetate and water (4:1) (Xiong et al., 2022).

Why untargeted analysis?

Untargeted approaches are a versatile toll for investigating a diverse array of phytohormonal groups, as shown in Fig. 3F. This analytical technique routinely detects stress-related hormones such as salicylates, JAs, and ABA, alongside "growth hormones" including auxins, CKs, and GAs. Moreover, in the context of drought and nitrogen deficiency stress, several studies have highlighted the analysis of BRs (Carlson et al., 2020; Squeri et al., 2021), while others have contributed to the identification of their novel metabolites (Xin et al., 2016; Xiong et al., 2022).

Predominant applications in untargeted metabolomics perform comparative analyses of two distinct metabolomes in plants exposed to biotic or abiotic stressors (Fig. 3B). Notably, observable shifts in concentrations of JAs, ABA, and salicylates under stress conditions have been documented, demonstrating their consistent up or down-regulation across multiple studies (Cao J et al., 2016; Pétriacq et al., 2016; Thomason et al., 2018; Kattupalli et al., 2021). Accurate annotation of these metabolites requires comprehensive measurement of their accurate molecular weights and fragmentation patterns, pivotal for

their integration into databases. Multiple HRMS studies, particularly focusing on phytohormones, have been performed as a basis for the subsequent development of untargeted MS-based methodologies in plant extracts (Zhao et al., 2013; Revelou et al., 2019). In addition, numerous studies measure different metabolomes of honey (Kečkeš et al., 2013; Li et al., 2017), plants (Van Meulebroek et al., 2015; Zhang et al., 2019; Welling et al., 2021; He et al., 2022), and microorganisms (Fiore et al., 2015; Aoki et al., 2019).

Overall, the untargeted analysis represents an excellent tool for screening and the semi-quantitative analysis. The advantages of this method are rapid extraction and the possibility to avoid sample preparation and MS method development. Moreover, it enables easy identification of new, uncharacterised phytohormone-related compounds in plants. However, HRMS exhibits approximately 2-5 times lower sensitivity compared to targeted MRM approaches (Nováková, 2013). This can be critical in detecting low levels of phytohormones. Furthermore, accurate quantification requires the addition of the internal standards (as discussed above), which can be a problem given their limited availability, especially for newly identified metabolites. Moreover, the price of Q-TOF or Q-orbitrap is approximately two times higher than that of QqQ (Schwaiger-Haber et al., 2021).

From organs to organelles

Substantial progress in mass spectrometry, particularly its enormous developments in recent decade, has greatly increased sensitivity and selectivity of newly developed MS-based protocols. This made it possible to reduce the required sample weight, allowing for the downsizing of phytohormonal analyses from entire plants to specific anatomical components (Fig. 4).

Organ-specific profiling of phytohormones

In recent years, various MS-based methods have been introduced to enable the simultaneous monitoring of multiple phytohormones with organ resolution. These hormonomic studies typically focus on analytes such as ABA, IAA, JA, SA, selected representatives of CKs and GAs, and/or their various derivatives. For example, a method designed to profile ten phytohormones in roots was developed and applied to investigate the effect of salinity stress in barley (Cao et al., 2017). The spatiotemporal distribution of phytohormones in rice was examined using the rapid profiling by targeted hormonomic approach (Cai et al., 2016). To elucidate hormone dynamics during the flowering stage, the organ-specific phytohormone analysis was conducted in model ornamental plants, specifically Agapanthus praecox (Zhang et al., 2014), and Petunia axillaris (Iftikhar et al., 2020). Šimura et al. (2018) introduced a methodology enabling the simultaneous screening of 101 phytohormones and related substances, including biosynthetic precursors and metabolites. A sample quantity requirement of a mere 20 milligrams makes the method suitable for conducting organ-specific studies.

Downscaling hormone profiling through advancements in sample pretreatment methods

Sample pretreatment plays a crucial role in improving MS detection by addressing various challenges associated with the complexity of plant sample matrices and extremely low endogenous concentrations of phytohormones. Implementation of suitable and efficient purification methods can significantly enhance the performance and sensitivity of MS detection of phytohormones and allows further reduction of sample size towards sub-milligram samples. A highly efficient strategy is the application of direct derivatization, as demonstrated in the quantification of GAs in minute plant structures as individual *Arabidopsis* flowers or dissected stamens (Li et al., 2016). Furthermore, selective sample purification based on highly specific immunoaffinity extraction was used to accurately quantify indole-3-acetic acid (IAA), addressing the directional aspects of auxin transport in Arabidopsis root tip (Zhang et al., 2010). Microscale magnetic microparticle-based immunopurification also enabled profiling of CK metabolites in 50 pieces of Arabidopsis root apices (Plačková et al., 2017). The reduction in analyte losses and the increase in recovery achieved through the miniaturization of SPE purification are very beneficial in the analysis of small tissue samples. Analytical protocols based on µSPE have been developed for high-throughput profiling of various phytohormonal groups, including CKs (Svačinová et al., 2012), auxins (Liu et al., 2012) and stress-related hormones (Široká et al., 2022). While these protocols efficiently quantify targeted analytes in less than 10 milligrams of fresh tissue, the downsizing of the sample preparation procedure, particularly when coupled with ultra-sensitive MS, enables the analysis even at the sub-milligram level. For example, the application µSPE-based method (Pěnčík et al, 2018) for the quantification of IAA and its metabolites (IAA-aspartate and 2-oxoindole-3-acetic acid, oxIAA) in dissected *Arabidopsis* ovules highly supported the finding that early embryo patterning is coordinated by auxin supply from the mother plant (Robert et al., 2018).

Tissue-/cell type-specific and live-single cell phytohormone analysis

Phytohormones often have cell-specific functions that contribute to overall plant development and response to environmental stimuli. The study of plant hormones at the tissue or cellular levels helps reveal the complexities of plant growth, organ formation, and responses to external factors, contributing to a comprehensive understanding of plant development. The critical and highly challenging part of such a specialized analysis is the precise separation of specific cell types within plant tissues and organs. Cryosectioning, enabling very precise slicing of plant tissues, represents an efficient approach to isolating specific tissue regions. IAA, CKs and GAs were quantified in stem cryo-fractions ranging from 100 to 300 µm to elucidate hormonal distribution across the poplar cambial zone, providing insights into the regulatory processes governing cambial activity in poplar trees (Immanen et al., 2016). Alternatively, the preparation of intact protoplast populations from plant tissues by enzymatic digestion of surrounding cell walls was utilized for the cell type-specific determination of phytohormones. The ABA-responsive metabolome including 22 phytohormone-related metabolites was studied in isolated guard cell protoplasts using a targeted

metabolomics approach (Jin et al., 2013). A high-resolution distribution map within the *Arabidopsis* primary root apex was generated for IAA (Petersson et al., 2009), its catabolite oxIAA (Pěnčík et al., 2013) and CK metabolites (Antoniadi et al., 2015). This was achieved by combining the ultra-sensitive MS-based analysis with fluorescence-activated cell sorting of cell types marked with green fluorescent protein (GFP), providing a sophisticated approach to elucidate the spatial patterns of plant hormones.

To achieve an even more precise understanding of localized distribution of phytohormones and to enable real-time monitoring of dynamic fluctuations in their levels within individual cells, the live single-cell analysis is needed. The in vivo single-cell MS analysis of phytohormones faces challenges in terms of sensitivity, as the minute quantities present in individual cells require highly sensitive instrumentation. In a pioneering study in this field, Shimizu et al. (2015) demonstrated the ability to monitor the stress-induced accumulation of ABA and jasmonoyl-isoleucine (JA-Ile) in living single cells of *Vicia faba* leaves using nano-ESI tips and direct infusion of single-cell content into a HRMS analyser.

Profiling phytohormones in cell compartments

Plant hormone profiling with organelle-resolution is essential to gain insights into the precise localization and distribution of phytohormones within plant cells. This is crucial to understanding the intracellular hormone homeostasis, the cornerstone of fundamental regulatory processes at the cellular level.

For an accurate hormonal analysis with high resolution at the subcellular level, it is essential to obtain highly pure fractions of intact organelles. Multiple approaches for cell fractionation have been designed, however, only a few have been combined with MS to determine phytohormones in cell compartments. The majority of studies dealing with the subcellular analysis are based on conventional biochemical protocols of organelle isolation, mostly employing density-gradient (ultra)centrifugation (Table 2). Using this approach, auxins, ABA and CKs were determined in chloroplasts (Benková et al., 1999; Polanská et al, 2007; Tamizhselvan et al., 2024), and full CK profiles were analysed in vacuoles isolated from Arabidopsis and barley (Jiskrová et al., 2016). Moreover, the determination of IAA and its metabolites in isolated Arabidopsis vacuoles, along with the discovery of a novel transport function of the tonoplast membrane, provided new insight into the complex intracellular auxin transport network in plants (Ranocha et al., 2013). Conventional biochemical protocols for organelle isolation were originally designed for distinct purposes that do not necessarily have such high requirements on the quality of isolated fractions. However, the intactness and high purity of isolated organelles are essential for reliable hormonal subcellular profiling. Therefore, the improvement of the protocol in order to enhance the parameters of the isolated fractions is crucial. Včelařová et al. (2021) analysed the profile of auxin metabolites in Arabidopsis endoplasmic reticulum (ER) using an optimised isolation protocol. Its high effectiveness was confirmed by immunoblot and proteomic analyses of isolated ER-enriched fractions. Skalický et al. (2021) tested and compared several published nucleus isolation protocols based on differential centrifugation or flow cytometry. This study demonstrated that flow

cytometry provides superior performance in terms of the purity and intactness of isolated organelles. The optimized sorting protocol was coupled with the MS-based analysis to determine the nuclear auxin metabolite profile in *Arabidopsis* and tobacco. So far, all studies dealing with organelle-specific phytohormone determination have concerned only one type of organelles. A novel breakthrough flow cytometry-based technique for fluorescence-activated sorting of multiple organelles was recently introduced (Skalický et al. 2023). This approach enables the simultaneous fractionation of chloroplasts, nuclei, ER and mitochondria from a single sample. Using proteomics and metabolomics assays, rapid isolation has been shown to ensure stability of hormone profiles throughout the sorting procedure. Moreover, quantification of auxin and CK profiles in sorted organelle populations by ultra-sensitive LC–MS/MS resulted in the first high-resolution intracellular hormonal map (Skalický et al. 2023).

In vivo visualisation

High spatial resolution measurements using mass-spectrometry

Mass spectrometry imaging (MSI) is an advanced biomolecule mapping method that has been widely used for the *in-situ* metabolomics and proteomics analysis of plant samples in the past years (McDonnell & Heeren, 2007; Horn & Chapman, 2024). With increasing requirements for targeted spatial information and high-throughput visualisation, MSI has demonstrated stronger competitiveness in the phytohormone analysis than any other imaging methods (Shimizu et al., 2015). MALDI-MSI is an organic matrix-based method that can visualize phytohormones together with related metabolites on tissues without extra labelling. Recently, visualization of ABA and CKs was achieved *via* MALDI-MSI from the root sections (Shiono et al., 2017). Interestingly, replacement of organic matrices with iron nanoparticles enabled the detection of auxins, BRs, JAs and SA. Noteworthy, the very low molecular weight ethylene biosynthetic precursor, 1-aminocyclopropane-1-carboxylic acid (ACC), was also reported from the same cross-sectioned root (Shiono et al., 2020). Another MSI technique, secondary ion mass spectrometry (SIMS)-MSI can establish metabolite images at the single-cell or even subcellular levels with a spatial resolution of up to 0.15 µm (Thomen et al., 2020). However, this powerful method has not been applied to characterise small plant molecules such as phytohormones. Recently, desorption electrospray ionization (DESI)-MSI has been introduced to plant imaging. Compared with other MSI methods, it has the unique advantages of simple sample preparation and ambient data acquisition. The DESI-MSI analysis revealed alternative distributions of ABA and JA biosynthetic precursor 12-oxo-phytodienoic acid (OPDA) from a 20 µm thick intact bean section, and the results were further validated by MS/MS imaging (Enomoto et al., 2017). Due to the limitation of standard MS-based libraries, there are still many other interesting phytohormone metabolites that could potentially be identified from the same MSI data set. For example, unique localizations of JA-related metabolites were identified after matching *m/z* values from common bean samples with later acquired standard masses (Enomoto & Miyamoto, 2021). Moreover, the DESI-MSI protocol was further modified to visualize major wound-induced

phytohormone species. JA and ABA together with their precursors, were detected in a single wounded *Arabidopsis* leaf using both intact leaf samples and thin-layer chromatography imprints (Zhang et al., 2021). Currently, *in-situ* separation of isomeric and isobaric compounds from targeted phytohormones is the biggest challenge in phytohormone MSI studies. Therefore, ion mobility (IM) is applied as an additional analytical dimension to separate compounds based on their molecular size through drifting gas. The use of IM in the innovative MSI analysis significantly increases results the coverage and reliability of the results (McLean et al., 2007). Recent work combined the IM separation with DESI-MSI achieved direct separation and visualization of two isomeric auxin derivatives with endogenous auxins from *Arabidopsis*. The results revealed different distributions of isomers in primary roots and hypocotyls from a treated plant sample (Zhang et al., 2024). Although MSI has demonstrated its advantages in the characterization of various molecules ranging from small phytohormones to extra-large polymers, this novel technique is still not considered in the majority of hormonomic and proteomic analyses due to the lack of sophisticated methods.

High spatiotemporal measurements with in vivo biosensors

Finally, an increasingly popular method for detecting phytohormones in living organisms involves the use of MS-free methodology based on biosensors (Fig. 1). Devices designed to detect specific substances and translate this biological recognition into measurable electrical signals, directly proportional to the substance concentration (Bhalla et al., 2016). Leveraging our understanding of how phytohormones are perceived and the knowledge of the signalling pathways, biosensors either targeted these downstream cascades or directly targeted phytohormones to estimate their concentration within cells. These biosensors are divided into various types based on their biological recognition mechanisms: enzyme-based, tissue-based, genetically-encoded, DNA, thermal, immune- and piezoelectric biosensors. Moreover, fluorescent biosensors are a great tool for near-real-time observation of phytohormones at subcellular resolution. However, the obtained signals depend not only on the hormone concentration, but also on the activities and levels of other signalling components, and therefore the results must be interpreted with caution (Balcerowitz et al., 2021). In recent years, several reviews focusing on this topic have been published, consolidating the latest methodological advances (Novák et al., 2017; Pařízková et al., 2017; Naqvi et al., 2023).

Currently, biosensors including reporter genes, fluorescent or other chemically modified antibodies and probes are the predominant tools for *in-situ* visualization of small molecules such as phytohormones from samples with high sensitivities and specificity. For example, the real-time abundance and localization of GAs in Arabidopsis can be monitored via encoded Gibberellin Perception Sensors (Rizza et al., 2019), while fluorescent conjugates of 2,4-dichlorophenoxyacetic acid can be apply to represent auxin distributions using confocal microscopy (Pařízková et al., 2021). Although biosensor-based plant hormone analysis has achieved spatiotemporal resolution at the single-cell or even organelle-level, it also has many limitations compared to MS-based imaging tools. First, MSI has a significantly higher analytical throughput due to the detection of

hundreds of metabolites including plant hormones from the same experiment. Conversely, most biosensors are specific for only a very few targeted hormones. Introducing a reporter to plant models normally requires previous knowledge of the targeted genes. Moreover, establishing a new reporter is laborious, intensive and time-consuming. On the other hand, labelled biosensors are frequently used for small molecule imaging (Pařízková et al., 2017), but the *in vivo* consumption, transport and degradation of xenobiotic compounds in plants are largely unclear. As an untargeted and label-free approach, MSI does not need any genome information and applies to various plant models with very fast and simple sample preparation steps, which allows plant hormone imaging from their untainted location (Hu et al., 2021). Recently, immunofluorescent biosensors have been combined with MSI to characterise individual myeloid phenotype cells with a molecular micro-environment (Goossens et al., 2022), but the method of multiplex imaging integration has not yet been applied in plant research.

Conclusion

The significance of MS-based technologies in plant hormone analysis is constantly rising. The comprehensive plant hormonomics is based on rigorous and complex analytical workflows requiring highly sensitive mass spectrometers, normalization on the stable isotope-labelled internal standards and removal of the plant matrix by effective sample purification procedures. Furthermore, the tremendous progress in downscaling the complex targeted analysis from organs to cellular compartments is also remarkable. The last decade of the plant hormone analysis is futher characterised by the increasing influence of untargeted metabolomic approaches that follow simple and fast sample preparation procedures. Despite problematic quantification, the untargeted analysis offers a great tool for the identification of uncharacterised phytohormone-related compounds from not only plant extracts. Complementary to biosensor applications, protocols using MSI have become emerging approaches for in vivo detection of plant hormones. With the accumulation of MSI analysis of phytohormones together with other metabolites, lipids and proteins from consecutive plant sections, further spatial correlation analysis will deliver single-cell multi-omic references for the plant signalling network and complement current knowledge in phytohormone homeostasis. These high-resolution spatial maps will also benefit future plant histological and genetic research. Importantly, the increasing capability of plant hormonomics in conjunction with other 'omics' disciplines yields large integrated datasets. Therefore, there is a strong demand for advanced statistical approaches including multivariate data analysis. Methods such as dimensionality reduction, multivariate regression or discriminant analysis will be critical to convert huge tables of plain values into compact and clear results elucidating coplex relationships in the plant hormonome, proteome, transcriptome or metabolome. The qrowing capabilities of artificial intelligence and the performance of machine learning offer an effective tool to find these hidden patterns.

Acknowledgements

The authors would like to thank Danuše Tarkowská for critical proof-reading and useful comments, and Helena Mazáčová for careful language revision.

Conflict of interest

No conflict of interest declared.

Funding

This work was supported by Internal Grant Agency of Palacky University (IGA_PrF_2024_013), by the Czech Science Foundation (GACR) (22-17435S) and by the EU Horizon-2020 project ADAPT (grant number 862858).

Repository Files

Repository File 1. Statistical methods

Repository File 2. Raw data from Web of Science for targeted plant hormone analysis

Repository File 3. Raw data from Web of Science for untargeted plant hormone analysis

References

Adigun OA, Pham T, Grapov D, Nadeem M, Jewell LE, Cheema M, Galagedara L, Thomas R. 2023. Phyto-oxylipin mediated plant immune response to colonization and infection in the soybean-Phytophthora sojae pathosystem. Frontiers in Plant Science 14, 1141823.

Antoniadi I, Plačková L, Simonovik B, Doležal K, Turnbull C, Ljung K, Novák O. 2015. Cell-type specific cytokinin distribution within the Arabidopsis primary root apex. Plant Cell 27, 1955–1967.

Aoki MM, Kisiala AB, Li S, Stock NL, Brunetti CR, Huber RJ, Emery RJN. 2019. Cytokinin Detection during the Dictyostelium discoideum Life Cycle: Profiles Are Dynamic and Affect Cell Growth and Spore Germination. Biomolecules 9(11), 702.

Arnold MD, Gruber C, Floková K, Miersch O, Strnad M, Novák O, Wasternack C, Hause B. 2016. The Recently Identified Isoleucine Conjugate of *cis*-12-Oxo-Phytodienoic Acid Is Partially Active in *cis*-12-Oxo-Phytodienoic Acid-Specific Gene Expression of *Arabidopsis thaliana*. PLoS One 11(9), e0162829.

Balcerowitz M, Shetty KN, Jones AM. 2021. Fluorescent biosensors illuminating plant hormone research. Plant Physiology 187(2), 590-602.

Benková E, Witters E, Van Dongen W, Kolár J, Motyka V, Brzobohaty B, Van Onckelen HA, Macháčková I. 1999. Cytokinins in tobacco and wheat chloroplasts. Occurrence and changes due to light/dark treatment. Plant Physiology 121, 245–252.

Bhalla N, Jolly P, Formisano N, Estrela P. 2016. Introduction to biosensors. Essays in Biochemistry 60(1), 1-8.

Bourmaud A, Gallien S, Domon B. 2016. Parallel reaction monitoring using quadrupole-Orbitrap mass spectrometer: Principle and applications. Proteomics 16, 2146–2159.

Brunetti C, George RM, Tattini M, Field K, Davey MP. 2013. Metabolomics in plant environmental physiology. Journal of Experimental Botany 64(13), 4011-4020.

Cai BD, Zhu JX, Shi ZG, Yuan BF, Feng YQ. 2013. A simple sample preparation approach based on hydrophilic solid-phase extraction coupled with liquid chromatography-tandem mass spectrometry for determination of endogenous cytokinins. Journal of Chromatography B (942), 31-36.

Cai BD, Yin J, Hao YH, Li YN, Yuan BF, Feng YQ. 2015. Profiling of phytohormones in rice under elevated cadmium concentration levels by magnetic solid-phase extraction coupled with liquid chromatography tandem mass spectrometry. Journal of Chromatography A 1406, 78-86.

Cai WJ, Ye TT, Wang Q, Cai BD, Feng YQ. 2016. A rapid approach to investigate spatiotemporal distribution of phytohormones in rice. Plant Methods 12, 47.

Cai WJ, Yu L, Wang W, Sun MX, Feng YQ. 2019. Simultaneous determination of multiclass phytohormones in submilligram plant samples by one-pot multifunctional derivatization-assisted liquid chromatography-tandem mass spectrometry. Analytical Chemistry 91(5), 3492-3499.

Cao D, Lutz A, Hill CB, Callahan DL, Roessner U. 2017. A quantitative profiling method of phytohormones and other metabolites applied to barley roots subjected to salinity stress. Frontiers in Plant Science 7, 2070.

Cao J, Li M, Chen J, Liu P, Li Z. 2016. Effects of MeJA on Arabidopsis metabolome under endogenous JA deficiency. Scientific Reports 6(1), 1 – 13.

Cao ZY, Sun LH, Mou RX, Zhang LP, Lin XY, Zhu ZW, Chen MX. 2016. Profiling of phytohormones and their major metabolites in rice using binary solid-phase extraction and liquid chromatography-triple quadrupole mass spectrometry. Journal of Chromatography A 1451, 67-74.

Cappiello A, Famiglini G, Palma P, Pierini E, Termopoli V, Trufelli H. 2008. Overcoming matrix effects in liquid chromatography−mass spectrometry. Analytical Chemistry 80(23), 9343-9348.

Carlson R, Tugizimana F, Steenkamp PA, Dubery IA, Hassen A, Labuschagne N. 2020. Rhizobacteria-induced systemic tolerance against drought stress in Sorghum bicolor (L.) Moench. Microbiological Research 232, 126388.

Chernonosov AA, Karpova EA, Karakulov AV. 2023. Metabolomic profiling of three Rhododendron species from Eastern Siberia by liquid chromatography with high-resolution mass spectrometry. South African Journal of Botany 157, 622-634.

Contreras-Gutierrez PK, Hurtado-Fernández E, Gómez-Romero M, Hormaza JI, Carrasco-Pancorbo A, Fernández-Gutiérrez A. 2013. Determination of changes in the metabolic profile of avocado fruits (Persea americana) by two CE-MS approaches (targeted and non-targeted). Electrophoresis 34(19), 2928-2942.

Di Masi S, De Benedetto GE, Malitesta C, Saponari M, Citti C, Cannazza G, Ciccarella G. 2022. HPLC-MS/MS method applied to an untargeted metabolomics approach for the diagnosis of "olive quick decline syndrome". Analytical and Bioanalytical Chemistry 414(1), 465-473.

Dziurka K, Dziurka M, Warchol M, Czyczylo-Mysza I, Marcinska I, Noga A, Kaploniak K, Skrzypek E. 2019. Endogenous phytohormone profile during oat (Avena sativa L.) haploid embryo development. In Vitro Cellular & Developmental Biology - Plant 55(2), 221-229.

Enomoto H, Sensu T, Sato K, Sato F, Paxton T, Yumoto E, Miyamoto K, Asahina M, Yokota T, Yamane H. 2017. Visualisation of abscisic acid and 12-oxo-phytodienoic acid in immature Phaseolus vulgaris L. seeds using desorption electrospray ionisation-imaging mass spectrometry. Scientific Reports 7, 42977.

Enomoto H, Miyamoto K. 2021. Unique localization of jasmonic acid-related compounds in developing Phaseolus vulgaris L. (common bean) seeds revealed through desorption electrospray ionization-mass spectrometry imaging**.** Phytochemistry 188, 112812.

Erland L, Turi C, Saxena P, Murch S. 2020. Metabolomics and hormonomics to crack the code of filbert growth. Metabolomics 16(5), 1-15.

Fenn JB, Mann M, Meng CK, Wong SF, Whitehouse CM. 1989. Electrospray Ionization for Mass Spectrometry of Large Biomolecules. Science 246(4926), 64-71.

Fernie AR, Tohge T. 2017. The genetics of plant metabolism. Annual Review of Genetics 51, 287-310.

Fiore CL, Longnecker K, Kido Soule MC, Kujawinski EB. 2015. Release of ecologically relevant metabolites by the cyanobacterium Synechococcus elongatus CCMP 1631. Environmental Microbiology 17(10), 3949-3963.

Fonseca S, Chini A, Hamberg M, Adie B, Porzel A, Kramell R, Miersch O, Wasternack C, Solano R. 2009. (+)-7-iso-Jasmonoyl-L-isoleucine is the endogenous bioactive jasmonate. Nature Chemical Biology 5(5), 344-350.

Fresno DH, Munne-Bosch S. 2023. Organ-specific responses during acclimation of mycorrhizal and non-mycorrhizal tomato plants to a mild water stress reveal differential local and systemic hormonal and nutritional adjustments. Planta 258(2), 32.

Fu L, Li Q, Chen C, Zhang Y, Liu Y, Xu L, Zhou Y, Li C, Zhou D, Rittmann BE. 2021. Benzoic and salicylic acid are the signaling molecules of Chlorella cells for improving cell growth. Chemosphere 265, 129084.

García-Pérez P, Miras-Moreno B, Lucini L, Gallego PP. 2021. The metabolomics reveals intraspecies variability of bioactive compounds in elicited suspension cell cultures of three Bryophyllum species. Industrial Crops and Products 163, 113322.

Glauser G, Grata E, Dubugnon L, Rudaz S, Farmer EE, Wolfender JL. 2008. Spatial and temporal dynamics of jasmonate synthesis and accumulation in Arabidopsis in response to wounding. Journal of Biological Chemistry 283(24), 16400-16407.

Gong MX, Luo HL, Wang AQ, Zhou YY, Huang WJ, Zhu PC, He LF. 2017. Phytohormone profiling during tuber development of Chinese yam by Ultra-high performance liquid chromatography-triple quadrupole tandem mass spectrometry. Journal of Plant Growth Regulation 36(2), 362-373.

Goossens P, Lu C, Cao J, et al. 2022. Integrating multiplex immunofluorescent and mass spectrometry imaging to map myeloid heterogeneity in its metabolic and cellular context. Cell Metabolism 34(8), 1214-1225.

Guo J, Huan T. 2020. Comparison of Full-Scan, Data-Dependent, and Data-Independent Acquisition Modes in Liquid Chromatography-Mass Spectrometry Based Untargeted Metabolomics. Analytical Chemistry 92(12), 8072-8080.

Hashiguchi T, Hashiguchi M, Tanaka H, Fukushima K, Gondo T, Akashi R. 2021. Quantitative analysis of seven plant hormones in Lotus japonicus using standard addition method. PLoS One 16(2), e0247276.

Hayashi KI, Arai K, Aoi Y, et al. (2021) The main oxidative inactivation pathway of the plant hormone auxin. Nature Communication 12(1), 6752.

He P, Huang Y, Qiu J, Zhang H, Shao L, Lü F. 2022. Molecular diversity of liquid digestate from anaerobic digestion plants for biogenic waste. Bioresource Technology 347, 126373.

Horn PJ, Chapman KD. 2024. Imaging Plant Metabolism in situ. Journal of Experimental Botany 75(6), 1654-1670.

Hu J, Liu F, Chen Y, Shangguan G, Ju H. 2021. Mass Spectrometric Biosensing: A Powerful Approach for Multiplexed Analysis of Clinical Biomolecules. ACS Sensors 6(10), 3517-3535.

Iftikhar J, Lyu M, Liu Z, Mehmood N, Munir N, Ahmed MAA, Batool W, Aslam MM, Yuan Y, Wu B. 2020. Sugar and hormone dynamics and the expression profiles of SUT/SUC and SWEET sugar transporters during flower development in *Petunia axillaris*. Plants 9(12), 1770.

Immanen J, Nieminen K, Smolander OP, et al. 2016. Cytokinin and auxin display distinct but interconnected distribution and signaling profiles to stimulate cambial activity. Current Biology 26, 1990–1997.

Jia H, Wang L, Li J, Sun P, Lu M, Hu J. 2020. Comparative metabolomics analysis reveals different metabolic responses to drought in tolerant and susceptible poplar species. Physiologia Plantarum 168(3), 531-546.

Jin X, Wang RS, Zhu M, Jeon BW, Albert R, Chen S, Assmann SM. 2013. Abscisic acid-responsive guard cell metabolomes of Arabidopsis wild-type and gpa1G-protein mutants. Plant Cell 25, 4789–4811.

Jiskrová E, Novák O, Pospíšilová H, Holubová K, Karády M, Galuszka P, Robert S, Frébort I. 2016. Extra- and intracellular distribution of cytokinins in the leaves of monocots and dicots. New Biotechnology 33, 735–774.

Kasote DM, Ghosh R, Chung JY, Kim J, Bae I, Bae H. 2016. Multiple reaction monitoring mode based liquid chromatography-mass spectrometry method for simultaneous quantification of brassinolide and other plant hormones involved in abiotic stresses. International Journal of Analytical Chemistry, 7214087.

Kattupalli D, Pinski A, Sreekumar S, Usha A, Girija A, Beckmann M, Mur LAJ, Eppurathu Vasudevan S. 2021. Non-targeted metabolite profiling reveals host metabolomic reprogramming during the interaction of black pepper with phytophthora capsici. International Journal of Molecular Sciences 22(21), 11433.

Kaufmann A. 2018. Analytical performance of the various acquisition modes in Orbitrap MS and MS/MS. Journal of Mass Spectrometry 53(8), 725-738.

Kebert M, Kostic S, Vuksanovic V, Markic AG, Kiprovski B, Zoric M, Orlovic S. 2022. Metal- and organ-specific response to heavy metal-induced stress mediated by antioxidant enzymes' activities, polyamines, and plant hormones levels in *Populus deltoides*. Plants 11(23), 3246.

Kečkeš S, Gašić U, Gašić TĆ, Milojković-Opsenica D, Natić M, Tešić Ž. 2013. The determination of phenolic profiles of Serbian unifloral honeys using ultra-high-performance liquid chromatography/high resolution accurate mass spectrometry. Food Chemistry 138(1), 32-40.

Kim HK, Choi YH, Verpoorte R. 2011. NMR-based plant metabolomics: where do we stand, where do we go? Trends in Biotechnology 29(6), 267-275.

Kisiala A, Kambhampati S, Stock NL, Aoki M, Emery RJN. 2019. Quantification of cytokinins using high-resolution accurate-mass orbitrap mass spectrometry and parallel reaction monitoring (PRM). Analytical Chemistry 91(23), 15049-15056.

Kojima K, Andou D, Ito M. 2021. Plant hormone changes in growing small watermelon fruit. The Horticulture Journal 90(2), 202-208.

Landi M, Misra BB, Muto A, Bruno L, Araniti F. 2020. Phytotoxicity, morphological, and metabolic effects of the sesquiterpenoid nerolidol on *Arabidopsis thaliana* Seedling Roots. Plants 9(10), 1347.

Leng F, Cao JP, Wang SP, Jiang L, Li X, Sun CD. 2018. Transcriptomic Analyses of Root Restriction Effects on Phytohormone Content and Signal Transduction during Grape Berry Development and Ripening. Int. J. Mol. Sci. 19(8).

Li D, Guo Z, Chen Y. 2016. Direct derivatization and quantitation of ultra-trace gibberellins in submilligram fresh plant organs. Molecular Plant 9, 175–177.

Li WB, Li CQ, Sun JB, Peng M. 2017. Metabolomic, Biochemical, and Gene Expression Analyses Reveal the Underlying Responses of Resistant and Susceptible Banana Species during Early Infection with Fusarium oxysporum f. sp cubense. PLANT DIS. 101(4), 534-543.

Li Y, Jin Y, Yang S, et al. 2017. Strategy for comparative untargeted metabolomics reveals honey markers of different floral and geographic origins using ultrahigh-performance liquid chromatography-hybrid quadrupole-orbitrap mass spectrometry. Journal of Chromatography A 1499, 78-89.

Lin HA, Coker HR, Howe JA, Tfaily MM, Nagy EM, Antony-Babu S, Hague S, Smith AP. 2023. Progressive drought alters the root exudate metabolome and differentially activates metabolic pathways in cotton (*Gossypium hirsutum*). Frontiers in Plant Science 14, 1244591.

Liu SC, Chen WQ, Qu L, Gai Y, Jiang XN. 2013. Simultaneous determination of 24 or more acidic and alkaline phytohormones in femtomole quantities of plant tissues by high-performance liquid chromatography-electrospray ionization-ion trap mass spectrometry. Anal. Bioanal. Chem. 405(4), 1257-1266.

Liu X, Hageman AD, Gardner G, Cohen JD. 2012. Protocol: High-throughput and quantitative assays of auxin and auxin precursors from minute tissue samples. Plant Methods 8, 31.

Liu JF, Ding J, Yuan BF, Feng YQ. 2014. Magnetic solid phase extraction coupled with in situ derivatization for the highly sensitive determination of acidic phytohormones in rice leaves by UPLC-MS/MS. Analyst 139(21), 5605-5613.

Lopez-Guerrero MG, Wang P, Phares F, Schachtman DP, Alvarez S, van Dijk K. 2022. A glass bead semi-hydroponic system for intact maize root exudate analysis and phenotyping. Plant Methods 18, 25.

Lu QM, Zhang WM, Gao J, Lu MH, Zhang L, Li JR. 2015. Simultaneous determination of plant hormones in peach based on dispersive liquid-liquid microextraction coupled with liquid chromatography-ion trap mass spectrometry. Journal of Chromatography B 992, 8-13.

Luo SS, Lin L, Wang XW, Zou SC, Luan TG. 2013. Determination of phytohormones in plant extracts using in-matrix ethyl chloroformate derivatization and DLLME-GC-MS. LCGC Europe 26(6), 310.

Luo ZF, Xu MW, Wang RZ, Liu XB, Huang YK, Xiao LT. 2021. Magnetic Ti3C2 MXene functionalized with beta-cyclodextrin as magnetic solid-phase extraction and in situ derivatization for determining 12 phytohormones in oilseeds by ultra-performance liquid chromatography-tandem mass spectrometry. Phytochemistry 183, 112611.

Majchrzak T, Wojnowski W, Rutkowska M, Wasik A. 2020. Real-Time Volatilomics: A Novel Approach for Analyzing Biological Samples. Trends in Plant Science 25(3), 302-312.

Mandal S, Poi R, Banerjee K, Ansary I, Bhattacharyya S, Hazra DK, Ghosh R, Karmakar R. 2021. Bioefficacy, residue dynamics and dietary risk assessment of gibberellic acid in improving the potential yield of tomato (*Solanum lycopersicum L*.). Environmental Monitoring and Assessment 193(10).

Martinez AG, Liebanas FJA, Valverde RS, Torres MEH, Casinello JR, Frenich AG. 2020. Multifamily determination of phytohormones and acidic herbicides in fruits and vegetables by liquid chromatography-tandem mass spectrometry under accredited conditions. Foods 9(7), 906.

Matsuura T, Mori IC, Himi E, Hirayama T. 2019. Plant hormone profiling in developing seeds of common wheat (Triticum aestivum L.). Breeding Science 69(4), 601-610.

McDonnell LA, Heeren RM. 2007. Imaging mass spectrometry. Mass spectrometry reviews 26, 606-643.

McLean JA, Ridenour WB, Caprioli RM. 2007. Profiling and imaging of tissues by imaging ion mobility-mass spectrometry. Journal of mass spectrometry 42, 1099-1105.

Misra BB. 2021. Advances in high resolution GC-MS technology: a focus on the application of GC-Orbitrap-MS in metabolomics and exposomics for FAIR practices. Analytical Methods 13(20), 2265-2282.

Mogal CS, Solanki VH, Kansara RV, Jha S, Singh S, Parekh VB, Rajkumar BK. 2022. UHPLC-MS/MS and QRT-PCR profiling of PGP agents and Rhizobium spp. of induced phytohormones for growth promotion in mungbean (var. Co4). Heliyon 8(5), e09532.

Mohnike L, Rekhter D, Huang W, Feussner K, Tian H, Herrfurth C, Zhang Y, Feussner I. 2021. The glycosyltransferase UGT76B1 modulates N-hydroxy-pipecolic acid homeostasis and plant immunity. The Plant Cell 33(3), 735-749.

Naqvi S, Zhang Y, Tahir M, et al. 2023. Advanced strategies of the in-vivo plant hormone detection. Trends in Analytical Chemistry 166, 117186.

Novák O, Napier R, Ljung K. 2017. Zooming in on plant hormone analysis: Tissue- and cell-specific approaches. Annual Review of Plant Biology 68, 323-348.

Nováková L. 2013. Challenges in the development of bioanalytical liquid chromatography–mass spectrometry method with emphasis on fast analysis. Journal of Chromatography A 1292, 25-37.

Oklešťková J, Tarkowská D, Eyer L, Elbert T, Marek A, Smržová Z, Novák O, Franěk M, Zhabinskii VN, Strnad M. 2017. Immunoaffinity chromatography combined with tandem mass spectrometry: A new tool for the selective capture and analysis of brassinosteroid plant hormones. Talanta 170, 432-440.

Pařízková B, Pernisová M, Novák O. 2017. What has been seen cannot be unseen—detecting auxin in vivo. International Journal of Molecular Sciences 18(12), 2736.

Pařízková B, Žukauskaite A, Vain T, Grones P, Raggi S, Kubeš MF, Kieffer M, Doyle SM, Strnad M, Kepinski S, Napier R, Doležal K, Robert S, Novák O. 2021. New fluorescent auxin probes visualise tissue-specific and subcellular distributions of auxin in Arabidopsis. New Phytologist 230(2), 535-549.

Pěnčík A, Simonovik B, Petersson SV, et al. 2013. Regulation of auxin homeostasis and gradients in Arabidopsis roots through the formation of the IAA catabolite oxIAA. Plant Cell 25, 3858-3870.

Pěnčík A, Casanova-Saez R, Pilařová V, Žukauskaite A, Pinto R, Micol JL, Ljung K, Novák O. 2018. Ultra-rapid auxin metabolite profiling for high-throughput mutant screening in Arabidopsis. Journal of Experimental Botany 69(10), 2569-2579.

Pereira L, Pujol M, Garcia-Mas J, Phillips MA. 2017. Non-invasive quantification of ethylene in attached fruit headspace at 1p.p.b. by gas chromatography-mass spectrometry. The Plant Journal 91(1), 172-183.

Perez de Souza L, Alseekh S, Scossa F, Fernie AR. 2021. Ultra-high-performance liquid chromatography high-resolution mass spectrometry variants for metabolomics research. Nature Methods 18(7), 733-746.

Perin EC, Crizel RL, Galli V, Messias RD, Rombaldi CV, Chaves FC. 2018. Extraction and quantification of abscisic acid and derivatives in strawberry by LC-MS. Food Analytical Methods 11(9), 2547-2552.

Petersson SV, Johansson AI, Kowalczyk M, Makoveychuk A, Wang JY, et al. 2009. An auxin gradient and maximum in the Arabidopsis root apex shown by high-resolution cell-specific analysis of IAA distribution and synthesis. Plant Cell 21, 1659–1668.

Pétriacq P, Stassen JHM, Ton J. 2016. Spore density determines infection strategy by the plant pathogenic fungus *Plectosphaerella cucumerina*. Plant Physiology 170(4), 2325-2339.

Petřík I, Pěnčík A, Stýskala J, Tranová L, Amakorová P, Strnad M, Novák O. 2024. Rapid profiling of cytokinins using supercritical fluid chromatography coupled with tandem mass spectrometry. Analytica Chimica Acta 1285, 1-10.

Plačková L, Oklešťková J, Pospíšková K, et al. 2017. Microscale magnetic microparticle-based immunopurification of cytokinins from Arabidopsis root apex. The Plant Journal 89(5), 1065-1075.

Polanská L, Vičánková A, Nováková M, Malbeck J, Dobrev PI, Brzobohatý B, Vaňková R, Macháčková I. 2007. Altered cytokinin metabolism affects cytokinin, auxin, and abscisic acid contents in leaves and chloroplasts, and chloroplast ultrastructure in transgenic tobacco. Journal of Experimental Botany 58, 637–649.

Porfirio S, Sonon R, da Silva MDRG, Peixe A, Cabrita MJ, Azadi P. 2016. Quantification of free auxins in semi-hardwood plant cuttings and microshoots by dispersive liquid-liquid microextraction/microwave derivatization and GC/MS alysis. Analytical Methods 8(31), 6089-6098.

Ranocha P, Dima O, Nagy R, et al. 2013. Arabidopsis WAT1 is a vacuolar auxin transport facilitator required for auxin homoeostasis. Nature Communication 4, 2625.

Rawlinson C, Kamphuis LG, Gummer JPA, Singh KB, Trengove RD. 2015. A rapid method for profiling of volatile and semi-volatile phytohormones using methyl chloroformate derivatisation and GC-MS. Metabolomics 11(6), 1922-1933.

Revelou M, Kokotou MG, Constantinou-Kokotou V. 2019. Identification of auxin metabolites in *Brassicaceae* by Ultra-Performance liquid chromatography coupled with high-Resolution mass Spectrometry. Molecules 24(14), 2615.

Rittenberg D, Foster GL. 1940. A new procedure for quantitative analysis by isotope dilution, with application to the determination of amino acids and fatty acids. Journal of Biological Chemistry 133, 737-744.

Rizza A, Walia A, Tang B and Jones AM. 2019. Visualizing Cellular Gibberellin Levels Using the nlsGPS1 Forster Resonance Energy Transfer (FRET) Biosensor. Journal of visualized experiments 143.

Robert HS, Park C, Gutièrrez CL, et al. 2018. Maternal auxin supply contributes to early embryo patterning in Arabidopsis. Nature Plants 4, 548–553.

Roberts LD, Souza AL, Gerszten RE, Clish CB. 2012. Targeted Metabolomics. Current Protocols in Molecular Biology 30, 1-24.

Rogach VV; Kuryata VG; Kosakivska IV; Voitenko LV; Shcherbatiuk MM; Rogach TI. 2021. Morphogenesis, pigment content, phytohormones and productivity of sweet pepper under the action of gibberellin and tebuconazole. Regulatory Mechanisms in Biosystems 12(2), 294-300.

Schwaiger-Haber M; Stancliffe E; Arends V; Thyagarajan B; Sindelar M; Patti GJ. 2021. A Workflow to Perform Targeted Metabolomics at the Untargeted Scale on a Triple Quadrupole Mass Spectrometer. ACS Measurement Science Au. 1(1), 35-45.

Shimizu T, Miyakawa S, Esaki T, Mizuno H, Masujima T, Koshiba T, Seo M. 2015. Live single-cell plant hormone analysis by video-mass spectrometry. Plant Cell Physiology 56, 1287–1296.

Shiono K, Hashizaki R, Nakanishi T, Sakai T, Yamamoto T, Ogata K, Harada K, Ohtani H, Katano H, Taira S. 2017. Multi-imaging of Cytokinin and Abscisic Acid on the Roots of Rice (Oryza sativa) Using Matrix-Assisted Laser Desorption/Ionization Mass Spectrometry. Journal of Agricultural and Food Chemistry 65, 7624-7628.

Shiono K, Taira S. 2020. Imaging of Multiple Plant Hormones in Roots of Rice (Oryza sativa) Using Nanoparticle-Assisted Laser Desorption/Ionization Mass Spectrometry. Journal of Agricultural and Food Chemistry, 68, 6770-6775.

Skalický V, Vojtková T, Pěnčík A, Vrána J, Juzoń K, Koláčková V, Sedlářová M, Kubeš MF, Novák O. 2021. Auxin metabolite profiling in isolated and intact plant nuclei. International Journal of Molecular Sciences 22(22), 12369.

Skalický V, Antoniadi I, Pěnčík A, et al. 2023. Fluorescence-activated multi-organelle mapping of subcellular plant hormone distribution. The Plant Journal 116(6), 1825 – 1841.

Skalska A, Beckmann M, Corke F, Savas Tuna G, Tuna M, Doonan JH, Hasterok R, Mur LAJ. 2021. Metabolomic variation aligns with two geographically distinct subpopulations of *Brachypodium Distachyon* before and after drought stress. Cells 10(3), 683.

Squeri C, Miras-Moreno B, Gatti M, Garavani A, Poni S, Lucini L, Trevisan M. 2021. Gas exchange, vine performance and modulation of secondary metabolism in Vitis vinifera L. cv Barbera following long-term nitrogen deficit. Planta 253(3), 1-13.

Sugahara K, Kitao K, Yamagaki T, Koyama T. 2020. Practical optimization of liquid chromatography/mass spectrometry conditions and pretreatment methods toward the sensitive quantification of auxin in plants. Rapid Communications in Mass Spectrometry 34(7), e8625.

Svačinová J, Novák O, Plačková L, Lenobel R, Holík J, Strnad M, Doležal K. 2012. A new approach for cytokinin isolation from Arabidopsis tissues using miniaturized purification: pipette tip solid-phase extraction. Plant Methods 8, 17.

Šimura J, Antoniadi I, Široká J, Tarkowská D, Strnad M, Ljung K, Novák O. 2018. Plant hormonomics: Multiple phytohormone profiling by targeted metabolomics. Plant Physiology 177(2), 476-489.

Široká J, Brunoni F, Pěnčík A, Mik V, Žukauskaite A, Strnad M, Novák O, Floková K. 2022. High-throughput interspecies profiling of acidic plant hormones using miniaturised sample processing. Plant Methods 18, 122.

Tadić Đ, Gramblicka M, Mistrik R, Bayona JM. 2022. Systematic identification of trimethoprim metabolites in lettuce 414(9), 3121-3135.

Tamizhselvan P, Madhavan S, Constan-Aguilar C, Elrefaay ER, Liu J, Pěnčík A, Novák O, Cairó A, Hrtyan M, Geisler M, et al. 2024. Chloroplast auxin efflux mediated by ABCB28 and ABCB29 fine-tunes salt and drought stress responses in Arabidopsis. Plants. 13(1), 7.

Tang L, Kebarle P. 1993. Dependence of ion intensity in electrospray mass spectrometry on the concentration of the analytes in the electrosprayed solution. Analytical Chemistry 65(24), 3654-3668.

Tang J, Tian X, Mei E, et al. 2022. WRKY53 negatively regulates rice cold tolerance at the booting stage by fine-tuning anther gibberellin levels. Plant Cell 34(11), 4495-4515.

Tarkowská D, Novák O, Floková K, Tarkowski P, Turečková V, Grúz J, Rolčík J, Strnad M. 2014. Quo vadis plant hormone analysis? Planta 240, 55–76.

Thomason K, Babar MA, Erickson JE, Mulvaney M, Beecher Ch, MacDonald G. 2018. Comparative physiological and metabolomics analysis of wheat (Triticum aestivum L.) following post-anthesis heat stress, 13(6), e0197919.

Thomen A, Najafinobar N, Penen F, et al. 2020. Subcellular Mass Spectrometry Imaging and Absolute Quantitative Analysis across Organelles. ACS Nano 14, 4316-4325.

Tranová L, Buček J, Zatloukal M, Cankař P, Stýskala J. 2019. Synthesis of [15N4] purine labeled cytokinin glycosides derived from zeatins and topolins with 9-β-D, 7-β-D-glucopyranosyl, or 9-β-D-ribofuranosyl group, Journal of Labelled Compounds and Radiopharmaceuticals 62(3), 118-125.

Trapp MA, De Souza GD, Rodrigues E, Boland W, Mithofer A. 2014. Validated method for phytohormone quantification in plants. Frontiers in Plant Science 5, 417.

Tsugawa H, Cajka T, Kind T, Ma Y, Higgins B, Ikeda K, Kanazawa M, Vandergheynst J, Fiehn O, Arita M. 2015. MS-DIAL: data-independent MS/MS deconvolution for comprehensive metabolome analysis. Nature Methods 12(6), 523-526.

Van Meulebroek L, Bussche JV, DeClerq N, Steppe K, Vanhaecke L. 2015. A metabolomics approach to unravel the regulating role of phytohormones towards carotenoid metabolism in tomato fruit. Metabolomics 11(3), 667-683.

Včelařová L, Skalický V, Chamrád I, Lenobel R, Kubeš MF, Pěnčík A, Novák O. 2021. Auxin metabolome profiling in the Arabidopsis endoplasmic reticulum using an optimised organelle isolation protocol. International Journal of Molecular Sciences 22(17), 9370.

Viant MR, Kurland IJ, Jones MR, Dunn WB. 2017. How close are we to complete annotation of metabolomes? Current Opinion in Chemical Biology 36, 64-69.

Vrobel, O; Tarkowski, P. 2023. Can plant hormonomics be built on simple analysis? A review. Plant Methods 19, 107.

Watson JD, Crick FHC. 1953. Molecular Structure of Nucleic Acids: A Structure for Deoxyribose Nucleic Acid. Nature 171, 737-738.

Welling M, Deseo M, Bacic A, Doblin M. 2021. Untargeted metabolomic analyses reveal chemical complexity of dioecious Cannabis flowers. Australian Journal of Chemistry 74(6), 463-479.

Went F.W. 1926. On growth-accelerating substances in the coleoptile of Avena sativa. Proceedings of the Section of Sciences 30, 10-19.

Wu TB, Liang Y, Zhu XC, Zhao MP, Liu HW. 2014. Separation and quantification of four isomers of indole-3-acetyl-myo-inositol in plant tissues using high-performance liquid chromatography coupled with quadrupole time-of-flight tandem mass spectrometry. Analytical and Bioanalytical Chemistry 406(13), 3239-3247.

Xiao HM, Cai WJ, Ye TT, Ding J, Feng YQ. 2018. Spatio-temporal profiling of abscisic acid, indoleacetic acid and jasmonic acid in single rice seed during seed germination. Analytica Chimica Acta 1031, 119-127.

Xie HB, Zhou MY, Zhao HF, Wang YG, Jiang WF, Zhao S. 2014. Determination of three exogenous plant hormone residues in bean sprout by high performance liquid chromatography-quadrupole-time of flight mass spectrometry. Chinese Journal of Chromatography 32(5), 493-498.

Xin P, Yan J, Li B, Fang S, Fan J, Tian H, Shi Y, Tian W, Yan C, Chu J. 2016. A comprehensive and effective mass spectrometry-based screening strategy for discovery and identification of new brassinosteroids from rice tissues. Frontiers in Plant Science 7, 233601.

Xiong CF, Bai YL, Yin XM, Ye TT, Feng YQ. 2022. Use of chemical labeling-assisted liquid chromatography-mass spectrometry for discovering derivatives of brassinosteroids. Journal of Chromatography A 1685, 463639.

Yang XH, Brown SK, Davies PJ. 2013. The content and in vivo metabolism of gibberellin in apple vegetative tissues. Journal of the American Society for Horticultural Science 138(3), 173-183.

Yao XC, Xia NY, Meng X, Duan CQ, Pan QH. 2022. A one-step polyphenol removal approach for detection of multiple phytohormones from grape berry. Horticulturae 8(6), 548.

Yonny ME, Ballesteros-Gomez A, Adamo MLT, Torresi AR, Nazareno MA, Rubio S. 2020. Supramolecular solvent-based high-throughput sample treatment for monitoring phytohormones in plant tissues. Talanta 219, 121249.

Záveská Drábková L, Dobrev PI, Motyka V. 2015. Phytohormone profiling across the Bryophytes. PLoS One 10(5), e0125411.

Zemanová V, Pavlíková D, Dobrev PI, Motyka V, Pavlík M. 2019. Endogenous phytohormone profiles in Pteris fern species differing in arsenic accumulating ability. Environmental and Experimental Botany 166, 103822.

Zhang C, Žukauskaitė A, Petřík I, Pěnčík A, Hönig M, Grúz J, Široká J, Novák O, Doležal K. 2021. In situ characterisation of phytohormones from wounded Arabidopsis leaves using desorption electrospray ionisation mass spectrometry imaging. Analyst 146, 2653-2663.

Zhang C, Bieleszová K, Žukauskaitė A, Hladík P, Grúz J, Novák O, Doležal K. 2024. In situ separation and visualization of isomeric auxin derivatives in Arabidopsis by ion mobility mass spectrometry imaging. Analytical and Bioanalytical Chemistry 416, 125-139.

Zhang D, Ren L, Yue J, Wang L, Zhuo L, Shen X. 2014. GA4 and IAA were involved in the morphogenesis and development of flowers in Agapanthus praecox ssp. Orientalis. Journal of Plant Physiology 171(14), 966-976.

Zhang J, Nodzyński T, Pěnčík A, Rolčík J, Friml J. 2010. PIN phosphorylation is sufficient to mediate PIN polarity and direct auxin transport. Proceedings of the National Academy of Sciences 107, 918–922.

Zhang N, Jing T, Zhao M, Jin J, Xu M, Chen Y, Zhang S, Wan X, Schwab W, Song C. 2019. Untargeted metabolomics coupled with chemometrics analysis reveals potential non-volatile markers during oolong tea shaking. Food Research International 123, 125-134.

Zhang QC, Chen Y, Yang YQ, Liu YL, Wen M, Wang XY. 2023. Fabrication of magnetic ordered mesoporous carbon for quantitative analysis of acidic phytohormones in mushroom samples prior to their determination by ultra-high-performance liquid chromatography-tandem mass spectrometry. Acta Chromatographica 35(1), 60-69.

Zhao H, Jiang M, Liang Q, Xie C, Song S, Wang J, Bai G, Luo G. 2013. Fragmentation pathway studies of several plant hormones using an electrospray ionization-quadrupole/time-of-flight mass spectrometer. International Journal of Mass Spectrometry 335, 7-15.

Zou YL, Meng LY, Cui MY, Zhao JH, He M, Kim J, Quinto M, Shang HB, Li DH. 2019. Fast on-fiber derivatization and GC/MS analysis of phytohormones in wheat based on pencil-type coated carbon fibers. Food Chemistry 274, 254-260.

Tables

Table 1. Sample extraction solutions used in untargeted analysis in recently published studies.

Extraction solution	Reference
Methanol	*Xin et al., 2016*
	Carlson et al., 2020
	Garciá-Pérez et al., 2021
Acetonitrile	*Bai et al., 2022*
	Xiong et al., 2022
	Adigun et al., 2023
Water	*Li Y et al., 2017*
Ethanol	*Erland et al., 2020*
	Chernonosov et al., 2023
Ethyl acetate	*Kečkeš et al., 2013*
	Fu et al., 2021
	Di Masi et al., 2022
Methyl tert-butyl ether	*Mohnike et al., 2021*
Methanol:Acetonitrile	*Fiore et al., 2015*
	Cao J et al., 2016
Methanol:Chloroform	*Jia et al., 2020*
Calcium chloride	*Lin et al., 2023*

Table 2. Subcellular profiling of phytohormones.

Organelle isolation approach	Organelle (Plant material)	Analyzed phytohormones	Reference
Density-gradient (ultra)centrifugation	Chloroplasts (*Nicotiana tabacum, Triticum aestivum*)	Cytokinins	*Benková et al, 1999*
	Chloroplasts (*Nicotiana tabacum*)	Auxins, Cytokinins, ABA	*Polanská et al, 2007*
	Chloroplasts (*Arabidopsis*)	Auxins (IAA, precursors and metabolites)	*Tamizhselvan et al., 2024*
	Vacuole (*Arabidopsis)*	Auxins (IAA, precursors and metabolites)	*Ranocha el al., 2013*
	Vacuole (*Arabidopsis, Hordeum vulgare*)	Cytokinins	*Jiskrová et al, 2016*
	ER (*Arabidopsis*)	Auxins (IAA and metabolites)	*Včelařová et al, 2021*
	Nucleus (*Arabidopsis, Nicotiana tabacum*)	Auxins (IAA, precursors and metabolites)	*Skalický et al, 2021*
	Vacuole (*Arabidopsis cell culture*)	Auxins (IAA and metabolites), Cytokinins	*Skalický et al., 2023*
Flow cytometry	Nucleus (*Arabidopsis, Nicotiana tabacum*)	Auxins (IAA, precursors and metabolites)	*Skalický et al, 2021*
	Nucleus, Mitochondria, Chloroplasts, ER, (*Arabidopsis cell culture*)	Auxins (IAA and metabolites), Cytokinins	*Skalický et al., 2023*

Figures

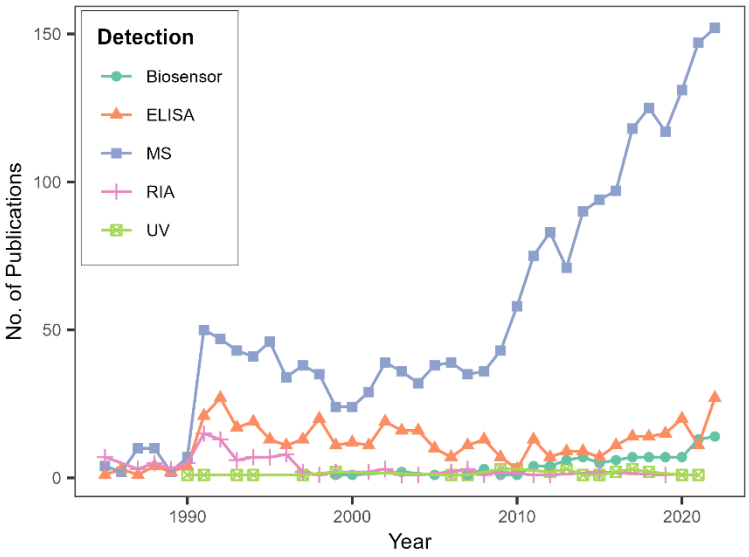

Fig. 1. Timeline of the publication activity related to a plant hormone analysis. The colour of a particular line corresponds with a following detection method: biosenzor (dark green), enzyme-linked immunosorbent assay (ELISA, red), mass spectrometry (MS, blue), radioimmunoassay (RIA, violet), ultraviolet spectrophotometry detection (UV, light green). Data were retrieved from the Web of Science.

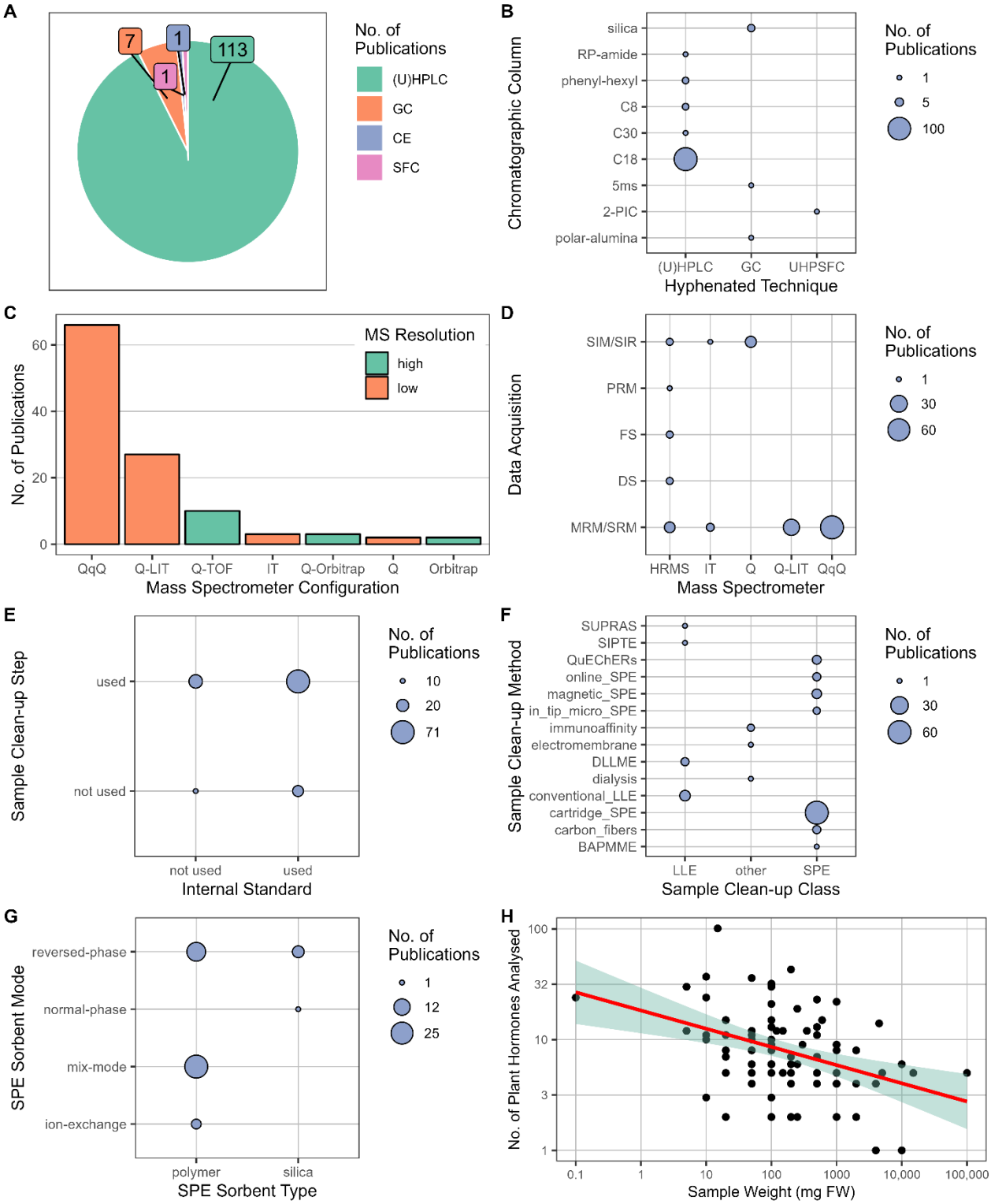

Fig. 2. Overview of the current trends in mass-spectrometry based targeted plant hormones analysis. Proportion of publications (n = 122) based on the hyphenated technique (A). Frequency of chromatographic column types. A bubble size corresponds with the number of publications. Amide column used in reversed phase mode (RP-amide), octyl (C8), octadecyl (C18), triacontyl (C30), (5%-phenyl)-methylpolysiloxane (5ms), 2-picolylamine (2-PIC) (B). Frequency of mass spectrometry configuration. The colour corresponds with mass-spectrometry (MS) resolution. Triple quadrupole (QqQ), quadrupole-linear ion trap (Q-LIT), quadrupole-time-of-flight analyser (Q-TOF), ion-trap (IT), quadrupole-Orbitrap (Q-Orbitrap), single quadrupole (Q) (C). Frequency of data acquisition mode based on mass spectrometer configuration. Single ion monitoring or single ion reaction (SIM/SIR), parallel reaction monitoring (PRM),

full scan (FS), product ion scan (daughter scan; DS), multiple or single reaction monitoring (MRM/SRM) (D). Frequency of internal standard and/or sample clean-up step use (E). Frequency of sample clean-up methods use. Supramolecular solvents (SUPRAS), sequential solvent-induced phase transition extraction (SIPTE), “Quick, Easy, Cheap, Effective, Rugged, and Safe” extraction (QuEChERs), solid phase extraction (SPE), dispersive liquid-liquid microextraction (DLLME), liquid-liquid extraction (LLE), boronate affinity polymer monolith microextraction (BAPMME) (F). Frequency of SPE sorbent mode based on sorbent type/material (G). Number of plant hormones analysed as a function of sample weight in milligram of fresh weight (mg FW). Each point represents one publication. The red line shows a linear dependency. Green shade enveloping the regression line represents the confidence interval at 95% significance level.

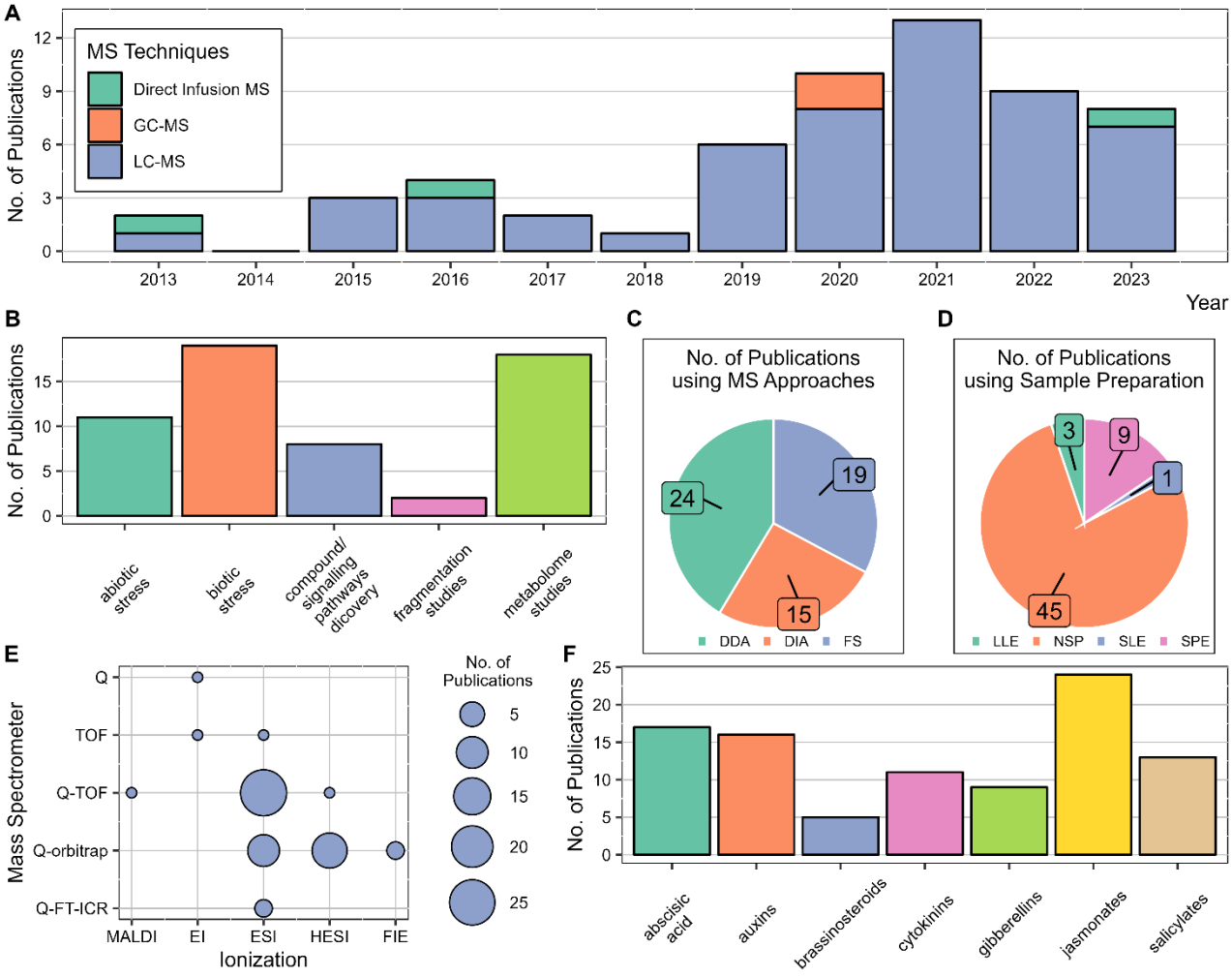

Fig. 3. Overview of the current trends in mass-spectrometry based untargeted plant hormones analysis. A comprehensive search of the Web of Science database was conducted to identify publications utilizing phytohormone analysis and untargeted mass spectrometry methods. Subsequently, all generated publications underwent manual processing, resulting in the selection of a subset of 58 publications from the past decade. The timeline depicts the publication activity related to plant hormone analysis, with a focus on mass spectrometry techniques (A). Various trends in the application of these techniques are highlighted, including their biological applications (B), types of analysis approaches (C), and sample preparation techniques (D). The combination of ionization methods and mass spectrometers is depicted (E), with the size of each bubble representing the number of publications. Additionally, the number of publications focused on each distinct type of plant hormone studied through untargeted analysis is illustrated (F). List of variables: DDA, data-dependent analysis; DIA, data-independent analysis; EI, electron impact; ESI, electrospray ionization; FIE, flow infusion electrospray; FS, full scan; GC-MS, gas chromatography-mass spectrometry; HESI, heated electrospray ionization; LC-MS, liquid chromatography-mass spectrometry; LLE, liquid-liquid extraction; SLE, solid-liquid extraction; SPE, solid phase extraction; MALDI, matrix-assisted laser desorption/ionization; NSP, no sample preparation; Q, single quadrupole; Q-FT-ICR, quadrupole-Fourier transform ion cyclotron resonance; Q-orbitrap, quadrupole-orbitrap; Q-TOF, quadrupole-time of flight; TOF, time of flight.

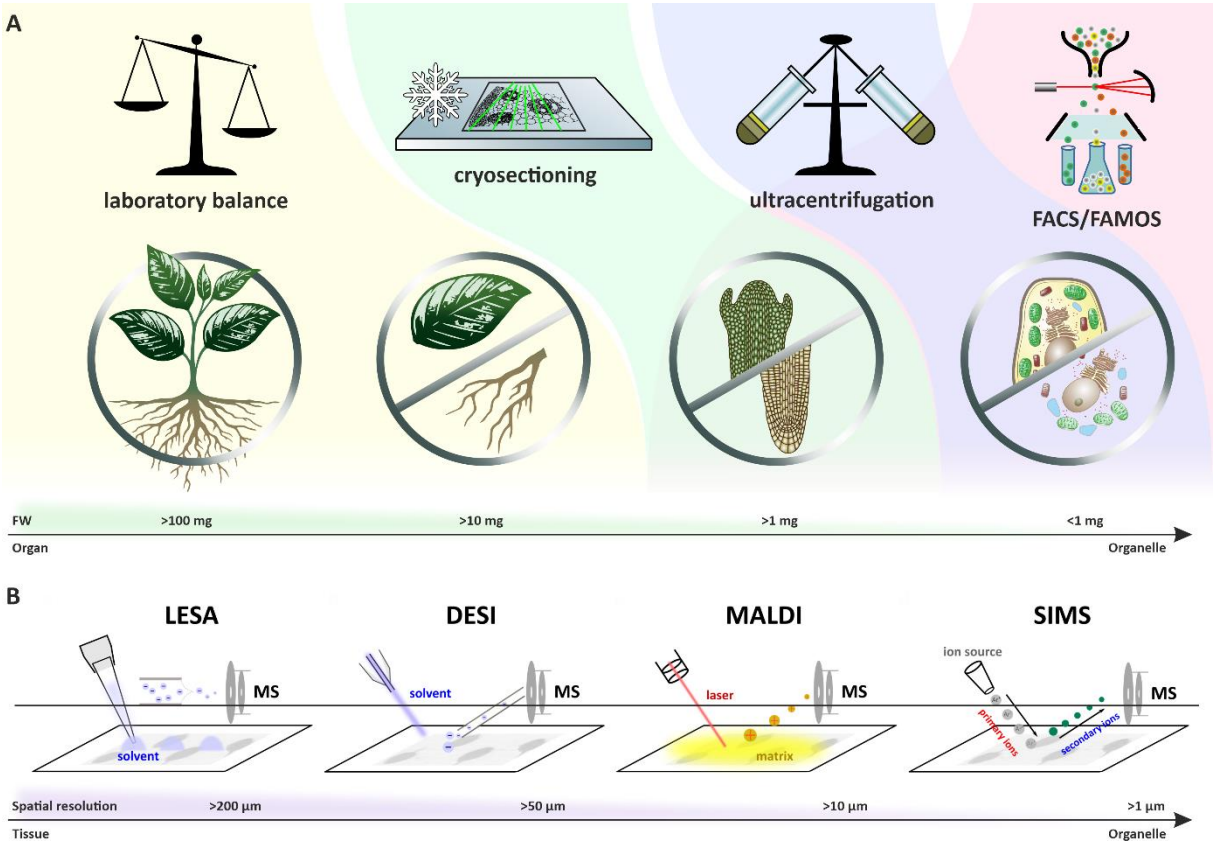

Fig. 4. From organ to organelle. The size and mass scale ordered from the left: whole plant, organ, tissue, cell/organelles and methods used to obtain their exact amount (A). Application of various ionization methods used for mass spectrometry imaging of phytohormones based on the spatial resolution scale. Liquid extraction surface analysis (LESA), desorption electrospray ionization (DESI), matrix assisted laser desorption ionization (MALDI), secondary ion mass spectrometry (SIMS) (B).

Supplement I

Supplement II

Supplement III

Supplement IV

Supplement V

Supplement VI

Supplement VII

Supplement VIII

Petřík I, Valníčková A, Stýskala J, Strnad M, Ljung K, Novák O. [In preparation]. DisperSpin solid phase micro-extraction: next generation micro-purification method for UHPLC-MS/MS determination of naturally occurring phytohormones.

DisperSpin solid phase micro-extraction: next generation micro-purification method for UHPLC-MS/MS determination of naturally occurring phytohormones

Petřík Ivan[1], Valníčková Anna[1], Stýskala Jakub[2], Strnad Miroslav[1], Ljung Karin[3], Novák Ondřej[1,3]

[1] *Laboratory of Growth Regulators, The Czech Academy of Sciences, Institute of Experimental Botany & Palacký University, Faculty of Science, Šlechtitelů 27, CZ-78371 Olomouc, Czech Republic*

[2] *Department of Organic Chemistry, Palacký University, Faculty of Science, 17. listopadu 1192/12, CZ-77146 Olomouc, Czech Republic*

[3] *Umeå Plant Science Centre, Department of Forest Genetics and Plant Physiology, Swedish University of Agricultural Sciences, SE-90183 Umeå, Sweden*

Abstract

Background

Phytohormones are naturally occurring compounds, which regulate development and stress responses in living plants. Their natural concentrations are very low (pmol – fmol per gram of fresh weight). Therefore, very sensitive instrumentation is crucial to use for the analysis of phytohormones in plant extracts. Nowadays, state-of-the-art technology used for this purpose is ultra-high performance chromatography coupled with tandem mass spectrometry (UHPLC-MS/MS). However, plant extract is very complex mixture containing plethora of contaminating compounds. These contaminants can suppress the signal of phytohormones and thus make the analysis impossible. Therefore, purification of plant sample is one of the most important step in analytical workflow to achieve high quality data. One of the most prominent method for purification of phytohormones is solid phase extraction (SPE). The classic format of SPE is cartridge extraction using flow of liquid sample through fixed sorbent. However, dispersive SPE has been introduced several years ago as an alternative approach using dispersion of free sorbent in liquid sample. Several variations of dispersive SPE have been published (magnetic, non-magnetic, centrifugal, matrix dispersion format etc.).

Results

Our effort was dedicated to develop a novel dispersive SPE method for purification of several tens of main phytohormonal classes: cytokinins, auxins and abscisic acid. Method uses commercially available non-magnetic mixed-mode SPE sorbent. Method was characterized, optimized, validated and tested on various types of plant species across the plant kingdom. For these purposes, design of experiment combined with multi-variate regression modelling was used. It was proved that method is efficient, reproducible and reliable.

Conclusions

We developed a DisperSpin SPE method for purification of 51 phytohormones and metabolites including cytokinins, auxins and abscisic acid. This novel technique is miniature, efficient, robust and practical. DisperSpin SPE can be adapted further for purification of other bioactive compounds.

1. Introduction

Phytohormones play an important role in regulation of plant growth, development and environmental responses. Nowadays, about ten classes of plant hormones are known (Novak et al., 2017). Our work was focused on cytokinins (CKs), auxins and abscisic acid (ABA). CKs and auxins represent the phytohormones closely related to organ development, cell proliferation and elongation, root and shoot formation, apical dominance, inhibition of senescence and many others developmental processes (Zurcher and Muller, 2016; Casanova-Saez and Voss, 2019). ABA participates on growth development and water management including bud and seed dormancy, stomatal regulation and responses to abiotic stress (Cutler et al., 2010). These and other phytohormones cooperate in sophisticated cross-talking network (Vanstraelen and Benkova, 2012). Knowledge about this network helps to understand the complex plant physiological processes with impact on agriculture, forestry or horticulture. Actual progress in research of phytohormones is remarkable. However, plethora of physiological, metabolic or molecular mechanisms that plant hormones participate still remains unexplained. Therefore, determination of phytohormones in plant tissue, cells or subcellular compartments can shed the light on so far unexplored processes.

Phytohormones occur in plants in very low concentrations (10^{-12} to 10^{-15} mol/g of fresh weight; FW) and determination of their concentration levels requires very sensitive approaches (Simura et al., 2018). One of the most prominent tool for this purpose is ultra-high performance liquid chromatography coupled with tandem mass spectrometry (UHPLC-MS/MS) (Novak et al., 2017). However, a plant sample usually contains plenty of high abundant contaminants leading to signal suppression of targeted compounds. Therefore, a sample purification step before UHPLC-MS/MS analysis of phytohormones should be involved in analytical workflow (Tarkowska et al., 2014).

Solid phase extraction (SPE) represents very popular technology for purification of plant hormones. SPE based on reverse phase, ion exchange or combination of both is well established in phytohormonal analysis for many years (Dobrev and Kaminek, 2002; Tureckova et al., 2009; Novak et al., 2012; Flokova et al., 2014). Nowadays, development of novel advanced methods tends to miniaturization. The last decade, stop-and-go-microextraction in pipette tip (StageTip) became a state-of-the-art technology allowing purification of phytohormones from less than 1 mg FW of plant material (Rappsilber et al., 2007; Svacinova et al., 2012; Pencik et al., 2018). Recently, auxin profile on subcellular level was determined in endoplasmic reticulum using StageTips (Vcelarova et al., 2021).

In addition, miniaturized purification methods of phytohormones has been introduced with magnetic SPE (mSPE) (Cai et al., 2015; Zhang et al., 2016; Luo et al., 2017). Unlike the previously mentioned techniques, mSPE is based on a dispersion of magnetic SPE particles in a liquid plant extract. However, the production of magnetic particles is difficult and requires collaboration with highly expertized laboratories. Therefore, a family of non-magnetic dispersive SPE methods have been introduced as well, like matrix solid phase dispersion (MSPD) and QuEChERS (an acronym of Quick, Easy, Cheap, Effective, Rugged and Safe) (Barker, 2000; Anastassiades et al., 2003). Several works showed that these techniques can be used for extraction of selected plant growth regulators (Flores et al., 2011; Yan et al., 2012; Deng et al., 2017; Chen et al., 2018; Martinez et al., 2020). We developed a novel, advanced and miniaturized method for purification of CKs, auxins and ABA based on non-magnetic dispersive SPE. The method combines high efficiency of mixed-mode SPE purification in cartridge format (Dobrev and Kaminek, 2002) with practical benefits of QuEChERS and MSPD.

2. Results and discussion

2.1. Optimization of extraction solvent composition

The early step of UHPLC-MS/MS analysis of phytohormones in plants is extraction to solvent. The composition of extraction solvent is usually designed regarding the solubility and chemical stability of targeted compounds. However, the complex plant sample contains plethora of extractable species including enzymes contributing phytohormonal metabolism. Consequently, unwanted changes in concentrations of endogenous phytohormones could emerge during the extraction (Tarkowska et al., 2014). Therefore, the inhibition of enzymatic activity should be considered while extraction solvent is designed. Beileski buffer is one of the well-established solvent for extraction of CKs. It consists from 60% methanol, 15% chloroform, 5% formic acid and 20% water (Bieleski, 1964). Alternatively, modified Bieleski buffer, which is free of chloroform, has been also well established (Singh et al., 1988; Hoyerova et al., 2006).

We selected modified Bieleski buffer (75% methanol, 20% water, 5% formic acid) as a first choice extraction solvent. However, high concentration of methanol in extraction solvent can be problematic when purification with SPE follows. Therefore, the organic content should be reduced. Evaporation or dilution of extract is usually performed for this purpose (Horgan, 1975; Dobrev and Kaminek, 2002). However, both can lead to increase of sample volume or process time. Hence, we decided to decrease the initial concentration of methanol from 75 % to 10 %. To test the efficiency, we compared endogenous profile of CKs, auxins and ABA obtained by innovated extraction solvent with profile achieved by modified Bieleski buffer. Profiles of *Arabidopsis* seedlings and T89 poplar leaves were compared.

It was shown that both extraction solvents provided similar phytohormonal profiles (Figure 1a). The obvious difference in concentration level was observed for oxIAA in T89 poplar extract. Weak extraction solvent provided higher mean value compared to control. One of the possible explanation was conversion of free IAA to oxIAA during the extraction. However, the level of IAA was equal in both extracts. Therefore, higher yield of oxIAA was probably not caused by oxidation during sample preparation. Rather, higher extractability of oxIAA in polar solvent was suggested as a more likely reason. Polar aqueous solvent has been also recommended for extraction of auxins from plant material (Novak et al., 2012; Pencik et al., 2018). Hence, 10% methanol with 5% formic acid was assumed reasonable for extraction of CKs, auxins and ABA from *Arabidopsis* seedlings and T89 poplar leaves.

2.2. Development of DisperSpin SPE

Recently, mixed-mode polymer sorbents has become a prominent tool for SPE (Poole, 2003). Oasis MCX® extraction cartridges (Waters, Milford, USA) represents a mixed-mode combining strong cation exchange and reverse phase. Robust protocol for purification of CKs, auxins and ABA based on MCX was established several decades ago (Dobrev and Kaminek, 2002). Our initial effort was aimed to utilize MCX bulk sorbent in centrifugal dispersive format similarly to QuEChERS protocol (Anastassiades et al., 2003). In pilot experiment, *Arabidopsis* seedlings were extracted and purified with centrifugal dispersive SPE using MCX sorbent (Dobrev and Kaminek, 2002). Data were compared to purification with classic cartridge SPE.

It was shown that centrifugal dispersive SPE was not reasonable format for purification of CKs, auxins and ABA. The peak areas of isotopically labelled internal standards achieved by centrifugal dispersive SPE was dramatically decreased compared to classic cartridge SPE (Figure S1). Moreover, the reproducibility of dispersive method was poor as the variability among technical replicates was tremendous. Insufficient process efficiency was caused by losses of bulk SPE sorbent (visible by the eye) during the purification procedure. Previously described cartridge method is complex multi-step methodology including loading, wash and several elutions (Dobrev and Kaminek, 2002). Transferred to dispersive format, each step requires a separation of sorbent particles and liquid supernatant. In centrifugal dispersive SPE, collection of maximal volume of supernatant is critical to achieve high process efficiency. However, it can be counterproductive when the sorbent is lost concurrently. This challenging task has been already resolved with magnetic particles in mSPE (Zhang et al., 2010; Cai et al., 2015; Luo et al., 2017) or magnetic immunopurification (Plackova et al., 2017). However, magnetic-based separation method is not possible to use with non-magnetic MCX sorbent. Thus, we had to find another solution for separation of supernatant. Finally, filtration was suggested as a promising way. Centrifugation filters were utilized and this innovation was proved to be efficient, fast and easy to use. As the dispersion of bulk SPE sorbent was performed on a “spin filter”, a novel method was called DisperSpin SPE.

The reproducibility of DisperSpin SPE was comparable with reproducibility of classic cartridge SPE (Figure 1b). Significant differences were observed in yield of auxin metabolites, ABA and CK ribosides. Surprisingly, a tremendous improvement in yield of CK nucleotides and CK *O*-glucosides was observed in DisperSpin format. These differences in process efficiency could be explained variously regarding parameters of SPE procedure. For instance,

different format, loading time, elution volume, matrix effect and other factors could affect the process efficiency. As these characteristics of DisperSpin SPE had been entirely unexplored, method was characterized to understand the relationship between factors and process efficiency.

2.3. Characterization of DisperSpin SPE

As the composition of solvents was already characterized in cartridge SPE protocol (Dobrev and Kaminek, 2002), the characterization of DisperSpin SPE was focused on factors related to SPE kinetics. The following factors were screened: incubation time, sorbent amount, elution volume and number of elution cycles. The effectivity of these factors on process efficiency of DisperSpin SPE was calculated in partial least square (PLS) regression model (Figure 2a). The model describes association between factors and yield of phytohormonal standards.

The effect of incubation time was neglectable, as the position of incubation time was situated near the origin of PLS loading plot. This observation suggested that retention of phytohormonal standards on MCX bulk sorbent was fast and was not changing in the time. Therefore, incubation time was assumed as the most robust examined factor.

The position of sorbent amount in PLS loading plot was the most distant from the origin. Hence, the sorbent amount was identified as the most important factor in terms of process efficiency. Surprisingly, CK bases, CK ribosides, non-polar CK-glucosides and IAA were negatively associated with sorbent amount. The yield of these compounds was higher when low amount of sorbent was used and vice versa. On the other hand, the highest yield of CK nucleotides was achieved with high amount of sorbent (Figure 2).

This contradicting observation was probably the result of different interaction mechanisms of each individual compound with MCX sorbent. It has been described previously that CK nucleotides prefer electrostatic forces as the elution fraction has been obtained mainly by change of pH (Dobrev and Kaminek, 2002). On the other hand, IAA is retained primarily by hydrophobic interactions as majority of IAA has been eluted with methanol. Compounds preferring both types of interactions (CK bases, ribosides and glucosides) have been eluted with combination of pH change and methanol. A similar elution concept has been described in StageTip purification protocol as well (Svacinova et al., 2012).

The importance of elution cycles was also demonstrated (Figure 2a). Auxin metabolites and ABA were eluted more effectively with repeated elution cycles. However, the importance of elution cycles dropped when high elution volume was used (Figure 2b). Therefore, one elution cycle with maximal elution volume (400 µl) was reasonable to achieve acceptable process efficiency. These results explain lower yields of auxin metabolites and ABA purified by DisperSpin SPE compared to cartridge SPE as the elution volume differed in both methods (Figure 1b).

We concluded that process efficiency of DisperSpin SPE depends on balance between sorbent amount and elution volume. Low volume is enough for elution of CK nucleotides even from high amount of sorbent. Relatively low yield of auxin metabolites and ABA can be compensated with higher elution volume. However, some compounds like CK bases or IAA are problematic to elute even a high elution volume is used. Therefore, decrease of sorbent amount is crucial to obtain reasonable process efficiency.

2.4. Optimization of DisperSpin SPE

Presence of plant matrix in sample is additional factor affecting the process efficiency. This factor has been described as matrix effect, which alters the ionization of analysed compounds in UHPLC-MS/MS analysis. The effect can be negative (signal suppression) or positive (signal enhancement) (Gosetti et al., 2010; Novakova, 2013). It is known that matrix effect can be suppressed by purification procedure (Choi et al., 2001; Marchi et al., 2010). Therefore, we optimized amount of plant material and sorbent amount as one of the most important factor of SPE. For this purpose, *Arabidopsis* seedlings and T89 poplar leaves were tested. The main goal was to find the optimal setpoint to obtain acceptable response of endogenous phytohormones.

It was not surprise that overall response was increasing with increasing amount of plant material (Figure 3). Relationship between response, sorbent amount and sample amount corresponded to pattern discussed in section 2.3. This pattern corresponds with theory of SPE capacity. It has been estimated that capacity is about 1 to 5 % of total mass of SPE sorbent. (Poole, 2003). However, plant matrix can dramatically decrease the capacity as competes with phytohormones for functional groups of sorbent. It has several consequences. The process efficiency can be lower due to the losses during the loading step. However, lower capacity of SPE can facilitate the elution and thus increase the process efficiency. Moreover, some

components of matrix can be retained and eluted with phytohormones simultaneously and thus contribute on matrix effects in ion source (Zhou et al., 2017). All of these effects related to matrix and capacity of SPE contribute to final process efficiency (Matuszewski et al., 2003). In general, capacity of polymer mixed-mode sorbents is relatively high allowing purification of high amount of sample (Fontanals et al., 2020). Our experience corresponded with this statement. When 2 mg of sorbent were used for purification of 20 mg FW, no overload was observed (Figure 3). Finally, 10 mg of sorbent combined with 10 mg FW of sample was selected as a compromise to reach reasonable limits of quantification.

2.5. Method validation

Optimized method was validated according to recommended guidelines (Matuszewski et al., 2003). Validation was performed with 10 mg FW of *Arabidopsis* seedlings at three different concentration levels. The concentration levels were determined with standard isotope dilution method. Calculated values were compared with known amounts of spiked phytohormones (Table S1). A relative difference between theoretical and estimated value was presented as a bias defining method accuracy. Median value of method accuracy was 2.9 % ranged between quartiles -6.9 % and 9.3 % (Figure 4). Method precision was estimated as a relative standard deviation (RSD). Median value of RSD was 3.6 % ranging between quartiles 2.0 % and 15.4 %. Process efficiency was calculated as a product of recovery and matrix effect. Median process efficiency was 45.8 % with quartiles 30.4 % and 57.0 %. These results of validation indicated that method is reliable to use for determination of naturally occurring CKs, auxins and ABA.

2.6. Robustness test

Plant extracts of various plant tissues and plant species differs in chemical complexity. Oils, sugars, pigments, proteins, secondary metabolites and other compounds are present in tissues in different proportions. Consequently, various matrix effects can make a UHPLC-MS/MS analysis difficult (Tarkowska et al., 2014). Therefore, we tested the robustness of DisperSpin SPE for determination of phytohormonal profile in green material of various plant species. Representative plants were selected across the plant kingdom. *Nostoc* culture represented algae. Gametophytes of *Merchantia polymorpha* were used as a bryophyte material. Norway spruce seedlings were representative of conifers and wheat leaves of monocots. Finally,

T89 poplar leaves and *Arabidopsis* seedlings represented dicots. The profiles of naturally occurring phytohormones were determinated. Method was proved to be robust as profiles of CKs, auxins and ABA were determinated in all investigated types of plant matrix (Figure 5).

3. Material and methods

3.1. Chemicals

Deionized water was produced with Millipore Direct-Q® 3 UV system (Millipore, Bedford, MA, USA). Methanol (gradient grade), formic acid were purchased from Merck (Darmstadt, Germany) and 25% ammonia hydroxide solution (v/v) was obtained from Honeywell Fluka™ (Bucharest, Romania). Methanol, formic acid and ammonia hydroxide in hypergrade purity for UHPLC-MS/MS analysis were obtained from Merck (Darmstadt, Germany). Phytohormone standards and isotopically labelled internal standards (IS) were obtained from Olchemim Ltd. (Olomouc, Czech Republic) and from Faculty of Science, Palacký University in Olomouc (Czech Republic). The collection of standards and isotopically labelled internal standards is listed in Table 1.

3.2. Preparation of plant material

Arabidopsis thaliana (ecotype Col-0) seeds were planted on Petri dishes with solid medium consisting from 2.2 g/l Murashige & Skoog medium, 7 g/l agar (both Duchefa Biochemie, Haarlem, Netherlands), 10 g/L sucrose and 0.05 g/l morpholinoethanesulfonic acid (both Sigma Aldrich, St. Louis, MO, USA). The planted seeds were stratified for two days in dark at 4 °C. After 2 days of stratification the seedlings were transfered to long-day conditions accounting for 16 hours light, 8 hours dark and 22 °C. 10-day-old seedlings and 21-day-old seedlings were harvested and immediatelly disrupted under liquid nitrogen with pestle and mortar to the powder. The homogenized material was collected in falcon tube and stored at -70 °C.

Populus tremula x Populus tremuloides hybrid clones T89 were grown *in vitro* by cloning procedure. The stem of 3-month-old aspen tree was cut between the internodes below the apex. Each cutting was transferred to the jar containing 20 mL media consisting from 2.183 g/L MS 1A media, 1 g/L glucose and 8 g/L plant agar (Duchefa Biochemie, Haarlem,

Netherlands). Autoclaved media was enriched with 112 mg/L Gamborg's B5 vitamin mixture (Duchefa Biochemie, Haarlem, Netherlands), L-Glutamine 20 mg/L, panthotenate 0.1 mg/L, L-cysteine chlorhydrate 0.1 mg/L and biotine 0.001 mg/L (all purchased from Sigma Aldrich, St. Louis, MO, USA). The jar was enclosed with the lid and placed to the culture chamber with schedule 16 h light (22 °C), 8 h dark (18 °C). The leaves of 90-day-old seedling were cut at petiole 3 hours after start of light period to maximize the level of endogenous aromatic cytokinins (Edwards et al., 2018). Harvested leaves were stored at –70 °C.

Triticum aestivum (winter type, variety *Turandot*) dormant seeds were soaked in tap water for 5 hours at room temperature. Afterwards, seeds were sown onto wet vermiculite and grown in long-day conditions (16 h light, 8 h dark) at room temperature. Irrigation was performed once per two days with 0.5 l of modified Hoagland's nutrient solution (Arnon and Hoagland, 1940). The nutrient solution for plant growth was prepared as follows. Micronutrients including 280 mg boric acid, 340 mg manganese sulfate monohydrate, 10 mg copper sulfate pentahydrate, 22 mg zinc sulfate heptahydrate and 10 mg ammonium heptamolybdate tetrahydrate were dissolved in 100 mL deionized water. Stock solution was divided to 10 ml aliquots and stored in –20 °C. Macronutrients consisting from 9.4 g calcium nitrate tetrahydrate, 5.2 g magnesium sulfate heptahydrate, 6.6 g potassium nitrate and 1.2 g ammonium dihydrogen phosphate were dissolved separately, each in 10 ml deionized water. Macronutrient individual solutions and micronutrient stock aliquote were combined and diluted in 1.0 l water acidified with 5 µl of concentrated sulphuric acid. The final irrigating solution was prepared from 100 ml of combined solution, 895 ml of deionized water and 5 ml of iron sulfate heptahydrate in concentration 27.25 g/l previously dissolved in 7.45 g/l ethylenediaminetetraacetic acid. The leaves of 7-day-old seedlings were cut at a base and homogenized with pestle and mortar supported by liquid nitrogen. Homogenate was stored in –70 °C.

Samples of Norway spruce (*Pinea abies*) were prepared according to previously described procedure (Brunoni et al., 2020). Briefly, seeds were incubated in tap water for 12 h at 4 °C and planted in well soaked vermiculite. Substrate with seeds was transferred to growth chamber with long-day schedule 16 h light at 22 °C with light intensity 150 µmol m^{-2} s^{-1} and 8 h night at 18 °C. Seedlings were harvested 14 days after sowing and 10 mg of cotyledons were collected (Brunoni et al., 2020).

Merchantia polymorpha (WT strain *Tak1*) gametophytes were obtained from Center for Research in Agricultural Genomics (Barcelona, Spain). Plants were cultivated on half

Gamborg's B5 media containing 1% agar and no sucrose in long-day photo-period conditions (16 h light. 8 h dark) at 22 °C. After 3 weeks, gametophytes were harvested and lyophilized.

Cyanobacterium *Nostoc sp.* CCAP 1453/38 was cultivated according to procedure described in (Chmelik et al., 2019).

3.3. Extraction of plant material

Homogenized plant material was weighed into 2ml Eppendorf tube. Sample was covered with 0.5 ml of weak extraction solution consisted from 10% methanol, 5% formic acid and 85% water (v/v). Mixture of internal standards and four ceramic homogenization beads were added into tube. Sample was shaken in Retsch MM400 oscilation mill (Haan, Germany) at 27 Hz for 5 minutes, sonicated for 3 minutes and incubated for 30 minutes in refrigerator. Afterwards, sample was centrifuged with chilled Allegra 64R benchtop centrifuge (Beckman Coulter, USA) at 20,000 rpm for 15 minutes. Supernatant was collected.

3.4. Cartridge SPE

Cartridge SPE was performed according to modified protocol for purification of CKs, auxins and ABA (Dobrev and Kaminek, 2002). Oasis® MCX extraction cartridges (30 mg/1 ml) (Waters, Milford, USA) were conditioned with 1 ml methanol, 1 ml water and 1 ml formic acid (1 mol/l). Then, samples were loaded into cartridge and washed with 1 ml formic acid (1 mol/l). Subsequently, elution of fraction A containing auxins and ABA was performed with 2 ml of 80% methanol (v/v). CKs were eluted in fraction B with 1 ml ammonia (0.35 mol/l) in water and 2 ml ammonia (0.35 mol/l) in 60% methanol (v/v). Eluates were evaporated in vacuum evaporator to dryness.

3.5. Centrifugal dispersive SPE

Oasis MCX® bulk sorbent (30 μm) was weighed per 10 mg into 2ml Eppendorf tube. Sorbent was conditioned with 0.5 ml methanol, stirred shortly and centrifuged at 20,000 rpm for 2 minutes. Supernatant was removed with pipette and replaced with 0.5 ml formic acid (1 mol/l). Sorbent was stirred, centrifuged and conditioning with formic acid was repeated once again. After removal of supernatant, 0.5 ml of plant extract was loaded and incubated for 5 minutes at 4 °C. Sample was centrifuged, supernatant was removed and sorbent was washed

with 0.5 ml formic acid (1 mol/l). Sample was stirred, centrifuged, solvent was pipetted out and 0.5 ml 80% methanol was applied. After short stirring and centrifugation, eluate was collected as fraction A. Subsequently, 0.5 ml ammonia (0.35 mol/l) in water was pipetted onto a sorbent, sample was stirred, centrifuged and eluate was collected as a fraction B. Finally, 0.5 ml ammonia (0.35 mol/l) in 60% methanol (v/v) was applied, stirred and centrifuged. Eluate was collected as an additional fraction B. Both fractions were evaporated to dryness.

3.6. DisperSpin SPE

Procedure was performed as depicted in Figure S2. 100 mg of Oasis MCX® bulk sorbent (30 μm) was weighed into 2ml Eppendorf tube. Sorbent was conditioned with 1 ml of methanol, stirred shortly and centrifuged at 20,000 rpm for 2 minutes. Supernatant was pipetted out and replaced with 1 ml of formic acid (1 mol/l). Sorbent was stirred and centrifuged. Supernatant was removed and 1 ml formic acid (1 mol/l) was applied again. Tube was stirred and suspension of sorbent (100 mg/ml) was aliquot with pipette per 10 mg onto MicroSpin centrifuge filters (nylon, 0.2 μm, Chromservis, Czech Republic).

Plant extract (0.5 ml) was loaded onto sorbent and suspension was mixed. Samples were spin in chilled centrifuge at 2000 rpm for 3 minutes. Liquid filtrate was removed from collection tube. Sorbent was washed with 0.4 ml formic acid (1 mol/l), mixed and centrifuged at the same conditions. Then, centrifugation filter with SPE sorbent was transferred into fresh 2ml collection tube labelled as fraction A.

Sorbent was covered with 0.4 ml 80% methanol (v/v), mixed, centrifuged and eluate was collected. Centrifugation filter was transferred into another fresh 2ml tube marked as fraction B. Sorbent was covered with 0.4 ml ammonia (0.35 mol/l) in water, mixed and spin. Afterwards, 0.4 ml ammonia (0.35 mol/l) in 60% methanol (v/v) was applied mixed and sample was centrifuged once again to collect an additional fraction B. Both fractions were evaporated to dryness.

3.7. UHPLC-MS/MS analysis

Evaporated samples were reconstructed with 40 μl of 10% methanol (v/v) and transferred into LC vial (2 ml, 12×32 mm) equipped with glass insert (250 μl, 5.8×29 mm) (Chromservis, Czech Republic). Acquity UPLC® I-Class (Waters, Millford, USA) coupled

with Xevo TQ-S equipped with electrospray ionization (Waters, Manchester, UK) was utilized. Analysis of CKs was performed according to previously described methodology (Svacinova et al., 2012). Analysis of auxins and ABA was performed with previously described method (Pencik et al., 2018). Data were processed with MassLynx v4.2 and TargetLynx V4.2 software (both Waters, Manchester, UK).

3.9. Optimization of extraction solvent composition

Plant extracts from 10 mg FW *Arabidopsis* seedlings and 10 mg FW T89 poplar leaves were prepared according to section 3.3. Each plant extract was prepared in three independent replicates. Additionally, identical plant extracts were prepared using modified Bieleski buffer instead (75% methanol, 20% water and 5% formic acid (v/v)). Collected supernatants were diluted with 2.5 ml formic acid (1 mol/l) and purified as described in section 3.4. Purified samples were analysed with UHPLC-MS/MS (see section 3.7). Endogenous concentration levels of plant hormones were calculated by standard isotope dilution method.

3.10. Development of DisperSpin SPE

Six independent extracts of 1 mg FW of *Arabidopsis* seedlings (section 3.3) were devided into two groups. The first group of three replicates was purified with cartridge SPE (section 3.4.) and second group with centrifugal dispersive SPE working with 10 mg of MCX sorbent (section 3.5.). Samples were analysed with UHPLC-MS/MS (section 3.7). Peak areas of internal standards recovered after purification were evaluated and compared.

Plant extracts were obtained from 10 mg FW *Arabidopsis* seedlings and 10 mg FW T89 poplar leaves (section 3.3). Three independent samples were purified with cartridge SPE and three replicates with DisperSpin SPE using 30 mg of MCX sorbent (section 3.6). Samples were analysed with UHPLC-MS/MS. Yields of internal standards were calculated and compared.

3.11. Characterization of DisperSpin SPE

Characterization of DisperSpin SPE was performed with full factorial design of experiment (Plackett and Burman, 1946). Four factors represented dimensions in four-dimensional experimental space. Incubation time was characterized in range 5 to 25 minutes, sorbent amount ranged between 2 and 30 mg, elution volume between 0.1 and 0.4 ml and elution

cycles were performed in number 1, 2 and 3. 16 samples and 3 center points prepared as follows represented this design of experiment. 0.5 ml of extraction solvent was spiked with mixture of phytohormonal standards (Table 1). Each sample was purified with DisperSpin SPE procedure with individual settings of factors (section 3.6). Samples were analysed with UHPLC-MS/MS. Yields of phytohormonal standards were calculated and obtained data were processed by multivariate analysis (Simca 17, Sartorius Stedim Data Analytics AB, Umeå, Sweden). Data were centered and standardized with unit-variance scaling. Principle component analysis (PCA) was performed to reveal data structure and check for outliers. Then, predicting variables (factors) were assigned to matrix X and predicted variables (yields of standards) to matrix Y. Partial least square (PLS) regression was used to calculate covariance between X and Y matrix and thus estimate association between factors and yields (Wold et al., 2001). Representative compounds were selected from each quadrant of PLS loading plot. Multiple linear regression (MLR) was used upon these representatives to estimate interaction between yield and investigated factors (Bauer and Curran, 2005). MLR model and design of experiment were calculated with Modde 13 software (Sartorius Stedim Data Analytics AB, Umeå, Sweden). Regression models were cross-validated and assessed in terms of goodness of fit (R^2) and goodness of prediction (Q^2).

3.12. Optimization of DisperSpin SPE

The optimization was performed with two types of extracts: *Arabidopsis* seedlings and T89 poplar leaves (see *Extraction of plant material*) purified with DisperSpin SPE procedure. Response surface methodology was used for the optimization (Box and Hunter, 1957; Bezerra et al., 2008). D-Optimal design of experiment with 6 degrees of freedom including 11 samples and 3 center points was selected. Following factors were optimized: Oasis® MCX sorbent amount in range of 2 to 30 mg and plant matrix amount in range of 2 to 20 mg FW. Samples including center points were analysed with UHPLC-MS/MS and signal to noise ratio (S/N) was monitored as a response. S/N = 10 was set as the minimal value. Response contours were calculated by quadratic model for each individual compound. All quadratic models were assessed regarding goodness of fit (R^2), goodness of prediction (Q^2). All calculations were performed with Modde 13 software (Sartorius Stedim Data Analytics AB, Umeå, Sweden). S/N was estimated by TargetLynx V4.2 software (Waters, Manchester, UK). Peak to peak algorithm with average noise level was used to calculate S/N.

3.13. Method validation

DisperSpin SPE method was validated according to guideline described in (Matuszewski et al., 2003). Solution of phytohormonal standards was prepared in following concentrations. High concentration level contained 1 pmol CKs, 50 pmol auxins and 50 pmol ABA per 10 µl of 10% methanol. The middle concentration level contained 0.1 pmol CKs, 10 pmol auxins and 10 pmol ABA per 10 µl. And finally, low concentration level contained 0.01 pmol CKs, 1 pmol auxins and 1 pmol ABA per 10 µl. Similarly, mixture of isotopically labelled standards in 10% MeOH was prepared. 10 µl of internal standard mixture contained 0.2 pmol CK bases, CK ribosides and CK *N*-glucosides, 0.5 pmol CK nucleotides and CK *O*-glucosides, 5 pmol auxins and 5 pmol ABA. Set of twelve independent technical replicates containing 10 mg FW *Arabidopsis* seedlings was extracted with 0.5 ml of weak extraction solvent (10% MeOH 5% FA). Four replicates were spiked with 10 µl of low level, four samples with 10 µl of middle level and four samples with 10 µl of high concentration level of phytohormonal standards. Additionally, each sample was spiked with 10 µl of mixture with isotopically labelled internal standards. All samples were processed by DisperSpin SPE purification procedure with 10 mg of sorbent. Another set of twelve replicates was prepared and spiked with phytohormonal standards after purification. Each sample was evaporated, dissolved in 40 µl of 10% MeOH and 10 µl was injected for UHPLC-MS/MS analysis. Validation parameters were calculated with following indicators: A = peak area of standard injected from neat solution, B = peak area of standard spiked before purification, C = peak area of standard spiked after purification. D = theoretical molar amount of standard. E = estimated molar amount of standard. Validation parameters were calculated as follows: Recovery = C/B, Process efficiency = C/A, Matrix effect = B/A, Relative matrix effect = 1 – B/A, Method accuracy = E/D – 1, Method precision = relative standard deviation of E (n = 6).

3.14. Robustness test

Following plant material (prepared according to section 3.2) was weighed into 2ml Eppendorf tubes. *Arabidopsis* seedlings (10 mg FW), T89 poplar leaves (10 mg FW), *Triticum aestivum* (10 mg FW), Norway spruce (10 mg FW), *Merchantia polymorpha* (2 mg DW) and *Nostoc sp.* (2 mg DW). Each material was prepared in four independent replicates. Samples were extracted (section 3.3) and purified with DisperSpin SPE (section 3.6). Purified samples were analysed with UHPLC-MS/MS and endogenous phytohormones were determined with isotope standard dilution method.

4. Conclusion and perspectives

We developed novel miniaturized method for extraction and purification of endogenous CKs, auxins and ABA in plants before UHPLC-MS/MS analysis. The method is based on dispersive mix-mode SPE. As the dispersion of bulk sorbent is designed in centrifugation filters, method was named "DisperSpin SPE". This novel purification technique was well characterised and optimized with modern approach of design of experiment. It was shown that DisperSpin SPE is practical, comfortable, fast, robust and cheap. High accuracy and precission was reported in method validation. Process efficiency of the method depends on balance of amount of SPE sorbent, plant tissue and elution volume. Whereas response of IAA and non-polar CKs is the best with low amount of sorbent, response of CK nucleotides is highest with high amount of sorbent. One of the benefit of DisperSpin SPE is easy and precise dosing of sorbent amount. Therefore, method can be adjusted simply and highly specifically according to analytical needs of targeted compounds. Thus, DisperSpin SPE represents versatile technique following the modern trends of plant hormone analysis. For the future perspectives, any other type of bulk SPE sorbent can be utilized. Hence, DisperSpin SPE can be included in analytical workflow for determination not only plant hormones but also any other bioactive compounds.

References

Bieleski, R.L. (1964). The problem of halting enzyme action when extracting plant tissues. Anal. Biochem. **9,** 431-442.

Anastassiades, M., Lehotay, S.J., Stajnbaher, D., and Schenck, F.J. (2003). Fast and easy multiresidue method employing acetonitrile extraction/partitioning and "dispersive solid-phase extraction" for the determination of pesticide residues in produce. Journal of Aoac International **86,** 412-431.

Arnon, D.I., and Hoagland, D.R. (1940). Crop production in artificial culture solutions and in soils with special reference to factors influencing yields and absorption of inorganic nutrients. Soil Science **50,** 463-485.

Barker, S.A. (2000). Matrix solid-phase dispersion. Journal of Chromatography A **885,** 115-127.

Bauer, D.J., and Curran, P.J. (2005). Probing interactions in fixed and multilevel regression: Inferential and graphical techniques. Multivariate Behavioral Research **40,** 373-400.

Bezerra, M.A., Santelli, R.E., Oliveira, E.P., Villar, L.S., and Escaleira, L.A. (2008). Response surface methodology (RSM) as a tool for optimization in analytical chemistry. Talanta **76,** 965-977.

Box, G.E.P., and Hunter, J.S. (1957). MULTI-FACTOR EXPERIMENTAL-DESIGNS FOR EXPLORING RESPONSE SURFACES. Annals of Mathematical Statistics **28,** 195-241.

Brunoni, F., Collani, S., Casanova-Saez, R., Simura, J., Karady, M., Schmid, M., Ljung, K., and Bellini, C. (2020). Conifers exhibit a characteristic inactivation of auxin to maintain tissue homeostasis. New Phytologist **226,** 1753-1765.

Cai, B.D., Yin, J., Hao, Y.H., Li, Y.N., Yuan, B.F., and Feng, Y.Q. (2015). Profiling of phytohormones in rice under elevated cadmium concentration levels by magnetic solid-phase extraction coupled with liquid chromatography tandem mass spectrometry. Journal of Chromatography A **1406,** 78-86.

Casanova-Saez, R., and Voss, U. (2019). Auxin Metabolism Controls Developmental Decisions in Land Plants. Trends in Plant Science **24,** 741-754.

Chen, Y.L., Wu, X., Li, Y.X., Yang, Y., Yang, D.N., Yin, S., Liu, L., and Sun, C.J. (2018). Simultaneous Determination of Seven Plant Growth Regulators in Melons and Fruits by Modified QuEChERS Coupled with Capillary Electrophoresis. Food Analytical Methods **11,** 2788-2798.

Chmelik, D., Hrouzek, P., Fedorko, J., Vu, D.L., Urajova, P., Mares, J., and Cerveny, J. (2019). Accumulation of cyanobacterial oxadiazine nocuolin A is enhanced by temperature shift during cultivation and is promoted by bacterial cohabitants in the culture. Algal Research-Biomass Biofuels and Bioproducts **44,** 8.

Choi, B.K., Hercules, D.M., and Gusev, A.I. (2001). Effect of liquid chromatography separation of complex matrices on liquid chromatography-tandem mass spectrometry signal suppression. Journal of Chromatography A **907,** 337-342.

Cutler, S.R., Rodriguez, P.L., Finkelstein, R.R., and Abrams, S.R. (2010). Abscisic Acid: Emergence of a Core Signaling Network. In Annual Review of Plant Biology, Vol 61, S. Merchant, W.R. Briggs, and D. Ort, eds (Palo Alto: Annual Reviews), pp. 651-679.

Deng, T., Wu, D.P., Duan, C.F., Yan, X.H., Du, Y., Zou, J., and Guan, Y.F. (2017). Spatial Profiling of Gibberellins in a Single Leaf Based on Microscale Matrix Solid-Phase Dispersion and Precolumn Derivatization Coupled with Ultraperformance Liquid Chromatography-Tandem Mass Spectrometry. Analytical Chemistry **89,** 9537-9543.

Dobrev, P.I., and Kaminek, M. (2002). Fast and efficient separation of cytokinins from auxin and abscisic acid and their purification using mixed-mode solid-phase extraction. Journal of Chromatography A **950,** 21-29.

Edwards, K.D., Takata, N., Johansson, M., Jurca, M., Novak, O., Henykova, E., Liverani, S., Kozarewa, I., Strnad, M., Millar, A.J., Ljung, K., and Eriksson, M.E. (2018). Circadian clock components control daily growth activities by modulating cytokinin levels and cell division-associated gene expression in Populus trees. Plant Cell and Environment **41,** 1468-1482.

Flokova, K., Tarkowska, D., Miersch, O., Strnad, M., Wasternack, C., and Novak, O. (2014). UHPLC-MS/MS based target profiling of stress-induced phytohormones. Phytochemistry **105,** 147-157.

Flores, M.I.A., Romero-Gonzalez, R., Frenich, A.G., and Vidal, J.L.M. (2011). QuEChERS-based extraction procedure for multifamily analysis of phytohormones in vegetables by UHPLC-MS/MS. Journal of Separation Science **34,** 1517-1524.

Fontanals, N., Borrull, F., and Marce, R.M. (2020). Mixed-mode ion-exchange polymeric sorbents in environmental analysis. Journal of Chromatography A **1609,** 13.

Gosetti, F., Mazzucco, E., Zampieri, D., and Gennaro, M.C. (2010). Signal suppression/enhancement in high-performance liquid chromatography tandem mass spectrometry. Journal of Chromatography A **1217,** 3929-3937.

Horgan, R. (1975). NEW CYTOKININ METABOLITE. Biochemical and Biophysical Research Communications **65,** 358-363.

Hoyerova, K., Gaudinova, A., Malbeck, J., Dobrev, P.I., Kocabek, T., Solcova, B., Travnickova, A., and Kaminek, M. (2006). Efficiency of different methods of extraction and purification of cytokinins. Phytochemistry **67,** 1151-1159.

Luo, X.T., Cai, B.D., Chen, X., and Feng, Y.Q. (2017). Improved methodology for analysis of multiple phytohormones using sequential magnetic solid-phase extraction coupled with liquid chromatography-tandem mass spectrometry. Analytica Chimica Acta **983,** 112-120.

Marchi, I., Viette, V., Badoud, F., Fathi, M., Saugy, M., Rudaz, S., and Veuthey, J.L. (2010). Characterization and classification of matrix effects in biological samples analyses. Journal of Chromatography A **1217,** 4071-4078.

Martinez, A.G., Liebanas, F.J.A., Valverde, R.S., Torres, M.E.H., Casinello, J.R., and Frenich, A.G. (2020). Multifamily Determination of Phytohormones and Acidic Herbicides in Fruits and Vegetables by Liquid Chromatography-Tandem Mass Spectrometry under Accredited Conditions. Foods **9,** 21.

Matuszewski, B.K., Constanzer, M.L., and Chavez-Eng, C.M. (2003). Strategies for the assessment of matrix effect in quantitative bioanalytical methods based on HPLC-MS/MS. Analytical Chemistry **75,** 3019-3030.

Novak, O., Napier, R., and Ljung, K. (2017). Zooming In on Plant Hormone Analysis: Tissue- and Cell-Specific Approaches. In Annual Review of Plant Biology, Vol 68, S.S. Merchant, ed (Palo Alto: Annual Reviews), pp. 323-348.

Novak, O., Henykova, E., Sairanen, I., Kowalczyk, M., Pospisil, T., and Ljung, K. (2012). Tissue-specific profiling of the Arabidopsis thaliana auxin metabolome. Plant Journal **72,** 523-536.

Novakova, L. (2013). Challenges in the development of bioanalytical liquid chromatography-mass spectrometry method with emphasis on fast analysis. Journal of Chromatography A **1292,** 25-37.

Pencik, A., Casanova-Saez, R., Pilarova, V., Zukauskaite, A., Pinto, R., Micol, J.L., Ljung, K., and Novak, O. (2018). Ultra-rapid auxin metabolite profiling for high-throughput mutant screening in Arabidopsis. Journal of Experimental Botany **69,** 2569-2579.

Plackett, R.L., and Burman, J.P. (1946). The design of optimum multifactorial experiments. Biometrika **33,** 305-325.

Plackova, L., Oklestkova, J., Pospiskova, K., Polakova, K., Bucek, J., Styskala, J., Zatloukal, M., Safarik, I., Zboril, R., Strnad, M., Dolezal, K., and Novak, O. (2017). Microscale magnetic microparticle-based immunopurification of cytokinins from Arabidopsis root apex. Plant Journal **89,** 1065-1075.

Poole, C.F. (2003). New trends in solid-phase extraction. Trac-Trends in Analytical Chemistry **22,** 362-373.

Rappsilber, J., Mann, M., and Ishihama, Y. (2007). Protocol for micro-purification, enrichment, pre-fractionation and storage of peptides for proteomics using StageTips. Nature Protocols **2,** 1896-1906.

Simura, J., Antoniadi, I., Siroka, J., Tarkowska, D., Strnad, M., Ljung, K., and Novak, O. (2018). Plant Hormonomics: Multiple Phytohormone Profiling by Targeted Metabolomics. Plant Physiology **177,** 476-489.

Singh, S., Letham, D.S., Jameson, P.E., Zhang, R., Parker, C.W., Bandenochjones, J., and Nooden, L.D. (1988). CYTOKININ BIOCHEMISTRY IN RELATION TO LEAF SENESCENCE .4. CYTOKININ METABOLISM IN SOYBEAN EXPLANTS. Plant Physiology **88,** 788-794.

Svacinova, J., Novak, O., Plackova, L., Lenobel, R., Holik, J., Strnad, M., and Dolezal, K. (2012). A new approach for cytokinin isolation from Arabidopsis tissues using miniaturized purification: pipette tip solid-phase extraction. Plant Methods **8,** 14.

Tarkowska, D., Novak, O., Flokova, K., Tarkowski, P., Tureckova, V., Gruz, J., Rolcik, J., and Strnad, M. (2014). Quo vadis plant hormone analysis? Planta **240,** 55-76.

Tureckova, V., Novak, O., and Strnad, M. (2009). Profiling ABA metabolites in Nicotiana tabacum L. leaves by ultra-performance liquid chromatography-electrospray tandem mass spectrometry. Talanta **80,** 390-399.

Vanstraelen, M., and Benkova, E. (2012). Hormonal Interactions in the Regulation of Plant Development. In Annual Review of Cell and Developmental Biology, Vol 28, R. Schekman, ed (Palo Alto: Annual Reviews), pp. 463-487.

Vcelarova, L., Skalicky, V., Chamrad, I., Lenobel, R., Kubes, M.F., Pencik, A., and Novak, O. (2021). Auxin Metabolome Profiling in the Arabidopsis Endoplasmic Reticulum Using an Optimised Organelle Isolation Protocol. International Journal of Molecular Sciences **22,** 18.

Wold, S., Sjostrom, M., and Eriksson, L. (2001). PLS-regression: a basic tool of chemometrics. Chemometrics and Intelligent Laboratory Systems **58,** 109-130.

Yan, H.Y., Wang, F., Wang, H., and Yang, G.L. (2012). Miniaturized molecularly imprinted matrix solid-phase dispersion coupled with high performance liquid chromatography for rapid determination of auxins in orange samples. Journal of Chromatography A **1256,** 1-8.

Zhang, Q.C., Li, G.K., Xiao, X.H., Zhan, S., and Gao, Y.J. (2016). Efficient and Selective Enrichment of Ultratrace Cytokinins in Plant Samples by Magnetic Perhydroxy-Cucurbit 8 uril Microspheres. Analytical Chemistry **88,** 4055-4062.

Zhang, Y., Li, Y.W., Hu, Y.L., Li, G.K., and Chen, Y.Q. (2010). Preparation of magnetic indole-3-acetic acid imprinted polymer beads with 4-vinylpyridine and beta-cyclodextrin as binary monomer via microwave heating initiated polymerization and their application to trace analysis of auxins in plant tissues. Journal of Chromatography A **1217,** 7337-7344.

Zhou, W.L., Yang, S., and Wang, P.G. (2017). Matrix effects and application of matrix effect factor. Bioanalysis **9,** 1839-1844.

Zurcher, E., and Muller, B. (2016). Cytokinin Synthesis, Signaling, and Function-Advances and New Insights. In International Review of Cell and Molecular Biology, Vol 324 (San Diego: Elsevier Academic Press Inc), pp. 1-38.

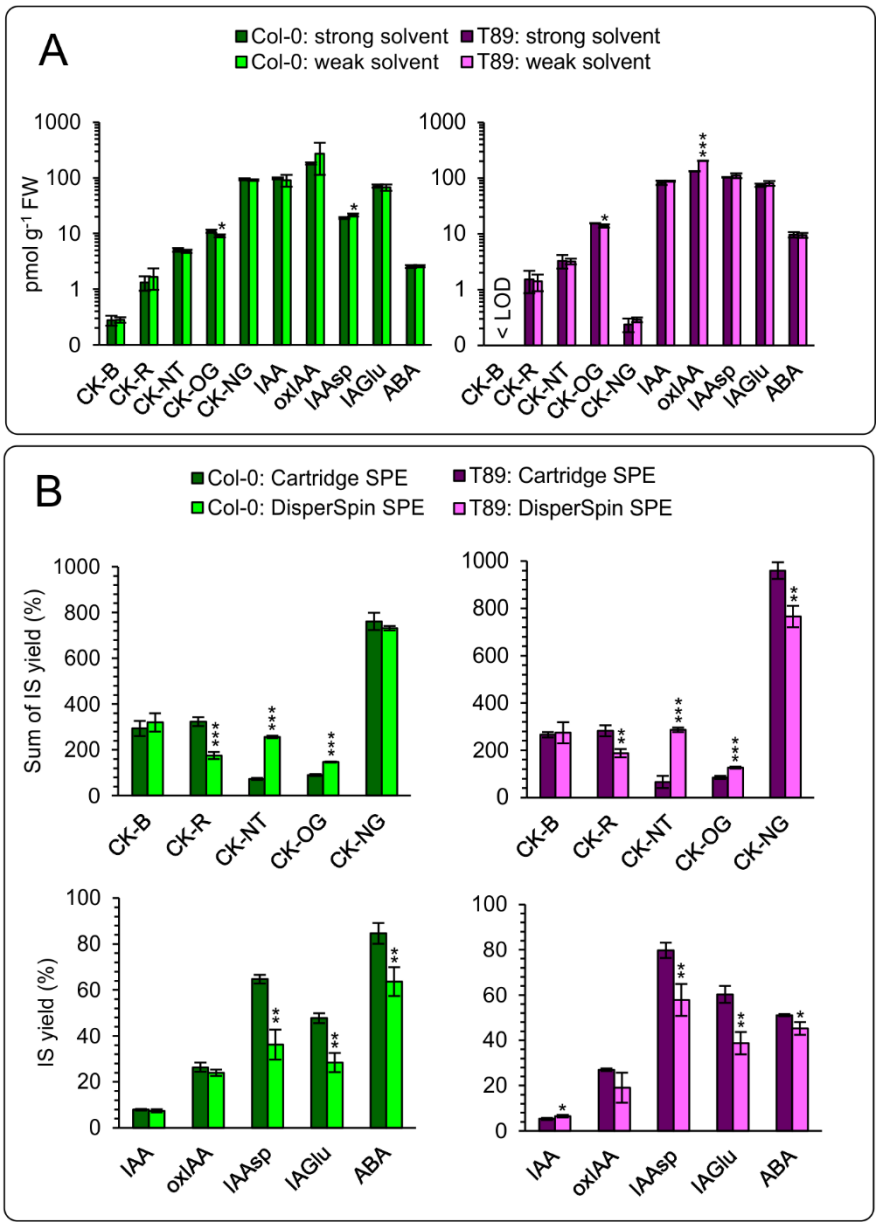

Figure 1. (A) Profile of endogenous phytohormones (pmol/g FW) extracted from 10 mg FW Col-0 *Arabidopsis* seedlings (green bars) and 10 mg FW T89 poplar leaves (violet bars) by strong solvent (75% MeOH, 5% FA, 20% water; dark bars) and weak solvent (10% MeOH, 5% FA, 85% water; light bars). **(B)** Yields of internal standards added into extracts of 10 mg FW Col-0 *Arabidopsis* seedlings (green bars) and 10 mg FW T89 poplar leaves (violet bars) purified by cartridge SPE (dark bars) and DisperSpin SPE (light bars). All values show mean ± SD (n = 3). Asterisks are result of independent two-sample student's t-test. Significance levels α = 0.05 (*), α = 0.01 (**) and α = 0.001 (***). < LOD refers to statement that concentration of compound was under limit of detection.

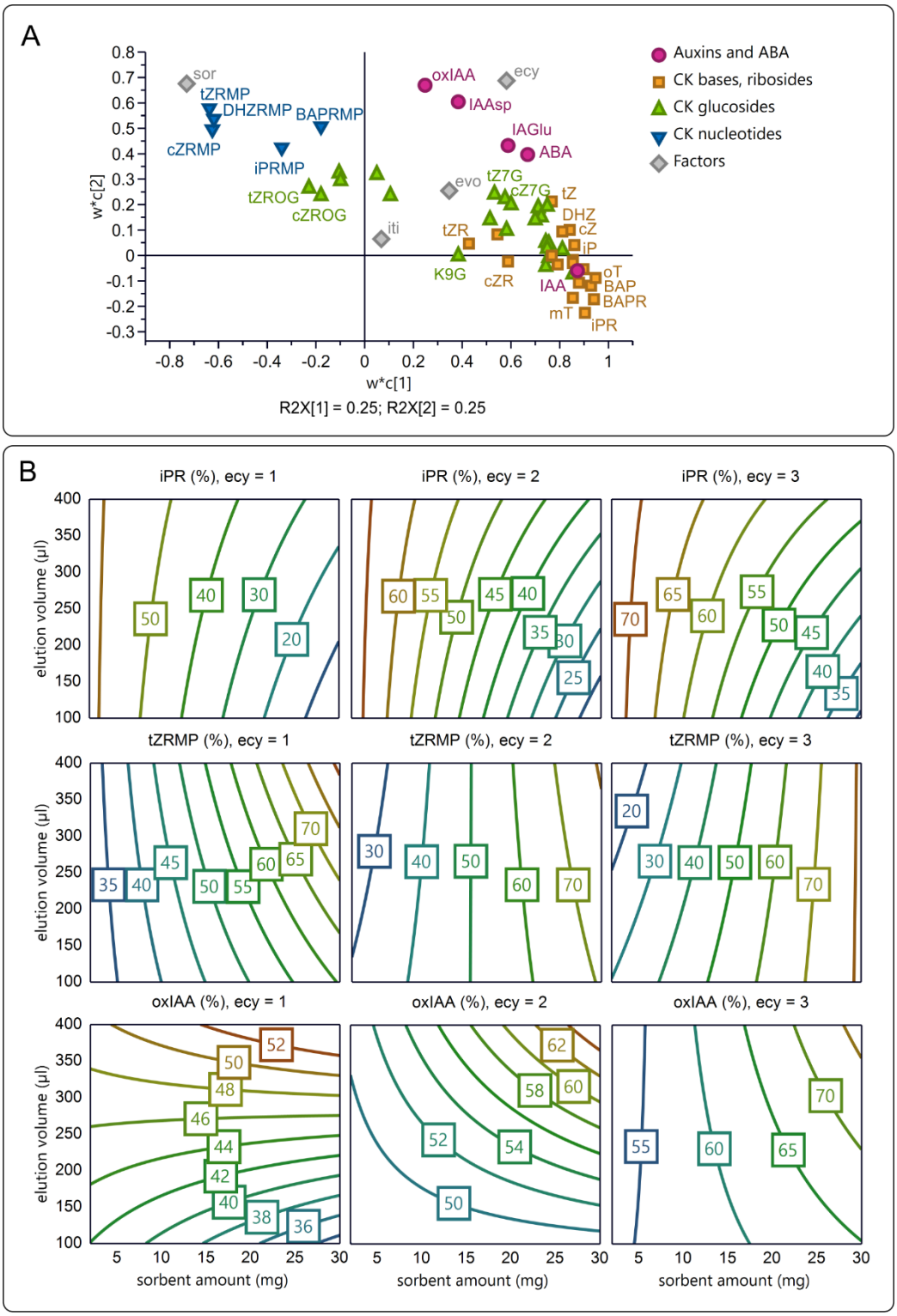

Figure 2. Characterization of DisperSpin SPE method. (A) PLS loading plot of covariance between factors and yield of phytohormonal standards purified with DisperSpin SPE. Abbreviations refer to following factors: incubation time (iti), sorbent amount (sor), elution volume (evo), elution cycles (ecy). R2X values refer to total variance explained by x- and y-axis. (B) Contour plots of phytohormonal standard yields (%) predicted by sor, evo and ecy factors calculated by MLR. All values were predicted using 19 independent samples prepared in respect with full factorial design of experiment.

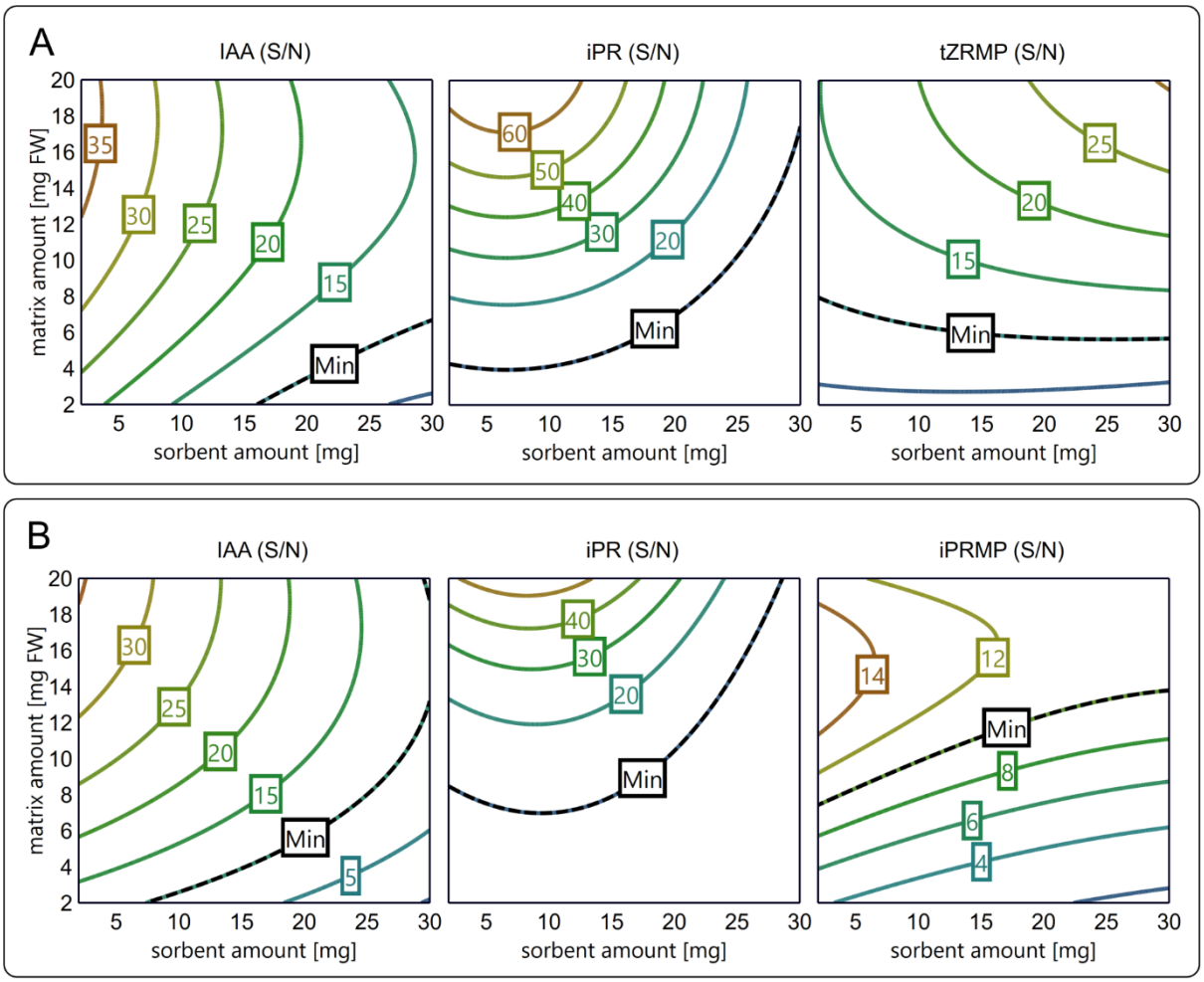

Figure 3. Optimization of DisperSpin SPE. S/N of endogenous phytohormones predicted by sorbent amount and matrix amount in *Arabidopsis* seedlings **(A)** and T89 poplar leaves **(B)**. "Min" lines refer to limit of quantification (S/N = 10). Regression models were calculated by MLR with 14 independent samples prepared regarding to response surface methodology.

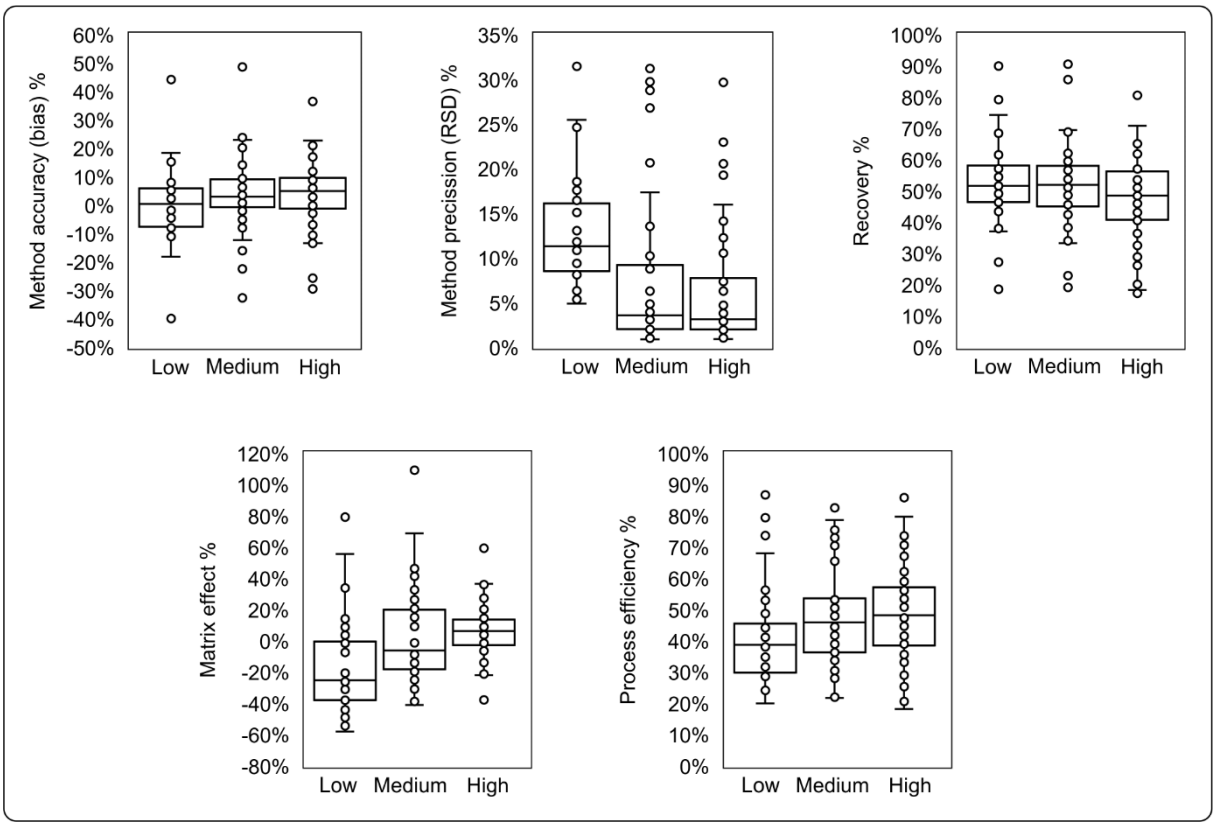

Figure 4. Validation of DisperSpin SPE method. Data points refer to values of validation parameters calculated for each individual compound. Box plots refer to overall median value at low, medium and high concentration levels ranged by quartiles and standard deviation as whiskers. Validation parameters were calculated according to recommended guideline.

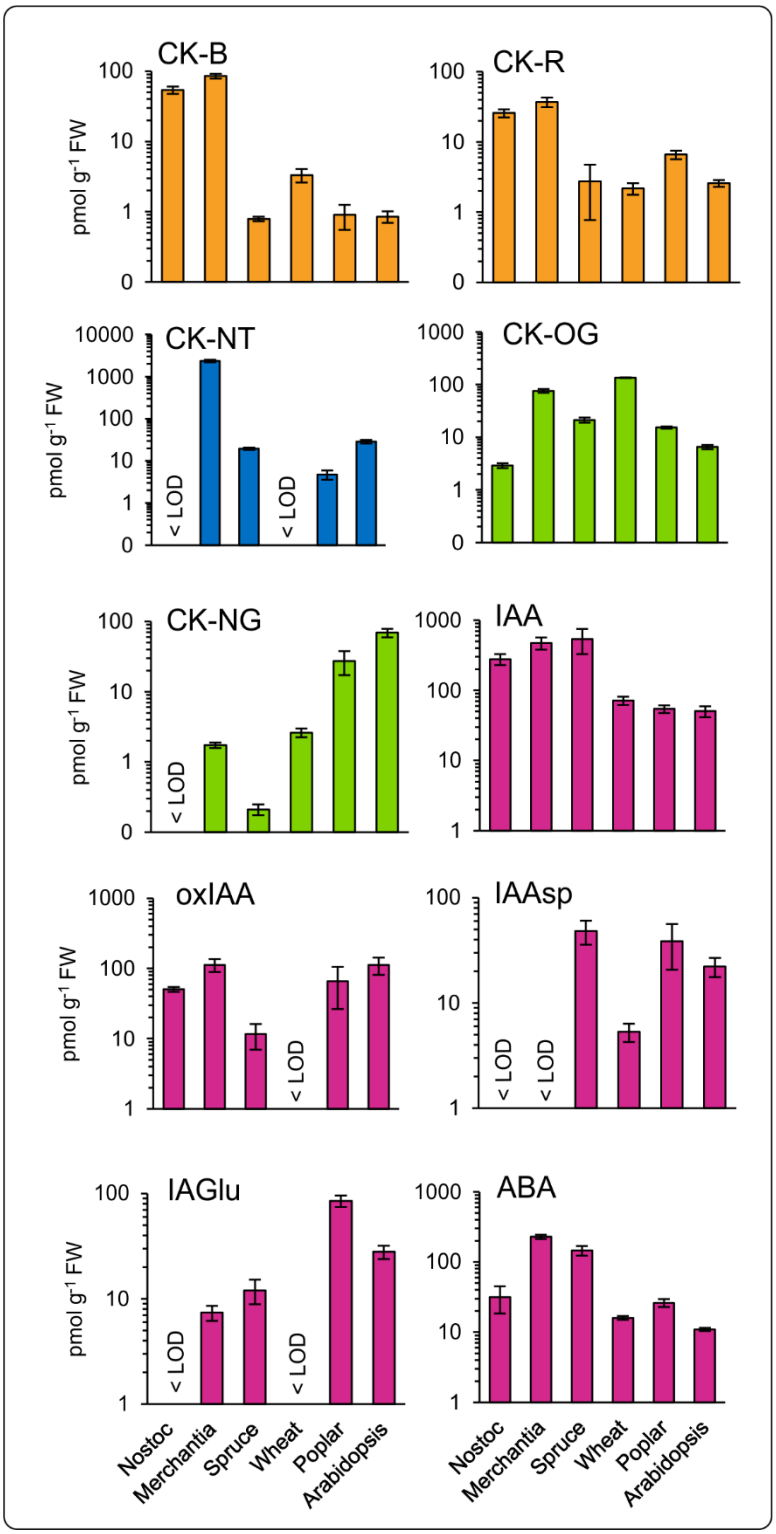

Figure 5. Robustness test of DisperSpin SPE. Relative endogenous concentration levels of phytohormones profiled in various plant species (pmol/g FW). Values show mean (n = 4). < LOD refers to statement that concentration of compound was under limit of detection.

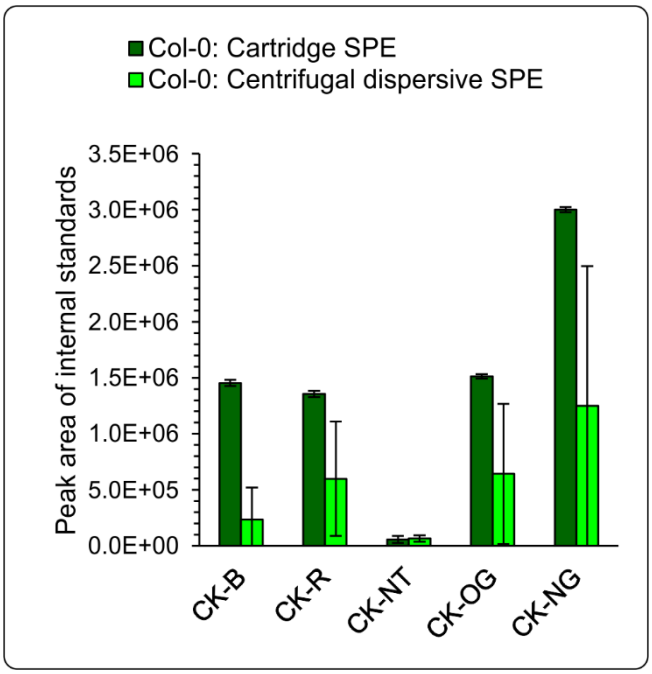

Figure S1. Comparison of peak areas of internal standards recovered from Arabidopsis seedling extract (1 mg FW) after purification with Cartridge SPE (dark bars) and centrifugal dispersive SPE (light bars). Values show mean ± SD (n = 3).

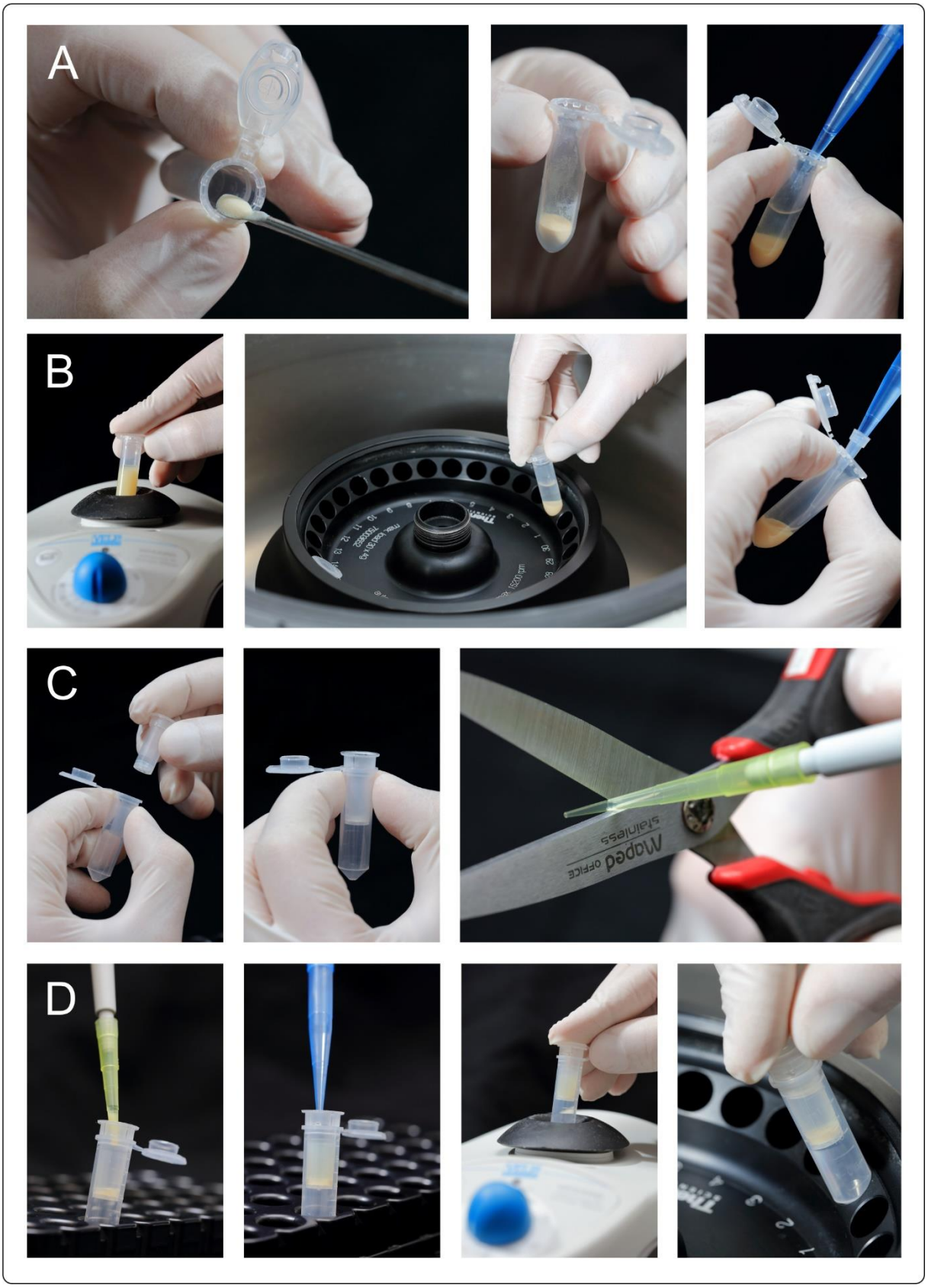

Figure S2. Workflow of DisperSpin SPE method. (A) Weighing of bulk sorbent. (B) Conditioning of bulk sorbent. (C) Assembling of centrifugation filter. (D) Dosing of bulk sorbent onto a centrifugation filter. (E) Loading of sample and filtration of bulk sorbent.

Table 1. List of targeted compounds and isotopic labelled internal standards. Compounds marked with asterisk (IAGlc and oxIAGlc) were used only in the validation step.

ID	Abbreviation	Compound name	IS abbreviation	IS pmol per sample
1	tZ	*trans*-zeatin	[13C5]-tZ	0.2
2	cZ	*cis*-zeatin	[13C5]-cZ	0.2
3	DHZ	dihydrozeatin	[2H3]-DHZ	0.2
4	iP	isopentenyladenine	[2H6]-iP	0.2
5	BAP	benzyladenine	[2H7]-BAP	0.2
6	oT	*ortho*-topolin	[15N4]-oT	0.2
7	mT	*meta*-topolin	[15N4]-mT	0.2
8	pT	*para*-topolin	[15N4]-pT	0.2
9	K	kinetin	[15N4]-K	0.2
10	tZR	*trans*-zeatin riboside	[2H5]-tZR	0.2
11	cZR	*cis*-zeatin riboside	(see tZR)	
12	DHZR	dihydrozeatin riboside	[2H3]-DHZR	0.2
13	iPR	isopentenyladenosine	[2H6]-iPR	0.2
14	BAPR	benzyladenine riboside	[2H7]-BAPR	0.2
15	oTR	*ortho*-topolin riboside	[15N4]-oTR	0.2
16	mTR	*meta*-topolin riboside	[15N4]-mTR	0.2
17	pTR	*para*-topolin riboside	[15N4]-pTR	0.2
18	KR	kinetin riboside	(see BAPR)	
19	tZRMP	*trans*-zeatin riboside-5'-monophosphate	[2H5]-tZRMP	0.5
20	cZRMP	*cis*-zeatin riboside-5'-monophosphate	(see tZRMP)	
21	DHZRMP	dihydrozeatin riboside-5'-monophosphate	[2H3]-DHZRMP	0.5
22	iPRMP	isopentenyladenine riboside-5'-monophosphate	[2H6]-iPRMP	0.5
23	BAPRMP	benzyladenine riboside-5'-monophosphate	(see iPRMP)	
24	tZOG	*trans*-zeatin-*O*-glucoside	[2H5]-tZOG	0.5
25	cZOG	*cis*-zeatin-*O*-glucoside	(see tZOG)	
26	DHZOG	dihydrozeatin-*O*-glucoside	[2H7]-DHZOG	0.5
27	tZROG	*trans*-zeatin riboside-*O*-glucoside	[2H5]-tZROG	0.5
28	cZROG	*cis*-zeatin riboside-*O*-glucoside	(see tZROG)	
29	DHZROG	dihydrozeatin riboside-*O*-glucoside	[2H3]-DHZROG	0.5
30	tZ7G	*trans*-zeatin-*N7*-glucoside	[2H5]-tZ7G	0.2
31	cZ7G	*cis*-zeatin-*N7*-glucoside	[15N4]-cZ7G	0.2
32	DHZ7G	dihydrozeatin-*N7*-glucoside	(see tZ7G)	
33	iP7G	isopentenyladenine-*N7*-glucoside	[2H6]-iP7G	0.2
34	BAP7G	benzyladenine-*N7*-glucoside	(see iP7G)	
35	oT7G	*ortho*-topolin-*N7*-glucoside	[15N4]-oT7G	0.2
36	mT7G	*meta*-topolin-*N7*-glucoside	[15N4]-mT7G	0.2
37	pT7G	*para*-topolin-*N7*-glucoside	[15N4]-pT7G	0.2
38	tZ9G	*trans*-zeatin-*N9*-glucoside	[2H5]-tZ9G	0.2
39	cZ9G	*cis*-zeatin-*N9*-glucoside	(see tZ9G)	
40	DHZ9G	dihydrozeatin-*N9*-glucoside	[2H3]-DHZ9G	0.2
41	iP9G	isopentenyladenine-*N9*-glucoside	[2H6]-iP9G	0.2
42	BAP9G	benzyladenine-*N9*-glucoside	[2H7]-BAP9G	0.2
43	oT9G	*ortho*-topolin-*N9*-glucoside	[15N4]-oT9G	0.2
44	mT9G	*meta*-topolin-*N9*-glucoside	[15N4]-mT9G	0.2
45	pT9G	*para*-topolin-*N9*-glucoside	[15N4]-pT9G	0.2
46	K9G	kinetin-*N9*-glucoside	(see K9G)	
47	IAA	indole-3-acetic acid	[13C6]-IAA	5.0
48	oxIAA	2-oxo-indole-3-acetic acid	[13C6]-oxIAA	5.0
49	IAAsp	indole-3-acetyl-L-aspartic acid	[13C6]-IAAsp	5.0
50	IAGlu	indole-3-acetyl-L-glutamic acid	[13C6]-IAGlu	5.0
51	IAGlc *	indole-3-acetic acid glucosyl ester	[13C6]-IAGlc	5.0
52	oxIAGlc *	2-oxo-indole-3-acetic acid glucosyl ester	[13C6]-oxIAGlc	5.0
51	ABA	abscisic acid	[2H6]-ABA	5.0

Table S1. Validation of DisperSpin SPE method. Values represent the mean result (n = 6) of particular validation parameter obtained after extraction of 10 mg FW of 10-days old Arabidopsis seedlings spiked with low/middle/high concentration level of phytohormonal standard.

Compound	Accuracy (%)	Precision (%)	Recovery (%)	Process efficiency (%)	Relavive matrix effect (%)
tZ	6/15/23	11/2/2	56/62/67	56/73/80	0/18/19
cZ	18/23/23	10/2/3	68/63/63	68/82/86	-1/30/36
DHZ	6/4/7	6/3/3	53/58/57	58/65/68	9/12/20
iP	-11/3/12	12/2/2	27/35/48	42/51/57	56/46/18
BAP	-4/1/3	18/4/3	74/33/47	38/44/51	-49/33/8
oT	5/1/6	15/2/2	38/38/48	40/42/47	6/9/-2
mT	-10/-2/8	12/1/3	44/46/59	44/55/62	-2/22/6
pT	3/7/8	9/6/2	46/52/65	53/66/75	14/26/16
K	15/26/21	9/1/2	62/53/55	57/70/71	-8/33/27
tZR	-40/-12/-5	25/6/4	44/49/43	20/39/43	-54/-19/-1
cZR	-18/4/8	16/2/4	49/51/46	29/47/48	-42/-8/5
DHZR	3/2/-6	8/2/1	48/50/44	38/48/48	-21/-4/9
iPR	-/-7/-5	-/4/2	-/45/43	-/36/41	-/-19/-4
BAPR	8/20/7	13/4/4	37/42/36	25/32/34	-31/-25/-6
oTR	-7/3/14	8/1/1	39/48/52	29/36/45	-27/-23/-14
mTR	0/0/-2	9/1/2	51/54/49	41/46/51	-20/-16/4
pTR	-3/1/1	8/1/1	53/56/51	38/45/49	-28/-20/-4
KR	44/49/36	13/5/7	47/49/45	35/40/44	-26/-18/-3
tZRMP	-/-16/3	-/3/8	-/19/17	-/22/18	-/15/5
cZRMP	-/12/17	-/3/5	-/23/20	-/28/21	-/22/3
DHZRMP	10/7/7	12/4/7	19/23/18	33/28/21	79/21/16
iPRMP	-/-23/-13	-/27/12	-/34/26	-/71/36	-/109/36
BAPRMP	-/-/-26	-/-/30	-/-/29	-/-/33	-/-/14
tZOG	-/6/10	-/3/5	-/55/51	-/50/56	-/-8/10
tZROG	-11/-33/-30	19/10/14	46/41/33	26/24/25	-45/-41/-22
cZOG	-40/-8/-11	31/1/11	58/54/51	24/44/45	-58/-18/-12
cZROG	-2/-2/-5	18/4/5	50/42/35	25/35/35	-49/-18/0
DHZOG	0/2/4	9/3/2	58/57/52	44/53/56	-24/-6/8
DHZROG	16/14/10	9/1/4	51/46/38	36/41/40	-30/-11/7
tZ7G	-/0/1	-/17/3	-/51/45	-/51/51	-/0/14
cZ7G	-8/-1/2	81/9/1	56/52/47	32/51/53	-43/-1/13
DHZ7G	-11/4/4	25/3/3	56/54/48	31/51/52	-45/-5/8
iP7G	-/1/-3	-/14/2	-/57/52	-/54/51	-/-6/-1
BAP7G	1/3/3	8/1/2	57/58/53	43/52/54	-25/-12/0
oT7G	0/7/17	6/3/2	57/62/62	42/54/63	-26/-13/2
mT7G	8/-2/-7	6/5/4	62/57/49	46/49/48	-26/-14/-2
pT7G	-5/-8/-13	12/10/11	61/63/57	40/46/46	-35/-27/-19
tZ9G	-/24/18	-/9/3	-/43/36	-/39/39	-/-9/7
cZ9G	9/10/5	12/3/2	52/48/41	39/46/45	-24/-4/9
DHZ9G	2/8/5	12/2/2	49/47/40	36/45/45	-26/-5/10
iP9G	1/11/9	25/3/2	57/55/48	32/45/46	-44/-19/-4
BAP9G	-5/0/3	9/2/3	48/51/48	29/35/41	-38/-31/-14
oT9G	3/3/0	13/1/2	52/54/48	31/33/38	-40/-39/-21
mT9G	-9/3/8	9/5/2	63/61/55	49/54/59	-23/-12/6
pT9G	-2/3/8	9/5/5	54/59/58	41/52/60	-25/-13/3
K9G	-10/-5/-12	19/5/6	46/48/37	29/34/35	-38/-30/-7
IAA	-/10/9	-/29/21	-/69/71	-/22/29	-/69/59
oxIAA	-/-1/0	-/31/20	-/69/62	-/52/57	-/25/9
IAAsp	-8/6/0	7/30/20	90/92/81	87/79/74	4/15/10
IAGlu	-3/10/8	5/29/19	91/91/82	74/65/67	19/28/18
IAGlc	5/4/11	32/14/16	43/52/49	29/30/35	34/41/29
oxIAGlc	-/-3/2	-/21/23	-/23/22	-/28/31	-/-23/-38
ABA	17/9/21	5/9/14	79/86/81	79/75/75	0/12/7

Supplement I

Supplement II

Supplement III

Supplement IV

Supplement V

Supplement VI

Supplement VII

Supplement VIII

Petřík I, Pěnčík A, Stýskala J, Tranová L, Amakorová P, Strnad M, Novák O. 2024. Rapid profiling of cytokinins using supercritical fluid chromatography coupled with tandem mass spectrometry. Anal Chim Acta 1285, 342010.

Analytica Chimica Acta 1285 (2024) 342010

Contents lists available at ScienceDirect

Analytica Chimica Acta

journal homepage: www.elsevier.com/locate/aca

Rapid profiling of cytokinins using supercritical fluid chromatography coupled with tandem mass spectrometry

Ivan Petřík [a], Aleš Pěnčík [a], Jakub Stýskala [b], Lenka Tranová [b], Petra Amakorová [a], Miroslav Strnad [a], Ondřej Novák [a,*]

[a] Laboratory of Growth Regulators, The Czech Academy of Sciences, Institute of Experimental Botany & Palacký University, Faculty of Science, Šlechtitelů 27, CZ-78371, Olomouc, Czech Republic

[b] Department of Organic Chemistry, Palacký University, Faculty of Science, 17. listopadu 1192/12, CZ-77146, Olomouc, Czech Republic

HIGHLIGHTS

- 37 cytokinins analysed in 9 min.
- Limits of detection close to 0.03 fmol.
- Accuracy and precision close to 15 %.
- Low matrix effect for key metabolites.
- Endogenous cytokinins determined in *Arabidopsis* seedlings.

GRAPHICAL ABSTRACT

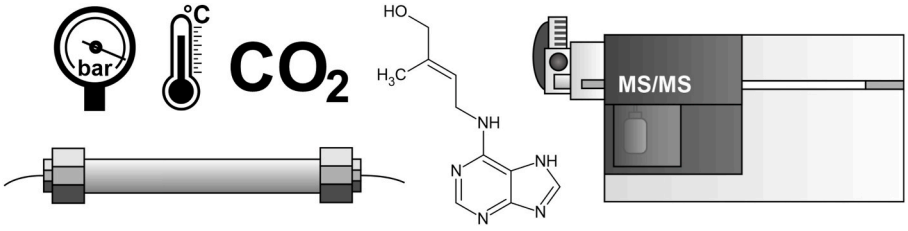

ARTICLE INFO

Keywords:
UHPSFC-MS/MS
Separation
Quantification
Phytohormone
Cytokinin
Arabidopsis

ABSTRACT

Background: The determination of plant hormones is still a very challenging analytical discipline, mainly due to their low concentration in complex plant matrices. Therefore, the involvement of very sensitive high-throughput techniques is required. Cytokinins (CKs) are semi-polar basic plant hormones regulating plant growth and development. Modern methods for CK determination are currently based on ultra-high performance liquid chromatography-tandem mass spectrometry (UHPLC-MS/MS), which enables the separation of CK isomeric forms occurring endogenously in plants. Here, ultra-high performance supercritical fluid chromatography coupled with tandem mass spectrometry (UHPSFC-MS/MS) was used for the simultaneous determination of 37 CK metabolites.

Results: The chromatographic conditions were tested on three different columns with various retention mechanisms. Hybrid silica modified with 2-picolylamine was selected as the stationary phase. Several parameters such as column temperature, back pressure regulation, mobile phase composition and make-up solvent were investigated to achieve efficient separation of CK isomers and reasonable sensitivity. Compared to UHPLC-MS/MS, a 9-min chromatographic analysis using a mobile phase of supercritical CO_2 and 5 mM ammonia in methanol represents a three-fold acceleration of total run time. The quantification limit of UHPSFC-MS/MS method was in the range of 0.03–0.19 fmol per injection and the method validation showed high accuracy and precision (below 15 % for most analytes). The method was finally applied to the complex plant matrix of the model plant *Arabidopsis thaliana* and the obtained profiles of CK metabolites were compared with the results from the conventional UHPLC-MS/MS method.

* Corresponding author.
E-mail address: novako@ueb.cas.cz (O. Novák).

https://doi.org/10.1016/j.aca.2023.342010
Received 19 July 2023; Received in revised form 10 October 2023; Accepted 7 November 2023
Available online 15 November 2023

Significance: The presented work offers a novel approach for quantification of endogenous CKs in plants. Compared to the conventional UHPLC-MS/MS, the total run time is shorter and the matrix effect lower for the key CK metabolites. This approach opens the opportunity to utilize UHPSFC-MS/MS instrumentation for targeted plant hormonomics including other plant hormone families.

1. Introduction

Cytokinins (CKs) are naturally occurring low-molecular-weight bioactive compounds. As a prominent class of plant hormones, they play an irreplaceable role in the regulation of cell division, growth, organ development, leaf expansion or plant senescence. From a chemical point of view, CKs are N^6-substituted derivatives of adenine, where the substituent on N^6 position determines the CK-type. Nowadays, several naturally occurring types of CK are known in the major plant model *Arabidopsis thaliana*: isopentenyl adenine (iP) and its hydroxylated forms *trans*-zeatin (*t*Z), *cis*-zeatin (*c*Z) and dihydrozeatin (DHZ). Moreover, CK types with aromatic N^6-substituents, such as benzylaminopurine (BA) and its hydroxylated variants *ortho*-topolin (*o*T) and *meta*-topolin (*m*T), have also been well known for several decades [1]. Furthermore, N^6-furfuryl-adenine known as kinetin (K) was discovered as the first CK in the middle of 20th century [2]. However, the natural occurrence of K and aromatic CKs have never been proven in *Arabidopsis*, they are important plant growth regulators for micropropagation and in vitro cultivation [3,4].

Substitution at the N^7 and N^9 positions of the adenine moiety determines the metabolic groups. CK bases have been described as bioactive compounds, while CK N^9-ribosides are considered as a transport form with low CK activity in bioassays [5]. CK homeostasis in plants is maintained by glycosylation. CK N^7 glucosides and N^9-glucosides lead to irreversible metabolism. CK *O*-glucosides, whose glucosyl moiety is localised on the hydroxylated N^6-side chain, are considered as storage products of reversible metabolism [6–8]. The combination of all these substitutions provides a group of 37 CK compounds (Figure 1, Table A.1). Knowledge of their endogenous levels in various plant organs and tissues, together with the distribution of CK metabolites during plant growth and development, may shed the light on so far unexplored physiological processes. Therefore, determination of CKs in plants is important part of plant research.

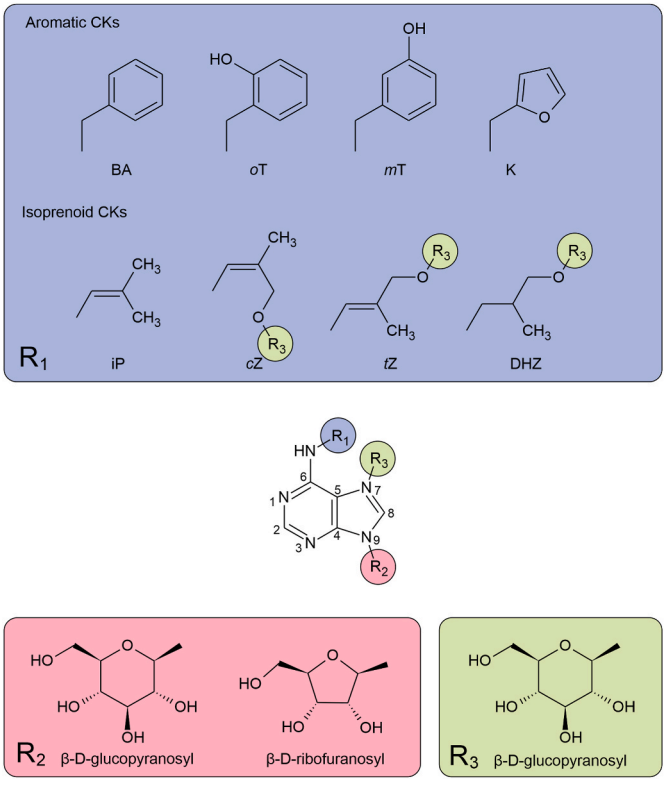

Fig. 1. Chemical structure of endogenous cytokinins.

Analysis of CKs, as well as other plant hormones, is a very challenging task. Firstly, their endogenous concentrations are usually very low (fmol to pmol per gram of fresh weight; FW) and highly sensitive instruments such as tandem mass spectrometers (MS/MS) must be used to overcome this limitation [9,10]. Second, due to the complexity of the plant matrix, at least one-step purification of the plant extract is crucial to obtain sufficient signal responses. Moreover, the addition of labelled internal standards ensures an accurate estimation of phytohormonal content. Lastly, frequent structural isomers in the CK portfolio require high-efficient separation techniques such as ultra-high performance liquid chromatography (UHPLC).

It is well known that separation efficiency depends on the stationary phase (SP) diameter and the mobile phase velocity in the chromatographic system [11]. UHPLC combines high velocity and sub-2μm SPs and therefore represents one of the most efficient chromatographic techniques. However, increasing efficiency and reducing analysis time are not infinitive. Modern CK profiling methods based on UHPLC-MS/MS, including efficient separation of their isomers, therefore take at least 20–30 min per run [12,13].

A new generation of MS/MS-compatible supercritical fluid chromatographs (SFCs) has recently been introduced. These systems utilize supercritical CO_2 ($scCO_2$) as the mobile phase, which can be modified with miscible organic co-solvents. Ultra-high performance supercritical fluid chromatography (UHPSFC) combines the advantages of UHPLC (high separation efficiency) and gas chromatography (low viscosity of mobile phase), resulting in a breakthrough of chromatographic performance. Since the polarity of mobile phase can be altered by co-solvent, semi-polar analytes such as CKs can be separated with SFC.

Despite evident benefits, UHPSFC-MS/MS is still a pioneering technology compared to UHPLC-MS/MS. Over the last decade, barely 200 studies have been published utilizing SFC coupled with MS detectors [14]. Majority of them dealt with the determination of compounds important for pharmaceutics, industry, environment, food or natural products. However, none of them focused on plant hormone research. Here we present that UHPSFC-MS/MS enables rapid screening of the CK profile in plants. Importantly, maintaining the separation efficiency despite the higher speed of analysis allowed sufficient separation of all CK isomers. In addition, the use of highly sensitive MS/MS-based detection ensured a reasonable sensitivity of the method. Our data also show a comparison with the conventional UHPLC-MS/MS method and suggest another possible direction of SFC applicability in plant hormone research.

2. Material and methods

2.1. Chemicals and reagents

A bottle of pressurised liquid CO_2 5.3 grade (99,9993 %) was purchased from Linde Gas, a.s. (Czech Republic). Methanol, ethanol, acetonitrile (ACN), isopropanol, formic acid and acetic acid, all in LC-MS grade, were purchased from Merck (Darmstadt, Germany). Ammonia hydroxide solution 25 % (v/v) was obtained from Honeywell Fluka™ (Bucharest, Romania). Deionised water was produced in lab by Millipore Direct-Q® 3 UV system (Millipore, Bedford, MA, USA). A collection of

CK standards and isotopic labelled internal standards were obtained from Olchemim Ltd. (Olomouc, Czech Republic) and from Faculty of Science, Palacký University in Olomouc (Czech Republic). CK N^7-glucoside and CK N^9-glucoside isotopic labelled standards were prepared according to a previously published procedure [15]. All standards in analytical purity are listed in Table A.1. Murashige & Skoog medium and agar were purchased from Duchefa Biochemie (Haarlem, Netherlands), sucrose and morpholinoethanesulfonic acid from Sigma Aldrich (St. Louis, MO, USA).

2.2. UHPSFC-MS/MS instrumentation and conditions

All experiments were performed with an Agilent 1260 Infinity II LC/SFC hybrid system equipped with binary solvent delivery pumps operating at a pressure limit of 600 bar in SFC mode and 800 bar in LC mode (Agilent Technologies, Santa Clara, CA, USA). The multisampler contained a sample loop allowing injection in the range 0.1–90 μL in SFC mode and 0.1–100 μL in LC mode. All samples in SFC mode were injected at a draw speed of 0.1 mL min^{-1}, an eject speed of 0.5 mL min^{-1} and then waited 1.2 s after draw. Feed injection was not used. The flushing pump for washing the sample loop in SFC mode was filled with methanol. The 4-position multicolumn thermostat was equipped with two independent temperature zones. The backpressure regulator has been integrated into the SFC control module operating in the pressure range of 90–400 bar. After chromatography separation, the sample was delivered into the transfer line using the split flow mode via T-splitter interface. The sample in the transfer line was dissolved in make-up solvent delivered by isocratic pump.

The chromatographic system was coupled to an Agilent 6495B Triple Quadrupole equipped with electrospray ionization (ESI). Nitrogen was used as the ion source and collision gas. Source and iFunnel parameters were optimised using the Agilent MassHunter Source Optimizer tool for 6400 series Triple quadrupoles, version 9.00. The optimal gas temperature was 130 °C, gas flow 14 L min^{-1} and nebulizer pressure 25 psi. The sheath gas flowed 12 L min^{-1} and the sheath temperature was 400 °C. All compounds were analysed in ESI+ polarity. The capillary voltage was set at 2800 V. The low pressure voltage in iFunnel was set at 80 V and the high pressure voltage at 130 V. The MS/MS system was operated

Table 1
Validation of SFC-MS/MS method.

	Compound	LOD[a]	LOQ[b]	Linear range[c]	R^2[d]	Accuracy[e] (%)	Precision[f] (%)
CK bases							
1	*t*Z	0.168	0.563	0.5–1000	0.9994	3/9/5	11/6/5
2	*c*Z	0.057	0.189	0.5–1000	0.9996	1/2/6	5/2/4
3	DHZ	0.133	0.445	0.5–1000	0.9988	15/6/2	8/3/2
4	iP	0.102	0.340	0.5–1000	0.9995	14/11/12	13/6/3
5	BA	0.080	0.268	0.5–1000	0.9998	54/3/5	24/4/2
6	*o*T	0.074	0.246	0.5–1000	0.9995	28/2/3	13/7/2
7	*m*T	0.028	0.093	0.5–1000	0.9999	5/4/2	15/3/4
8	K	0.068	0.228	0.5–1000	0.9999	24/1/1	8/5/2
CK ribosides							
9	*tZR*	0.100	0.333	0.1–1000	0.9986	8/1/9	1/3/3
10	*c*ZR	0.029	0.095	0.1–1000	0.9995	–/44/36	–/2/2
11	DHZR	0.072	0.240	0.1–100	0.9991	19/6/12	2/2/3
12	iPR	0.031	0.104	0.5–1000	0.9996	33/15/15	14/6/2
13	BAR	0.024	0.079	0.05–1000	0.9995	9/2/6	6/5/5
14	*o*TR	0.030	0.100	0.5–1000	0.9998	6/7/9	11/5/5
15	*m*TR	0.044	0.145	0.5–1000	0.9994	1/6/8	9/4/8
16	KR	0.080	0.253	0.1–1000	0.9997	54/59/60	8/4/7
CK *O*-glucosides							
17	*t*ZOG	0.022	0.073	0.5–1000	0.9998	–/4/5	–/9/3
18	*c*ZOG	0.038	0.128	0.5–1000	0.9998	25/4/4	8/9/3
19	DHZOG	0.112	0.372	0.5–1000	0.9998	4/2/2	9/2/2
20	*t*ZROG	0.137	0.446	0.5–1000	0.9995	–/26/17	–/6/5
21	*c*ZROG	0.179	0.596	0.5–1000	0.9993	–/2/9	–/14/4
22	DHZROG	0.173	0.578	0.5–1000	0.9999	10/3/9	15/10/2
CK N^7-glucosides							
23	*t*Z7G	0.067	0.225	0.5–1000	0.9995	–/7/7	–/34/9
24	*c*Z7G	0.123	0.410	0.5–500	0.9988	–/15/4	–/9/6
25	DHZ7G	0.093	0.310	0.5–1000	0.9996	20/2/6	53/9/4
26	iP7G	0.060	0.200	0.5–1000	0.9989	–/12/7	–/15/9
27	BA7G	0.028	0.093	1–1000	0.9992	–/43/9	–/6/21
28	*o*T7G	0.087	0.290	0.1–1000	0.9991	10/1/1	5/2/2
29	*m*T7G	0.190	0.634	0.5–1000	0.9999	7/4/1	3/3/2
CK N^9-glucosides							
30	*t*Z9G	0.035	0.116	0.5–1000	0.9995	–/29/10	–/20/3
31	*c*Z9G	0.013	0.042	0.1–1000	0.9990	2/13/1	12/10/1
32	DHZ9G	0.012	0.039	0.5–1000	0.9997	9/7/4	19/12/3
33	iP9G	0.041	0.136	0.1–1000	0.9998	16/17/8	30/11/8
34	BA9G	0.074	0.248	0.1–1000	0.9991	25/1/3	8/3/4
35	*oT9G*	0.075	0.251	0.5–100	0.9998	–/11/8	–/10/8
36	*m*T9G	0.023	0.076	0.1–1000	0.9990	1/1/3	21/2/3
37	K9G	0.063	0.210	0.1–1000	0.9993	83/84/84	6/4/4

[a] Limit of detection (LOD) in fmol on column.
[b] Limit of quantification (LOQ) in fmol on column.
[c] Linear range in fmol on column.
[d] Coefficient of determination.
[e] Method accuracy calculated as a mean bias of estimated concentration at 10/100/1000 fmol validation level.
[f] Method precision calculated as a relative standard deviation at 10/100/1000 fmol validation level.

in dynamic multiple reaction monitoring (MRM) mode using unit resolution and a cycle time of 600 ms. The fragmentor voltage was 380 V and the cell accelerator voltage was 5 V. The fragment ions were selected and all collision energies were tuned to obtain the highest sensitivity and optimal values summarised in Table A.2.

Data were acquired using MassHunter LC/MS Data Acquisition for 6400 Series Triple Quadrupole version B.09.00. Chromatograms were evaluated in MassHunter Qualitative Analysis version B.07.00. Automatic integration was performed and peak areas were calculated using MassHunter Quantitative Analysis for QQQ version B.09.00 (all Agilent Technologies, Santa Clara, CA USA).

2.3. Development of UHPSFC chromatography

Four different chromatographic columns were tested (a-d), each under different conditions depending on the SP type and column geometry (a) Torus DIOL, 3.0 × 100 mm, 1.7 μm (Waters, Milford, CT, USA); (b) Zorbax RX-SIL, 4.6 × 150 mm, 5.0 μm (Agilent Technologies, Santa Clara, CA USA); (c) Torus 2-PIC, 3.0 × 100 mm, 1.7 μm (Waters, Milford, CT USA). Certain conditions are described in Method A.3. In all cases, 2 μL of 10^{-7} M mixture of CK standards dissolved in methanol were injected. Make-up solvent consisted of methanol flowing at a rate of 0.25 mL min^{-1}.

2.4. Selected chromatography conditions

A 2-PIC column was employed for the final UHPSFC-MS/MS method. The back pressure regulator maintained 300 bar and the column was heated at 60 °C. The mobile phase consisted of $scCO_2$ (A) combined with 5 mM ammonia in methanol (B) and was pumped at a flow rate of 1.5 mL min^{-1}. A 9-min gradient elution program was set up as follows: 0 min 5 % B, 7 min 40 % B, 7.5 min 5 % B and then 2 min column equilibration. Methanol was employed as a make-up solvent flowing at a rate of 0.25 mL min^{-1}.

2.5. Investigation of make-up solvent

The binary solvent delivery pump, back pressure regulator, multisampler and column thermostat were set as described in the final chromatography conditions (section 2.4). Different flow rate of methanol (0.10, 0.25 and 0.40 mL min^{-1}), different solvents (methanol, ethanol, 2-propanol and ACN) and different additives in methanol (15 mM formic acid, acetic acid and respective ammonia salts) at flow rate of 0.25 mL min^{-1} were tested. Each variant was examined with three independent injections of 2 μL 10^{-7} M CK mixture dissolved in methanol. The effectivity of make-up solvent was estimated from the peak area of each CK standard normalised by mean of control sample (methanol at flow rate of 0.25 mL min^{-1}).

2.6. Investigation of sample diluent

Solutions of CK standards were diluted in 10 %, 50 % and 90 % ACN or methanol (v/v) at concentrations as follows: A: 50 fmol μL^{-1}, B: 10 fmol μL^{-1} and C: 5 fmol μL^{-1}. All samples were prepared in four independent replicates and injected under the final chromatography conditions described above. The injection volume tested was 1 μL (samples A), 5 μL (samples B) and 10 μL (samples C) to obtain a response of 50 fmol of each CK standard.

2.7. Preparation of plant samples

Arabidopsis thaliana seeds (ecotype Col-0) were planted on full strength Murashige & Skoog solid medium in Petri dishes. The medium consisted of 2.2 g L^{-1} Murashige & Skoog, 7 g L^{-1} agar, 10 g L^{-1} sucrose and 50 mg L^{-1} morpholinoethanesulfonic acid. After 2 days of stratification in dark at 4 °C, seeds were grown in a chamber with long-day conditions accounting for 16 h light, 8 h dark and 22 °C. Whole seedlings were harvested after 10 days and ground to a fine powder using mortar and pestle in liquid nitrogen. Homogenised material was stored at −70 °C.

2.8. Sample extraction and purification

10 mg FW of *Arabidopsis* homogenate was weighed into a 2 mL microtube. The sample was extracted with 1 mL of cold modified Bieleski solution consisting 75 % methanol, 20 % water and 5 % formic acid (all v/v). Three ceramic beads and a mixture of isotopic labelled internal standards (0.1 pmol CK bases, ribosides and *N*-glucosides, 1 pmol CK *O*-glucosides) were added. The sample was shaken in an oscillation bead mill (Retsch MM400, Haan, Germany) at 27 Hz for 5 min, sonicated for 3 min and incubated for 30 min at 4 °C. The sample was then centrifuged at 20,000 rpm, 4 °C for 15 min (Allegra 64R benchtop centrifuge, Beckman Coulter, USA). After extraction, the supernatant was collected and purified by mixed-mode SPE using Oasis MCX® extraction cartridges 30 mg mL^{-1} (Waters, Milford, USA) according to a previously published protocol [16]. Briefly, extraction cartridge was subsequently conditioned with 1 mL of methanol, water and 1 M formic acid. The plant extract was loaded onto the cartridge and washed with 1 mL of 1 M formic acid and 1 mL of methanol. Finally, CKs were eluted with 1 mL of 0.35 M ammonia in water and 2 mL of 0.35 M ammonia in 60 % methanol (v/v). The eluate was collected into 5 mL glass vial and evaporated to dryness using SpeedVac concentrator (RC1010 Centrivap Jouan, ThermoFisher, USA). The sample was reconstituted in 30 μL of 50 % ACN (v/v) and transferred into an LC vial equipped with a glass insert (Chromservis Ltd., Czech Republic).

2.9. UHPLC-MS/MS method

The method was based on a previously published methodology for the determination of CKs by UHPLC-MS/MS [12]. Briefly, 5 μL of sample dissolved in 10 % methanol (v/v) was injected into Kinetex C18, 150 × 2.1 mm, 1.8 μm column (Phenomenex, Torrance, CA, USA) heated at 70 °C. Mobile phase consisted from methanol (A) and 15 mM ammonium formate, pH 3.95 (B). Sample was separated by linear gradient elution as follows: 0 min 5 % A, 7 min 5 % A, 16 min 20 % A, 23 min 50 % A, 23.5 min 99 % A, 24 min 99 % A, 24.5 min 5 % A and the chromatographic run was finished at 28 min. The flow rate of mobile phase was 0.25 mL min^{-1}. MS conditions were identical to the UHPSFC-MS/MS method (section 2.2).

2.10. Method validation

A set of 18 independent *Arabidopsis* extracts (each per 10 mg FW mL^{-1}) was prepared. Before extraction, samples were spiked with internal standards and then divided into three equal volumes. The first third was spiked with non-labelled CK standards of theoretical concentration (CT) 10 fmol mL^{-1}, the second third was spiked with 100 fmol mL^{-1} and the last third was spiked with 1000 fmol mL^{-1}. The samples were processed by the extraction and purification procedure described above. Evaporated samples were dissolved in 30 μL of 50 % ACN, 5 μL were injected and analysed by the final UHPSFC-MS/MS method (section 2.4). The estimated concentration (CE) of each compound was determined by the isotopic dilution method. Method accuracy (MA) was calculated as follows: MA = (CE – CT)/CT. Method precision was calculated as relative standard deviation (RSD) of CE in six independent replicates. Ten-point calibration curve ranged by 0.01 and 1000 fmol per injection was prepared and analysed in three independent replicates. The slope and intercept were calculated by linear regression and used to calculate the instrumental limit of detection (LOD) and instrumental limit of quantification (LOQ) as follows: LOD = 3 · (SD intercept/mean slope), LOQ = 10 · (SD intercept/mean slope). The matrix effect (ME) was evaluated using a matrix-matched calibration prepared by spiking a

purified extract of 10 mg FW *Arabidopsis* seedlings compared to a calibration in neat solvent. The ME was calculated in terms of slope ratios as followed: ME = matrix-matched slope/neat solvent slope [17,18].

2.11. Comparison of UHPSFC and UHPLC chromatography

The performance of the chromatographic methods was evaluated based on the following parameters. Retention time (RT), full width at half maximum (FWHM) and peak symmetry were calculated using MassHunter Quantitative for QQQ version B.09.00 (Agilent Technologies, Santa Clara, CA USA). The column efficiency was calculated for each compound as 5.54 · (RT/FWHM). The chromatographic resolution (Rs) was determined according to equation $Rs = 1.18 \cdot (RT_1 - RT_2)/(FWHM_1 + FWHM_2)$ for two closely eluting peaks with the same MRM transition and/or all eluted analytes.

2.12. Proof of concept

Six independent *Arabidopsis* extracts (10 mg FW) spiked with internal standards were prepared and purified as mentioned above. Evaporated samples were reconstructed in 30 μL of 50 % ACN (v/v) and 5 μL was injected and analysed by the final SFC-MS/MS method. Afterwards, the remaining volume was evaporated and dissolved in 25 μL of 10 % methanol (v/v). Additional 5 μL were the analysed with UHPLC-MS/MS method. The CK content was determined by the isotopic dilution method and the endogenous CK profiles obtained in UHPLC-MS/MS and UHPSFC-MS/MS were compared.

3. Results and discussion

3.1. Development of SFC separation

In general, SFC systems suffer from higher dead volumes compared to LC instruments. As previously recommended, the ratio between the extra-column volume and the total volume of chromatographic system should be less than 10 % to avoid a peak broadening [19]. To follow this rule, we tested columns with a relatively large inner diameter (ID ≥ 3.0 mm). Retention and separation efficiency and peak shape in SFC mode were the most important criteria for selection of the chromatographic column. For this reason, we examined: a) hybrid silica modified with diol group (DIOL), b) bare fully porous silica (RX-SIL) and c) hybrid silica modified with 2-picolylamine group (2-PIC).

DIOL embedded hybrid silica has been recommended as a possible SP for the separation of polar basic compounds [19,20]. Thus, our next efforts were dedicated to apply DIOL for the analysis of CKs exhibiting high polarity and basic pK. A linear gradient elution using ammonium formate in methanol as a co-solvent was employed in 15-min chromatographic run. As shown in Figure A.4, high separation efficiency and reasonable peak shape were obtained with the DIOL column. Compared to the classic RPLC-MS/MS described in Svačinová et al., the order of peaks in UHPSFC-MS/MS on a DIOL column was reversed [12]. Semi-polar CKs were eluted from the column first in order and polar analytes at the end of the linear gradient. As already mentioned in previously published studies, the opposite elution order was caused by the different retention mechanisms of SFC, which is similar to the normal LC phase [21–23].

Despite the relatively high separation efficiency of the DIOL column, zeatin glucosides were revealed as the most problematic compounds. As already mentioned in the introduction, zeatin occurs naturally in two different isoforms (*trans*- and *cis*-) and both can be glucosyled at the N^9-, N^7- and *O*-positions [7]. In all combinations, six isomers should be distinguished in a common MRM transition 382 > 220. However, two pairs (*c*ZOG/*c*Z9G and *t*ZOG/*t*Z9G) were highly demanding to separate using a DIOL column. In order to improve the separation efficiency of zeatin glucosides, the column temperature and the concentration of ammonia in the co-solvent were tested. Our data showed that both parameters changed the selectivity of the DIOL sorbent (Figure A.5). Interestingly, variation in column temperature affected the separation of CK N^7- and N^9-glucosides, whereas the addition of ammonia had an impact on the separation of CK *O*- and N^9-glucosides. *c*ZOG was separated from *c*Z9G at low concentration of ammonia, however, the respective *trans*-isoforms co-eluted. Conversely, separation of *t*ZOG and *t*Z9G was obtained at high ammonia content, while the *cis*-isoforms shared an identical retention time. As discussed earlier, hydrogen bonding plays the most important role in the retention of polar compounds onto DIOL or silanol groups [24,25]. Additives in the co-solvent, such as acids or their ammonia salts, activate or inactivate these functional groups and thereby affect the bonding capacity. Furthermore, the additives promote a formation of ion-pairs with the analytes. The combination of these effects alters the analyte retention and thus the sorbent selectivity. Regarding our experience with DIOL, we decided to resolve the separation of zeatin glucosides by choosing a silica RX-SIL column exhibiting similar retention mechanisms.

It is well known that column temperature and back pressure regulation play an important role in SFC selectivity [26]. Both of these parameters affect $scCO_2$ density and thus analyte retention. The selectivity of zeatin glucosides on the RX-SIL column as a function of column temperature and back pressure effect is shown in Figure A.6.Variation in column temperature had a stronger impact on the separation of zeatin glucosides compared to back pressure effect. The mechanism of this action is related to the physical properties of the mobile phase. A high portion of organic co-solvent at the end of the gradient (40 %) reduced the compressibility of the mobile phase and altered the critical point of $scCO_2$. Consequently, the end of the gradient operated under subcritical conditions, which was still effective since the properties of subcritical CO_2 and $scCO_2$ are continuous [27]. Although the lower compressibility of the mobile phase should suppress the importance of back pressure effect [19], we surprisingly achieved the best selectivity for zeatin glucosides with a combination of the highest values of column temperature (60 °C) and back pressure (300 bar). Our next effort was dedicated to resolving the persistent co-elution of *t*ZOG and *t*Z9G, which could be problematic in the presence of a plant matrix.

It has been reported that the addition of a small amount of water in the mobile phase co-solvent can have a strong impact on the peak shape, peak intensity and selectivity [28]. Water as an additive is effectively used for the separation of polar compounds such as monosaccharides, nucleobases, nucleosides or amino acids [29–32]. Therefore, we added water into the methanolic co-solvent to address the issue of zeatin glucoside. Even the presence of 2.5 % water in methanol had a positive effect on the separation of zeatin glucosides (Figure A.7). Baseline separation was achieved with 5.0 % of water. However, addition of water resulted in co-elution in MRM channel 384 > 222, referring to dihydrozeatin glucosides. This contradicting effect indicates the limited use of the water-based additive in the co-solvent combined with the RX-SIL column.

Previously, the Torus 2-PIC column was introduced into SFC as a suitable SP for the retention of polar compounds [26]. The 2-PIC sorbent is equipped with a heterocyclic functional group with a minimal amount of residual silanols providing a different retention mechanism compared to DIOL [33]. Recently, 2 PIC was used for the determination of skin protectans [34]. In this study, several columns of the Torus series were tested for the separation of weak bases (similar to CKs). The problematic CK co-elutions observed on the DIOL column were therefore solved using 2 PIC sorbent. Based on previous knowledge of the effect of water, ammonia or ammonia salts on the chromatography of polar basic metabolites [35], we used a 5 mM aqueous solution of ammonia in methanol as a co-solvent to improve the peak shape and overall MS/MS response (Figure A.8). To obtain a satisfactory analysis time, we shortened the method by using a 7 min gradient from 5 % to 40 % co-solvent, followed by a 2 min equilibration step.

Using our chromatographic settings applied onto a Torus 2-PIC column, the first compound (iP) was eluted at a retention time of 1.00 min

and the last analyte (*m*T7G) at 7.60 min (Figure 2). Altogether, in a 9-min analytical run, the total time for the separation of 37 CK metabolites was 6.60 min.

3.2. Composition of sample diluent

Competition between sample diluent, analytes and mobile phase modifier for the stationary phase adsorption centres plays an important role in the integrity of chromatographic peaks. This may be related to the viscosity of the solvents used. The gap in viscosity between the sample diluent and the mobile phase can lead to an effect known as viscous fingering. The less viscous fluid tends to penetrate the other liquid, resulting in distortion of the chromatographic peaks [36,37] Viscous fingering in LC can be overcome by dissolving the samples in a diluent identical to the mobile phase. However, this is not possible in SFC with a mobile phase containing mainly $scCO_2$. Recently, an extensive study investigated the association between viscous fingering and various sample diluents in SFC [38]. The results showed that low-viscosity liquids such as ACN were suitable sample diluents due to their viscosity close to $scCO_2$. On the other hand, highly viscous water as a diluent resulted in peak distortion. This does not necessarily mean that the sample cannot be dissolved in aqueous solvents for SFC analysis. However, viscous fingering must be compensated by reducing the injection volume [39]. Based on these conclusions, we focused on the composition of the sample diluent and the injection volume.

We investigated the peak integrity of zeatin glucosides as a function of ACN concentration in water and injection volume. The results are illustrated in Figure 3. The strongest effect of viscous fingering was observed when 10 μL of 10 % ACN (v/v) were injected. On the other hand, peak symmetry improved with increasing portion of ACN and/or with decreasing injection volume. Our results were consistent with the observations described previously [38]. However, we should apply the lowest possible portion of ACN in the sample diluent to avoid the difficulties with CK solubility. Moreover, a high injection volume from a preconcentrated sample was also preferred to obtain a sufficient signal response of low-abundance plant hormones. To preserve peak integrity, a reasonable compromise between injection volume and diluent composition was 5 μL of 50 % ACN (v/v).

3.3. Composition of make-up solvent

Modern SFC-MS/MS systems are equipped with an isocratic pump introducing make-up solvent to the stream of decompressed mobile phase in the transfer line. The role of make-up solvent is (i) to avoid precipitation of the separated sample and (ii) to affect the electrospray ionization, which depends on the solvent composition and the flow rate [19,40]. The effectiveness of these parameters was evaluated by the relative change in the peak area compared to the control (methanol at a flow rate of 0.25 mL min^{-1}). As shown in Figure 4A, the variation in flow rate did not affect the response of all CK metabolic groups. The total transferred volume consisted of the make-up solvent and co-solvent in the mobile phase, the effect of flow rate was probably attenuated by the high portion of co-solvent. Obviously, the importance of make-up solvent volume is strongest with no or low transferred volume of co-solvent [38]. However, the CK analysis in our study operated at a high flow rate of a mobile phase containing a high portion of co-solvent. Therefore, the flow rate of the make-up solvent had a neglectable effect on the CK response.

Subsequently, the effect of four organic solvent (methanol, ACN, ethanol and 2-propanol) on signal enhancement was tested (Figure 4B). Using our conditions, methanol provided up to two-fold higher relative peak areas of all CK compounds compared to other solvent types. Moreover, pure methanol was enriched by the following 15 mM additives: ammonia, formic acid, ammonium acetate and ammonium formate (Figure 4C). All additives provided similar or worse MS signals compared to pure methanol. As shown in Figure A.8, the addition of ammonia into the mobile phase increased dramatically the signal of CK metabolites. However, further addition of ammonia into the make-up solvent did not significantly enhance this effect. This observation indicated that the concentration of ammonia ions in the mobile phase was sufficient for effective ionization and no further increase of ammonia in the transfer line was necessary. Our findings were consistent with a broad systematic study dealing with the ionization effectivity of drug analytes in combination with various make-up solvents [41]. In this work, methanol, ethanol or isopropanol were tested in combination with several additives such as water, ammonium hydroxide, formic acid or ammonium formate. Although the use of additives resulted in signal enhancement of several compounds, signal suppression was also observed for other analytes. Therefore, methanol was considered as the first-choice make-up solvent for generic analysis. This was later confirmed by several published results, e.g., a method for screening of impurities in pharmaceutically active mixtures [42]. With regard to the findings discussed above, methanol was accepted as the make-up solvent for CK analysis in our UHPFSC-MS/MS method.

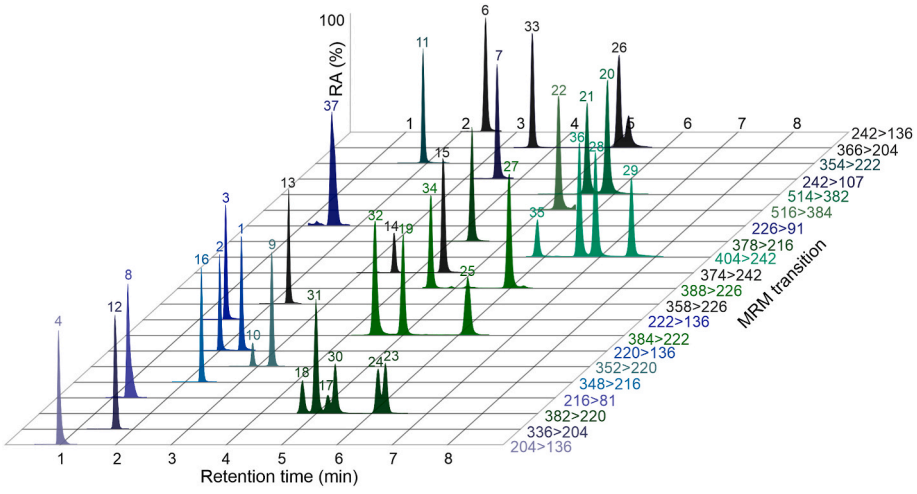

Fig. 2. Separation of cytokinin standards by UHPSFC-MS/MS method using a Torus 2-PIC (3.0 × 100 mm, 1.7 μm) column. Multi-MRM chromatograms of 22 isoprenoid and 15 aromatic cytokinins including bases, ribosides, and *N*-/*O*-glucosides containing 0.1 pmol of each metabolite per injection. Relative abundance (RA %) is function of retention time (min) and MRM transition.

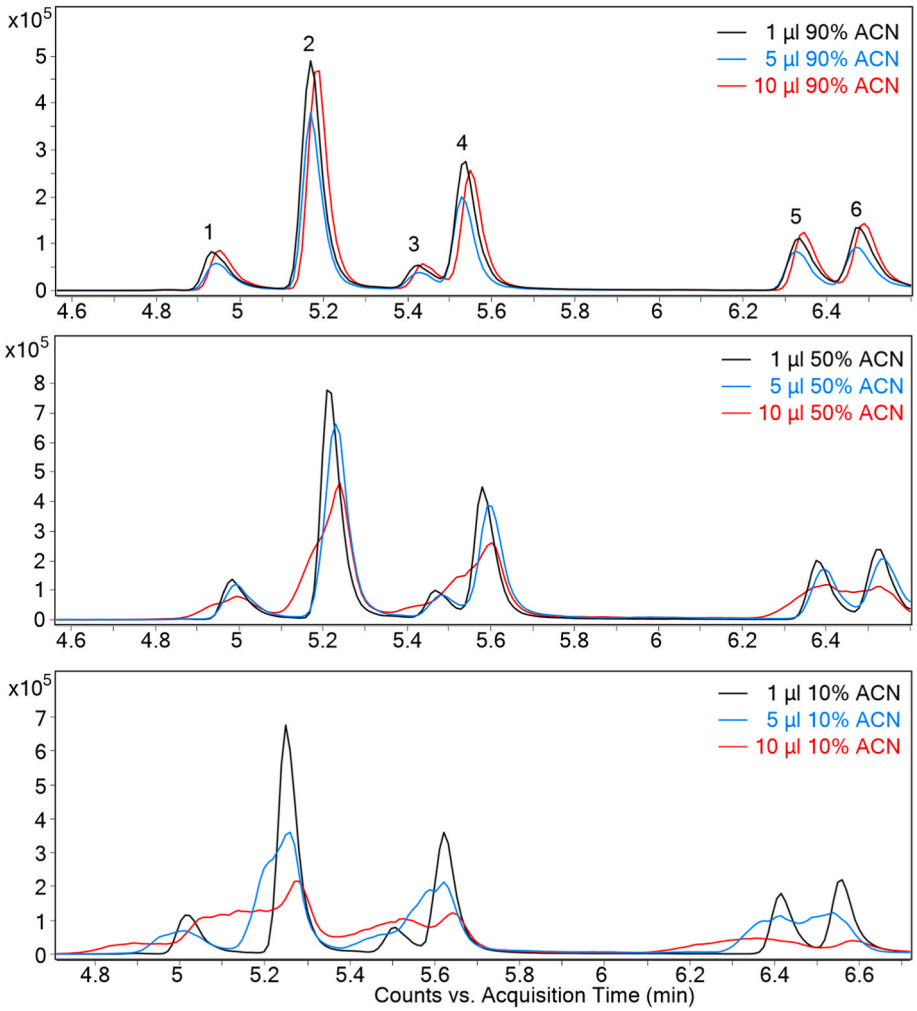

Fig. 3. Effect of sample diluent. Chromatograms show MRM transition (382 > 220) of compounds as follows: *c*ZOG (1), *c*Z9G (2), *t*ZOG (3) *t*Z9G (4), *c*Z7G (5) and *t*Z7G (6). CK standards were dissolved in 10 % ACN (bottom box), 50 % ACN (middle box) and 90 % ACN (upper box) and injected in volumes of 1 µL (black line), 5 µL (blue line) and 10 µL (red line). Each injection contained 50 fmol of CK standards. (For interpretation of the references to colour in this figure legend, the reader is referred to the Web version of this article.)

3.4. Method validation

Complete results of method validation are summarised in Table 1. Overall, the calibration curves showed a coefficient of determination (R^2) close to 0.999, indicating reasonable linearity. The working range of the method was set to the lower value of the quantification limit corresponding to 0.1–0.6 fmol per injection. The upper bound was defined by the highest concentration point of the linear range, which was 1000 fmol per injection for most compounds. This represents a range of five orders of magnitude that is wide enough to cover the endogenous CK concentrations in plant tissues [12,13].

Method accuracy and precision were estimated at three concentration levels in a linear range (10/100/1000 fmol mL^{-1}) spiked to 1 mL of 10 mg FW *Arabidopsis* seedling extract. Due to the natural occurrence of CKs in the plant extract (e. g. *t*ZOG, *t*Z7G, *t*Z9G, *c*Z7G, DHZ7G, iP7G), the estimation of some analytes at the lowest level was highly biased. The accuracy of UHPSFC-MS/MS was satisfactory for most CK metabolites except *c*ZR, BA7G, KR and K9G, probably due to the lack of isotopically labelled internal standards. These compounds were quantified using structurally similar analogues, namely [$^2H_3$]DHZR, [$^{15}N_4$]*c*Z7G, [$^2H_7$]BAR and [$^2H_7$]BA9G, respectively. For example, [$^2H_3$]DHZR, which differs from *c*ZR only in the absence a double bond on the hydroxylated isopentyl side chain, was probably unable to fully compensate for the effect of the complex plant matrix and losses during sample ionization. Altogether, method accuracy was lower than recommended cut-off value (15 %) for majority of compounds, indicating a reasonable trueness of the method. Method precision was evaluated as the relative standard deviation (RSD) of the estimated concentrations. Most of the compounds reported RSD <15 %, which corresponds to the high reproducibility of the method.

3.5. Evaluation of matrix effect

The matrix effect (ME) plays an important role in the development of bioanalytical methods. It can influence the MS response and thus method accuracy and precision. ME mechanisms are mainly associated with ionization yield, whereby components from the matrix can compete with analytes for charge. Furthermore, the matrix can alter the viscosity of the mobile phase, affect droplet evaporation and thus charge transfer leading to signal suppression or enhancement [21,43]. The role of ME has been well described for LC-MS/MS, however, only a few studies have addressed the influence of ME in SFC-MS/MS [44–46].

We compared the ME in CK-enriched plant extracts analysed by UHPSFC-MS/MS and UHPLC-MS/MS (Figure 5). Lines at the 100 % limit indicate no matrix effect. Values above or below the limit suggest positive or negative ME, respectively. Both chromatographic methods showed mostly negative ME, indicating ion suppression. The strongest ME was observed for CK N^7-glucosides, reaching up to 70 % in UHPSFC-

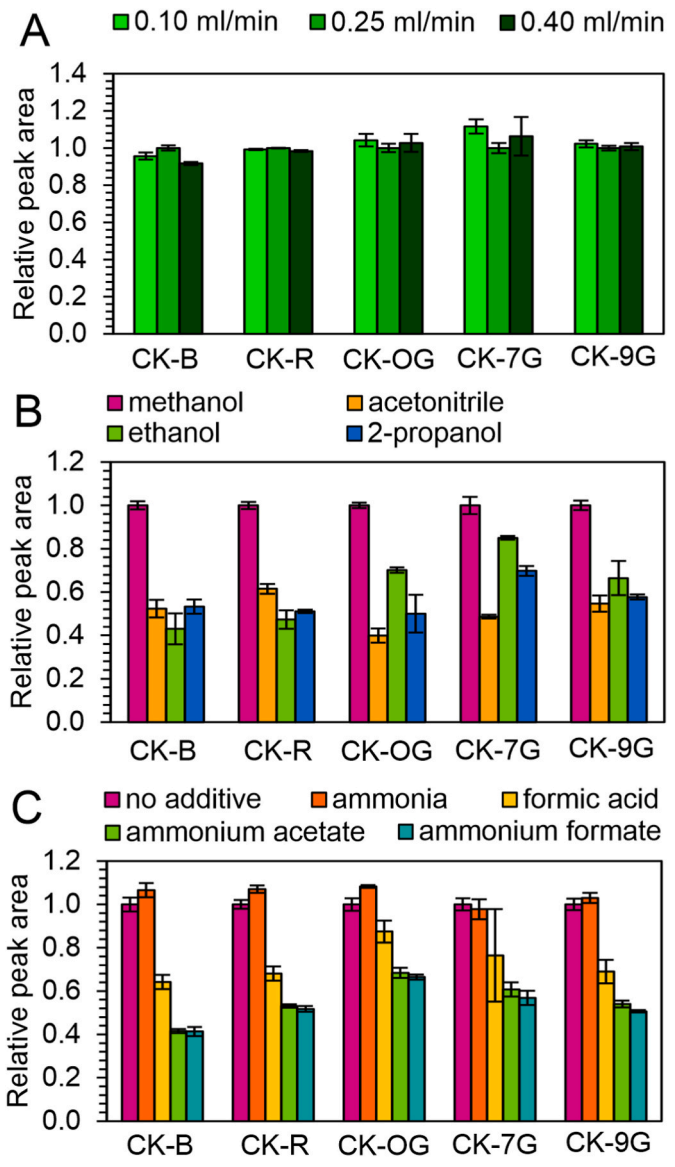

Fig. 4. Investigation of make-up solvent. The following parameters were tested: (A) methanol flow rate (0.10, 0.25 and 0.40 mL min^{-1}), (B) solvent types (methanol, ethanol, acetonitrile and 2-propanol) and (C) additives in methanol (15 mM formic acid and 15 mM acetic acid with appropriate ammonium salts). Signal enhancement/suppression were estimated from the peak area of each CK standard normalised with a control sample (methanol at a flow rate of 0.25 mL min^{-1}). All values are mean ± SD (n = 3).

MS/MS and 52 % in UHPLC-MS/MS. Interestingly, isoprenoid N^7-glucosides handled the *Arabidopsis* matrix better in UHPSFC-MS/MS, but aromatic N^7-glucosides were less affected by the sample matrix in UHPLC-MS/MS. This observation could be related to the different elution pattern of the chromatographic modes. Whereas the isoprenoid N^7-glucosides were predominately eluted in the first half of the UHPLC-MS/MS gradient, the aromatic counterparts were eluted by a higher proportion of the organic phase, which can positively affect the ionization yield. On the other hand, UHPSFC-MS/MS provided elution of both groups at the very end of analysis (Table A.9).

A comparison of ME in SFC-MS/MS and LC-MS/MS analysis of plant tissue samples has not been published yet. However, recent studies have reported ME for pharmaceutically important compounds in human urine and plasma using LC or SFC coupled to ESI-MS/MS [44,45]. The application of SFC-MS/MS to the human fluid matrix showed lower ME compared to LC-MS/MS, which was partially in acceptance with our observations in the *Arabidopsis* matrix. However, this comparison has several limitations. Importantly, the ME in the urine and plasma matrix was estimated by post-extraction addition, whereas the ME in the plant extract was calculated by matrix-matched calibration. Matrix-matching compares the slopes of the regression lines and, importantly, is robust to the presence of naturally occurring analytes in the samples (as mentioned above). Therefore, matrix-matching was preferred over post-extraction addition in our ME study. Moreover, urine and plasma contain primarily salts and polar nitrogen-rich compounds, whereas our purified plant matrix consists mainly of non-polar substances [44]. First, the plant sample were extracted with aqueous acidified methanol, which also co-extracted of non-polar compounds. Second, majority of salts and polar contaminants were removed by mixed-mode SPE-based purification. The effect of non-polar interferences in ESI-equipped SFC-MS and LC-MS systems was previously explained on the analysis of doping agents in wastewaters enriched by non-polar contaminants [46]. Importantly, similar to the *Arabidopsis* matrix, the wastewater SFC-based analysis also showed a predominant negative ME.

3.6. Comparison of UHPSFC and UHPLC chromatography

To compare both separation methods, we examined several basic chromatographic parameters. First, the chromatographic resolution was calculated against the nearest peak with the same MRM transition (Table A.9). Most of the compounds showed a baseline separation, which was defined as a resolution value of 1.5 [47]. The resolution in the range of 1.93–12.68 was observed for fast 7-min UHPSFC chromatography, except for the pairs *t*ZOG/*t*Z9G and *c*Z7G/*t*Z7G with lower resolutions of 0.91 and 0.93, respectively. On the other hand, the 25-min UHPLC chromatography gave a mean resolution of 10.48 (Table A.9). We also calculated the overall resolution for each CK metabolite compared to all other eluted compounds (Figure A.10). Our findings showed that UHPSFC method achieved sufficient resolution similar to UHPLC, despite its short analytical time. Importantly, we also ensured the recognition of overlapping peaks by choosing an appropriate MRM transition for each compound (Table A.2). Both UHPSFC and UHPLC methods produced similar peak symmetry, with average values of 1.4 and 1.3, respectively (Table A.9). However, as indicated by the FWHM values, the peaks under UHPSFC separation conditions were up to twice narrower than those under UHPLC conditions. Finally, we calculated the column efficiency based on both FWHM and retention time, and found that it was higher for the conventional UHPLC separation. This was not surprising, since UHPLC was a slower generic method for accurate quantification of cytokinins [12] whereas the UHPSFC method was designed as a fast-screening method for CK metabolites.

3.7. Rapid cytokinin profiling

The reliability of the developed method was finally tested using CK profiling in 10-day-old *Arabidopsis* seedlings. CK levels were determined by UHPSFC-MS/MS and conventional UHPLC-MS/MS [12]. The list of detected CK metabolites and concentration levels are summarised in Table A.11. In accordance with previous publications, only isoprenoid CKs were determined [12,48]. The annotation of each endogenous CK metabolite was confirmed by the retention time of the corresponding stable isotopically labelled internal standard (Table A.2). As shown in Figure A.12, we also compared the retention time stability of the injected plant extract with a solution of CK standards. Furthermore, number of misannotated peaks was minimised by incorporating a one-step SPE that removed the complex plant matrix (Figure A.12). The chromatograms demonstrate that both UHPSFC and UHPLC methods provide consistent retention times and symmetrical peaks for all CK metabolites. Specifically, 18 CK compounds were detected by UHPSFC-MS/MS and 15 CKs by UHPLC-MS/MS. The slight difference in the number of detected CK metabolites as well as their levels may be due to the ME as described above (Figure 5A). CK *N*-glucosides were

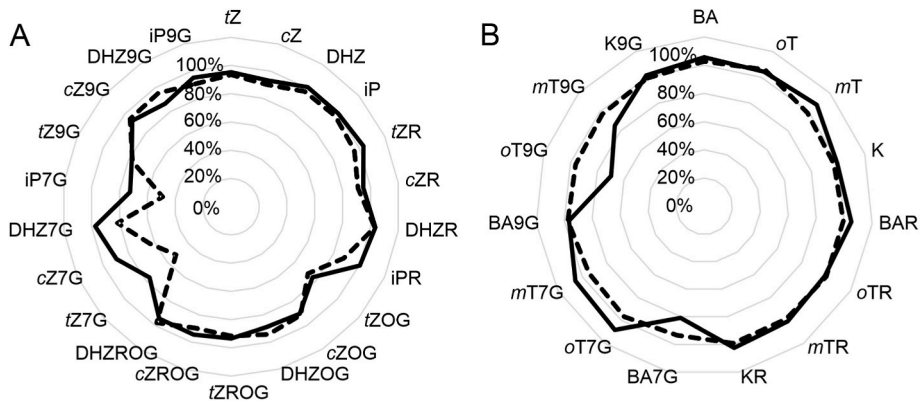

Fig. 5. Matrix effect. Isoprenoid (panel A) and aromatic (panel B) CKs were analysed in the spiked extract of 10-day-old *Arabidopsis* by UHPSFC-MS/MS (full line) and UHPLC-MS/MS (dashed line). The ME was calculated as the ratio of the slope of the matrix-matched calibration curve to the slope of the neat solvent calibration curve.

identified as the most abundant compounds (~84 %), followed by CK *O*-glucosides (~8 %), CK ribosides (~2 %) and biologically active CK bases (~1 %). The relative distribution of estimated concentrations was similar in both methods and the results obtained were consistent with a previous publication describing the dominancy of *N*-glucosides in the CK pool of young *Arabidopsis* seedlings [49].

4. Conclusions

We have developed a new rapid method for the determination of endogenous CKs in plant tissues based on rapid and highly sensitive UHPSFC-MS/MS. The work brings new knowledge about SFC chromatography of semi-polar basic compounds on different types of columns in combination with various composition of the mobile phase, column temperature, back pressure effect, injection parameters and the composition of make-up solvent. The developed method was validated with reasonable accuracy and precision. Compared to the well-established UHPLC-MS/MS method for CK profiling, the UHPSFC-MS/MS method proposed in this study offers a 7-min separation while maintaining sufficient resolution of all isomers of endogenous CK metabolites. Our data also showed that chromatographic parameters, such as peak symmetry and FWHM, are satisfactory for a rapid screening of CK metabolites using UHFSC as an analytical tool. Surprisingly, we detected a lower matrix effect for naturally occurring isoprenoid CKs in *Arabidopsis* samples in the novel UHPSFC mode rather than the conventional UHPLC method. Our findings open the opportunity to use the UHPSFC-MS/MS instrumentation for fast target plant hormonomics including other (not only non-polar) families of plant hormone.

CRediT authorship contribution statement

Ivan Petřík: Methodology, Investigation, Formal analysis, Validation, Visualization, Writing – original draft. **Aleš Pěnčík:** Investigation, Formal analysis, and. **Jakub Stýskala:** Resources, and. **Lenka Tranová:** Resources. **Petra Amakorová:** Investigation, Formal analysis. **Miroslav Strnad:** Funding acquisition. **Ondřej Novák:** Conceptualization, Funding acquisition, Supervision, Writing – review & editing.

Declaration of competing interest

The authors declare that they have no known competing financial interests or personal relationships that could have appeared to influence the work reported in this paper.

Data availability

Data will be made available on request.

Acknowledgement

This work was supported by Internal Grant Agency of Palacky University (IGA_PrF_2023_020 and IGA_PrF_2023_031) and by the EU Horizon-2020 project ADAPT (grant number 862858).

Appendix A. Supplementary data

Supplementary data to this article can be found online at https://doi.org/10.1016/j.aca.2023.342010.

References

[1] M. Strnad, The aromatic cytokinins, Physiol. Plantarum 101 (1997) 674–688.
[2] C.O. Miller, F. Skoog, M.H. Von Saltza, F.M. Strong, Kinetin, a cell division factor from deoxyribonucleic acid, J. Am. Chem. Soc. 77 (1955) 1392.
[3] J. Holub, J. Hanus, D.E. Hanke, M. Strnad, Biological activity of cytokinins derived from Ortho- and Meta-Hydroxybenzyladenine, Plant Growth Regul. 26 (1998) 109–115.
[4] E. Baroja-Fernandez, J. Aguirreolea, H. Martinkova, J. Hanus, M. Strnad, Aromatic cytokinins in micropropagated potato plants, Plant Physiol. Biochem. 40 (2002) 217–224.
[5] S.N. Lomin, D.M. Krivosheev, M.Y. Steklov, D.V. Arkhipov, D.I. Osolodkin, T. Schmülling, G.A. Romanov, Plant membrane assays with cytokinin receptors underpin the unique role of free cytokinin bases as biologically active ligands, J. Exp. Bot. 66 (2015) 1851–1863.
[6] T. Werner, T. Schmülling, Cytokinin action in plant development, Curr. Opin. Plant Biol. 12 (2009) 527–538.
[7] L. Spichal Funct, Cytokinins - recent news and views of evolutionally old molecules, Plant Biol. 39 (2012) 267–284.
[8] E. Zurcher, B. Muller, Cytokinin synthesis, signaling, and function—advances and new insights, Int. Rev. Cell Mol. Biol. 324 (2016) 1–38.
[9] D. Tarkowska, O. Novak, K. Flokova, P. Tarkowski, V. Tureckova, J. Gruz, J. Rolcik, M. Strnad, Quo vadis plant hormone analysis? Planta 240 (2014) 55–76.
[10] O. Novak, R. Napier, K. Ljung, Zooming in on plant hormone analysis: tissue- and cell-specific approaches, Annu. Rev. Plant Biol. 68 (2017) 323–348.
[11] J.J. Van Deemter, F.J. Zuiderweg, A. Klinkenberg, Longitudinal diffusion and resistance to mass transfer as causes of nonideality in chromatography, Chem. Eng. Sci. 5 (1956) 271–289.
[12] J. Svacinova, O. Novak, L. Plackova, R. Lenobel, J. Holik, M. Strnad, K. Dolezal, A new approach for cytokinin isolation from Arabidopsis tissues using miniaturized purification: pipette tip solid-phase extraction, Plant Methods 8 (2012) 17.
[13] J. Simura, I. Antoniadi, J. Siroka, D. Tarkowska, M. Strnad, K. Ljung, O. Novak, Plant hormonomics: multiple phytohormone profiling by targeted metabolomics, Plant Physiol. 177 (2018) 476–489.
[14] T. Gazarkova, K. Plachka, F. Svec, L. Novakova, Current state of supercritical fluid chromatography-mass spectrometry, Trends Anal. Chem. 142 (2022), 116544.
[15] L. Tranova, J. Bucek, M. Zatloukal, P. Cankar, J. Styskala, Synthesis of [15N4] purine labeled cytokinin glycosides derived from zeatins and topolins with 9-β-D, 7-β-D-glucopyranosyl, or 9-β-D-ribofuranosyl group, J. Label. Compd. Radiopharm. 62 (2019) 118–125.
[16] P.I. Dobrev, M. Kamínek, Fast and efficient separation of cytokinins from auxin and abscisic acid and their purification using mixed-mode solid-phase extraction, J. Chromatogr. A 950 (2002) 21–29.
[17] J. Quin, Y. Fu, Q. Lu, X. Dou, J. Luo, M. Yang, Matrix-matched monitoring ion selection strategy for improving the matrix effect and qualitative accuracy in

pesticide detection based on UFLC-ESI-MS/MS: a case of Chrysanthemum, Microchem. J. 160 (2021), 105681.
[18] B.K. Matuszewski, M.L. Constanzer, C.M. Chavez-Eng, Strategies for the assessment of matrix effect in quantitative bioanalytical methods based on HPLC-MS/MS, Anal. Chem. 75 (2003) 3019–3030.
[19] V. Desfontaine, D. Guillarme, E. Francotte, L. Novakova, Supercritical fluid chromatography in pharmaceutical analysis, J. Pharm. Biomed. Anal. 113 (2015) 56–71.
[20] L. Novakova, V. Desfontaine, F. Ponzetto, R. Nicoli, M. Saugy, J. Veuthey, D. Guillarme, Fast and sensitive supercritical fluid chromatography - tandem mass spectrometry multi-class screening method for the determination of doping agents in urine, Anal. Chim. Acta 915 (2016) 102–110.
[21] A.G. Perrenoud, J. Veuthey, D. Guillarme, Comparison of ultra-high performance supercritical fluid chromatography and ultra-high performance liquid chromatography for the analysis of pharmaceutical compounds, J. Chromatogr. A 1266 (2012) 158–167.
[22] M.A. Khalikova, D. Satinsky, P. Solich, L. Novakova, Development and validation of ultra-high performance supercritical fluid chromatography method for determination of illegal dyes and comparison to ultra-high performance liquid chromatography method, Anal. Chim. Acta 874 (2015) 84–96.
[23] L. Zhu, Y. Zhao, Y. Xu, Q. Sun, X. Sun, L. Kang, R. Yan, J. Zhang, L. Chao, B. Ma, Comparison of ultra-high performance supercritical fluid chromatography and ultra-high performance liquid chromatography for the separation of spirostanol saponins, J. Pharm. Biomed. Anal. 120 (2016) 72–78.
[24] J. Zheng, J.D. Pinkston, P.H. Zoutendam, L.T. Taylor, Feasibility of supercritical fluid chromatography/mass spectrometry of polypeptides with up to 40-mers, Anal. Chem. 78 (2006) 1535–1545.
[25] A. Cazenave-Gassiot, R. Boughtflower, J. Caldwell, L. Hitzel, C. Holyoak, S. Lane, P. Oakley, F. Pullen, S. Richardson, J. Langley, Effect of increasing concentration of ammonium acetate as an additive in supercritical fluid chromatography using CO2-methanol mobile phase, J. Chromatogr. A 1216 (2009) 6441–6450.
[26] E. Lesellier, Usual, unusual and unbelievable retention behavior in achiral supercritical fluid chromatography: review and discussion, J. Chromatogr. A 1614 (2020), 460582.
[28] M. Xhaferaj, E. Naegele, M.K. Parr, Ion exchange in supercritical fluid chromatography tandem mass spectrometry (SFC-MS/MS): application for polar and ionic drugs and metabolites in forensic and anti-doping analysis, J. Chromatogr. A 1614 (2020), 460726.
[27] G. Guiochon, A.J. Tarafder, Fundamental challenges and opportunities for preparative supercritical fluid Chromatography, J. Chromatogr. A 1218 (2011) 1037–1114.
[29] D. Roy, A. Tarafder, L. Miller, Effect of water addition to super/sub-critical fluid mobile-phases for achiral and chiral separations, Trends Anal. Chem. 145 (2021), 116464.
[30] Y. Hsieh, F. Li, J.G. Duncan, Supercritical fluid chromatography and high-performance liquid chromatography/tandem mass spectrometric methods for the determination of cytarabine in mouse plasma, Anal. Chem. 79 (2007) 3856–3861.
[31] V. Desfontaine, G.L. Losacco, Y. Gagnebin, J. Pezzatti, W.P. Farrell, V. Gonzalez-Ruiz, S. Rudaz, J. Veuthey, D. Guillarme, Applicability of supercritical fluid chromatography - mass spectrometry to metabolomics. I - optimization of separation conditions for the simultaneous analysis of hydrophilic and lipophilic substances, J. Chromatogr. A 1562 (2018) 96–107.
[32] Y. Huang, T. Wang, M. Fillet, J. Crommen, Z. Jiang, Simultaneous determination of amino acids in different teas using supercritical fluid chromatography coupled with single quadrupole mass spectrometry, J. Pharm. Anal. 9 (2019) 254–258.
[33] G.L. Losacco, E. Marconetto, R. Nicoli, T. Kuuranne, J. Boccard, S. Rudaz, J. Veuthey, D. Guillarme, Supercritical fluid chromatography-mass spectrometry in routine anti-doping analyses: estimation of retention time variability under reproducible conditions, J. Chromatogr. A 1616 (2020), 460780.
[34] M.A. Khalikova, E. Lesellier, E. Chapuzet, D. Satinsky, C. West, Development and validation of ultra-high performance supercritical fluid chromatography method for quantitative determination of nine sunscreens in cosmetic samples, Anal. Chim. Acta 1034 (2018) 184–194.
[35] A. Sen, C. Knappy, M. Lewis, R.S. Plumb, I.D. Wilson, J.K. Nicholson, N.W. Smith, Analysis of polar urinary metabolites for metabolic phenotyping using supercritical fluid chromatography and mass spectrometry, J. Chromatogr. A 1449 (2016) 141–155.
[36] G. Rosseaux, A. De Wit, M. Martin, Viscous fingering in packed chromatographic columns: linear stability analysis, J. Chromatogr. A 1149 (2007) 254–273.
[37] G. Rosseaux, M. Martin, A. De Wit, Viscous fingering in packed chromatographic columns: non-linear dynamics, J. Chromatogr. A 1218 (2011) 8353–8361.
[38] V. Desfontaine, A. Tarafder, J. Hill, J. Fairchild, A.G. Perrenoud, J. Veuthey, D. Guillarme, A systematic investigation of sample diluents in modern supercritical fluid chromatography, J. Chromatogr. A 1511 (2017) 122–131.
[39] P.R. Fields, T.L. Chester, A.M. Stalcup, Viscosity estimation in binary and ternary supercritical fluid mixtures containing carbon dioxide using a supercritical fluid chromatograph, J. Liq. Chromatogr. Relat. 34 (2011) 995–1003.
[40] A.G. Perrenoud, J. Veuthey, D. Guillarme, Coupling state-of-the-art supercritical fluid chromatography and mass spectrometry: from hyphenation interface optimization to high-sensitivity analysis of pharmaceutical compounds, J. Chromatogr. A 1339 (2014) 174–184.
[41] L. Novakova, A.G. Perrenoud, R. Nicoli, M. Saugy, J. Veuthey, D. Guillarme, Ultra high performance supercritical fluid chromatography coupledwith tandem mass spectrometry for screening of doping agents. I: investigation of mobile phase and MS conditions, Anal. Chim. Acta 853 (2015) 637–646.
[42] K. Plachka, F. Svec, L. Novakova, Ultra-high performance supercritical fluid chromatography in impurity control: searching for generic screening approach, Anal. Chim. Acta 1039 (2018) 149–161.
[43] V. Pilarova, K. Plachka, M.A. Khalikova, F. Svec, L. Novakova, Recent developments in supercritical fluid chromatography - mass spectrometry: is it a viable option for analysis of complex samples? Trends Anal. Chem. 112 (2019) 212–225.
[44] L. Novakova, M. Rentsch, A.G. Perrenoud, R. Nicoli, M. Saugy, J. Veuthey, D. Guillarme, Ultra high performance supercritical fluid chromatography coupled with tandem mass spectrometry for screening of doping agents. II: analysis of biological samples, Anal. Chim. Acta 853 (2015) 647–659.
[45] V. Desfontaine, L. Novakova, F. Ponzetto, R. Nicoli, M. Saugy, J. Veuthey, D. Guillarme, Liquid chromatography and supercritical fluid chromatography as alternative techniques to gas chromatography for the rapid screening of anabolic agents in urine, J. Chromatogr. A 1451 (2016) 145–155.
[46] A. Svan, M. Hedeland, T. Arvidsson, C.E. Pettersson, The differences in matrix effect between supercritical fluid chromatography and reversed phase liquid chromatography coupled to ESI/MS, Anal. Chim. Acta 1000 (2018) 163–171.
[47] L.R. Snyder, J.J. Kirkland, J.W. Dolan, Introduction to Modern Liquid Chromatography, third ed., Wiley, New York, 2009.
[48] L. Plackova, J. Oklestkova, K. Pospiskova, K. Polakova, J. Bucek, J. Styskala, M. Zatloukal, I. Safarik, R. Zboril, M. Strnad, K. Dolezal, O. Novak, Microscale magnetic microparticle-based immunopurification of cytokinins from Arabidopsis root apex, Plant J. 89 (2017) 1065–1075.
[49] P. Hosek, K. Hoyerova, N.S. Kiran, P.I. Dobrev, L. Zahajska, R. Filepova, V. Motyka, K. Muller, M. Kaminek, Distinct metabolism of N-glucosides of isopentenyladenine and trans-zeatin determines cytokinin metabolic spectrum in Arabidopsis, New Phytol. 225 (2020) 2423–2438.

Appendix A. Supplementary Figures:

Rapid profiling of cytokinins using supercritical fluid chromatography coupled with tandem mass spectrometry

Ivan Petřík [a], Aleš Pěnčík [a], Jakub Stýskala [b], Lenka Tranová [b], Petra Amakorová [a], Miroslav Strnad [a], Ondřej Novák [a,*]

[a] Laboratory of Growth Regulators, The Czech Academy of Sciences, Institute of Experimental Botany & Palacký University, Faculty of Science, Šlechtitelů 27, CZ-78371 Olomouc, Czech Republic.

[b] Department of Organic Chemistry, Palacký University, Faculty of Science, 17. listopadu 1192/12, CZ-77146 Olomouc, Czech Republic

*Corresponding author: novako@ueb.cas.cz

Contents:

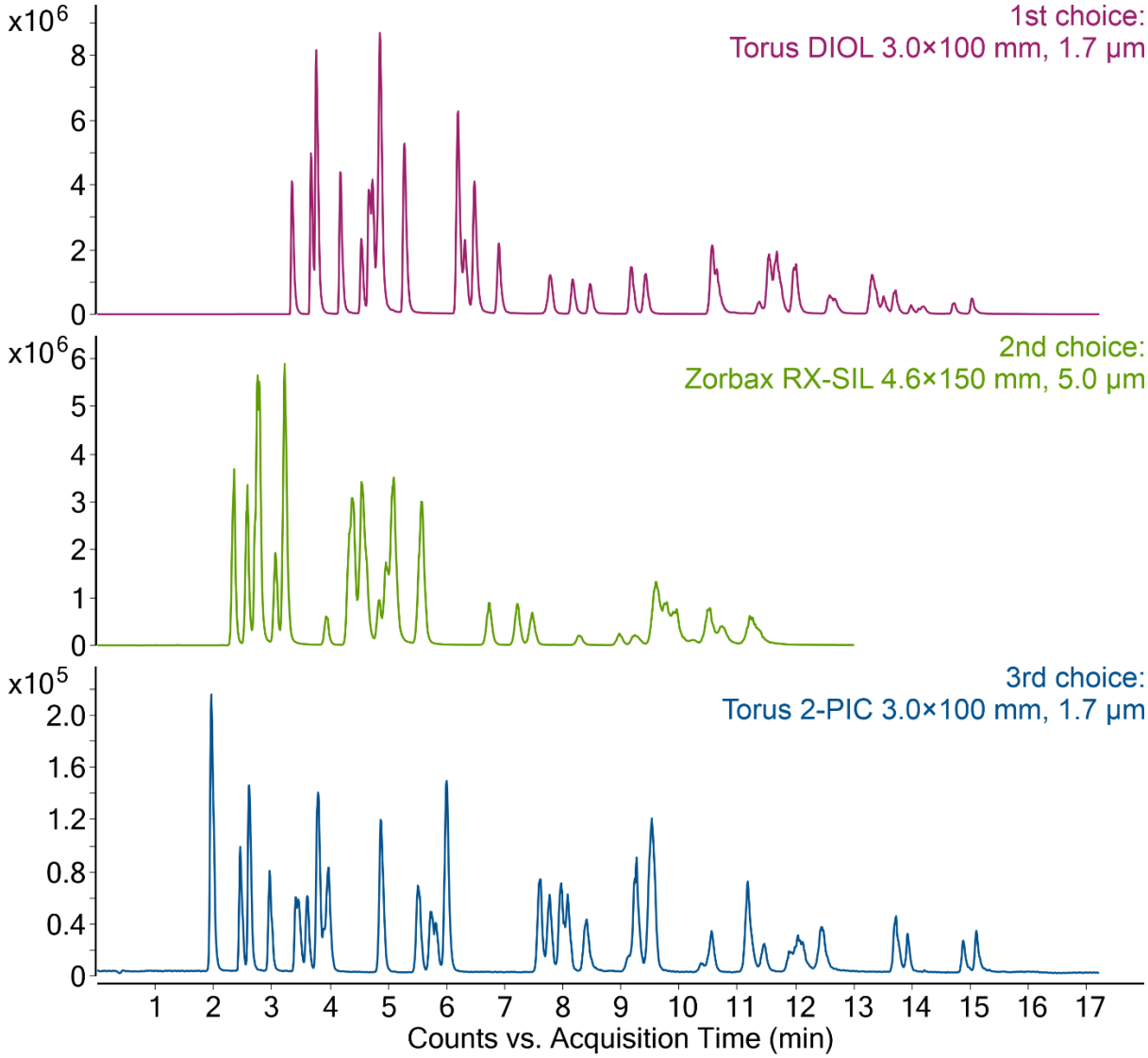

Figure A.4. Elution profiles of chromatographic columns tested – Zorbax Eclipse Plus C18 (red), Torus DIOL (yellow), Zorbax RX SIL (green) and Torus 2-PIC (blue). The vertical axis represents the total ion current of the MS/MS signal. 2 µL of 10^{-7} M mixture of CK standards dissolved in methanol were injected.

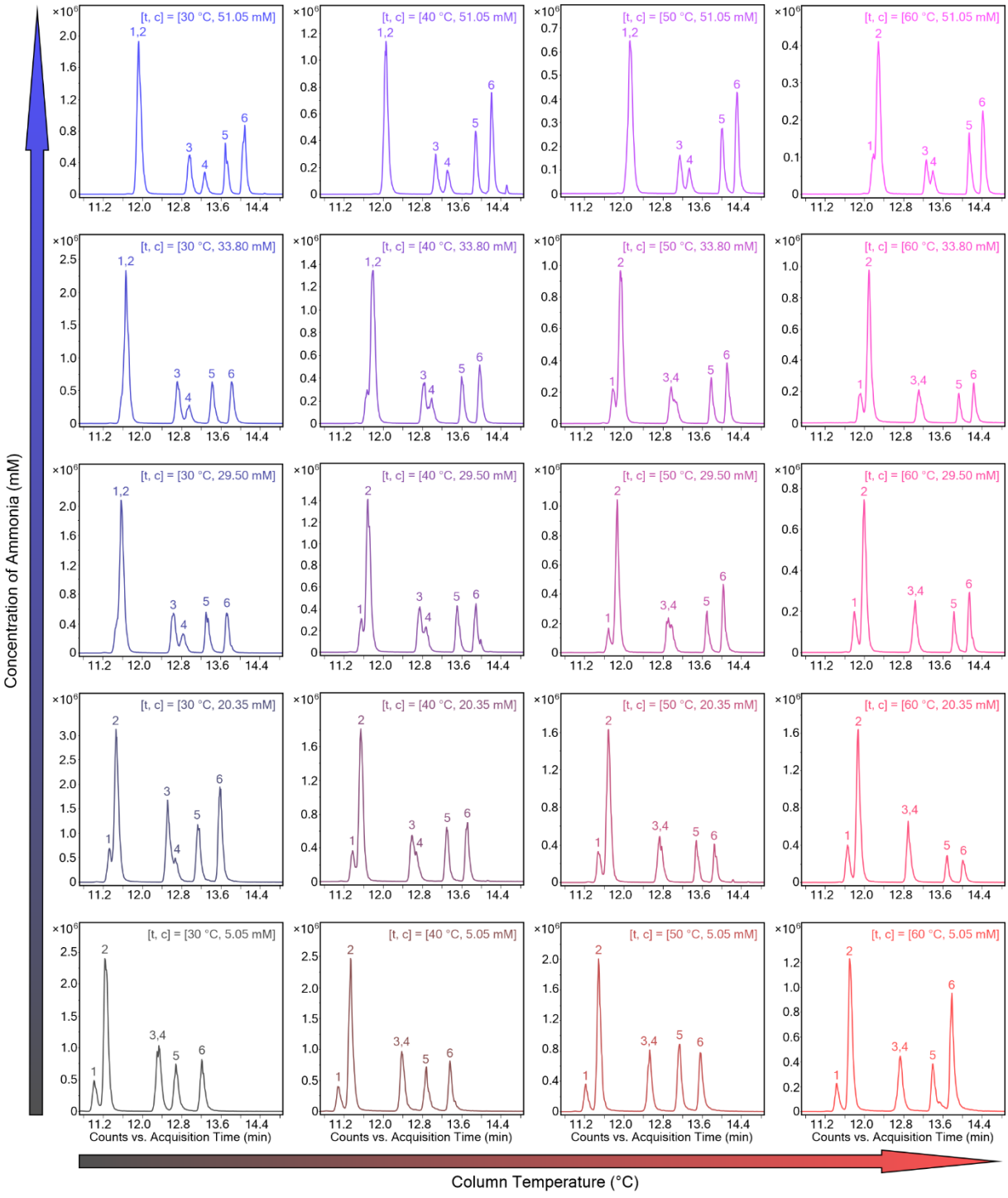

Figure A.5. Chromatographic selectivity of Torus DIOL column as a function of column temperature (t = 30, 40, 50 and 60 °C) and ammonia concentration (c = 5.05, 20.35, 29.50, 33.80 and 51.05 mM) in mobile phase B consisting of 15 mM formic acid in 5% water and 95% methanol (v/v). 2 µL of 10^{-7} M mixture of CK standards dissolved in methanol were injected. The order of CK metabolite was as follows: (1) *c*ZOG, (2) *c*Z9G, (3) *t*ZOG, (4) *t*Z9G, (5) *c*Z7G and (6) *t*Z7G.

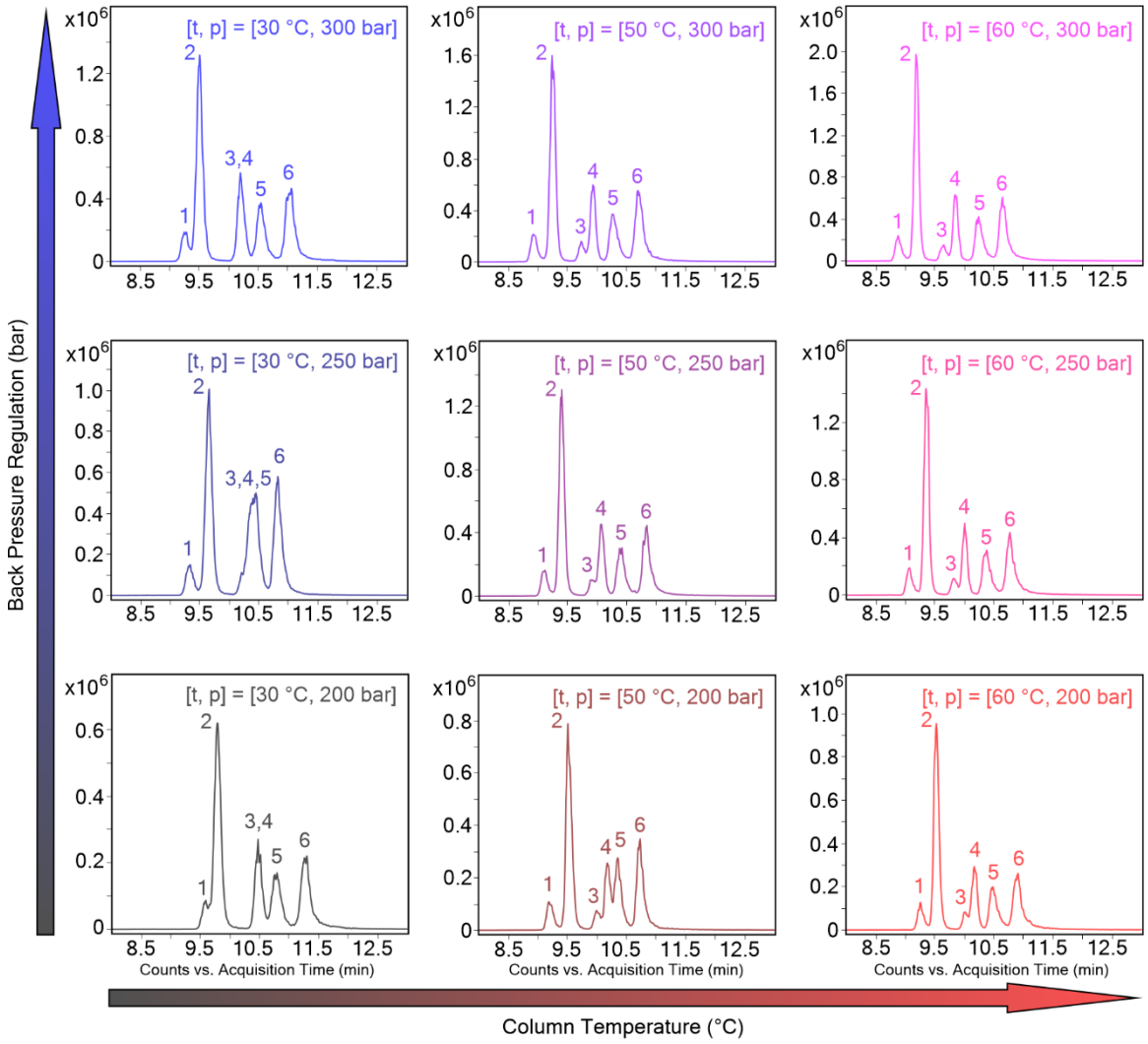

Figure A.6. Chromatographic selectivity of Zorbax RX-SIL column as a function of column temperature (t = 30, 40 and 60) and BPR (p = 200, 250 and 300 bar). 2 µL of 10^{-7} M mixture of CK standards dissolved in methanol were injected. The order of CK metabolite was as follows: (1) *c*ZOG, (2) *c*Z9G, (3) *t*ZOG, (4) *t*Z9G, (5) *c*Z7G and (6) *t*Z7G.

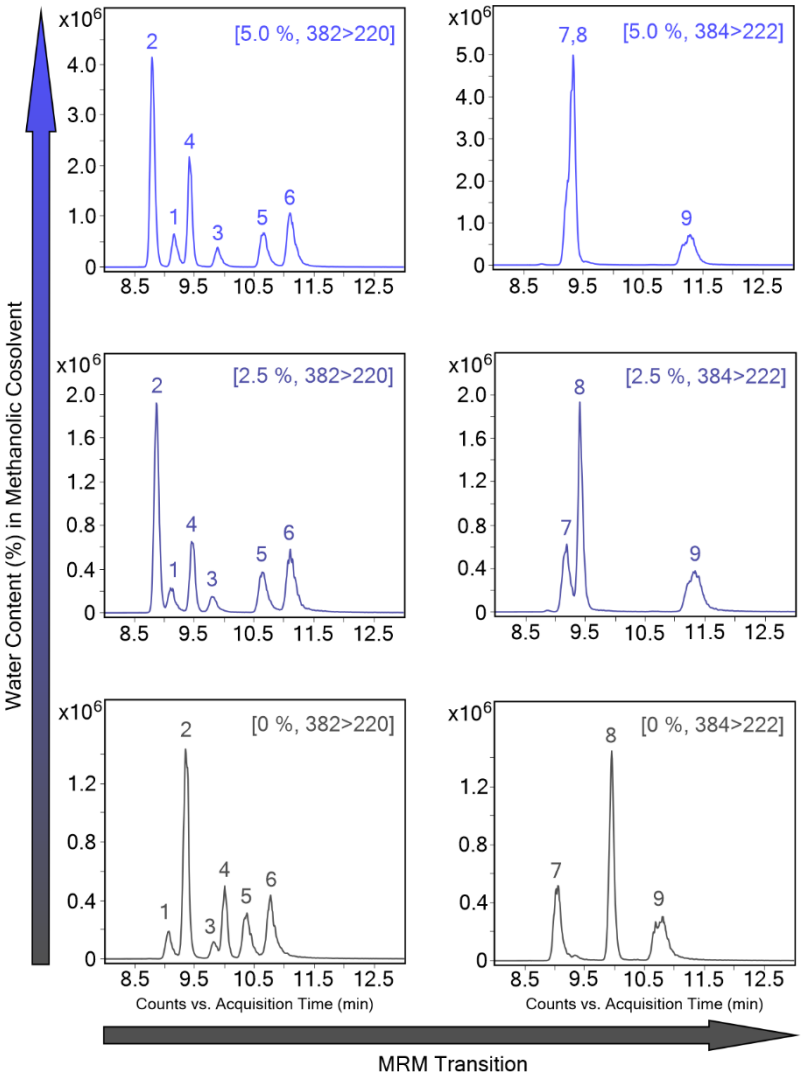

Figure A.7. Effect of water content (0%, 2.5% and 5.0%) in the methanolic co-solvent of the mobile phase on the chromatographic selectivity of the Zorbax RX-SIL column. 2 µL of 10^{-7} M mixture of CK standards dissolved in methanol were injected. The order of CK metabolite was as follows: (1) *c*ZOG, (2) *c*Z9G, (3) *t*ZOG, (4) *t*Z9G, (5) *c*Z7G, (6) *t*Z7G, (7) DHZOG, (8) DHZ9G and (9) DHZ7G.

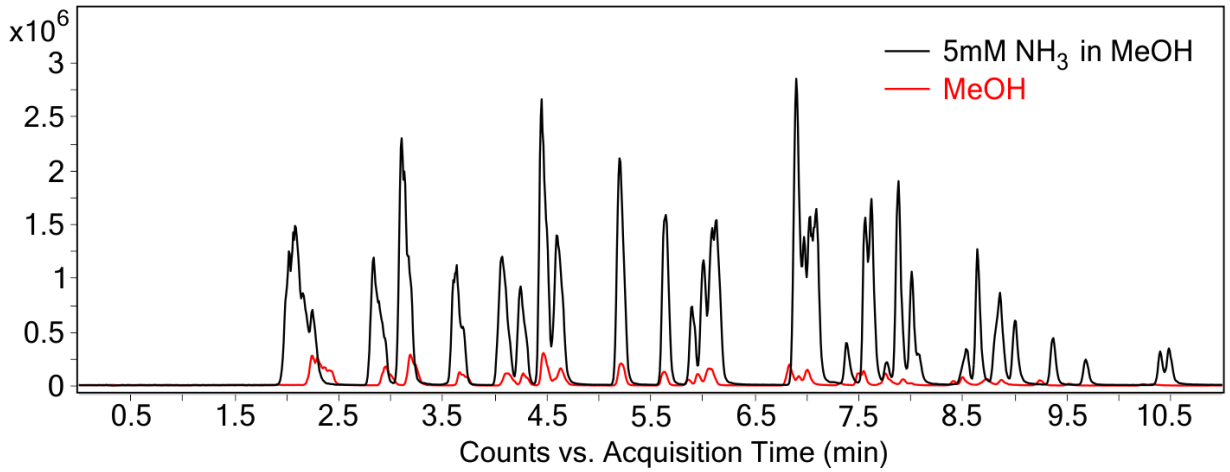

Figure A.8. Effect of ammonia (5 mM) added to the methanolic mobile phase on the total ion current of the MS/MS signal using a Torus 2-PIC column.

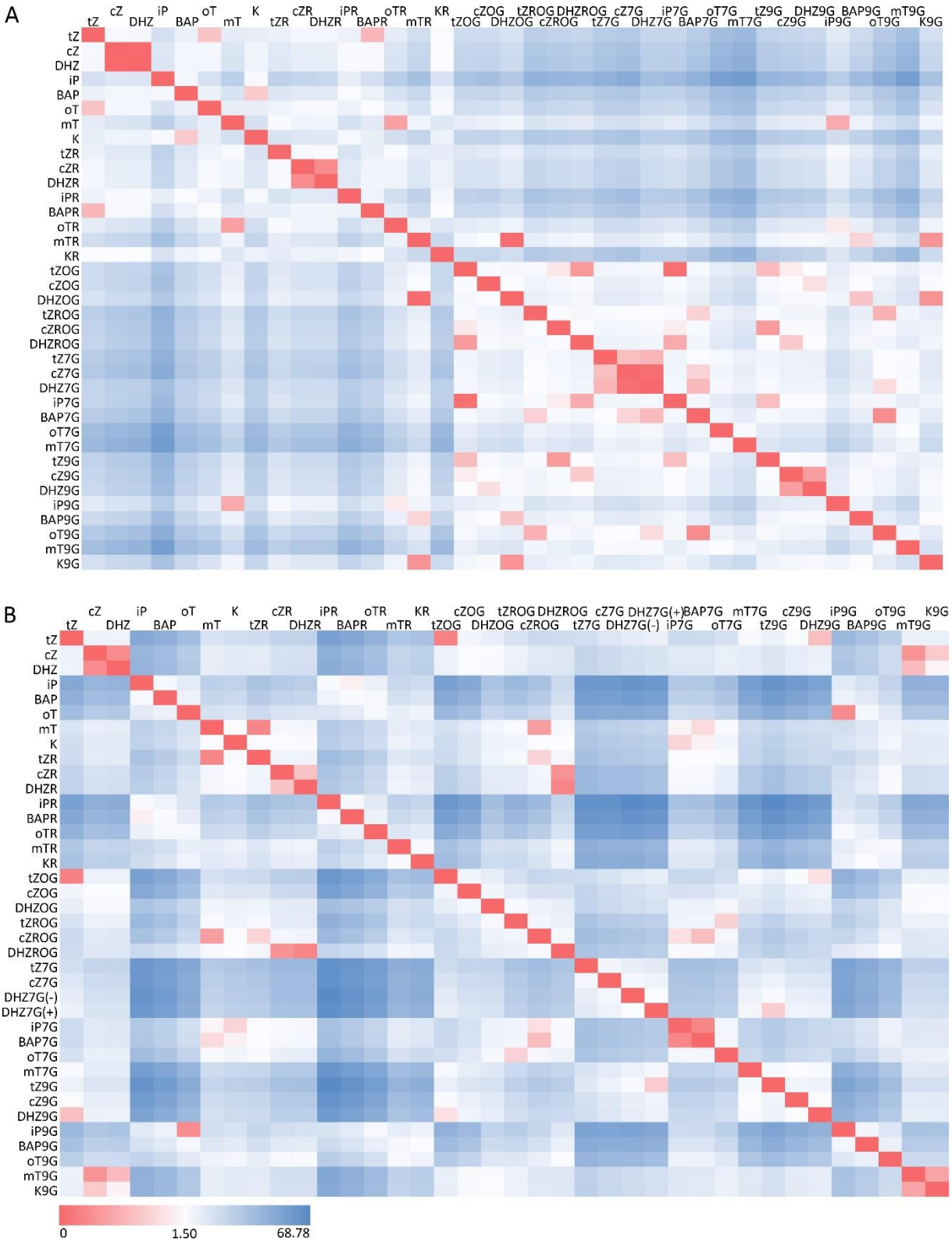

Figure A.10. Overall chromatographic resolution in UHPSFC (A) and UHPLC (B) modes. Value 1.5 (white) represents baseline separation. Values < 1.5 (red) show overlapping peaks and > 1.5 (blue) peaks up to maximal observed resolution (68.78).

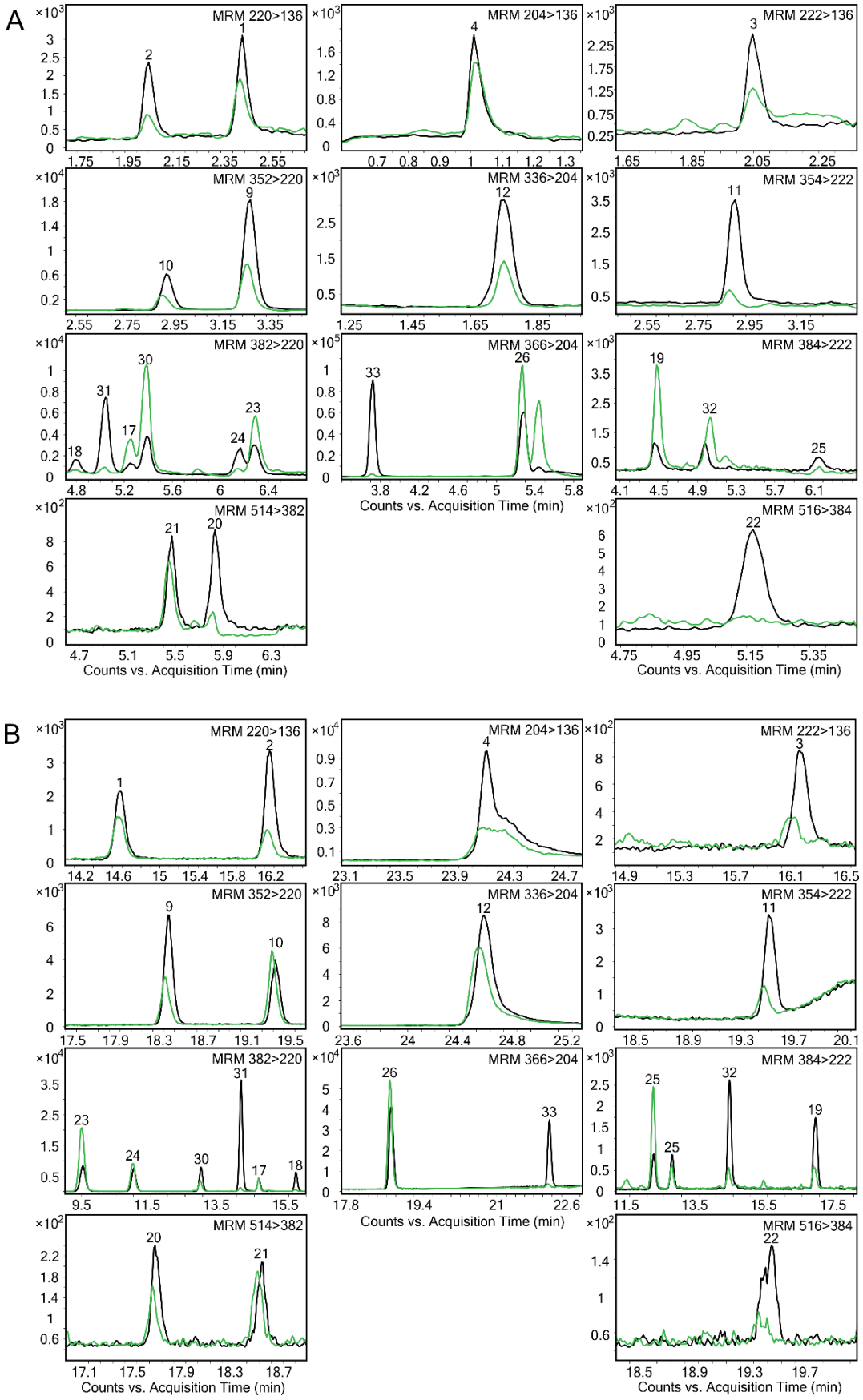

Figure A.12. Chromatograms of CK metabolites detected in purified *Arabidopsis* extract (green line) and in neat standard (black line) using UHPSFC-MS/MS (A) and UHPLC-MS/MS (B). The signal intensity of appropriate CK standard is represented by the nearest calibration point of the respective endogenous concentration.

Appendix A. Supplementary data:

Rapid profiling of cytokinins using supercritical fluid chromatography coupled with tandem mass spectrometry

Ivan Petřík [a], Aleš Pěnčík [a], Jakub Stýskala [b], Lenka Tranová [b], Petra Amakorová [a], Miroslav Strnad [a], Ondřej Novák [a,*]

[a] Laboratory of Growth Regulators, The Czech Academy of Sciences, Institute of Experimental Botany & Palacký University, Faculty of Science, Šlechtitelů 27, CZ-78371 Olomouc, Czech Republic.

[b] Department of Organic Chemistry, Palacký University, Faculty of Science, 17. listopadu 1192/12, CZ-77146 Olomouc, Czech Republic

*Corresponding author: novako@ueb.cas.cz

Contents:

Method A.3. Development of chromatographic method.

First, a Torus DIOL (3.0×100 mm, 1.7 μm; Waters, Milford, CT, USA) was utilized in combination with a mobile phase consisting of $scCO_2$ (A) and 15 mM ammonium formate in 5% water and 95% methanol (v/v) (B). A linear gradient from 0% to 40% B in 15 min was applied to elute all CK metabolites. The flow rate of the mobile phase was 1.5 mL min^{-1}, the column temperature was 40 °C and the back pressure was 160 bar. Mobile phase B was prepared as follows: an aqueous solution 300 mM formic acid was prepared and adjusted with 25% ammonium hydroxide (v/v) to concentration 0.10, 0.41, 0.59, 0.68 and 1.02 M. Each solution was then diluted 20-fold in methanol.

Second, the sample was injected into a Zorbax RX-SIL (4.6×150 mm, 5.0 μm; Agilent Technologies, Santa Clara, CA USA). The generic conditions were applied as followed: linear gradient elution of $scCO_2$ (A) and methanol (B) raising 15–45% B in 12 min at a constant flow rate of 2.5 mL min^{-1}. The column temperature was 30 °C and BPR was set to 200 bar.

Third, a Torus 2-PIC (3.0×100 mm, 1.7 μm; Waters, Milford, CT USA) was combined with a mobile phase consisting of $scCO_2$ (A) and 5% water in methanol (v/v) (B). CK metabolites were eluted with 0–40% B in 15 min. The flow rate was 1.5 mL min^{-1}, the column was heated to 50 °C and the back pressure was set to 160 bar. The effect on MS signal enhancement was tested by adding 5 mM ammonia to mobile phase B.

Appendix A. Supplementary data:

Rapid profiling of cytokinins using supercritical fluid chromatography coupled with tandem mass spectrometry

Ivan Petřík [a], Aleš Pěnčík [a], Jakub Stýskala [b], Lenka Tranová [b], Petra Amakorová [a], Miroslav Strnad [a], Ondřej Novák [a,*]

[a] Laboratory of Growth Regulators, The Czech Academy of Sciences, Institute of Experimental Botany & Palacký University, Faculty of Science, Šlechtitelů 27, CZ-78371 Olomouc, Czech Republic.

[b] Department of Organic Chemistry, Palacký University, Faculty of Science, 17. listopadu 1192/12, CZ-77146 Olomouc, Czech Republic

*Corresponding author: novako@ueb.cas.cz

Contents:

Table A.1. List of compounds and their physicochemical properties.

No	Name	Acronym	Formula	Mw [a]	logP [b]	pK_a [c]	pK_b [d]	H donors/ acceptors
CK bases								
1	*trans*-zeatin	*t*Z	$C_{10}H_{13}N_5O$	219.11	−0.15	9.87	4.03	2/2
2	*cis*-zeatin	*c*Z	$C_{10}H_{13}N_5O$	219.11	−0.15	9.87	4.03	2/2
3	dihydrozeatin	DHZ	$C_{10}H_{15}N_5O$	221.12	0.02	9.87	4.07	2/2
4	isopentenyl adenine	iP	$C_{10}H_{13}N_5$	203.12	1.13	9.87	4.03	1/2
5	benzyladenine	BA	$C_{12}H_{11}N_5$	225.10	1.50	9.87	4.03	1/2
6	*ortho*-topolin	*o*T	$C_{12}H_{11}N_5O$	241.10	1.19	9.14	4.03	2/2
7	*meta*-topolin	*m*T	$C_{12}H_{11}N_5O$	241.10	1.19	9.28	4.03	2/2
8	kinetin	K	$C_{10}H_9N_5O$	215.08	0.56	9.86	4.01	1/2
CK ribosides								
9	*trans*-zeatin riboside	*t*ZR	$C_{15}H_{21}N_5O_5$	351.15	−1.71	12.45	3.72	4/2
10	*cis*-zeatin riboside	*c*ZR	$C_{15}H_{21}N_5O_5$	351.15	−1.71	12.45	3.72	4/2
11	dihydrozeatin riboside	DHZR	$C_{15}H_{23}N_5O_5$	353.17	−1.54	12.45	3.76	4/2
12	isopentenyladenosine	iPR	$C_{15}H_{21}N_5O_4$	335.16	−0.43	12.45	3.72	3/2
13	benzyladenine riboside	BAR	$C_{17}H_{19}N_5O_4$	357.14	−0.06	12.45	3.72	3/2
14	*ortho*-topolin riboside	*o*TR	$C_{17}H_{19}N_5O_5$	373.14	−0.37	9.23	3.72	4/2
15	*meta*-topolin riboside	*m*TR	$C_{17}H_{19}N_5O_5$	373.14	−0.37	9.42	3.72	4/2
16	kinetin riboside	KR	$C_{15}H_{17}N_5O_5$	347.12	−1.00	12.45	3.70	4/2
CK *O*-glucosides								
17	*trans*-zeatin *O*-glucoside	*t*ZOG	$C_{16}H_{23}N_5O_6$	381.16	−1.92	9.86	4.03	5/2
18	*cis*-zeatin *O*-glucoside	*c*ZOG	$C_{16}H_{23}N_5O_6$	381.16	−1.92	9.86	4.03	5/2
19	dihydrozeatin *O*-glucoside	DHZOG	$C_{16}H_{25}N_5O_6$	383.18	−1.75	9.87	4.07	5/2
20	*trans*-zeatin riboside *O*-glucoside	*t*ZROG	$C_{21}H_{31}N_5O_{10}$	513.21	−3.48	12.01	4.70	7/1
21	*cis*-zeatin riboside *O*-glucoside	*c*ZROG	$C_{21}H_{31}N_5O_{10}$	513.21	−3.48	12.01	4.70	7/1
22	dihydro-zeatin riboside *O*-glucoside	DHZROG	$C_{21}H_{33}N_5O_{10}$	515.22	−3.31	12.01	4.74	7/1
CK N^7-glucosides								
23	*trans*-zeatin N^7-glucoside	*t*Z7G	$C_{16}H_{23}N_5O_6$	381.16	−2.38	12.36	3.33	5/1
24	*cis*-zeatin N^7-glucoside	*c*Z7G	$C_{16}H_{23}N_5O_6$	381.16	−2.38	12.36	3.33	5/1
25	dihydrozeatin N^7-glucoside	DHZ7G	$C_{16}H_{25}N_5O_6$	383.18	−2.21	12.36	3.37	5/1
26	isopentenyladenine N^7-glucoside	iP7G	$C_{16}H_{23}N_5O_5$	365.17	−1.10	12.36	3.33	4/1
27	benzyladenine N^7-glucoside	BA7G	$C_{18}H_{21}N_5O_5$	387.15	−0.74	12.36	3.33	4/1
28	*ortho*-topolin N^7-glucoside	*o*T7G	$C_{18}H_{21}N_5O_6$	403.15	−1.04	9.23	3.33	5/1
29	*meta*-topolin N^7-glucoside	*m*T7G	$C_{18}H_{21}N_5O_6$	403.15	−1.04	9.42	3.33	5/1
CK N^9-glucosides								
30	*trans*-zeatin N^9-glucoside	*t*Z9G	$C_{16}H_{23}N_5O_6$	381.16	−2.34	12.36	3.72	5/2
31	*cis*-zeatin N^9-glucoside	*c*Z9G	$C_{16}H_{23}N_5O_6$	381.16	−2.34	12.36	3.72	5/2
32	dihydrozeatin N^9-glucoside	DHZ9G	$C_{16}H_{25}N_5O_6$	383.18	−2.17	12.36	3.76	5/2
33	isopentenyladenine N^9-glucoside	iP9G	$C_{16}H_{23}N_5O_5$	365.17	−1.06	12.36	3.72	4/2
34	benzyladenine N^9-glucoside	BA9G	$C_{18}H_{21}N_5O_5$	387.15	−0.70	12.36	3.72	4/2
35	*ortho*-topolin N^9-glucoside	*o*T9G	$C_{18}H_{21}N_5O_6$	403.15	−1.00	9.23	3.72	5/2
36	*meta*-topolin N^9-glucoside	*m*T9G	$C_{18}H_{21}N_5O_6$	403.15	−1.00	9.42	3.72	5/2
37	kinetin N^9-glucoside	K9G	$C_{16}H_{19}N_5O_6$	377.13	−1.63	12.36	3.70	5/2

All properties were predicted by MarvinSketch 19.10 (ChemAxon Ltd., Budapest, Hungary).

[a] exact molecular weight

[b] octanol-water partition coefficient

[c] the most basic pKa

[d] the most acidic pKb

Table A.2. Optimized MS parameters for CK metabolites and appropriate isotopic labeled internal standards.

	Compound	MRM transition	CE [a] (eV)	Internal standard	
				Compound	MRM transition
CK bases					
1	*t*Z	220.1>136.0	18	[$^{13}C_5$]-*t*Z	225.1>141.0
2	*c*Z	220.1>136.0	18	[$^{13}C_5$]-*c*Z	225.1>141.0
3	DHZ	222.1>136.0	22	[$^{2}H_3$]-DHZ	225.1>136.0
4	iP	204.3>136.1	18	[$^{2}H_6$]-iP	210.3>137.1
5	BA	226.3>91.0	26	[$^{2}H_7$]-BAP	233.3>98.0
6	*o*T	242.1>140.0	18	[$^{15}N_4$]-*o*T	246.1>140.0
7	*m*T	242.1>107.0	24	[$^{15}N_4$]-*m*T	246.1>107.0
8	K	216.1>81.0	22	[$^{15}N_4$]-K	220.1>81.0
CK ribosides					
9	*t*ZR	352.2>220.1	20	[$^{2}H_5$]-*t*ZR	357.2>225.1
10	*c*ZR	352.2>220.1	20	[$^{2}H_3$]-DHZR	357.2>225.1
11	DHZR	354.2>222.1	22	[$^{2}H_3$]-DHZR	357.2>225.1
12	iPR	336.4>204.1	20	[$^{2}H_6$]-iPR	342.4>210.1
13	BAR	358.4>226.2	20	[$^{2}H_7$]-BAR	365.4>233.2
14	*o*TR	374.2>242.1	22	[$^{15}N_4$]-*o*TR	378.4>246.2
15	*m*TR	374.2>242.1	22	[$^{15}N_4$]-*m*TR	378.4>246.2
16	KR	348.2>216.1	20	[$^{2}H_7$]-BAR	365.4>233.2
CK *O*-glucosides					
17	*t*ZOG	382.2>220.1	20	[$^{2}H_5$]-*t*ZOG	387.2>225.1
18	*c*ZOG	382.2>220.1	20	[$^{2}H_5$]-*t*ZOG	387.2>225.1
19	DHZOG	384.2>222.1	24	[$^{2}H_7$]-DHZOG	391.2>229.1
20	*t*ZROG	514.2>382.1	22	[$^{2}H_5$]-*t*ZROG	519.2>387.1
21	*c*ZROG	514.2>382.1	22	[$^{2}H_3$]-DHZ9G	387.2>225.1
22	DHZROG	516.2>384.1	22	[$^{2}H_3$]-DHZ9G	387.2>225.1
CK *N*7-glucosides					
23	*t*Z7G	382.2>220.1	20	[$^{2}H_5$]-*t*Z7G	387.2>225.1
24	*c*Z7G	382.2>220.1	20	[$^{15}N_4$]-*c*Z7G	386.2>224.1
25	DHZ7G	384.2>222.1	24	[$^{15}N_4$]-*c*Z7G	386.2>224.1
26	iP7G	366.2>204.1	20	[$^{2}H_6$]-iP7G	372.2>210.1
27	BA7G	388.2>226.1	24	[$^{15}N_4$]-*cZ7G*	386.2>224.1
28	*o*T7G	404.2>242.1	20	[$^{15}N_4$]-*o*T7G	408.2>246.1
29	*m*T7G	404.2>242.1	20	[$^{15}N_4$]-*m*T7G	408.2>246.1
CK *N*9-glucosides					
30	*t*Z9G	382.2>220.1	20	[$^{2}H_3$]-DHZ9G	387.2>225.1
31	*c*Z9G	382.2>220.1	20	[$^{2}H_3$]-DHZ9G	387.2>225.1
32	DHZ9G	384.2>222.1	24	[$^{2}H_3$]-DHZ9G	387.2>225.1
33	iP9G	366.2>204.1	20	[$^{2}H_6$]-iP9G	372.2>210.1
34	BA9G	388.2>226.1	24	[$^{2}H_7$]-BA9G	395.2>233.1
35	*o*T9G	404.2>242.1	20	[$^{15}N_4$]-*o*T9G	408.2>246.1
36	*m*T9G	404.2>242.1	20	[$^{15}N_4$]-*m*T9G	408.2>246.1
37	K9G	378.2>216.1	20	[$^{2}H_7$]-BA9G	395.2>233.1

[a] CE - collision energy

Table A.9. Chromatography parameters in UHPSFC and UHPLC determined at 50 fmol per injection.

#	Compound	RT [a]		Peak Symmetry		FWHM [b]		Column Efficiency		Resolution [c]	
		UHPSFC	UHPLC	UHPSFC	UHPLC	UHPSFC	UHPLC	UHPSFC	UHPLC	UHPSFC	UHPLC
CK bases											
1	tZ	2.43	14.58	1.60	1.39	0.050	0.118	13126	84681	4.66	7.94
2	cZ	2.05	16.15	1.45	1.28	0.046	0.116	10791	107221	4.66	7.94
3	DHZ	2.05	16.08	1.63	1.46	0.040	0.111	14292	117246	-	-
4	iP	1.01	24.09	2.43	1.34	0.036	0.089	4359	409680	-	-
5	BAP	1.47	23.39	2.00	1.52	0.074	0.092	2223	360210	-	-
6	oT	2.52	22.07	1.19	1.66	0.059	0.096	9965	292420	10.15	18.51
7	mT	3.62	18.39	1.50	1.94	0.068	0.138	15501	97868	10.15	18.51
8	K	1.34	18.92	2.63	1.21	0.072	0.130	1932	117177	-	-
CK ribosides											
9	tZR	3.26	18.33	1.22	1.20	0.058	0.092	17690	218631	3.72	6.53
10	cZR	2.92	19.31	1.08	1.02	0.051	0.085	18077	286575	3.72	6.53
11	DHZR	2.88	19.46	1.50	0.94	0.052	0.088	16855	270929	-	-
12	iPR	1.76	24.51	1.26	1.21	0.046	0.080	8006	519654	-	-
13	BAPR	2.36	23.87	1.30	1.23	0.046	0.082	14421	465043	-	-
14	oTR	3.55	22.73	1.45	1.77	0.059	0.081	19974	440578	8.32	15.77
15	mTR	4.44	20.55	1.19	1.52	0.066	0.082	24891	345682	8.32	15.77
16	KR	2.21	20.98	1.46	1.29	0.045	0.080	13315	381913	-	-
CK O-glucosides											
17	tZOG	5.23	14.63	0.79	1.34	0.099	0.098	15463	123093	0.91	3.03
18	cZOG	4.78	15.71	1.20	1.08	0.076	0.093	22089	157597	1.93	6.69
19	DHZOG	4.45	16.86	1.86	1.49	0.082	0.142	16124	78084	3.76	11.58
20	tZROG	5.80	17.64	1.23	1.37	0.081	0.084	28387	246513	2.77	6.15
21	cZROG	5.43	18.50	1.47	1.22	0.076	0.082	28099	279760	2.77	6.15
22	DHZROG	5.15	19.40	1.04	0.82	0.071	0.142	28799	102815	-	-
CK N7-glucosides											
23	tZ7G	6.25	9.54	1.41	1.12	0.091	0.175	26083	16421	0.93	5.36
24	cZ7G	6.11	11.01	1.09	1.11	0.078	0.150	33847	29833	0.93	5.36
25	DHZ7G*	6.10	12.21	1.33	1.07	0.114	0.119	15934	57834		2.69
			12.75		0.94		0.118		65124	7.23	2.69
26	iP7G	5.24	18.70	1.62	1.09	0.080	0.096	23711	208340	12.68	22.64
27	BAP7G	5.96	18.64	1.68	1.44	0.084	0.096	27867	208904	11.11	17.35
28	oT7G	6.94	17.80	1.56	1.19	0.082	0.088	40052	227978	2.17	9.93
29	mT7G	7.58	13.82	1.69	1.17	0.089	0.110	40356	87543	6.76	13.71
CK N9-glucosides											
30	tZ9G	5.36	12.96	0.87	1.29	0.074	0.107	28951	81802	0.91	6.70
31	cZ9G	5.02	14.12	0.92	1.08	0.070	0.099	28242	113418	1.93	3.03
32	DHZ9G	4.95	14.40	1.24	1.05	0.075	0.109	24176	96390	3.76	8.58
33	iP9G	3.70	22.13	1.28	1.16	0.063	0.083	19019	397954	12.68	22.64
34	BAP9G	4.57	21.32	1.14	1.58	0.063	0.086	28928	337810	11.11	17.35
35	oT9G	5.90	19.94	1.26	1.13	0.076	0.089	33702	278151	5.93	14.26
36	mT9G	6.65	16.24	1.15	1.53	0.074	0.098	45144	151283	2.17	9.93
37	K9G	4.39	16.34	1.26	1.19	0.067	0.099	23404	151768	-	-

[a] Retention time (min)

[b] Full width at half maximum

[c] Resolution against the nearest peak with the same MRM transition

* DHZ7G was separated in UHPLC-MS/MS as (+) and (–) isomers

Table A.11. Endogenous levels of cytokinin metabolites in 10-day-old *Arabidopsis* seedlings determined by UHPLC-MS/MS and UHPSFC-MS/MS.

	Compound	UHPSFC-MS/MS	UHPLC-MS/MS
CK bases			
1	*t*Z	1.74 ± 0.39	1.99 ± 0.25
2	*c*Z	1.97 ± 0.22	0.87 ± 0.14
3	DHZ	n. d.	n. d.
4	iP	n. d.	n. d.
CK ribosides			
9	*t*ZR	3.02 ± 0.35	2.94 ± 0.42
10	*c*ZR	4.42 ± 0.31	7.49 ± 0.87
11	DHZR	n. d.	n. d.
12	iPR	6.48 ± 1.16	n. d.
CK *O*-glucosides			
17	*t*ZOG	34.57 ± 3.86	49.45 ± 6.50
18	*c*ZOG	2.78 ± 0.23	4.50 ± 0.21
19	DHZOG	8.64 ± 0.55	n. d.
20	*t*ZROG	3.91 ± 1.44	5.53 ± 0.75
21	*c*ZROG	23.57 ± 2.99	8.34 ± 0.40
22	DHZROG	n. d.	n. d.
CK N^7-glucosides			
23	*t*Z7G	204.07 ± 22.43	132.42 ± 14.41
24	*c*Z7G	71.71 ± 7.49	64.46 ± 3.73
25	DHZ7G	11.19 ± 2.41	19.80 ± 2.18
26	iP7G	174.04 ± 12.88	183.48 ± 17.14
CK N^9-glucosides			
30	*t*Z9G	27.31 ± 2.50	27.78 ± 2.45
31	*c*Z9G	2.25 ± 0.28	1.10 ± 0.10
32	DHZ9G	8.57 ± 1.11	n. d.
33	iP9G	12.04 ± 0.78	11.12 ± 1.04

Values are pmol g^{-1} FW (mean ± SD; n = 6).
n. d. - not detected compounds.

Supplement I

Supplement II

Supplement III

Supplement IV

Supplement V

Supplement VI

Supplement VII

Supplement VIII

Tan S, Abas M, Verstraeten I, Glanc M, Molnár G, Hajný J, Lasák P, **Petřík I**, Russinova E, Petrášek J, Novák O, Pospíšil J, Friml J. 2020. Salicylic acid targets protein phosphatase 2A to attenuate growth in plants. Curr Biol 30(3), 381–395.

Article

Current Biology

Salicylic Acid Targets Protein Phosphatase 2A to Attenuate Growth in Plants

Graphical Abstract

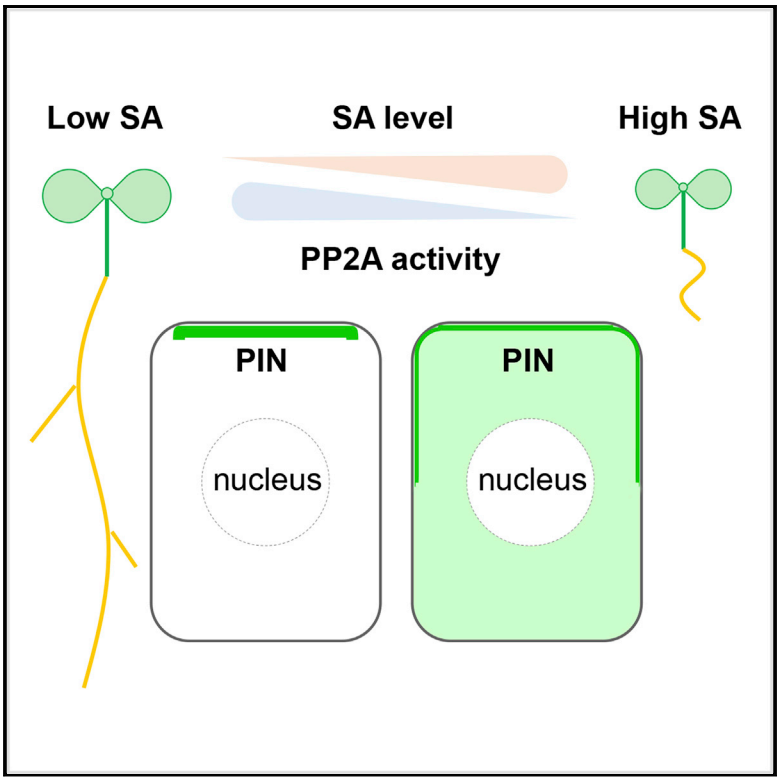

Authors

Shutang Tan, Melinda Abas, Inge Verstraeten, ..., Ondřej Novák, Jiří Pospíšil, Jiří Friml

Correspondence

jiri.friml@ist.ac.at

In Brief

Besides the canonical role in immunity, the defense hormone salicylic acid also shapes plant growth and development. Tan et al. show that salicylic acid regulates *Arabidopsis* growth through directly binding to A subunits of the PP2A enzyme and thereby modulating its activity.

Highlights

- SA modulates root development independently of NPR1-mediated canonical signaling
- SA attenuates growth through crosstalk with the auxin transport network
- SA upregulates the phosphorylation status of PIN auxin efflux carriers through PP2A
- SA directly targets A subunits of PP2A, inhibiting the activity of the complex

Tan et al., 2020, Current Biology *30*, 381–395
February 3, 2020
https://doi.org/10.1016/j.cub.2019.11.058

CellPress

Current Biology
Article

Salicylic Acid Targets Protein Phosphatase 2A to Attenuate Growth in Plants

Shutang Tan,[1] Melinda Abas,[1,2] Inge Verstraeten,[1] Matouš Glanc,[1,3] Gergely Molnár,[1,2] Jakub Hajný,[1,4] Pavel Lasák,[4] Ivan Petřík,[4] Eugenia Russinova,[6,7] Jan Petrášek,[3,8] Ondřej Novák,[4] Jiří Pospíšil,[4,5] and Jiří Friml[1,9,*]
[1]Institute of Science and Technology Austria (IST Austria), Am Campus 1, 3400 Klosterneuburg, Austria
[2]Department of Applied Genetics and Cell Biology, University of Natural Resources and Life Sciences (BOKU), Muthgasse 18, 1190 Vienna, Austria
[3]Department of Experimental Plant Biology, Faculty of Science, Charles University, Viničná 5, 128 44 Prague 2, Czech Republic
[4]Laboratory of Growth Regulators, The Czech Academy of Sciences, Institute of Experimental Botany & Palacký University, Faculty of Science, Šlechtitelů 27, 783 71 Olomouc, Czech Republic
[5]Department of Organic Chemistry, Faculty of Science, Palacký University, tř. 17. listopadu 1192/12, CZ-771 46 Olomouc, Czech Republic
[6]Department of Plant Biotechnology and Bioinformatics, Ghent University, 9052 Ghent, Belgium
[7]Center for Plant Systems Biology, VIB, 9052 Ghent, Belgium
[8]Institute of Experimental Botany, The Czech Academy of Sciences, Rozvojová 263, 165 02 Prague 6, Czech Republic
[9]Lead Contact
*Correspondence: jiri.friml@ist.ac.at
https://doi.org/10.1016/j.cub.2019.11.058

SUMMARY

Plants, like other multicellular organisms, survive through a delicate balance between growth and defense against pathogens. Salicylic acid (SA) is a major defense signal in plants, and the perception mechanism as well as downstream signaling activating the immune response are known. Here, we identify a parallel SA signaling that mediates growth attenuation. SA directly binds to A subunits of protein phosphatase 2A (PP2A), inhibiting activity of this complex. Among PP2A targets, the PIN2 auxin transporter is hyperphosphorylated in response to SA, leading to changed activity of this important growth regulator. Accordingly, auxin transport and auxin-mediated root development, including growth, gravitropic response, and lateral root organogenesis, are inhibited. This study reveals how SA, besides activating immunity, concomitantly attenuates growth through crosstalk with the auxin distribution network. Further analysis of this dual role of SA and characterization of additional SA-regulated PP2A targets will provide further insights into mechanisms maintaining a balance between growth and defense.

INTRODUCTION

Life of multicellular organisms is a permanent trade-off to allocate resources between growth and defense against pathogens. Salicylic acid (SA) is a classical plant hormone traditionally connected with plant immunity, and its levels increase in response to pathogen attack [1]. SA functions as an endogenous signal mediating local and systemic defense responses against pathogens by upregulating the production of pathogenesis-related (PR) proteins. The best characterized components of the SA immunity pathway are the NPR (NONEXPRESSOR OF PR GENES) proteins that include four close isoforms, NPR1–NPR4 [2–4]. Following increase in SA levels, NPR1 translocates from cytoplasm into nucleus [5–7], thereby allowing binding to the downstream transcription factors and regulation of the expression of downstream genes [8]. NPR1, together with NPR3/NPR4, were shown to be bona fide SA receptors for the immune pathway [7, 9, 10]. NPR1 functions as a transcriptional activator, whereas NPR3 and NPR4 are transcriptional repressors, all working independently and harmoniously to regulate the expression of downstream genes [7].

Much less understood is the role of SA beyond plant immunity, in particular in modulating plant growth and development. SA has been implicated in the regulation of photosynthesis, respiration, flowering, senescence, seed germination, and growth. Nevertheless, whether SA signaling for these functions depends on the NPR-mediated pathway or other, so far molecularly uncharacterized mechanism(s) remains unclear [8, 11–15]. Biochemical approaches have identified numerous potential SA binding proteins (SABPs), but their potential roles in SA physiological functions remain unclear [16–19].

SA, similarly to other endogenous signals in plants, executes its effect in concert with other plant hormones. In particular, the SA-auxin signaling crosstalk has been proposed to be important for SA roles in balancing plant defense and development [15]. This notion was strengthened by the observation that SA affects the constitutive subcellular dynamics of PIN (PIN FORMED) auxin transporters [14, 20], which are important regulators of many developmental processes [21]. Nonetheless, the physiological relevance of this SA regulation or the underlying signaling mechanism remains elusive.

Here, we demonstrate an alternative SA signaling mechanism, by which SA, in addition to activating plant immunity, attenuates root growth through regulating PIN-dependent auxin distribution network.

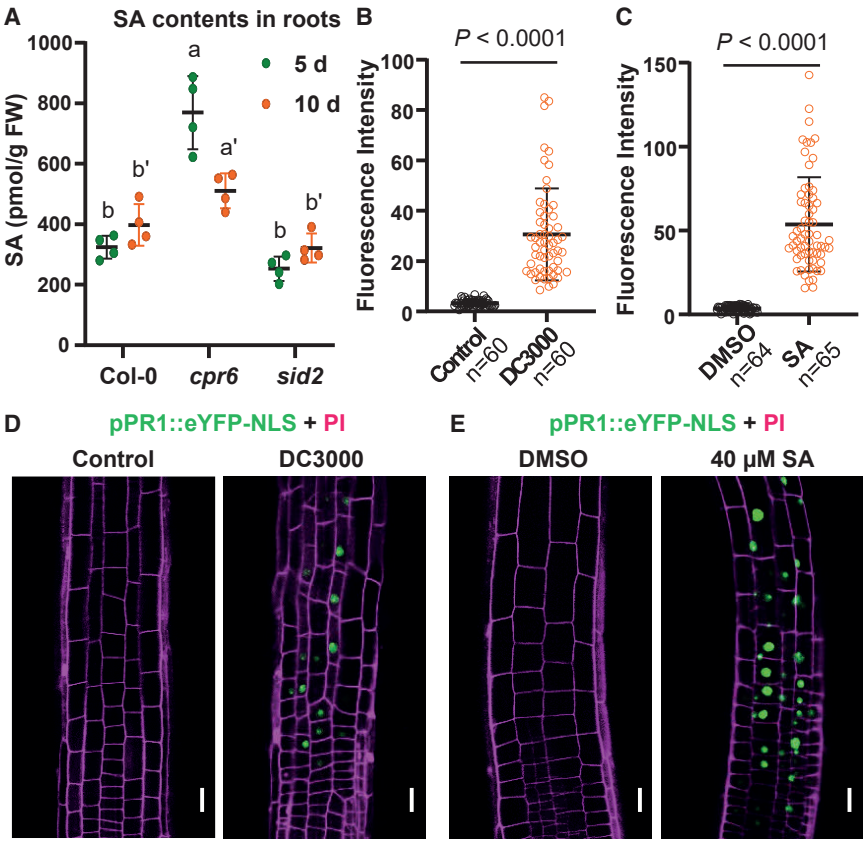

Figure 1. Pathogen-Induced SA Response in Roots, Revealed by the *pPR1::eYFP-NLS* Reporter

(A) SA contents in the roots of 5- or 10-day-old seedlings of Col-0, *cpr6*, and *sid2* (*sid2-3*) measured by LC/MS-MS. n = 4 replicates, with multiple seedlings for each. Dots represent individual values, and lines indicate mean ± SD. Different letters represent significant difference; $p < 0.05$; by one-way ANOVA with a Tukey multiple comparison test.

(B–E) Induced *pPR1::eYFP-NLS* expression by *P. syringae* DC3000 (B and D) or SA (C and E) in roots.

(B and D) 5-day-old *pPR1::eYFP-NLS* seedlings were treated with *P. syringae* DC3000 (optical density 600 [OD_{600}] = 0.01, ~5 × 10^6 colony-forming units [CFUs]/mL) or with resuspension buffer (control) for 48 h and were then imaged by confocal laser scanning microscope (CLSM).

(C and E) For SA treatment, 5-day-old *pPR1::eYFP-NLS* seedlings were transferred to plates with DMSO or 40 μM SA for 24 h and were then imaged by CLSM. Scale bars, 10 μm. For quantification, the average GFP florescence of 5–10 representative cells from 10 seedlings for each treatment was measured by Fiji. The data points were shown as dot plots. Dots represent individual values, and lines indicate mean ± SD. p values were calculated by a two-tailed t test.

See also Figure S1.

RESULTS

SA Regulates Root Growth Independently of Canonical NPR Receptors

The majority of SA physiology studies have focused on adult-stage shoots and so far it remains unclear whether there are significant levels of SA in the root. Therefore, we examined the SA contents by liquid chromatography-tandem mass spectrometry (LC-MS/MS) first. SA production is typically highly elevated after pathogen attack [22], and thus, the basal SA levels in the roots were relatively low but detectable (Figure 1A). There was a small decrease in the SA-biosynthesis-deficient mutant, *sid2-3* [1], and a corresponding increase in the SA overproduction mutant, *cpr6* [23]. Moreover, using *pPR1::eYFP-NLS* reporter line for the NPR1 pathway [24], we detected an induced *PR1* expression in both shoots (Figures S1A–S1D) and roots (Figures 1B–1E) following treatment with either a plant pathogen, *Pseudomonas syringe* DC3000 (Figures 1B and 1D), or SA (Figures 1C and 1E), confirming that pathogen- or SA-mediated activation of NPR1 pathway occurs also in roots.

Given detectable levels of SA in roots and previous indications about a physiological role of SA in roots [14, 25], we examined the effect of exogenously applied SA on root growth. Compared to the control conditions, seedlings growing on 20 or 40 μM SA exhibited shorter (Figures 2A and 2B) and partially agravitropic roots (Figures 2C–2H), as well as fewer lateral roots (Figure 2I). Two inactive SA isomers, 3-hydroxybenzoic acid (3-OH-BA) and 4-hydroxybenzoic acid (4-OH-BA) [26], did not show any obvious effects at comparable concentrations (Figures S1E–S1J). These observations show that SA impacts root development at concentrations equal to or below those established in shoots [7] and its activity is specific to its active structure.

Next, we addressed the requirement of the SA receptors, NPR1/NPR3/NPR4, which are well established in the immune response, for the observed root response [2–4, 7, 10]. NPR1 is a central regulator of the canonical immune pathway, and the downstream transcriptional responses are completely blocked by *npr1* deficiency [3]. Unexpectedly, the well-characterized corresponding mutants *npr1*, *npr3,4* double, and *npr1,3,4* triple mutants did not show a decreased sensitivity to SA in terms of root elongation, gravitropic growth, and lateral root formation (Figures 2B–2I and S1K–S1R). It is noteworthy that the *npr1,3,4* triple mutant exhibited even a pronounced SA-hypersensitive phenotype (Figures S1K–S1R), which might come from downregulation of multiple genes involved in auxin biosynthesis, transport, or signaling.

In conclusion, SA regulates multiple aspects of root development by a signaling mechanism not requiring the established NPR receptors.

SA Regulates PIN-Dependent Auxin Transport and PIN2 Phosphorylation

The root phenotypes generated by SA treatment are reminiscent of defective auxin homeostasis because auxin and its distribution have been shown to regulate primary root growth, gravitropic bending, and lateral root formation [21, 27]. To test the

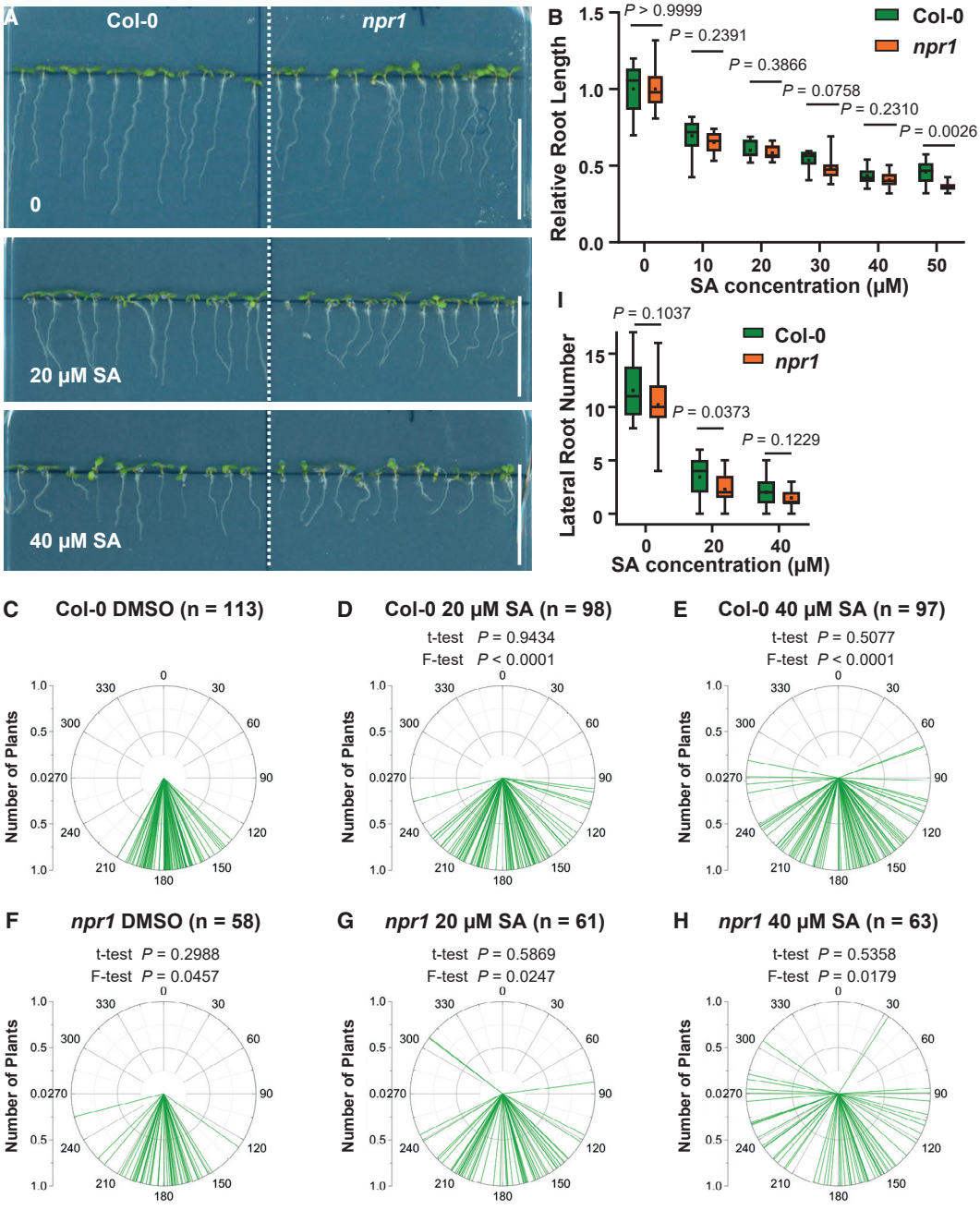

Figure 2. SA Regulates Root Growth and Development in a *NPR1*-Independent Manner

(A) Representative images showing the morphological changes of Col-0 and *npr1* under SA treatment. DMSO is the solvent control. Scale bars, 2 cm.

(B) SA inhibited the primary root elongation in a *NPR1*-independent manner. Root length of 7-day-old Col-0 and *npr1* seedlings grown on MS plates with different concentrations of SA was measured. Relative length was calculated by dividing the values with the root length at SA = 0. Boxplots show the first and third quartiles, with whiskers indicating maximum and minimum, the line for median, and the black dot for mean. n = 11–28; p values were calculated by a two-tailed t test for indicated pairs of Col-0 and *npr1* at a certain concentration of SA.

(C–H) SA interfered with root gravitropism independently of *NPR1*. Root tip angles of 7-day-old Col-0 (C–E) and *npr1* (F–H) seedlings were measured and shown as polar bar charts. Two-tailed t tests were performed to indicate the difference of mean value, and F-tests indicate the difference of variances. For Col-0, SA treatments were compared with the DMSO control, and the *npr1* groups were compared with Col-0 under the same SA treatment, respectively.

(I) Inhibition of lateral root formation by SA does not involve *NPR1*. The number of emerged lateral roots for 10-day-old plants was counted. n = 20–25. p values were calculated by a two-tailed t test.

See also Figure S1.

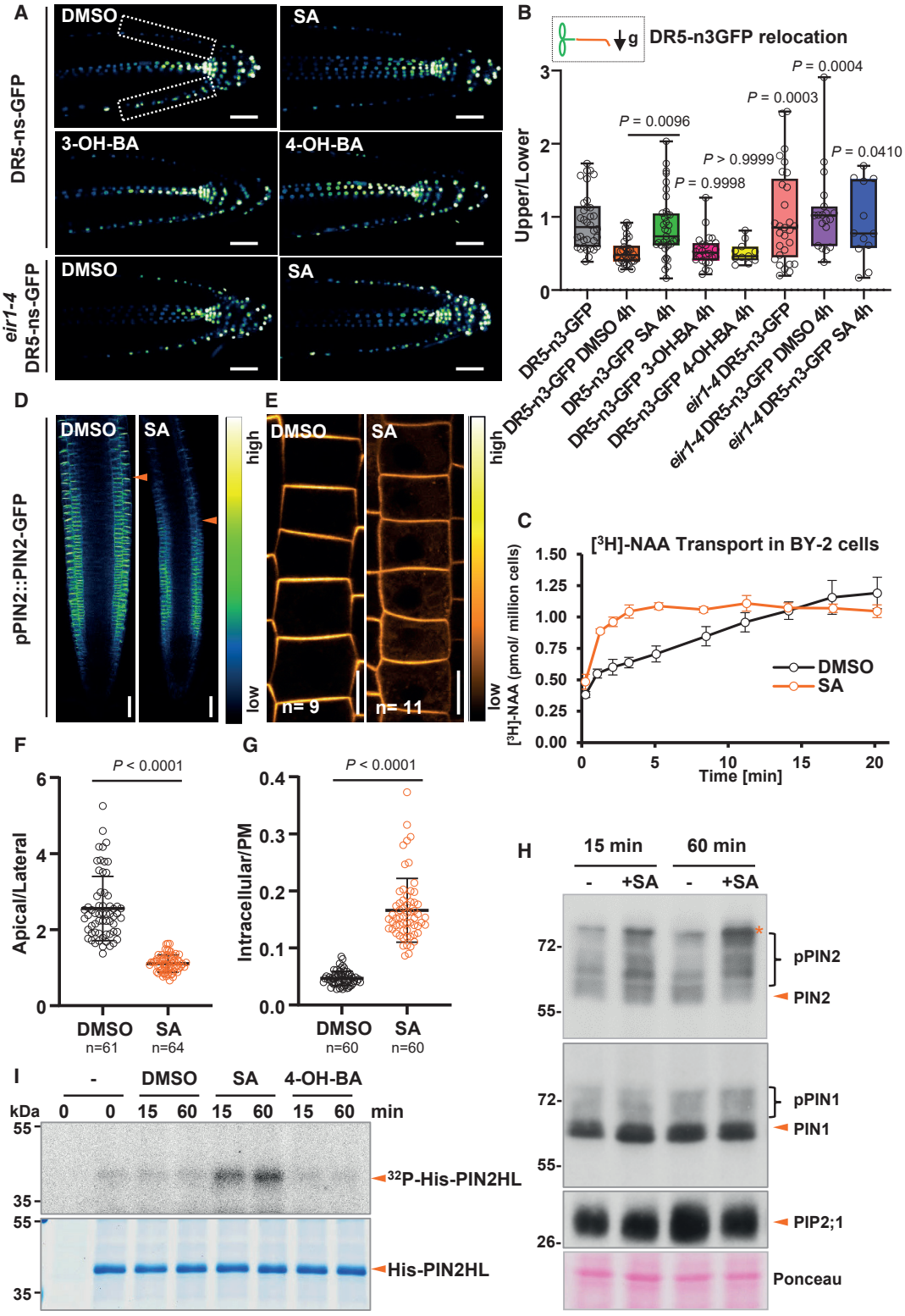

Figure 3. SA Regulates Auxin Transport via Modulating PIN2 Phosphorylation

(A) SA inhibited the relocation of DR5-n3GFP. 5-day-old *DR5v2* and *eir1-4 DR5v2* seedlings were transferred to different plates with DMSO, 40 μM SA, 40 μM 3-OH-BA, or 40 μM 4-OH-BA, respectively, and then turned 90 degrees for gravistimulation. After 4 h, the roots were imaged by CLSM. The GFP channel (DR5-n3GFP) was shown. Scale bars, 10 μm.

(legend continued on next page)

potential effect of SA on auxin response and distribution, we used an auxin-responsive marker DR5-n3GFP (the GFP channel of DR5v2) [28], which monitors auxin response in plant tissues, including the gravity-induced auxin translocation to the lower root side [28]. After 4-h gravistimulation by 90° reorientation, the seedlings treated with SA, unlike the DMSO-treated controls, failed to show a pronounced DR5-n3GFP asymmetry with the stronger signal at the lower root side, in line with the SA-induced gravitropism defect (Figures 3A, 3B, and S2A), as observed before [14]. This suggests that SA interferes with auxin distribution either at the level of transport [21] or local auxin biosynthesis [29]. Recently, SA has been proposed to increase auxin levels in root tips [30]. Nonetheless, this upregulation of iIndole-3-acetic acid (IAA) biosynthesis cannot explain the auxin-related phenotypes described here, such as agravitropic root growth and the reduced lateral root number, because increased auxin levels have rather opposite effects. It is likely that increased IAA biosynthesis after SA treatment is rather the consequence, but not the cause, of the auxin transport regulations by SA, presumably due to a feedback regulatory mechanism.

To test a possible effect of SA on auxin transport, we measured the basipetal (rootward) auxin transport in etiolated hypocotyls, which revealed that SA can inhibit the rootward transport of [^{3}H]-IAA, similar to widely used PIN-dependent auxin transport inhibitors NPA (1-N-naphthylphthalamic acid) and TIBA (2,3,5-triiodobenzoic acid) (Figure S2B). With tobacco BY-2 cultured cells [31], we tested the effect of SA on transport of different auxin analogs, [^{3}H]-NAA and [^{3}H]-2,4-D. SA treatment increased the cellular accumulation of [^{3}H]-NAA (Figure 3C), but not of [^{3}H]-2,4-D or [^{3}H]-BA (Figures S2C and S2D). Despite possible effect on auxin metabolism, this selective effect of SA on accumulation of NAA, which is a good substrate of PIN auxin exporters [32], strongly suggests a regulatory role of SA in PIN-dependent auxin transport. Overall, these observations show that SA, exhibiting distinct activities for different tissues, directly or indirectly regulates auxin transport.

To investigate the mechanism underlying the role of SA in regulating root growth and development, we focus on the root gravitropic phenotype. PIN2 and AUX1 auxin transporters play a prominent role in shootward auxin transport in the root and thus in the auxin redistribution during the gravitropic response [33–37]. Therefore, we analyzed the response of *eir1-4* [36] loss-of-function mutant, which exhibits strongly agravitropic roots. After SA treatment, *eir1-4* showed a slight SA hypersensitivity in primary root elongation but no further enhancement of the gravitropic defect at 40 μM SA (Figures S2E–S2J). These observations suggest that SA acts in the gravitropic response through the auxin efflux carrier PIN2. Using the *eir1-4 DR5-n3-GFP* cross, we could not see gravity-induced DR5-n3-GFP asymmetry and SA treatment had no additional effect (Figures 3A and 3B). Furthermore, we examined the SA effect on the localization of these proteins using *pAUX1::AUX1-YFP* and *pPIN2::PIN2-GFP* marker lines. Whereas we observed no obvious effect of SA treatment on AUX1-YFP except a slight decrease in the overall intensity (Figures S2K–S2M), PIN2-GFP incidence in the plasma membrane of the root epidermis cells upon SA treatment was visibly decreased with higher intracellular signal and less pronounced polar distribution as compared to the control (Figures 3D–3G).

Reversible phosphorylation plays an important role in regulating PIN polarity, subcellular dynamics, and activity. PIN proteins can be phosphorylated by multiple kinases, most prominently PID (PINOID)/WAGs (WAVY ROOT GROWTHs), D6PK/D6PKLs, and PAX (PROTEIN KINASE ASSOCIATED WITH BRX), and dephosphorylated by various phosphatases, including protein phosphatase 2A (PP2A), PP1, and PP6 [38–40]. We examined the PIN2 phosphorylation status by western blot. When roots were extracted with a protocol [36, 41] specifically modified to preserve phosphorylation, PIN2 appeared as a smear of bands (Figure 3H). Phosphatase treatment shifted the slower migrating bands toward the faster migrating band at the base of the smear (Figure S3A), indicating that the upper parts of the smear comprise phosphorylated species. We found that

(B) The ratio of fluorescence between the upper side and the lower side was measured, as shown in (A). n = 34, 30, 35, 24, 11, 29, 19, and 12, respectively. p values are calculated by a two-tailed t test, comparing different datasets with the DR5-n3-GFP DMSO control (t = 4 h), as shown with the horizontal line in the case of DR5-n3-GFP SA 4 h.

(C) SA treatment increased the accumulation of [^{3}H]-NAA in tobacco BY-2 cells, suggesting a decrease in auxin export. DMSO and 200 μM SA were added to the cell culture and then the radioactivity inside of cells was measured at indicated time points after the addition of [^{3}H]-NAA to the DMSO- and SA-treated cell cultures. n = 3.

(D–G) SA treatment impaired the polar localization and promoted the internalization of PIN2-GFP in root epidermis (D and E). *pPIN2::PIN2-GFP* seedlings were grown on plates with DMSO and 40 μM SA for 4 days and were then imaged by CLSM. Scale bars, 20 μm (D) and 10 μm (E), respectively. Arrowheads in (D) indicate the beginning of root transition zone.

(F) The intensity ratio of apical/lateral was measured by Fiji to assess PIN2 polarity.

(G) Quantification of the PIN2-GFP intensity ratio of intracellular/PM.

(F and G) Dots represent individual values, and lines indicate mean ± SD. p values are calculated by a two-tailed t test.

(H) SA treatment enhanced the phosphorylation of PIN2. Roots of 7-day seedlings were treated with DMSO or 40 μM SA for 15 min and 60 min and then analyzed by western blot with an anti-PIN2 antibody (upper panel). Phosphorylation of the multiple phosphorylation sites in PIN2 causes slower migrating species. The more highly phosphorylated, the slower the migration. The same membrane was stripped and detected by anti-PIN1 (second panel) and anti-PIP2;1 (third panel) antibodies, sequentially. The molecular weight (MW) of PIN2 and PIN1 is 69 and 67 kDa, respectively. For unknown reasons, PIN2 runs faster than expected, perhaps due to incomplete denaturing when heated only at 50°C. The shifted bands indicate the phosphorylated PIN proteins. Bottom panel: Ponceau staining is shown. Asterisk indicates partial contribution by a non-specific band (see also in Figure 4A).

(I) SA treatment increased the phosphorylation of His-PIN2-HL in plant extracts. Roots of 7-day seedlings were treated with DMSO or 40 μM SA for 15 min and 60 min, respectively, and then were subject to protein extraction. Crude plant extracts were incubated with recombinant His-PIN2-HL for 60 min with ^{32}P-ATP and $MgCl_2$. The first lane was without His-PIN2-HL as negative control. Reaction samples were analyzed by SDS-PAGE and the subsequent autoradiography. Upper panel: autoradiography is shown; lower panel: Coomassie Brilliant Blue (CBB) staining is shown.

See also Figures S2 and S3.

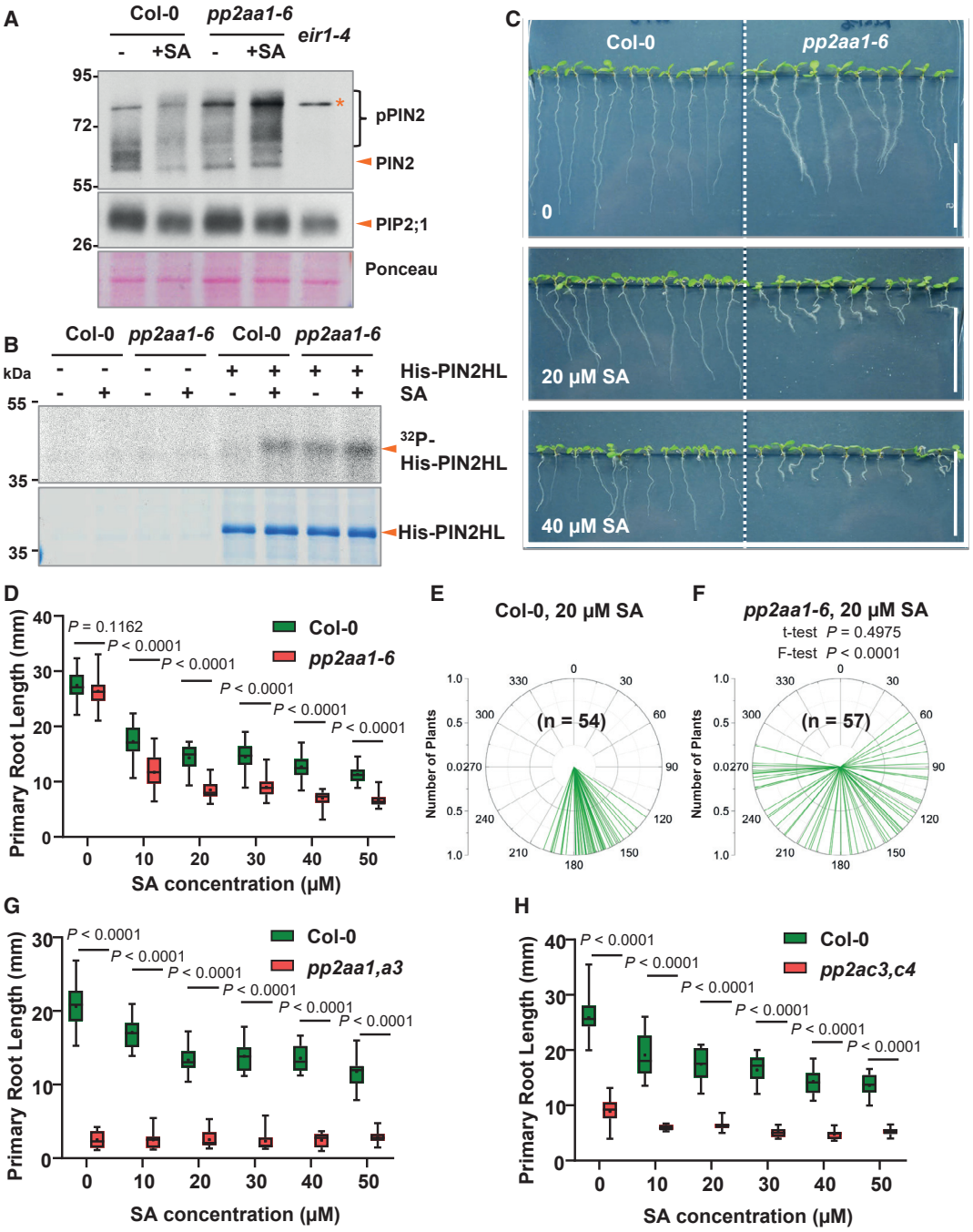

Figure 4. SA Functions through PP2A in Regulating Root Development

(A) SA treatment promoted the phosphorylation of PIN2 in Col-0 to a similar degree as that in *pp2aa1-6*. Roots of 7-day-old Col-0 and *pp2aa1-6* seedlings were treated with DMSO or 40 μM SA for 60 min and were then sampled for protein isolation and western blot. The shifted bands indicate the phosphorylated PIN proteins (upper panel). Asterisk indicates a non-specific band that contributes partially to the signal. The same membrane was stripped and probed with a PIP2;1 antibody to indicate the loading (upper panel). Ponceau staining is shown in the bottom panel.

(B) Phosphorylation with ^{32}P-ATP revealed that SA treatment increased the phosphorylation of His-PIN2-HL in Col-0, whereas this increase was attenuated in *pp2aa1-6*. Upper panel: autoradiography is shown; lower panel: CBB is shown.

(C) Representative images revealing the hypersensitivity of *pp2aa1-6* to SA. Col-0 and *pp2aa1-6* seedlings were grown on plates with SA. Scale bars, 2 cm.

(D) *pp2aa1-6* was hypersensitive to SA in root growth inhibition. Col-0 and *pp2aa1-6* seedlings grew on plates with SA for 7 days and then the primary root length was measured. n = 11–28. p values were calculated by a two-tailed t test for indicated pairs of Col-0 and *pp2aa1-6* at a certain concentration of SA.

(E and F) *pp2aa1-6* was hypersensitive to SA in terms of interfering with root gravitropism. Col-0 (E) and *pp2aa1-6* (F) seedlings grew on plates containing different concentrations of SA for 7 days, and the root tip angles were measured by ImageJ and shown as polar bar charts. p values were calculated by a two-tailed t test in (E) and (F) and indicate differences of variances by a further F-test in (F).

(legend continued on next page)

SA treatment led to a more pronounced shift of PIN2 protein mobility to slower migrating species than seen in control, indicating an increase in phosphorylation status. This occurred as rapidly as after 15 min and more pronounced after 60 min (Figures 3H and S3A). To confirm the SA effect on the change of PIN2 phosphorylation, we expressed and purified the PIN2 hydrophilic loop with His tag (His-PIN2HL) and incubated it with the protein extract from seedlings treated with SA or the inactive isomers in a ^{32}P-ATP phosphorylation reaction (Figure 3I). There was more phosphorylation of the His-PIN2HL with SA. This confirmed that SA treatment led to an increase in PIN2 phosphorylation level, either through stimulating phosphorylation or suppressing dephosphorylation.

Taken together, the physiological, microscopic, and biochemical observations collectively suggest that SA regulates PIN-dependent auxin transport, presumably by changing the phosphorylation status and thus the cellular localization and the activity of PIN proteins. Such mechanism would explain the observed physiological SA effects on root development.

PP2A Is Required for SA Regulation of PIN2 Phosphorylation and Root Development

To gain insight into the mechanism by which SA modulates PIN phosphorylation and root development, we focused on the potential regulators of PIN phosphorylation. Of those, the A subunit of PP2A (PP2AA1/RCN1, ROOTS CURL IN NPA1), an established regulator of PIN phosphorylation and auxin transport [42, 43], came to our attention, as it also appeared in a high-throughput proteomics study as potentially associated with SA binding [44].

We first tested whether PP2AA1 is involved in SA-induced increase of PIN phosphorylation status. Western blot showed that SA treatment could increase the phosphorylation level of PIN2 in wild-type (WT), whereas in PP2AA1 loss-of-function mutant, *pp2aa1* (also known as *pp2aa1-6 and rcn1-6*), there was already a higher level of PIN2 phosphorylation, consistent with PP2AA1 involvement in PIN2 dephosphorylation (Figures 4A and S3B). This phosphorylation was still increased further by SA treatment (Figure 4A), suggesting that the other PP2AA homologs can play a role in the absence of PP2AA1. Accordingly, the ^{32}P-ATP phosphorylation reaction using purified His-PIN2HL incubated with the protein extracts from SA-treated WT and *pp2aa1* seedlings (Figure 4B) confirmed at least partial PP2AA1 requirement for the SA effect on PIN2 phosphorylation.

In line with this, *pp2aa1* mutants (*pp2aa1-6* and *pp2aa1-1*) roots showed hypersensitivity to SA in terms of primary root growth and gravitropic bending (Figures 4C–4F and S3C–S3I). In addition, SA treatment at higher concentrations (50 μM) often led to a slight swelling in WT root tips, whereas in *pp2aa1*, a much stronger root tip swelling was observed even at a lower SA concentration (20 μM; Figure S3C).

PP2A is a heterotrimeric complex composed of A, B, and C subunits with three homologs for the PP2A A subunits, PP2AA1/RCN1, PP2AA2, and PP2AA3 [45]. Notably, overexpression of *PP2AA1* (*35S::myc-PP2AA1*) alone did not lead to obvious changes in SA sensitivity (Figures S3J–S3L), suggesting importance of the whole heterotrimeric PP2A holoenzyme integrity. Single mutants of *pp2aa2* and *pp2aa3* did not show any visible difference in SA sensitivity compared to WT (Figures S4A–S4C). The double mutant of *pp2aa1 pp2aa2-3* (*pp2aa1,a2*) showed a much stronger response to SA than WT or *pp2aa1/rcn1* single mutant (Figures 4D and S4D). The *pp2aa1,a3* double mutant had severe defects in growth and development with a short primary root already without any treatment (Figures S4E–S4H) [43, 45], which is reminiscent to WT treated by higher concentration of SA, and subsequent SA treatment could not further enhance this phenotype (Figure 4G). Similar results were observed for the *pp2ac3,c4* double mutant of the catalytic C subunits [46]. The roots of *pp2ac3,c4* were short without any treatment, and higher exogenous SA treatment did again not further enhance this phenotype (Figure 4H). The mutant in the regulatory subunit, *fass/tonneau2* (*ton2*), has been reported to show a similar phenotype as *pp2aa1,a3* [46]. However, *fass* [46], the double knockout mutant *pp2aa1-1 pp2aa2-1* [43, 45], and triple *pp2aa1-1 pp2aa2-1 pp2aa3-1* [43, 45] were too sick to perform meaningful SA sensitivity assays. It has been well described that these mutants exhibited severe growth defects, with swelling root morphology [45, 46], which are similar to seedlings treated with SA. Thus, loss-of-function mutants in all PP2A subunits perturbed plant sensitivity to SA in terms of root growth. Importantly, phenotypes of the stronger higher order mutants could be phenocopied by SA treatment. The SA-overproducing *cpr6* mutants show a severe dwarf phenotype [8] and increased SA levels in roots (Figure 1A) but no obvious changes in root development (Figure 5A). On the other hand, the *pp2aa1-6 cpr6* double mutant had shorter roots and increased sensitivity to SA (Figures 5A and 5B) as well as exhibited a much more severe dwarf phenotype than *cpr6* alone (Figures 5C and 5D). This provides a genetic confirmation that PP2A is involved in the SA-mediated developmental regulation.

In summary, these biochemical and genetic analyses suggest that the PP2A complex is involved in SA regulation of PIN (de) phosphorylation and root growth.

SA Inhibits PP2A Activity

To further confirm whether SA is an endogenous regulator of PP2A, we tested the sensitivity of *pp2aa1-1* to a known PP2A inhibitor, cantharidin, that binds the C subunits in both animals and plants [45, 47–49]. When grown on media with cantharidin, WT seedlings exhibited shorter, agravitropic roots and root tip swelling as observed for SA treatment, and notably, *pp2aa1* mutants were hypersensitive to cantharidin (Figures S4I and

(G) The *pp2aa1, a3* double mutant exhibited decreased sensitivity to SA. Col-0 and *pp2aa1, a3* seedlings grew on plates with SA for 7 days and then the primary root length was measured. n = 11–25. p values were calculated by a two-tailed t test for indicated pairs of Col-0 and *pp2aa1, a3* at the given concentration of SA.
(H) The *pp2ac3, c4* double mutant exhibited decreased sensitivity to SA. Col-0 and *pp2ac3, c4* seedlings grew on plates with SA for 7 days and then the primary root length was measured. n = 10–21. p values were calculated by a two-tailed t test for indicated pairs of Col-0 and *pp2ac3, c4* at the given concentration of SA.
See also Figures S3 and S4.

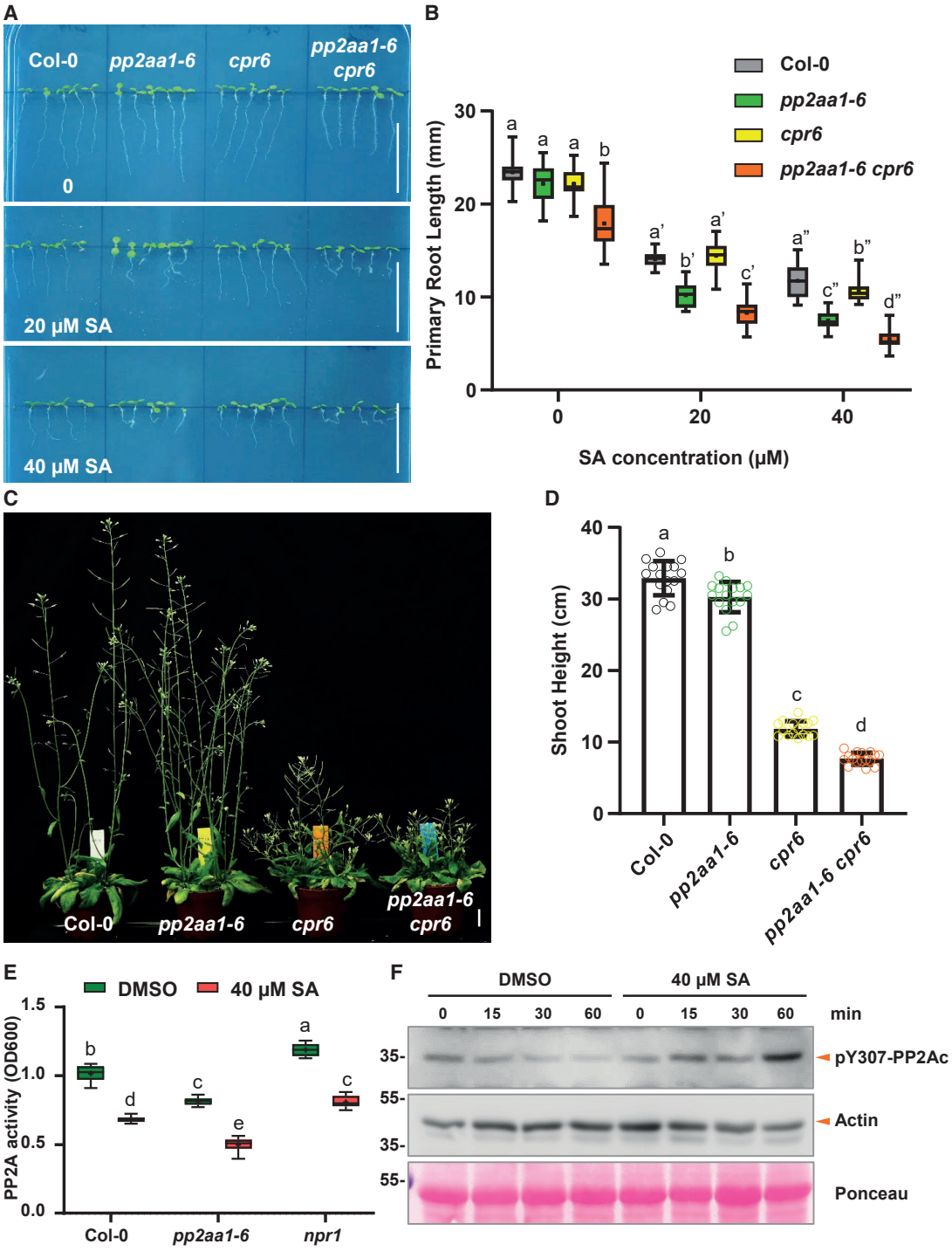

Figure 5. Genetic Analysis of *pp2aa1-6* and *cpr6* Mutations, and SA Inhibits PP2A Activity *In Planta*

(A) Representative images showing the enhanced sensitivity of *pp2aa1-6* to SA. Col-0, *pp2aa1-6*, *cpr6*, and *pp2aa1-6 cpr6* seedlings were grown on plates with different concentrations of SA for 7 days. Scale bars, 2 cm.

(B) The root growth analysis revealed that the *cpr6* mutation decreased the primary root length and increased the SA sensitivity of *pp2aa1-6*. n = 16. Different letters represent significant difference; $p < 0.05$; by one-way ANOVA with a Tukey multiple comparison test.

(C and D) The *pp2aa1-6* mutation enhances the stunted shoot phenotype of *cpr6*. Col-0, *pp2aa1-6*, *cpr6*, and *pp2aa1-6 cpr6* plants were grown for 38 days, and representative plants are shown (C). Scale bar, 2 cm.

(D) The height of plants was measured and shown as dot plots. Dots represent individual values, and lines indicate mean ± SD. n = 16. Different letters represent significant difference; $p < 0.05$; by one-way ANOVA with a Tukey multiple comparison test.

(legend continued on next page)

S4J) as they were to SA. The identical physiological effects of SA to an established PP2A inhibitor and similarities between the SA effects and stronger loss-of-function phenotypes of the PP2A complex indicated that SA may act as an endogenous inhibitor of PP2A.

Therefore, we analyzed PP2A activity in the protein extracts of *Arabidopsis* seedlings using the established colorimetric method with phospho-Ser/Thr peptides as PP2A substrates [50]. This revealed that the *pp2aa1* mutant had lower PP2A activity than WT [48] and that SA treatment decreased PP2A activity in WT (Figure 5E). Notably, the *npr1* mutant defective in an established SA receptor still showed high sensitivity to SA in the PP2A activity assay (Figure 5E). Next, we established an independent method to assess the PP2A activity. In mammalian cells, phosphorylation at Tyr307 (pY307) of the catalytic subunit PP2Ac is used as a measure of PP2A activity and can be detected by a phospho-Tyr307 (pY307)-PP2Ac antibody [51]. Alignment of the five *Arabidopsis* PP2AC subunits with the human and mice homologs indicated that the antigen motif recognized by this antibody is highly conserved across different homologs (Figure S4K), which makes it feasible to use the same antibody to evaluate the PP2A activity *in planta*. The phosphorylation status of PP2ACs, monitored by this method, was robust and stable under control treatments, whereas treating seedlings with SA led to an increased PP2AC phosphorylation (Figure 5F) indicative of decreased PP2A activity.

Taken together, our physiological and biochemical observations show that SA inhibits PP2A activity, indicating that the PP2A complex could be a direct target of SA.

SA Binds to the A Subunits of PP2A

Next, we addressed a mechanism by which SA inhibits PP2A activity. The finding that established SA receptors from the NPR family are not required for this SA effect on root growth and on PP2A activity supported a possibility that SA targets PP2A directly.

To test for a direct SA binding to PP2A, we first used the drug affinity responsive target stability (DARTS) method based on the fact that ligand binding to its protein target typically causes a conformational change, which affects the exposure of protease recognition sites and thus influences protein stability in the presence of the ligand [52]. DARTS using extracts of *pPP2AA1::PP2AA1-GFP* seedlings revealed that SA treatment led to an obvious protection of PP2AA1-GFP against Pronase (mixture of proteases) degradation, but 4-OH-BA did not (Figures 6A, S5A, and S5B). This suggests that SA targets PP2AA1 *in planta*. Notably, although SA concentration as high as 500 μM still showed pronounced protective effects toward PP2AA1-GFP, the 50 μM SA was more effective (Figure 6A). This suggests a more complicated regulatory effect of SA on PP2AA1-GFP stability for the high concentrations.

Differential scanning calorimetry (DSC) is a method to detect thermostability of a protein by measuring the heat release during denaturing [53]. We expressed and purified from *E. coli* His-PP2AA1 (Figures S5C–S5F) and used the recombinant protein for DSC. We detected a denaturing temperature (Tm) of His-PP2AA1 at 48.01°C, but following SA treatment, the Tm shifted to 45.03°C (Figure 6B), suggesting that SA treatment changed PP2AA1 stability, which might be due to conformational changes. A further control with the inactive SA isomer, 4-OH-BA, did not show any effect on PP2AA1 thermostability, confirming this specific activity of SA (Figure S5G). Usually ligand binding stabilizes the target protein [54], but in some well characterized cases, such as receptors for the plant hormone strigolactone, ligand binding caused the destabilization of the protein, which is similar to what we observed for SA and PP2AA1 [55]. Thus, DSC also supports the hypothesis of direct SA binding to PP2AA1.

To further confirm SA binding to PP2AA1 and to measure the binding affinity, we employed the surface plasmon resonance (SPR) method [56]. We first designed a SA analog with a linker, SA-f, which can be immobilized on the SPR sensory chip. A set of SA derivatives have been synthesized with modifications at the meta- and para- positions in the benzoic ring and then we first tested their bioactivity in terms of PIN2-GFP endocytic trafficking as an output of NPR-receptors-independent SA activity [14], as well as the physiological effects on root morphology that we describe here. These tests indicated that modifications at the meta- position did not affect this SA bioactivity (Figure S5H), thus identifying C-10 moiety as being most promising for further modification (Figures S6A, S6B, and S6D–S6F). For the second round, we added a -$(CH_2)_6$-O- linker at the meta-position, SA-1∼3 (Figure S5H), with different groups at the end of the linker to mimic the matrix of sensor chips. SA-2 and SA-3 still kept the activity on PIN2-GFP trafficking (Figures S6C and S7A–S7C) and root development similar to non-modified SA (Figures S6C, S6D, and S7A–S7C). Finally, we synthesized SA-f, with an NH_2- group for immobilization on the SPR sensor chips. Then, we used recombinant His-PP2AA1 and His-PP2AA3 proteins and measured their binding affinity to immobilized SA (Figures S5C–S5F). Indeed, we detected a concentration-dependent binding of His-PP2AA1 to immobilized SA. Plotted with the steady-state binding with different concentrations of the protein, we obtained a K_D of 3.623 μM (Figures 6D and S7D). Performing the same experiment for His-PP2AA3, we also detected binding with an even smaller K_D value of 1.916 μM (Figures 6E and S7E). In a different, single-cycle SPR experimental setup, including 0.1% BSA in the SPR flow to prevent unspecific binding, a similar K_D value (2.374 μM) for PP2AA1 was obtained (Figures S7F and S7G).

(E) SA treatment decreased the total PP2A activity *in planta*. Col-0, *pp2aa1-6*, and *npr1* seedlings were grown on plates containing DMSO or 40 μM SA for 5 days and then sampled for protein isolation and PP2A activity measurement. n = 6. Different letters represent significant difference; $p < 0.05$; by one-way ANOVA with a Tukey multiple comparison test.

(F) SA treatment increased the phosphorylation of the PP2A catalytic subunits (PP2Ac), suggesting the decrease in PP2A activity. 7-day-old Col-0 seedlings were treated with DMSO or 40 μM SA for 0, 15 min, 30 min, and 60 min respectively, and were then collected for protein extraction and the subsequent western blot. A pY307-PP2Ac antibody was used, 1:1,000 (upper panel). The anti-actin blot (medium panel; 1:2,000) and Ponceau staining (bottom panel) indicate the loading amounts.

See also Figure S4.

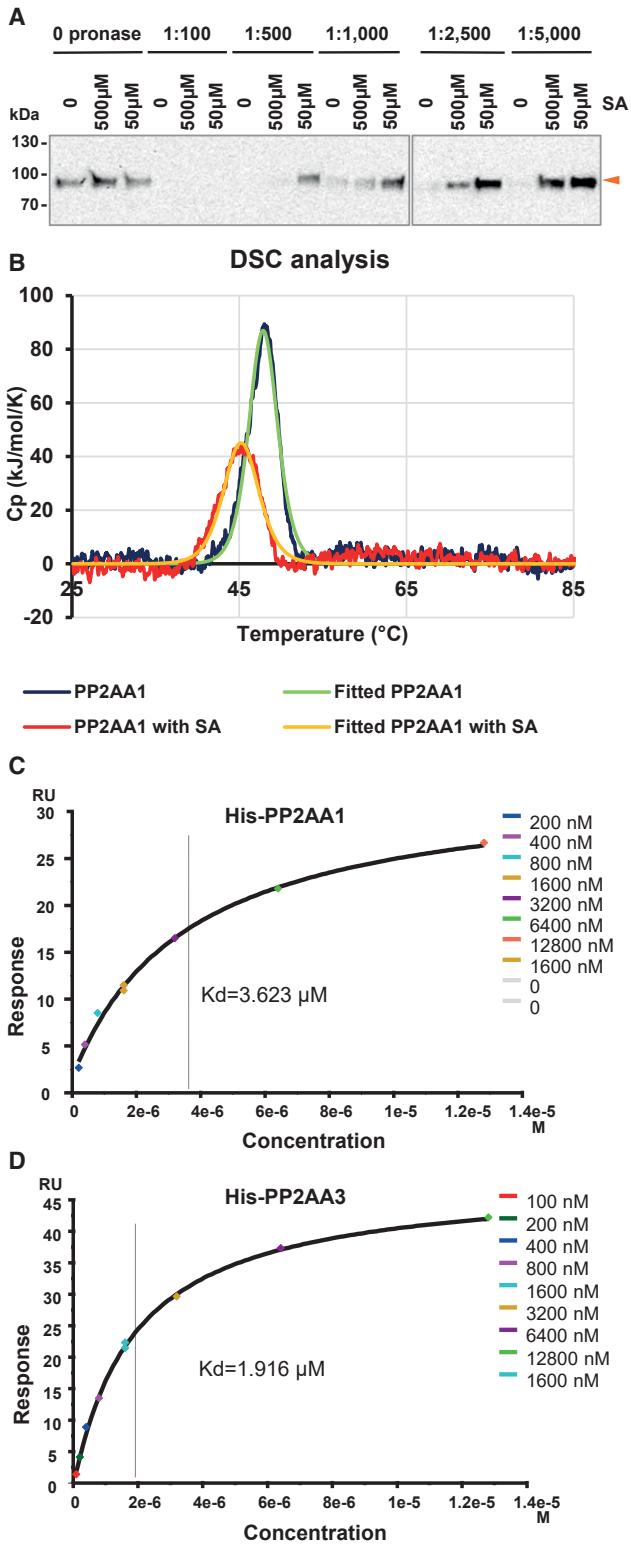

Figure 6. SA Binds to the A Subunit of PP2A

(A) DARTS assay suggests that PP2AA1 is potential target of SA. *pPP2AA1::PP2AA1-GFP* seedlings were used for the protein isolation. Samples were treated with DMSO (mock) and SA and digested by different concentrations of Pronase. Samples were further analyzed by western blot with an anti-GFP antibody.

(B) DSC analysis suggesting the potential binding of SA to recombinant His-PP2AA1. 5 μM of purified His-PP2AA1 protein was analyzed by DSC with or without 50 μM SA. Tm = 48.01°C and 45.03°C for His-PP2AA1+DMSO and His-PP2AA1+SA, respectively.

(C) SPR analysis of the His-PP2AA1 and SA interaction. An active synthetic SA analog (SA-f) was immobilized on a CM-5 sensor chip, and different concentrations of His-PP2AA1 were applied. The binding curve was plotted by values at the steady state, for which the sensorgram is shown is Figure S7D. A K_D value of 3.623 μM was detected.

(D) SPR assay reveals the binding of His-PP2AA3 to SA. The same sensor chip as above was used, and different concentrations of His-PP2AA3 were applied. The binding curve was plotted by values at the steady state, with the data points shown in the sensorgram in Figure S7E. A K_D value of 1.916 μM was detected.

See also Figures S5, S6, and S7.

Thus, all these methodically distinct approaches have confirmed a direct binding of SA to A subunits of PP2A at concentrations well matching the SA physiological activity. The binding of SA to PP2AAs is in line with observations on SA regulating PP2A activity, downstream PIN2 (de)phosphorylation, and auxin-mediated root development.

DISCUSSION

Balancing allocation of resources between growth and defense against pathogens is a common challenge in multicellular organisms [57]. It has been long proposed that, except for the canonical roles as stress hormones, both SA and jasmonic acid (JA) also regulate plant growth and development [12, 15]. Meanwhile, another phytohormone, auxin, well recognized as an essential signaling molecule for growth and development and seemingly involved in almost every aspect of plant life, was proposed to also participate in plant defense against pathogens [11, 15, 58]. Here, we revealed a dual role for the plant hormone SA, which by two parallel perception and signaling mechanisms concomitantly activates immunity and represses growth.

SA is a well-established defense signal of plants; its levels rapidly rise following pathogen attack, and it acts via the NPR-type receptors on transcription of defense genes (Figure 7A) [1]. Here, we identify a parallel signaling pathway that leads to regulation of growth. Both *in vivo* and *in vitro* experiments show that SA specifically binds to the A subunit of the PP2A complex and inhibits its activity. PP2A is a protein phosphatase important for many cellular processes through dephosphorylating various protein substrates [43, 45, 48]. Prominent among its substrates are PIN auxin transporters that play key roles in many developmental processes, and multiple aspects of PIN activity, localization, and subcellular dynamics are mediated by different phosphorylation states [27, 39]. In line with our observation that SA inhibits PP2A activity, increased SA levels lead to an increase in PIN phosphorylation and thus to a change in subcellular PIN distribution and decrease in auxin export activity (Figure 7B). This leads to attenuation of auxin-mediated growth as manifested by a decrease in primary root elongation, inhibition of gravitropic response, and repression of lateral root organogenesis. Identification of SA as direct regulator of PP2A highlights a role for this phosphatase complex as a molecular hub for the trade-off between immune response and

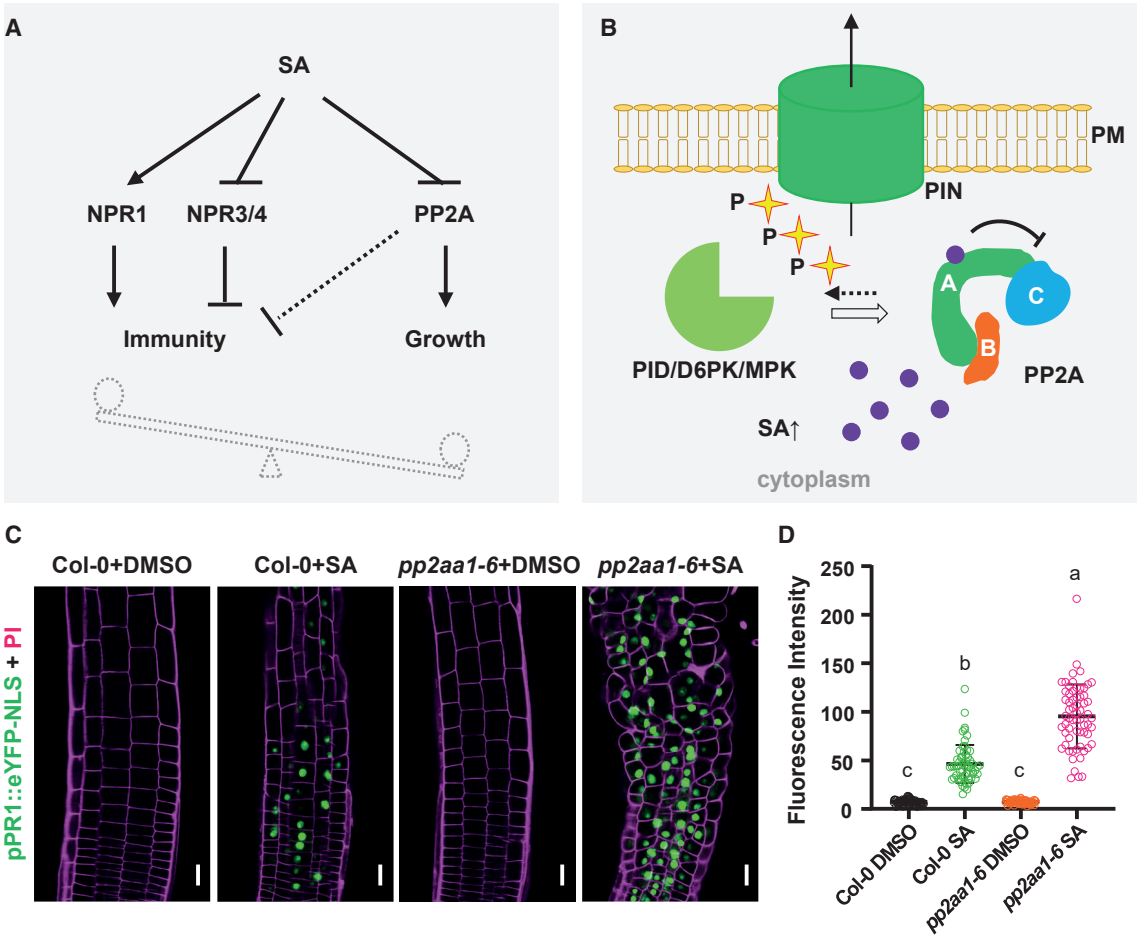

Figure 7. Model for the Parallel SA Action in Immunity and Growth Regulation

(A) SA plays a key role in the growth-immunity transition following pathogen attack: on one hand, SA activates the immune response, through stimulating NPR1 and repressing NPR3/4, all together increasing the expression of downstream defense genes; on the other hand, SA inhibits growth via suppressing PP2A activity and the subsequent dephosphorylation of substrates.

(B) The auxin efflux carrier PIN2 is phosphorylated by different kinases, including PINOID/WAGs, D6PK/D6PKLs, and MAPKs, and dephosphorylated by PP2A. Following pathogen attack, the SA levels increase. SA binds to the A subunits of PP2A and thereafter represses its dephosphorylation activity toward PIN proteins, which leads to hyperphosphorylation of PIN, thereby a decrease in PIN activity ultimately resulting in a decrease in auxin export and attenuation of growth.

(C and D) Induced stronger expression of *pPR1::eYFP-NLS* by SA was detected in *pp2aa1-6*.

(C) *pPR1::eYFP-NLS* seedlings were constantly grown on plates with DMSO or 40 μM SA for 5 days from germination and were then imaged by CLSM. Scale bars, 10 μm.

(D) For quantification, the average GFP florescence of 5–10 representative cells from 10 seedlings for each treatment was measured by Fiji. The data points were showed as dot plots, and lines indicate mean ± SD. Different letters represent significant difference; $p < 0.05$; by one-way ANOVA with a Tukey multiple comparison test.

growth. It is noteworthy that SA does not completely inhibit the PP2A activity, perhaps because PP2AAs are solely the scaffold proteins for the PP2A holoenzyme. This regulatory mode may present a mechanism to fine-tune PP2A activity under different conditions. Notably, we demonstrate that this hyperphosphorylation by PP2A inhibition leads to mislocalization of PIN2, suggesting more kinases, other than PID, involved in apical versus basal PIN targeting [43]. Phosphorylation by mitogen-activated protein kinase (MAPK) gives rise to a decreased PIN polarity and plasma membrane (PM) targeting [59]; thus, it would be interesting to investigate whether PP2A also antagonizes with MAPK in directing PIN localization.

Our previous study revealed that SA interferes with the internalization of PIN proteins, which depends on the clathrin-mediated endocytosis pathway [14]. It has been also reported that *pp2a* mutants, including *pp2aa1*, show decreased PIN internalization [60, 61]. Our proposed SA-PP2A model further clarifies the molecular mechanism underlying the SA effect on PIN trafficking [14]. A recent study shows that SA has an impact on the root meristem patterning via auxin distribution through both upregulating auxin biosynthesis and interfering with transport [30]. Though elevated auxin levels do not typically lead to agravitropic root growth and therefore are likely a result of a regulatory feedback from the blocked auxin transport, it would

still be interesting to test whether PP2A is also involved in this SA effect. Likewise, the observed developmental abnormalities in SA-treated root columella cells [30] were also reported in PP2A mutants [48], further supporting our hypothesis that this SA-PP2A pathway plays more roles in plant growth and development. Here, this study focuses on the SA action on root development, especially PIN2-mediated gravitropism. It is likely that more PP2A substrates, other PIN proteins, or even non-PIN substrates are also involved in these effects.

Previous studies uncovered that plant pathogens interfere with the auxin pathway at the level of the signaling. For example, flagellin of pathogen can induce a microRNA (miRNA) to negatively regulate the expression of auxin receptors, TRANSPORT INHIBITOR RESISTANT1 (TIR1)/ AUXIN SINGNALING F BOX (AFB) [58]. Moreover, SA also stabilizes the negative regulators of auxin signaling pathway, AUXIN/IAA (AUX/IAA) [8], or interferes with auxin biosynthesis [11]. Notably, the *npr1* mutation suppresses the immune response, but not the growth attenuation phenotype of *snc2-1D*, which shows constitutive defense response [62]. Recently, a gain-of-function mutation of *NPR4*, *npr4-4D*, was identified to work together with *npr1-1* and additively to regulate immune response as well as the growth pathway [7]. In view of these observations, we conclude that SA regulates plant growth and development through multiple mechanisms, many of which involve auxin. Generally, it remains unclear whether these other SA effects are mediated by the canonical, NPR1-mediated pathway or require here identified SA-PP2A signaling module.

Notably, by investigating the NPR1-mediated immune response with *pPR1::eYFP-NLS*, we found that *pp2aa1* mutation leads to an increased SA sensitivity (Figures 7C and 7D). It has been reported that bacterial type-III effector proteins could target PP2A to facilitate infection and that multiple *pp2a* loss-of-function mutants, including *pp2aa1*, exhibit elevated response to pathogen attack [63]. Together with our findings, we hypothesize that PP2A, as an essential regulator for multiple pathways, might play a central role in coordinating plant immune response with attenuation of growth and development.

Previous studies demonstrated that NPR1/NPR3/NPR4 are genuine SA receptors, mediating the downstream transcriptional response. NPR proteins share sequence similarity with the mammalian master regulator in the inflammatory response, nuclear factor κB (NF-κB), and specifically its subunit, inhibitor protein I-κB (IκB) [3, 4]. IκB is phosphorylated by an IκB kinase (IKK) complex, whose activity is directly inhibited by salicylates, the active breakdown compound of the common anti-inflammatory drug Aspirin (2-acetoxybenzoic acid), thus providing mechanism of their well-known anti-inflammatory effects [64]. These interesting analogies between plant and mammalian pathogen defense mechanisms, both at the sequence level of involved regulators as well as at structural level of the involved ligands, point to possible evolutionary conservation between these otherwise seemingly unrelated pathogen defense strategies. Given the fact that PP2A regulates the dephosphorylation of numerous substrates, it would be interesting to investigate whether the SA-PP2A signaling module is a part of this evolutionary conserved mechanism and also regulates the NPR-mediated immunity in plants or NF-κB-controlled inflammatory response in mammals.

STAR★METHODS

Detailed methods are provided in the online version of this paper and include the following:

- KEY RESOURCES TABLE
- LEAD CONTACT AND MATERIALS AVAILABILITY
- EXPERIMENTAL MODEL AND SUBJECT DETAILS
  - Plant Materials and Growth Conditions
- METHOD DETAILS
  - Pseudomonas syringae treatment of *Arabidopsis* seedlings
  - Pharmacological treatments
  - Free SA measurement by liquid chromatography-tandem mass spectrometry (LC-MS/MS)
  - Auxin transport in hypocotyls and tobacco BY-2 cells
  - Imaging with Confocal Laser Scanning Microscopy (CLSM)
  - Image analysis and morphological analysis
  - Molecular cloning
  - PP2A activity assay
  - Protein extraction and immunoblot
  - PIN2 phosphorylation assays
  - PIN2-HL phosphorylation assay with [γ-^{32}P]-ATP
  - Drug Affinity Responsive Target Stability (DARTS) assay
  - Recombinant protein expression and purification
  - Differential Scanning Calorimetry (DSC) analysis
  - Chemical synthesis of SA derivatives
  - SPR analysis
  - Accession Numbers
- QUANTIFICATION AND STATISTICAL ANALYSIS
- DATA AND CODE AVAILABILITY

SUPPLEMENTAL INFORMATION

Supplemental Information can be found online at https://doi.org/10.1016/j.cub.2019.11.058.

ACKNOWLEDGMENTS

We thank Shigeyuki Betsuyaku (University of Tsukuba), Alison Delong (Brown University), Xinnian Dong (Duke University), Dolf Weijers (Wageningen University), Yuelin Zhang (UBC), and Martine Pastuglia (Institut Jean-Pierre Bourgin) for sharing published materials; Jana Riederer for help with cantharidin physiological analysis; David Domjan for help with cloning pET28a-PIN2HL; Qing Lu for help with DARTS; Hana Kozubíková for technical support on SA derivative synthesis; Zuzana Vondráková for technical support with tobacco cells; Lucia Strader (Washington University), Bert De Rybel (Ghent University), Bartel Vanholme (Ghent University), and Lukas Mach (BOKU) for helpful discussions; and bioimaging and life science facilities of IST Austria for continuous support. We gratefully acknowledge the Nottingham Arabidopsis Stock Center (NASC) for providing T-DNA insertional mutants. The DSC and SPR instruments were provided by the EQ-BOKU VIBT GmbH and the BOKU Core Facility for Biomolecular and Cellular Analysis, with help of Irene Schaffner. The research leading to these results has received funding from the European Union's Horizon 2020 program (ERC grant agreement no. 742985 to J.F.) and the People Programme (Marie Curie Actions) of the European Union's Seventh Framework Programme (FP7/2007-2013) under REA grant agreement no. 291734. S.T. was supported by a European Molecular Biology Organization (EMBO) long-term postdoctoral fellowship (ALTF 723-2015). O.N. was supported by the Ministry of Education, Youth and Sports of the Czech Republic (European Regional Development Fund-Project "Centre for Experimental Plant Biology" no.

CZ.02.1.01/0.0/0.0/16_019/0000738). J. Pospíšil was supported by European Regional Development Fund Project "Centre for Experimental Plant Biology" (no. CZ.02.1.01/0.0/0.0/16_019/0000738). J. Petrášek was supported by EU Operational Programme Prague-Competitiveness (no. CZ.2.16/3.1.00/21519).

AUTHOR CONTRIBUTIONS

S.T. and J.F. designed research and analyzed data. S.T., M.A., I.V., M.G., G.M., and J.H. performed experiments. I.P. and O.N. provided the SA analyses. P.L. and J. Pospíšil synthesized the SA derivatives. E.R. contributed to the DARTS assay. J. Petrášek contributed to auxin transport assays with BY-2 cells. S.T. and J.F. wrote the manuscript with input from other authors, and all authors revised it.

DECLARATION OF INTERESTS

The authors declare no competing interests.

Received: July 9, 2019
Revised: October 22, 2019
Accepted: November 19, 2019
Published: January 16, 2020

REFERENCES

1. Wildermuth, M.C., Dewdney, J., Wu, G., and Ausubel, F.M. (2001). Isochorismate synthase is required to synthesize salicylic acid for plant defence. Nature *414*, 562–565.
2. Cao, H., Bowling, S.A., Gordon, A.S., and Dong, X. (1994). Characterization of an *Arabidopsis* mutant that is nonresponsive to inducers of systemic acquired resistance. Plant Cell *6*, 1583–1592.
3. Cao, H., Glazebrook, J., Clarke, J.D., Volko, S., and Dong, X. (1997). The *Arabidopsis NPR1* gene that controls systemic acquired resistance encodes a novel protein containing ankyrin repeats. Cell *88*, 57–63.
4. Ryals, J., Weymann, K., Lawton, K., Friedrich, L., Ellis, D., Steiner, H.Y., Johnson, J., Delaney, T.P., Jesse, T., Vos, P., and Uknes, S. (1997). The *Arabidopsis* NIM1 protein shows homology to the mammalian transcription factor inhibitor I kappa B. Plant Cell *9*, 425–439.
5. Mou, Z., Fan, W., and Dong, X. (2003). Inducers of plant systemic acquired resistance regulate NPR1 function through redox changes. Cell *113*, 935–944.
6. Spoel, S.H., Mou, Z., Tada, Y., Spivey, N.W., Genschik, P., and Dong, X. (2009). Proteasome-mediated turnover of the transcription coactivator NPR1 plays dual roles in regulating plant immunity. Cell *137*, 860–872.
7. Ding, Y., Sun, T., Ao, K., Peng, Y., Zhang, Y., Li, X., and Zhang, Y. (2018). Opposite roles of salicylic Acid receptors NPR1 and NPR3/NPR4 in transcriptional regulation of plant immunity. Cell *173*, 1454–1467.e15.
8. Wang, D., Pajerowska-Mukhtar, K., Culler, A.H., and Dong, X. (2007). Salicylic acid inhibits pathogen growth in plants through repression of the auxin signaling pathway. Curr. Biol. *17*, 1784–1790.
9. Fu, Z.Q., Yan, S., Saleh, A., Wang, W., Ruble, J., Oka, N., Mohan, R., Spoel, S.H., Tada, Y., Zheng, N., and Dong, X. (2012). NPR3 and NPR4 are receptors for the immune signal salicylic acid in plants. Nature *486*, 228–232.
10. Wu, Y., Zhang, D., Chu, J.Y., Boyle, P., Wang, Y., Brindle, I.D., De Luca, V., and Després, C. (2012). The *Arabidopsis* NPR1 protein is a receptor for the plant defense hormone salicylic acid. Cell Rep. *1*, 639–647.
11. Yuan, H.M., Liu, W.C., and Lu, Y.T. (2017). CATALASE2 coordinates SA-mediated repression of both auxin accumulation and JA biosynthesis in plant defenses. Cell Host Microbe *21*, 143–155.
12. Rivas-San Vicente, M., and Plasencia, J. (2011). Salicylic acid beyond defence: its role in plant growth and development. J. Exp. Bot. *62*, 3321–3338.
13. Zhang, X., Dai, Y., Xiong, Y., DeFraia, C., Li, J., Dong, X., and Mou, Z. (2007). Overexpression of *Arabidopsis MAP kinase kinase 7* leads to activation of plant basal and systemic acquired resistance. Plant J. *52*, 1066–1079.
14. Du, Y., Tejos, R., Beck, M., Himschoot, E., Li, H., Robatzek, S., Vanneste, S., and Friml, J. (2013). Salicylic acid interferes with clathrin-mediated endocytic protein trafficking. Proc. Natl. Acad. Sci. USA *110*, 7946–7951.
15. Kazan, K., and Manners, J.M. (2009). Linking development to defense: auxin in plant-pathogen interactions. Trends Plant Sci. *14*, 373–382.
16. Klessig, D.F., Tian, M., and Choi, H.W. (2016). Multiple targets of salicylic acid and its derivatives in plants and animals. Front. Immunol. *7*, 206.
17. Slaymaker, D.H., Navarre, D.A., Clark, D., del Pozo, O., Martin, G.B., and Klessig, D.F. (2002). The tobacco salicylic acid-binding protein 3 (SABP3) is the chloroplast carbonic anhydrase, which exhibits antioxidant activity and plays a role in the hypersensitive defense response. Proc. Natl. Acad. Sci. USA *99*, 11640–11645.
18. Choi, H.W., Manohar, M., Manosalva, P., Tian, M., Moreau, M., and Klessig, D.F. (2016). Activation of plant innate immunity by extracellular High Mobility Group Box 3 and its inhibition by salicylic acid. PLoS Pathog. *12*, e1005518.
19. Manohar, M., Wang, D., Manosalva, P.M., Choi, H.W., Kombrink, E., and Klessig, D.F. (2017). Members of the abscisic acid co-receptor PP2C protein family mediate salicylic acid-abscisic acid crosstalk. Plant Direct *1*, e00020.
20. Wang, C., Hu, T., Yan, X., Meng, T., Wang, Y., Wang, Q., Zhang, X., Gu, Y., Sánchez-Rodríguez, C., Gadeyne, A., et al. (2016). Differential regulation of clathrin and its adaptor proteins during membrane recruitment for endocytosis. Plant Physiol. *171*, 215–229.
21. Adamowski, M., and Friml, J. (2015). PIN-dependent auxin transport: action, regulation, and evolution. Plant Cell *27*, 20–32.
22. Lebeis, S.L., Paredes, S.H., Lundberg, D.S., Breakfield, N., Gehring, J., McDonald, M., Malfatti, S., Glavina del Rio, T., Jones, C.D., Tringe, S.G., and Dangl, J.L. (2015). PLANT MICROBIOME. Salicylic acid modulates colonization of the root microbiome by specific bacterial taxa. Science *349*, 860–864.
23. Clarke, J.D., Liu, Y., Klessig, D.F., and Dong, X. (1998). Uncoupling *PR* gene expression from NPR1 and bacterial resistance: characterization of the dominant *Arabidopsis cpr6-1* mutant. Plant Cell *10*, 557–569.
24. Betsuyaku, S., Katou, S., Takebayashi, Y., Sakakibara, H., Nomura, N., and Fukuda, H. (2018). Salicylic acid and Jasmonic acid pathways are activated in spatially different domains around the infection site during effector-triggered immunity in *Arabidopsis thaliana*. Plant Cell Physiol. *59*, 8–16.
25. Zhao, X., Wang, J., Yuan, J., Wang, X.L., Zhao, Q.P., Kong, P.T., and Zhang, X. (2015). NITRIC OXIDE-ASSOCIATED PROTEIN1 (AtNOA1) is essential for salicylic acid-induced root waving in *Arabidopsis thaliana*. New Phytol. *207*, 211–224.
26. Conrath, U., Chen, Z., Ricigliano, J.R., and Klessig, D.F. (1995). Two inducers of plant defense responses, 2,6-dichloroisonicotinec acid and salicylic acid, inhibit catalase activity in tobacco. Proc. Natl. Acad. Sci. USA *92*, 7143–7147.
27. Naramoto, S. (2017). Polar transport in plants mediated by membrane transporters: focus on mechanisms of polar auxin transport. Curr. Opin. Plant Biol. *40*, 8–14.
28. Liao, C.-Y., Smet, W., Brunoud, G., Yoshida, S., Vernoux, T., and Weijers, D. (2015). Reporters for sensitive and quantitative measurement of auxin response. Nat. Methods *12*, 207–210, 2, 210.
29. Brumos, J., Robles, L.M., Yun, J., Vu, T.C., Jackson, S., Alonso, J.M., and Stepanova, A.N. (2018). Local auxin biosynthesis is a key regulator of plant development. Dev. Cell *47*, 306–318.e5.
30. Pasternak, T., Groot, E.P., Kazantsev, F.V., Teale, W., Omelyanchuk, N., Kovrizhnykh, V., Palme, K., and Mironova, V.V. (2019). Salicylic acid affects root meristem patterning via auxin distribution in a concentration-dependent manner. Plant Physiol. *180*, 1725–1739.

31. Petrásek, J., Elčkner, M., Morris, D.A., and Zazímalová, E. (2002). Auxin efflux carrier activity and auxin accumulation regulate cell division and polarity in tobacco cells. Planta *216*, 302–308.

32. Petrásek, J., Mravec, J., Bouchard, R., Blakeslee, J.J., Abas, M., Seifertová, D., Wiśniewska, J., Tadele, Z., Kubeš, M., Covanová, M., et al. (2006). PIN proteins perform a rate-limiting function in cellular auxin efflux. Science *312*, 914–918.

33. Bennett, M.J., Marchant, A., Green, H.G., May, S.T., Ward, S.P., Millner, P.A., Walker, A.R., Schulz, B., and Feldmann, K.A. (1996). *Arabidopsis AUX1* gene: a permease-like regulator of root gravitropism. Science *273*, 948–950.

34. Swarup, R., Friml, J., Marchant, A., Ljung, K., Sandberg, G., Palme, K., and Bennett, M. (2001). Localization of the auxin permease AUX1 suggests two functionally distinct hormone transport pathways operate in the *Arabidopsis* root apex. Genes Dev. *15*, 2648–2653.

35. Luschnig, C., Gaxiola, R.A., Grisafi, P., and Fink, G.R. (1998). EIR1, a root-specific protein involved in auxin transport, is required for gravitropism in *Arabidopsis thaliana*. Genes Dev. *12*, 2175–2187.

36. Abas, L., Benjamins, R., Malenica, N., Paciorek, T., Wiśniewska, J., Moulinier-Anzola, J.C., Sieberer, T., Friml, J., and Luschnig, C. (2006). Intracellular trafficking and proteolysis of the *Arabidopsis* auxin-efflux facilitator PIN2 are involved in root gravitropism. Nat. Cell Biol. *8*, 249–256.

37. Baster, P., Robert, S., Kleine-Vehn, J., Vanneste, S., Kania, U., Grunewald, W., De Rybel, B., Beeckman, T., and Friml, J. (2013). SCF(TIR1/AFB)-auxin signalling regulates PIN vacuolar trafficking and auxin fluxes during root gravitropism. EMBO J. *32*, 260–274.

38. Habets, M.E.J., and Offringa, R. (2014). PIN-driven polar auxin transport in plant developmental plasticity: a key target for environmental and endogenous signals. New Phytol. *203*, 362–377.

39. Armengot, L., Marquès-Bueno, M.M., and Jaillais, Y. (2016). Regulation of polar auxin transport by protein and lipid kinases. J. Exp. Bot. *67*, 4015–4037.

40. Marhava, P., Bassukas, A.E.L., Zourelidou, M., Kolb, M., Moret, B., Fastner, A., Schulze, W.X., Cattaneo, P., Hammes, U.Z., Schwechheimer, C., and Hardtke, C.S. (2018). A molecular rheostat adjusts auxin flux to promote root protophloem differentiation. Nature *558*, 297–300.

41. Abas, L., and Luschnig, C. (2010). Maximum yields of microsomal-type membranes from small amounts of plant material without requiring ultracentrifugation. Anal. Biochem. *401*, 217–227.

42. Garbers, C., DeLong, A., Deruére, J., Bernasconi, P., and Söll, D. (1996). A mutation in protein phosphatase 2A regulatory subunit A affects auxin transport in *Arabidopsis*. EMBO J. *15*, 2115–2124.

43. Michniewicz, M., Zago, M.K., Abas, L., Weijers, D., Schweighofer, A., Meskiene, I., Heisler, M.G., Ohno, C., Zhang, J., Huang, F., et al. (2007). Antagonistic regulation of PIN phosphorylation by PP2A and PINOID directs auxin flux. Cell *130*, 1044–1056.

44. Manohar, M., Tian, M., Moreau, M., Park, S.-W., Choi, H.W., Fei, Z., Friso, G., Asif, M., Manosalva, P., von Dahl, C.C., et al. (2015). Identification of multiple salicylic acid-binding proteins using two high throughput screens. Front. Plant Sci. *5*, 777.

45. Zhou, H.-W., Nussbaumer, C., Chao, Y., and DeLong, A. (2004). Disparate roles for the regulatory A subunit isoforms in *Arabidopsis* protein phosphatase 2A. Plant Cell *16*, 709–722.

46. Spinner, L., Gadeyne, A., Belcram, K., Goussot, M., Moison, M., Duroc, Y., Eeckhout, D., De Winne, N., Schaefer, E., Van De Slijke, E., et al. (2013). A protein phosphatase 2A complex spatially controls plant cell division. Nat. Commun. *4*, 1863.

47. Li, Y.M., and Casida, J.E. (1992). Cantharidin-binding protein: identification as protein phosphatase 2A. Proc. Natl. Acad. Sci. USA *89*, 11867–11870.

48. Yue, K., Sandal, P., Williams, E.L., Murphy, E., Stes, E., Nikonorova, N., Ramakrishna, P., Czyzewicz, N., Montero-Morales, L., Kumpf, R., et al. (2016). PP2A-3 interacts with ACR4 and regulates formative cell division in the *Arabidopsis* root. Proc. Natl. Acad. Sci. USA *113*, 1447–1452.

49. Blakeslee, J.J., Zhou, H.-W., Heath, J.T., Skottke, K.R., Barrios, J.A.R., Liu, S.-Y., and DeLong, A. (2008). Specificity of RCN1-mediated protein phosphatase 2A regulation in meristem organization and stress response in roots. Plant Physiol. *146*, 539–553.

50. Ekman, P., and Jäger, O. (1993). Quantification of subnanomolar amounts of phosphate bound to seryl and threonyl residues in phosphoproteins using alkaline hydrolysis and malachite green. Anal. Biochem. *214*, 138–141.

51. Bos, C.L., Kodach, L.L., van den Brink, G.R., Diks, S.H., van Santen, M.M., Richel, D.J., Peppelenbosch, M.P., and Hardwick, J.C.H. (2006). Effect of aspirin on the Wnt/β-catenin pathway is mediated via protein phosphatase 2A. Oncogene *25*, 6447–6456.

52. Lomenick, B., Hao, R., Jonai, N., Chin, R.M., Aghajan, M., Warburton, S., Wang, J., Wu, R.P., Gomez, F., Loo, J.A., et al. (2009). Target identification using drug affinity responsive target stability (DARTS). Proc. Natl. Acad. Sci. USA *106*, 21984–21989.

53. Gill, P., Moghadam, T.T., and Ranjbar, B. (2010). Differential scanning calorimetry techniques: applications in biology and nanoscience. J. Biomol. Tech. *21*, 167–193.

54. Niesen, F.H., Berglund, H., and Vedadi, M. (2007). The use of differential scanning fluorimetry to detect ligand interactions that promote protein stability. Nat. Protoc. *2*, 2212–2221.

55. Hamiaux, C., Drummond, R.S.M., Janssen, B.J., Ledger, S.E., Cooney, J.M., Newcomb, R.D., and Snowden, K.C. (2012). DAD2 is an α/β hydrolase likely to be involved in the perception of the plant branching hormone, strigolactone. Curr. Biol. *22*, 2032–2036.

56. Karlsson, R., Michaelsson, A., and Mattsson, L. (1991). Kinetic analysis of monoclonal antibody-antigen interactions with a new biosensor based analytical system. J. Immunol. Methods *145*, 229–240.

57. Belkhadir, Y., Yang, L., Hetzel, J., Dangl, J.L., and Chory, J. (2014). The growth-defense pivot: crisis management in plants mediated by LRR-RK surface receptors. Trends Biochem. Sci. *39*, 447–456.

58. Navarro, L., Dunoyer, P., Jay, F., Arnold, B., Dharmasiri, N., Estelle, M., Voinnet, O., and Jones, J.D.G. (2006). A plant miRNA contributes to antibacterial resistance by repressing auxin signaling. Science *312*, 436–439.

59. Jia, W., Li, B., Li, S., Liang, Y., Wu, X., Ma, M., Wang, J., Gao, J., Cai, Y., Zhang, Y., et al. (2016). Mitogen-activated protein kinase cascade MKK7-MPK6 plays important roles in plant development and regulates shoot branching by phosphorylating PIN1 in *Arabidopsis*. PLoS Biol. *14*, e1002550.

60. Kleine-Vehn, J., Huang, F., Naramoto, S., Zhang, J., Michniewicz, M., Offringa, R., and Friml, J. (2009). PIN auxin efflux carrier polarity is regulated by PINOID kinase-mediated recruitment into GNOM-independent trafficking in *Arabidopsis*. Plant Cell *21*, 3839–3849.

61. Karampelias, M., Neyt, P., De Groeve, S., Aesaert, S., Coussens, G., Rolčík, J., Bruno, L., De Winne, N., Van Minnebruggen, A., Van Montagu, M., et al. (2016). ROTUNDA3 function in plant development by phosphatase 2A-mediated regulation of auxin transporter recycling. Proc. Natl. Acad. Sci. USA *113*, 2768–2773.

62. Zhang, Y., Yang, Y., Fang, B., Gannon, P., Ding, P., Li, X., and Zhang, Y. (2010). *Arabidopsis snc2-1D* activates receptor-like protein-mediated immunity transduced through WRKY70. Plant Cell *22*, 3153–3163.

63. Jin, L., Ham, J.H., Hage, R., Zhao, W., Soto-Hernández, J., Lee, S.Y., Paek, S.M., Kim, M.G., Boone, C., Coplin, D.L., and Mackey, D. (2016). Direct and indirect targeting of PP2A by conserved bacterial type-III effector proteins. PLoS Pathog. *12*, e1005609.

64. Yin, M.J., Yamamoto, Y., and Gaynor, R.B. (1998). The anti-inflammatory agents aspirin and salicylate inhibit the activity of I(κ)B kinase-β. Nature *396*, 77–80.

65. Suga, S., Imagawa, S., and Maeshima, M. (2001). Specificity of the accumulation of mRNAs and proteins of the plasma membrane and tonoplast aquaporins in radish organs. Planta *212*, 294–304.

66. Fischer, U., Ikeda, Y., Ljung, K., Serralbo, O., Singh, M., Heidstra, R., Palme, K., Scheres, B., and Grebe, M. (2006). Vectorial information for *Arabidopsis* planar polarity is mediated by combined AUX1, EIN2, and GNOM activity. Curr. Biol. *16*, 2143–2149.

67. Swarup, R., Kargul, J., Marchant, A., Zadik, D., Rahman, A., Mills, R., Yemm, A., May, S., Williams, L., Millner, P., et al. (2004). Structure-function analysis of the presumptive *Arabidopsis* auxin permease AUX1. Plant Cell *16*, 3069–3083.

68. Zhang, Y., Cheng, Y.T., Qu, N., Zhao, Q., Bi, D., and Li, X. (2006). Negative regulation of defense responses in *Arabidopsis* by two *NPR1* paralogs. Plant J. *48*, 647–656.

69. Gross, J., Cho, W.K., Lezhneva, L., Falk, J., Krupinska, K., Shinozaki, K., Seki, M., Herrmann, R.G., and Meurer, J. (2006). A plant locus essential for phylloquinone (vitamin K1) biosynthesis originated from a fusion of four eubacterial genes. J. Biol. Chem. *281*, 17189–17196.

70. Xu, J., and Scheres, B. (2005). Dissection of Arabidopsis ADP-RIBOSYLATION FACTOR 1 function in epidermal cell polarity. Plant Cell *17*, 525–536.

71. Bowling, S.A., Guo, A., Cao, H., Gordon, A.S., Klessig, D.F., and Dong, X. (1994). A mutation in *Arabidopsis* that leads to constitutive expression of systemic acquired resistance. Plant Cell *6*, 1845–1857.

72. Bowling, S.A., Clarke, J.D., Liu, Y., Klessig, D.F., and Dong, X. (1997). The *cpr5* mutant of *Arabidopsis* expresses both NPR1-dependent and NPR1-independent resistance. Plant Cell *9*, 1573–1584.

73. Ishiga, Y., Ishiga, T., Uppalapati, S.R., and Mysore, K.S. (2011). *Arabidopsis* seedling flood-inoculation technique: a rapid and reliable assay for studying plant-bacterial interactions. Plant Methods *7*, 32.

74. Floková, K., Tarkowská, D., Miersch, O., Strnad, M., Wasternack, C., and Novák, O. (2014). UHPLC-MS/MS based target profiling of stress-induced phytohormones. Phytochemistry *105*, 147–157.

75. Lewis, D.R., and Muday, G.K. (2009). Measurement of auxin transport in Arabidopsis thaliana. Nat. Protoc. *4*, 437–451.

76. Schindelin, J., Arganda-Carreras, I., Frise, E., Kaynig, V., Longair, M., Pietzsch, T., Preibisch, S., Rueden, C., Saalfeld, S., Schmid, B., et al. (2012). Fiji: an open-source platform for biological-image analysis. Nat. Methods *9*, 676–682.

77. Kania, U., Nodzyński, T., Lu, Q., Hicks, G.R., Nerinckx, W., Mishev, K., Peurois, F., Cherfils, J., De Rycke, R., Grones, P., et al. (2018). The inhibitor endosidin 4 targets SEC7 domain-type ARF GTPase exchange factors and interferes with subcellular trafficking in eukaryotes. Plant Cell *30*, 2553–2572.

78. Mishev, K., Lu, Q., Denoo, B., Peurois, F., Dejonghe, W., Hullaert, J., De Rycke, R., Boeren, S., Bretou, M., De Munck, S., et al. (2018). Nonselective chemical inhibition of Sec7 domain-containing ARF GTPase exchange factors. Plant Cell *30*, 2573–2593.

79. Kong, X., He, Z., Zhang, Y., Mu, L., Liang, C., Chen, B., Jing, X., and Cammidge, A.N. (2011). A mesogenic triphenylene-perylene-triphenylene triad. Org. Lett. *13*, 764–767.

STAR★METHODS

KEY RESOURCES TABLE

REAGENT or RESOURCE	SOURCE	IDENTIFIER
Antibodies		
Rabbit anti-PIN1	[37]	N/A
Rabbit anti-PIN2	[36]	N/A
Mouse anti-His-tag monoclonal Antibody	Agrisera	Cat# AS11 1771
Mouse anti-myc-tag monoclonal Antibody, clone 4A6	Millipore (Merck)	Cat# 05-724
Phospho-PP2A alpha (Tyr307) Polyclonal Antibody	Thermo Scientific	Cat# PA5-36874; RRID:AB_2553794
Anti-GFP-HRP	Miltenyi Biotec	Cat# 130-091-833; RRID:AB_247003
Monoclonal anti-GFP antibody produced in mouse	Sigma	Cat# G6539; RRID:AB_259941
Anti-PIP2;1	[65]	N/A
Bacterial and Virus Strains		
Escherichia coli DH5α	Lab stock	N/A
E.coli BL21 (DE3)	New England Biolabs	Cat# C2527H
Agrobacterium tumefaciens GV3101	Lab stock	N/A
Pseudomonas syringae pv. tomato DC3000	Armin Djamei lab	N/A
Chemicals, Peptides, and Recombinant Proteins		
brefeldin A	Sigma	Cat# B7651
Propidium Iodide	Sigma	Cat# P3566
PBS Buffer 10 × (1000 mL)	GE Healthcare	Cat# BR100672
PhosSTOP	Sigma/Roche	Cat# 4906837001
cOmplete protease inhibitor cocktail	Sigma/Roche	Cat# 4693124001
Benzoic acid (BA)	Sigma	Cat# 242381
Salicylic Acid (SA)	Sigma	Cat# 247588
3-Hydroxybenzoic acid (3-OH-BA)	Sigma	Cat# H20008
4-Hydroxybenzoic acid (4-OH-BA)	Sigma	Cat# H20059
N-(1-Naphthyl)phthalamidic acid	Sigma	Cat# N12507
2,3,5-Triiodobenzoic acid (TIBA)	Sigma	Cat# T5910
[3H]-IAA (([5-^{3}H]-Indole-3-acetic acid)	American Radiolabeled Chemicals	Cat# ART 0340
[3H]- NAA ([4-^{3}H]-1-Naphthylacetic acid)	American Radiolabeled Chemicals	Cat# ART 0610
[3H]-2,4-D (([5-^{3}H]-2,4-Dichlorophenoxy acetic acid)	American Radiolabeled Chemicals	Cat# ART 0559
Cantharidin	Sigma	Cat# C7632
Imidazole	Sigma	Cat# I5513
FastDigest Hin1II	Thermo Fisher Scientific	Cat# FD1834
FastDigest EcoRI	Thermo Fisher Scientific	Cat# FD0274
FastDigest XhoI	Thermo Fisher Scientific	Cat# FD0694
FastDigest BamHI	Thermo Fisher Scientific	Cat# FD0054
FastDigest SalI	Thermo Fisher Scientific	Cat# FD0644
T4 DNA Ligase Buffer	Thermo Fisher Scientific	Cat# 46300-018
T4 DNA Ligase (1 U/μL)	Thermo Fisher Scientific	Cat# 15224-017
GeneJET Plasmid Miniprep Kit	Thermo Fisher Scientific	Cat# K0503
GeneJET Gel extraction kit	Thermo Fisher Scientific	Cat# K0692
BSA (Bovine Serum Albumin)	Sigma	Cat# A2153
His-PP2AA1	This study	N/A
His-PP2AA3	This study	N/A

(*Continued on next page*)

Continued

REAGENT or RESOURCE	SOURCE	IDENTIFIER
His-PIN2HL	This study	N/A
Critical Commercial Assays		
Bio-Safe Coomassie Stain #1610786	Bio-Rad	Cat# 1610786
Non-Radioactive Phosphatase Assay Systems	Promega	Cat# V2460
HisPur Ni-NTA Resin	Thermo Fisher Scientific	Cat# 88222
γ-[^{32}P]-ATP	PerkinElmer	Cat# NEG502A001MC
Experimental Models: Cell Lines		
Nicotiana tabacum L., cv. Bright Yellow-2 (BY-2)	N/A	N/A
Experimental Models: Organisms/Strains		
Arabidopsis thaliana Col-0	N/A	N/A
A. thaliana Ws-4	NASC	N5390
A. thaliana eir1-4 (pin2-T)	[36]	SALK_091142
A. thaliana aux1-T (aux1)	[66]	SALK_020355
A. thaliana pAUX1::AUX1-YFP	[67]	N/A
A. thaliana pPR1::eYFP-NLS	[24]	N/A
A. thaliana npr1-1	[2]	N/A
A. thaliana npr3-1 npr4-3	[68]	N/A
A. thaliana npr1-1 npr3-1 npr4-3	[68]	N/A
A. thaliana cpr6	[23]	N/A
A. thaliana sid2-3	[69]	SALK_042603
A. thaliana rcn1-1 (rcn1, pp2aa1-1)	[42]	N/A
A. thaliana rcn1-6 (pp2aa1-6)	[49]	SALK_059903
A. thaliana pp2aa2-2	[45]	SALK_037095
A. thaliana pp2aa2-3	[45]	SALK_017541
A. thaliana pp2aa3-2	[45]	SALK_099550
A. thaliana pp2aa1 pp2aa2-3	[45]	N/A
A. thaliana pp2aa1 pp2aa3-1	[45]	N/A
A. thaliana pPIN2::PIN2-GFP	[70]	N/A
A. thaliana pPP2AA1::PP2AA1-GFP	[45]	N/A
A. thaliana DR5v2	[28]	N/A
A. thaliana eir1-4 DR5v2	This study	N/A
A. thaliana pPR1::eYFP-NLS	[24]	N/A
A. thaliana pp2aa1-6 pPR1::eYFP-NLS	This study	N/A
A. thaliana 35S::4 × myc-PP2AA1	This study	N/A
A. thaliana pp2aa1-6 cpr6	This study	N/A
Oligonucleotides		
Primers used in this study, see Table S1	This study	N/A
Recombinant DNA		
Plasmid pET28a-PP2AA1	This study	N/A
Plasmid pET28a-PP2AA3	This study	N/A
Plasmid pET28a-PIN2HL	This study	N/A
Plasmid pEGAD-35S::4 × myc-PP2AA1	This study	N/A
Software and Algorithms		
Arabidopsis Information Resource (TAIR)	http://www.arabidopsis.org/	N/A
ImageJ	https://imagej.nih.gov/ij/	NIH
Fiji	https://fiji.sc/	N/A

(*Continued on next page*)

Continued

REAGENT or RESOURCE	SOURCE	IDENTIFIER
ZEN	https://www.zeiss.com/microscopy/int/products/microscope-software/zen-lite.html	ZEISS
DNA MAN	https://www.lynnon.com/	N/A
ChemSketch	https://www.acdlabs.com/resources/freeware/chemsketch/	N/A

LEAD CONTACT AND MATERIALS AVAILABILITY

Requests for resources and reagents such as plasmids, compounds, mutant and transgenic lines should be directed to and will be fulfilled by the Lead Contact, Jiří Friml (jiri.friml@ist.ac.at).

EXPERIMENTAL MODEL AND SUBJECT DETAILS

Plant Materials and Growth Conditions

Arabidopsis thaliana (L.) mutants or transgenic lines are in Columbia-0 (Col-0) background if not particularly mentioned. The mutants and marker lines *pPIN2::PIN2-GFP* in *eir1-1* [70], *pAUX1::AUX1-YFP* [67], *aux1-T* [66], *eir1-4* (*pin2-T*) [36], *npr1-1* [2, 3], *sid2-3* (*sid2*) [69], *npr3-1 npr4-3* [68], *npr3-2 npr4-2* [68], *npr1-1 npr3-1 npr4-3* [68], *cpr1* [71], *cpr5* [72], *cpr6* [23], *rcn1-1* (*pp2aa1-1*, in Ws) [42], *rcn1-6* (*pp2aa1-6*) [49], *pp2aa2-2* [45], *pp2aa2-3* [45], *pp2aa3-2* [45], *pp2aa1,a2* (*pp2aa1, pp2aa2-3*) [45], *pp2aa1,a3* [45], *pp2aa2,a3* [45], *pPP2AA1::PP2AA1-GFP in Col-0* [45] and *DR5v2* [28] were published previously. The detailed information of plant lines, including mutants and marker lines, used in this study is listed in Key Resources Table. The primers used for genotyping the mutants were listed in Table S1.

For physiological experiments, surface-sterilized seeds were sown on Murashige and Skoog (1/2 MS) medium, supplemented with 1% sucrose, 0.8% phytoagar (pH 5.9), stratified at 4°C for 3 days (d), and then grown vertically in a growth chamber at 21°C with a 16-h-light/8-h-dark photoperiod.

METHOD DETAILS

Pseudomonas syringae treatment of *Arabidopsis* seedlings

P. syringae treatment was performed as reported previously [73]. A single colony of *P. syringae pv. tomato DC3000* (kind gift from Dr. Armin Djamei, IPK- Gatersleben) was cultured in 20 mL King's B (KB) liquid media overnight, to get OD_{600} between 0.4 and 0.6. The DC3000 cells were collected by spinning down at 1600 g, and were then resuspended in infection buffer (0.025% Silwet L-77, and 10 mM $MgCl_2$). The concentration was adjusted to OD_{600} = 0.01 (= ~5 × 10^6 CFU/mL) for treatment. The DC3000 suspension was dispensed into the plates with 5-day-old *pPR1::eYFP-NLS* seedlings and incubated for 3 min at 25°C. Afterward, the suspension was decanted, and seedlings were grown for another 2 days before imaging.

Pharmacological treatments

For long-term growth experiments, seeds were sown on MS plates containing indicated chemicals, including benzoic acid (Sigma, 242381), SA (Sigma, 247588), 3-OH-BA (Sigma, H20008), 4-OH-BA (Sigma, H20059), cantharidin (Sigma, C7632), NPA (Sigma, N12507), and TIBA (Sigma, T5910). After 3-d stratification at 4°C, they were moved to grow in a growth chamber as mentioned in the ''Plant material and growth conditions'' section, for 7 d or 10 d.

For short-term treatment, 4-d-old seedlings were incubated in liquid MS medium containing indicated chemicals for a certain time course as described in the Figure Legends. Detailed information of all chemicals used in this study is listed in Key Resources Table.

Free SA measurement by liquid chromatography-tandem mass spectrometry (LC-MS/MS)

Free SA contents was measured by LC-MS/MS as previously reported [74]. Approximately 10 mg fresh weight (FW) of roots from Col-0, *sid2-3*, and *cpr6* were collected and frozen in liquid nitrogen for LC-MS/MS. SA contents were calculated by the whole amount divided by the fresh weight (pmol/g FW).

Auxin transport in hypocotyls and tobacco BY-2 cells

The basipetal (rootward) transport assay of [^{3}H]-IAA in etiolated hypocotyls was performed according to a previous report [75], with a few modifications. 6-day-old etiolated Col-0 seedlings were placed on MS plates containing indicated chemicals, with 15 seedlings as one biological replicate, and 3 replicates per treatment. The [^{3}H]-IAA (PerkinElmer, ART-0340) droplets were prepared in MS medium with 1.25% agar and 500 μM [^{3}H]-IAA (1.45 μL in 10 mL), supplemented with same concentration of the chemicals as in the respective plate. The seedlings were decapitated and then covered with a [^{3}H]-IAA droplet at the shootward end. After incubation

for 6 hours in the dark, the lower part of the hypocotyls was cut and collected and were then ground completely in liquid nitrogen and homogenized in 1 mL scintillation solution (PerkinElmer, 6013199). The samples were incubated overnight to allow the radioactivity to evenly diffuse into the whole volume of the scintillation cocktail. Finally the radioactivity was measured with a scintillation counter (Hidex 300XL), with each sample counted for 100 s, 3 times. 3 samples with only the scintillation solution were used as background controls.

The transport of [^{3}H]-NAA, [^{3}H]-2,4-D, and [^{3}H]-BA in tobacco BY-2 cells was performed as published previously [32].

Imaging with Confocal Laser Scanning Microscopy (CLSM)

Fluorescence imaging was performed using a Zeiss LSM800 confocal laser scanning microscope (CLSM) with a GaAsP detector (Zeiss, Germany). The manufacturer's default settings (smart mode) were used for imaging GFP (excitation, 488 nm; emission, 495-545 nm)-, and tdTomato (excitation 561 nm; emission, 571-630 nm)-tagged proteins respectively. To image FM4-64-stained cells, a laser line of 543 nm was used for excitation, and an emission light with a wavelength of 600-700 nm was collected. For PI staining, excitation of 561 nm was used and emission signal was collected using a filter of 580- 680 nm. All images were recorded in 8 bit depth, 2 × line averaging. The images were analyzed and visualized with Fiji program [76].

Image analysis and morphological analysis

For root length measurement, photos were taken with a scanner (Epson Perfection V800 Photo) and then the root length was measured with ImageJ. The representative photos were taken by a camera (Sony A600 with a macro lens, 30mm/F3.5).

Molecular cloning

For pET28a-PIN2HL, pET28a-PP2AA1 and pET28a-PP2AA3 constructs, coding regions of *PIN2HL*, *PP2AA1* (primers PP2AA1-1/ PP2AA1-2) and *PP2AA3* (primers PP2AA3-1/ PP2AA3-2) were amplified and subcloned into vector pET28a (Novagen) with EcoRI/ SalI, EcoRI/*Xho*I, and EcoRI/*Xho*I respectively.

All the plasmids were identified by PCR and confirmed by sequencing (LGC). The primers used were listed in Table S1.

PP2A activity assay

The total PP2A activity assay was performed as previously reported with a Ser/Thr protein phosphatase assay kit (Promega, V2460) [48]. Approximately 1g of 7-d-old seedlings were ground in liquid nitrogen. Phosphatase storage buffer (250 mM imidazole, 1 mM EGTA, 0.1% β-mercaptoethanol, and 0.5mg/ml BSA, pH7.2) was added (1/2, volume/weight, hereafter short as v/w) to the frozen tissues and centrifuged to remove cell debris. Endogenous free phosphate was removed with the supplied Sephadex G-25 columns. PP2A phosphatase activity was measured using a molybdate dye-based phosphatase assay kit (Promega, V2460). The reactions were incubated at 37°C for 30 min before being terminated by the molybdate dye and additive mixture. The transparent 96-well plate was read on a Biotek Synergy H1 plate reader at 25°C at 600 nm, with 4 reads per well. The experiment was performed in three independent biological replicates for each treatment.

Protein extraction and immunoblot

To examine the expression level of myc-PP2AA1 in the *35S::myc-PP2AA1* overexpression line, or the phosphorylation level at Tyr307 (Y307) of PP2A C subunits, 100 mg of 7-d-old Col-0 seedlings were frozen in liquid nitrogen, ground totally, and homogenized in plant extraction buffer (20 mM Tris-HCl, pH 7.5, 150 mM NaCl, 0.5% Tween-20, 1 mM EDTA (ethylenediaminetetraacetic acid), 1 mM DTT (1,4-dithiothreitol)) containing a protease inhibitor cocktail (cOmplete, Roche). After addition of an equal volume of 3 × SDS (sodium dodecyl sulfate) loading buffer, the samples were boiled for 5 min, fractionated by 10% SDS-PAGE (sodium dodecyl sulfate-polyacrylamide gel electrophoresis) and transferred to a PVDF membrane by wet blotting. The membrane were incubated with a mouse anti-myc antibody (Millipore) or a mouse pY307-PP2Ac antibody (Millipore) and then with a bovine anti-mouse IgG HRP (horseradish peroxidase)-conjugated secondary antibody (GE Healthcare). HRP activity was detected by the Supersignal Western Detection Reagents (Thermo Scientific) and imaged with a GE Healthcare Amersham 600RGB system.

PIN2 phosphorylation assays

Roots from Col-0 and *pp2aa1-6* were treated with 40 μM SA or DMSO for 15 min, 1 h and 2 h. Untreated roots were also collected at time zero from Col-0, *pp2aa1-6* and *eir1-4* respectively. Protein extraction was performed as previously [41], with modifications for preserving phosphorylation status. The extraction buffer (EB) was: 50 mM Na_2HPO_4 (pH 7.4), 25% w/w sucrose, 7.5% glycerol, 20 mM betaglycerolphosphate, 5 mM Na_2MoO_4, 50 mM NaF, 0.1% casein, 10 mM EDTA (pH 8), 5 mM EGTA (pH 8), 20 mM borate/10 mM Tris-HCl (pH 8.2), 1 mM Na_3VO_4, 10 nM okadaic acid, 1 × PhosStop (Roche). Protease inhibitors (1 mM PMSF (phenylmethanesulfonyl fluoride), 1 mM Pefabloc-SC, 2 μg/mL E64, 0.7 μg/mL pepstatin A, 1 μg/mL aprotinin, and 1 μg/mL leupeptin) and insoluble PVPP (polyvinylpolypyrrolidone) were used. Samples were milled in liquid N_2, extracted with 4 volumes of EB, transferred to PVPP and spun at 500 g (2 min, 4°C). The supernatant was cleared again at 400 g (3 min, 4°C). The supernatant was saved as a total protein fraction, or diluted with 2 volumes of water and spun at 21, 000 g (20 min, 4°C) or 55, 000 g (10 min, 4°C) to obtain a membrane fraction pellet. All samples were solubilized with 0.5% SDS plus 20 mM DTE (Dithioerythritol), and precipitated with chloroform/methanol. Samples (corresponding to 2 or 3 mg original root weight) were denatured by heated only at 50°C to avoid aggregation, and were separated by SDS-PAGE and blotted. Blots were Ponceau stained to confirm loading, probed with rabbit anti-PIN2 [36],

stripped and reprobed with anti-PIN1 [37] or anti-PIP2;1 [65]. HRP activity was detected by the Supersignal Western Detection Reagents (Thermo Scientific) and imaged with Biorad XRS Chemidoc or conventional film.

PIN2-HL phosphorylation assay with [γ-^{32}P]-ATP

The phosphorylation assay of PIN2-HL with [γ-^{32}P]-ATP was performed as previously described [43], with a few modifications. Roots from Col-0 and *pp2aa1-6* (approximately 100 mg) were treated with 40 μM SA or DMSO for 1 h, and harvested for protein extraction. The samples were ground in liquid nitrogen and homogenized in 100 μL protein extraction buffer (20 mM Tris-HCl, pH 7.5, 150 mM NaCl, 0.5% Tween-20, 1 mM DTT, cOmplete protease inhibitor cocktail). 20 μL ($\sim$10 μg) recombinant His-PIN2HL protein was added with 4 μL plant extract, and then the reaction was initiated by adding 10 mM $MgCl_2$ and 2 μL (20 μCi) [γ-^{32}P]-ATP (NEG502A001MC, Perkin-Elmer). After incubation at 25°C for 1h, the reaction was terminated by adding 10 μL SDS loading buffer. The protein samples were separated by SDS-PAGE. The gel was rinsed with deionized H_2O, covered with a thin transparent plastic membrane, and developed with a phosphor plate overnight. The phosphor plate was finally scanned with a Fujifilm FLA 3000 plus DAGE system.

Drug Affinity Responsive Target Stability (DARTS) assay

The DARTS assay to test the binding of SA to PP2AA1-GFP was performed as previously reported [77, 78]. *pPP2AA1::PP2AA1-GFP* seedlings (7d) were used for total protein extraction. After harvesting, the samples were ground in liquid nitrogen, resuspended in protein extraction buffer (25 mM Tris-HCl, pH 7.5; 150 mM NaCl; 0.1% IGEPAL CA-630, Roche cOmplete protease inhibitor cocktail, EDTA free) with a 1:2 (w/v) ratio, and spun down to discard the cell debris. After quantifying the protein concentration (Quick Start Bradford Reagent, Bio-Rad), the cell lysate was aliquoted and incubated with 0, 50 μM or 500 μM SA respectively for 30 min at 25°C, mixing at a low speed. The treated extracts were further aliquoted, and mixed with different concentrations of Pronase (Roche) in Pronase buffer (25 mM Tris-HCl, pH 7.5; 150 mM NaCl). After incubation at 25°C for 30 min, the proteolytic digestion was terminated by adding protease inhibitor cocktail (cOmplete, Roche) and the samples were kept on ice for 10 min. The protein samples were then analyzed by western blot. PP2AA1-GFP was detected by an anti-GFP antibody (JL8, Clontech, 1:2000). HRP activity was detected by the Supersignal Western Detection Reagents (Thermo Scientific) and imaged with a GE Healthcare Amersham 600RGB system.

Recombinant protein expression and purification

Recombinant proteins were expressed in the *E. coli* strain BL21 (DE3) with induction by 0.5 mM IPTG (Isopropyl β-D-1-Thiogalactopyranoside, 16°C, 12 h) and then purified using Ni-NTA His binding resin (Thermo Scientific) according to the manufacturer's manual. The eluted samples were then purified with size exclusion chromatography, with a Superdex 200 increase column, on an ÄKTA pure chromatography system (GE Healthcare). Fractions were collected by 500 μL, and then analyzed by SDS-PAGE, followed by Coomassie brilliant blue (CBB, Bio-Safe Coomassie Stain #1610786 from BioRad) staining to check the protein quality.

Differential Scanning Calorimetry (DSC) analysis

The DSC analysis was performed with a MicroCal PEAQ-DSC Automated instrument (Malvern Panalytical). 5 μM PP2AA1 in 1 × PBS, with or without 50 μM SA, were heated from 25°C to 85°C at a heating rate of 1°C /min, cooled *in situ* and heated again under the same conditions. Data was obtained and analyzed with the provided program.

Chemical synthesis of SA derivatives

General information

All starting materials were used as received from commercial sources (Sigma-Aldrich, Merck, and Lach-Ner) without further purification. 2-(6-bromohexyl)isoindoline-1,3-dione was prepared using published procedure. THF [79] was distilled under argon from sodium benzophenone ketyl. All reactions were performed in round-bottom flasks fitted with rubber septa using the standard laboratory techniques. Reactions sensitive to air and/or moisture were performed under a positive pressure of argon. Analytical thin-layer chromatography (TLC) was performed using aluminum plates pre-coated with silica gel (silica gel 60 F^{254}). TLC plates were visualized by exposure to ultraviolet light and then were stained by submersion in basic potassium permanganate solution or in ethanolic phosphomolybdic acid solution followed by brief heating. Column chromatography was performed on silica gel 60 (40-63 μm). Melting points (mp) were tested on a capillary melting point apparatus. ^{1}H NMR and ^{13}C NMR spectra were recorded on 500 and 125 MHz in $CDCl_3$, CD_3OD, acetone-d_6 and DMSO-d_6; chemical shifts (δ ppm) and coupling constants (Hz) of ^{1}H NMR are reported in a standard fashion with relative to the remaining $CHCl_3$ present in $CDCl_3$ (δH = 7.27 ppm), central line of pentet in CHD_2OD present in CD_3OD (δH = 3.31 ppm), central line of pentet in $CHD_2C(O)CD_3$ present in acetone-d_6 (δH = 2.05 ppm), and central line of pentet in CHD_2SOCD_3 present in DMSO-d_6 (δH = 2.50 ppm). ^{13}C NMR chemical shifts (δ ppm) are reported relative to $CDCl_3$ (δC = 77.23 ppm, central line of triplet), CD_3OD (δC = 49.0 ppm, central line of heptet), $CD_3C(O)CD_3$ (δC = 29.84 ppm, central line of heptet), and DMSO-d_6 (δC = 39.52 ppm, central line of heptet). Proton coupling patterns are represented as singlet (s), doublet (d), doublet of doublet (dd), triplet (t), triplet of triplet (tt), pentet (p), and multiplet (m). HRMS data were obtained using quadrupole/ion trap mass analyzer. Analysis and assignments were made by comparison with literature spectroscopic data or using 2D-COSY, HSQC, HMBC, 2D-NOESY and 1D-NOEdiff experiments. Purity of final compounds was determined using the following protocol: Compound (1 mg) was dissolved in 1 mL of 1% methanol and injected (10 μL) onto a reverse-phased column (Symmetry C18, 5 μm, 150 mm × 2.1 mm; Waters, Milford, MA, USA) incubated at 25°C. Solvent (A) consisted of 15 mM ammonium formate adjusted to pH 4.0. Solvent (B) consisted of

methanol. At flow-rate of 200 μL/min, following binary gradient was used: 0 min, 10% B; 0-24 min. linear gradient to 90% B; 25-34 min. isocratic elution of 90% B; 35-45 min. linear gradient to 10% B. The effluent was introduced then to PDA detector (scanning range 210-700 nm with 1.2 nm resolution) and an electrospray source (source temperature 120°C, desolvation temperature 300°C, capillary voltage 3 kV, cone voltage 20 V). Nitrogen was used as well as cone gas (50 L/h) and desolvation gas (500 L/h). Data acquisition was performed in the full scan mode (50-1000 Da), scan time of 0.5 s. and collision energy of 6 V. Analyses were performed in positive mode (ESI^+) or in negative mode (ESI^-), therefore data were collected as quasi-molecular ions of $[M+H]^+$ and $[M-H]^-$, respectively.

C-10 (5-(allyloxy)-2-hydroxybenzoic acid)

Successively, K_2CO_3 (1.23 g, 8.93 mmol, 1.5 equiv) and allyl bromide (0.643 mL, 7.4 mmol, 1.25 equiv) were added to a solution of methyl 2,5-dihydroxybenzoate (1.0 g, 6.0 mmol, 1.0 equiv) in dry acetone (60 mL) and the resulting mixture was heated up to 60°C. After 5h at 60°C, the reaction mixture was cooled to 25°C (room temperature) and diluted with H_2O (50 mL). The whole mixture was extracted with CH_2Cl_2 (3 × 75 mL). Organic layers were combined and washed with brine (50 mL), dried over $MgSO_4$, filtered and volatiles were removed under reduced pressure. The residue was purified by flash column chromatography (SiO_2; hexane:EtOAc = 20:1 - > 10:1) and yielded 5-O-allylated ester (0.719 g, 58%). ^1H NMR (500 MHz, $CDCl_3$) δ (ppm): 3.95 (s, 3H), 4.52 (dt, *J* = 5.2, 1.8 Hz, 2H), 5.32 (dd, *J* = 10.5, 1.6 Hz, 1H), 5.43 (dd, *J* = 17.2, 1.7 Hz, 1H), 6.06 (ddt, *J* = 17.6, 10.5, 5.3 Hz, 1H), 6.92 (d, *J* = 9.2 Hz, 1H), 7.11 (dd, *J* = 9.2, 3.2 Hz, 1H), 7.32 (d, *J* = 3.2 Hz, 1H), 10.39 (s, 1H); 13C NMR (126 MHz, $CDCl_3$) δ (ppm): 52.3, 69.5, 111.7, 113.1, 117.8, 118.4, 124.6, 133.1, 150.8, 156.1, 170.2; MS (ESI^+), *m/z* (%): 209 $[M+H]^+$ (100); HRMS (ESI^+) *calcd.* for $C_{11}H_{13}O_4$ $[M+H]^+$: 209.0808, found 209.0808. 5-O-allylated ester (0.5 g, 2.4 mmol, 1.0 equiv) was dissolved in dry THF (24 mL) at 25°C. Potassium trimethylsilanolate (TMSOK, 0.924 g, 7.2 mmol, 3.0 equiv) was added and the resulting mixture was stirred at 25°C for 24 h. After this period of time, pH of the reaction mixture was adjusted to 2 with help of 10% aq. HCl. Organic solvents were removed under reduced pressure and additional H_2O (20 mL) was added. The whole mixture was extracted with CH_2Cl_2 (2 × 50 mL) and combined organic layers were washed with brine (30 mL), dried over $MgSO_4$ and evaporated to dryness under reduced pressure. The residue was purified by column chromatography (SiO_2; hexan:EtOAc:AcOH = 2:1:0.1 - > 1:1:0.1) to yield the desired compound C-10 (364 mg, 78%). ^1H NMR (500 MHz, $CDCl_3$) δ (ppm): 4.53 (dt, *J* = 5.3, 1.7 Hz, 2H), 5.32 (dd, *J* = 10.6, 1.5 Hz, 1H), 5.43 (dd, *J* = 17.4, 1.6 Hz, 1H), 6.06 (ddt, *J* = 17.5, 10.6, 5.4 Hz, 1H), 6.96 (d, *J* = 9.2 Hz, 1H), 7.19 (dd, *J* = 9.0, 3.1 Hz, 1H), 7.39 (d, *J* = 3.3 Hz, 1H), 10.03 (s, 1H); ^{13}C NMR (126 MHz, $CDCl_3$) δ (ppm): 69.8, 110.9, 113.8, 118.2, 119.1, 126.6, 133.2, 151.4, 157.1, 174.7; MS (ESI^+), *m/z* (%): 195 $[M+H]^+$; HRMS (ESI^+) *calcd.* for $C_{10}H_{11}O_4$ $[M+H]^+$: 195.0652, found 195.0651.

SA-1 (5-((6-aminohexyl)oxy)-2-hydroxybenzaldehyde hydrochlorid)

SA-3 (0.4 g, 1.09 mmol, 1.0 equiv) was dissolved in THF/H_2O = 2:1 (9.0 mL) and the resulting solution was cooled to 0°C. A solution of $HSO_3(NH_2)$ (0.211 g, 2.2 mmol, 2.0 equiv) in H_2O (2.2 mL) followed by $NaClO_2$ (0.108 g, 1.2 mmol, 1.1 equiv) in H_2O (1.2 mL) was added, and the resulting mixture was stirred at 0°C for 2 h. H_2O (20 mL) was added and the resulting solution was extracted with CH_2Cl_2 (3 × 50 mL). Organic layers were combined and washed with brine (25 mL), dried over Na_2SO_4, filtered and volatiles were removed under reduced pressure to yield carboxylic acid (0.343 g, 82%) sufficiently pure to be used in the next step. ^1H NMR (500 MHz, acetone-d_6) δ (ppm): 1.37 – 1.50 (m, 2H), 1.49 – 1.60 (m, 2H), 1.67 – 1.75 (m, 2H), 1.81 – 1.92 (m, 2H), 3.66 (t, J = 7.1 Hz, 2H), 4.20 (t, *J* = 6.6 Hz, 2H), 7.04 (dd, *J* = 8.9, 3.1 Hz, 1H), 7.11 (d, *J* = 9.0 Hz, 1H), 7.42 (d, *J* = 3.1 Hz, 1H), 7.92 (dd, *J* = 6.0, 3.3 Hz, 2H), 8.20 (dd, *J* = 6.0, 3.3 Hz, 2H); MS (ESI^+), *m/z* (%): 384 $[M+H]^+$; HRMS (ESI^+) *calcd.* for $C_{21}H_{21}NO_6Na$ $[M+Na]^+$: 406.1261, found 406.1262. Carboxylic acid (0.300 g, 0.78 mmol, 1.0 equiv) was dissolved in EtOH (8 mL) and hydrazine hydrate (0.076 mL, 1.56 mmol, 2.0 equiv) was added. The resulting mixture was stirred at 60°C for 6 h. White precipitate formed upon heating was filtered off and the filtrate was concentrated under reduced pressure to yield viscose oil. EtOH (10 mL) and H_2O (10 mL) were added and the pH was adjusted to 2 with help of 2.0 M aq. HCl. Concentration of the resulting mixture under reduced pressure and subsequent co-evaporation of the residue with EtOH (2 × 10 mL) and toluene (2 × 15 mL) yielded desired compound SA-1 (0.052 g, 27%). Mp: > 190°C (dec.); ^1H NMR (500 MHz, CD_3OD) δ (ppm): 1.44 – 1.51 (m, 2H), 1.51 – 1.62 (m, 2H), 1.65 – 1.75 (m, 2H), 1.82 (ddt, *J* = 14.2, 7.9, 4.2 Hz, 2H), 2.94 (t, *J* = 7.6 Hz, 3H), 4.07 (t, *J* = 6.3 Hz, 2H), 6.96 (dd, *J* = 8.9, 3.0 Hz, 1H), 7.00 (d, *J* = 8.9 Hz, 1H), 7.24 (d, *J* = 3.0 Hz, 1H); ^{13}C NMR (126 MHz, CD_3OD) δ (ppm): 26.6, 27.1, 28.5, 30.1, 40.7, 70.8, 116.9, 118.1, 121.3, 122.3, 152.1, 157.8, 168.5; MS (ESI^+), *m/z* (%): 254 $[M-Cl]^+$; HRMS (ESI^+) *calcd.* for $C_{13}H_{20}NO_4$ $[M-Cl]^+$: 254.1387, found 254.1388.

SA-2 (5-((5-(1,3-dioxoisoindolin-2-yl)pentyl)oxy)-2-hydroxybenzaldehyde)

2,5-dihydroxybenzaldehyde (0.5 g, 3.62 mmol, 1.0 equiv) was dissolved in dry DMF (36 mL) and K_2CO_3 (0.6 g, 4.3 mmol, 1.2 equiv) and 2-(6-bromohexyl)isoindoline-1,3-dione (1.07 g, 3.62 mmol, 1.0 equiv) were added. The resulting mixture was heated at 70°C for 4 h. All volatiles were removed under reduced pressure and the residue was dissolved in H_2O (50 mL). The whole mixture was extracted with EtOAc (3 × 50 mL) and combined organic layers were washed with brine (25 mL), dried over Na_2SO_4, filtered and evaporated to dryness. The residue was purified by flash column chromatography (SiO_2; hexane:EtOAc = 4:1- > 2:1) to yield SA-2 (0.627 g, 49%) as a yellowish viscose oil. ^1H NMR (500 MHz, $CDCl_3$) δ(ppm): 1.48 – 1.60 (m, 2H), 1.77 (p, *J* = 7.3 Hz, 2H), 1.82 – 1.93 (m, 2H), 3.73 (dd, *J* = 7.8, 6.5 Hz, 2H), 4.01 (t, *J* = 6.3 Hz, 2H), 6.85 (d, *J* = 9.0 Hz, 1H), 7.08 (dd, *J* = 8.9, 3.2 Hz, 1H), 7.28 (d, *J* = 3.1 Hz, 1H), 7.72 (dd, *J* = 5.5, 3.1 Hz, 2H), 7.85 (dd, *J* = 5.5, 3.1 Hz, 2H), 10.40 (s, 1H); ^{13}C NMR (126 MHz, $CDCl_3$) δ (ppm): 23.5, 28.4, 28.9, 37.9, 68.9, 113.5, 114.4, 123.4, 123.7, 125.4, 132.2, 134.2, 150.8, 155.8, 168.7, 189.9; MS (ESI^+), *m/z* (%): 354 $[M+H]^+$; HRMS (ESI^+) *calcd.* for $C_{20}H_{20}NO_5$ $[M+H]^+$: 354.1336, found 354.1335.

SA-3 (5-((6-(1,3-dioxoisoindolin-2-yl)hexyl)oxy)-2-hydroxybenzaldehyde)

Using the same procedure as for SA-2 synthesis. The residue was purified by flash column chromatography (SiO_2; hexane:EtOAc = 4:1- > 2:1) to yield SA-3 (1.04 g, 78%) as a white solid. Mp = 148-149°C; ^1H NMR (500 MHz, $CDCl_3$) δ (ppm): 1.41 (dd, *J* = 15.3, 7.9 Hz,

2H), 1.46 – 1.56 (m, 2H), 1.70 (dt, *J* = 15.0, 7.6 Hz, 2H), 1.74 – 1.84 (m, 2H), 3.69 (t, *J* = 7.3 Hz, 2H), 3.98 (t, *J* = 6.4 Hz, 2H), 6.83 (d, *J* = 9.2 Hz, 1H), 7.07 (dd, *J* = 8.9, 3.1 Hz, 1H), 7.28 (d, *J* = 3.3 Hz, 1H), 7.70 (dd, *J* = 5.3, 2.9 Hz, 2H), 7.82 (dd, *J* = 5.3, 2.9 Hz, 2H), 7.90 (s, 1H), 10.40 (s, 1H); ^{13}C NMR (126 MHz, $CDCl_3$) δ (ppm): 25.8, 26.7, 28.6, 29.2, 38.0, 69.1, 113.4, 114.4, 123.4, 123.7, 125.4, 132.2, 134.1, 150.9, 155.7, 168.7, 190.0; MS (ESI^+), *m/z* (%): 368 $[M+H]^+$; HRMS (ESI^+) *calcd.* for $C_{21}H_{22}NO_5$ $[M+H]^+$: 368.1492, found 368.1492.

SA-f (5-((5-aminopentyl)oxy)-2-hydroxybenzoic acid)

Methyl 2,5-dihydroxybenzoate (4.1 g, 24.4 mmol, 1.0 equiv) was dissolved in acetone/H_2O = 3.3:1 (190 mL) and K_2CO_3 (13.48 g, 98 mmol, 4 equiv) followed by 1,5-dibromopentane (10.0 mL, 73.4 mmol, 3.0 equiv) were added. The resulting mixture was refluxed for 4h, allowed to cool to 25°C and volatiles were removed under reduced pressure. Residue was extracted with CH_2Cl_2 (540 mL) and the organic layer was washed with H_2O (220 mL), brine (150 mL), dried over $MgSO_4$, filtered and evaporated to dryness yielding crude methyl 5-((5-bromopentyl)oxy)-2-hydroxybenzoate (16.5 g) as a brown oil. Crude ester was dissolved in acetone/H_2O = 3.3:1 (190 mL) and NaN_3 (7.9 g, 121.8 mmol, 5.0 equiv) was added. The resulting mixture was refluxed for 24 h before being allowed to cool to 25°C. Volatile solvents were removed under reduced pressure and the resulting mixture was extracted with CH_2Cl_2 (500 mL). Organic layer was washed with H_2O (150 mL), brine (100 mL), dried over $MgSO_4$, filtered and evaporated under reduced pressure. Resulting crude product was purified by flash column chromatography (SiO_2; hexan:EtOAc = 20:1- > 10:1) and yielded the desired methyl 5-((5-azidopentyl)oxy)-2-hydroxybenzoate (6.8 g, 99%) as a colorless oil. ^{1}H NMR (500 MHz, $CDCl_3$) δ (ppm): 1.40 – 1.53 (m, 2H), 1.60 – 1.67 (m, 2H), 1.81 (dt, *J* = 14.6, 6.5 Hz, 2H), 3.30 (t, *J* = 6.8 Hz, 2H), 3.93 (t, *J* = 6.3 Hz, 2H), 3.96 (s, 3H), 6.92 (d, *J* = 9.0 Hz, 1H), 7.08 (dd, *J* = 9.0, 3.1 Hz, 1H), 7.29 (d, *J* = 3.1 Hz, 1H), 10.37 (s, 1H); ^{13}C NMR (126 MHz, $CDCl_3$) δ (ppm): 23.6, 28.8, 29.0, 51.5, 52.5, 68.5, 112.1, 113.0, 118.7, 124.7, 151.6, 156.2, 170.5; MS (ESI^+), *m/z* (%): 280 $[M+H]^+$; HRMS (ESI^+) *calcd.* for $C_{13}H_{18}N_3O_4$ $[M+H]^+$: 280.1292, found 280.1291. Azide (6.79 g, 24.4 mmol, 1.0 equiv) was dissolved in dry THF (234 mL) and TMSOK (10.4 g, 73.2 mmol, 3 equiv; 90% purity) was added. The resulting mixture was stirred at 25°C for 24 h, cooled to 0°C and the pH of the mixture was adjusted to pH = 2 by 10% aq. HCl. The volume of the resulting mixture was in vacuo reduced to ½ of its original volume, and H_2O (100 mL) was added. The whole mixture was extracted with CH_2Cl_2 (2 × 400 mL) and combined organic layers were washed with H_2O (120 mL), brine (180 mL), dried over $MgSO_4$, and organic solvents were removed under reduced pressure. Crude product was dissolved in CH_2Cl_2 (20 mL) and hexane (60 mL) was added. Two third of the resulting solvent mixture were removed under reduced pressure and the desired 5-((5-azidopentyl)oxy)-2-hydroxybenzoic acid crystalized off the solution upon prolonged standing (24 h) at 25°C in form of white needles (5.89 g, 91%). Mp = 81-82.5°C; ^{1}H NMR (500 MHz, $CDCl_3$) δ (ppm): 1.53 – 1.63 (m, 2H), 1.64 – 1.75 (m, 2H), 1.82 (dq, *J* = 8.0, 6.3 Hz, 2H), 3.33 (t, *J* = 6.9 Hz, 2H), 3.95 (t, *J* = 6.3 Hz, 2H), 6.95 (d, *J* = 9.1 Hz, 1H), 7.15 (dd, *J* = 9.1, 3.1 Hz, 1H), 7.35 (d, *J* = 3.1 Hz, 1H), 10.08 (s, 1H); ^{13}C NMR (126 MHz, $CDCl_3$) δ (ppm): 23.6, 28.9, 29.0, 51.6, 68.6, 110.9, 113.3, 119.0, 126.2, 151.8, 157.0, 173.6; MS (ESI^-), *m/z* (%): 264 $[M-H]^-$; HRMS (ESI^+) *calcd.* for $C_{12}H_{15}N_3O_4Na$ $[M+Na]^+$: 288.0955, found 288.0956. 5-((5-azidopentyl)oxy)-2-hydroxybenzoic acid (0.75 g, 2.83 mmol, 1.0 equiv) was dissolved in EtOAc (14 mL) and 10% of palladium on carbon (3.8 mg, 0.05 equiv) was added. The whole mixture was placed under the hydrogen atmosphere (1.0 atm) and stirred for 24h. The whole mixture was filtered through microfilter (0.5 μm) and the filter was washed with MeOH (2 × 15 mL). Combined filtrates were evaporated under reduced pressure to give 5-((5-aminopentyl)oxy)-2-hydroxybenzoic acid SA-f (0.664 g, 98%) as a viscose oil. ^{1}H NMR (500 MHz, DMSO-d_6) δ (ppm): 1.42 (p, *J* = 7.7 Hz, 2H), 1.57 (p, *J* = 7.6 Hz, 2H), 1.64 (p, *J* = 7.3, 6.8 Hz, 2H), 2.78 (t, *J* = 7.4 Hz, 2H), 3.80 (t, *J* = 6.2 Hz, 2H), 6.69 (d, *J* = 8.8 Hz, 1H), 6.86 (dd, *J* = 8.8, 3.1 Hz, 1H), 7.36 (d, *J* = 3.2 Hz, 1H); ^{13}C NMR (126 MHz, DMSO-d_6) δ (ppm): 22.6, 26.8, 28.3, 38.8, 67.7, 114.4, 116.3, 119.5, 120.2, 149.4, 156.4, 171.5; MS (ESI^-), *m/z* (%): 238 $[M-H]^-$; HRMS (ESI^+) *calcd.* for $C_{12}H_{15}N_3O_4Na$ $[M+Na]^+$: 262.1050, found 262.1050. Purity 98+% (LC-MS), R_t = 11.93 min.

SPR analysis

SPR analysis of SA binding to His-PP2AA1 or His-PP2AA3 was performed with a Biacore T200 instrument (GE Healthcare). A synthesized active SA analog, SA-f, was immobilized on a CM5 sensor chip (GE Healthcare) first: the carboxyl group of the CM5 sensor chip was activated using a mixture of 1-ethyl-3-(3-dimethyl aminopropyl) carbodiimide hydrochloride (EDC) and N-hydroxy-succinimide (NHS) for 7 min at a flow rate of 5 μL/min. After activation, 1 mM of SA-f dissolved in 0.1 M borate buffer (pH 10) was passed over for a period of 3 min at 5 μL/min for immobilization. Then excess reactive groups were inactivated by flowing ethanolamine hydrochloride-NaOH pH 8.5 for 7 min, at 5 μL/min. 1 × PBS buffer (GE Healthcare) was used as running buffer in all assays. To test SA binding of His-PP2AA1 or His-PP2AA3, proteins were diluted in 1 × PBS buffer, and then flowed through the flow cell of sensor chip with SA-f immobilized or through the reference cell. The binding signal was generated by subtracting the signal of reference cell from that generated with the SA-f flow cell. The flow cells were regenerated with flowing 250 mM NaOH solution. Details about the chemical synthesis of SA derivatives are described in the Supplemental Information.

Accession Numbers

Sequence data from this article can be found in the *Arabidopsis* Genome Initiative or GenBank/EMBL databases under the following accession numbers: PIN1 (AT1G73590), PIN2 (AT5G57090), NPR1 (AT1G64280), NPR2 (AT4G26120), NPR3 (AT5G45110), NPR4 (AT4G19660), PINOID (AT2G34650), PP2AA1 (AT1G25490), PP2AA2 (AT3G25800), PP2AA3 (AT1G13320), PP2AC3 (AT3G58500), and PP2AC4 (AT2G42500).

QUANTIFICATION AND STATISTICAL ANALYSIS

For measurement of primary root length and root tip angles, photos were analyzed with ImageJ (https://imagej.nih.gov/ij/download.html). Fluorescence intensity of marker lines were quantified by Fiji (https://fiji.sc/).

Most data plotting and statistics were performed with Graphpad Prism8. A two-tailed t test was used for comparing two datasets. One-way ANOVA with a Tukey multiple comparison test was performed to evaluate the differences of multiple datasets. For root gravitropic responses, polar bar charts were generated by Origin 8.0, and both two-tailed t test and F-test were used to evaluate the mean value and variances respectively.

DATA AND CODE AVAILABILITY

This study did not generate/analyze datasets/code.

Current Biology, Volume *30*

Supplemental Information

Salicylic Acid Targets Protein Phosphatase 2A to Attenuate Growth in Plants

Shutang Tan, Melinda Abas, Inge Verstraeten, Matouš Glanc, Gergely Molnár, Jakub Hajný, Pavel Lasák, Ivan Petřík, Eugenia Russinova, Jan Petrášek, Ondřej Novák, Jiří Pospíšil, and Jiří Friml

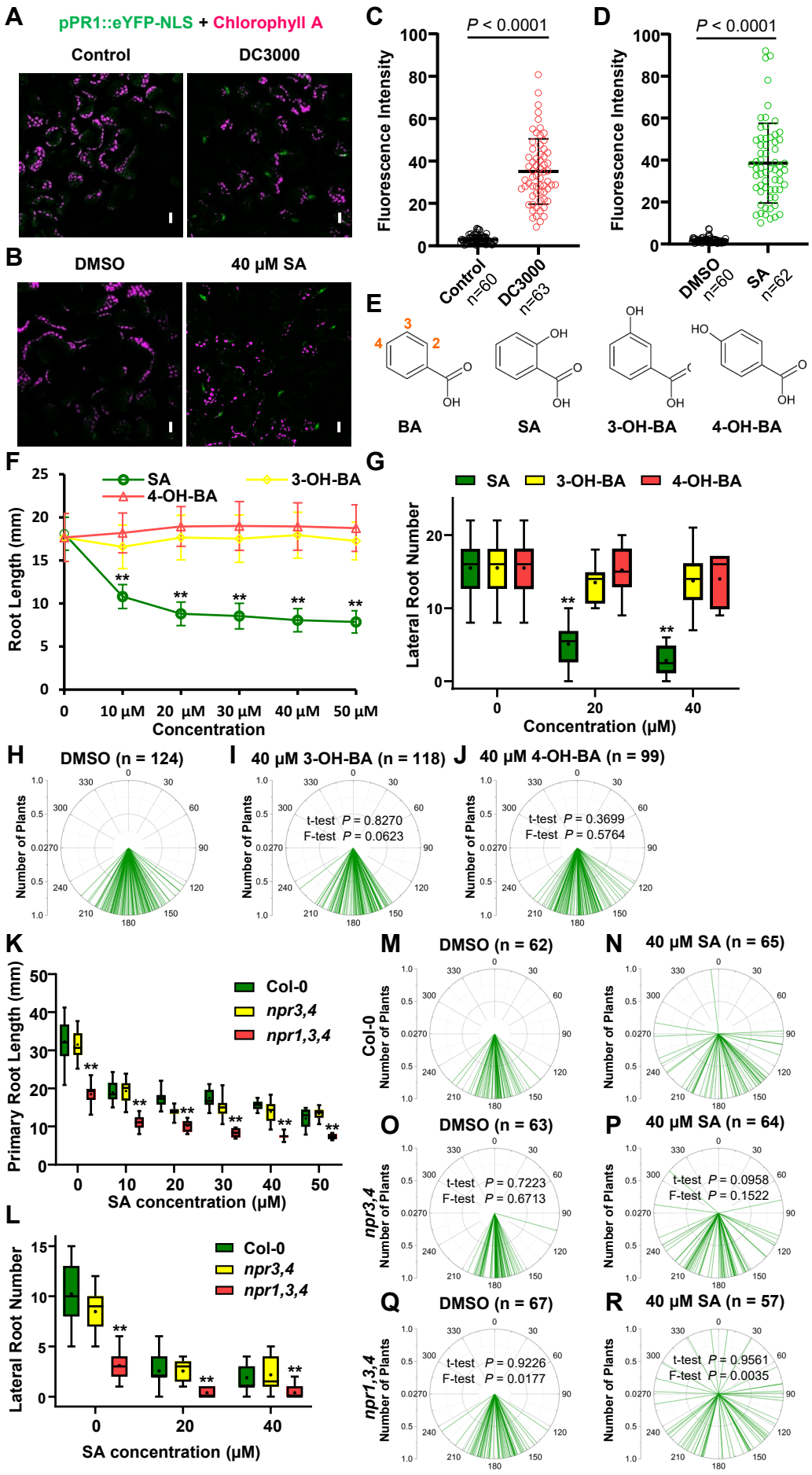
A
pPR1::eYFP-NLS + Chlorophyll A
Control
DC3000
B
DMSO
40 μM SA
C
P < 0.0001
Fluorescence Intensity
Control n=60
DC3000 n=63
D
P < 0.0001
Fluorescence Intensity
DMSO n=60
SA n=62
E
BA
SA
3-OH-BA
4-OH-BA
F
SA
4-OH-BA
3-OH-BA
Root Length (mm)
0 10 μM 20 μM 30 μM 40 μM 50 μM
Concentration
G
SA
3-OH-BA
4-OH-BA
Lateral Root Number
Concentration (μM)
H
DMSO (n = 124)
I
40 μM 3-OH-BA (n = 118)
t-test P = 0.8270
F-test P = 0.0623
J
40 μM 4-OH-BA (n = 99)
t-test P = 0.3699
F-test P = 0.5764
Number of Plants
K
Col-0
npr3,4
npr1,3,4
Primary Root Length (mm)
SA concentration (μM)
L
Col-0
npr3,4
npr1,3,4
Lateral Root Number
SA concentration (μM)
M
DMSO (n = 62)
N
40 μM SA (n = 65)
O
DMSO (n = 63)
t-test P = 0.7223
F-test P = 0.6713
P
40 μM SA (n = 64)
t-test P = 0.0958
F-test P = 0.1522
Q
DMSO (n = 67)
t-test P = 0.9226
F-test P = 0.0177
R
40 μM SA (n = 57)
t-test P = 0.9561
F-test P = 0.0035
Col-0
npr3,4
npr1,3,4
Number of Plants

Figure S1. Structural isomers and the specific role of SA in the root growth regulation. Related to Figures 1 & 2.

(A-D) Induced *pPR1::eYFP-NLS* expression by *P. syringae* DC3000 (A, C) or SA (B, D) in cotyledons. (A, C) 5-d-old *pPR1::eYFP-NLS* seedlings were treated with *P. syringae* DC3000 (OD_{600} = 0.01, ~5×10^6 CFU/mL) or with resuspension buffer (control) for 48 h, and were then imaged by CLSM. Scale bars, 10 μm. (B, D) Induced *pPR1::eYFP-NLS* expression by SA in cotyledons. 5-d-old *pPR1::eYFP-NLS* seedlings were transferred to plates with DMSO or 40 μM SA for 24h, and were then imaged by CLSM. Scale bars, 10 μm. For quantification, the average GFP fluorescence of 5-10 representative cells from 10 seedlings for each treatment was measured by Fiji. The data points were shown as dot plots. Dots represent individual values, and lines indicate mean ± SD. *P* values were calculated by a two-tailed t-test.

(E) Structures of benzoic acid analogues, including benzoic acid (BA), 2-hydroxybenzoic acid (also known as ortho-salicylic acid, SA), 3-hydroxybenzoic acid (3-OH-BA, also known as meta-salicylic acid), and 4-hydroxybenzoic acid (4-OH-BA, also known as para-salicylic acid). Chemical structures were illustrated with the ChemSketch program.

(F) 3-OH-BA and 4-OH-BA do not inhibit primary root elongation. Root length of 7-d-old Col-0 seedlings grown on MS plates containing different concentrations of SA, 3-OH-BA or 4-OH-BA was measured. Note that the same DMSO control was used for all the indicated chemicals. n = 100-129. **, $P < 0.01$, by a two-tailed t-test.

(G) 3-OH-BA and 4-OH-BA do not repress lateral root formation. The lateral root number of 10-d-old plants was counted. The same DMSO control was used for all the indicated chemicals. n = 10-22. **, $P < 0.01$, by a two-tailed t-test.

(H-J) 3-OH-BA and 4-OH-BA do not have a significant effect on root gravitropism. The root tip angles of 7-d-old Col-0 seedlings on different plates were measured. *P* values were calculated by a two-tailed t-test to evaluate the mean value and by a further F-test to indicate differences of variances.

(K) SA inhibited primary root elongation, which was not suppressed by NPR deficiency. Root length of 7-d-old Col-0, *npr3,4* and *npr1,3,4* seedlings grown on MS plates containing different concentrations of SA was measured. n = 10-26. **, $P < 0.01$. *P* values were calculated by one-way ANOVA with a Tukey multiple comparison test, compared to Col-0 in each treatment.

(L) Inhibition of lateral root formation by SA does not depend on *NPRs*. The lateral root number of 10-d-old Col-0, *npr3,4* and *npr1,3,4* plants was counted. n = 9-24. **, $P < 0.01$. *P* values were calculated by one-way ANOVA with a Tukey multiple comparison test, compared to Col-0.

(M-R) SA repressed root gravitropism independently of *NPRs*. The angles of root tips of 7-d-old Col-0 (M, N), *npr3,4* (O, P) and *npr1,3,4* (Q, R) seedlings were measured. *P* values were calculated by a two-tailed t-test to evaluate the mean value and by a further F-test to indicate differences of variances.

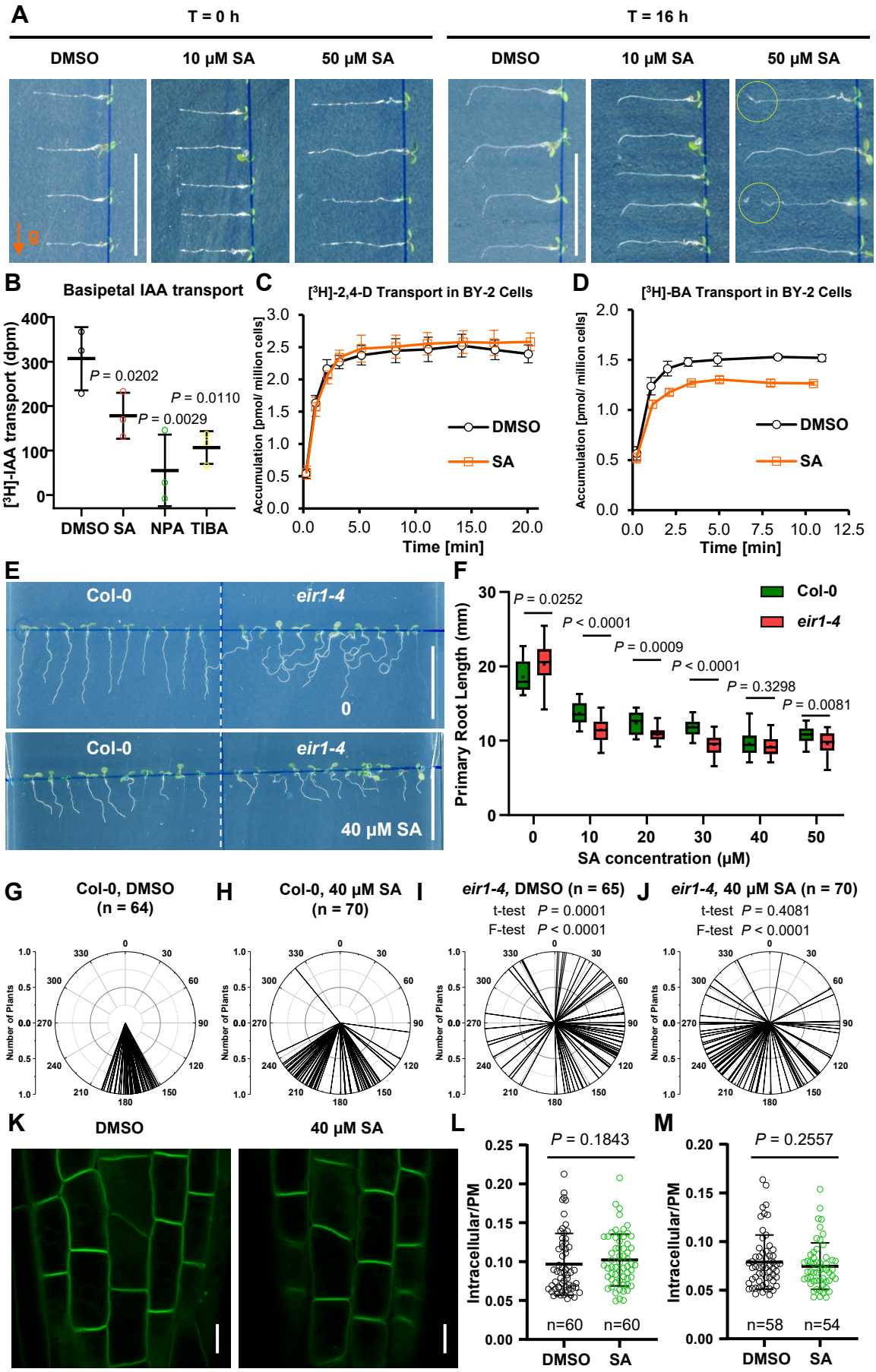
A
T = 0 h
T = 16 h
DMSO
10 µM SA
50 µM SA
DMSO
10 µM SA
50 µM SA
g
B
Basipetal IAA transport
[3H]-IAA transport (dpm)
P = 0.0202
P = 0.0110
P = 0.0029
DMSO SA
NPA
TIBA
C
[3H]-2,4-D Transport in BY-2 Cells
Accumulation [pmol/ million cells]
Time [min]
DMSO
SA
D
[3H]-BA Transport in BY-2 Cells
Accumulation [pmol/ million cells]
Time [min]
DMSO
SA
E
Col-0
eir1-4
0
Col-0
eir1-4
40 µM SA
F
Col-0
eir1-4
Primary Root Length (mm)
P = 0.0252
P < 0.0001
P = 0.0009
P < 0.0001
P = 0.3298
P = 0.0081
SA concentration (µM)
G
Col-0, DMSO
(n = 64)
H
Col-0, 40 µM SA
(n = 70)
I
eir1-4, DMSO (n = 65)
t-test P = 0.0001
F-test P < 0.0001
J
eir1-4, 40 µM SA (n = 70)
t-test P = 0.4081
F-test P < 0.0001
Number of Plants
K
DMSO
40 µM SA
L
P = 0.1843
Intracellular/PM
n=60
n=60
DMSO
SA
M
P = 0.2557
Intracellular/PM
n=58
n=54
DMSO
SA

Figure S2. Specific SA action on root gravitropic response and auxin export, in a PIN-dependent manner. Related to Figure 3.

(A) Representative images showing the gravitropic response of WT seedlings on different concentrations of SA. 5-d-old seedlings were transferred to indicated plates, and grown for additional 16 h. DMSO as the solvent control. Agravitropic roots are marked. Scale bars, 2 cm.

(B) SA inhibited the basipetal transport of [^{3}H]-IAA in etiolated hypocotyls. DMSO, 10 μM NPA, 10 μM TIBA, and 500 μM SA were added to both the [^{3}H]-IAA droplets and the medium. 15 seedlings were pooled as a biological replicate; n = 3. Dots represent individual values, and lines indicate mean ± SD. *P* values were calculated by one-way ANOVA with a Tukey multiple comparison test, compared to DMSO.

(C-D) SA has no effect on the accumulation of [^{3}H]-2,4-D (C) or [^{3}H]-BA (D) in tobacco BY-2 cells, suggesting no effect on export, as controls for [^{3}H]-IAA. DMSO (the solvent control) and 200 μM SA were added to the cell culture, and then the radioactivity of ^{3}H was measured at indicated timepoints after the addition of [^{3}H]-2,4-D (C) or [^{3}H]-BA (D) to the DMSO- and SA-treated cell cultures. n = 3.

(E) Representative images show the sensitivity of *eir1-4* to SA. Col-0 and *eir1-4* seedlings were grown on plates with different concentrations of SA for 7 d. Scale bars, 2 cm.

(F) *eir1-4* shows slightly increased sensitivity to SA in root growth inhibition. Col-0 and *eir1-4* seedlings were grown on plates with concentrations of SA for 7 d, and the primary root length was measured. n = 16-23; *P* values were calculated by a two-tailed t-test for indicated pairs of Col-0 and *eir1-4* at a certain concentration of SA.

(G-J) *eir1-4* showed agravitropic roots, which were not further enhanced by SA treatment. Col-0 and *eir1-4* seedlings were grown on plates with different concentrations of SA for 7 d, and the root tip angles were measured by Image J, and shown by polar bar charts. *P* values were calculated by a two-tailed t-test to evaluate the mean value and by a further F-test to indicate differences of variances. The *eir1-4* groups were compared with Col-0 under treatment with the same concentration of SA respectively.

(K) The localization of AUX1-YFP. Plants were grown for 4 d on DMSO or 40 μM SA. Scale bars, 10 μm.

(L-M) Quantification of AUX1-YFP subcellular distribution revealed by its intracellular/PM fluorescence ratio. The average AUX1-YFP fluorescence of the intracellular area and PM of 5-10 representative cells from 10 seedlings for each treatment was measured by Fiji. The data points were shown as dot-plots. Dots represent individual values, and lines indicate mean ± s.d.. *P* values were calculated by a two-tailed t-test. (L) 4-d-old seedling grown on plates with 40 μM SA are shown in (K); (M) 4-d-old seedling were treated with 40 μM SA for 12 h.

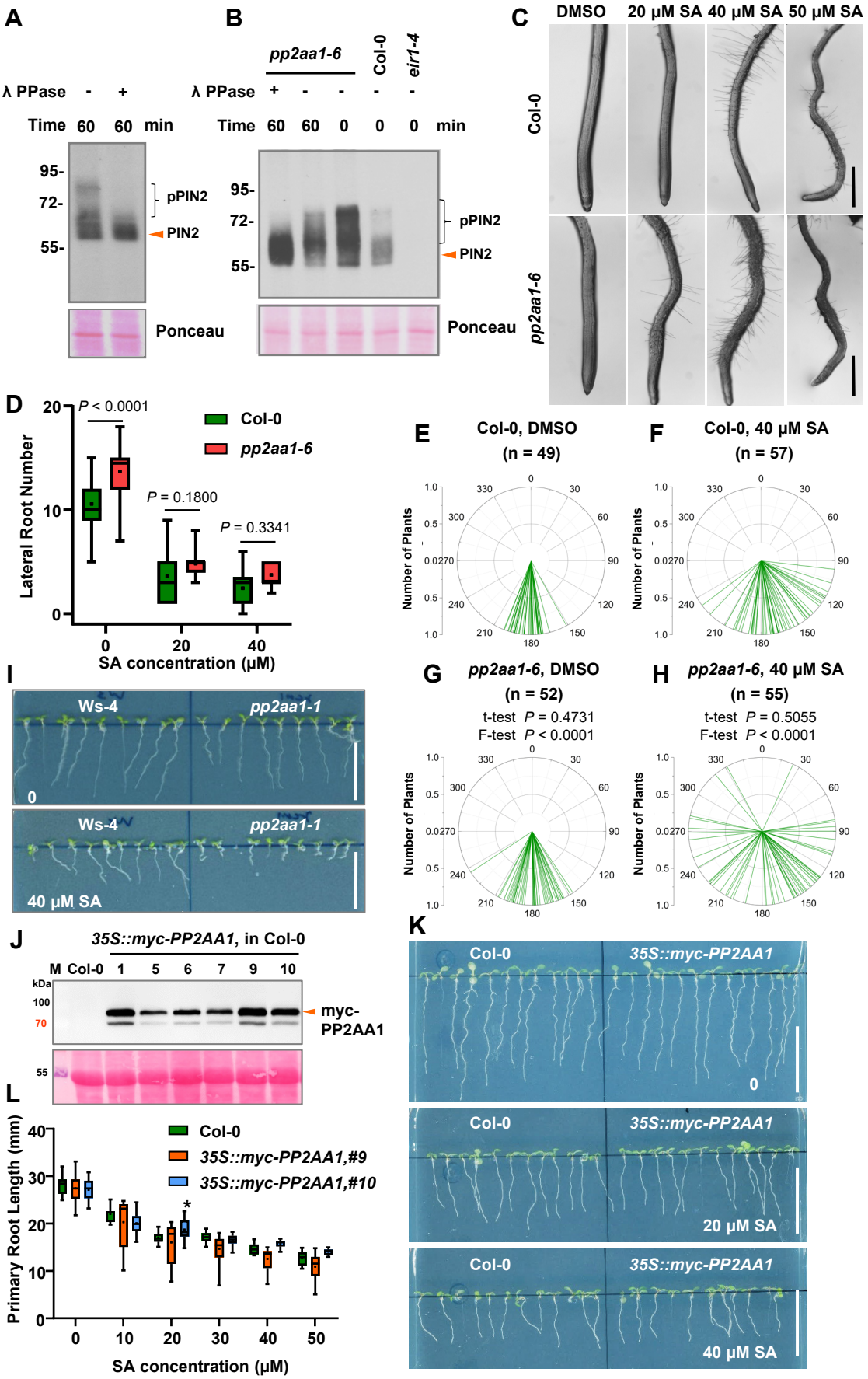
A
λ PPase - +
Time 60 60 min
95-
72-
55-
pPIN2
PIN2
Ponceau
B
pp2aa1-6
Col-0
eir1-4
λ PPase + - - - -
Time 60 60 0 0 0 min
95-
72-
55-
pPIN2
PIN2
Ponceau
C
DMSO
20 μM SA
40 μM SA
50 μM SA
Col-0
pp2aa1-6
D
P < 0.0001
P = 0.1800
P = 0.3341
Col-0
pp2aa1-6
Lateral Root Number
SA concentration (μM)
E
Col-0, DMSO
(n = 49)
F
Col-0, 40 μM SA
(n = 57)
Number of Plants
G
pp2aa1-6, DMSO
(n = 52)
t-test P = 0.4731
F-test P < 0.0001
H
pp2aa1-6, 40 μM SA
(n = 55)
t-test P = 0.5055
F-test P < 0.0001
I
Ws-4
pp2aa1-1
0
40 μM SA
J
35S::myc-PP2AA1, in Col-0
M Col-0 1 5 6 7 9 10
kDa
100
70
55
myc-PP2AA1
K
Col-0
35S::myc-PP2AA1
0
20 μM SA
40 μM SA
L
Col-0
35S::myc-PP2AA1,#9
35S::myc-PP2AA1,#10
Primary Root Length (mm)
SA concentration (μM)

Figure S3. Deficiency of the PP2A A subunit, PP2AA1 (RCN1), leads to SA hypersensitivity, and SA treatment inhibits PP2A activity *in planta*. Related to Figure 4.

(A) PIN2 phosphorylation gave rise to shifted smears, revealed by dephosphorylation of PIN2 by lambda phosphatase (λ PPase) *in vitro*. Total membrane extracts were incubated with or without 2 U of λ PPase for the indicated time, and samples were then analysed by Western blot with an anti-PIN2 antibody. Upper, anti-PIN2; bottom, Ponceau staining.

(B) Increase of PIN2 phosphorylation in *pp2aa1-6*. Total membrane extracts from Col-0, *pp2aa1-6*, and *eir1-4* were incubated with or without 5 U λ PPase for the indicated time, and samples were analysed by Western blot with an anti-PIN2 antibody. Upper, anti-PIN2; bottom, Ponceau staining.

(C) Close views of the morphology of Col-0 and *pp2aa1-6* roots under different concentrations of SA. Seedlings were observed by a differential interference contrast (DIC) microscopy. Scale bars, 1 mm.

(D) Sensitivity of *pp2aa1-6* to SA in terms of inhibiting lateral root formation. Col-0 and *pp2aa1-6* seedlings were grown on plates containing different concentrations of SA for 10 d, and the number of emerged lateral root was counted. *P* values were calculated by a two-tailed t-test.

(E-H) Following Figure 4F. *pp2aa1-6* is hypersensitive to SA in terms of interfering with the gravitropic response. Col-0 (E-F) and *pp2aa1-6* (G-H) seedlings were grown on plates containing different concentrations of SA for 7 d, and the root tip angles were measured by Image J, and shown as polar bar charts. *P* values were calculated by a two-tailed t-test to evaluate the mean value and by a further F-test to indicate differences of variances. The *pp2aa1-6* groups were compared with Col-0 under treatment with the same concentration of SA respectively.

(I) Representative images showing hypersensitivity of *pp2aa1-1* to SA. WT (Ws-4) and *pp2aa1-1* seedlings were grown on plates with different concentrations of SA for 7 d. Scale bars, 2 cm.

(J) Western blot verified the expression of myc-PP2AA1. 7-d-old seedlings were subjected to protein extraction and the subsequent Western blot with an anti-myc antibody (1:2000). Upper panel, anti-myc; lower panel, Ponceau staining to show the loading. Lines 9 and 10 (T_3 generation, homozygous lines) were used for further analysis.

(K) Representative images showing the sensitivity of *35S::myc-PP2AA1* to SA. Col-0 and *35S::myc-PP2AA1* seedlings were grown on plates with different concentrations of SA for 7 d. Scale bars, 2 cm.

(L) *35S::myc-PP2AA1* did not show any difference in sensitivity to SA in root growth inhibition. Col-0 and *35S::myc-PP2AA1* seedlings were grown on plates with concentrations of SA for 7 d, and the primary root length was measured. n = 11-30; *, $P < 0.05$, by one-way ANOVA with a Tukey multiple comparison test, compared to Col-0.

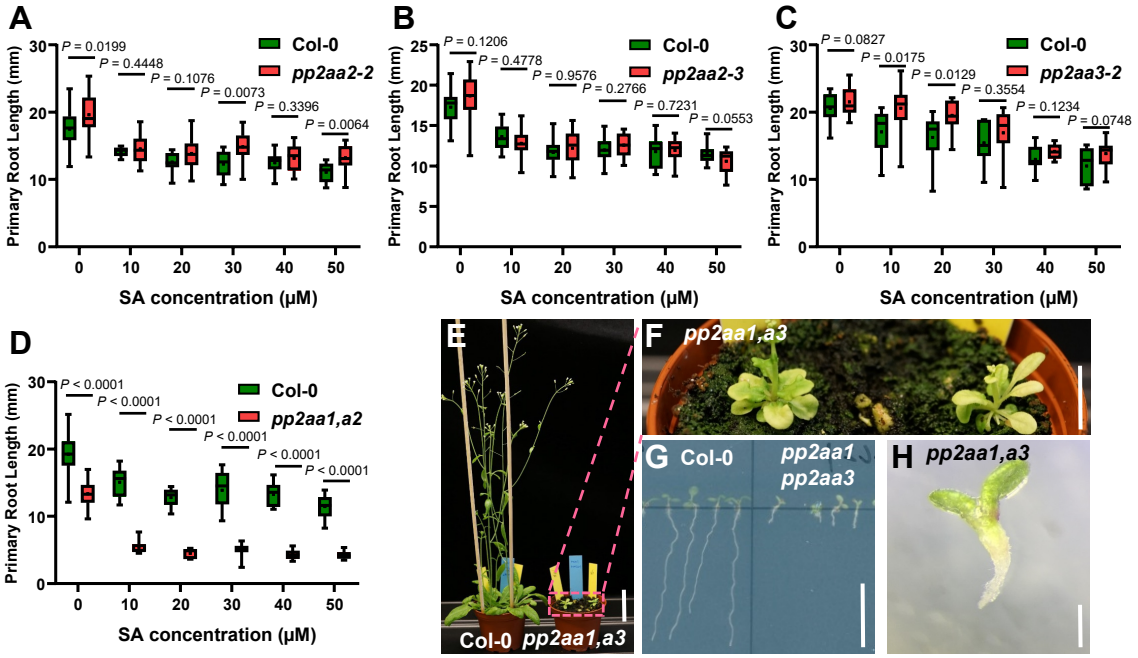
A
Primary Root Length (mm)
Col-0
pp2aa2-2
P = 0.0199
P = 0.4448
P = 0.1076
P = 0.0073
P = 0.3396
P = 0.0064
SA concentration (μM)
B
Col-0
pp2aa2-3
P = 0.1206
P = 0.4778
P = 0.9576
P = 0.2766
P = 0.7231
P = 0.0553
SA concentration (μM)
C
Col-0
pp2aa3-2
P = 0.0827
P = 0.0175
P = 0.0129
P = 0.3554
P = 0.1234
P = 0.0748
SA concentration (μM)
D
Col-0
pp2aa1,a2
P < 0.0001
P < 0.0001
P < 0.0001
P < 0.0001
P < 0.0001
P < 0.0001
SA concentration (μM)
E
Col-0
pp2aa1,a3
F
pp2aa1,a3
G
Col-0
pp2aa1
pp2aa3
H
pp2aa1,a3

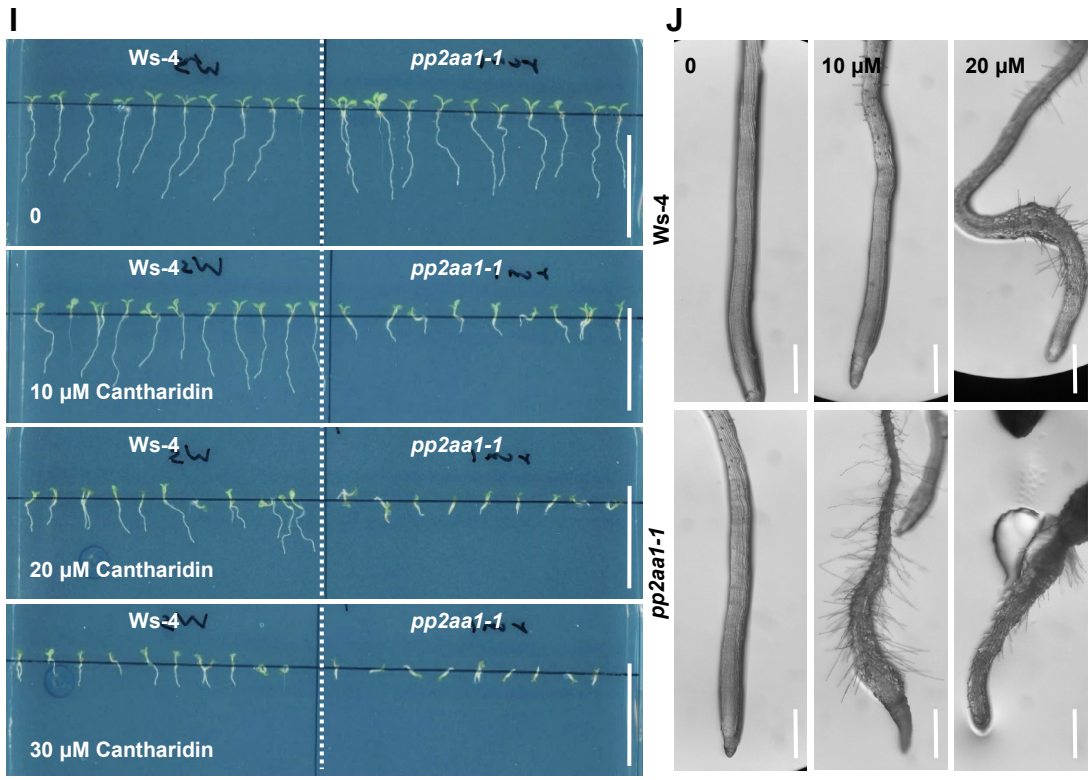
I
Ws-4
pp2aa1-1
0
10 μM Cantharidin
20 μM Cantharidin
30 μM Cantharidin
J
0
10 μM
20 μM
Ws-4
pp2aa1-1

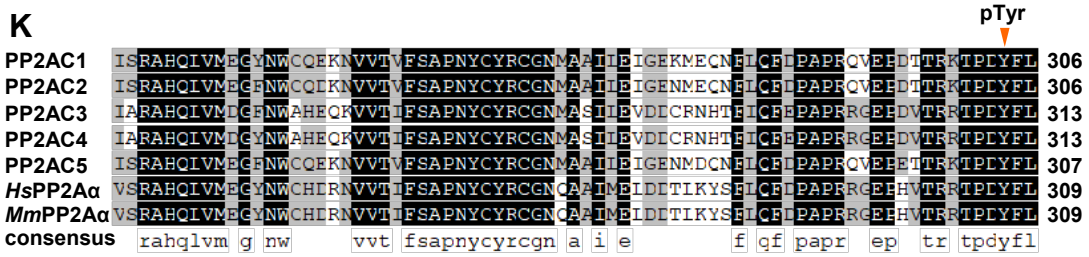
K
pTyr
PP2AC1 306
PP2AC2 306
PP2AC3 313
PP2AC4 313
PP2AC5 307
HsPP2Aα 309
MmPP2Aα 309
consensus

Figure S4. SA sensitivity of the loss-of-function mutants of PP2A subunits, and deficiency of the PP2A A subunit, PP2AA1 (RCN1), leads to hypersensitivity to a known PP2A inhibitor, cantharidin. Related to Figures 4 & 5.

(A-D) The sensitivity of different PP2A mutants to SA in primary root elongation. Col-0, *pp2aa2-2*, *pp2aa2-3* (a knock-down line), *pp2aa3-2*, and *pp2aa1 pp2aa2-3* (short as *pp2aa1,a2*) seedlings were grown on plates with different concentrations of SA for 7 d, and the primary root length was measured. (A) n = 11-27，(B) n = 12-30，(C) n = 10-28，(D) n = 13-28. *P* values were calculated by a two-tailed t-test for indicated pairs of Col-0 and *pp2aa1, a3* at the given concentration of SA.

(E-H) The double mutant of *pp2aa1 pp2aa3* exhibited deficiency in growth and development with severe root defects, reminiscent of SA- or cantharidin- treatment. Scale bar, 5 cm (E), 1 cm (F), 1 cm (G), and 1 mm (H) respectively.

(I) Representative images showing the hypersensitivity of *pp2aa1-1* to cantharidin. Ws-4 and *pp2aa1-1* seedlings were grown on plates containing different concentrations of cantharidin for 7 d. Scale bars, 2 cm.

(J) Close view of the morphology of Ws-4 and *pp2aa1-1* roots under different concentrations of cantharidin. Scale bars, 1 mm.

(K) Sequence alignment of *Arabidopsis* PP2A C subunits, with their homologues in human (*Homo sapiens*) and mice (*Mus musculus*). All the sequences share 87.13% similarity. The arrowhead indicates the conserved phosphorylation site, which is responsible for PP2Ac activity and is recognized by the pY307-PP2Ac antibody.

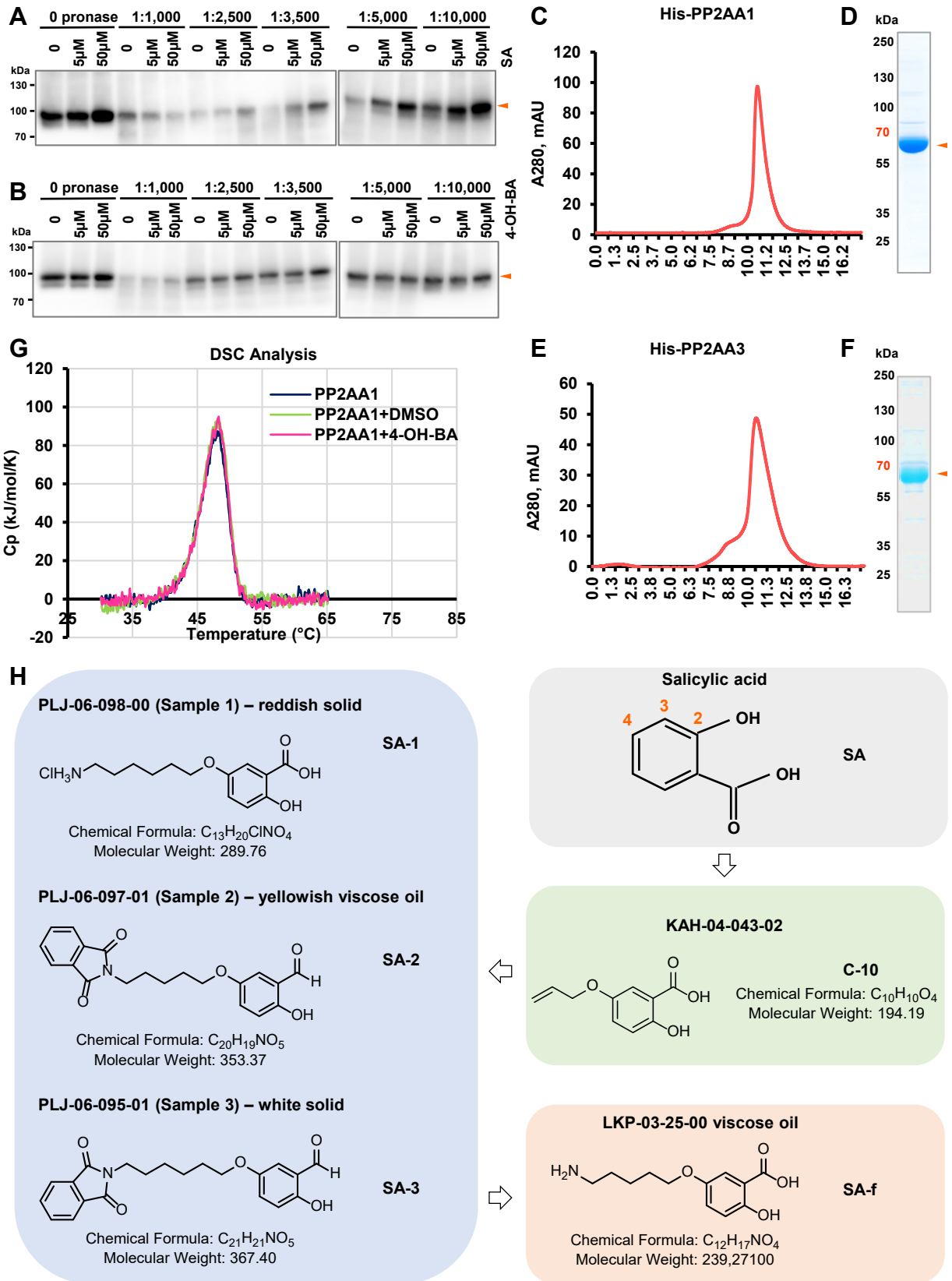
A
0 pronase
1:1,000
1:2,500
1:3,500
1:5,000
1:10,000
0
5μM
50μM
kDa
130
100
70
SA
B
4-OH-BA
C
His-PP2AA1
A280, mAU
D
kDa
250
130
100
70
55
35
25
E
His-PP2AA3
F
G
DSC Analysis
PP2AA1
PP2AA1+DMSO
PP2AA1+4-OH-BA
Cp (kJ/mol/K)
Temperature (°C)
H
PLJ-06-098-00 (Sample 1) – reddish solid
SA-1
Chemical Formula: C13H20ClNO4
Molecular Weight: 289.76
PLJ-06-097-01 (Sample 2) – yellowish viscose oil
SA-2
Chemical Formula: C20H19NO5
Molecular Weight: 353.37
PLJ-06-095-01 (Sample 3) – white solid
SA-3
Chemical Formula: C21H21NO5
Molecular Weight: 367.40
Salicylic acid
SA
KAH-04-043-02
C-10
Chemical Formula: C10H10O4
Molecular Weight: 194.19
LKP-03-25-00 viscose oil
SA-f
Chemical Formula: C12H17NO4
Molecular Weight: 239,27100

Figure S5. DARTS assay suggests potential binding of SA to PP2AA1, protein purification of His-PP2AA1 and His-PP2AA3 by Size exclusion chromatography (SEC), and the design flow of the SA analogue, SA-f, for the SPR. Related to Figure 6.

(A-B) DARTS assay suggests PP2AA1 is potential target of SA. *pPP2AA1::PP2AA1-GFP* seedlings were used for the protein isolation, and Samples were treated with DMSO (mock) and SA (0, 5 μM, and 50 μM respectively, in A), with 4-OH-BA as a negative control (B), and digested by different concentrations of pronase.

(C) SEC purification of His-PP2AA1 with a Superdex 200 increase column. A representative run is shown here to indicate the purity of recombinant His-PP2AA1 used for DSC and SPR analyses.

(D) SDS-PAGE to check the quality of His-PP2AA1, visualized by CBB staining.

(E) SEC purification of His-PP2AA3.

(F) SDS-PAGE to check the quality of His-PP2AA3, by CBB staining.

(G) DSC analysis of the effect of 4-OH-BA, an inactive SA isomer, on His-PP2AA1 stability. 5 μM of purified His-PP2AA1 protein were added with or without DMSO, or 50 μM 4-OH-BA, and were then analysed by DSC. Tm = 47.57°C, 47.69°C, and 47.69°C, for His-PP2AA1, His-PP2AA1+DMSO, and His-PP2AA1+4-OH-BA respectively.

(H) Workflow for the design of the synthetic SA analogue, SA-f, which can be immobilized on a CM-5 SPR sensor chip. Multiple SA analogues with different groups at different positions of the benzoic ring were synthesized, tested, with C-10 coming out as the best one with activity and the possibility to immobilize it. Further analysis for SA-1/2/3 with a linker and a group to mimic the surface of the matrix of SPR sensor chips, revealed that the linker does not affect the bioactivity of SA.

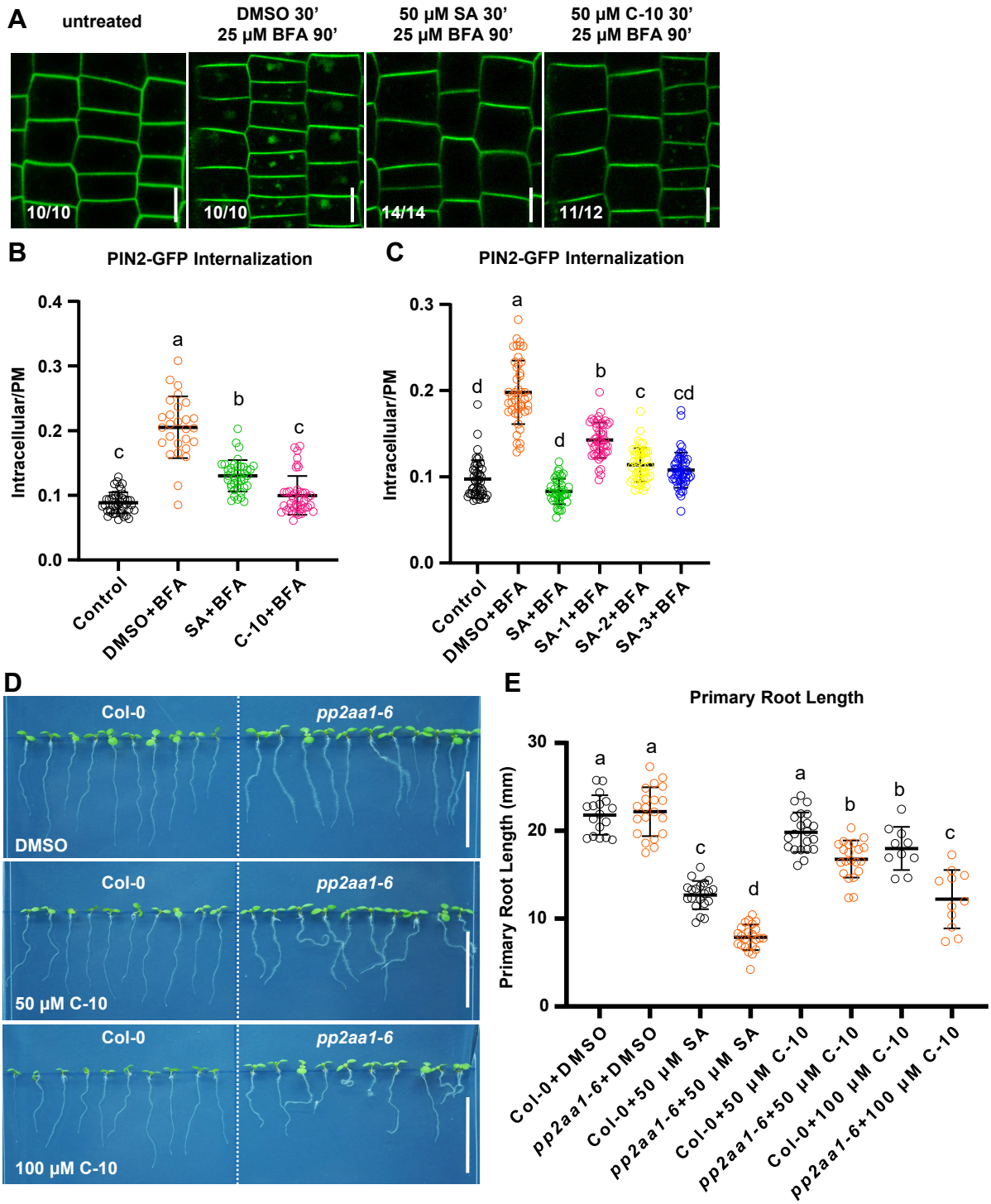
A
untreated
DMSO 30'
25 μM BFA 90'
50 μM SA 30'
25 μM BFA 90'
50 μM C-10 30'
25 μM BFA 90'
10/10
10/10
14/14
11/12
B
PIN2-GFP Internalization
Intracellular/PM
Control
DMSO+BFA
SA+BFA
C-10+BFA
C
PIN2-GFP Internalization
Intracellular/PM
Control
DMSO+BFA
SA+BFA
SA-1+BFA
SA-2+BFA
SA-3+BFA
D
Col-0
pp2aa1-6
DMSO
50 μM C-10
100 μM C-10
E
Primary Root Length
Primary Root Length (mm)
Col-0+DMSO
pp2aa1-6+DMSO
Col-0+50 μM SA
pp2aa1-6+50 μM SA
Col-0+50 μM C-10
pp2aa1-6+50 μM C-10
Col-0+100 μM C-10
pp2aa1-6+100 μM C-10
F
DMSO (n = 60)
50 μM C-10 (n = 48)
t-test P = 0.2521
F-test P < 0.0001
DMSO (n = 61)
50 μM C-10 (n = 47)
t-test P = 0.3365
F-test P < 0.0001
t-test P = 0.4076
F-test P < 0.0001
Col-0
pp2aa1-6
Number of Plants

Figure S6. Bioactivity test of the synthetic SA analogues. Related to Figure 6.

(A-B) Cellular activity of the synthetic compound, C-10, with the SA moiety, in terms of inhibiting BFA (brefeldin A) body formation. 4-d-old *pPIN2::PIN2-GFP* seedlings were treated with indicated chemicals and imaged by CLSM. (A), representative images, Scale bars, 10 μm; (B), quantification of the BFA body formation by calculating the intracellular/PM ratio for the PIN2-GFP fluorescence intensity.

(C) Cellular activity of the synthetic compounds, SA-1 to SA-3, in terms of inhibiting BFA body formation. 4-d-old *pPIN2::PIN2-GFP* seedlings were treated with indicated chemicals and imaged by CLSM. Quantification of the BFA body formation by calculating the intracellular/PM ratio for the PIN2-GFP fluorescence intensity.

Dots represent individual values, and lines indicate mean ± SD. (B) n = 27-42; (C) n = 41-50. Different letters represent significant difference, $P < 0.05$, by one-way ANOVA with a Tukey multiple comparison test.

(D) Physiological activity of the synthetic SA analogue C-10, in terms of root morphology. 7-d-old Col-0 seedlings were grown on plates with indicated chemicals. Scale bars, 2 cm.

(E) C-10 inhibits primary root elongation. Dots represent individual values, and lines indicate mean ± SD. n =10-23; *P* values were calculated by a two-tailed t-test.

(F) Treatment with C-10 gave rise to less gravitropic roots. The angles of root tips were measured by Image J, and shown as polar bar charts. *P* values were calculated by a two-tailed t-test to evaluate the mean value and by a further F-test to indicate differences of variances. For Col-0, C-10 treatments were compared with the DMSO control, and the *pp2aa1-6* groups were compared with Col-0 under treatment with the same concentration of C-10 respectively.

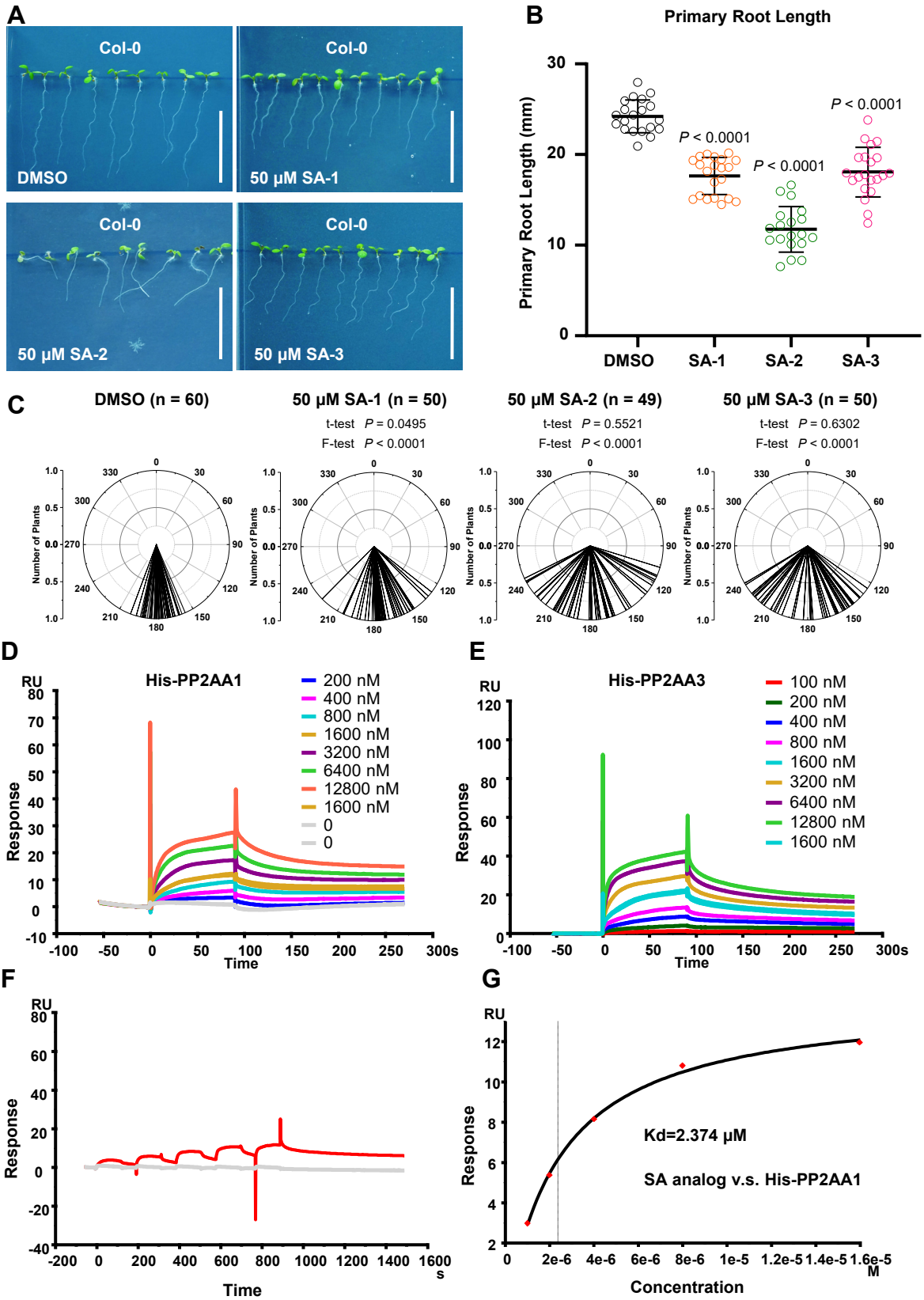
A
Col-0
DMSO
Col-0
50 μM SA-1
Col-0
50 μM SA-2
Col-0
50 μM SA-3
B
Primary Root Length
Primary Root Length (mm)
P < 0.0001
P < 0.0001
P < 0.0001
DMSO
SA-1
SA-2
SA-3
C
DMSO (n = 60)
50 μM SA-1 (n = 50)
t-test P = 0.0495
F-test P < 0.0001
50 μM SA-2 (n = 49)
t-test P = 0.5521
F-test P < 0.0001
50 μM SA-3 (n = 50)
t-test P = 0.6302
F-test P < 0.0001
Number of Plants
D
His-PP2AA1
RU
Response
Time
200 nM
400 nM
800 nM
1600 nM
3200 nM
6400 nM
12800 nM
1600 nM
0
0
E
His-PP2AA3
RU
Response
Time
100 nM
200 nM
400 nM
800 nM
1600 nM
3200 nM
6400 nM
12800 nM
1600 nM
F
RU
Response
Time
G
RU
Response
Kd=2.374 μM
SA analog v.s. His-PP2AA1
Concentration
M

Figure S7. Physiological test of the SA analogues, and additional data for the binding between SA and His-PP2AA1. Related to Figure 6.

(A) Physiological activity of the synthetic SA analogues SA-1 to SA-3, in terms of root morphology. 7-d-old Col-0 seedlings were grown on plates with indicated chemicals. Scale bars, 2 cm.

(B) SA analogues (SA-1 to SA-3) inhibit the primary root elongation. Dots represent individual values, and lines indicate mean ± SD. n =17-21; *P* values were calculated by a two-tailed t-test.

(C) Treatment with SA analogues (SA-1 to SA-3) gave rise to less gravitropic roots. The angles of root tips were measured by Image J, and shown as polar bar charts. *P* values were calculated by a two-tailed t-test to evaluate the mean value and by a further F-test to indicate differences of variances in comparison to mock treatment.

(D) SPR assay reveals the binding of His-PP2AA1 to SA. The sensorgram shows the kinetics for the interaction between His-PP2AA1 and SA, used for generating Figure 6C.

(E) SPR assay reveals the binding of His-PP2AA3 to SA. Sensorgram showing the kinetics for the interaction between His-PP2AA3 and SA.

(F-G) SPR revealing the binding between SA and His-PP2AA1. Single cycle binding kinetics was conducted, without regeneration between different concentrations of His-PP2AA1. 0.1% BSA (~15 μM) was included in the His-PP2AA1 flow. (F), sensorgram; (G), plotted by the values at steady state. A Kd value of 2.374 μM was detected.

Primers	**Oligonucleotide (5’ to 3’)**	**use**
For Genotyping		
Oligo Name	**Sequence**	**Mutants**
pp2aa1-1 _LP	AGCACATCCTTCCTTGTGTGAAGG	*pp2aa1-1*
pp2aa1-1 _RP	AACTTGCTTATGATGTTAAGGCGC	
pp2aa1-1 _RB	TGTCCCGCGTCATCGGCGGGGGTC	
*pp2aa1-6*_LP	GGCCAGCCAGTTAGGTATAGG	*pp2aa1-6*
*pp2aa 1-6*_RP	AAACATAGCCACACGCATTTC	
*pp2aa2-1*_LP	CGATGTTACGTGCCCTCTTAC	*pp2aa2-1*
*pp2aa2-1*_RP	TCTACCGAATGACCATTTTGC	
*pp2aa2-3*_LP	ATTGGTTATTTGGGATCGGAG	*pp2aa2-3*
*pp2aa2-3*_RP	ACTCTCCCTCATCTGAGAGCC	
*pp2aa3-1*_LP	TATTTCCAAACTTTGGGGGAC	*pp2aa3-1*
*pp2aa3-1*_RP	ATGGACACAGCTTGAAGATGG	
*pp2aa3-2*_LP	GCACCAAGCTTCTCATCAAAG	*pp2aa3-2*
*pp2aa3-2*_RP	GACCGGAGCCAACTAGGTAAG	
LB1	GCCTTTTCAGAAATGGATAAATAGCCTTGCTTCC	SAIL lines
LBb1.3	ATTTTGCCGATTTCGGAAC	SALK lines
pp2ac3-1-LP	GCTTGAAAGAACAGCATTTCG	*pp2ac3-1*
pp2ac3-1-RP	GTGGATTATCACCATCCATCG	
pp2ac4-1-LP	TAATTGGTATCAGGGCACTGC	*pp2ac4-1*
pp2ac4-1-RP	TGTTTCCTGATCTGTTTTCCG	
npr1-1-F	CGTGTGCTCTTCATTTCGCTGT	*npr1-1*
npr1-1-R	GTGCGGTTCTACCTTCCAAAGTT	
npr3-1-F	GAGTCAGATATCACTCTAGATCAAGC	*npr3-1*
npr3-1-R	GGAAAGAACAACTGAGCAAGCCCCA	
npr4-3-F	CGGATCTTGTTTCGTCATTTCAG	*npr4-1*
npr4-3-R	CAAACGTGAAATCTGAAGCATTAGC	
sid2-3-LP	ACCCTAATTTGGATTTGGTGC	*sid2-3*
sid2-3-RP	AGCTCTAGGCCTAGTTGCAGC	
For Cloning		
Oligo Name	**Sequence**	**Plasmid**

PIN2HL-1(EcoRI)	TGGAATTCGCTAAGCTTCTCATCTCCGAGC	pET28a-PIN2HL
PIN2HL-2(SalI)	CCGGTCGACACTCGCCGGCGGCATCTGCTG	
PP2AA1-1(EcoRI)	GGAATTCATGGCTATGGTAGATGAACCGTTG	pET28a-PP2AA1
PP2AA1-2(XhoI)	CCGCTCGAGGGATTGTGCTGCTGTGGAACCATC	
PP2AA3-1(EcoRI)	GGAATTCATGTCTATGGTTGATGAGCCTTTA	pET28a-PP2AA3
PP2AA3-2(XhoI)	CCGCTCGAGGCTAGACATCATCACATTGTC	

Table S1. List of primers used in this study. Related to STAR METHODS and Key Resources Table.

Supplement I

Supplement II

Supplement III

Supplement IV

Supplement V

Supplement VI

Supplement VII

Supplement VIII

Poitout A, Crabos A, **Petřík I**, Novák O, Krouk G, Lacombe B, Ruffel S. 2018. Responses to systemic nitrogen signaling in arabidopsis roots involve trans-zeatin in shoots. Plant Cell 30(6), 1243–1257.

The Plant Cell, Vol. 30: 1243–1257, June 2018, www.plantcell.org © 2018 ASPB.

Responses to Systemic Nitrogen Signaling in Arabidopsis Roots Involve *trans*-Zeatin in Shoots

Arthur Poitout,[a] Amandine Crabos,[a] Ivan Petřík,[b] Ondrej Novák,[b] Gabriel Krouk,[a] Benoît Lacombe,[a] and Sandrine Ruffel[a,1]

[a]BPMP, INRA, CNRS, Université de Montpellier, Montpellier SupAgro, 34090 Montpellier, France
[b]Laboratory of Growth Regulators, Centre of the Region Haná for Biotechnological and Agricultural Research, Institute of Experimental Botany CAS and Faculty of Science of Palacký University, CZ-78371 Olomouc, Czech Republic

ORCID IDs: 0000-0003-4228-9351 (A.P.); 0000-0003-3693-6735 (G.K.); 0000-0001-9924-3093 (B.L.); 0000-0002-5651-8349 (S.R.)

Plants face temporal and spatial variation in nitrogen (N) availability. This includes heterogeneity in soil nitrate (NO_3^-) content. To overcome these constraints, plants modify their gene expression and physiological processes to optimize N acquisition. This plasticity relies on a complex long-distance root-shoot-root signaling network that remains poorly understood. We previously showed that cytokinin (CK) biosynthesis is required to trigger systemic N signaling. Here, we performed split-root experiments and used a combination of CK-related mutant analyses, hormone profiling, transcriptomic analysis, NO_3^- uptake assays, and root growth measurements to gain insight into systemic N signaling in *Arabidopsis thaliana*. By comparing wild-type plants and mutants affected in CK biosynthesis and ABCG14-dependent root-to-shoot translocation of CK, we revealed an important role for active *trans*-zeatin (*tZ*) in systemic N signaling. Both rapid sentinel gene regulation and long-term functional acclimation to heterogeneous NO_3^- supply, including NO_3^- transport and root growth regulation, are likely mediated by the integration of *tZ* content in shoots. Furthermore, shoot transcriptome profiling revealed that glutamate/glutamine metabolism is likely a target of *tZ* root-to-shoot translocation, prompting an interesting hypothesis regarding shoot-to-root communication. Finally, this study highlights *tZ*-independent pathways regulating gene expression in shoots as well as NO_3^- uptake activity in response to total N deprivation.

Continuous functional and morphological organ plasticity is one of the most fascinating differences between plants and animals. Indeed, plants employ a range of strategies to tolerate fluctuating resource availability, with plant roots particularly malleable, since they may be exposed to either a scarcity or excess of nutrients and/or water. The signaling networks controlling root adaptation are an important focus for a new green revolution aimed at optimizing root function for the benefit of aerial plant tissue development (Den Herder et al., 2010; Kong et al., 2014; Bishopp and Lynch, 2015).

Nitrogen (N) is a basic building block in the biosynthesis of proteins, nucleic acids, and essential pigments such as chlorophyll. Thus, plants need to deploy strategies to avoid N limitation and to optimize N use during their life cycle. The strong responsiveness of roots to N availability reflects the crucial capacity of plants to maintain N homeostasis. This is reflected, for example, by the plasticity of root system architecture to respond to N deficiency conditions (Gruber et al., 2013) and differentially to N availability based on the presence of other nutrients (Kellermeier et al., 2014).

Root responsiveness relies on the plant's capacity to sense N availability. This N sensing is commonly divided into two major branches, namely, local perception of N in the vicinity of the root (particularly in the form of nitrate [NO_3^-]) and systemic perception of internal N/NO_3^- availability at the whole organism level. The latter relies on root-shoot-root signaling and the integration of information from different parts of the plant (Gansel et al., 2001; Walch-Liu et al., 2005; Alvarez et al., 2012; Li et al., 2014). This dual N sensing is integrated through an intricate signaling network that permits the reciprocal control of root N acquisition and plant growth to ensure N homeostasis (Krouk et al., 2011; Krouk, 2016).

In *Arabidopsis thaliana*, the perception and propagation of local NO_3^- signaling has been the focus of considerable research. The molecular players involved include the NO_3^- transceptor NPF6.3/NRT1.1/CHL1 (Ho et al., 2009; Krouk et al., 2010b), a number of kinases (CIPK8, CIPK23, CPK10, CPK30, and CPK32), the phosphatase ABI2 (Ho et al., 2009; Hu et al., 2009; Léran et al., 2015; Liu et al., 2017), the cleavage and polyadenylation factor CPSF30-L (Li et al., 2017), and several transcription factors (NLP6/7, TGA1/4, NRG2, and SPL9) (Castaings et al., 2009; Krouk et al., 2010a; Konishi and Yanagisawa, 2013; Marchive et al., 2013; Alvarez et al., 2014; Xu et al., 2016). Upon NO_3^- treatment, these transcription factors trigger the expression of genes involved in NO_3^- transport and assimilation, a molecular response also known as the primary nitrate response (PNR) (Medici and Krouk, 2014). Additionally, Ca^{2+} is a crucial secondary messenger in the establishment of this response (Riveras et al., 2015; Krouk, 2017; Liu et al., 2017). Plant responses to N provision involve additional molecular actors. For example, transcription factors such as ANR1, ARF8, and NAC4, as well as CLE peptides, are implicated in N-dependent root development (Zhang and Forde, 1998; Gifford et al., 2008; Vidal et al., 2013; Araya et al., 2014). The transcription factors bZIP1, LBD37/38/39, BT2,

[1]Address correspondence to sandrine.ruffel@inra.fr.
The author responsible for distribution of materials integral to the findings presented in this article in accordance with the policy described in the Instructions for Authors (www.plantcell.org) is: Sandrine Ruffel (sandrine.ruffel@inra.fr).
www.plantcell.org/cgi/doi/10.1105/tpc.18.00011

IN A NUTSHELL

Background: Nitrate, NO_3^- (the preferential nitrogen [N] source for most of higher plants) is spread unevenly in the soil due to its high mobile property, a phenomenon known as spatial NO_3^- heterogeneity. To face this constraint, plants regulate root growth and NO_3^- uptake/assimilation in different parts of the root system according to the spatial NO_3^- availability and the N needs of the whole plant. This optimization of N acquisition is the result of a dual regulation involving (1) a local signaling related to external NO_3^- supply and (2) a root-shoot-root long-distance signaling related to whole plant N/NO_3^- needs. The molecular basis of this long-distance signaling is poorly understood. However, the plant hormone cytokinin was previously shown to be important for the root responses to soil NO_3^- availability.

Question: Do cytokinins play a role as a root-to-shoot messenger of NO_3^- systemic signaling, and how do shoots optimize N acquisition in response to spatial NO_3^- heterogeneity?

Findings: We found that mutant plants that are impaired in cytokinin biosynthesis or in root-to-shoot translocation also are strongly impaired to face spatial NO_3^- heterogeneity. Both rapid molecular responses (regulation of N-responsive genes) and long-term functional acclimation (regulation of NO_3^- transport and root growth) to spatial NO_3^- heterogeneity were strongly reduced in mutant plants compared to the wild type. Shoot transcriptomic profiling showed important transcriptomic changes in response to spatial NO_3^- heterogeneity that are dependent on cytokinin biosynthesis and transport. We also found that these transcriptomic changes are likely mediated by the active form of cytokinin, *trans*-Zeatin, in shoots and that glutamate/glutamine metabolism could be a target of *trans*-Zeatin root-to-shoot translocation in the context of spatial NO_3^- heterogeneity.

Next steps: When plants face spatial NO_3^- heterogeneity, long-distance signals originating from both NO_3^--supplied and N-deprived roots are integrated in the shoots in order to optimize N acquisition. We wish to decipher the molecular details of the shoot-to-root messenger system of cytokinin-dependent long-distance signaling and to use this information to improve nutrient foraging in plants.

and HRS1/HHOs control N use (Baena-González et al., 2007; Rubin et al., 2009; Araus et al., 2016; Safi et al., 2018). The transcription factor TCP20, which is not involved in the PNR per se, physically interacts with NLP6/7 and regulates the expression of NO_3^--responsive genes and a cell cycle marker gene (Li et al., 2005; Guan et al., 2014, 2017). Interestingly, TCP20 also regulates root foraging under heterogeneous NO_3^- supply conditions (Guan et al., 2014) and thus may serve as a gateway to understanding how local and systemic N regulation is integrated (Guan et al., 2017).

Unlike local N signaling, the mechanistic details of the systemic signaling cascade are still poorly understood. This knowledge gap may be attributed to the necessity for complex experimental approaches, such as split-root systems or grafting, to specifically address research questions about long-distance signaling. Indeed, split-root experiments provide a relevant framework to uncouple local and systemic signaling via comparisons of roots experiencing similar local hydro-mineral conditions but different distant media (i.e., in another part of the root) (Li et al., 2014). In this system, any differences in the properties of roots in the same local environment should be due to the effects of long-distance signals. Such an approach has helped to define the landscape of the systemic N-related signaling response and has revealed at least two coexisting systemic signaling pathways (Gansel et al., 2001; Ruffel et al., 2011; Li et al., 2014). The N-demand long-distance signal conveys the message that the whole plant is experiencing a distal N deprivation, whereas the N-supply long-distance signal conveys the message that some N has been found by the plant (Ruffel et al., 2011). Two major aspects of these signaling pathways have been elucidated, namely, the involvement of C-terminally encoded peptides (CEPs) (Tabata et al., 2014) and cytokinin (CK) biosynthesis (Ruffel et al., 2011, 2016).

The role of CEPs in systemic N-demand signaling was recently demonstrated. Upon N deprivation, CEPs are translocated to the shoots, where they are recognized by two leucine-rich repeat receptor kinases known as CEP Receptor 1 and 2 (Tabata et al., 2014). Within the shoot vascular system, this recognition leads to the expression of glutaredoxin-like small polypeptides that translocate toward the roots and, in combination with local NO_3^- sensing, participate in the specific control of the expression of *NRT2.1*, encoding the main high-affinity NO_3^- transporter in roots (Ohkubo et al., 2017; Ruffel and Gojon, 2017). However, in response to heterogeneous NO_3^- supply, roots display a wide range of responses, including the transcriptional regulation of hundred of genes, enhanced lateral root development, and enhanced NO_3^- acquisition (Gansel et al., 2001; Remans et al., 2006; Ruffel et al., 2008, 2011; Mounier et al., 2014). The roles for CEP-derived long-distance signals in these processes remain to be demonstrated.

In response to NO_3^- supply, CKs are synthesized in roots and translocated to the shoots, leading to the control of shoot growth (Takei et al., 2001, 2004; Sakakibara et al., 2006; Osugi et al., 2017). CKs also play crucial roles in root responses to long-distance signals (Ruffel et al., 2011). However, an important question remains concerning the role of CK in shoots in triggering root responses in a systemic context. In other words, are active CKs in shoots a component of the long-distance signaling that controls molecular and/or physiological responses to NO_3^- heterogeneity in roots? And which CK form in particular is involved?

Isoprenoid CKs, including N^6-(Δ^2-isopentenyl)adenine (iP), *trans*-zeatin (*tZ*), dihydrozeatin (DHZ), and *cis*-zeatin (*cZ*), are more abundant in plants than aromatic CKs, with the first two being the major forms in Arabidopsis. Briefly, the prenylation of adenosine mono-, di-, or tri-phosphate by the adenosine

phosphate-isopentenyltransferase (IPT) enzymes leads first to the formation of iP-ribotides using the dimethylallyl diphosphate substrate predominantly from the methylerythritol phosphate pathway. These iP-ribotides are subsequently hydroxylated to synthetize *t*Z-ribotides. On the other hand, the prenylation of adenine on tRNA leads to the formation of *c*Z-ribotides, using the dimethylallyl diphosphate substrate from the mevalonate pathway. Therefore, *t*Z-type and *c*Z-type CKs have different metabolic origins, albeit they can be enzymatically interconverted by zeatin *cis-trans* isomerase. CK ribotides can be dephosphorylated to synthetize riboside-type CK precursors, which are considered to be the major translocation forms (Sakakibara, 2006). This does not exclude the possibility that free-base forms of CK, which are the actual active forms, are also translocated long-distance. Indeed, systemic transport of *t*Z was recently shown to regulate leaf size, whereas *t*ZR controls meristem activity (Osugi et al., 2017). Ultimately, CK homeostasis is also modulated by sugar conjugation through *O*- or *N*-glycosylation, deactivating CK in a reversible (inactive storage) and irreversible manner, respectively (Sakakibara, 2006).

In this study, we further investigated the role of CK in systemic N signaling. We used genetic approaches to manipulate CK content and translocation combined with detailed measurements of CK forms and shoot transcriptome analysis. We show that *t*Z in shoots is required for the appropriate responses of roots to heterogeneous NO_3^- conditions. Specifically, the integration of *t*Z content in shoots likely plays an essential role in long-distance signaling that controls (1) transcriptional reprogramming of roots and shoots, (2) root growth, and (3) NO_3^- transport activity.

RESULTS

Root-to-Shoot Translocation of Cytokinin Controls Transcriptional Responses to Systemic N-Demand Signaling

To investigate the role of root-to-shoot translocation of CK in N systemic signaling, we characterized an Arabidopsis mutant lacking the ATP Binding Cassette Transporter Subfamily G (ABCG14) transporter, which is impaired in delivering CK to the shoot (Ko et al., 2014; Zhang et al., 2014). Wild-type and mutant plants were grown in a hydroponic split-root system. Our experimental system consisted of three N supply conditions: (1) a heterogeneous split environment (Sp.KNO_3/Sp.KCl: one compartment containing 1 mM KNO_3 and the other containing 1 mM KCl), (2) a control homogeneous N-replete environment (C.KNO_3: both compartments containing 1 mM KNO_3), and (3) a control homogeneous N-deprived environment (C.KCl: both compartments containing 1 mM KCl), which thus provided four different root samples and three different shoot samples (Figure 1A). Any difference recorded between root C.KNO_3 and Sp.KNO_3 samples is indicative of a N-demand long-distance signal, whereas any difference recorded between root Sp.KCl and C.KCl samples is indicative of a N-supply long-distance signal. This logic was applied throughout the study (Figure 1A). This system was used to test the specific and rapid responses of systemic N-signaling sentinel genes that were identified previously in a root transcriptomic analysis following plant transfer to homogeneous or heterogeneous conditions (Ruffel et al., 2011). These sentinel genes have important functions, including roles in NO_3^- transport, i.e., *NITRATE TRANSPORTER2.1* (*NRT2.1*; Filleur et al., 2001) and its functional partner *NRT3.1*/*NAR2.1* (also known as *WOUND-RESPONSIVE3*; Yong et al., 2010), and NO_3^- assimilation, i.e., *NITRITE REDUCTASE* (*NiR*), *GLUCOSE-6-PHOSPHATE DEHYDROGENASE3* (*G6PD3*), *UROPHORPHYRIN METHYLASE1* (*UPM1*), and *FERREDOXIN-NADP(+)-OXIDOREDUCTASE2* (*FNR2*).

In wild-type (Col-0) plants, the expression levels of these sentinel genes were globally higher in Sp.KNO_3 roots compared with roots grown under the homogeneous control condition, C.KNO_3. This result indicates that wild-type roots respond to heterogeneous NO_3^- availability through a systemic N-demand signal (Figure 1B) (Ruffel et al., 2011). Under these hydroponic split-root conditions, the isopentenyltransferase triple mutant *ipt3 ipt5 ipt7* (*ipt3,5,7*), with altered CK biosynthesis (Miyawaki et al., 2006), displayed an altered response to systemic N-demand signaling (Figure 1B), as previously shown (Ruffel et al., 2011). In *abcg14*, the expression levels of sentinel genes in roots supplied with NO_3^- were lower compared with those in the wild type and *ipt3,5,7*, but more importantly, Sp.KNO_3 roots did not display any significant increase in sentinel gene expression compared with C.KNO_3 control roots. This demonstrates that *abcg14* is also impaired in its response to systemic N-demand signaling (Figure 1B). Therefore, root-to-shoot translocation of CK may be essential for transcriptional plant responses to heterogeneous NO_3^- environments. Notably, for both mutants, some sentinel genes, such as *G6PD3*, were still responsive to local NO_3^- availability (C.KNO_3 and Sp.KNO_3 versus Sp.KCl and C.KCl; Figure 1B), indicating that these mutants have maintained their ability to detect NO_3^- per se.

CK Partitioning Is under the Control of the Combined Effect of NO_3^-, IPTs, and ABCG14

To determine how CK partitioning/homeostasis control root-specific responses to heterogeneous NO_3^- supply, we measured the levels of the four basic isoprenoid CK forms (iP, *t*Z, DHZ, and *c*Z) and their derivatives (ribotides, ribosides, *O*-glucosides, and *N*-glucosides) in roots and shoots. These measurements were performed at the same time point used to evaluate the responses of sentinel genes (Figure 1). To validate our experimental system, we first determined if the accumulation patterns of the four CK forms were indeed affected in *ipt3,5,7* and *abcg14* (Miyawaki et al., 2006; Ko et al., 2014) (Figure 2A). Moreover, we also explored the responses of CK accumulation to NO_3^- provision in the wild type and these mutants (C.KNO_3 versus C.KCl; Figure 2A).

As expected, the triple mutation of *IPT* genes led to a drastic decrease in the levels of *t*Z and iP-type CKs in both roots and shoots (Figure 2A). In accordance with the predominant role of *IPT3* and *IPT5* in NO_3^--dependent CK biosynthesis (Takei et al., 2004), *t*Z and iP-type CKs were still synthetized in *ipt3,5,7* and were not regulated by NO_3^- provision (Figure 2A). Contrary to previous observations, the *ipt3,5,7* mutations did not lead to a compensatory accumulation of *c*Z-type CK (Miyawaki et al., 2006) but rather led to a significant decrease in the accumulation

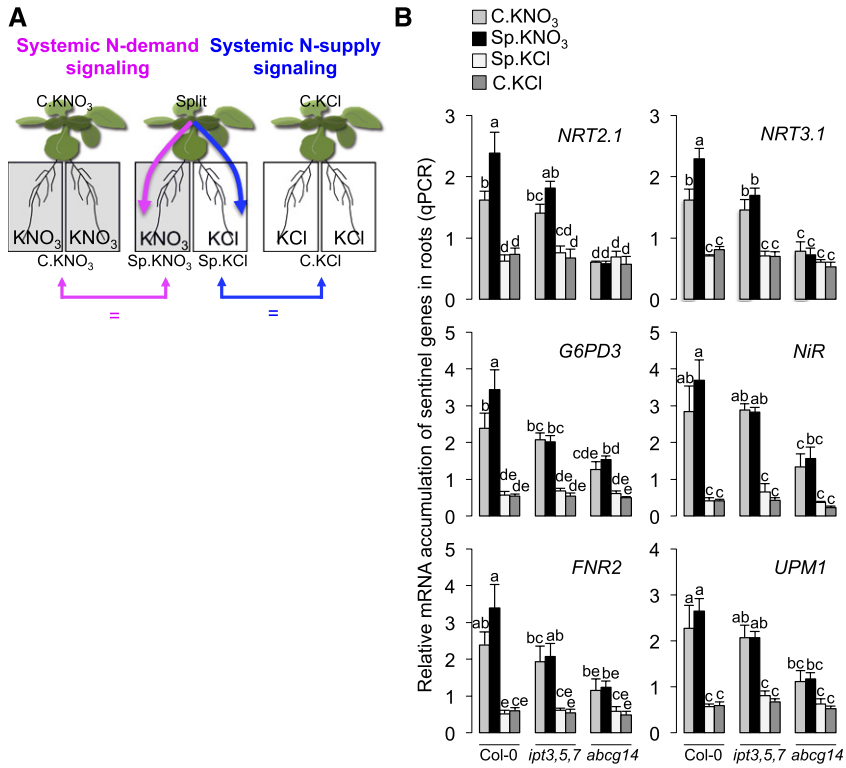

Figure 1. Perturbation of Root-to-Shoot Translocation of CK Impairs the Response of Sentinel Genes to Systemic N-Demand Signaling.

(A) Wild-type and mutant plants were grown under split-root conditions to decipher systemic N-demand and N-supply signaling by comparing root responses (molecular and integrated traits) in plants treated with the same local environment, as indicated by the equal signs. C.KNO_3 and C.KCl indicate control conditions (homogeneous KNO_3 or KCl supply). Sp.KNO_3 and Sp.KCl indicate heterogeneous conditions with KNO3 supply for one-half of the root system and KCl supply for the other part.

(B) Relative mRNA accumulation of sentinel genes in wild-type (Col-0), *ipt3,5,7*, and *abcg14* roots measured by qPCR 6.5 h after transfer to C.KNO_3, Sp.KNO_3/Sp.KCl, and C.KCl conditions. Bar graphs display the expression values of the six sentinel genes *NRT2.1*, *NRT3.1*, *G6PD3*, *NiR*, *FNR2*, and *UPM1*. Values are means (±SE) of three independent experiments, each consisting of two biological replicates corresponding to a pool of three plants grown for 27 d under hydroponic conditions. Different letters indicate significant difference (two-way ANOVA, Tukey post-hoc test, $P < 0.1$).

of this CK-type in roots under our conditions (Figure 2A). Interestingly, an increase in global *c*Z-type accumulation was instead observed in *abcg14* shoots in response to N deprivation (C.KCl) (Figure 2A). A more detailed analysis of *c*Z-type CK revealed that only the levels of *O*-glucosylated forms of *c*Z increased in *ipt3,5,7* under all conditions (Supplemental Data Set 1), whereas in *abcg14*, the levels of all *c*Z-forms, except ribotides, increased in shoots as soon as N provision was limited (Supplemental Data Set 1). Altogether, these results demonstrate that *c*Z-type homeostasis is indeed modified when methylerythritol phosphate pathway-dependent CKs are perturbed. In addition, our experimental setup provides an interesting framework to investigate the role of *c*Z forms in maintaining the minimal CK activity in shoots required for abiotic stress responses (Schäfer et al., 2015).

The perturbations of CK partitioning and accumulation observed in the *abcg14* mutant were consistent with previous data (Ko et al., 2014; Zhang et al., 2014). We indeed observed an increase in the accumulation of *t*Z-, iP-, and DHZ-type CKs in roots and a decrease in the accumulation of *t*Z-type CKs in shoots, in accordance with the role of ABCG14 in root-to-shoot translocation of CK (Figure 2A). Moreover, iP accumulation in the *abcg14* mutant increased in response to NO_3^- provision (Supplemental Data Set 1). Interestingly, the shoot iP content of wild-type plants followed the level of root N provision, and this aspect was very strongly affected in the *abcg14* mutant (Supplemental Data Set 1). In more detail, the *abcg14* mutant exhibited reduced accumulation of active iP forms in C.KNO3 and higher accumulation of all iP-forms in C.KCl (Supplemental Data Set 1). Therefore, taken together, these results demonstrate that the dynamic accumulation of *t*Z in shoots is under the control of the ABCG14 protein and that this differential accumulation also controls the N-responsive accumulation of iP-type CKs.

The Levels of the Active Forms of *t*Z in Shoots Control Root Responses to Systemic N-Demand Signaling

To investigate the early responses of sentinel genes to systemic N-demand signaling and their perturbations in the mutant backgrounds (Figure 1B), we analyzed the accumulation of active

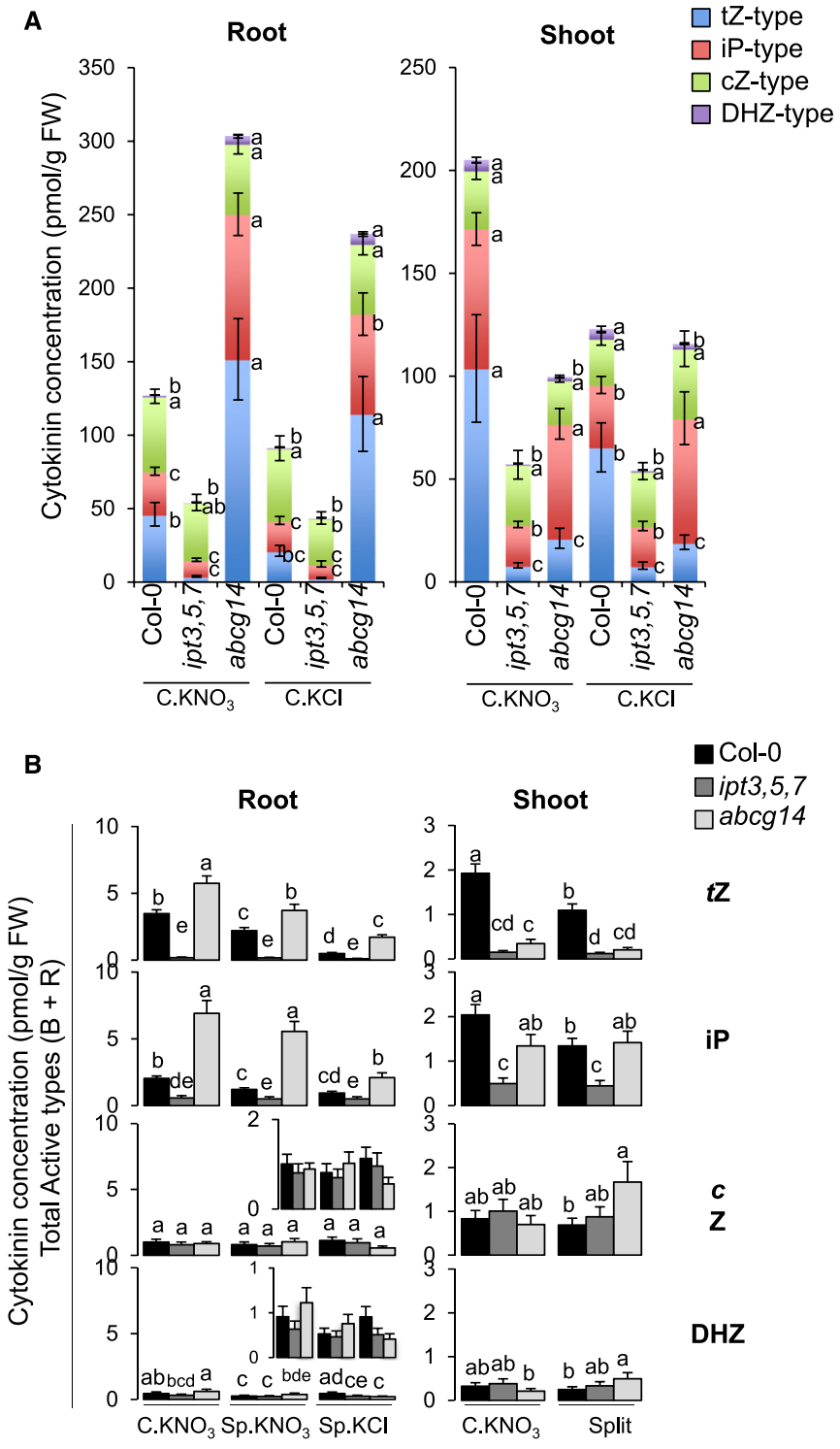

Figure 2. Root and Shoot Concentrations of Various Types of CK Points to a Role for *t*Z Accumulation in Shoots.

(A) Stacked bar graphs showing total CK concentrations and distribution of *t*Z, iP, *c*Z, and DHZ types of CK in the roots (left graph) and shoots (right graph) of wild-type (Col-0) and mutant (*ipt3,5,7* and *abcg14*) plants exposed to homogeneous $C.KNO_3$ or C.KCl conditions for 6.5 h.

(B) Bar graphs showing the concentrations of active and transported (base and riboside) CK (*t*Z, iP, *c*Z, and DHZ) in the roots (left graphs) and shoots (right graphs) of wild-type (Col-0) and mutant (*ipt3,5,7* and *abcg14*) plants exposed to homogeneous $C.KNO_3$ and heterogeneous $Sp.KNO_3$ or Sp.KCl conditions. The two insets in the two graphs at the bottom left are magnified versions of the corresponding graphs below.

In both panels, values are means (±SE) of four to five biological replicates collected from four independent experiments, each consisting of a pool of three plants grown for 27 d under hydroponic conditions. Different letters indicate significant differences between treated plants (two-way ANOVA, Tukey post-hoc test, $P < 0.05$).

and transported forms of CK (Base and Riboside) in roots and shoots in the split-root system (Figure 1A). No obvious correlation was detected between gene expression (Figure 1B) and the accumulation of active forms of CK in roots (Figure 2B, left panel). Indeed, *ipt3,5,7* and *abcg14* plants displayed opposite phenotypes concerning *t*Z and iP accumulation, whereas under the same conditions, both genotypes displayed the same gene expression profile (i.e., the loss of N-demand signaling). We thus conclude that CK accumulation in roots cannot explain sentinel gene expression. However, *t*Z accumulation in shoots could explain the results of root transcriptomic profiling. Indeed, *t*Z accumulation in shoots was reduced in both *ipt3,5,7* and *abcg14* (Figure 2B, right panel). Moreover, iP concentrations in shoots could not explain sentinel gene expression patterns, since *ipt3,5,7* but not *abcg14* displayed a significant decrease in the expression of these genes compared with the wild type. Similarly, *c*Z and DHZ concentrations could not explain root responses, since *abcg14* but not *ipt3,5,7* showed a significant increase in these concentrations compared with the wild type. In conclusion, our analysis of *ipt3,5,7* and *abcg14* indicated that *t*Z accumulation in shoots likely mediates gene expression in roots in response to long-distance N-signaling.

Moreover, it is noteworthy that differential accumulation of *t*Z in roots between C.KNO_3 and Sp.KNO_3 conditions was observed in both the wild type and *abcg14* (Figure 2B, left panel). This indicates that CK accumulation in roots is controlled by systemic N-demand signaling that is independent of CK itself. This resembles what we observed previously for lateral root elongation, which includes both CK-dependent and -independent branches (Ruffel et al., 2016).

Genetic Reprogramming in Shoots in Response to Heterogeneous NO_3^- Supply Is Perturbed in Cytokinin Biosynthesis and Translocation Mutants

Since we demonstrated that *t*Z accumulation in shoots likely mediates molecular responses in roots to long-distance N-demand signaling, we decided to evaluate how the shoot transcriptome response in plants under homogeneous or heterogeneous NO_3^- supply is affected in *ipt3,5,7* and *abcg14* (Figure 3A), using Arabidopsis Gene1.1 ST Affymetrix array strips (see Methods for details on samples, arrays, and data analysis). By specifically analyzing gene expression data in the wild type, we found 745 nonambiguous significant differentially expressed genes between C.KNO_3 and Split conditions in shoots (Supplemental Data Set 2). Among these, we found 397 upregulated genes under Split conditions compared with the control C.KNO_3 and 348 downregulated genes under Split conditions compared with the control C.KNO_3. Notably, we based our gene selection only on the results of the statistical test because at this stage of the analysis, we did not make any assumption about the level of gene expression differences that would functionally affect the shoot response. Hierarchical clustering of their expression level in the two treatments (homogeneous and heterogeneous NO_3^- supply) and the three genotypes revealed that the regulation of gene expression by heterogeneous NO_3^- provision detected in the wild type was strongly affected in the two mutants (Figure 3B). Therefore, in addition to being impaired in *t*Z accumulation in response to NO_3^- supply, the two CK mutants are affected in their capacity to reprogram gene expression in response to NO_3^- supply, which likely disrupts systemic N-signaling controlling root responses. Interestingly, the annotation of these genes revealed the enrichment of some functional terms, revealing biological functions likely under the control of CK accumulation in shoots. Among the genes upregulated under heterogeneous compared with homogeneous NO_3^- conditions, we found a significant enrichment of two interpro domains, ipr000583 and ipr017932, which both correspond to a glutamine amidotransferase class II domain found in three genes involved in glutamate biosynthesis (i.e., AT2G41220, AT3G24090, and AT5G04140) (Figure 3B, gene cluster c1, and Figure 3D, word cloud c1). Moreover, overrepresentation of the glutamine term was also found for four other genes annotated as glutamine amidotransferase class I and glutamate-ammonia ligase (i.e., AT1G53280, AT3G53180, AT4G26900, and AT4G30550) (Figure 3B, gene cluster c1, and Figure 3D, word cloud c1). These results suggest that, even if NO_3^- is the genuine signal that triggers systemic N-demand signaling (Ruffel et al., 2011), its heterogeneous supply triggers the modification of a N assimilation pathway in shoots in a CK-dependent manner. Similarly, we observed functional term enrichment among the genes downregulated under heterogeneous compared with homogeneous NO_3^- conditions that corresponded to the interpro domain ipr006688 found in three ADP-ribosylation factors (i.e., AT3G49860, AT5G14670, and AT1G02440) and duo1 (or germline-specific) found in two genes annotated as encoding C2H2 zinc-finger proteins and the *HAPLESS2* gene (i.e., AT4G35280, AT4G35700, and AT4G11720) (Figure 3B, gene cluster c2, and Figure 3D word cloud c2).

By integrating the expression levels of the whole genome data set (i.e., three genotypes and two treatments), we also identified 669 unique genes that responded similarly to NO_3^- treatment in the shoots of the three genotypes, without making any assumptions about gene expression ratios between the conditions (Supplemental Data Set 3). These genes are those whose regulation is likely not related to CK-dependent long-distance signaling. Hierarchical clustering displayed a first level of classification based on differential regulation under NO_3^- heterogeneous versus homogeneous conditions (Figure 3C). Functional term enrichment analysis of these genes revealed a variety of meaningful terms, including, for example, the term "uba-like" for three genes related to ubiquitination processes (i.e., AT2G17190, AT4G11740, and AT5G50870) (Figure 3D, word cloud c3).

Altogether, this shoot transcriptomic analysis revealed the massive and rapid reprogramming of gene expression accompanying the accumulation of distinct CKs in response to NO_3^- supply. Moreover, this allowed us to confirm the occurrence of CK-dependent and CK-independent branches of systemic N signaling (Ruffel et al., 2011, 2016) and shed light on the biological pathways associated with the respective signals.

ipt3,5,7 and *abcg14* Plants Are Affected in Integrated Root Traits in Response to Heterogeneous NO_3^- Supply

At the molecular level, sentinel genes that respond specifically and rapidly to a CK-dependent systemic N-demand signaling

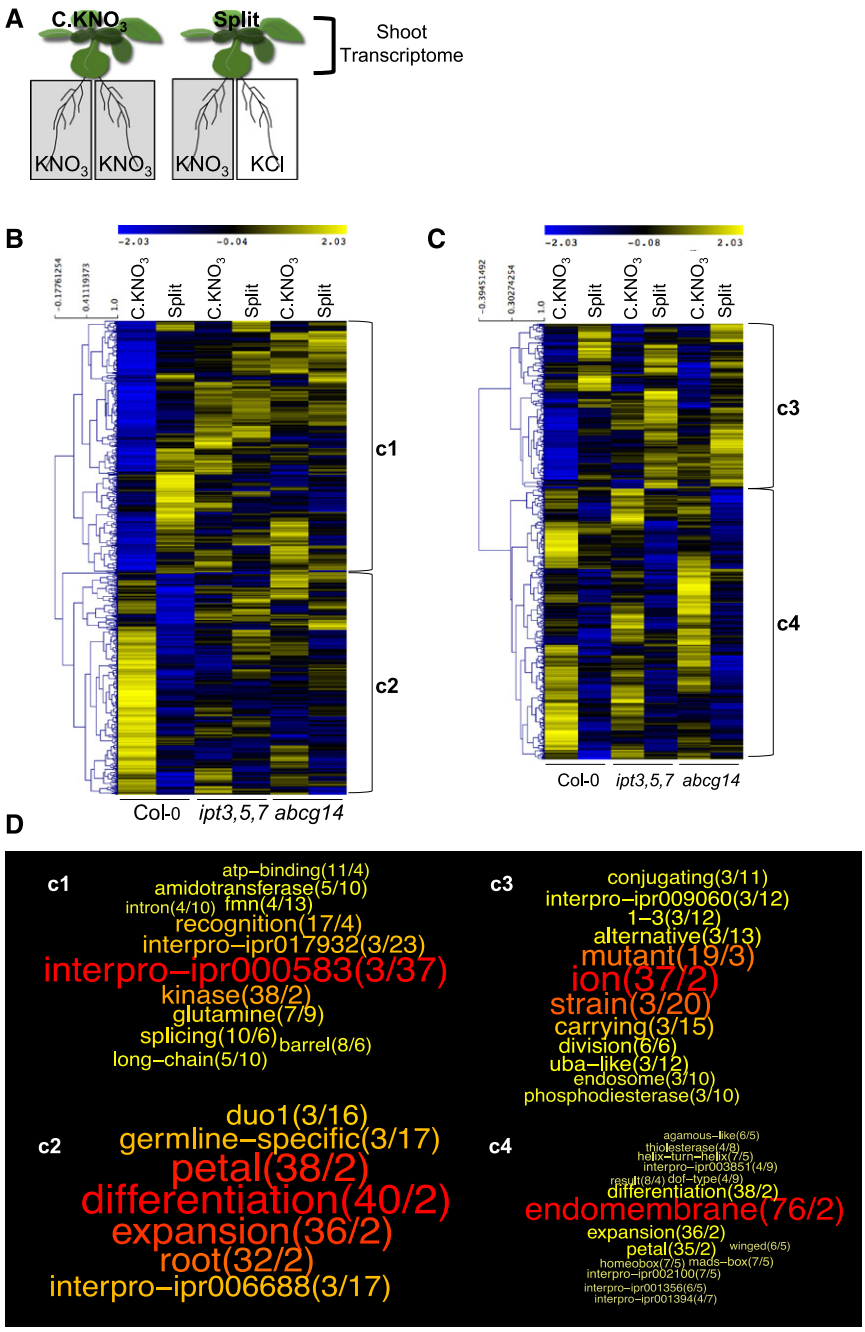

Figure 3. CK-Dependent and -Independent Changes in the Shoot Transcriptome in Response to Heterogeneous NO_3^- Supply to Roots.

(A) Schematic diagram of the experimental design. Transcriptomic analysis of gene expression was performed in shoots of wild-type (Col-0) and mutant (*ipt3,5,7* and *abcg14*) plants following 24 h incubation under NO_3^- homogeneous ($C.KNO_3$) or heterogeneous (split) conditions. Samples of four biological replicates, each consisting of a pool of three plants grown for 18 d in in vitro conditions, from four independent experiments were used to perform the microarray analysis using Arabidopsis Gene1.1 ST Array Strips (Affymetrix GeneAtlas).

(B) Hierarchical clustering of the 745 genes identified as differentially expressed under homogeneous versus heterogeneous conditions specifically in the wild type (Supplemental Data Set 2) was performed with MeV software (http://mev.tm4.org/). The scale on the left of the cluster indicates the distance threshold between gene expression levels based on Pearson correlation. The tree was drawn using the average linkage method. Each cluster is divided in two gene populations according to the most distant node, resulting in two subclusters named c1 and c2.

(C) Hierarchical clustering of the 669 genes identified as differentially expressed under homogeneous versus heterogeneous conditions in the three genotypes (Supplemental Data Set 3). Clustering was performed exactly as described in **(B)**. The two subclusters are named c3 and c4.

(D) Word clouds based on functional term enrichment of the four subclusters examined via GeneCloud analysis (https://m2sb.org). The first number next to each term (in parentheses) corresponds to the number of genes containing the term and the second number indicates the fold enrichment. The words (or terms) are displayed in a range from red to yellow in order to highlight the different sizes of text, which are proportional to the product between the occurrence of the word and the enrichment ratio.

are largely involved in NO_3^- transport and assimilation (e.g., *NRT2.1* and *NiR*) (Figure 1B). Therefore, we asked to what extent genetic perturbation of biosynthesis and root-to-shoot translocation of CK could affect the associated long-term acclimation of root physiology to variable N supply. We specifically assayed root NO_3^- influx capacity and biomass (e.g., root dry weight). We also investigated the relationship between these two components of N acquisition. To do so, we combined root traits on single graphs, which allowed us to take into account the variability of plant growth between independent biological replicates (independent plants and experiments) (Figure 4A).

In the wild type, both components (root dry weight and NO_3^- transport) responded significantly to systemic N-signaling (N-demand and N-supply), since the mean values were significantly higher under Sp.KNO_3 (5.8 mg and 92 μmol $N{\cdot}h^{-1}{\cdot}g^{-1}$ root dry weight [DW]) compared with C.KNO_3 (3.6 mg and 56 μmol $N{\cdot}h^{-1}{\cdot}g^{-1}$ root DW) conditions and lower under Sp.KCl (2.9 mg and 28 μmol $N{\cdot}h^{-1}{\cdot}g^{-1}$ root DW) compared with C.KCl (4.3 mg and 74 μmol $N{\cdot}h^{-1}{\cdot}g^{-1}$ root DW) conditions (Figure 4A, upper graphs). Interestingly, this analysis revealed the existence of a relationship between the two regulated processes measured in NO_3^- supplied roots (i.e., transport and biomass). Indeed, wild-type plants that had a strong developmental response displayed a lower NO_3^- transport response and vice versa, suggesting that the global level of NO_3^- acquisition by roots results from an interaction between development and transport (Figure 4A, top left).

In the CK mutants, root biomass and NO_3^- influx responses to systemic N-demand signaling were strongly perturbed (Figure 4A, left panel), suggesting that CK and especially root-to-shoot translocation of CK is a limiting factor in root responses to a heterogeneous NO_3^- environment. The stimulation of root biomass production observed in the wild type under Sp.KNO_3 conditions compared with C.KNO_3 conditions was abolished in the CK mutants (Figure 4A, left panel). According to the strategy of wild-type plants described above, one would expect that the smallest root systems would display a greater increase in NO_3^- influx as an alternative strategy to compensate for distal N deprivation. Thus, the CK mutants might compensate for their root biomass phenotype by increasing their NO_3^- transport activity. However, this effect was not observed. Indeed, if we consider only roots with a dry biomass under 2 mg (those with the greatest adaptations in NO_3^- transport in the wild type), wild-type roots under Sp.KNO_3 conditions displayed a significant (2-fold) increase in NO_3^- influx. By contrast, the CK mutants did not display any response to this treatment (Figure 4B, top left graph). However, when the dry biomass was >2 mg, the *ipt3,5,7* mutant displayed a NO_3^- influx response (Figure 4B, top right graph). This suggests that despite the dramatic alteration of CK contents (Figure 2), signaling pathways can still operate to some extent in the triple mutant to trigger an acclimated NO_3^- transport response to heterogeneous NO_3^- supply. Overall, CK appears to be central for the two intertwined long-term responses to heterogeneous NO_3^- supply, namely, NO_3^- transport and root development.

The two CK mutants did not behave similarly in response to systemic N-supply signaling (Figure 4A, right panel). Whereas CK biosynthesis was required to stimulate root proliferation and NO_3^- influx when N was completely absent from the medium (Figure 4A, graph on middle right), *abcg14* still maintained a NO_3^- influx capacity similar to that in the wild type (i.e., 71 and 74 μmol $N{\cdot}h^{-1}{\cdot}g^{-1}$ root, respectively), albeit *abcg14* displayed higher variability than the wild type (Figure 4A, graphs on top and bottom right).

Given that CK mutants displayed reduced shoot biomass (Figure 4C, *y* axis), we exploited the phenotypic variability in order to rule out the notion that their response defect was due to their small size. Specifically, we extracted biological repeats among the three genotypes displaying the same shoot biomass for each condition (i.e., the smallest in Col-0 and largest in the mutants). Using these samples, we confirmed the trend in NO_3^- influx responses described above (Figure 4A). Indeed, the *ipt3,5,7* mutant displayed the systemic regulation of NO_3^- influx based on its increased capacity only in roots under Sp.KNO_3 conditions, whereas *abcg14* displayed an increased capacity only in roots under C.KCl conditions (Figure 4B, bottom graph). These results confirm that the two mutants are affected in their response to systemic N signaling, which cannot be explained by their shoot growth defects (Figure 4B, bottom graph).

Unambiguously, root growth responses to systemic N demand and N supply are impaired by the alteration of CK biosynthesis or partitioning. Therefore, we looked at the impact of CK mutation on the modulation of an even more integrative trait controlled by N provision, that is, the shoot/root ratio (Figure 4C). Compared with the wild type, whose shoot/root ratio varied according to the level of N supply, alterations in CK biosynthesis and partitioning resulted in an unchanged shoot/root ratio in the mutants. This result suggests that these mutants would not be able to direct their growth toward the shoots or roots to acclimate the growth of the whole plant to fluctuating environmental conditions, i.e., variations in NO_3^- availability in the soil.

We conclude that CKs are likely integral to the control of long-term plant acclimation to NO_3^- heterogeneity, but with some specificity according to the type of systemic N signaling. For instance, root-to-shoot *tZ* translocation or *tZ* levels in shoots are not likely involved in regulating NO_3^- uptake capacity in roots when plants are totally N-deprived (Figure 4A, graph bottom right).

Local NO_3^- Response Is Not Impaired in Cytokinin Mutants

We previously showed that root responses to heterogeneous NO_3^- supply depend on a long-distance signaling network triggered by NO_3^- per se (Ruffel et al., 2011). Indeed, the regulation of the specific and early sentinel genes under heterogeneous conditions is similar between wild-type and NR-null (nitrate reductase-null) mutant plants, leading to the conclusion that the perception of NO_3^- is a prerequisite to trigger the response to systemic signaling (Ruffel et al., 2011). Thus, we performed further experiments to rule out the possibility that *ipt3,5,7* and *abcg14* plants are impaired in their molecular and physiological responses to heterogeneous NO_3^- conditions only because they cannot perceive local NO_3^- supply. We first tested the PNR (Medici and Krouk, 2014) in the two mutants by transferring plants from N-free solution to 1 mM KNO_3 or 1 mM KCl for 30 min. In the two mutants, the activation of PNR was similar

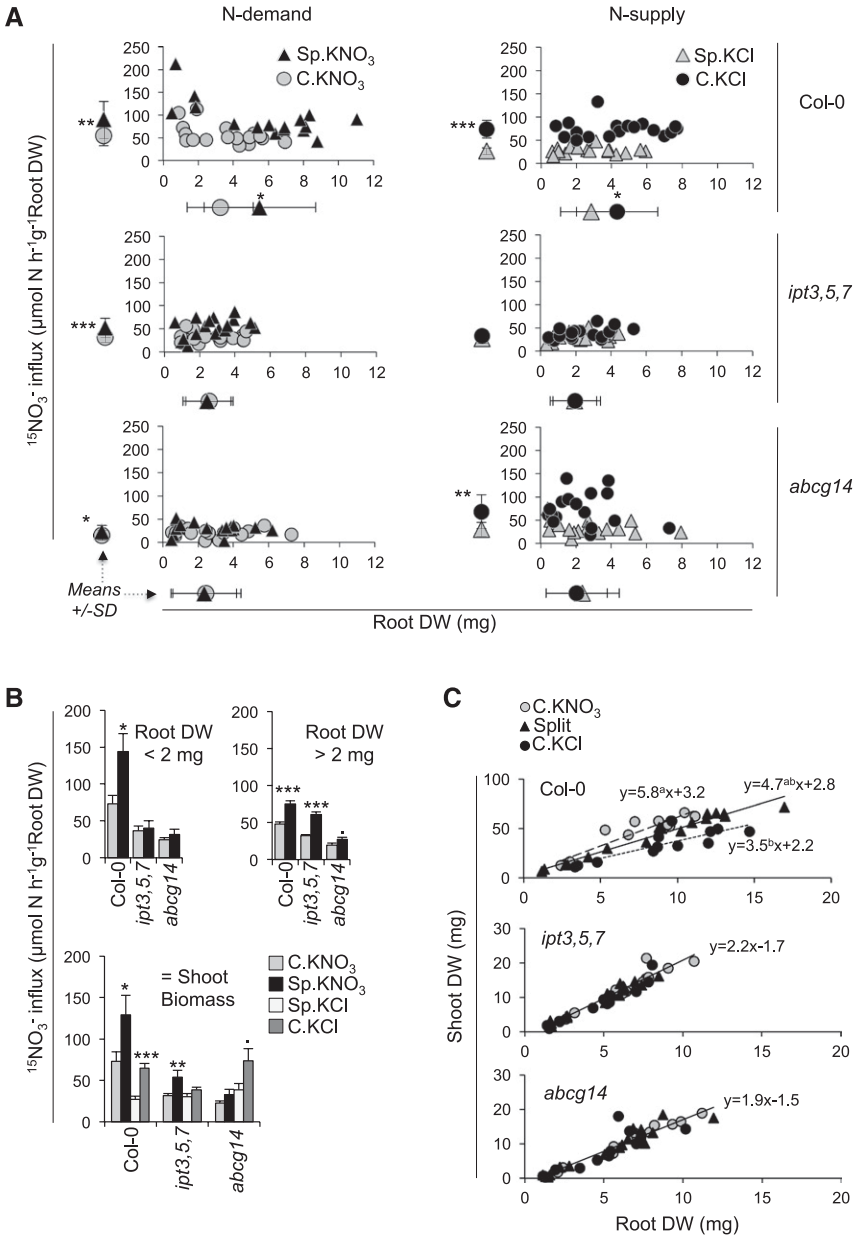

Figure 4. Responses of Integrated Traits to Systemic N Signaling Are Affected in CK Mutants.

(A) Individual $^{15}NO_3^-$ influx in roots plotted against individual root biomass in wild-type (Col-0), *ipt3,5,7*, and *abcg14* plants under $C.KNO_3$, split, or C.KCl conditions for 4 d. Average (±SE) root biomass and average (±SE) root $^{15}NO_3^-$ influx are shown below and to the left of each plot, respectively. In the left column plots, the effects of systemic N-demand signaling are shown via a comparison of $C.KNO_3$ and $Sp.KNO_3$ roots. In the right column plots, the effects of systemic N-supply signaling are shown via a comparison of C.KCl and Sp.KCl roots. Top, middle, and bottom row plots correspond to Col-0, *ipt3,5,7*, and *abcg14*, respectively. Data were obtained from five to six biological replicates of plants grown for 31 (27+4) d and collected from three independent experiments. Asterisks indicate significant differences (Student's *t* test, *P < 0.05, **P < 0.01, and ***P < 0.001).

(B) Average (±SE) root NO_3^- influx in wild-type (Col-0), *ipt3,5,7*, and *abcg14* plants under NO_3^- homogeneous ($C.KNO_3$), heterogeneous ($Sp.KNO_3$/Sp.KCl) conditions or N-deprived homogeneous (C.KCl) conditions for a selected subset of plants presented in **(A)**. To generate the two bar graphs on top, we used NO_3^- influx measurements from roots displaying dry weight less than (to the left) or greater than (to the right) 2 mg. This threshold was chosen according to the biomass distribution observed in Col-0 (graph on top left in **[A]**). For the third bar graph, we used root NO_3^- influx measurements from plants displaying an equivalent shoot biomass for the three genotypes for each condition. Asterisks indicate significant differences between $C.KNO_3$ and $Sp.KNO_3$ or between Sp.KCl and C.KCl (Student's *t* test, ·P < 0.1, *P < 0.05, **P < 0.01, and ***P < 0.001).

(C) Shoot/root ratio in response to NO_3^- availability under split-root conditions. Scatterplots indicate the relationship between root and shoot dry biomass in wild-type (Col-0), *ipt3,5,7*, and *abcg14* plants treated in $C.KNO_3$, split, or C.KCl conditions using plants from **(A)**. For each genotype and each condition, linear regression modeling was performed. Statistical differences between the slopes and the intercepts were tested by covariance analysis. For Col-0, the three equations are displayed beside each model. Different letters above the value of each slope indicate significant differences between the slopes (no differences between the intercepts). For the two CK mutants, no significant differences were observed between the linear models. Therefore, the equation corresponds to a linear regression including the three conditions.

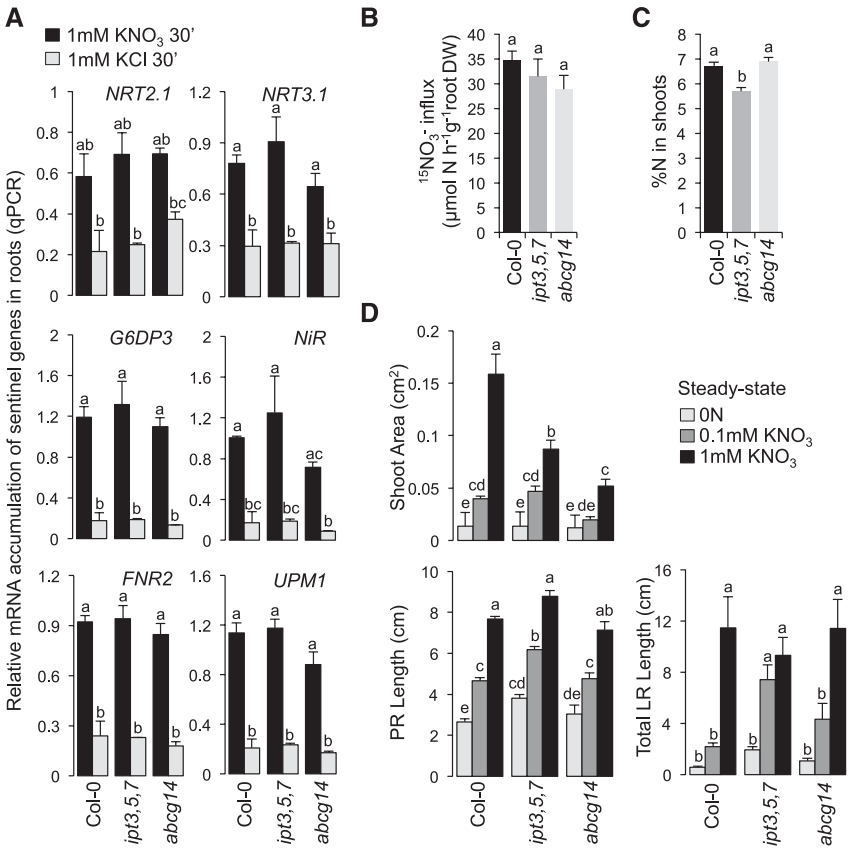

Figure 5. The Primary NO_3^- Response, NO_3^- Transport, Shoot N Status, and N-Dependent Root Development Are Not Impaired in CK Mutants.

(A) Relative mRNA accumulation of six sentinel genes of the primary NO_3^- response (*NRT2.1*, *NRT3.1*, *G6PD3*, *NiR*, *FNR2*, and *UPM1*) in roots of wild-type (Col-0), *ipt3,5,7*, and *abcg14* plants following 30 min incubation in medium containing 1 mM KNO_3 (dark bars) or 1 mM KCl (gray bars) as the control. Data are means (±SE) obtained from two independent experiments, each including two pools of five to six plants grown for 27 d under hydroponic conditions.

(B) Root $^{15}NO_3^-$ influx in 0.2 mM $K^{15}NO_3$ in wild-type (Col-0), *ipt3,5,7*, and *abcg14* plants after being exposed to KNO_3 1 mM for 30 min. Data are means (±SE) obtained from two independent experiments, each including 12 individual plants grown for 27 d under hydroponic conditions.

(C) Percentage of N in shoots of the three genotypes from plants collected at a stage corresponding to time 0 of the split-root treatments. Data are means (±SE) obtained from two independent experiments, each including 12 individual plants grown for 27 d under hydroponic conditions.

(D) Shoot area, lengths of primary and total lateral roots (PR and LR, respectively) in wild-type (Col-0) and mutant (*ipt3,5,7* and *abcg14*) plants grown for 17 d in N-free (0 N) or 0.1 mM or 1 mM KNO_3-containing medium. Data are means (±SE) determined from 6 to 12 plants.

Different letters indicate a significant difference (two-way ANOVA, Tukey post-hoc test, $P < 0.05$ for **[A]** and **[C]** and one-way ANOVA for **[B]**).

to that observed in wild-type plants (Figure 5A). The capacity of *ipt3,5,7* and *abcg14* plants to react to NO_3^- addition was also supported by the similar root NO_3^- influx level between the three genotypes at the same time point selected to evaluate PNR (Figure 5B).

Also, in order to rule out the possibility that *ipt3,5,7* and *abcg14* are impaired in their responses to heterogeneous NO_3^- conditions only because the N status of the shoots is different from the wild type, we determined the percentage of N in the shoots of the three genotypes. To do so, we used plants at the stage corresponding to the beginning of the split-root treatments. Interestingly, *ipt3,5,7* and *abcg14* displayed significantly different N% from each other (Figure 5C). Moreover, *abcg14* and wild-type plants displayed the same N% (Figure 5C), although their responses to heterogeneous NO_3^- conditions were the most different (Figures 1B and 4). These results suggest that the loss of responses to systemic N signaling in *ipt3,5,7* and *abcg14* mutants cannot be explained by some differences of the N status of the mutant plants.

Similarly, the absence of changes in root biomass in response to systemic N signaling in the mutants (Figure 4A) prompted us to verify that they are not simply restrained in their capacity to grow, independent of N supply conditions. When wild-type and mutant plants were grown on N-free, 0.1 mM KNO_3, or 1 mM KNO_3 containing medium, the primary root length and total lateral root length increased with increasing N concentration for all three genotypes (Figure 5D, bottom graphs), with a longer primary root observed in *ipt3,5,7*, as previously reported (Miyawaki et al., 2006). Moreover, under steady state conditions of N supply, wild-type and *abcg14* plants were similarly able to direct

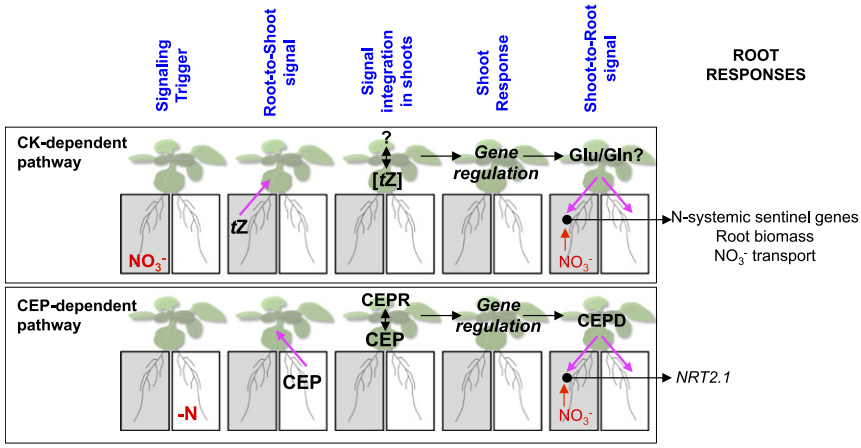

Figure 6. Multiple Systemic Signaling Pathways Likely Coexist to Coordinate Plant Responses to a Heterogeneous NO_3^- Environment.

In the CK-dependent pathway, NO_3^- itself appears to be the triggering signal of systemic N-demand signaling, since NO_3^- supplied roots are the main providers of *t*Z. The integration of *t*Z concentrations in shoots would lead to the differential regulation of genes under heterogeneous compared with homogeneous NO_3^- conditions, including the regulation of genes involved in glutamate and glutamine biosynthesis. Our model hypothesizes that these amino acids correspond to a shoot-to-root signal that, in combination with local NO_3^- presence, would enhance the expression of N-systemic sentinel genes as well as root biomass and NO_3^- transport. This proposed model diverges from the CEP-dependent pathway because CEP synthesis is triggered in N-deprived roots. These peptides, moving from roots to shoots, are perceived by CEPR (CEP receptor) kinase receptors. This recognition in shoots triggers the synthesis of CEPD (CEP downstream) peptides (glutaredoxin-like) corresponding to a shoot-to-root signal that, in combination with local NO_3^- presence, enhances *NRT2.1* expression (Tabata et al., 2014; Ohkubo et al., 2017; Ruffel and Gojon, 2017).

root growth matching the level of N provided to the plant (Figure 5D, bottom graphs), even though shoot growth was particularly impaired in the mutant background (Figure 5D, top graph). Thus, we confirmed that these mutants have the capacity for increased growth with increasing N supply.

Altogether, we conclude that CK biosynthesis and root-to-shoot translocation of CK do not affect NO_3^- perception, the potential to use N, or plant growth rates in accordance with N supply. Therefore, we confirmed that CK plays an important role in the fine-tuned functional root response to systemic N signaling that operates in a heterogeneous NO_3^- environment.

DISCUSSION

Functional root responses to NO_3^- availability are the result of a complex signaling network that integrates localized sensing of root NO_3^- availability with long-distance signaling aimed at coordinating the needs of different parts of the plant. Here, we showed that the integration of *t*Z content in shoots is likely an essential component of the long-distance N-signaling network controlling root responses. Our results, supported by previous works focusing on the functional characterization of genes involved in CK biosynthesis (Sakakibara et al., 2006; Kiba et al., 2013; Osugi et al., 2017), suggest that NO_3^- triggers *t*Z biosynthesis mainly in roots. This *t*Z would then be transported to the shoots via ABCG14, where it modifies gene expression and possibly associated metabolic processes. Therefore, our model proposes that NO_3^- provision leads to *t*Z accumulation in roots, which is subsequently transported to the shoots. Under this scenario, *t*Z translocation could even constitute part of the systemic signal itself. The accumulation of *t*Z, which differs between homogeneous and heterogeneous NO_3^- conditions, would then be interpreted in the shoots. This would lead to differential control of root responses according to NO_3^- supply to the roots through a shoot-to-root signal that still needs to be identified (Figure 6). Recently, major advances have been made regarding the role of CK in shoot growth and development, including some links with NO_3^- availability (Osugi et al., 2017; Landrein et al., 2018). These works shed light on the roles of *t*Z and *t*ZR in signaling mechanisms controlling leaf expansion or shoot apical meristem development through the regulation of *WUSCHEL* (regulator of stem cell homeostasis) expression. Therefore, it would be interesting to understand the extent to which these pathways are connected to the transcriptional regulation in shoots that we described here and how they play a role in adjusting molecular responses in roots to N availability.

The regulatory pathways of physiological and developmental acclimation to systemic N signaling (N demand and N supply) in roots and the role of CK in this signaling appear to be complex. For instance, the plant will compensate for a small root system by increasing NO_3^- uptake capacity (Figure 4A, top left graph), suggesting tight and reciprocal control of the regulatory pathways downstream of systemic N-demand signaling. This control does not seem to occur for root acclimation to total N deprivation, since NO_3^- uptake was stable across various sizes of root systems under C.KCl conditions (Figure 4A, top right graph). This tends to confirm the genetic uncoupling of signaling pathways that control the same root responses in roots under Sp.KNO_3 and C.KCl conditions (Ruffel et al., 2011). If on one hand, the role of CK in the control of root growth by systemic N signaling is clearly required, on the other hand, the role of CK in regulating NO_3^- transport capacity is more complex. Indeed, the

ipt3,5,7 triple mutant displayed an altered root response to systemic N-demand signaling, except for NO_3^- transport capacity (Figure 4A). This could be the result of a compensatory mechanism in the *ipt3,5,7* background. A more detailed analysis of CK concentrations in *ipt3,5,7* across the duration of split-root treatment could allow us to determine if CK biosynthesis by other IPT members or IPT-independent CK biosynthesis could be responsible for the acclimation of the NO_3^- uptake response. Similarly, the two mutants displayed different NO_3^- uptake levels under total N-deprivation conditions (C.KCl roots). In this case, we would be tempted to speculate that the stimulation of NO_3^- influx capacity in *abcg14* plants depends on the CK species, whose concentrations do not dramatically differ between the wild type and *abcg14*. Therefore, it would be interesting to assess the role of *c*Z level in roots (Figure 2A, left graph, C.KCl condition) to determine, specifically under this condition, the extent to which this particular CK-type participates to responses to growth limitation (Schäfer et al., 2015).

In shoots, glutamine biosynthesis is a functional term likely influenced by *t*Z accumulation (Figure 3D). Interestingly, amino acids are thought to serve as reporters of the N status of a plant (Cooper and Clarkson, 1989; Muller and Touraine, 1992). We therefore hypothesize that CK-dependent N-related signals might modify glutamine and/or glutamate metabolism in shoots and that this might be part of a branch of the shoot-to-root signal, as previously proposed by others (Imsande and Touraine, 1994; Girin et al., 2010; Gent and Forde, 2017). Of course, further studies are needed to validate this hypothesis, but our work provides experimental and genome-wide clues about the potential roles of amino acids in shoot-to-root N signaling.

We confirmed that CK accumulation is considerably affected in *ipt3,5,7* and *abcg14* plants (Figure 2) (Miyawaki et al., 2004; Ko et al., 2014; Zhang et al., 2014). Despite the strong repressive effect of local CK status on root development (Laplaze et al., 2007; Werner et al., 2010), we found that these mutants, particularly *abcg14*, still maintain a certain growth plasticity, particularly in response to homogenous NO_3^- supply (Figure 5C). This could be explained by recent findings regarding CK partitioning between the apoplasm and the cytosol. Indeed, an important aspect of CK signaling is that CKs are perceived in the apoplasm and that the PUP14 transporter is crucial for importing bioactive CKs into the cytosol and suppressing the CK response (Zürcher et al., 2016). In this regard, we believe that CK accumulation is important but active CK transport at the cellular level in roots can, to some extent, explain the responsiveness of *ipt3,5,7* and *abcg14* plants.

Finally, this work refines the model of the integration of different N-related long-distance signaling pathways, which displays some differences to the CEP-related long-distance pathway. Indeed, CEPs are synthesized in N-deprived roots and transported to the shoots where they are recognized by the related receptor kinase, CEPR (Tabata et al., 2014). This recognition activates the biosynthesis of CEPD polypeptides, which are transported to the root where they activate *NRT2.1* expression (Ohkubo et al., 2017). Thus, signaling in the CEP-dependent pathway is triggered by N deprivation. In our model, we suggest that the long-distance signal is generated by NO_3^- itself. Indeed, we observed that *t*Z accumulation is correlated with NO_3^- supply (Figure 2B). We thus hypothesize that the two pathways likely rely on different signaling modules (Figure 6). In nature, the shoot of a plant that is experiencing heterogeneous NO_3^- conditions in roots likely receives a combination of different long-distance signals arising from the different parts of the plant, which include CEP from N-deprived roots and CK from N-supplied roots. Future investigations will aim to resolve how plants integrate these different signaling pathways in shoots to enact a coherent response in roots.

METHODS

Plant Materials

Arabidopsis thaliana in the Col-0 background was used as the wild type. The *abcg14* (SK_15918) mutant line was kindly provided by Donghwi Ko (The Sainsbury Laboratory, Cambridge, UK). The *ipt3,5,7* triple mutant line was kindly provided by Sabrina Sabatini (University La Sapienza, Rome).

Plant Growth Conditions

All plants were grown under a short-day photoperiod (8 h light 23°C/16 h dark 21°C) at 260 μmol m^{-2} s^{-1} light intensity using a mix of sodium-vapor and metal halide 400-W lamps (in growth chambers used for hydroponic culture) and Osram 18-W 840 Lumilux neon tubes (for in vitro plant growth). Split-root in vitro culture was performed as previously described (Ruffel et al., 2011). Briefly, plants were grown on solid (1% agar type A) N-free modified basal Murashige and Skoog (MS) medium supplemented with 0.5 mM NH_4-succinate and 0.1 mM KNO_3 as N sources. On day 10, the primary root was cut off below the second lateral root in order to obtain two new primary roots. On day 14, the plants were transferred to 1 mM NH_4-succinate split medium in order to separate the root system into two isolated parts. On day 18, the plants were transferred to new split plates containing basal MS medium supplemented with (1) 1 mM KNO_3 on one side (Sp.KNO_3) and 1 mM KCl on the other side (Sp. KCl), (2) 1 mM KNO_3 on both sides (C.KNO_3), or (3) 1 mM KCl on both sides (C.KCl). For the split-root assay in the hydroponic system, seeds were sown on upside down Eppendorf caps with 1-mm holes filled with water-agar 0.7% solution and grown for 7 d on tap water. The seedlings were grown in nutrient solution containing KH_2PO_4 1 mM; $MgSO_4$,$7H_2O$ 1 mM; K_2SO_4 0.25 mM; $CaCl_2$,$2H_2O$ 2.5 mM; Na-Fe-EDTA 0.1 mM; KCl 50 μM; H_3BO_3 7.5 μM; $MnSO_4$,H_2O 1.25 μM; $ZnSO_4$,$7H_2O$ 0.25 μM; $CuSO_4$, $5H_2O$ 0.25 μM; and $(NH_4)6$ Mo_7 O_{24}, $4H_2O$ 0.025 μM supplemented with 1 mM NH_4Cl and 0.1 mM KNO_3 as N sources, pH 5.8. Nutrient solution was renewed every 4 d. At 17 d after sowing, the primary root was cut off below the second lateral root in order to obtain two root systems. Four days later, the plants were transferred to a split root system with 1 mM NH_4Cl as the sole N source for an additional 4 d to let the roots grow under split conditions. Twenty-four hours before treatment, the nutrient solution was replaced with N-free nutrient solution. Treatments were then applied by adding concentrated KNO_3 or KCl solution to each compartment up to a final concentration of 1 mM. For PNR analysis, plants were grown exactly as described for the split-root experiments, except that the primary root was not cut and, thus, the root system was not split into two parts at the time of treatment. To analyze root developmental traits, seeds were sown and plants grown for 17 d in vitro in square plates containing modified N-free basal MS containing 0.3 mM sucrose, 0.5 g/L MES, and 1% agar type A, supplemented with either 0, 0.1, or 1 mM KNO_3. Collection and analysis of plants tissues were performed as indicated in Results.

Gene Expression Analysis

Total RNA was extracted from frozen and ground root or shoot tissue using TRIzol reagent (15596026; Thermo Fisher Scientific) following

the manufacturer's instructions. RNA integrity and concentration were determined using a 2100 Bioanalyzer Instrument (Agilent) and Agilent RNA 6000 Nano kit (5067-1511). DNA contamination was removed by digestion with DNase I (AMPD1; Sigma-Aldrich). For RT-qPCR analysis, reverse transcription of mRNAs was done using ThermoScript RT-PCR (11146016; Thermo Fisher Scientific) according to the manufacturer's protocol. Gene expression levels were determined using a LightCycler 480 Instrument (Roche) and SYBR Premix Ex Taq (RR420L; TaKaRa). Expression levels of the tested genes were normalized using the expression levels of *ACTIN2/8* and *CLATHRIN*. All specific primers used in this study are listed in Supplemental Data Set 4. Genome-wide expression analysis in shoots was based on four biological replicates obtained from four independent experiments including the three treatments (i.e., C.KNO_3, Split, and C.KCl) and the three genotypes (i.e., Col-0, *ipt3,5,7*, and *abcg14*). Gene expression measurements were performed using Arabidopsis Affymetrix Gene 1.1 ST array strips designed to measure whole transcript accumulation of 28,501 genes (or transcripts clusters), based on 600,941 probes designed based on TAIR10 genome annotation. Biotin labeled and fragmented cRNAs were obtained using a GeneChip WT PLUS Reagent kit (902280; Thermo Fisher Scientific) following the manufacturer's instructions. Hybridization on array strips was performed for 16 h at 48°C. The arrays were washed, stained, and scanned using a GeneAtlas HWS Kit (901667; Thermo Fisher Scientific) on the GeneAtlas Fluidics and Imaging Station.

Statistical Analysis and Bioinformatics

All data analysis was performed using the program R and the ANOVA, TukeyHSD, or t.test functions (Supplemental Table 1). Microarrays raw data were processed with GCRMA available in the Expression Console Software package developed by Affymetrix. Genes differentially expressed specifically in the wild type were identified using Student's *t* test (P value < 0.05). Genes responding to the treatment in the three genotypes were identified using a two-way ANOVA that was modeled as follows: $Y = \mu + \alpha^{genotype} + \beta^{treatment} + (\alpha\beta)^{genotype*\,treatment} + \varepsilon$, where Y is the normalized expression signal of a gene, μ is the global mean, the α and β coefficients correspond to the effects of NO_3^- availability (homogeneous or heterogeneous) of the genotype and of the interaction between both factors, and ε represents unexplained variance. All genes for which at least the $\beta_{treatment}$ was significant (P value<0.05) to explain variation of expression were selected. Hierarchical clustering of gene expression was performed using Multiple Experiment Viewer v4.8 (MeV) software (Saeed et al., 2003). Functional analysis of gene lists was performed using the GeneCloud platform, and functional term enrichment was displayed using word clouds (https://m2sb.org; Krouk et al., 2015).

Determination of Cytokinin Levels

CK purification was performed according to previously described methods (Svačinová et al., 2012) with some modifications (Šmehilová et al., 2016). Briefly, CKs were extracted from 30 mg of frozen powdered tissue in modified Bieleski buffer (methanol/water/formic acid, 15/4/1, v/v/v) containing a cocktail of stable isotope-labeled internal standards (0.25 pmol of CK bases, ribosides, and *N*-glucosides; 0.5 pmol of CK *O*-glucosides and nucleotides added per sample) and purified using two solid phase extraction columns. CK concentration was determined by UHPLC-MS/MS (ultra-high-performance liquid chromatography coupled to a triple quadrupole mass spectrometer equipped with an electrospray interface). Quantification was performed with Masslynx software (v4.1; Waters) using a standard isotope dilution method. The ratio of endogenous CK to the appropriate labeled standard was determined and used to quantify the level of endogenous compounds in the original extract according to the known quantity of the added internal standard.

Determination of Root Biomass and Nitrate Influx Capacity

Root $^{15}NO_3^-$ influx was assayed as described previously (Muños et al., 2004). Root systems were rinsed with 0.1 mM $CaSO_4$ solution for 1 min, transferred to nutrient solution containing 0.2 mM $^{15}NO_3^-$ (99% atom excess ^{15}N), pH 5.8, for 5 min, and washed with 0.1 mM $CaSO_4$ solution for 1 min. Roots and shoots were harvested separately and dried in an oven at 70°C for 48 h. Dry weight was determined and the total N and atom % ^{15}N were determined by continuous-flow isotope ratio mass spectrometry using a Euro-EA Euro Vector elemental analyzer coupled with an IsoPrime mass spectrometer (GV Instruments).

Measurement of Shoot and Root Developmental Traits

Scans of square plates containing plants were performed at 600 dpi in TIFF format using an HP scanner. Shoot area, primary and lateral root length, and the number of lateral roots were measured using ImageJ software (https://imagej.nih.gov/ij/).

Accession Numbers

Sequence data for the genes mentioned in this article can be found in the Arabidopsis Genome Initiative database under the following accession numbers: *IPT3* (AT3G63110), *IPT5* (AT5G19040), *IPT7* (AT3G23630), *ABCG14* (AT1G31770), *NRT2.1* (AT1G08090), *NRT3.1* (AT5G50200), *G6PD3* (AT1G24280), *NiR* (AT2G15620), *FNR2* (AT1G30510), and *UPM1* (AT5G40850). The Affymetrix GeneChip data have been deposited in NCBI's Gene Expression Omnibus in compliance with MIAME standards (http://www.ncbi.nlm.nih.gov/geo/) and are accessible through Gene Expression Omnibus Series accession number GSE114162.

Supplemental Data

Supplemental Table 1. ANOVA, Tukey, and Student's *t* test tables.

Supplemental Data Set 1. Detailed CK concentrations (pmol/gFW), organized by type and form, in shoots and roots of Col-0, *ipt3,5,7*, and *abcg14.*

Supplemental Data Set 2. 745 genes significantly regulated by heterogeneous NO_3^- provision (split) compared with homogeneous NO_3^- conditions (C.KNO_3) specifically in Col-0 shoots.

Supplemental Data Set 3. 669 genes significantly regulated by heterogeneous NO_3^- provision (split) compared with homogeneous NO_3^- conditions (C.KNO_3) in the shoots of the three genotypes.

Supplemental Data Set 4. RT-qPCR primers used in this study.

ACKNOWLEDGMENTS

We thank Hugues Baudot and his team for taking care of the plant culture system, Franck Lecocq and Chantal Brachet for technical support, Pascal Tillard for ^{15}N measurements, and Hana Martínková for her help with phytohormone analyses. We also thank Denis Vile for his help for statistical analysis of the data. This work was supported by the Institut National de La Recherche Agronomique (CJS Fellowship to A.P. and BAP project VARNET to S.R.), by the National Science Foundation (IOS 1339362-NutriNet with a fellowship to A.C.), and by Agence Nationale de la Recherche (IMANA ANR-14-CE19-0008). I.P and O.N. were supported by the Czech Science Foundation (Project GA17-06613S) and the Ministry of Education, Youth, and Sports of the Czech Republic (National Program for Sustainability I; Grant LO1204).

AUTHOR CONTRIBUTIONS

A.P., A.C., I.P., and O.N. performed the research. A.P. and S.R. analyzed the data. G.K., B.L., and S.R. designed the research and wrote the manuscript.

Received January 8, 2018; revised March 19, 2018; accepted May 14, 2018; published May 15, 2018.

REFERENCES

Alvarez, J.M., Vidal, E.A., and Gutiérrez, R.A. (2012). Integration of local and systemic signaling pathways for plant N responses. Curr. Opin. Plant Biol. **15:** 185–191.

Alvarez, J.M., Riveras, E., Vidal, E.A., Gras, D.E., Contreras-López, O., Tamayo, K.P., Aceituno, F., Gómez, I., Ruffel, S., Lejay, L., Jordana, X., and Gutiérrez, R.A. (2014). Systems approach identifies TGA1 and TGA4 transcription factors as important regulatory components of the nitrate response of *Arabidopsis thaliana* roots. Plant J. **80:** 1–13.

Araus, V., Vidal, E.A., Puelma, T., Alamos, S., Mieulet, D., Guiderdoni, E., and Gutiérrez, R.A. (2016). Members of BTB gene family of scaffold proteins suppress nitrate uptake and nitrogen use efficiency. Plant Physiol. **171:** 1523–1532.

Araya, T., Miyamoto, M., Wibowo, J., Suzuki, A., Kojima, S., Tsuchiya, Y.N., Sawa, S., Fukuda, H., von Wirén, N., and Takahashi, H. (2014). CLE-CLAVATA1 peptide-receptor signaling module regulates the expansion of plant root systems in a nitrogen-dependent manner. Proc. Natl. Acad. Sci. USA **111:** 2029–2034.

Baena-González, E., Rolland, F., Thevelein, J.M., and Sheen, J. (2007). A central integrator of transcription networks in plant stress and energy signalling. Nature **448:** 938–942.

Bishopp, A., and Lynch, J.P. (2015). The hidden half of crop yields. Nat. Plants **1:** 15117.

Castaings, L., Camargo, A., Pocholle, D., Gaudon, V., Texier, Y., Boutet-Mercey, S., Taconnat, L., Renou, J.P., Daniel-Vedele, F., Fernandez, E., Meyer, C., and Krapp, A. (2009). The nodule inception-like protein 7 modulates nitrate sensing and metabolism in Arabidopsis. Plant J. **57:** 426–435.

Cooper, H.D., and Clarkson, D.T. (1989). Cycling of amino-nitrogen and other nutrient between shoots and roots in cereals: a possible mechanism integrating shoot and root in the regulation of nutrient uptake. J. Exp. Bot. **40:** 753–762.

Den Herder, G., Van Isterdael, G., Beeckman, T., and De Smet, I. (2010). The roots of a new green revolution. Trends Plant Sci. **15:** 600–607.

Filleur, S., Dorbe, M.F., Cerezo, M., Orsel, M., Granier, F., Gojon, A., and Daniel-Vedele, F. (2001). An Arabidopsis T-DNA mutant affected in Nrt2 genes is impaired in nitrate uptake. FEBS Lett. **489:** 220–224.

Gansel, X., Muños, S., Tillard, P., and Gojon, A. (2001). Differential regulation of the NO3– and NH4+ transporter genes AtNrt2.1 and AtAmt1.1 in Arabidopsis: relation with long-distance and local controls by N status of the plant. Plant J. **26:** 143–155.

Gent, L., and Forde, B.G. (2017). How do plants sense their nitrogen status? J. Exp. Bot. **68:** 2531–2539.

Gifford, M.L., Dean, A., Gutierrez, R.A., Coruzzi, G.M., and Birnbaum, K.D. (2008). Cell-specific nitrogen responses mediate developmental plasticity. Proc. Natl. Acad. Sci. USA **105:** 803–808.

Girin, T., El-Kafafi, S., Widiez, T., Erban, A., Hubberten, H.M., Kopka, J., Hoefgen, R., Gojon, A., and Lepetit, M. (2010). Identification of Arabidopsis mutants impaired in the systemic regulation of root nitrate uptake by the nitrogen status of the plant. Plant Physiol. **153:** 1250–1260.

Gruber, B.D., Giehl, R.F., Friedel, S., and von Wirén, N. (2013). Plasticity of the Arabidopsis root system under nutrient deficiencies. Plant Physiol. **163:** 161–179.

Guan, P., Wang, R., Nacry, P., Breton, G., Kay, S.A., Pruneda-Paz, J.L., Davani, A., and Crawford, N.M. (2014). Nitrate foraging by Arabidopsis roots is mediated by the transcription factor TCP20 through the systemic signaling pathway. Proc. Natl. Acad. Sci. USA **111:** 15267–15272.

Guan, P., Ripoll, J.-J., Wang, R., Vuong, L., Bailey-Steinitz, L.J., Ye, D., and Crawford, N.M. (2017). Interacting TCP and NLP transcription factors control plant responses to nitrate availability. Proc. Natl. Acad. Sci. USA **114:** 2419–2424.

Ho, C.H., Lin, S.H., Hu, H.C., and Tsay, Y.F. (2009). CHL1 functions as a nitrate sensor in plants. Cell **138:** 1184–1194.

Hu, H.C., Wang, Y.Y., and Tsay, Y.F. (2009). AtCIPK8, a CBL-interacting protein kinase, regulates the low-affinity phase of the primary nitrate response. Plant J. **57:** 264–278.

Imsande, J., and Touraine, B. (1994). N demand and the regulation of nitrate uptake. Plant Physiol. **105:** 3–7.

Kellermeier, F., Armengaud, P., Seditas, T.J., Danku, J., Salt, D.E., and Amtmann, A. (2014). Analysis of the root system architecture of Arabidopsis provides a quantitative readout of crosstalk between nutritional signals. Plant Cell **26:** 1480–1496.

Kiba, T., Takei, K., Kojima, M., and Sakakibara, H. (2013). Side-chain modification of cytokinins controls shoot growth in Arabidopsis. Dev. Cell **27:** 452–461.

Ko, D., et al. (2014). Arabidopsis ABCG14 is essential for the root-to-shoot translocation of cytokinin. Proc. Natl. Acad. Sci. USA **111:** 7150–7155.

Kong, X., Zhang, M., De Smet, I., and Ding, Z. (2014). Designer crops: optimal root system architecture for nutrient acquisition. Trends Biotechnol. **32:** 597–598.

Konishi, M., and Yanagisawa, S. (2013). Arabidopsis NIN-like transcription factors have a central role in nitrate signalling. Nat. Commun. **4:** 1617.

Krouk, G., et al. (2010b). Nitrate-regulated auxin transport by NRT1.1 defines a mechanism for nutrient sensing in plants. Dev. Cell **18:** 927–937.

Krouk, G. (2016). Hormones and nitrate: a two-way connection. Plant Mol. Biol. **91:** 599–606.

Krouk, G. (2017). Nitrate signalling: Calcium bridges the nitrate gap. Nat. Plants **3:** 17095.

Krouk, G., Mirowski, P., LeCun, Y., Shasha, D.E., and Coruzzi, G.M. (2010a). Predictive network modeling of the high-resolution dynamic plant transcriptome in response to nitrate. Genome Biol. **11:** R123.

Krouk, G., Ruffel, S., Gutiérrez, R.A., Gojon, A., Crawford, N.M., Coruzzi, G.M., and Lacombe, B. (2011). A framework integrating plant growth with hormones and nutrients. Trends Plant Sci. **16:** 178–182.

Krouk, G., Carré, C., Fizames, C., Gojon, A., Ruffel, S., and Lacombe, B. (2015). GeneCloud reveals semantic enrichment in lists of gene descriptions. Mol. Plant **8:** 971–973.

Landrein, B., Formosa-Jordan, P., Malivert, A., Schuster, C., Melnyk, C.W., Yang, W., Turnbull, C., Meyerowitz, E.M., Locke, J.C.W., and Jönsson, H. (2018). Nitrate modulates stem cell dynamics in *Arabidopsis* shoot meristems through cytokinins. Proc. Natl. Acad. Sci. USA **115:** 1382–1387.

Laplaze, L., et al. (2007). Cytokinins act directly on lateral root founder cells to inhibit root initiation. Plant Cell **19:** 3889–3900.

Léran, S., Edel, K.H., Pervent, M., Hashimoto, K., Corratgé-Faillie, C., Offenborn, J.N., Tillard, P., Gojon, A., Kudla, J., and Lacombe, B. (2015). Nitrate sensing and uptake in Arabidopsis are enhanced by ABI2, a phosphatase inactivated by the stress hormone abscisic acid. Sci. Signal. **8:** ra43.

Li, C., Potuschak, T., Colón-Carmona, A., Gutiérrez, R.A., and Doerner, P. (2005). Arabidopsis TCP20 links regulation of growth and cell division control pathways. Proc. Natl. Acad. Sci. USA **102:** 12978–12983.

Li, Y., Krouk, G., Coruzzi, G.M., and Ruffel, S. (2014). Finding a nitrogen niche: a systems integration of local and systemic nitrogen signalling in plants. J. Exp. Bot. **65:** 5601–5610.

Li, Z., Wang, R., Gao, Y., Wang, C., Zhao, L., Xu, N., Chen, K.E., Qi, S., Zhang, M., Tsay, Y.F., Crawford, N.M., and Wang, Y. (2017). The Arabidopsis CPSF30-L gene plays an essential role in nitrate signal-

ing and regulates the nitrate transceptor gene NRT1.1. New Phytol. **16:** 1205–1222.

Liu, K.H., et al. (2017). Discovery of nitrate-CPK-NLP signalling in central nutrient-growth networks. Nature **545:** 311–316.

Marchive, C., Roudier, F., Castaings, L., Bréhaut, V., Blondet, E., Colot, V., Meyer, C., and Krapp, A. (2013). Nuclear retention of the transcription factor NLP7 orchestrates the early response to nitrate in plants. Nat. Commun. **4:** 1713.

Medici, A., and Krouk, G. (2014). The primary nitrate response: a multifaceted signalling pathway. J. Exp. Bot. **65:** 5567–5576.

Miyawaki, K., Matsumoto-Kitano, M., and Kakimoto, T. (2004). Expression of cytokinin biosynthetic isopentenyltransferase genes in Arabidopsis: tissue specificity and regulation by auxin, cytokinin, and nitrate. Plant J. **37:** 128–138.

Miyawaki, K., Tarkowski, P., Matsumoto-Kitano, M., Kato, T., Sato, S., Tarkowska, D., Tabata, S., Sandberg, G., and Kakimoto, T. (2006). Roles of Arabidopsis ATP/ADP isopentenyltransferases and tRNA isopentenyltransferases in cytokinin biosynthesis. Proc. Natl. Acad. Sci. USA **103:** 16598–16603.

Mounier, E., Pervent, M., Ljung, K., Gojon, A., and Nacry, P. (2014). Auxin-mediated nitrate signalling by NRT1.1 participates in the adaptive response of Arabidopsis root architecture to the spatial heterogeneity of nitrate availability. Plant Cell Environ. **37:** 162–174.

Muller, B., and Touraine, B. (1992). Inhibition of NO3– uptake by various phloem-translocated amino acids in soybean seedlings. J. Exp. Bot. **43:** 617–623.

Muños, S., Cazettes, C., Fizames, C., Gaymard, F., Tillard, P., Lepetit, M., Lejay, L., and Gojon, A. (2004). Transcript profiling in the *chl1-5* mutant of Arabidopsis reveals a role of the nitrate transporter NRT1.1 in the regulation of another nitrate transporter, NRT2.1. Plant Cell **16:** 2433–2447.

Ohkubo, Y., Tanaka, M., Tabata, R., Ogawa-Ohnishi, M., and Matsubayashi, Y. (2017). Shoot-to-root mobile polypeptides involved in systemic regulation of nitrogen acquisition. Nat. Plants **3:** 17029.

Osugi, A., Kojima, M., Takebayashi, Y., Ueda, N., Kiba, T., and Sakakibara, H. (2017). Systemic transport of trans-zeatin and its precursor have differing roles in Arabidopsis shoots. Nat. Plants **3:** 17112.

Remans, T., Nacry, P., Pervent, M., Filleur, S., Diatloff, E., Mounier, E., Tillard, P., Forde, B.G., and Gojon, A. (2006). The Arabidopsis NRT1.1 transporter participates in the signaling pathway triggering root colonization of nitrate-rich patches. Proc. Natl. Acad. Sci. USA **103:** 19206–19211.

Riveras, E., Alvarez, J.M., Vidal, E.A., Oses, C., Vega, A., and Gutiérrez, R.A. (2015). The calcium ion is a second messenger in the nitrate signaling pathway of Arabidopsis. Plant Physiol. **169:** 1397–1404.

Rubin, G., Tohge, T., Matsuda, F., Saito, K., and Scheible, W.R. (2009). Members of the LBD family of transcription factors repress anthocyanin synthesis and affect additional nitrogen responses in Arabidopsis. Plant Cell **21:** 3567–3584.

Ruffel, S., et al. (2008). Systemic signaling of the plant nitrogen status triggers specific transcriptome responses depending on the nitrogen source in *Medicago truncatula*. Plant Physiol. **146:** 2020–2035.

Ruffel, S., and Gojon, A. (2017). Systemic nutrient signalling: On the road for nitrate. Nat. Plants **3:** 17040.

Ruffel, S., Krouk, G., Ristova, D., Shasha, D., Birnbaum, K.D., and Coruzzi, G.M. (2011). Nitrogen economics of root foraging: transitive closure of the nitrate-cytokinin relay and distinct systemic signaling for N supply vs. demand. Proc. Natl. Acad. Sci. USA **108:** 18524–18529.

Ruffel, S., Poitout, A., Krouk, G., Coruzzi, G.M., and Lacombe, B. (2016). Long-distance nitrate signaling displays cytokinin dependent and independent branches. J. Integr. Plant Biol. **58:** 226–229.

Saeed, A.I., et al. (2003). TM4: a free, open-source system for microarray data management and analysis. Biotechniques **34:** 374–378.

Safi, A., Medici, A., Szponarski, W., Marshall-Colon, A., Ruffel, S., Gaymard, F., Coruzzi, G., Lacombe, B., and Krouk, G. (2018). HRS1/HHOs GARP transcription factors and reactive oxygen species are regulators of Arabidopsis nitrogen starvation response. bioRxiv doi/10.1101/164277.

Sakakibara, H. (2006). Cytokinins: activity, biosynthesis, and translocation. Annu. Rev. Plant Biol. **57:** 431–449.

Sakakibara, H., Takei, K., and Hirose, N. (2006). Interactions between nitrogen and cytokinin in the regulation of metabolism and development. Trends Plant Sci. **11:** 440–448.

Schäfer, M., Brütting, C., Meza-Canales, I.D., Großkinsky, D.K., Vankova, R., Baldwin, I.T., and Meldau, S. (2015). The role of cis-zeatin-type cytokinins in plant growth regulation and mediating responses to environmental interactions. J. Exp. Bot. **66:** 4873–4884.

Šmehilová, M., Dobrůšková, J., Novák, O., Takáč, T., and Galuszka, P. (2016). Cytokinin-specific glycosyltransferases possess different roles in cytokinin homeostasis maintenance. Front. Plant Sci. **7:** 1264.

Svačinová, J., Novák, O., Plačková, L., Lenobel, R., Holík, J., Strnad, M., and Doležal, K. (2012). A new approach for cytokinin isolation from Arabidopsis tissues using miniaturized purification: pipette tip solid-phase extraction. Plant Methods **8:** 17.

Tabata, R., Sumida, K., Yoshii, T., Ohyama, K., Shinohara, H., and Matsubayashi, Y. (2014). Perception of root-derived peptides by shoot LRR-RKs mediates systemic N-demand signaling. Science **346:** 343–346.

Takei, K., Sakakibara, H., Taniguchi, M., and Sugiyama, T. (2001). Nitrogen-dependent accumulation of cytokinins in root and the translocation to leaf: implication of cytokinin species that induces gene expression of maize response regulator. Plant Cell Physiol. **42:** 85–93.

Takei, K., Ueda, N., Aoki, K., Kuromori, T., Hirayama, T., Shinozaki, K., Yamaya, T., and Sakakibara, H. (2004). AtIPT3 is a key determinant of nitrate-dependent cytokinin biosynthesis in Arabidopsis. Plant Cell Physiol. **45:** 1053–1062.

Vidal, E.A., Moyano, T.C., Riveras, E., Contreras-López, O., and Gutiérrez, R.A. (2013). Systems approaches map regulatory networks downstream of the auxin receptor AFB3 in the nitrate response of *Arabidopsis thaliana* roots. Proc. Natl. Acad. Sci. USA **110:** 12840–12845.

Walch-Liu, P., Filleur, S., Gan, Y., and Forde, B.G. (2005). Signaling mechanisms integrating root and shoot responses to changes in the nitrogen supply. Photosynth. Res. **83:** 239–250.

Werner, T., Nehnevajova, E., Köllmer, I., Novák, O., Strnad, M., Krämer, U., and Schmülling, T. (2010). Root-specific reduction of cytokinin causes enhanced root growth, drought tolerance, and leaf mineral enrichment in Arabidopsis and tobacco. Plant Cell **22:** 3905–3920.

Xu, N., Wang, R., Zhao, L., Zhang, C., Li, Z., Lei, Z., Liu, F., Guan, P., Chu, Z., Crawford, N.M., and Wang, Y. (2016). The Arabidopsis NRG2 protein mediates nitrate signaling and interacts with and regulates key nitrate regulators. Plant Cell **28:** 485–504.

Yong, Z., Kotur, Z., and Glass, A.D. (2010). Characterization of an intact two-component high-affinity nitrate transporter from Arabidopsis roots. Plant J. **63:** 739–748.

Zhang, H., and Forde, B.G. (1998). An Arabidopsis MADS box gene that controls nutrient-induced changes in root architecture. Science **279:** 407–409.

Zhang, K., Novak, O., Wei, Z., Gou, M., Zhang, X., Yu, Y., Yang, H., Cai, Y., Strnad, M., and Liu, C.J. (2014). Arabidopsis ABCG14 protein controls the acropetal translocation of root-synthesized cytokinins. Nat. Commun. **5:** 3274.

Zürcher, E., Liu, J., di Donato, M., Geisler, M., and Müller, B. (2016). Plant development regulated by cytokinin sinks. Science **353:** 1027–1030.

Supplemental Data. Poitout et al. Plant Cell (2018) 10.1105/tpc.18.00011

Supplemental Table 1. ANOVA, Tukey and Student's *t*.test tables

Sum Sq = Sum of squares; df = degrees of freedom; Mean Sq = Mean Squares;
p adj = p-value adjusted for multiple comparisons

Figure 1B

NRT2.1	df	Sum Sq	Mean Sq	F value	Pr(>F)
PCGenotype	2	3.5	1.7	27.4	6.38E-07
PCTreatment	3	5.4	1.8	28.4	4.54E-08
PCGenotype:PCTreatment	6	3.4	0.6	9.0	3.44E-05
Residuals	24	1.5	0.1		
Total	35	13.8			

NRT3.1	Df	Sum Sq	Mean Sq	F value	Pr(>F)
PCGenotype	2	3.0	1.5	38.5	3.22E-08
PCTreatment	3	5.4	1.8	45.8	4.40E-10
PCGenotype:PCTreatment	6	2.0	0.3	8.5	5.08E-05
Residuals	24	0.9	0.0		
Total	35	11.4			

G6PD3	Df	Sum Sq	Mean Sq	F value	Pr(>F)
PCGenotype	2	3.5	1.7	11.5	3.11E-04
PCTreatment	3	22.3	7.4	49.6	1.95E-10
PCGenotype:PCTreatment	6	4.4	0.7	4.9	2.06E-03
Residuals	24	3.6	0.2		
Total	35	33.8			

NiR	Df	Sum Sq	Mean Sq	F value	Pr(>F)
PCGenotype	2	6.5	3.3	11.5	3.21E-04
PCTreatment	3	40.3	13.4	47.2	3.25E-10
PCGenotype:PCTreatment	6	5.3	0.9	3.1	2.21E-02
Residuals	24	6.8	0.3		
Total	35	58.9			

FNR2	Df	Sum Sq	Mean Sq	F value	Pr(>F)
PCGenotype	2	4.4	2.2	8.7	1.47E-03
PCTreatment	3	20.3	6.8	26.4	9.04E-08
PCGenotype:PCTreatment	6	5.0	0.8	3.3	1.72E-02
Residuals	24	6.2	0.3		
Total	35	35.9			

UPM1	Df	Sum Sq	Mean Sq	F value	Pr(>F)
PCGenotype	2	3.0	1.5	11.3	3.40E-04
PCTreatment	3	14.3	4.8	36.6	4.08E-09
PCGenotype:PCTreatment	6	2.7	0.5	3.5	1.28E-02
Residuals	24	3.1	0.1		
Total	35	23.2			

Figure 1B (Continuation)

Tukey multiple comparisons of means	p adj *NRT2.1*	*NRT3.1*	*G6PD3*	*NiR*	*FNR2*	*UPM1*
ipt:C.KNO3-Col:C.KNO3	9.95E-01	9.96E-01	9.97E-01	1.00E+00	9.91E-01	1.00E+00
abcg:C.KNO3-Col:C.KNO3	2.33E-03	1.37E-03	5.79E-02	6.91E-02	1.68E-01	2.53E-02
Col:Sp.KNO3-Col:C.KNO3	3.95E-02	1.51E-02	8.54E-02	7.14E-01	4.33E-01	9.78E-01
ipt:Sp.KNO3-Col:C.KNO3	9.97E-01	1.00E+00	9.90E-01	1.00E+00	1.00E+00	1.00E+00
abcg:Sp.KNO3-Col:C.KNO3	1.69E-03	5.72E-04	3.00E-01	1.91E-01	2.44E-01	3.83E-02
Col:Sp.KCl-Col:C.KNO3	2.94E-03	4.56E-04	3.42E-04	5.00E-04	6.09E-03	2.95E-04
ipt:Sp.KCl-Col:C.KNO3	1.42E-02	4.39E-04	7.91E-04	1.92E-03	1.00E-02	2.16E-03
abcg:Sp.KCl-Col:C.KNO3	6.08E-03	9.84E-05	4.63E-04	3.93E-04	8.74E-03	4.78E-04
Col:C.KCl-Col:C.KNO3	9.93E-03	2.07E-03	2.92E-04	5.24E-04	9.23E-03	3.65E-04
ipt:C.KCl-Col:C.KNO3	5.12E-03	3.98E-04	2.83E-04	5.62E-04	7.16E-03	7.11E-04
abcg:C.KCl-Col:C.KNO3	1.54E-03	3.35E-05	1.97E-04	1.93E-04	4.87E-03	2.11E-04
abcg:C.KNO3-ipt:C.KNO3	2.67E-02	1.45E-02	3.56E-01	5.41E-02	7.55E-01	1.12E-01
Col:Sp.KNO3-ipt:C.KNO3	3.56E-03	1.43E-03	9.61E-03	7.80E-01	5.90E-02	7.18E-01
ipt:Sp.KNO3-ipt:C.KNO3	6.93E-01	9.45E-01	1.00E+00	1.00E+00	1.00E+00	1.00E+00
abcg:Sp.KNO3-ipt:C.KNO3	1.98E-02	6.22E-03	8.59E-01	1.55E-01	8.61E-01	1.60E-01
Col:Sp.KCl-ipt:C.KNO3	3.32E-02	4.97E-03	3.65E-03	3.79E-04	7.49E-02	1.59E-03
ipt:Sp.KCl-ipt:C.KNO3	1.33E-01	4.79E-03	8.35E-03	1.45E-03	1.15E-01	1.14E-02
abcg:Sp.KCl-ipt:C.KNO3	6.42E-02	1.07E-03	4.94E-03	2.97E-04	1.02E-01	2.58E-03
Col:C.KCl-ipt:C.KNO3	9.83E-02	2.15E-02	3.12E-03	3.97E-04	1.07E-01	1.97E-03
ipt:C.KCl-ipt:C.KNO3	5.50E-02	4.34E-03	3.03E-03	4.25E-04	8.62E-02	3.83E-03
abcg:C.KCl-ipt:C.KNO3	1.81E-02	3.54E-04	2.10E-03	1.47E-04	6.15E-02	1.13E-03
Col:Sp.KNO3-abcg:C.KNO3	4.49E-07	1.18E-07	2.18E-05	7.25E-04	7.17E-04	1.31E-03
ipt:Sp.KNO3-abcg:C.KNO3	2.33E-04	4.75E-04	4.36E-01	7.41E-02	5.52E-01	1.17E-01
abcg:Sp.KNO3-abcg:C.KNO3	1.00E+00	1.00E+00	9.99E-01	1.00E+00	1.00E+00	1.00E+00
Col:Sp.KCl-abcg:C.KNO3	1.00E+00	1.00E+00	5.72E-01	6.19E-01	9.19E-01	7.64E-01
ipt:Sp.KCl-abcg:C.KNO3	1.00E+00	1.00E+00	7.82E-01	9.09E-01	9.69E-01	9.94E-01
abcg:Sp.KCl-abcg:C.KNO3	1.00E+00	9.92E-01	6.51E-01	5.56E-01	9.58E-01	8.64E-01
Col:C.KCl-abcg:C.KNO3	1.00E+00	1.00E+00	5.31E-01	6.31E-01	9.63E-01	8.11E-01
ipt:C.KCl-abcg:C.KNO3	1.00E+00	1.00E+00	5.23E-01	6.49E-01	9.39E-01	9.24E-01
abcg:C.KCl-abcg:C.KNO3	1.00E+00	9.09E-01	4.32E-01	3.80E-01	8.85E-01	6.82E-01
ipt:Sp.KNO3-Col:Sp.KNO3	2.58E-01	4.07E-02	6.84E-03	6.93E-01	1.16E-01	7.06E-01
abcg:Sp.KNO3-Col:Sp.KNO3	3.39E-07	5.71E-08	1.70E-04	2.54E-03	1.19E-03	2.05E-03
Col:Sp.KCl-Col:Sp.KNO3	5.51E-07	4.74E-08	1.82E-07	5.09E-06	1.92E-05	1.54E-05

Figure 1B (Continuation)

Tukey multiple comparisons of means	p adj *NRT2.1*	*NRT3.1*	*G6PD3*	*NiR*	*FNR2*	*UPM1*
ipt:Sp.KCl-Col:Sp.KNO3	2.32E-06	4.59E-08	3.75E-07	1.81E-05	3.13E-05	1.06E-04
abcg:Sp.KCl-Col:Sp.KNO3	1.05E-06	1.37E-08	2.36E-07	4.06E-06	2.74E-05	2.44E-05
Col:C.KCl-Col:Sp.KNO3	1.65E-06	1.67E-07	1.59E-07	5.32E-06	2.89E-05	1.88E-05
ipt:C.KCl-Col:Sp.KNO3	9.02E-07	4.24E-08	1.55E-07	5.67E-06	2.25E-05	3.59E-05
abcg:C.KCl-Col:Sp.KNO3	3.12E-07	5.84E-09	1.14E-07	2.11E-06	1.55E-05	1.12E-05
abcg:Sp.KNO3-ipt:Sp.KNO3	1.69E-04	1.99E-04	9.14E-01	2.03E-01	6.83E-01	1.66E-01
Col:Sp.KCl-ipt:Sp.KNO3	2.94E-04	1.59E-04	5.15E-03	5.43E-04	3.69E-02	1.67E-03
ipt:Sp.KCl-ipt:Sp.KNO3	1.46E-03	1.53E-04	1.17E-02	2.08E-03	5.81E-02	1.19E-02
abcg:Sp.KCl-ipt:Sp.KNO3	6.12E-04	3.50E-05	6.95E-03	4.26E-04	5.14E-02	2.70E-03
Col:C.KCl-ipt:Sp.KNO3	1.01E-03	7.18E-04	4.40E-03	5.69E-04	5.40E-02	2.07E-03
ipt:C.KCl-ipt:Sp.KNO3	5.13E-04	1.39E-04	4.28E-03	6.10E-04	4.28E-02	4.02E-03
abcg:C.KCl-ipt:Sp.KNO3	1.54E-04	1.22E-05	2.97E-03	2.10E-04	2.99E-02	1.19E-03
Col:Sp.KCl-abcg:Sp.KNO3	1.00E+00	1.00E+00	1.51E-01	3.15E-01	8.35E-01	6.53E-01
ipt:Sp.KCl-abcg:Sp.KNO3	9.99E-01	1.00E+00	2.79E-01	6.42E-01	9.19E-01	9.80E-01
abcg:Sp.KCl-abcg:Sp.KNO3	1.00E+00	1.00E+00	1.91E-01	2.68E-01	8.99E-01	7.72E-01
Col:C.KCl-abcg:Sp.KNO3	1.00E+00	1.00E+00	1.34E-01	3.25E-01	9.07E-01	7.07E-01
ipt:C.KCl-abcg:Sp.KNO3	1.00E+00	1.00E+00	1.31E-01	3.39E-01	8.66E-01	8.55E-01
abcg:C.KCl-abcg:Sp.KNO3	1.00E+00	9.85E-01	9.69E-02	1.60E-01	7.87E-01	5.66E-01
ipt:Sp.KCl-Col:Sp.KCl	1.00E+00	1.00E+00	1.00E+00	1.00E+00	1.00E+00	9.99E-01
abcg:Sp.KCl-Col:Sp.KCl	1.00E+00	1.00E+00	1.00E+00	1.00E+00	1.00E+00	1.00E+00
Col:C.KCl-Col:Sp.KCl	1.00E+00	1.00E+00	1.00E+00	1.00E+00	1.00E+00	1.00E+00
ipt:C.KCl-Col:Sp.KCl	1.00E+00	1.00E+00	1.00E+00	1.00E+00	1.00E+00	1.00E+00
abcg:C.KCl-Col:Sp.KCl	1.00E+00	9.92E-01	1.00E+00	1.00E+00	1.00E+00	1.00E+00
abcg:Sp.KCl-ipt:Sp.KCl	1.00E+00	1.00E+00	1.00E+00	1.00E+00	1.00E+00	1.00E+00
Col:C.KCl-ipt:Sp.KCl	1.00E+00	1.00E+00	1.00E+00	1.00E+00	1.00E+00	1.00E+00
ipt:C.KCl-ipt:Sp.KCl	1.00E+00	1.00E+00	1.00E+00	1.00E+00	1.00E+00	1.00E+00
abcg:C.KCl-ipt:Sp.KCl	9.98E-01	9.93E-01	1.00E+00	9.97E-01	1.00E+00	9.97E-01
Col:C.KCl-abcg:Sp.KCl	1.00E+00	9.76E-01	1.00E+00	1.00E+00	1.00E+00	1.00E+00
ipt:C.KCl-abcg:Sp.KCl	1.00E+00	1.00E+00	1.00E+00	1.00E+00	1.00E+00	1.00E+00
abcg:C.KCl-abcg:Sp.KCl	1.00E+00	1.00E+00	1.00E+00	1.00E+00	1.00E+00	1.00E+00
ipt:C.KCl-Col:C.KCl	1.00E+00	1.00E+00	1.00E+00	1.00E+00	1.00E+00	1.00E+00
abcg:C.KCl-Col:C.KCl	1.00E+00	8.40E-01	1.00E+00	1.00E+00	1.00E+00	1.00E+00
abcg:C.KCl-ipt:C.KCl	1.00E+00	9.95E-01	1.00E+00	1.00E+00	1.00E+00	1.00E+00

Figure 2A

Left graph

tZ Root	Df	Sum Sq	Mean Sq	F value	Pr(>F)
PCGenotype2	2	74510.2	37255.1	123.2	5.67E-12
PCTreatment2	1	2963.5	2963.5	9.8	5.26E-03
PCGenotype2:PCTreatment2	2	1352.3	676.2	2.2	1.33E-01
Residuals	20	6046.4	302.3		
Total	25	84872.4			

iP Root	Df	Sum Sq	Mean Sq	F value	Pr(>F)
PCGenotype2	2	24200.9	12100.4	137.8	2.01E-12
PCTreatment2	1	1148.3	1148.3	13.1	1.72E-03
PCGenotype2:PCTreatment2	2	930.9	465.5	5.3	1.42E-02
Residuals	20	1756.0	87.8		
Total	25	28036.2			

cZ Root	Df	Sum Sq	Mean Sq	F value	Pr(>F)
PCGenotype2	2	1089.4	544.7	10.5	7.67E-04
PCTreatment2	1	63.6	63.6	1.2	2.82E-01
PCGenotype2:PCTreatment2	2	63.8	31.9	0.6	5.51E-01
Residuals	20	1038.6	51.9		
Total	25	2255.3			

DHZ Root	Df	Sum Sq	Mean Sq	F value	Pr(>F)
PCGenotype2	2	190.6	95.3	118.6	8.10E-12
PCTreatment2	1	1.0	1.0	1.3	2.70E-01
PCGenotype2:PCTreatment2	2	3.3	1.7	2.1	1.51E-01
Residuals	20	16.1	0.8		
Total	25	211.0			

Figure 2A (Continuation)

Right graph

tZ Shoot	Df	Sum Sq	Mean Sq	F value	Pr(>F)
PCGenotype2	2	31142.2	15571.1	72.6	6.79E-10
PCTreatment2	1	1536.2	1536.2	7.2	1.45E-02
PCGenotype2:PCTreatment2	2	2146.1	1073.0	5.0	1.73E-02
Residuals	20	4291.4	214.6		
Total	25	39115.9			

iP Shoot	Df	Sum Sq	Mean Sq	F value	Pr(>F)
PCGenotype2	2	6548.0	3274.0	50.0	1.64E-08
PCTreatment2	1	1129.8	1129.8	17.3	4.89E-04
PCGenotype2:PCTreatment2	2	2426.1	1213.1	18.5	2.79E-05
Residuals	20	1308.6	65.4		
Total	25	11412.5			

cZ Shoot	Df	Sum Sq	Mean Sq	F value	Pr(>F)
PCGenotype2	2	37.2	18.6	0.5	5.93E-01
PCTreatment2	1	5.5	5.5	0.2	6.94E-01
PCGenotype2:PCTreatment2	2	402.4	201.2	5.8	1.03E-02
Residuals	20	693.0	34.7		
Total	25	1138.2			

DHZ Shoot	Df	Sum Sq	Mean Sq	F value	Pr(>F)
PCGenotype2	2	99.2	49.6	53.2	9.78E-09
PCTreatment2	1	0.0	0.0	0.0	9.84E-01
PCGenotype2:PCTreatment2	2	1.4	0.7	0.8	4.76E-01
Residuals	20	18.6	0.9		
Total	25	119.2			

Figure 2A (Continuation)

Left graph

	p adj			
Tukey multiple comparisons of means	*t*Z Root	iP Root	cZ Root	DHZ Root
Col:C.KCl-abcg:C.KCl	1.62E-06	4.01E-06	9.99E-01	1.82E-08
ipt:C.KCl-abcg:C.KCl	2.16E-07	3.45E-07	4.69E-02	8.94E-09
abcg:C.KNO3-abcg:C.KCl	6.35E-02	1.91E-03	1.00E+00	2.31E-01
Col:C.KNO3-abcg:C.KCl	1.29E-04	6.74E-05	9.73E-01	2.58E-08
ipt:C.KNO3-abcg:C.KCl	2.53E-07	5.56E-07	5.67E-01	9.33E-09
ipt:C.KCl-Col:C.KCl	6.19E-01	5.05E-01	1.55E-02	8.98E-01
abcg:C.KNO3-Col:C.KCl	6.58E-09	1.04E-09	9.99E-01	1.35E-06
Col:C.KNO3-Col:C.KCl	2.55E-01	6.98E-01	9.98E-01	1.00E+00
ipt:C.KNO3-Col:C.KCl	6.77E-01	6.71E-01	3.23E-01	9.09E-01
abcg:C.KNO3-ipt:C.KCl	1.63E-09	2.46E-10	4.57E-02	4.62E-07
Col:C.KNO3-ipt:C.KCl	1.49E-02	5.06E-02	6.42E-03	8.05E-01
ipt:C.KNO3-ipt:C.KCl	1.00E+00	1.00E+00	6.64E-01	1.00E+00
Col:C.KNO3-abcg:C.KNO3	2.29E-07	8.08E-09	9.75E-01	2.03E-06
ipt:C.KNO3-abcg:C.KNO3	1.86E-09	3.49E-10	5.59E-01	4.86E-07
ipt:C.KNO3-Col:C.KNO3	1.83E-02	8.75E-02	1.69E-01	8.20E-01

Right Graph

	p adj			
Tukey multiple comparisons of means	tZ Shoot	iP Shoot	cZ Shoot	DHZ Shoot
Col:C.KCl-abcg:C.KCl	1.69E-03	2.67E-04	8.29E-02	1.32E-02
ipt:C.KCl-abcg:C.KCl	8.77E-01	8.06E-06	5.42E-01	9.41E-02
abcg:C.KNO3-abcg:C.KCl	1.00E+00	9.62E-01	6.52E-02	9.34E-01
Col:C.KNO3-abcg:C.KCl	5.15E-07	7.33E-01	7.06E-01	2.37E-03
ipt:C.KNO3-abcg:C.KCl	8.82E-01	1.01E-05	8.58E-01	1.04E-01
ipt:C.KCl-Col:C.KCl	1.30E-04	3.56E-01	8.80E-01	1.92E-05
abcg:C.KNO3-Col:C.KCl	2.61E-03	1.79E-03	1.00E+00	1.48E-03
Col:C.KNO3-Col:C.KCl	5.84E-03	5.89E-06	6.43E-01	9.60E-01
ipt:C.KNO3-Col:C.KCl	1.34E-04	4.17E-01	5.55E-01	2.15E-05
abcg:C.KNO3-ipt:C.KCl	7.91E-01	4.31E-05	7.80E-01	4.34E-01
Col:C.KNO3-ipt:C.KCl	6.64E-08	2.70E-07	9.99E-01	4.02E-06
ipt:C.KNO3-ipt:C.KCl	1.00E+00	1.00E+00	9.92E-01	1.00E+00
Col:C.KNO3-abcg:C.KNO3	7.39E-07	2.63E-01	5.24E-01	2.66E-04
ipt:C.KNO3-abcg:C.KNO3	7.97E-01	5.44E-05	4.47E-01	4.63E-01
ipt:C.KNO3-Col:C.KNO3	6.78E-08	3.33E-07	1.00E+00	4.47E-06

Figure 2B

Left graph

tZ Root		Df	Sum Sq	Mean Sq	F value	Pr(>F)
	PCGenotype2B	2	154.01	77.01	121.46	2.49E-23
	PCTreatment2B	2	75.98	37.99	59.92	8.22E-16
	PCGenotype2B:PCTreatment2B	4	34.30	8.57	13.52	3.43E-08
	Residuals	69	43.75	0.63		
	Total	77	308.04			

iP Root		Df	Sum Sq	Mean Sq	F value	Pr(>F)
	PCGenotype2B	2	255.92	127.96	88.55	8.86E-20
	PCTreatment2B	2	48.77	24.38	16.87	1.08E-06
	PCGenotype2B:PCTreatment2B	4	56.18	14.05	9.72	2.71E-06
	Residuals	69	99.71	1.45		
	Total	77	460.59			

cZ Root		Df	Sum Sq	Mean Sq	F value	Pr(>F)
	PCGenotype2B	2	0.47	0.24	0.57	5.67E-01
	PCTreatment2B	2	0.07	0.03	0.08	9.19E-01
	PCGenotype2B:PCTreatment2B	4	1.59	0.40	0.96	4.37E-01
	Residuals	69	28.63	0.41		
	Total	77	30.76			

DHZ Root		Df	Sum Sq	Mean Sq	F value	Pr(>F)
	PCGenotype2B2	2	0.13	0.07	7.03	3.14E-03
	PCTreatment2B2	2	0.22	0.11	11.73	1.72E-04
	PCGenotype2B2:PCTreatment2B2	4	0.25	0.06	6.51	6.77E-04
	Residuals	30	0.29	0.01		
	Total	38	0.89			

Figure 2B (Continuation)

Tukey multiple comparisons of means	p adj *tZ* Root	iP Root	cZ Root	DHZ Root
Col:C.KNO3-abcg:C.KNO3	2.56E-06	2.32E-11	1.00E+00	3.25E-01
ipt:C.KNO3-abcg:C.KNO3	0.00E+00	0.00E+00	1.00E+00	4.94E-03
abcg:Sp.KCl-abcg:C.KNO3	0.00E+00	6.59E-10	9.82E-01	5.91E-05
Col:Sp.KCl-abcg:C.KNO3	0.00E+00	0.00E+00	9.97E-01	3.15E-01
ipt:Sp.KCl-abcg:C.KNO3	0.00E+00	0.00E+00	1.00E+00	4.17E-04
abcg:Sp.KNO3-abcg:C.KNO3	9.49E-05	3.84E-01	1.00E+00	4.35E-02
Col:Sp.KNO3-abcg:C.KNO3	0.00E+00	0.00E+00	1.00E+00	2.86E-04
ipt:Sp.KNO3-abcg:C.KNO3	0.00E+00	0.00E+00	1.00E+00	1.65E-04
ipt:C.KNO3-Col:C.KNO3	0.00E+00	2.18E-01	9.99E-01	4.85E-01
abcg:Sp.KCl-Col:C.KNO3	4.67E-04	1.00E+00	8.72E-01	1.55E-02
Col:Sp.KCl-Col:C.KNO3	9.04E-11	5.24E-01	1.00E+00	1.00E+00
ipt:Sp.KCl-Col:C.KNO3	0.00E+00	1.71E-01	1.00E+00	8.95E-02
abcg:Sp.KNO3-Col:C.KNO3	9.99E-01	1.41E-06	1.00E+00	9.52E-01
Col:Sp.KNO3-Col:C.KNO3	1.76E-02	8.36E-01	9.99E-01	8.31E-02
ipt:Sp.KNO3-Col:C.KNO3	0.00E+00	1.74E-01	9.84E-01	4.04E-02
abcg:Sp.KCl-ipt:C.KNO3	7.51E-03	2.28E-01	9.98E-01	7.84E-01
Col:Sp.KCl-ipt:C.KNO3	9.96E-01	9.99E-01	9.79E-01	4.97E-01
ipt:Sp.KCl-ipt:C.KNO3	1.00E+00	1.00E+00	1.00E+00	9.90E-01
abcg:Sp.KNO3-ipt:C.KNO3	0.00E+00	1.58E-10	9.99E-01	9.93E-01
Col:Sp.KNO3-ipt:C.KNO3	3.53E-05	9.68E-01	1.00E+00	9.95E-01
ipt:Sp.KNO3-ipt:C.KNO3	1.00E+00	1.00E+00	1.00E+00	9.37E-01
Col:Sp.KCl-abcg:Sp.KCl	4.51E-02	5.25E-01	6.49E-01	1.63E-02
ipt:Sp.KCl-abcg:Sp.KCl	4.09E-03	1.82E-01	9.48E-01	9.98E-01
abcg:Sp.KNO3-abcg:Sp.KCl	1.17E-04	7.77E-06	8.86E-01	2.73E-01
Col:Sp.KNO3-abcg:Sp.KCl	9.28E-01	8.23E-01	9.96E-01	9.92E-01
ipt:Sp.KNO3-abcg:Sp.KCl	6.73E-03	1.85E-01	1.00E+00	1.00E+00
ipt:Sp.KCl-Col:Sp.KCl	9.83E-01	9.97E-01	1.00E+00	9.32E-02
abcg:Sp.KNO3-Col:Sp.KCl	2.05E-11	4.33E-10	1.00E+00	9.56E-01
Col:Sp.KNO3-Col:Sp.KCl	2.75E-04	1.00E+00	9.74E-01	8.69E-02
ipt:Sp.KNO3-Col:Sp.KCl	9.94E-01	9.98E-01	8.94E-01	4.22E-02
abcg:Sp.KNO3-ipt:Sp.KCl	0.00E+00	8.09E-11	1.00E+00	6.90E-01
Col:Sp.KNO3-ipt:Sp.KCl	1.63E-05	9.43E-01	1.00E+00	1.00E+00
ipt:Sp.KNO3-ipt:Sp.KCl	1.00E+00	1.00E+00	9.97E-01	1.00E+00
Col:Sp.KNO3-abcg:Sp.KNO3	4.40E-03	3.50E-09	9.99E-01	7.18E-01
ipt:Sp.KNO3-abcg:Sp.KNO3	0.00E+00	8.55E-11	9.85E-01	4.77E-01
ipt:Sp.KNO3-Col:Sp.KNO3	3.07E-05	9.46E-01	1.00E+00	1.00E+00

Figure 2B (Continuation)

Right graph

tZ Shoot	Df	Sum Sq	Mean Sq	F value	Pr(>F)
PCGenotype2BS	2	21.01	10.51	72.51	6.01E-15
PCTreatment2BS	1	1.80	1.80	12.44	9.63E-04
PCGenotype2BS:PCTreatment2BS	2	1.73	0.87	5.98	4.93E-03
Residuals	46	6.66	0.14		
Total	51	31.21			

iP Shoot	Df	Sum Sq	Mean Sq	F value	Pr(>F)
PCGenotype2BS	2	13.82	6.91	19.29	8.25E-07
PCTreatment2BS	1	0.88	0.88	2.47	1.23E-01
PCGenotype2BS:PCTreatment2BS	2	1.58	0.79	2.20	1.22E-01
Residuals	46	16.48	0.36		
Total	51	32.76			

cZ Shoot	Df	Sum Sq	Mean Sq	F value	Pr(>F)
PCGenotype2BS	2	1.60	0.80	1.36	2.66E-01
PCTreatment2BS	1	0.54	0.54	0.91	3.45E-01
PCGenotype2BS:PCTreatment2BS	2	3.40	1.70	2.89	6.60E-02
Residuals	46	27.07	0.59		
Total	51	32.61			

DHZ Shoot	Df	Sum Sq	Mean Sq	F value	Pr(>F)
PCGenotype2BS2	2	0.03	0.01	1.34	2.84E-01
PCTreatment2BS2	1	0.01	0.01	1.09	3.08E-01
PCGenotype2BS2:PCTreatment2BS2	2	0.17	0.08	7.62	3.46E-03
Residuals	20	0.22	0.01		
Total	25	0.43			

Figure 2B (Continuation)

Tukey multiple comparisons of means	p adj *tZ* Shoot	iP Shoot	cZ Shoot	DHZ Shoot
Col:C.KNO3-abcg:C.KNO3	3.73E-10	1.61E-01	9.99E-01	6.02E-01
ipt:C.KNO3-abcg:C.KNO3	9.08E-01	7.03E-02	9.66E-01	2.32E-01
abcg:Split-abcg:C.KNO3	9.75E-01	1.00E+00	1.37E-01	1.18E-02
Col:Split-abcg:C.KNO3	1.97E-03	1.00E+00	1.00E+00	9.94E-01
ipt:Split-abcg:C.KNO3	8.44E-01	4.68E-02	9.97E-01	5.73E-01
ipt:C.KNO3-Col:C.KNO3	1.04E-11	2.87E-05	9.97E-01	9.57E-01
abcg:Split-Col:C.KNO3	2.77E-11	2.63E-01	2.14E-01	1.97E-01
Col:Split-Col:C.KNO3	1.82E-04	1.17E-01	9.98E-01	8.59E-01
ipt:Split-Col:C.KNO3	5.86E-12	1.57E-05	1.00E+00	1.00E+00
abcg:Split-ipt:C.KNO3	1.00E+00	3.83E-02	5.22E-01	6.67E-01
Col:Split-ipt:C.KNO3	6.10E-05	4.93E-02	9.50E-01	4.25E-01
ipt:Split-ipt:C.KNO3	1.00E+00	1.00E+00	9.99E-01	9.84E-01
Col:Split-abcg:Split	1.61E-04	1.00E+00	9.52E-02	2.41E-02
ipt:Split-abcg:Split	9.98E-01	2.48E-02	3.23E-01	2.97E-01
ipt:Split-Col:Split	3.49E-05	3.15E-02	9.95E-01	8.26E-01

Figure 4A

Student's t test (p.val)		Col-0	*ipt3,5,7*	*abcg14*
C.KNO3 vs Sp.KNO3	Root DW	1.61E-02	7.79E-01	8.93E-01
	$^{15}NO_3^-$ influx	2.42E-03	8.51E-04	4.45E-02
C.KCl vs Sp.KCl	Root DW	4.06E-02	9.44E-01	6.04E-01
	$^{15}NO_3^-$ influx	3.33E-11	1.58E-01	3.59E-04

Figure 4B

Top Graphs

Student's t test (p.val)		Col-0	*ipt3,5,7*	*abcg14*
C.KNO3 vs Sp.KNO3	$^{15}NO_3^-$ influx (root DW<2mg)	1.88E-02	7.51E-01	3.64E-01
	$^{15}NO_3^-$ influx (root DW>2mg)	5.96E-05	2.70E-06	9.85E-02

Bottom Graph

Student's t test (p.val)		Col-0	*ipt3,5,7*	*abcg14*
C.KNO3 vs Sp.KNO3	$^{15}NO_3^-$ influx (=shoot biomass)	5.41E-02	9.00E-03	1.59E-01
C.KCl vs Sp.KCl	$^{15}NO_3^-$ influx (=shoot biomass)	6.26E-04	1.05E-01	6.95E-02

Figure 4C

Col-0	Estimate	Std. Error	t value	Pr(>|t|)
(Intercept)	2.18	5.40	0.40	6.89E-01
root_biomass	3.52	0.56	6.32	2.92E-07
conditionC.NO3	1.08	7.39	0.15	8.85E-01
conditionSplit	0.59	6.39	0.09	9.27E-01
root_biomass:conditionC.NO3	2.30	0.85	2.70	1.07E-02
root_biomass:conditionSplit	1.17	0.66	1.78	8.41E-02

ipt3,5,7	Estimate	Std. Error	t value	Pr(>|t|)
(Intercept)	-2.38	1.08	-2.20	3.46E-02
root_biomass	2.26	0.20	11.12	4.97E-13
conditionC.NO3	0.94	1.61	0.59	5.61E-01
conditionSplit	1.39	1.41	0.99	3.29E-01
root_biomass:conditionC.NO3	-0.03	0.27	-0.13	9.00E-01
root_biomass:conditionSplit	-0.15	0.26	-0.57	5.73E-01

abcg14	Estimate	Std. Error	t value	Pr(>|t|)
(Intercept)	-1.29	1.35	-0.95	3.48E-01
root_biomass	1.82	0.24	7.59	6.73E-09
conditionC.NO3	-0.42	1.98	-0.21	8.32E-01
conditionSplit	-0.12	1.72	-0.07	9.46E-01
root_biomass:conditionC.NO3	0.09	0.31	0.28	7.83E-01
root_biomass:conditionSplit	0.03	0.29	0.09	9.25E-01

Figure 5A

NRT2.1	Df	Sum Sq	Mean Sq	F value	Pr(>F)
PCGenotype5	2	0.04	0.02	1.50	2.96E-01
PCTreatment5	1	0.43	0.43	35.14	1.03E-03
PCGenotype5:PCTreatment5	2	0.01	0.00	0.32	7.41E-01
Residuals	6	0.07	0.01		
Total	11	0.54			

NRT3.1	Df	Sum Sq	Mean Sq	F value	Pr(>F)
PCGenotype5	2	0.04	0.02	1.28	3.45E-01
PCTreatment5	1	0.66	0.66	48.07	4.46E-04
PCGenotype5:PCTreatment5	2	0.03	0.02	1.24	3.53E-01
Residuals	6	0.08	0.01		
Total	11	0.82			

G6PD3	Df	Sum Sq	Mean Sq	F value	Pr(>F)
PCGenotype5	2	0.04	0.02	0.76	5.09E-01
PCTreatment5	1	3.22	3.22	128.12	2.85E-05
PCGenotype5:PCTreatment5	2	0.01	0.01	0.28	7.64E-01
Residuals	6	0.15	0.03		
Total	11	3.42			

NiR	Df	Sum Sq	Mean Sq	F value	Pr(>F)
PCGenotype5	2	0.20	0.10	2.11	2.02E-01
PCTreatment5	1	2.12	2.12	43.79	5.73E-04
PCGenotype5:PCTreatment5	2	0.10	0.05	0.99	4.24E-01
Residuals	6	0.29	0.05		
Total	11	2.70			

FNR2	Df	Sum Sq	Mean Sq	F value	Pr(>F)
PCGenotype5	2	0.01	0.01	0.98	4.29E-01
PCTreatment5	1	1.42	1.42	207.91	6.97E-06
PCGenotype5:PCTreatment5	2	0.00	0.00	0.08	9.24E-01
Residuals	6	0.04	0.01		
Total	11	1.48			

UPM1	Df	Sum Sq	Mean Sq	F value	Pr(>F)
PCGenotype5	2	0.07	0.04	3.86	8.35E-02
PCTreatment5	1	2.21	2.21	234.19	4.92E-06
PCGenotype5:PCTreatment5	2	0.03	0.02	1.79	2.46E-01
Residuals	6	0.06	0.01		
Total	11	2.38			

Figure 5A (Continuation)

	p adj					
Tukey multiple comparisons of means	*NRT2.1*	*NRT3.1*	*G6PD3*	*NiR*	*FNR2*	*UPM1*
ipt:C.KNO3-Col:C.KNO3	9.10E-01	8.70E-01	9.56E-01	8.55E-01	1.00E+00	9.98E-01
abcg:C.KNO3-Col:C.KNO3	9.02E-01	8.45E-01	9.89E-01	7.70E-01	9.30E-01	2.18E-01
Col:C.KCl-Col:C.KNO3	9.92E-02	4.33E-02	5.24E-03	6.15E-02	1.34E-03	6.05E-04
ipt:C.KCl-Col:C.KNO3	1.40E-01	5.06E-02	5.63E-03	6.69E-02	1.25E-03	6.98E-04
abcg:C.KCl-Col:C.KNO3	4.79E-01	4.97E-02	4.25E-03	4.15E-02	8.43E-04	4.79E-04
abcg:C.KNO3-ipt:C.KNO3	1.00E+00	3.40E-01	7.34E-01	2.73E-01	8.36E-01	1.42E-01
Col:C.KCl-ipt:C.KNO3	3.48E-02	1.48E-02	2.80E-03	1.95E-02	1.13E-03	4.85E-04
ipt:C.KCl-ipt:C.KNO3	4.81E-02	1.70E-02	3.00E-03	2.10E-02	1.05E-03	5.57E-04
abcg:C.KCl-ipt:C.KNO3	1.68E-01	1.67E-02	2.31E-03	1.38E-02	7.19E-04	3.88E-04
Col:C.KCl-abcg:C.KNO3	3.40E-02	1.52E-01	8.53E-03	2.64E-01	2.51E-03	3.57E-03
ipt:C.KCl-abcg:C.KNO3	4.70E-02	1.80E-01	9.21E-03	2.88E-01	2.33E-03	4.30E-03
abcg:C.KCl-abcg:C.KNO3	1.64E-01	1.76E-01	6.81E-03	1.75E-01	1.52E-03	2.64E-03
ipt:C.KCl-Col:C.KCl	9.99E-01	1.00E+00	1.00E+00	1.00E+00	1.00E+00	1.00E+00
abcg:C.KCl-Col:C.KCl	7.03E-01	1.00E+00	1.00E+00	9.99E-01	9.72E-01	9.98E-01
abcg:C.KCl-ipt:C.KCl	8.50E-01	1.00E+00	9.99E-01	9.96E-01	9.86E-01	9.83E-01

Figure 5B

$^{15}NO_3^-$ influx		Df	Sum Sq	Mean Sq	F value	Pr(>F)
	PCGenotype5B	2	406.96	203.48	1.09	3.41E-01
	Residuals	68	12669.30	186.31		
	Total	70	13076.26			

Figure 5C

%N in shoots		Df	Sum Sq	Mean Sq	F value	Pr(>F)
	PCGenotype5B	2	20.10	10.05	17.07	1.02E-06
	Residuals	67	39.44	0.59		
	Total	69	59.54			

Tukey multiple comparisons of means	p adj
Col-abcg	7.28E-01
ipt-abcg	2.99E-06
ipt-Col	5.38E-05

Figure 5D

		Df	Sum Sq	Mean Sq	F value	Pr(>F)
Shoot area	PCGenotype5D	2	0.02	0.01	27.13	4.05E-09
	PCTreatment5D	2	0.09	0.05	128.49	2.06E-22
	PCGenotype5D:PCTreatment5D	4	0.03	0.01	17.87	1.04E-09
	Residuals	60	0.02	0.00		
	Total	68	0.16			

PR Length		Df	Sum Sq	Mean Sq	F value	Pr(>F)
	PCGenotype5D	2	13.56	6.78	15.13	4.79E-06
	PCTreatment5D	2	254.69	127.34	284.11	2.52E-31
	PCGenotype5D:PCTreatment5D	4	2.38	0.60	1.33	2.69E-01
	Residuals	60	26.89	0.45		
	Total	68	297.52			

LR Length		Df	Sum Sq	Mean Sq	F value	Pr(>F)
	PCGenotype5D	2	9.59	4.79	0.48	6.24E-01
	PCTreatment5D	2	1044.02	522.01	51.79	8.55E-14
	PCGenotype5D:PCTreatment5D	4	105.80	26.45	2.62	4.34E-02
	Residuals	60	604.72	10.08		
	Total	68	1764.13			

Figure 5D (Continuation)

	p adj		
Tukey multiple comparisons of means	Shoot area	PR Length	LR Length
Col:0.1N-abcg:0.1N	5.34E-01	1.00E+00	9.29E-01
ipt:0.1N-abcg:0.1N	2.01E-01	1.04E-02	7.26E-01
abcg:0N-abcg:0.1N	9.98E-01	4.22E-04	6.05E-01
Col:0N-abcg:0.1N	1.00E+00	1.55E-05	4.59E-01
ipt:0N-abcg:0.1N	9.99E-01	1.31E-01	8.39E-01
abcg:1N-abcg:0.1N	8.94E-02	2.46E-06	8.15E-03
Col:1N-abcg:0.1N	1.99E-11	3.60E-09	4.60E-03
ipt:1N-abcg:0.1N	7.08E-07	2.00E-11	1.34E-01
ipt:0.1N-Col:0.1N	9.97E-01	1.00E-03	4.45E-02
abcg:0N-Col:0.1N	8.19E-02	2.22E-04	9.98E-01
Col:0N-Col:0.1N	1.45E-01	5.96E-06	9.84E-01
ipt:0N-Col:0.1N	6.05E-02	1.32E-01	1.00E+00
abcg:1N-Col:0.1N	9.42E-01	7.28E-08	2.64E-05
Col:1N-Col:0.1N	1.99E-11	6.05E-11	8.74E-06
ipt:1N-Col:0.1N	1.61E-04	1.99E-11	1.17E-03
abcg:0N-ipt:0.1N	1.78E-02	5.35E-11	8.03E-03
Col:0N-ipt:0.1N	3.53E-02	2.15E-11	4.81E-03
ipt:0N-ipt:0.1N	1.17E-02	1.99E-08	1.62E-02
abcg:1N-ipt:0.1N	1.00E+00	2.08E-01	3.76E-01
Col:1N-ipt:0.1N	1.99E-11	2.65E-03	3.02E-01
ipt:1N-ipt:0.1N	5.12E-03	2.89E-08	9.68E-01
Col:0N-abcg:0N	1.00E+00	9.68E-01	1.00E+00
ipt:0N-abcg:0N	1.00E+00	2.39E-01	1.00E+00
abcg:1N-abcg:0N	6.33E-03	1.99E-11	3.68E-06
Col:1N-abcg:0N	1.99E-11	1.99E-11	1.15E-06
ipt:1N-abcg:0N	5.11E-09	1.99E-11	1.62E-04
ipt:0N-Col:0N	1.00E+00	1.50E-02	9.92E-01
abcg:1N-Col:0N	1.31E-02	1.99E-11	2.52E-06
Col:1N-Col:0N	1.99E-11	1.99E-11	8.26E-07
ipt:1N-Col:0N	2.23E-08	1.99E-11	1.02E-04
abcg:1N-ipt:0N	3.93E-03	2.10E-11	4.67E-06
Col:1N-ipt:0N	1.99E-11	1.99E-11	1.22E-06
ipt:1N-ipt:0N	7.12E-10	1.99E-11	2.58E-04
Col:1N-abcg:1N	2.03E-11	8.77E-01	1.00E+00
ipt:1N-abcg:1N	3.35E-02	1.42E-03	9.56E-01
ipt:1N-Col:1N	5.14E-08	7.16E-02	9.34E-01

Supplement I

Supplement II

Supplement III

Supplement IV

Supplement V

Supplement VI

Supplement VII

Supplement VIII

Kocáb O, Jakšová J, Novák O, **Petřík I**, Lenobel R, Chamrád I, Pavlovič A. 2020. Jasmonate-independent regulation of digestive enzyme activity in the carnivorous butterwort Pinguicula × Tina. J Exp Bot 71(12), 3749–3758.

Journal of Experimental Botany, Vol. 71, No. 12 pp. 3749–3758, 2020
doi:10.1093/jxb/eraa159 Advance Access Publication 27 March 2020
This paper is available online free of all access charges (see https://academic.oup.com/jxb/pages/openaccess for further details)

RESEARCH PAPER

Jasmonate-independent regulation of digestive enzyme activity in the carnivorous butterwort *Pinguicula* × *Tina*

Ondřej Kocáb[1], Jana Jakšová[1], Ondřej Novák[2], Ivan Petřík[2], René Lenobel[3], Ivo Chamrád[3], and Andrej Pavlovič[1,*]

[1] Department of Biophysics, Centre of the Region Haná for Biotechnological and Agricultural Research, Faculty of Science, Palacký University, Šlechtitelů 27, Olomouc CZ-783 71, Czech Republic
[2] Laboratory of Growth Regulators, Institute of Experimental Botany, The Czech Academy of Sciences and Faculty of Science, Palacký University, Šlechtitelů 27, Olomouc CZ-783 71, Czech Republic
[3] Department of Protein Biochemistry and Proteomics, Centre of the Region Haná for Biotechnological and Agricultural Research, Faculty of Science, Palacký University, Šlechtitelů 27, Olomouc CZ-783 71, Czech Republic.

* Correspondence: andrej.pavlovic@upol.cz

Received 12 December 2019; Editorial decision 23 March 2020; Accepted 25 March 2020

Editor: John Lunn, Max Planck Institute of Molecular Plant Physiology, Germany

Abstract

Carnivorous plants within the order Caryophyllales use jasmonates, a class of phytohormone, in the regulation of digestive enzyme activities. We used the carnivorous butterwort *Pinguicula* × *Tina* from the order Lamiales to investigate whether jasmonate signaling is a universal and ubiquitous signaling pathway that exists outside the order Caryophyllales. We measured the electrical signals, enzyme activities, and phytohormone tissue levels in response to prey capture. Mass spectrometry was used to identify proteins in the digestive secretion. We identified eight enzymes in the digestive secretion, many of which were previously found in other genera of carnivorous plants. Among them, alpha-amylase is unique in carnivorous plants. Enzymatic activities increased in response to prey capture; however, the tissue content of jasmonic acid and its isoleucine conjugate remained rather low in contrast to the jasmonate response to wounding. Enzyme activities did not increase in response to the exogenous application of jasmonic acid or coronatine. Whereas similar digestive enzymes were co-opted from plant defense mechanisms among carnivorous plants, the mode of their regulation differs. The butterwort has not co-opted jasmonate signaling for the induction of enzyme activities in response to prey capture. Moreover, the presence of alpha-amylase in digestive fluid of *P.* × *Tina*, which has not been found in other genera of carnivorous plants, might indicate that non-defense-related genes have also been co-opted for carnivory.

Keywords: Butterwort, carnivorous plant, digestive enzymes, electrical signals, jasmonic acid, *Pinguicula*, protease, variation potential.

Introduction

The carnivorous plants have evolved specialized leaves or leaf parts that function as traps for prey capture and digestion to obtain scarce nutrients.This adaptation to low nutrient content in the soil has independently evolved by convergent evolution at least 10 times in several orders of flowering plants (Albert *et al.*, 1992; Givnish *et al.*, 2015; Fleischmann *et al.*, 2018). Whereas the mechanisms of prey capture have been studied in great detail during the past two centuries, the process of digestion

was almost completely unknown. The first endogenous enzyme in carnivorous plants was described only at the beginning of this century in the pitcher plant (genus *Nepenthes*), which resolved the longstanding question of whether prey digestion is mediated by symbiotic microorganisms or plant-derived enzymes (Athauda *et al.*, 2004). In the decade that followed, the development of mass spectrometry techniques enabled the discovery of over 20 other digestive enzymes in different species of carnivorous plants, which are surprisingly very similar across distantly related taxa (Eilenberg *et al.*, 2006; Hatano and Hamada, 2008; 2012; Rottloff *et al.*, 2011; 2016; Lee *et al.*, 2016; Fukushima *et al.*, 2017; Krausko *et al.*, 2017). Yet, the mechanism by which the secretion of these digestive enzymes is regulated by stimuli from prey remained unknown until Escalanté-Pérez *et al.* (2011) found that a phytohormone from the group of jasmonates, 12-oxo-phytodienoic acid (OPDA), was responsible for activation of the digestive process in Venus flytrap (*Dionaea muscipula*). An increased level of the true bioactive compound in jasmonate signaling, the isoleucine conjugate of jasmonic acid (JA-Ile), was later found in Venus flytrap, sundew plant (*Drosera capensis*), and the pitcher plant *Nepenthes alata* in response to prey capture (Nakamura *et al.*, 2013; Libiaková *et al.*, 2014; Yilamujiang *et al.*, 2016; Krausko *et al.*, 2017; Pavlovič *et al.*, 2017). The binding of JA-Ile to CORONATINE INSENSITIVE1 (COI1) protein as part of a co-receptor complex mediates the ubiquitin-dependent degradation of JASMONATE ZIM-DOMAIN (JAZ) repressors, resulting in the activation of jasmonate-dependent gene expression (Chini *et al.*, 2007; Thines *et al.*, 2007; Fonseca *et al.*, 2009; Sheard *et al.*, 2010). In ordinary plants, JA-Ile is responsible for the activation of defense mechanisms after herbivore attack or wounding, and it was postulated that the carnivorous plants co-opted the jasmonate signaling pathway for prey capture (Pavlovič and Saganová 2015; Bemm *et al.*, 2016; Pavlovič and Mithöfer, 2019). Unfortunately, the studies to date have generally been confined to three genera of carnivorous plants (*Drosera*, *Dionaea*, and *Nepenthes*), which all are within the order Caryophyllales (or, according to some authors, the separate order Nepenthales; Fleischmann *et al.*, 2018) and are monophyletic. Therefore, it remains unclear whether the jasmonate signaling pathway is a universal and ubiquitous signaling pathway in other phylogenetic lineages of carnivorous plants.

In this study, we focused on carnivorous plants of the genus *Pinguicula* (butterworts), which belongs to the order Lamiales and is distantly related to the Venus flytrap, sundew, and pitcher plant (Albert *et al.*, 1992; Givnish, 2015). Most species of *Pinguicula* have a basal rosette of compact leaves that are more or less broadly ovate, and only a few species (*Pinguicula heterophylla*, *Pinguicula gypsicola*) have filiform upright leaves. Some species can bend their leaf edges slightly in response to prey capture, while others have no such ability (Fleischmann and Roccia, 2018). The leaves are covered by two types of glands. The stalked glands produce sticky mucilage and serve mainly for prey capture, but with the capacity to produce their own digestive enzymes. The sessile glands are the main site for the production of digestive enzymes (Heslop-Harrison and Knox, 1971; Heslop-Harrison and Heslop-Harrison, 1980, 1981; Legendre, 2000; Heslop-Harrison, 2004). Both types of digestive glands of *Pinguicula* share a special characteristic with the Venus flytrap and sundew in that they do not secrete enzymes until stimulated by the presence of prey (Darwin, 1875). It has been postulated that the glands of *Pinguicula* undergo a type of total autophagy and are simply a sac of enzymes that are discharged in response to prey capture, in contrast to the jasmonate-mediated expression/secretion of digestive enzymes in the carnivorous plants within the order Caryophyllales. The initial event associated with the onset of secretion is the rapid movement of chloride ions followed by water across the glands, flushing out the stored enzymes from the cell walls of the glands (Heslop-Harrison and Knox, 1971; Heslop-Harrison and Heslop-Harrison, 1980). Contrary to this eccrine hypothesis, Vassilyev and Muravnik (1988a , b) showed that the glands remain highly active during the entire secretion process and additional digestive enzymes are synthesized and secreted into the digestive fluid after stimulation, much in common with the process in Venus flytrap. In this study, we aimed to shed light on this discrepancy in the view of jasmonate signaling within a less-studied genus of carnivorous plant, *Pinguicula*. We were interested in whether the jasmonate signaling pathway was co-opted for plant carnivory outside the order Caryophyllales. We measured electrical activity, analyzed the composition of the digestive fluid and its enzymatic activity in response to prey capture, and assessed endogenous phytohormone content. We did not find any evidence that butterworts use jasmonate signaling for the induction of enzyme activities.

Materials and methods

Plant material and experimental setup

We used a horticultural hybrid of *Pinguicula* × *Tina* (*Pinguicula agnata* × *Pinguicula zecheri*) purchased from Gartneriet Lammehave (Ringe, Denmark) and *Drosera capensis* in our experiments (Fig. 1A). *Pinguicula* × *Tina* is famous for being vigorous and easy to grow, with many flowers, and producing large leaves with a sufficient amount of digestive fluid for analyses. Plants were grown at the Department of Biophysics of Palacký University in Olomouc, Czech Republic, under standard greenhouse conditions. Plants were grown in plastic pots filled with well-drained peat moss, placed in a tray filled with distilled water to a depth of 1–2 cm. During the experiments the plants were placed in a growth chamber maintained at 21–22 °C and 100 μmol m^{-2} s^{-1} photosynthetically active radiation, with a 16/8 h light/dark period.

Fruit flies (*Drosophila melanogaster*) were used as a model prey. Flies were cultured from eggs in a carbohydrate-rich medium and were provided by the Department of Genetics, Faculty of Natural Sciences Comenius University in Bratislava, Slovakia. Before the experiments, adult flies were cooled in a refrigerator at 4 °C for 15 minutes to facilitate manipulation. Ten fruit flies were placed on one leaf surface or one flower stalk of plant under study (Fig. 1B, C). After 2 h and 24 h, 10 control and 10 fed leaves were cut off the plant using a scalpel, and leaf blades were submerged one at a time in 4 ml of 50 mM sodium acetate buffer solution (pH 5.0) for 3 min to collect the exudates. Because of seasonal blooming, the limited number and low biomass of flower stalks available were collected only after 24 h.

In the experiments with jasmonates (see below), plants were sprayed with 1 mM jasmonic acid or 100 μM coronatine in 0.001% Tween 20. Control plants were sprayed with 0.001% Tween 20 only. The leaf exudates were collected after 24 h as described above. For this experiment, sundew plants (*D. capensis*) were used as a positive control, as this species is known to increase digestive enzyme synthesis in response to the exogenous application of jasmonates (Krausko *et al.*, 2017). For experiments

Fig. 1. Butterwort *Pinguicula* × *Tina*. (A) Whole plant. (B) Flower stalk covered with digestive glands. (C) Leaf covered with stalked and sessile glands.

with hypertonic NaCl solution, 20 µl drops of 5% NaCl or distilled water (as a control) were applied on the glandular leaf surface and collected using a pipette after 15 min. This time point was chosen as sufficiently long to induce the flow of water from the glands but too short for the synthesis and secretion of digestive enzymes *de novo* (based on our experience with Venus flytrap; Jakšová *et al.*, 2020; Pavlovič *et al.*, 2020). For wounding experiments, a leaf was wounded with a needle once for electrical signal measurement or 10–15 times for phytohormone analyses (see below).

Extracellular recording of electrical signals

Changes in the surface potential were measured by using non-polarizable Ag–AgCl surface electrodes (Scanlab Systems, Prague, Czech Republic) moistened with a drop of conductive EV gel (Hellada, Prague, Czech Republic) that is commonly used in electrocardiography. The electrode was attached on the abaxial side of the leaf either beneath an applied fly (*D. melanogaster*) or 1 cm from a wounding site that was made with a needle. The electrical signals were recorded by a non-invasive device inside a Faraday cage according to Ilík *et al.* (2010). The reference electrode was taped to the side of the plastic pot containing the plant, submerged in 1–2 cm of water in a dish beneath the pot. The electrodes were connected to an amplifier [gain 1–1000, noise 2–3 µV, bandwidth (–3 dB) 10^5 Hz, response time 10 µs, input impedance 10^{12} Ω]. The signals from the amplifier were transferred to an analogue–digital PC data converter (eight analogue inputs, 12-bit converter, ±10 V, PCA-7228AL, supplied by TEDIA, Plzeň, Czech Republic), collected every 6 ms.

Measurements of enzyme activities

The proteolytic activity of digestive fluid was determined by incubating 150 µl of the collected sample of digestive fluid with 150 µl of 2% (w/v) bovine serum albumin in 200 mM glycine–HCl (pH 3.0) at 37 °C for 2 h. The reaction was stopped by the addition of 450 µl of 5% (w/v) trichloroacetic acid (TCA). Samples were incubated on ice for 10 min and then centrifuged at 20 000 *g* for 10 min at 4 °C. The amount of released non-TCA-precipitable peptides was used as a measure of proteolytic activity, which was determined by comparing the absorbance of the supernatant at 280 nm with that of a blank sample with a Specord 250 Plus double-beam spectrophotometer (Analytik Jena). One unit of proteolytic activity is defined as an increase of 0.001 min^{-1} in the absorbance at 280 nm (Matušíková *et al.*, 2005).

We used 5 mM 4-nitrophenyl phosphate (Sigma-Aldrich) in 50 mM acetate buffer (pH 5) to estimate the activity of acid phosphatases. A 50 µl sample of the collected digestive fluid was added to 500 µl of the acetate buffer and mixed with 400 µl of the substrate. As a control, 400 µl of substrate solution was added to 550 µl of buffer. Mixed samples were incubated at 25 °C for 2 h. Thereafter, 160 µl of 1.0 M NaOH was added to terminate the reaction. Absorbance was measured at 410 nm with a Specord 250 Plus double-beam spectrophotometer (Analytik Jena). The calibration curve was determined using 4-nitrophenol and the activities were expressed in µmol ml^{-1} h^{-1}.

Amylase activity was measured using an amylase assay kit (Sigma-Aldrich). Ethylidene-pNP-G7 was used as a substrate, which upon cleavage by amylase generates 4-nitrophenyl. A 20 µl aliquot of collected digestive fluid was added to a 96-well plate and adjusted to 50 µl with the amylase assay buffer. Then 100 µl of substrate was added, the reaction mixture was incubated at 25 °C, and absorbance at 405 nm was measured every 15 min for 2 h using a SynergyMx microplate reader (BioTek Instruments, Winooski, VT, USA). Positive control (amylase enzyme) and 4-nitrophenyl standard at different concentrations were incubated under the same conditions on the same microplate.

Chitinase activities were measured using a fluorimetric chitinase assay kit (Sigma Aldrich). We used 4-methylumbelliferyl *N*-acetyl-β-D-glucosaminide, 4-methylumbelliferyl *N*,*N*′-diacetyl-β-D-chitobioside, and 4-methylumbelliferyl β-D-*N*,*N*′,*N*″-triacetylchitotriose for the detection of β-*N*-acetylglucosaminidase (exochitinase), chitobiosidase, and endochitinase activities, respectively, according to the manufacturer's instructions. A 10 µl aliquot of collected digestive fluid was incubated with 90 µl of substrate working solution at 37 °C and after 2 h the reaction was stopped by the addition of 200 µl of sodium carbonate provided in the kit. The fluorescence of liberated 4-methylumbelliferone was measured in alkaline pH using a SynergyMx microplate reader (BioTek Instruments, Winooski, VT, USA) with excitation at 360 nm and emission at 450 nm. Chitinase from *Trichoderma viride* (positive control) and 4-methylumbelliferone standard at different concentrations were incubated under the same conditions on the same microplate.

All enzyme activities were measured on pooled samples from 10 leaves from 3 plants to have sufficiently concentrated samples within the limit of detection.

SDS-PAGE electrophoresis

Digestive fluid collected for the enzyme assays was subjected to SDS-PAGE. The samples were heated and denatured for 30 min at 70 °C and then mixed with modified Laemmli sample buffer to a final concentration of 50 mM Tris–HCl (pH 6.8), 2% SDS, 10% glycerol, 1% β-mercaptoethanol, 12.5 mM EDTA, and 0.02% bromophenol blue. The same volume of digestive fluid was electrophoresed in 10% (v/v) SDS-polyacrylamide gel (Schägger, 2006). The proteins in the gels were visualized by silver staining (ProteoSilver; Sigma Aldrich).

Proteomic analysis of digestive fluid

Freshly collected digested fluid from fed plants was divided into 1 ml aliquots, which were subsequently frozen in liquid nitrogen

and lyophilized overnight. The dry residue corresponding to one aliquot was adjusted to 100 µl with 10× cOmplete™ Protease Inhibitor Cocktail (Roche, Switzerland) in 100 mM NaCl, and proteins were precipitated using the TCA/acetone method. Briefly, the protein sample was thoroughly mixed with 8 volumes of ice-cold acetone and 1 volume of TCA, and the resulting solution was kept at −20 °C for 1 h. The protein pellet was recovered by centrifugation at 20 000 g and 4 °C for 10 min, rinsed twice with 2 volumes of ice-cold acetone (Kim *et al.*, 2006), dissolved in Laemmli sample buffer, and separated by SDS-PAGE (Laemmli, 1970). The resolved proteins were stained with colloidal Coomassie (Candiano *et al.*, 2004) and digested in-gel with raffinose-modified trypsin (Šebela *et al.*, 2006) as described elsewhere (Shevchenko *et al.*, 2006). Peptides were cleaned on home-made C18 StageTips (Rappsilber *et al.*, 2008), and mass spectrometry (MS) analysis was done on a UHR-QTOF maXis tandem mass spectrometer (Bruker Daltonik, Bremen, Germany) coupled to a RSLCnano nanoflow capillary liquid chromatography system (Dionex, Thermo Fisher Scientific, Sunnyvale, CA, USA) via online nanoESI source (Bruker Daltonik, Bremen, Germany). The specific settings of the chromatography system and the mass analyzer were identical to those described previously (Simerský *et al.*, 2017).

The acquired MS data were either processed by classical MASCOT searches against a selected database or subjected to *de novo* sequencing. In the first case, the precursor and fragmentation data were extracted from raw data using DataAnalysis v 4.3 x64 (Bruker Daltonik, Bremen, Germany), exported into MGF files, and uploaded to Protein Scape v. 2.1 (Bruker Daltonik, Bremen, Germany). Peptide and protein searches were performed employing the MASCOT algorithm (v2.2.07, in-house server; Matrix Science, London, UK) against an order Lamiales-specific protein database (NCBI; 325 526 sequences; downloaded 23 October 2017) that was supplemented with common protein contaminants. The following parameters were used for each MASCOT search: MS and MS/MS tolerance were set at ±25 ppm and ±0.03 Da, respectively; trypsin was selected as the protease and two missed cleavages were allowed; carbamidomethylation of cysteine was included as a fixed modification; and *N*-terminal protein acetylation and methionine oxidation were selected as variable modifications. A positively identified protein had to fulfil the following parameters: contain at least one peptide with identity score calculated by the MASCOT algorithm (a cut-off score required for the other assigned peptides was 25 with *P*-value of 0.05); pass over a protein cut-off score of 30. For *de novo* sequencing, the DeNovoGUI interface (v1.16.0; Muth *et al.*, 2014) containing the Novor (Ma, 2015), DirecTag (Tabb *et al.*, 2008), PepNovo (Frank and Pevzner, 2005), and pNovo (Chi *et al.*, 2010) algorithms was applied to generate full-length peptide sequences directly from raw data. The same settings were adopted as for the MASCOT searches described above. To assign all obtained *de novo* peptide sequences, a local pBLAST search was carried out against a compiled list of proteins identified in digestive fluids from all carnivorous plant species that have been examined to date. The BLAST hits were filtered by similarity with following requirements: an alignment length of at least five amino acids; cut-off values for overall identity and positivity were set at 75%. After manual quality control of peptide spectra, all assigned *de novo* peptides were considered as positive identifications.

Quantification of phytohormones

At 2 h and 24 h after prey feeding or wounding with a needle, leaves were collected from control and fed plants and immediately (within 10 s) frozen in liquid nitrogen and stored at −80 °C until analysis. Quantification of jasmonic acid (JA), JA-Ile, *cis*-12-oxo-phytodienoic acid (*cis*-OPDA), abscisic acid (ABA), salicylic acid (SA), and indole-3-acetic acid (IAA) was performed according to the modified method described by Floková *et al.* (2014). Briefly, frozen plant material (20 mg) was homogenized and extracted using 1 ml of ice-cold 10% methanol/H_2O (v/v). A cocktail of stable isotope-labeled standards was added as follows: 10 pmol of [$^2H_6$]JA, [$^2H_2$]JA-Ile, [$^2H_5$]OPDA, [$^2H_6$]ABA, and [$^{13}C_6$]-IAA, and 20 pmol of [$^2H_4$]SA (all from Olchemim Ltd, Czech Republic) per sample to validate the LC-MS/MS method. The extracts were purified using Oasis® HLB columns (30 mg 1 ml^{-1}, Waters) and hormones were eluted with 80% methanol. The eluent was evaporated to dryness under a stream of nitrogen. Phytohormone levels were determined by ultra-high performance liquid chromatography-electrospray tandem mass spectrometry (UPLC-MS/MS) using an Acquity UPLC® I-Class System (Waters, Milford, MA, USA) equipped with an Acquity UPLC CSH® C_{18} column (100 × 2.1 mm; 1.7 µm; Waters) coupled to a Xevo™ TQ-S MS triple quadrupole mass spectrometer equipped with electrospray ionization technique (Waters MS Technologies, Manchester, UK). Three independent technical measurements were performed on 5–15 biological replicates.

Statistical analyses

Throughout this paper, data are presented as means ±SD. To evaluate the significance of differences between the control and treated plants, two-tailed Student's *t*-tests was used (Origin 2015, Northampton, MA, USA). Before the statistical tests, the data were analyzed for normality and homogeneity of variance. When non-homogeneity was present, the *t*-test was used with the appropriate corrected degrees of freedom (Welch's *t*-test).

Results

Electrical signaling

The presence of live prey did not elicit any electrical signal in the leaf for the duration of measurements (6 h). By contrast, wounding with a needle elicited depolarization of membrane potential, a typical variation potential (VP) with amplitude 15–50 mV and duration 200–400 s (negative voltage shift recorded extracellularly, representing intracellular depolarization; Fig. 2).

Insect prey-induced enzyme activity

The activities of proteases, acid phosphatases, amylases, and exochitinases increased 2 h after prey feeding (Fig. 3A–D). After 24 h, all measured enzyme activities in leaf exudates were significantly increased (Fig. 3A–F). Surprisingly, the flower stalk exudates also had increased proteolytic, acid phosphatase, amylase, and exochitinase activities 24 h after feeding (Fig. 3A–D).

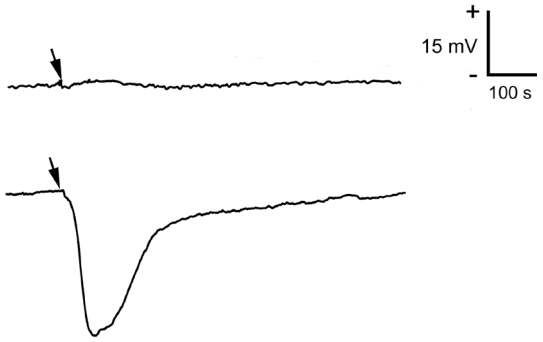

Fig. 2. Extracellular membrane potential in response to prey (*Drosophila melanogaster*) applied on the trap surface (upper trace) and wounding (lower trace) in *Pinguicula* × *Tina*. Arrows indicate the time point of stimulus application. These representative records are shown from five independent measurements.

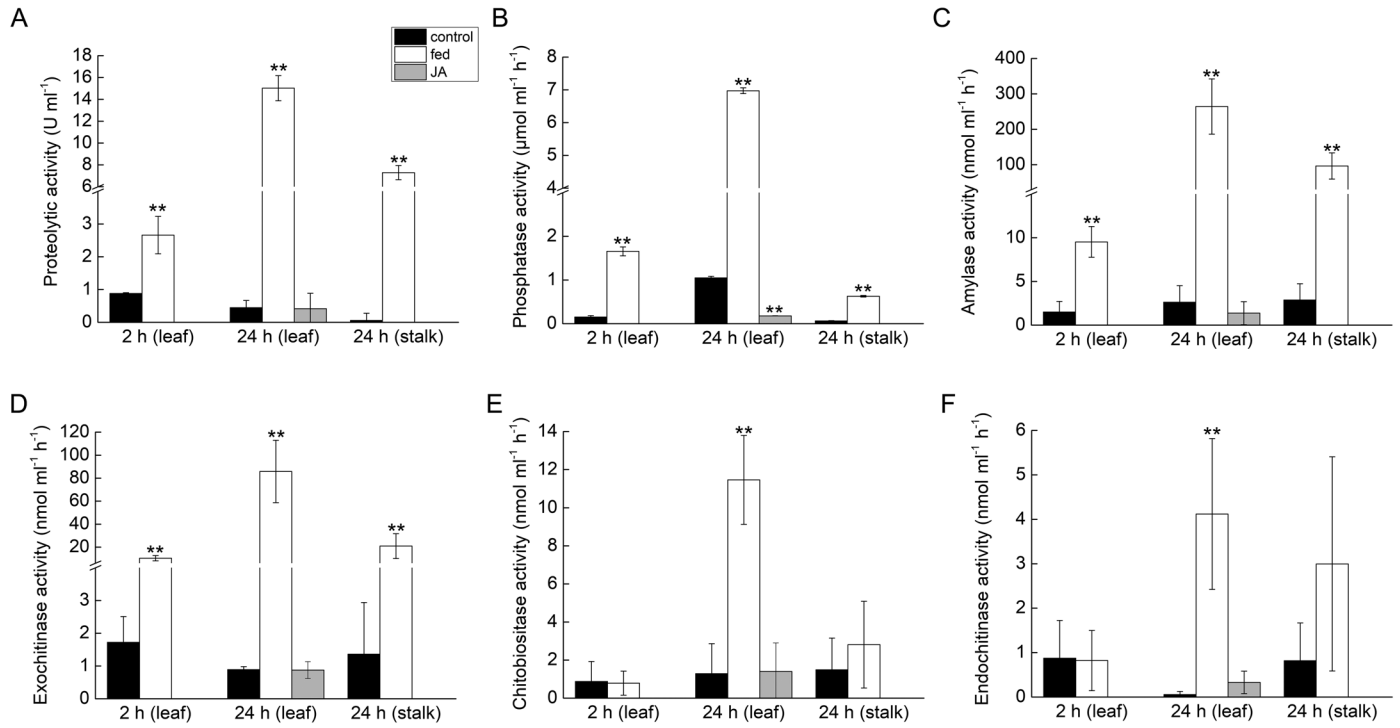

Fig. 3. Enzyme activities in *Pinguicula* × *Tina* in response to insect prey feeding and jasmonic acid (JA) application. Enzyme activities were measured 2 h and 24 h after feeding in leaf exudates, 24 h after feeding in flower stalk exudates, and 24 h after the application of 1 mM JA on the trap surface. (A) Proteolytic activity. (B) Phosphatase activity. (C) Amylase activity. (D) Exochitinase activity. (E) Chitobiosidase activity. (F) Endochitinase activity. Data are mean ±SD (n=5–6). Significant differences between control and fed plants, and between control and JA-applied plants, were evaluated by Student's t-test: $^{*}P<0.05$, $^{**}P<0.01$.

Composition of digestive fluid

Our homology based-identification strategy enabled the identification of 14 protein sequences covering 8 different catalytic activities, which included aspartic and cysteine proteases, peroxidases, esterase/lipase and endonuclease. Interestingly, the presence of alpha-amylase, an enzyme that has not been described before in the digestive fluids of the other carnivorous plants, was identified as well (Table 1; see also Supplementary Table S1 and Fig. S1 at *JXB* online).

Jasmonates are not responsible for induction of enzyme activity

The level of JA did not significantly increase at 2 h or 24 h after feeding plants with fruit flies. To investigate whether *Pinguicula* increases JA in response to damaging stimuli, leaves were wounded 10–15 times with a needle. Wounding resulted in a 10-fold increase of JA after 2 h; this increase was significant (Fig. 4A). While feeding resulted in a slight (1-fold) but significant increase of JA-Ile, wounding caused a 200-fold increase (Fig. 4B). The level of the JA precursor *cis*-OPDA was not altered significantly (Fig. 4C). Wounding also increased the level of ABA after 2 h and 24 h, whereas feeding increased the level of ABA only after 24 h (Fig. 4D). The level of SA did not increase in response to either stimulus, and only a significant decrease in response to wounding was detected at 24 h (Fig. 4E). The level of IAA level remained more or less constant in fed plants (Fig. 4F); IAA analysis in wounded leaves failed.

To confirm that jasmonates are not involved in enzyme secretion, we applied JA and coronatine (a molecular mimic of JA-Ile) exogenously. Neither JA nor coronatine was able to induce enzyme activity (Figs 3 and 5). SDS-PAGE confirmed that JA, ABA, and coronatine did not induce the secretion of proteins, and the protein profile of treated plants was comparable to that of control plants (Fig. 6). For control experiments, we used sundew plants (*D. capensis*), which are known to regulate enzyme production through jasmonates (Krausko *et al.*, 2017). Sundew plants showed a significant increase in enzyme activity in leaf exudates after coronatine treatment (Fig. 5). In response to exogenous coronatine, sundew plants folded their tentacles and traps not only locally to the site of coronatine application but also systemically, and both local and systemic leaves started to secrete digestive fluid. No such behaviour was observed in *Pinguicula* × *Tina* plants, which cannot fold their leaves.

Rapid efflux of water is responsible for induction of phosphatase activity

To induce a rapid efflux of water from the digestive glands of *Pinguicula* plants, we applied hypertonic 5% NaCl solution to the glandular leaf surface. The secretion was collected 15 min later for further analyses. Measurements of enzyme activity showed a 30-fold increase of phosphatase activity in digestive fluid within 15 min (Fig. 7B). The proteolytic activity was not significantly increased in comparison to controls (leaves treated with water) (Fig. 7C). Amylase and chitobiosidase

Table 1. Proteins identified by mass spectrometry analysis in *Pinguicula* × *Tina* digestive fluid collected 24 h after feeding on fruit flies

MS data processing method	**Identification characteristics**				
MASCOT search	**Detected sequence**	**Assigned protein**	**Accession[a]**	**MASCOT score**	**Peptides/PSMs/SC[b]**
	LAASILR	Peroxidase 10-like	KZV23101.1	33.5	1/3/2.1
	AVADIVINHR	Alpha-amylase	EPS60632.1	38.9	1/1/2.8
	GILQAAVQGELWR	Alpha-amylase	KZV28895.1	39.9	1/4/3.4
***De novo* sequencing pBLAST search**	**Detected sequence**	**Homologous protein**	**Accession[a]**	***De novo* score**	**pBLAST identity/ positivity[c]**
	TVPMVLNGAGLLNMGPPHMK	Nepenthesin II	BAD07475.1	30.28	77/88
	WESSLNWVLCMK	Asp protease	GAV80475.1	30.93	75/75
	HQMLVALQYYCNR	Cysteine protease	BAW35427.1	32.63	83/83
	MVQGGSGKVAQQTLAAN	Desiccation-related protein	BAW35440.1	31.03	75/100
	GRLMVAGLGGLGMKER	Cinnamyl alcohol dehydro-	-	35.07[d]	87/87[d]
	PNKFGVGLGGLGLMQR	genase		35.08[d]	100/100[d]
	MPVDFNVTATFHLQ	Leu-rich repeat protein NrLRR1	-	33.77	75/100
	SLNLNSLRGNVK	Peroxidase	BAM28609.1	32.28	100/100
	YYFNLNYPEGFTK	Beta-xylosidase	AAX92967.1	40.02	85/85
	TLLSDLVNSTTAMMK	Peroxidase	-	34.23	77/100
	ARMTNMRNKVQQVQQNMPR	GDSL esterase/lipase	XP_004232991.1	30.64	77/77
	AQKRNWVQQWQR	Endonuclease 2	-	32.59	100/100

[a] NCBI database accession. [b] PSMs, peptide-spectrum matches; SC, sequence coverage in %. [c] pBLAST identity and positivity in %. [d] Characteristics for two independent peptide hits acquired for the respective protein.

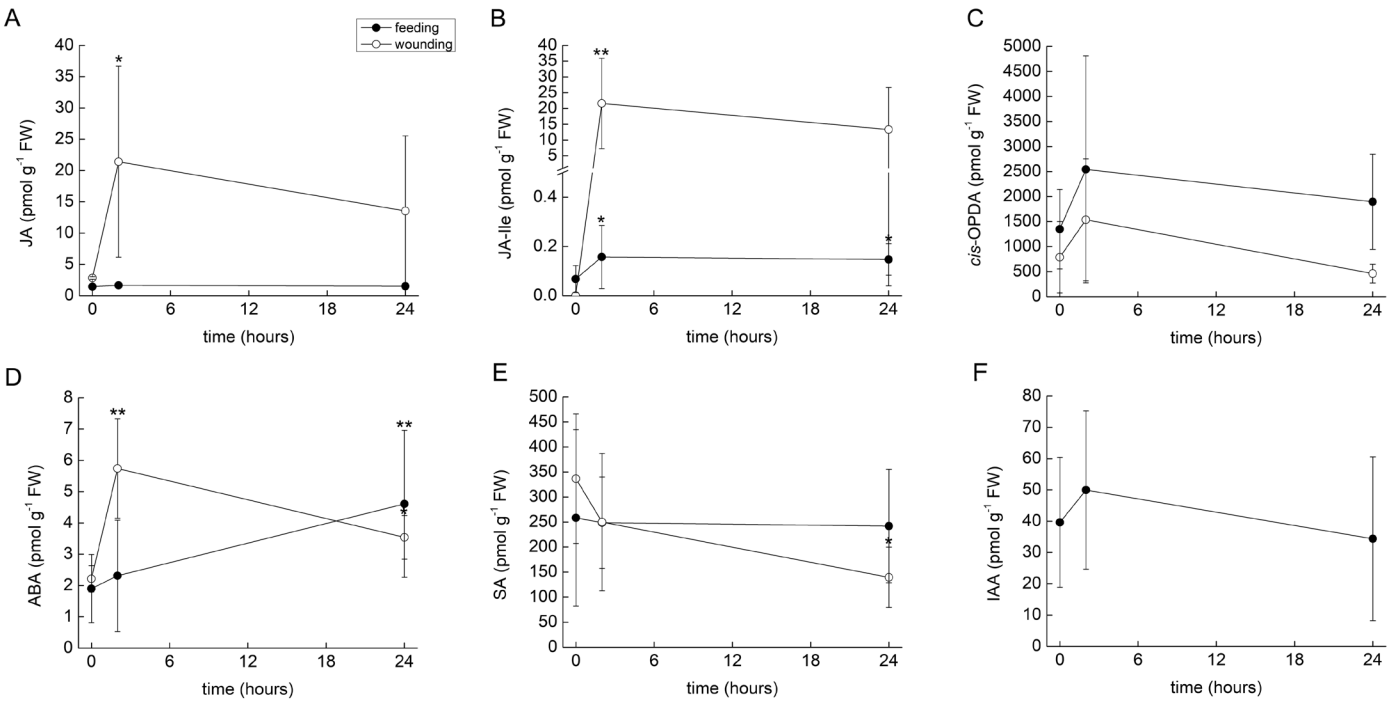

Fig. 4. Tissue levels of phytohormones in *Pinguicula* × *Tina* in response to feeding and wounding. (A) Jasmonic acid (JA). (B) Isoleucine conjugate of jasmonic acid (JA-Ile). (C) *cis*-12-oxophytodienoic acid (*cis*-OPDA). (D) Abscisic acid (ABA). (E) Salicylic acid (SA). (F) Indole-3-acetic acid (IAA). Data are mean ±SD (n=5–15). Significant differences between control (time 0) and fed plants after 2 h and 24 h were evaluated by Student's t-test: *P<0.05, **P<0.01.

activities were not detected. Exochitinase and endochitinase activities were slightly but significantly increased relative to controls (Fig. 7D, E). SDS-PAGE showed the clear appearance of some proteins in the digestive fluid of NaCl-treated leaves. The most prominent was the appearance of a band at ~20 kDa (Fig. 7A).

Discussion

In order to save available resources in nutrient-poor environments, carnivorous plants produce digestive enzymes not constitutively but in response to prey capture. Mechanical and chemical stimuli from insect prey have an indispensable role

in this process (for review, see Pavlovič and Mithöfer, 2019). The carnivorous plants with active trapping mechanisms (e.g. *Drosera* and *Dionaea* spp.) rely on both stimuli (Libiaková *et al.*, 2014; Bemm *et al.*, 2016; Krausko *et al.*, 2017; Jakšová *et al.*, 2020). The carnivorous plants with passive trapping mechanisms (*Nepenthes* and *Sarracenia* spp.) rely solely on chemical stimuli (Gallie and Chang, 1997; Yilamujiang *et al.*, 2016; Saganová *et al.*, 2018). The presence of chitin, protein, or different ions (e.g. NH_4^+) has been shown to be effective in induction processes (Libiaková *et al.*, 2014; Yilamujiang *et al.*, 2016; Saganová *et al.*, 2018; Jakšová *et al.*, 2020). All these stimuli increase the level of jasmonates, which transcriptionally activate the genes encoding digestive enzymes (Bemm *et al.*, 2016; Yilamujiang *et al.*, 2016; Pavlovič *et al.*, 2017; Jakšová *et al.*, 2020). However, all these studies were confined to carnivorous plants within the order Caryophyllales.

In this study, we showed that the butterwort (*Pinguicula* × *Tina*, order Lamiales) had increased enzyme activities in digestive fluid from leaves in response to prey capture. Interestingly, the enzyme activities were also increased in flower stalk exudate, which indicates that the flower stalk of *Pinguicula* is an additional carnivorous organ—a unique adaptation among carnivorous plants. This is consistent with the uptake of nitrogen from prey captured by the flower stalk, as was previously documented in *Pinguicula vulgaris* and *Pinguicula villosa* (Hanslin and Karlsson, 1996). After prey capture, MS revealed the presence of enzymes in leaf exudate well known from other non-related genera of carnivorous plants, such as cysteine and aspartic proteases, endonuclease, and peroxidase (Hatano and Hamada, 2008, 2012; Schulze *et al.*, 2012; Lee *et al.*, 2016; Rottloff *et al.*, 2016; Fukushima *et al.*, 2017; Krausko *et al.*, 2017). We propose the names 'pinguiculain' for cysteine protease and 'pinguiculasin' for aspartic protease, following the nomenclature of Takahashi *et al.* (2009, 2012). This finding supports the hypothesis that carnivorous plants with independent origins repeatedly co-opted the same plant defense protein lineages to acquire digestive physiology (Fukushima *et al.*, 2017). However, we also found one unique enzyme that has not been identified in the secretome of carnivorous plants before: alpha-amylase. Amylase is an enzyme that catalyzes the hydrolysis of starch, a polysaccharide produced by most green plants as an energy store. Our finding is consistent with the work of Heslop-Harrison and Knox (1971), which demonstrated amylase activity in the digestive glands of *Pinguicula*. The flat leaves of *Pinguicula* often trap significant amounts of plant material (Darwin, 1875) and amylases may help to digest this alternative source of carbon, implying that *Pinguicula* is a true mixotroph. When grown in axenic culture, plants of *Pinguicula lusitanica* showed significant increases in the numbers of leaves and flowers when fed with pine pollen (Harder and Zemlin, 1968). This 'vegetarianism' of carnivorous plants within the order Lamiales is not rare; on the contrary, it is very common in the genus *Utricularia* (Peroutka *et al.*, 2008, Koller-Peroutka *et al.*, 2015) and probably also in *Genlisea* (Plachno and Wolowski, 2008). The presence of alpha-amylase in digestive fluid might represent another example of non-defense-related genes that have been co-opted for the syndrome of carnivory. The class V β-1,3-glucanases in *Nepenthes* and *Dionaea*, like alpha-amylase, are involved in embryo and pollen development and germination rather than defense responses (Michalko *et al.*, 2017). The detection of phosphatase and chitinase activities (Fig. 3) but the absence of

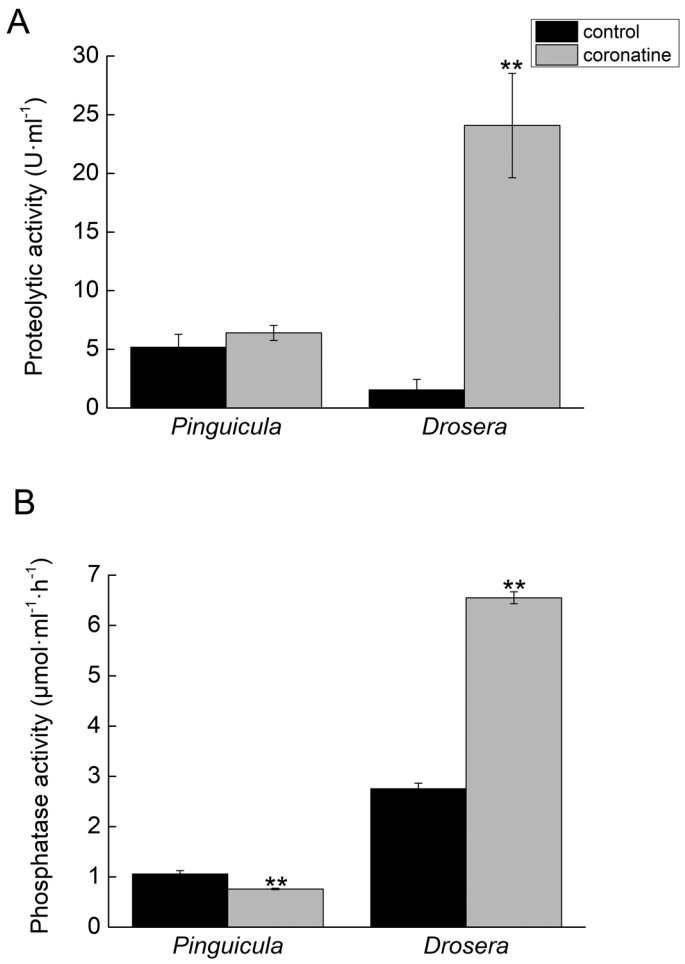

Fig. 5. Effect of application of 100 μM coronatine on enzyme activities in leaf exudates of *Pinguicula* × *Tina* and *Drosera capensis*. (A) Protease activity. (B) Phosphatase activity. Data are mean ±SD (n=5). Significant differences between control and coronatine-treated plants were evaluated by Student's t-test: *P<0.05, **P<0.01.

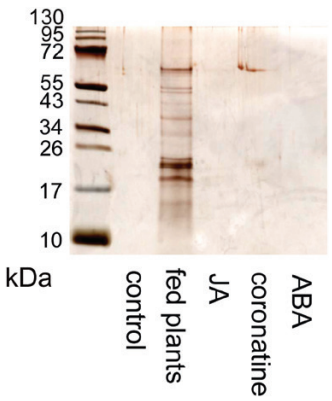

Fig. 6. Silver-stained SDS-PAGE of digestive fluid released in response to different stimuli in *Pinguicula* × *Tina*. The same volume of digestive fluid 24 h after different treatments was electrophoresed and the proteins were separated in 10% (v/v) SDS-polyacrylamide gel and silver stained. ABA, abscisic acid; JA, jasmonic acid.

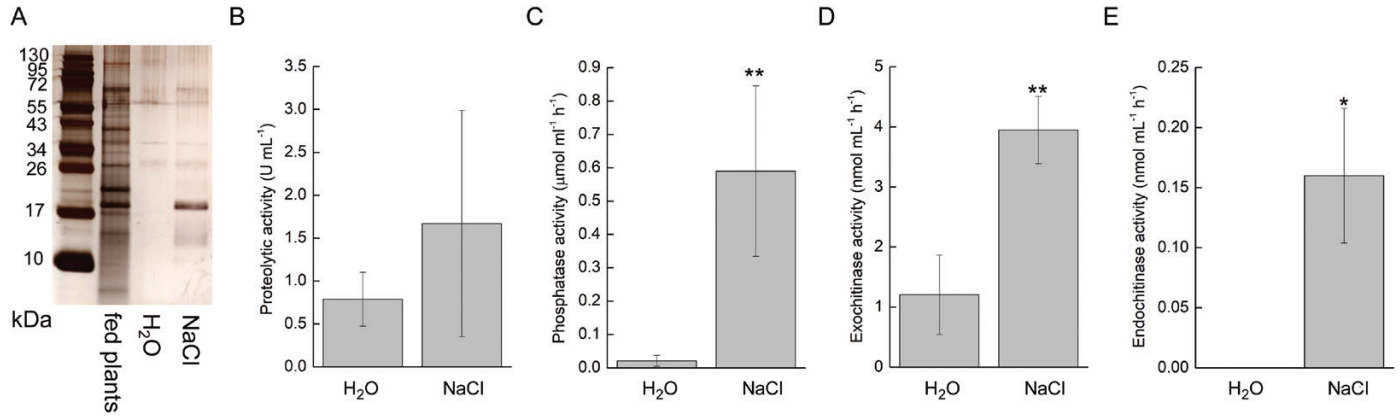

Fig. 7. Silver-stained SDS-PAGE and enzyme activities in the digestive fluid released in response to salt application in *Pinguicula* × *Tina*. (A) Protein profile resolved by SDS-PAGE. The same volume of digestive fluids 15 minutes after H_2O and 5% NaCl application and 24 h after feeding was electrophoresed and the proteins were separated in 10% (v/v) SDS-polyacrylamide gel and silver stained. (B) Proteolytic activity. (C) Phosphatase activity. (D) Exochitinase activity. (E) Endochitinase activity. Data are mean ±SD (n=3–6). Significant differences between H_2O and 5% NaCl treated plants were evaluated by Student's t-test: *P<0.05, **P<0.01

corresponding enzymes in the acquired dataset, together with rather modest coverages obtained for the assigned sequences, indicate that our proteomic analysis was not exhaustive and more enzymes could be present in the digestive fluid of *Pinguicula*. The most probable cause of this disparity is the lack of appropriate genomic background, which is a prerequisite for each protein identification experiment.

If these proteins were repeatedly co-opted for digestive physiology, it is tempting to assume that the signaling pathway would also be. Jasmonate signaling has been investigated in only three genera of carnivorous plants so far (*Dionaea*, *Drosera*, and *Nepenthes*), all of which are within the order Caryophyllales. All of these carnivorous plants increase their endogenous level of jasmonates (JA and JA-Ile) in response to prey capture and secrete enzymes in response to the exogenous application of these jasmonates (Nakamura *et al.*, 2013; Yilamujiang *et al.*, 2016; Krausko *et al.*, 2017; Pavlovič *et al.*, 2017). However, in this study we showed that neither of these phenomena occur in *Pinguicula*. A slight increase in JA-Ile was found in response to feeding (Fig. 4B), but such an increase could be caused by the presence of chitin in the applied insect exoskeleton and has probably no function in plant carnivory. This is supported by the fact that the exogenous application of JA and coronatine could not mimic insect prey and enzyme production was not increased in response to their application (Figs 3 and 5). The slight increase of endogenous ABA after feeding (Fig. 4B) was probably also caused by the presence of chitin in the insect exoskeleton, which may increase ABA concentrations (Iriti and Faoro, 2008; Iriti *et al.*, 2009, Jakšová *et al.*, 2020). The SDS-PAGE protein profiles in response to coronatine, JA, and ABA application strongly differ from those induced by insect prey and resemble control (unfed) plants, with no detectable protein bands (Fig. 6). In carnivorous plants of the genera *Drosera* and *Dionaea*, the exogenous application of jasmonates induces the same protein spectra as the application of live prey (compare Fig.7 in Krausko *et al.*, 2017, or Fig. 6 in Pavlovič *et al.*, 2017). In other words, the application of jasmonates to *Pinguicula* cannot mimic the presence of insect prey, which is in contrast to the response to exogenous jasmonates of carnivorous plants in the order Caryophyllales. To investigate whether other plant hormones might activate enzyme secretion by *Pinguicula*, we applied 100 μM gibberellic acid (GA_3), 250 μM SA, and 200 nM IAA, but none of these phytohormones was able to trigger significant enzyme activities in digestive fluid (data not shown).

The absence of jasmonate signaling in the genus *Pinguicula* could be explained by the absence of electrical signaling in its prey-detection system, in contrast to *Drosera* and *Dionaea* (Böhm *et al.*, 2016; Krausko *et al.*, 2017, Pavlovič *et al.*, 2017). In these genera, electrical and jasmonate signaling enable the coordinated activation of digestive processes in neighbouring glands that have not touched the insect prey. In *Pinguicula*, the activation of digestive glands is confined to the release of digestive fluid in response to chemical stimuli from the prey itself and the glands that have made contact with it (Heslop-Harrison and Knox, 1971). However, in some carnivorous plant species the presence of chemical signals from insect prey alone is able to trigger JA accumulation, as was documented in passive pitcher traps of *Nepenthes* (Yilamujiang *et al.*, 2016). This indicates that rapid electrical signals are not necessary for the induction of JA signaling in carnivorous plants. Thus, their absence in prey detection cannot account for the observation that *Pinguicula* does not use jasmonate signaling for the regulation of enzyme secretion.

The mechanism triggering enzyme secretion in the genus *Pinguicula* remains a subject for future research, given that our findings indicate that the jasmonates were not co-opted for plant carnivory in this genus. Heslop-Harrison and Knox (1971) proposed that the enzymes are pre-synthesized and stored in the vacuoles and cell walls of digestive glands, and are released only by the flux of water triggered by prey capture. They suggested total autolysis of the cells, in contrast to Vassilyev and Muravnik (1988a, b), who argued that secretory cells of the digestive glands remain highly active during the entire period of prey digestion. Vassilyev and Muravnik (1988a, b) also suggested that additional digestive enzymes are synthesized

de novo after stimulation, as occurs in Venus flytrap. Based on our experiments with NaCl, it seems that at least phosphatases are pre-synthesized and are only flushed away from the cell walls of the digestive glands by chloride ion movement (Heslop-Harrison and Heslop-Harrison, 1980). Indeed, a cytochemical study of the leaf gland enzymes in *Pinguicula* showed the presence of phosphatases in the spongy radial walls of the head of the unstimulated gland, which are clearly flushed away by the flux of water (Heslop-Harrison and Knox, 1971). However, some of the enzymes need to be synthesized *de novo* (e.g. proteases and amylases). The signal that triggers the expression of these enzymes remains unknown.

Conclusions

Our study clearly shows that whereas the proteomic composition of digestive fluid is similar among different orders of carnivorous plants (with the exception of alpha-amylase), the mode of their regulation may differ. This finding is consistent with the study of Nishimura *et al.* (2013), who found S-like RNases in three genera of carnivorous plants from two orders, but with different regulation of their expression. Although the genus *Pinguicula* shows strongly enhanced enzyme secretion in response to prey capture, jasmonates are not involved in this process. The hypothesis that the digestive enzymes are pre-synthesized and only flushed away by water outflow cannot be accepted entirely. The type of signal that is involved after prey capture in *Pinguicula* remains unknown.

Supplementary data

Supplementary data are available at *JXB* online.

Fig. S1. Protein profile of the digestive fluid from *Pinguicula* × *Tina* in response to feeding.

Table S1. Proteins identified in the digestive fluid of *Pinguicula* × *Tina*.

Acknowledgements

This work was supported by Internal Grant of Palacký University (IGA_PrF_2019_030 and IGA_PrF_2019_020) and grant no. CZ.02.1.01/0.0/0.0/16_019/0000827 (Plants as a Tool for Sustainable Global Development) from the Operational Programme Research, Development and Education, Ministry of Education Youth and Sports, Czech Republic. We thank Tanya Renner (Pennsylvania State University, USA) for critical reading of the early version of the manuscript.

Author contributions

AP designed the study and measured electrical signals; JJ, IP, and ON did phytohormone analysis; OK measured enzyme activities and SDS-PAGE; IC and RL analysed the composition of digestive fluid; OK and AP wrote the manuscript; AP and ON provided materials and financial support.

References

Albert VA, Williams SE, Chase MW. 1992. Carnivorous plants: phylogeny and structural evolution. Science **257**, 1491–1495.

Athauda SB, Matsumoto K, Rajapakshe S, *et al*. 2004. Enzymic and structural characterization of nepenthesin, a unique member of a novel subfamily of aspartic proteinases. Biochemical Journal **381**, 295–306.

Bemm F, Becker D, Larisch C, *et al*. 2016. Venus flytrap carnivorous lifestyle builds on herbivore defense strategies. Genome Research **26**, 812–825.

Böhm J, Scherzer S, Krol E, *et al*. 2016. The Venus flytrap *Dionaea muscipula* counts prey-induced action potentials to induce sodium uptake. Current Biology **26**, 286–295.

Candiano G, Bruschi M, Musante L, Santucci L, Ghiggeri GM, Carnemolla B, Orecchia P, Zardi L, Righetti PG. 2004. Blue silver: a very sensitive colloidal Coomassie G-250 staining for proteome analysis. Electrophoresis **25**, 1327–1333.

Chi H, Sun RX, Yang B, *et al*. 2010. pNovo: *de novo* peptide sequencing and identification using HCD spectra. Journal of Proteome Research **9**, 2713–2724.

Chini A, Fonseca S, Fernández G, *et al*. 2007. The JAZ family of repressors is the missing link in jasmonate signalling. Nature **448**, 666–671.

Darwin C. 1875. Insectivorous plants. London: John Murray.

Eilenberg H, Pnini-Cohen S, Schuster S, Movtchan A, Zilberstein A. 2006. Isolation and characterization of chitinase genes from pitchers of the carnivorous plant *Nepenthes khasiana*. Journal of Experimental Botany **57**, 2775–2784.

Escalante-Pérez M, Krol E, Stange A, Geiger D, Al-Rasheid KA, Hause B, Neher E, Hedrich R. 2011. A special pair of phytohormones controls excitability, slow closure, and external stomach formation in the Venus flytrap. Proceedings of the National Academy of Sciences, USA **108**, 15492–15497.

Fleischman A, Roccia A. 2018. Systematics and evolution of Lentibulariaceae: I. *Pinguicula*. In: Ellison AM, Adamec L, eds. Carnivorous plants. Physiology, ecology, and evolution. Oxford: Oxford University Press, 70–80.

Fleischmann A, Schlauer J, Smith SA, Givnish TJ. 2018. Evolution of carnivory in angiosperms. In: Ellison AM, Adamec L, eds. Carnivorous plants. Physiology, ecology, and evolution. Oxford: Oxford University Press, 22–41.

Floková K, Tarkowská D, Miersch O, Strnad M, Wasternack C, Novák O. 2014. UHPLC-MS/MS based target profiling of stress-induced phytohormones. Phytochemistry **105**, 147–157.

Fonseca S, Chini A, Hamberg M, Adie B, Porzel A, Kramell R, Miersch O, Wasternack C, Solano R. 2009. (+)-7-*iso*-Jasmonyl-L-isoleucine is the endogenous bioactive jasmonate. Nature Chemical Biology **5**, 344–350.

Frank A, Pevzner P. 2005. PepNovo: de novo peptide sequencing via probabilistic network modeling. Analytical Chemistry **77**, 964–973.

Fukushima K, Fang X, Alvarez-Ponce D, *et al*. 2017. Genome of the pitcher plant *Cephalotus* reveals genetic changes associated with carnivory. Nature Ecology Evolution **1**, 0059.

Gallie DR, Chang SC. 1997. Signal transduction in the carnivorous plant *Sarracenia purpurea*. Plant Physiology **115**, 1461–1471.

Givnish TJ. 2015. New evidence on the origin of carnivorous plants. Proceedings of the National Academy of Sciences, USA **112**, 10–11.

Hanslin HM, Karlsson PS. 1996. Nitrogen uptake from prey and substrate as affected by prey capture level and plant reproductive status in four carnivorous plant species. Oecologia **106**, 370–375.

Harder R, Zemlin I. 1968. Blütenbildung von *Pinguicula lusitanica in vitro* durch Fütterung mit pollen. Planta **78**, 72–78.

Hatano N, Hamada T. 2008. Proteome analysis of pitcher fluid of the carnivorous plant *Nepenthes alata*. Journal of Proteome Research **7**, 809–816.

Hatano N, Hamada T. 2012. Proteomic analysis of secreted protein induced by a component of prey in pitcher fluid of the carnivorous plant *Nepenthes alata*. Journal of Proteomics **75**, 4844–4852.

Heslop-Harrison Y. 2004. Pinguicula L. Journal of Ecology **92**, 1071–1118.

Heslop-Harrison Y, Heslop-Harrison J. 1980. Chloride ion movement and enzyme secretion from the digestive glands of *Pinguicula*. Annals of Botany **45**, 729–731.

Heslop-Harrison Y, Heslop-Harrison J. 1981. The digestive glands of *Pinguicula*: structure and cytochemistry. Annals of Botany **47**, 293–319.

Heslop-Harrison Y, Knox RB. 1971. A cytochemical study of the leaf-gland enzymes of insectivorous plants of the genus *Pinguicula*. Planta **96**, 183–211.

Ilík P, Hlaváčková V, Krchňák P, Nauš J. 2010. A low-noise multichannel device for the monitoring of systemic electrical signal propagation in plants. Biologia Plantarum **54**, 185–190.

Iriti M, Faoro F. 2008. Abscisic acid is involved in chitosan-induced resistance to tobacco necrosis virus (TNV). Plant Physiology and Biochemistry **46**, 1106–1111.

Iriti M, Valentina Picchi V, Rossoni M, Gomarasca S, Ludwig N, Gargano M, Faoro F. 2009. Chitosan antitranspirant activity is due to abscisic acid-dependent stomatal closure. Environmental and Experimental Botany **66**, 493–500.

Jakšová J, Libiaková M, Bokor B, Petřík I, Novák O, Pavlovič A. 2020. Taste for protein: chemical signal from prey activates jasmonate signalling in the carnivorous plant Venus flytrap (*Dionaea muscipula* Ellis). Plant Physiology and Biochemistry **146**, 90–97.

Kim SC, Chen Y, Mirza S, Xu Y, Lee J, Liu P, Zhao Y. 2006. A clean, more efficient method for in-solution digestion of protein mixtures without detergent or urea. Journal of Proteome Research **5**, 3446–3452.

Koller-Peroutka M, Lendl T, Watzka M, Adlassnig W. 2015. Capture of algae promotes growth and propagation in aquatic *Utricularia*. Annals of Botany **115**, 227–236.

Krausko M, Perutka Z, Šebela M, Šamajová O, Šamaj J, Novák O, Pavlovič A. 2017. The role of electrical and jasmonate signalling in the recognition of captured prey in the carnivorous sundew plant *Drosera capensis*. New Phytologist **213**, 1818–1835.

Laemmli UK. 1970. Cleavage of structural proteins during the assembly of the head of bacteriophage T4. Nature **227**, 680–685.

Legendre L. 2000. The genus *Pinguicula* L. (Lentibulariaceae): an overview. Acta Botanica Gallica **147**, 77–95.

Lee L, Zhang Y, Ozar B, Sensen CW, Schriemer DC. 2016. Carnivorous nutrition in pitcher plants (*Nepenthes* spp.) via an unusual complement of endogenous enzymes. Journal of Proteome Research **15**, 3108–3117.

Libiaková M, Floková K, Novák O, Slováková L, Pavlovič A. 2014. Abundance of cysteine endopeptidase dionain in digestive fluid of Venus flytrap (*Dionaea muscipula* Ellis) is regulated by different stimuli from prey through jasmonates. PLoS One **9**, e104424.

Ma B. 2015. Novor: real-time peptide de novo sequencing software. Journal of the American Society for Mass Spectrometry **26**, 1885–1894.

Matušíková I, Salaj J, Moravcíková J, Mlynárová L, Nap JP, Libantová J. 2005. Tentacles of in vitro-grown round-leaf sundew (*Drosera rotundifolia* L.) show induction of chitinase activity upon mimicking the presence of prey. Planta **222**, 1020–1027.

Michalko J, Renner T, Mészáros P, Socha P, Moravčíková J, Blehová A, Libantová J, Polóniová Z, Matušíková I. 2017. Molecular characterization and evolution of carnivorous sundew (*Drosera rotundifolia* L.) class V β-1,3-glucanase. Planta **245**, 77–91.

Muth T, Weilnböck L, Rapp E, Huber CG, Martens L, Vaudel M, Barsnes H. 2014. DeNovoGUI: an open source graphical user interface for *de novo* sequencing of tandem mass spectra. Journal of Proteome Research **13**, 1143–1146.

Nakamura Y, Reichelt M, Mayer VE, Mithöfer A. 2013. Jasmonates trigger prey-induced formation of 'outer stomach' in carnivorous sundew plants. Proceedingsof the Royal Society B: Biological Sciences **280**, 20130228.

Nishimura E, Kawahara M, Kodaira R, Kume M, Arai N, Nishikawa J, Ohyama T. 2013. S-like ribonuclease gene expression in carnivorous plants. Planta **238**, 955–967.

Pavlovič A, Jakšová J, Novák O. 2017. Triggering a false alarm: wounding mimics prey capture in the carnivorous Venus flytrap (*Dionaea muscipula*). New Phytologist **216**, 927–938.

Pavlovič A, Libiaková M, Bokor B, Jakšová J, Petřík I, Novák O, Baluška F. 2020. Anaesthesia with diethyl ether impairs jasmonate signalling in the carnivorous plant Venus flytrap (*Dionaea muscipula*). Annals of Botany **125**, 173–183.

Pavlovič A, Mithöfer A. 2019. Jasmonate signalling in carnivorous plants: copycat of plant defence mechanisms. Journal of Experimental Botany **70**, 3379–3389.

Pavlovič A, Saganová M. 2015. A novel insight into the cost–benefit model for the evolution of botanical carnivory. Annals of Botany **115**, 1075–1092.

Peroutka M, Adlassnig W, Volgger M, Lendl T, Url WG, Lichtscheidl IK. 2008. *Utricularia*: a vegetarian carnivorous plant? Plant Ecology **199**, 153–162.

Plachno BJ Wolowski K. 2008. Algae commensal community in *Genlisea* traps. Acta Societatis Botanicorum Poloniae **77**, 77–86.

Rappsilber J, Mann M, Ishihama Y. 2008. Protocol for micro-purification, enrichment, pre-fractionation and storage of peptides for proteomics using StageTips. Nature Protocols **2**, 1896–1906.

Rottloff S, Miguel S, Biteau F, *et al*. 2016. Proteome analysis of digestive fluids in *Nepenthes* pitchers. Annals of Botany **117**, 479–495.

Rottloff S, Stieber R, Maischak H, Turini FG, Heubl G, Mithöfer A. 2011. Functional characterization of a class III acid endochitinase from the traps of the carnivorous pitcher plant genus, *Nepenthes*. Journal of Experimental Botany **62**, 4639–4647.

Saganová M, Bokor B, Stolárik T, Pavlovič A. 2018. Regulation of enzyme activities in carnivorous pitcher plants of the genus *Nepenthes*. Planta **248**, 451–464.

Schägger H. 2006. Tricine-SDS-PAGE. Nature Protocols **1**, 16–22.

Schulze WX, Sanggaard KW, Kreuzer I, *et al*. 2012. The protein composition of the digestive fluid from the Venus flytrap sheds light on prey digestion mechanisms. Molecular and Cellular Proteomics **11**, 1306–1319.

Šebela M, Štosová T, Havlis J, Wielsch N, Thomas H, Zdráhal Z, Shevchenko A. 2006. Thermostable trypsin conjugates for high-throughput proteomics: synthesis and performance evaluation. Proteomics **6**, 2959–2963.

Sheard LB, Tan X, Mao H, *et al*. 2010. Jasmonate perception by inositol-phosphate-potentiated COI1-JAZ co-receptor. Nature **468**, 400–405.

Shevchenko A, Tomas H, Havlis J, Olsen JV, Mann M. 2006. In-gel digestion for mass spectrometric characterization of proteins and proteomes. Nature Protocols **1**, 2856–2860.

Simerský R, Chamrád I, Kania J, Strnad M, Šebela M, Lenobel R. 2017. Chemical proteomic analysis of 6-benzylaminopurine molecular partners in wheat grains. Plant Cell Reports **36**, 1561–1570.

Tabb DL, Ma ZQ, Martin DB, Ham AJ, Chambers MC. 2008. DirecTag: accurate sequence tags from peptide MS/MS through statistical scoring. Journal of Proteome Research **7**, 3838–3846.

Takahashi K, Matsumoto K, Nishi W, Muramatsu M, Kubota K, Shibata C, Athauda SBP. 2009. Comparative studies on the acid proteinase activities in the digestive fluids of *Nepenthes*, *Cephalotus*, *Dionaea*, and *Drosera*. Carnivorous Plant Newsletter **38**, 75–82.

Takahashi K, Nishii W, Shibata C. 2012. The digestive fluid of *Drosera indica* contains a cysteine endopeptidase ("Droserain") similar to dionain from *Dionaea muscipula*. Carnivorous Plant Newsletter **41**, 132–134.

Thines B, Katsir L, Melotto M, *et al*. 2007. JAZ repressor proteins are targets of the SCF (COI1) complex during jasmonate signalling. Nature **448**, 661–665.

Vassilyev AE, Muravnik LE. 1988a. The ultrastructure of the digestive glands in *Pinguicula vulgaris* L. (Lentibulariaceae) relative to their function. I. The changes during maturation. Annals of Botany **62**, 329–341.

Vassilyev AE, Muravnik LE. 1988b. The ultrastructure of the digestive glands in *Pinguicula vulgaris* L. (Lentibulariaceae) relative to their function. II. The changes on stimulation. Annals of Botany **61**, 343–351.

Yilamujiang A, Reichelt M, Mithöfer A. 2016. Slow food: insect prey and chitin induce phytohormone accumulation and gene expression in carnivorous *Nepenthes* plants. Annals of Botany **118**: 369–735.

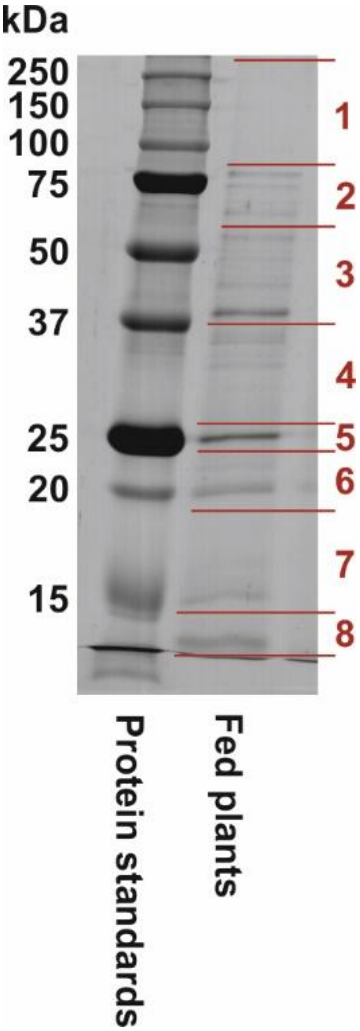

Fig. S1 Protein profile of the digestive fluid from *Pinguicula* x *Tina* in response to feeding. An aliquot (1 mL) of freshly collected digestive fluid secreted in response to feeding was frozen in liquid nitrogen and lyophilized overnight. The resulting dry residue was taken to 100 µL with 100mM NaCl, 10x cOmplete protease inhibitor cocktail (Roche, Switzerland) and proteins were precipitated using the TCA/acetone method. The obtained protein pellet was dissolved in Laemmli sample buffer, separated by SDS-PAGE and stained with colloidal Coomassie. Then, the gel was divided into 8 slices (shown with numbers) and the resolved proteins were digested in-gel with trypsin with raffinose-modified trypsin as described elsewhere. The resultant tryptic digest was cleaned on home-made C18 StageTips and analyzed by LC-ESI-MS/MS according to Simerský et al. (2017). For more detailed information, see Materials and Methods and the Supplementary Table 1.

Supplement I

Supplement II

Supplement III

Supplement IV

Supplement V

Supplement VI

Supplement VII

Supplement VIII

Jakšová J, Adamec L, **Petřík I**, Novák O, Šebela M, Pavlovič A. 2021. Contrasting effect of prey capture on jasmonate accumulation in two genera of aquatic carnivorous plants (Aldrovanda, Utricularia). Plant Physiol Biochem 166, 459–465.

Plant Physiology and Biochemistry 166 (2021) 459–465

Contents lists available at ScienceDirect

Plant Physiology and Biochemistry

journal homepage: www.elsevier.com/locate/plaphy

Short communication

Contrasting effect of prey capture on jasmonate accumulation in two genera of aquatic carnivorous plants (*Aldrovanda*, *Utricularia*)

Jana Jakšová [a], Lubomír Adamec [b], Ivan Petřík [c], Ondřej Novák [c], Marek Šebela [d], Andrej Pavlovič [a,*]

[a] Department of Biophysics, Centre of the Region Haná for Biotechnological and Agricultural Research, Faculty of Science, Palacký University, Šlechtitelů 27, CZ-783 71, Olomouc, Czech Republic
[b] Institute of Botany of the Czech Academy of Sciences, Department of Experimental and Functional Morphology, Dukelská135, CZ-379 82, Třeboň, Czech Republic
[c] Laboratory of Growth Regulators, Faculty of Science, Palacký University and Institute of Experimental Botany of the Czech Academy of Sciences, Šlechtitelů 27, CZ-783 71, Olomouc, Czech Republic
[d] Department of Biochemistry, Faculty of Science, and Centre of the Region Haná for Biotechnological and Agricultural Research, CATRIN, Palacký University, Šlechtitelů 27, CZ-783 71, Olomouc, Czech Republic

ARTICLE INFO

Keywords:
Abscisic acid
Aldrovanda vesiculosa
Carnivorous plant
Jasmonic acid
Salicylic acid
Utricularia reflexa

ABSTRACT

Terrestrial carnivorous plants of genera *Drosera*, *Dionaea* and *Nepenthes* within the order Caryophyllales employ jasmonates for the induction of digestive processes in their traps. Here, we focused on two aquatic carnivorous plant genera with different trapping mechanism from distinct families and orders: *Aldrovanda* (Droseraceae, Caryophyllales) with snap-traps and *Utricularia* (Lentibulariaceae, Lamiales) with suction traps. Using phytohormone analyses and simple biotest, we asked whether the jasmonates are involved in the activation of carnivorous response similar to that known in traps of terrestrial genera of Droseraceae (*Drosera*, *Dionaea*). The results showed that *Utricularia*, in contrast with *Aldrovanda*, does not use jasmonates for activation of carnivorous response and is the second genus in Lamiales, which has not co-opted jasmonate signalling for botanical carnivory. On the other hand, the nLC-MS/MS analyses revealed that both genera secreted digestive fluid containing cysteine protease homologous to dionain although the mode of its regulation may differ. Whereas in *Utricularia* the cysteine protease is present constitutively in digestive fluid, it is induced by prey and exogenous application of jasmonic acid in *Aldrovanda*.

1. Introduction

Carnivorous plants represent an ecological group of ca. 800 species which capture, kill and digest animal prey in specialised modified leaves called traps, and use the absorbed nutrients for growth and development (Ellison and Adamec, 2018). It has been documented that three genera of carnivorous plants (*Dionaea*, *Drosera*, and *Nepenthes*) from order Caryophyllales use jasmonates (JAs) for activation of the digestive process in their traps. Jasmonic acid (JA), its isoleucine conjugate (JA-Ile) as well as their biosynthetic precursor, *cis*-(+)-12-oxo-phytodienoic acid (*cis*-OPDA), significantly accumulated in traps over time after experimental feeding and their exogenous application triggered the secretion of digestive enzymes and formation of digestive cavity (Escalante-Pérez et al., 2011; Nakamura et al., 2013; Libiaková et al., 2014; Yilamujiang et al., 2016; Krausko et al., 2017; Pavlovič et al., 2017, 2020). In non-carnivorous plants, JAs accumulate in response to pathogen or herbivore attack and activate plant defense reactions by transcriptional activation (Wasternack and Hause, 2013). It has been suggested that the jasmonate signalling pathway as well as digestive enzymes, which belong to pathogenesis-related proteins, have been co-opted by carnivorous plants from plant defense to prey digestion during evolution (Mithöfer, 2011; Pavlovič and Saganová, 2015; Bemm et al., 2016; Pavlovič and Mithöfer, 2019). The true bioactive compound JA-Ile binds to the CORONATINE INSENSITIVE1 (COI1) protein as a part of a co-receptor complex, mediates the ubiquitin-dependent degradation of JASMONATE ZIM-DOMAIN (JAZ) repressors, resulting in the activation of jasmonate-dependent gene expression (Thines et al., 2007; Fonseca et al., 2009; Sheard et al., 2010); in carnivorous plants, it initiates the expression of carnivory-related genes, mainly for nutrient transport and digestive enzymes (Bemm et al., 2016; Böhm et al., 2016;

* Corresponding author.
E-mail address: andrej.pavlovic@upol.cz (A. Pavlovič).

https://doi.org/10.1016/j.plaphy.2021.06.014
Received 9 April 2021; Accepted 8 June 2021
Available online 16 June 2021

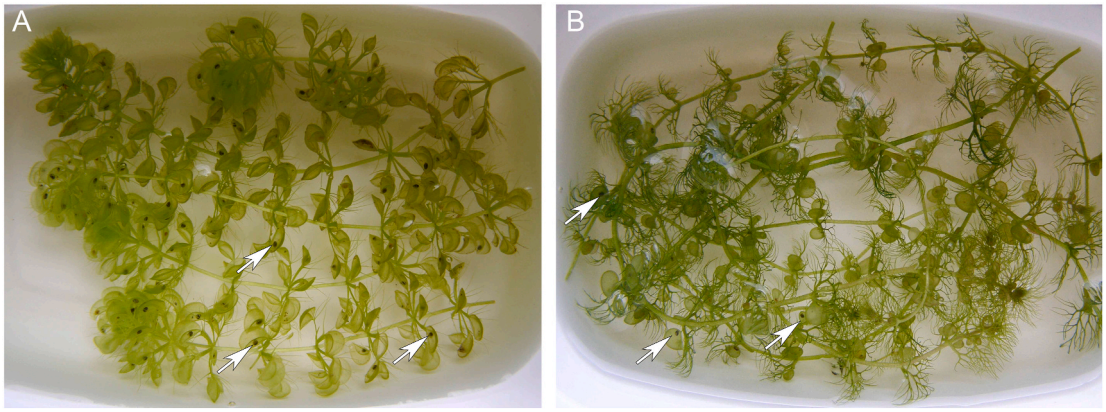

Fig. 1. Experimental setup. The plants were fed on aquatic prey for a short period. (A) *Aldrovanda vesiculosa*; (B) *Utricularia reflexa.* Arrows show the traps which successfully trapped prey and were used for analyses as fed traps.

Krausko et al., 2017; Pavlovič et al., 2017; Jakšová et al., 2020). However, all three genera mentioned above are closely related within the same order Caryophyllales. It has been recently reported that a carnivorous butterwort hybrid *Pinguicula* × *Tina* from the family Lentibulariaceae (order Lamiales) does not use jasmonate signalling for the induction of enzyme activities in response to prey capture, indicating that the jasmonate signalling is not a universal signalling pathway in all carnivorous plant genera (Kocáb et al., 2020).

In this study, we focused on two contrasting species of aquatic carnivorous plants. Aquatic carnivorous plants include monotypic *Aldrovanda vesiculosa* L. (Droseraceae, Caryophyllales) and about 60 submerged or amphibious species of *Utricularia* L. (Lentibulariaceae, Lamiales; Adamec, 2018). Although both genera of aquatic carnivores are ecologically very similar, the structures and functional principles of their motile traps are very different. *Aldrovanda* has 3–6 mm large snap-traps, reminiscent of those of the closely-related terrestrial Venus flytrap (*Dionaea muscipula*): two convex trap lobes are attached to a midrib and after mechanical irritation, generate action potentials and close within 14–50 ms (Iijima and Sibaoka, 1981, 1982; Poppinga et al., 2018; Westermeier et al., 2018, 2020). Although no digestive enzymes have been directly identified in the digestive fluid in *Aldrovanda* traps so far (Matušíková et al., 2018), exact ultrastructural studies on its digestive glands clearly revealed the stimulation mode of hydrolytic enzyme secretion after prey capture (Muravnik et al., 1995; Muravnik, 1996; Atsuzawa et al., 2020).

Suction traps of aquatic *Utricularia* species are 1–6 mm large, discoid hollow bladders with flexible side walls and contain a mobile sensitive trapdoor, hermetically sealing the trap. Continuous pumping of water out of the trap maintains a negative pressure inside the trap, which is the driving force for the prey capture (Adamec, 2018; Poppinga et al., 2016, 2018). The reset trap can open ('fire') very quickly after a mechanical stimulation or spontaneously after a critical negative pressure is reached (Adamec and Poppinga, 2016) and can repeatedly capture new prey every 30–60 min. Microbial commensal communities live inside the traps and function partly as digestion mutualists (Sirová et al., 2018a,b). Several classes of hydrolytic enzyme activities independent of prey capture have been reported from *Utricularia* traps (Sirová et al., 2003), but again no enzyme has been directly identified from the digestive fluid (Matušíková et al., 2018).

Analyses of phytohormones in traps were used in this study in two aquatic carnivores, *A. vesiculosa* and *Utricularia reflexa*, to find out whether their traps accumulate JAs in response to experimental feeding similar to terrestrial *Drosera*, *Dionaea* or *Nepenthes*. Simple biotests with JA, abscisic acid (ABA) and salicylic acid (SA) were conducted on the *Aldrovanda* trap closing reaction to reveal the possible regulatory effect of these metabolites on the activation of carnivory. In addition, LC-MS/MS analyses were used to identify new digestive enzymes in the digestive fluid.

2. Materials and methods

2.1. Plant material

Aldrovanda vesiculosa L. (origin from E Poland) and *Utricularia vulgaris* L. (from S Moravia, Czech Rep.) were grown outdoors in a 2 m^2 (volume 750 L) plastic container, while *Utricularia reflexa* Oliv. (from Botswana) and *Aldrovanda vesiculosa* (from N Australia) were grown indoors in naturally lit 3 L aquaria at the Institute of Botany in Třeboň (Czech Republic). A litter of robust *Carex* species was used as a substrate to mimic natural conditions. The water in both cultures was considered oligotrophic and moderately humic (for all details, see Sirová et al., 2003). Adult *Aldrovanda* plants were 12–20 cm long with traps 3–6 mm large, while *U. reflexa* plants were 20–30 cm long with traps 3–6 mm large and those of *U. vulgaris* were 60–80 cm long with traps 3.5–4.0 mm large. The use of *U. reflexa* was advantageous as this species has a small number of large traps.

2.2. Experimental design

Approximately 15 h before the feeding experiments, 25 robust plants of *A. vesiculosa* from the stock culture were shortened to 10 leaf whorls with mature traps (from the apex, shoot length 7—8 cm) and their branches were removed. Simultaneously, 10 plants of *U. reflexa* with large traps from the aquarium were shortened to10—15 leaf nodes (again from the apex, shoot length 6—8 cm) with mature traps; leaves bearing traps were excised from 3rd-12th mature leaf nodes (from the apex) of five *U. vulgaris* plants from the stock culture. The 15 h time period was chosen as sufficient based on the fact, that JA tissue level peaked 15–30 min after wounding in systemic tissue and then rapidly declined within 3 h to basal level (Koo et al., 2009). The plants or leaves were thoroughly washed in tap water and transferred to small plastic vessels with ca. 120 ml of filtered cultivation water taken from the outdoor plastic container. Five shoots (or seven excised leaves of *U. vulgaris*) were put in each small vessel. All traps with larger items of previously captured prey were removed. During ca. 15 h, most of the *Aldrovanda* traps were open and all *Utricularia* traps were reset and without air bubbles.

Relatively large zooplankton species (ostracods *Heterocypris incongruens* or diaptomids, copepods or daphnids) were added to the small vessels to feed the plants. After 20 min, at least 50% of *Aldrovanda* and 25% of *Utricularia* traps contained a prey (Fig. 1). Plants were then thoroughly washed in tap water again and put in small plastic vessels with ca. 200 ml of fresh filtered cultivation water without zooplankton. The vessels were transferred to a miniclimabox in continuous light (25

± 1 °C, fluorescent light 180 μmol m^{-2} s^{-1} PAR).

For phytohormone analyses, 2 and 24 h since prey addition, 12–20 traps (usually from 1 to 2 different shoots) with the captured prey, were cut as fast as possible for one sample and stored in ice-cold water during the manipulation. As a control, prey-free traps were sampled in parallel. The excised traps were then promptly (1–2 s) washed in tap water, blotted dry, weighed for fresh weight (FW), placed immediately in frozen 2 ml Eppendorf vials and stored in a freezer at −25 °C. Plant material was lyophilized immediately. Each sample had 1.5–3.7 mg of dry weight (DW). A DW/FW ratio (DW, 80 °C) was estimated in parallel material and each variant included 4–5 parallel samples from different plants. The zooplankton remained enclosed in the trap and it was not possible to remove it without causing trap damage. To estimate the hormone content in the prey, ostracods *Heterocypris incongruens* were also lyophilized for hormone analyses.

For protein determination experiment, the trap fluid was collected 24 h after feeding using the same set up from 240 fed traps of *A. vesiculosa* (unfed *A. vesiculosa* traps did not contain any digestive fluid and thus were not collected), 40 unfed and 50 fed traps of *U. reflexa*, and 26 unfed and 50 fed traps of *U. vulgaris*. The small glass capillary connected to peristaltic pump was inserted into *Utricularia* traps through the trap door or pierced through the *Aldrovanda* trap wall and digestive fluid was sampled. By this way, we obtained 130–400 μL of digestive fluid from different treatments.

2.3. Trap closing experiments

For studying the effect of JA, SA and ABA to induce trap closing, adult *Aldrovanda* plants from N Australia growing in indoor 3 L aquaria were used. Six short shoot segments containing 3rd–4th or 3rd–5th mature leaf whorls were cut, thoroughly washed in tap water, lightly blotted dry, and each segment was put in a transparent 30 mL plastic vial into 10 mL of the filtered cultivation water. The traps were left fully reopen for ca. 15 h. The individual phytohormones were added at a final concentration of 0.5 mM JA or 0.5 mM SA or 20 μM ABA at time 0 when each segment bore 15–23 open traps. These concentrations were chosen based on previous experiments on carnivorous plants, where they were found to be biologically active (Escalante-Perez et al., 2011; Nakamura et al., 2013; Buch et al., 2015; Krausko et al., 2017; Pavlovič et al., 2017). The segments were exposed under the same conditions as above. Closed traps were counted after 20, 40, 55, 120 and 180 min and observed for additional 48 h. Segments without added phytohormones were used as a control. Digestive fluid from JA-induced closed *Aldrovanda* traps was also collected as described above for MS analyses 24 h after the application of 0.5 mM JA. Due to spontaneous firing of *Utricularia* traps several times per day (Adamec, 2011; Vincent et al., 2011), it was pointless to repeat the same experiment with *U. reflexa* traps.

2.4. Quantification of phytohormones

The phytohormones were quantified in *A. vesiculosa* and *U. reflexa*. Quantification of phytohormones was performed according to the method described by Floková et al. (2014); the extraction process was modified for a small amount of dry plant tissue. One mL of ice-cold 10% MeOH/H_2O (v/v), internal standards and four small metallic beads were added to the dry biomass. Dry plant material was homogenized using a MM 301 vibration mill (Retsch GmbH & Co. KG, Haan, Germany) at a frequency of 27 Hz for 5 min. The samples were incubated at 4 °C by shaking using a laboratory rotator for 30 min and centrifuged (20,000 rpm, 4 °C, 15 min). The supernatant was transferred into a new Eppendorf vial, the volume was measured and the extract of most of the samples was subdivided (as dependent on the FW) into two aliquots. At the end, each sample contained stable isotope-labelled standards as follows: 10 pmol of [$^2H_6$]JA, [$^2H_5$]OPDA, [$^2H_6$]ABA, [$^{13}C_6$]IAA, 0.1 pmol of [$^2H_2$]JA-Ile and 20 pmol of [$^2H_4$]SA (all from Olchemim Ltd., Czech Republic) to validate the LC-MS/MS method. The extracts were purified using Oasis® HLB columns (30 mg mL^{-1}, Waters, Milford, MA, USA) and hormones were eluted with 80% methanol. The eluent was evaporated to dryness under a stream of nitrogen. Phytohormone levels were determined by ultra-high performance liquid chromatography-electrospray tandem mass spectrometry (UHPLC-MS/MS) using an Acquity UPLC I-Class System (Waters, Milford, MA, USA) equipped with an Acquity UPLC CSH C18 column (100 × 2.1 mm; 1.7 μm; Waters) coupled to a triple quadrupole mass spectrometer Xevo TQ-S MS (Waters MS Technologies, Manchester, UK).

2.5. Protein identification analysis

Protein concentration was determined by the bicinchoninic acid assay (Smith et al., 1985). Sample of fed *A. vesiculosa* showed the highest value of 2.1 mg ml^{-1} protein, sample of fed *U. vulgaris* contained 0.1 mg ml^{-1}; the others had even lower content. All samples were subjected to SDS-PAGE (Laemmli, 1970) in a 12% T/2.7% C resolving gel and 4% T/2.7% C stacking gel; 30-μL aliquots in Laemmli sample buffer were loaded per well onto an 8 × 7 cm minigel, 1-mm thick. Coomassie-stained protein bands were excised from the gel slab, which was followed by an in-gel digestion step (Shevchenko et al., 2006). The resulting digests were purified on ZipTip C18 pipette tips (Merck-Millipore, Ireland) and the recovered desalted peptides separated by nanoflow liquid chromatography coupled to electrospray ion trap tandem mass spectrometry (nLC-ESI-IT-MS/MS) on an amaZon speed ETD instrument (Bruker Daltonik, Bremen, Germany) as already described (Panáček et al., 2018).

MGF formatted nLC-ESI-IT-MS/MS data files were searched against Caryophyllales and Lamiales protein sequences downloaded from the NCBI Protein database (https://www.ncbi.nlm.nih.gov/protein/) in March 2021, and supplemented with CRAP contaminants database (https://www.thegpm.org/crap/), using PEAKS X software (Bioinformatics Solutions, Inc., Waterloo, ON, Canada). The data were also searched against the reviewed database Swiss-Prot (release 2021_01; https://www.uniprot.org/downloads), taxonomy Vidiriplantae. Parameters of the searches were as follows: monoisotopic masses; error tolerance for precursor mass of 50 ppm; error tolerance for fragment ions of 0.5 Da; semispecific trypsin digestion mode; up to three missed cleavages; carbamidomethylation of cysteine as a fixed modification; oxidation of methionine and acetylation of protein N-terminus as variable modifications; three maximum variable modifications per peptide.

Gel-based protein identification after the induction by 0.5 mM JA in *Aldrovanda* was not successful because of a low protein content. To overcome this, a 200-μl aliquot of the digestive fluid was dried out in a vacuum centrifuge. The solid residue was dissolved in 50 μl of 100 mM NH_4HCO_3 and alkalified by adding 1 μl of 25% (v/v) ammonia. Disulfides were reduced by adding 2 μl of 100 mM dithiothreitol (DTT) in 100 mM NH_4HCO_3 and incubating at 37 °C for 30 min. After cooling down, 5 μl of 100 mM iodoacetamide in 100 mM NH_4HCO_3 were added and the mixture incubated at 23 °C in the dark for 20 min. Then 2.5 μl of 100 mM DTT in 100 mM NH_4HCO_3 were added for quenching the unreacted alkylating reagent. After 20 min, the solution was adjusted to a total volume of 300 μl by 50 mM NH_4HCO_3. Digestion was initiated by 3 μL of SOLu trypsin (Merck, Germany) and proceeded at 37 °C for 24 h. The digest was evaporated to dryness in vacuum centrifuge and reconstituted in 10 μl of 0.1% (v/v) trifluoroacetic acid. Peptides from the digest were purified using a ZipTip C18 pipette tip. The procedure of protein identification was based on nLC coupled via an eluate-spotting device to MS/MS on a MALDI-TOF/TOF instrument as already described (Petrovská et al., 2014). MS/MS data were processed by database searches using PEAKS X as above (plus manually evaluated using flexAnalysis 3.4 and BioTools 3.2 by Bruker Daltonik); glutamine/asparagine deamidation was an additionally considered variable modification.

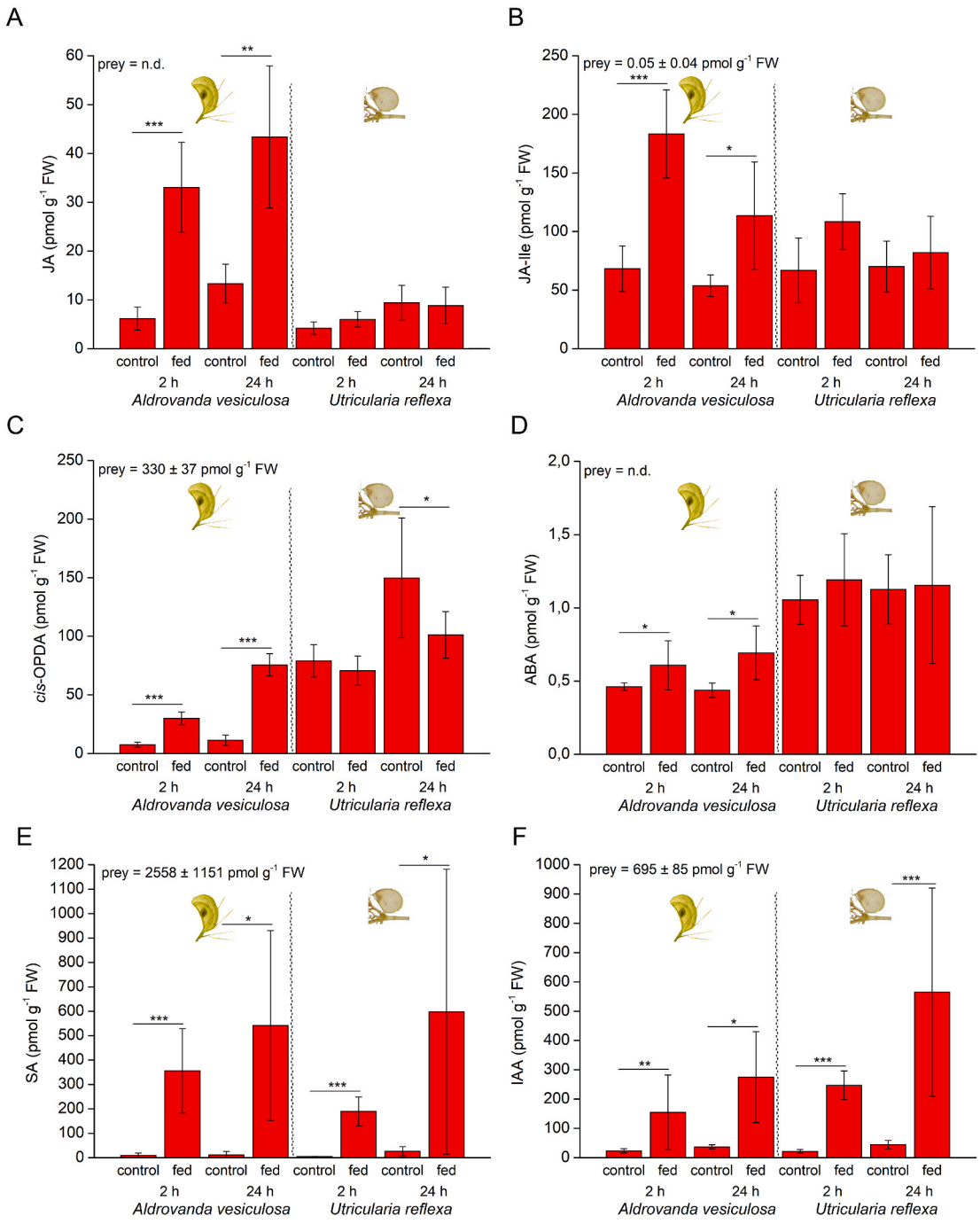

Fig. 2. Phytohormone trap tissue content. (A) Jasmonic acid, (B) jasmonic acid isoleucine conjugate, (C) *cis*-12-oxophytodienoic acid, (D) abscisic acid, (E) salicylic acid, (F) 3-indolacetic acid. Phytohormone content in the prey is shown in upper left corner. Means ± S.D., n = 4–10, n.d. – not determined (below detection limit).

2.6. Statistical analyses

Means ± SD intervals are shown. The statistically significant differences between fed variants and unfed controls were tested by the Student *t*-test. If non-homogeneity was present, the Welch *t*-test was used (Microsoft Excel).

3. Results and discussion

Morphological and physiological features and growth strategies of aquatic carnivorous plants are quite dissimilar from those of terrestrial ones (Adamec, 2018). The submerged aquatic or amphibious species of *Aldrovanda* and *Utricularia* are strictly rootless vascular plants that grow in dystrophic, barren waters. Here, we investigated whether the JAs accumulated in response to feeding in the traps of two distantly-related aquatic species of carnivorous plants, *Aldrovanda vesiculosa* and *Utricularia reflexa,* are similar to that in traps of some terrestrial species.

Aldrovanda vesiculosa accumulated significantly increased levels of JA, JA-Ile, *cis*-OPDA and ABA in trap tissues after both 2 and 24 h following experimental feeding on zooplankton. In contrast, *Utricularia reflexa* did not accumulate significant levels of these phytohormones in trap tissues after experimental feeding (Fig. 2A–D). The significant increase in the level of SA and indole-3-acetic acid (IAA) in fed traps of both species can be attributed to the high content of these phytohormones in the applied zooplankton, which remained enclosed in the traps and was thus analyzed together with trap tissue (Fig. 2E and F). To verify

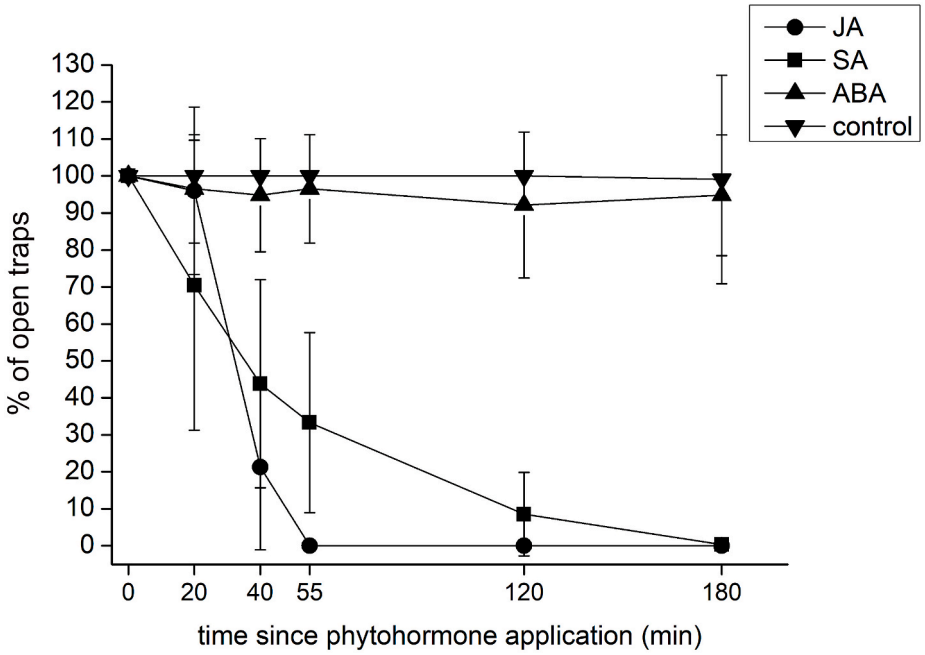

Fig. 3. Trap closing response in *Aldrovanda vesiculosa*. The phytohormones (0.5 mM JA, 0.5 mM SA, 20 μM ABA) were applied at time point 0 min, and numbers of closed traps were counted at regular time interval. Means ± S.D., n = 6 shoot segments.

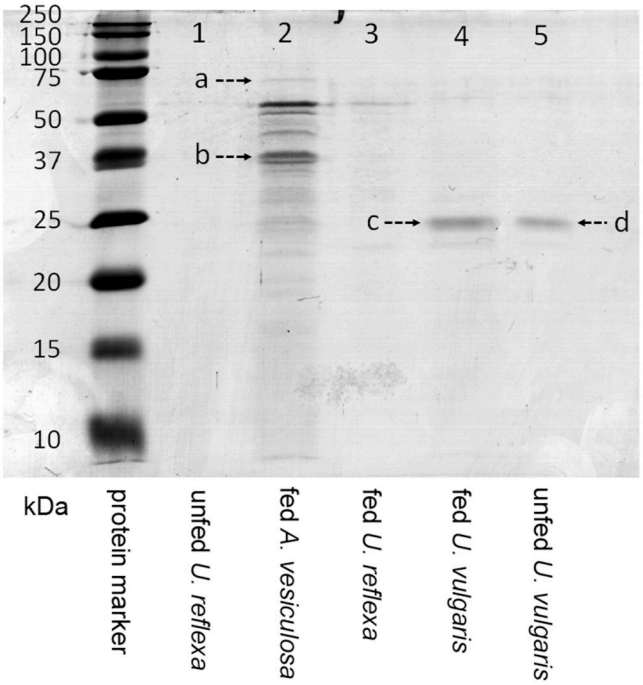

Fig. 4. Sodium dodecylsulfate polyacrylamide gel electrophoresis of digestive fluids. Protein samples were separated using a 12% resolving gel and 4% stacking gel. The resolving gel was stained afterwards by Coomassie Brilliant Blue G-250. The separation lanes show, from the left, a protein marker with the indicated molecular mass values of its components, and samples of digestive fluid from: 1 - unfed *U. reflexa*, 2 - fed *A. vesiculosa*, 3 – fed *U. reflexa*, 4 – fed *U. vulgaris*, 5 – unfed *U. vulgaris*. Arrows indicate the visualized proteins bands (2-a, 2-b, 4-c, 5-d), which were confirmed to contain hydrolytic enzymes as identified by nLC-ESI-IT-MS/MS.

the physiological effect of JAs; JA, SA and ABA were added into the cultivation water to a final concentration of 0.5 mM, 0.5 mM and 20 μM, respectively, and we observed the trap closing reaction. In the trap closing experiments on applied phytohormones, all *Aldrovanda* traps were closed after the application of JA after 55 min (Fig. 3) and stayed closed for a period of 48 h. Moreover, traps immersed in the JA medium for 10 h also stayed closed in the fresh medium without JA for the next 84 h (data not shown). The trap closing reaction was also induced by SA (Fig. 3), but after 44 h, all traps were damaged by SA and most probably were dead. After transfer into the fresh medium without SA, the traps only slightly re-opened but did not react to mechanical stimuli, indicating a pharmacologically damaging effect of SA. ABA was not able to induce the trap closing reaction at all (Fig. 3) and the traps fully closed upon mechanical stimulation after 44 h of the ABA treatment.

Despite its aquatic lifestyle, *Aldrovanda* accumulates JAs in response to prey capture and responds also to their exogenous application in a way similar to the terrestrial carnivorous members of Droseraceae, *Drosera capensis* and *Dionaea muscipula* (Nakamura et al., 2013; Libiaková et al., 2014; Krausko et al., 2017; Pavlovič et al., 2017). As *Aldrovanda* generates APs in response to mechanical stimulation (Iijima and Sibaoka, 1981, 1982) like its closest relative *Dionaea* (Hodick and Sievers, 1988), the downstream sequence of signalling events is probably similar and involves Ca^{2+} induced JAs accumulation as is well-known in non-carnivorous plants (Toyota et al., 2018; Farmer et al., 2020; Suda et al., 2020). In *Dionaea*, accumulated JAs activated the expression of digestive enzymes including cysteine protease dionain and VF chitinase I (Libiaková et al., 2014; Böhm et al., 2016; Pavlovič et al., 2017) and we found similar enzyme in *Aldrovanda.* Based on our nLC-MS/MS analysis and homology search, we identified a cysteine protease dionain3 from *Dionaea muscipula* (accession no. gi|794462956 assigned by a single peptide NSWGTSWGENGYIR to the band 2-b in Fig. 4) in the digestive fluid collected from fed *Aldrovanda* traps (we called it aldrovandain). Digestive fluid collected from hermetically closed traps induced by exogenously added 0.5 mM JA also contained cysteine protease in *Aldrovanda* (identification based on the same sequence as above). Therefore the mechanism of enzyme synthesis is the same as in *Dionaea*. Moreover, putative nucleotide pyrophosphatase/-phosphodiesterase from *Nepenthes mirabilis* (accession no. gi|1002635122) was assigned by a single peptide FLAFGDMGK to the protein band 2-a in Fig. 4. A recent genomic study has revealed that *Aldrovanda*, *Dionaea* and *Drosera* have significantly expanded gene

families related to jasmonate signalling (Palfalvi et al., 2020). Thus, our phytohormone analyses in *Aldrovanda*, *Drosera* (Krausko et al., 2017) and *Dionaea* (Libiaková et al., 2014; Pavlovič et al., 2017, 2020) are important physiological evidence to genome studies supporting the hypothesis that jasmonate signalling was co-opted for carnivory likely already in a common ancestor of the Droseraceae (Palfalvi et al., 2020). Based on the molecular evidence, it was proposed that the snap-traps of *Aldrovanda* and *Dionaea* were derived from a common terrestrial ancestor that had flypaper-traps (Cameron et al., 2002) which co-opted JA signalling from plant defense (Palfalvi et al., 2020). Later, probably terrestrial ancestor of *Aldrovanda* was becoming adapted to permanently aquatic lifestyle (Cameron et al., 2002).

On the other hand, the aquatic *Utricularia reflexa*, which uses different trapping mechanism and is not related to Droseraceae, does not accumulate significant amount of JAs in response to feeding. This is in accordance with genome analysis of *U. gibba*, where, in contrast with Droseraceae, gene families related to jasmonate signalling are not significantly expanded (Ibarra-Laclette et al., 2013; Carretero-Paulet et al., 2015; Lan et al., 2017). The findings that enzyme activity in *Utricularia* bladders is independent of prey capture and is rather constitutive (Sirová et al., 2003) question the necessity to possess a JA-inducible system for enzyme secretion. In the trap fluids of *Utricularia*, there are many species of living bacteria, algae, fungi and protozoa and it has been suggested that *Utricularia* are rather more 'farmers' than 'hunters' (Sirová et al., 2018a,b). Even more, putative losses of the defense response genes in *U. gibba* are apparent (Renner et al., 2018). Microbiome organisms certainly contribute to hydrolytic activities in the digestive fluid, but the plants also secrete their own digestive enzymes (Sirová et al., 2003). Using our nLC-MS/MS analyses and homology search we were unsuccessful to identify any secreted enzyme in *U. reflexa*. Therefore, we used another *Utricularia* species and found that the major bands in samples from fed and unfed *U. vulgaris* digestive fluid, i.e. 4-c and 5-d (Fig. 4), respectively, were assigned by a single peptide DQGQCGSCWAF to dionain 4 from *Dionaea muscipul*a (accession no. gi|1114672835) or cysteine protease from *Spinacia oleracea* (accession no. gi|222425026). Indeed, the *U. gibba* genome reveals large expansions of cysteine protease gene family which are predominantly expressed in trap tissue (Lan et al., 2017). It seems that different evolutionary lineages of carnivorous plants co-opted similar digestive enzymes with convergent amino acid changes (Fukushima et al., 2017), but the mode of their regulation may differ. Moreover, there is an obvious difference in the molecular mass (Fig. 4). Additional protein identifications in samples including abundant plant intracellular proteins such as actin, glyceraldehyde-3-phosphate dehydrogenase, fructose bisphosphate aldolase, triosephosphate isomerase, calmodulin, histones, and ubiquitin were considered contaminants arising from a mechanical injury of plants during the sample collection process.

In addition to our previous study on *Pinguicula* (Kocáb et al., 2020), *Utricularia* is the second genus of carnivorous plant in the order Lamiales, which has not co-opted jasmonate signalling for botanical carnivory. On the other hand, activation of digestive process in aquatic *Aldrovanda* is similar to terrestrial *Dionaea* and both rely on jasmonates. Interestingly, both genera of aquatic carnivorous plants used cysteine protease homologous to dionain for prey digestion, which is prey and JA-induced in *Aldrovanda* and constitutively present in *Utricularia*. Thus, although the similar digestive enzymes were co-opted for botanical carnivory, the mode of their regulation may differ in different taxa. How are the carnivory-related processes activated by prey in other genera of CPs remains to be investigated.

Author's contribution

AP and LA designed the experiments; JJ and LA collected samples and did the biotest; JJ, IP and ON analyzed phytohormone tissue level; MS performed nLC-MS/MS; JJ and AP wrote the manuscript.

Declaration of competing interest

The authors declare that they have no known competing financial interests or personal relationships that could have appeared to influence the work reported in this paper.

Acknowledgements

This study was partly supported (to LA) by the Long-term research development project No. RVO 67985939 and by the Internal Grant Agency of Palacký University (IGA_PrF_2021_011 and IGA_PrF_2020_028). Sincere thanks are due to Dr. Brian G. McMillan (Glasgow, Scotland) for correction of the language.

References

Adamec, L., 2011. The comparison of mechanically stimulated and spontaneous firings in traps of aquatic carnivorous *Utricularia* species. Aquat. Bot. 94, 44–49. https://doi.org/10.1016/j.aquabot.2010.09.004.

Adamec, L., 2018. Ecophysiology of aquatic carnivorous plants. In: Carnivorous Plants: Physiology, Ecology, and Evolution. Oxford University Press, pp. 256–269. https://doi.org/10.1093/oso/9780198779841.003.0019.

Adamec, L., Poppinga, S., 2016. Measurement of the critical negative pressure inside traps of aquatic carnivorous *Utricularia* species. Aquat. Bot. 133, 10–16. https://doi.org/10.1016/j.aquabot.2016.04.007.

Atsuzawa, K., Kanaizumi, D., Ajisaka, M., Kamada, T., Sakamoto, K., Matsushima, H., Kaneko, Y., 2020. Fine structure of *Aldrovanda vesiculosa* L: the peculiar lifestyle of an aquatic carnivorous plant elucidated by electron microscopy using cryo-techniques. Microscopy 69, 214–226. https://doi.org/10.1093/jmicro/dfaa019.

Bemm, F., Becker, D., Larisch, C., Kreuzer, I., Escalante-Perez, M., Schulze, W.X., Ankenbrand, M., Van De Weyer, A.L., Krol, E., Al-Rasheid, K.A.S., Mithöfer, A., Weber, A.P., Schultz, J., Hedrich, R., 2016. Venus flytrap carnivorous lifestyle builds on herbivore defense strategies. Genome Res. 26, 812–825. https://doi.org/10.1101/gr.202200.115.

Böhm, J., Scherzer, S., Krol, E., Kreuzer, I., Von Meyer, K., Lorey, C., Mueller, T.D., Shabala, L., Monte, I., Solano, R., Al-Rasheid, K.A.S., Rennenberg, H., Shabala, S., Neher, E., Hedrich, R., 2016. The Venus flytrap *Dionaea muscipula* counts prey-induced action potentials to induce sodium uptake. Curr. Biol. 26, 286–295. https://doi.org/10.1016/j.cub.2015.11.057.

Buch, F., Kaman, W.E., Bikker, F.J., Yilamujiang, A., Mithöfer, A., 2015. Nepenthesin protease activity indicates digestive fluid dynamics in carnivorous *Nepenthes* plants. PloS One 10. https://doi.org/10.1371/journal.pone.0118853 e0118853.

Cameron, K.M., Wurdack, K.J., Jobson, R.W., 2002. Molecular evidence for the common origin of snap-traps among carnivorous plants. Am. J. Bot. 89, 1503–1509. https://doi.org/10.3732/ajb.89.9.1503.

Carretero-Paulet, L., Librado, P., Chang, T.-H., Ibarra-Laclette, E., Herrera-Estrella, L., Rozas, J., Albert, V.A., 2015. High gene family turnover rates and gene space adaptation in the compact genome of the carnivorous plant *Utricularia gibba*. Mol. Biol. Evol. 32, 1284–1295. https://doi.org/10.1093/molbev/msv020.

Ellison, A.M., Adamec, L., 2018. Introduction: what is a carnivorous plant?. In: Carnivorous Plants: Physiology, Ecology, and Evolution. Oxford University Press, pp. 3–6. https://doi.org/10.1093/oso/9780198779841.003.0001.

Escalante-Perez, M., Krol, E., Stange, A., Geiger, D., Al-Rasheid, K.A.S., Hause, B., Neher, E., Hedrich, R., 2011. A special pair of phytohormones controls excitability, slow closure, and external stomach formation in the Venus flytrap. Proc. Natl. Acad. Sci. U.S.A. 108, 15492–15497. https://doi.org/10.1073/pnas.1112535108.

Farmer, E.E., Gao, Y., Lenzoni, G., Wolfender, J., Wu, Q., 2020. Wound- and mechano-stimulated electrical signals control hormone responses. New Phytol. 227, 1037–1050. https://doi.org/10.1111/nph.16646.

Floková, K., Tarkowská, D., Miersch, O., Strnad, M., Wasternack, C., Novák, O., 2014. UHPLC-MS/MS based target profiling of stress-induced phytohormones. Phytochemistry 105, 147–157. https://doi.org/10.1016/j.phytochem.2014.05.015.

Fonseca, S., Chini, A., Hamberg, M., Adie, B., Porzel, A., Kramell, R., Miersch, O., Wasternack, C., Solano, R., 2009. (+)-7-iso-Jasmonoyl-L-isoleucine is the endogenous bioactive jasmonate. Nat. Chem. Biol. 5, 344–350. https://doi.org/10.1038/nchembio.161.

Fukushima, K., Fang, X., Alvarez-Ponce, D., Cai, H., Carretero-Paulet, L., Chen, C., Chang, T.H., Farr, K.M., Fujita, T., Hiwatashi, Y., Hoshi, Y., Imai, T., Kasahara, M., Librado, P., Mao, L., Mori, H., Nishiyama, T., Nozawa, M., Pálfalvi, G., Pollard, S.T., Rozas, J., Sánchez-Gracia, A., Sankoff, D., Shibata, T.F., Shigenobu, S., Sumikawa, N., Uzawa, T., Xie, M., Zheng, C., Pollock, D.D., Albert, V.A., Li, S., Hasebe, M., 2017. Genome of the pitcher plant *Cephalotus* reveals genetic changes associated with carnivory. Nat. Ecol. Evol. 1, 59. https://doi.org/10.1038/s41559-016-0059.

Hodick, D., Sievers, A., 1988. The action potential of *Dionaea muscipula* Ellis. Planta 174, 8–18. https://doi.org/10.1007/BF00394867.

Ibarra-Laclette, E., Lyons, E., Hernández-Guzmán, G., Pérez-Torres, C.A., Carretero-Paulet, L., Chang, T.H., Lan, T., Welch, A.J., Juárez, M.J.A., Simpson, J., Fernández-Cortés, A., Arteaga-Vázquez, M., Góngora-Castillo, E., Acevedo-Hernández, G., Schuster, S.C., Himmelbauer, H., Minoche, A.E., Xu, S., Lynch, M., Oropeza-Aburto, A., Cervantes-Pérez, S.A., De Jesús Ortega-Estrada, M., Cervantes-

Luevano, J.I., Michael, T.P., Mockler, T., Bryant, D., Herrera-Estrella, A., Albert, V. A., Herrera-Estrella, L., 2013. Architecture and evolution of a minute plant genome. Nature 498, 94–98. https://doi.org/10.1038/nature12132.

Iijima, T., Sibaoka, T., 1981. Action potential in the trap-lobes of *Aldrovanda vesiculosa*. Plant Cell Physiol. 22, 1595–1601. https://doi.org/10.1093/oxfordjournals.pcp.a076312.

Iijima, T., Sibaoka, T., 1982. Propagation of action potential over the trap-lobes of *Aldrovanda vesiculosa*. Plant Cell Physiol. 23, 679–688. https://doi.org/10.1093/oxfordjournals.pcp.a076396.

Jakšová, J., Libiaková, M., Bokor, B., Petřík, I., Novák, O., Pavlovič, A., 2020. Taste for protein: chemical signal from prey stimulates enzyme secretion through jasmonate signalling in the carnivorous plant Venus flytrap. Plant Physiol. Biochem. 146, 90–97. https://doi.org/10.1016/j.plaphy.2019.11.013.

Kocáb, O., Jakšová, J., Novák, O., Petřík, I., Lenobel, R., Chamrád, I., Pavlovič, A., 2020. Jasmonate-independent regulation of digestive enzyme activity in the carnivorous butterwort *Pinguicula* × *Tina*. J. Exp. Bot. 71, 3749–3758. https://doi.org/10.1093/jxb/eraa159.

Koo, A.J.K., Gao, X., Jones, A.D., Howe, A.G., 2009. A rapid wound signal activates the systemic synthesis of bioactive jasmonates in *Arabidopsis*. Plant J. 59, 974–986. https://doi.org/10.1111/j.1365-313X.2009.03924.x.

Krausko, M., Perutka, Z., Šebela, M., Šamajová, O., Šamaj, J., Novák, O., Pavlovič, A., 2017. The role of electrical and jasmonate signalling in the recognition of captured prey in the carnivorous sundew plant *Drosera capensis*. New Phytol. 213, 1818–1835. https://doi.org/10.1111/nph.14352.

Lan, T., Renner, T., Ibarra-Laclette, E., Farr, K.M., Chang, T.H., Cervantes-Pérez, S.A., Zheng, C., Sankoff, D., Tang, H., Purbojati, R.W., Putra, A., Drautz-Moses, D.I., Schuster, S.C., Herrera-Estrella, L., Albert, V.A., 2017. Long-read sequencing uncovers the adaptive topography of a carnivorous plant genome. Proc. Natl. Acad. Sci. U.S.A. 114, E4435–E4441. https://doi.org/10.1073/pnas.1702072114.

Laemmli, U.K., 1970. Cleavage of structural proteins during the assembly of the head of bacteriophage T4. Nature 227, 680–685. https://doi.org/10.1038/227680a0.

Libiaková, M., Floková, K., Novák, O., Slováková, L., Pavlovič, A., 2014. Abundance of cysteine endopeptidase dionain in digestive fluid of venus flytrap (*Dionaea muscipula* Ellis) is regulated by different stimuli from prey through jasmonates. PloS One 9, e104424. https://doi.org/10.1371/journal.pone.0104424.

Matušíková, I., Pavlovič, A., Renner, T., 2018. Biochemistry of Prey Digestion and Nutrient Absorption, Carnivorous Plants: Physiology, Ecology, and Evolution. Oxford University Press, pp. 207–220. https://doi.org/10.1093/oso/9780198779841.003.0016.

Mithöfer, A., 2011. Carnivorous pitcher plants: insights in an old topic. Phytochemistry 72, 1678–1682. https://doi.org/10.1016/j.phytochem.2010.11.024.

Muravnik, L.E., 1996. Morphometric approach to the determination of secretory activity in digestive glands of *Aldrovanda vesiculosa* (Droseraceae). Bot. Zh. (Kiev) 81, 1–8.

Muravnik, L.J., Vasil'ev, A.J., Potapova, J.J., 1995. Ultrastructural aspects of digestive gland functioning in *Aldrovanda vesiculosa*. Russ. J. Plant Physiol. 42, 1–8.

Nakamura, Y., Reichelt, M., Mayer, V.E., Mithöfer, A., 2013. Jasmonates trigger prey-induced formation of "outer stomach" in carnivorous sundew plants. Proc. R. Soc. B Biol. Sci. 280 https://doi.org/10.1098/rspb.2013.0228, 20130228.

Palfalvi, G., Hackl, T., Terhoeven, N., Shibata, T.F., Nishiyama, T., Ankenbrand, M., Becker, D., Förster, F., Freund, M., Iosip, A., Kreuzer, I., Saul, F., Kamida, C., Fukushima, K., Shigenobu, S., Tamada, Y., Adamec, L., Hoshi, Y., Ueda, K., Winkelmann, T., Fuchs, J., Schubert, I., Schwacke, R., Al-Rasheid, K., Schultz, J., Hasebe, M., Hedrich, R., 2020. Genomes of the Venus flytrap and close relatives unveil the roots of plant carnivory. Curr. Biol. 30, 2312–2320. https://doi.org/10.1016/j.cub.2020.04.051.

Panáček, A., Kvítek, L., Smékalová, M., Večeřová, R., Kolář, M., Röderová, M., Dyčka, F., Šebela, M., Prucek, R., Tomanec, O., Zbořil, R., 2018. Bacterial resistance to silver nanoparticles and a way how to overcome it. Nat. Nanotechnol. 13, 65–71. https://doi.org/10.1038/s41565-017-0013-y.

Pavlovič, A., Jakšová, J., Novák, O., 2017. Triggering a false alarm: wounding mimics prey capture in the carnivorous venus flytrap (*Dionaea muscipula*). New Phytol. 216, 927–938. https://doi.org/10.1111/nph.14747.

Pavlovič, A., Libiaková, M., Bokor, B., Jakšová, J., Petřík, I., Novák, O., Baluška, F., 2020. Anaesthesia with diethyl ether impairs jasmonate signalling in the carnivorous plant Venus flytrap (*Dionaea muscipula*). Ann. Bot. 125, 173–183. https://doi.org/10.1093/aob/mcz177.

Pavlovič, A., Mithöfer, A., 2019. Jasmonate signalling in carnivorous plants: copycat of plant defence mechanisms. J. Exp. Bot. 70, 3379–3389. https://doi.org/10.1093/jxb/erz188.

Pavlovič, A., Saganová, M., 2015. A novel insight into the cost-benefit model for the evolution of botanical carnivory. Ann. Bot. 115, 1075–1092. https://doi.org/10.1093/aob/mcv050.

Petrovská, B., Jeřábková, H., Chamrád, I., Vrána, J., Lenobel, R., Uřinovská, J., Šebela, M., Doležel, J., 2014. Proteomic analysis of barley cell nuclei purified by flow sorting. Cytogenet. Genome Res. 143, 78–86. https://doi.org/10.1159/000365311.

Poppinga, S., Bauer, U., Speck, T., Volkov, A.G., 2018. Motile traps, in: Carnivorous Plants: Physiology, Ecology, and Evolution. Oxford University Press, pp. 180–193. https://doi.org/10.1093/oso/9780198779841.003.0014.

Poppinga, S., Weisskopf, C., Westermeier, A.S., Masselter, T., Speck, T., 2016. Fastest predators in the plant kingdom: functional morphology and biomechanics of suction traps found in the largest genus of carnivorous plants. AoB Plants 8, plv140. https://doi.org/10.1093/aobpla/plv140.

Renner, T., Lan, T., Farr, K.M., Ibarra-Laclette, E., Herrera-Estrella, L., Schuster, S.C., Hasebe, M., Fukushima, K., Albert, V.A., 2018. Carnivorous Plant Genomes, Carnivorous Plants: Physiology, Ecology, and Evolution. Oxford University Press, pp. 135–153. https://doi.org/10.1093/oso/9780198779841.003.0011.

Shevchenko, A., Tomas, H., Havliš, J., Olsen, J.V., Mann, M., 2006. In-gel digestion for mass spectrometric characterization of proteins and proteomes. Nat. Protoc. 1, 2856–2860. https://doi.org/10.1038/nprot.2006.468.

Sheard, L.B., Tan, X., Mao, H., Withers, J., Ben-Nissan, G., Hinds, T.R., Kobayashi, Y., Hsu, F.-F., Sharon, M., Browse, J., He, S.Y., Rizo, J., Howe, G.A., Zheng, N., 2010. Jasmonate perception by inositol-phosphate-potentiated COI1–JAZ co-receptor. Nature 468, 400–405. https://doi.org/10.1038/nature09430.

Smith, P.K., Krohn, R.I., Hermanson, G.T., Mallia, A.K., Gartner, F.H., Provenzano, M.D., Fujimoto, E.K., Goeke, N.M., Olson, B.J., Klenk, D.C., 1985. Measurement of protein using bicinchoninic acid. Anal. Biochem. 150, 76–85. https://doi.org/10.1016/0003-2697(85)90442-7.

Sirová, D., Adamec, L., Vrba, J., 2003. Enzymatic activities in traps of four aquatic species of the carnivorous genus *Utricularia*. New Phytol. 159, 669–675. https://doi.org/10.1046/j.1469-8137.2003.00834.x.

Sirová, D., Bárta, J., Borovec, J., Vrba, J., 2018a. The Utricularia-associated microbiome: composition, function, and ecology. In: Carnivorous Plants: Physiology, Ecology, and Evolution. Oxford University Press, pp. 349–358. https://doi.org/10.1093/oso/9780198779841.003.0025.

Sirová, D., Bárta, J., Šimek, K., Posch, T., Pech, J., Stone, J., Borovec, J., Adamec, L., Vrba, J., 2018b. Hunters or farmers? Microbiome characteristics help elucidate the diet composition in an aquatic carnivorous plant. Microbiome 6, 225. https://doi.org/10.1186/s40168-018-0600-7.

Suda, H., Mano, H., Toyota, M., Fukushima, K., Mimura, T., Tsutsui, I., Hedrich, R., Tamada, Y., Hasebe, M., 2020. Calcium dynamics during trap closure visualized in transgenic Venus flytrap. Nature Plants 6, 1219–1224. https://doi.org/10.1038/s41477-020-00773-1.

Thines, B., Katsir, L., Melotto, M., Niu, Y., Mandaokar, A., Liu, G., Nomura, K., He, S.Y., Howe, G.A., Browse, J., 2007. JAZ repressor proteins are targets of the SCFCOI1 complex during jasmonate signalling. Nature 448, 661–665. https://doi.org/10.1038/nature05960.

Toyota, M., Spencer, D., Sawai-Toyota, S., Jiaqi, W., Zhang, T., Koo, A.J., Howe, G.A., Gilroy, S., 2018. Glutamate triggers long-distance, calcium-based plant defense signaling. Science 361, 1112–1115. https://doi.org/10.1126/science.aat7744.

Vincent, O., Roditchev, I., Marmottant, P., 2011. Spontaneous firings of carnivorous aquatic *Utricularia* traps: temporal patterns and mechanical oscillations. PloS One 6, 20205. https://doi.org/10.1371/journal.pone.0020205.

Wasternack, C., Hause, B., 2013. Jasmonates: biosynthesis, perception, signal transduction and action in plant stress response, growth and development. An update to the 2007 review. Annals of Botany. Ann. Bot. 111, 1021–1058. https://doi.org/10.1093/aob/mct067.

Westermeier, A.S., Hiss, N., Speck, T., Poppinga, S., 2020. Functional–morphological analyses of the delicate snap-traps of the aquatic carnivorous waterwheel plant (*Aldrovanda vesiculosa*) with 2D and 3D imaging techniques. Ann. Bot. 126, 1099–1107. https://doi.org/10.1093/aob/mcaa135.

Westermeier, A.S., Sachse, R., Poppinga, S., Vögele, P., Adamec, L., Speck, T., Bischoff, M., 2018. How the carnivorous waterwheel plant (*Aldrovanda vesiculosa*) snaps. Proc. R. Soc. B Biol. Sci. 285 https://doi.org/10.1098/rspb.2018.0012 e20180012.

Yilamujiang, A., Reichelt, M., Mithöfer, A., 2016. Slow food: insect prey and chitin induce phytohormone accumulation and gene expression in carnivorous *Nepenthes* plants. Ann. Bot. 118, 369–375. https://doi.org/10.1093/aob/mcw110.

Supplement I

Supplement II

Supplement III

Supplement IV

Supplement V

Supplement VI

Supplement VII

Supplement VIII

Waidmann S, Ruiz Rosquete M, Schöller M, Sarkel E, Lindner H, LaRue T, **Petřík I**, Dünser K, Martopawiro S, Sasidharan R, Novak O, Wabnik K, Dinneny JR, Kleine-Vehn J. 2019. Cytokinin functions as an asymmetric and anti-gravitropic signal in lateral roots. Nat Commun 10(1), 3540.

nature COMMUNICATIONS

ARTICLE

https://doi.org/10.1038/s41467-019-11483-4 OPEN

Cytokinin functions as an asymmetric and anti-gravitropic signal in lateral roots

Sascha Waidmann[1], Michel Ruiz Rosquete[1], Maria Schöller[1], Elizabeth Sarkel[1], Heike Lindner[2], Therese LaRue[2,3], Ivan Petřík[4], Kai Dünser[1], Shanice Martopawiro[5], Rashmi Sasidharan[5], Ondrej Novak[4], Krzysztof Wabnik[6], José R. Dinneny[2,3] & Jürgen Kleine-Vehn[1]

Directional organ growth allows the plant root system to strategically cover its surroundings. Intercellular auxin transport is aligned with the gravity vector in the primary root tips, facilitating downward organ bending at the lower root flank. Here we show that cytokinin signaling functions as a lateral root specific anti-gravitropic component, promoting the radial distribution of the root system. We performed a genome-wide association study and reveal that signal peptide processing of Cytokinin Oxidase 2 (CKX2) affects its enzymatic activity and, thereby, determines the degradation of cytokinins in natural *Arabidopsis thaliana* accessions. Cytokinin signaling interferes with growth at the upper lateral root flank and thereby prevents downward bending. Our interdisciplinary approach proposes that two phytohormonal cues at opposite organ flanks counterbalance each other's negative impact on growth, suppressing organ growth towards gravity and allow for radial expansion of the root system.

[1] Department of Applied Genetics and Cell Biology, University of Natural Resources and Life Sciences, Vienna (BOKU), Muthgasse 18, 1190 Vienna, Austria. [2] Department of Biology, Stanford University, 260 Panama Street, Stanford, CA 94305, USA. [3] Department of Plant Biology, Carnegie Institution for Science, 260 Panama Street, Stanford, CA 94305, USA. [4] Laboratory of Growth Regulators, Centre of the Region Haná for Biotechnological and Agricultural Research, Faculty of Science of Palacký University and Institute of Experimental Botany of the Czech Academy of Sciences, Šlechtitelů 27, 78371 Olomouc, Czech Republic. [5] Plant Ecophysiology, Institute of Environmental Biology, Utrecht University, Padualaan 8, Utrecht 3584 CH, The Netherlands. [6] Centro de Biotecnología y Genómica de Plantas (Universidad Politécnica de Madrid - Instituto Nacional de Investigación y Tecnología Agraria y Alimentaria), Autopista M-40, Km 38-Pozuelo de Alarcón, 28223 Madrid, Spain. Correspondence and requests for materials should be addressed to J.K.-V. (email: juergen.kleine-vehn@boku.ac.at)

Root architectural traits define plant performance and yield[1]. The radial spreading of the root system depends on the directional growth of primary and secondary roots. The phytohormone auxin plays a central role in aligning root organ growth towards gravity[2]. In the root tip, columella cells perceive changes in gravity via statolith sedimentation[3]. The relative change in statolith positioning triggers a partial polarization of redundant PIN3, PIN4, and PIN7 auxin efflux carriers towards this side, leading to enhanced auxin transport along the gravity vector[4,5]. The asymmetric distribution of auxin eventually reduces cellular elongation rates at the lower root flank, which consequently leads to differential growth within the organ and bending towards gravity[6–8].

Lateral roots (LRs) substantially differ from main roots, establishing a distinct gravitropic set point angle (GSA)[9]. The divergent developmental programs of lateral and main (primary) roots allow the root system to strategically cover the surrounding substrate. In *Arabidopsis*, LRs emerge from the main root at a 90° angle (stage I LRs) and afterwards display maturation of gravity sensing cells, as well as the de novo formation of an elongation zone[7]. Transcription factors FOUR LIPS and MYB88 define PIN3 expression in columella cells of LRs[10] and its transient expression in columella cells temporally defines asymmetric auxin distribution as well as differential elongation rates in stage II LRs[7,11]. This developmental stage lasts about 8–9 h and is characterized by asymmetric growth towards gravity at a slower rate than in primary roots[7,12]. During this phase of development, the primary GSA of LRs is established. The subsequent repression of PIN3 in columella cells of stage III LRs coincides with symmetric elongation, maintaining this primary GSA[7]. Notably, the derepression of PIN3 and PIN4 in columella cells of older stage III LRs does not necessarily correlate with additional bending to gravity[8]. This finding illustrates that the primary GSA is developmentally maintained, determining an important root architectural trait. Moreover, a stage III LRs will return to its initial GSA if it is reoriented relative to the gravity vector[7,13,14]. Accordingly, the partial suppression of a full gravitropic response in recently emerged LRs is critical for establishing the primary growth direction of LRs, which importantly contributes to the root system architecture.

Despite the apparent importance of directional LR growth for radial exploration of the root system, the underlying suppressive mechanisms are largely unexplored. Using genetic, physiological, computational, biochemical, and cell biological approaches, we reveal that two opposing hormonal cues at the lower and upper lateral root flank counterbalance each other and set directional LR growth.

Results

Angular lateral root growth displays substantial natural variation. To examine the natural diversity in radial root growth, we screened 210 sequenced *Arabidopsis* accessions (Supplementary Fig. 1a, Supplemental Data 1) and quantified their primary GSA of LRs. When grown in vitro on the surface of the growth medium, we observed extensive variation for the mean GSA values, detecting a deviation of about 40° between most extreme natural accessions (Fig. 1a).

Because the in vitro approach allowed only two-dimensional analysis of root growth, we further assessed angular growth of LRs in three dimensional and soil systems. For this purpose, we studied a subset (depicted by red and blue lines in Fig. 1a) of hyper-responsive and hypo-responsive accessions in greater detail (Fig. 1b, c Supplementary Data 2). To allow three-dimensional root expansion in vitro, we grew this subset of accessions in growth medium-filled cylinders[8] (Supplementary Fig. 1b). In addition, we used the GLO-Roots system[15], which is a luciferase (LUC)-based imaging platform to visualize root systems in a soil-like environment (Supplementary Fig. 1c). Accordingly, we transformed the same subset of accessions with *pUBQ:LUC2o*[15], ubiquitously driving LUC expression. In the *Col-0* reference accession, about 60% of emerged LRs displayed a GSA between 51° and 70° in all three growth conditions (Fig. 1b–e, Supplementary Data 2). In all three systems, hypo-responsive and hyper-responsive accessions displayed a pronounced shift towards higher (71–90° and 91–110°) and lower (31–50° and 0–30°) angle categories, respectively (Fig. 1b–e, Supplementary Data 2). This suggests that our two-dimensional, in vitro screen was highly suitable to identify natural accessions with diverging GSA values of their root systems.

GWAS reveals a link between cytokinin and angular growth of LRs. Next, we sought to identify molecular players involved in the LR trait of our interest. To achieve this, we used our quantitative data on primary GSA of LRs and conducted a genome-wide association study (GWAS)[16]. We identified several chromosomal regions, displaying associations with our trait (Fig. 2a). A prominent peak at chromosome 2 drew our attention to a thymine (T)/guanine (G) single-nucleotide polymorphism (SNP) located in the *CYTOKININ OXIDASE 2* (*CKX2*) gene (position 8,447,233) (Fig. 2b). Importantly, the minor G allele, showing a frequency of 19.5% in all sequenced and 32.7% in our set of accessions, was associated with increased GSA values, reflecting more perpendicular LR growth to gravity (Fig. 2c). Notably, linkage disequilibrium analysis showed that adjacent SNPs display pronounced non-random association with our SNP of interest (Supplementary Fig. 2), suggesting that the *CKX2* gene could be linked to variations in angular growth of LRs.

CKX enzymes are responsible for the irreversible degradation of cytokinins (CKs) via the oxidative cleavage of their side chain[17]. iP-type CKs are the preferred substrate of CKXs[18] and were as expected increased in *ckx2-1* (*Col-0* background) mutant roots (Supplementary Fig. 3a). On the other hand, other types of CKs were downregulated in the *ckx2-1* mutant background (Supplementary Fig. 3a–e), presumably underlying a compensation mechanism. This measurement reveals that CK metabolism is indeed affected in *ckx2-1* mutant roots (Supplementary Fig. 3a–e). To test whether active CKs may modulate angular growth of LRs, we initially transferred 7-day-old seedlings of the reference accession *Col-0* to medium supplemented with CKs. We observed a strong concentration-dependent increase in GSA values of LRs emerging in presence of active CKs, such as 6-Benzylaminopurin (BAP) (Fig. 2d, Supplementary Data 2), *trans*-zeatin (tZ) and isopentenyladenine (iP) (Supplementary Fig. 3f, g, Supplementary Data 2). Conversely, CK receptor double mutant combinations showed a relatively mild, but statistically significant decrease in GSA of LRs (Fig. 2e, Supplementary Data 2), proposing functional redundancy among the cytokinin receptors.

This set of data suggests that cytokinin signaling interferes with downward bending of emerged LRs. Notably, emerging LRs of winter oilseed rape also displayed reduced bending of LRs when treated with BAP (Supplementary Fig. 3h, Supplementary Data 2), suggesting that the effect of CK on directional LR growth is likely to be conserved.

To further assess the importance of CKX2 in GSA establishment, we disrupted CKX activity in the reference accession *Col-0*. Treatments with the CKX inhibitor INCYDE[19] phenocopied the *ckx2-1* loss-of-function mutant, both displaying more horizontal LRs when compared to its respective controls (Fig. 2f, g, Supplementary Data 2). On the other hand, *CKX2* overexpressing (OX) plants showed accelerated bending of LRs, phenocopying

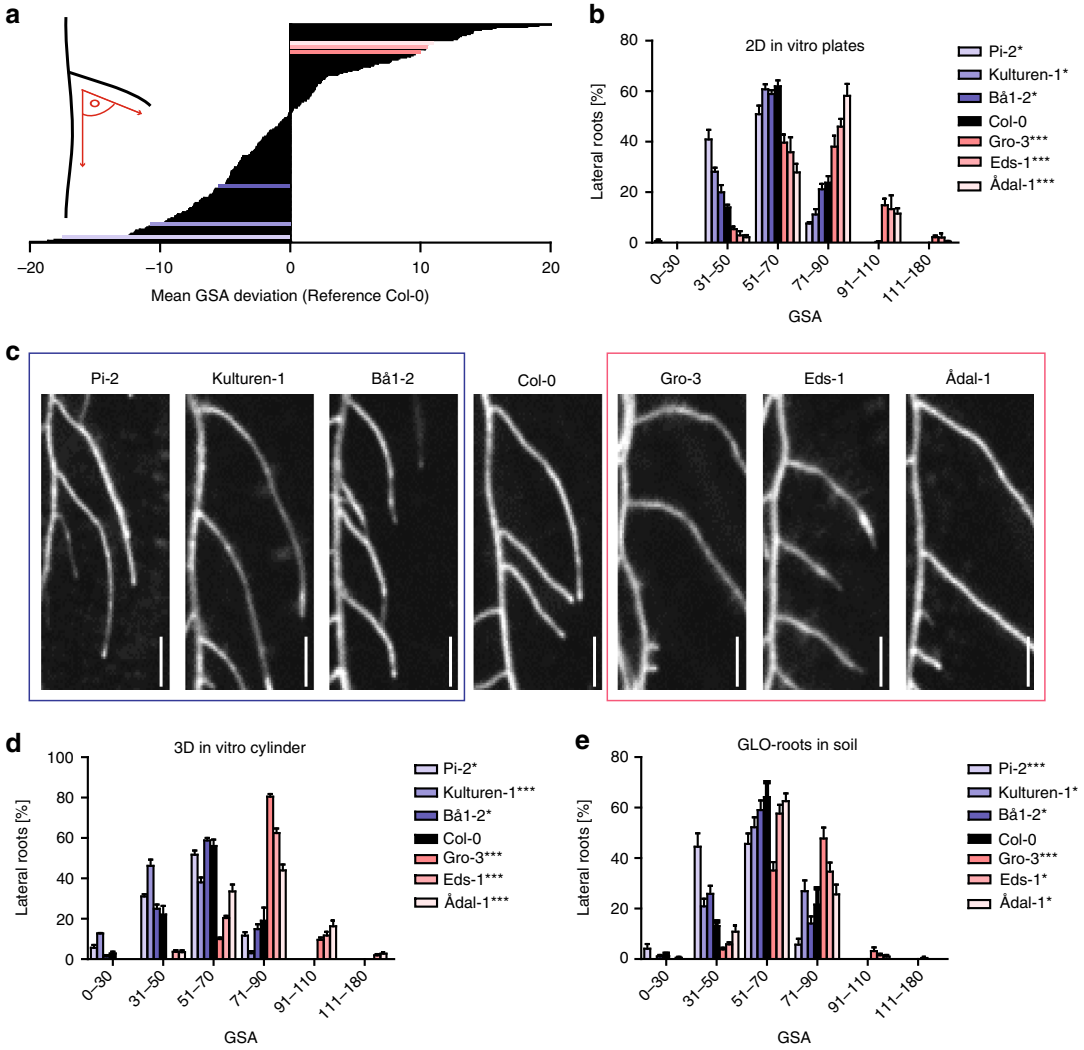

Fig. 1 Natural variation of the primary GSA of lateral roots in *Arabidopsis thaliana*. **a** Mean gravitropic set point angle (GSA) values are normalized to reference accession *Col-0*. Three hyper-responsive (blue colors) and hypo-responsive (red colors) accessions were selected for further analysis. **b** GSA distributions of hyper-responsive and hypo-responsive accessions grown on 2D agar plates. $n = 5$ plates (16 seedlings with 30–120 LRs per plate). **c** Representative images of hyper-responsive and hypo-responsive accessions grown on 2D agar plates. Scale bars, 20 mm. **d** GSA distribution of hyper-responsive and hypo-responsive accessions grown in 3D agar cylinders. $n = 5$ cylinders (25–120 LRs per cylinder). **e** GSA distribution of hyper-responsive and hypo-responsive accessions grown in soil. $n = 5$–10 plants (25–75 LRs per plant). **b**, **d**, **e** Kolmogorov–Smirnov test *P*-values: $^{*}P < 0.05$, $^{**}P < 0.01$, $^{***}P < 0.001$ (compared to *Col-0*). Mean ± SEM. Experiments were repeated at least three times

the CK receptor mutants (Fig. 2g, Supplementary Data 2). This set of data suggests that CK signaling defines directional lateral root growth by reducing LR bending after emergence.

Cytokinin response factors define angular growth of LRs. Our data indicates that CK signaling impacts the angular growth of emerged LRs. Therefore, we assessed whether CK-dependent transcription factors indeed have an impact on LR growth in the reference accession *Col-0*. It has been previously shown that CK signaling initiates transcriptional changes via the *Arabidopsis* response regulators (ARRs)[20–22] and the cytokinin response factors (CRFs)[23,24]. According to available LR organ-specific microarray data[25], type-B ARRs, such as ARR10 and ARR12, and type-A ARRs, such as *ARR3* and *ARR4* (Supplementary Fig. 4a, b) were strongly upregulated in mature LRs. However, we did not detect any expression of *ARR3*, *ARR4*, *ARR10*, and *ARR12* in young stage II LRs, using respective promoter GUS reporter lines (*pARR3::GUS*, *pARR4::GUS*, *pARR10::GUS*, *pARR12::GUS*; Supplementary Fig. 4d)). In agreement, angular growth of LRs was not altered in *arr3*, *arr4*, *arr10*, and *arr12* single mutants (Supplementary Fig. 4e, Supplementary Data 2). While this approach was not successful in identifying the responsible ARRs in young LRs, we in contrast could confirm expression of *CRF2* and *CRF3* ([25], Supplementary Fig. 4c) in the early stages of LR development (Fig. 3a and Supplementary Fig. 4f). *pCRF2::GFP-GUS* was ubiquitously expressed in young LRs, while *pCRF3::GFP-GUS* was preferentially expressed in cortical and epidermal cell files (Fig. 3a and Supplementary Fig. 4f). Notably, compared to emerged laterals, the main root displayed much weaker *CRF2* and *CRF3* expression (Supplementary Fig. 4g), suggesting that *CRF2* and *CRF3* expression is particularly high in young LRs.

In agreement with *CRF2* and *CRF3* expressions in emerged LRs, loss-of-function alleles of *crf2* and *crf3* displayed enhanced bending of LRs (Fig. 3b, Supplementary Fig. 4h, Supplementary Data 2). Conversely, we found that ubiquitous overexpression of either CRF2 or CRF3 led to more horizontal LRs (Fig. 3b, Supplementary Data 2). When we transferred *crf2* and *crf3* single

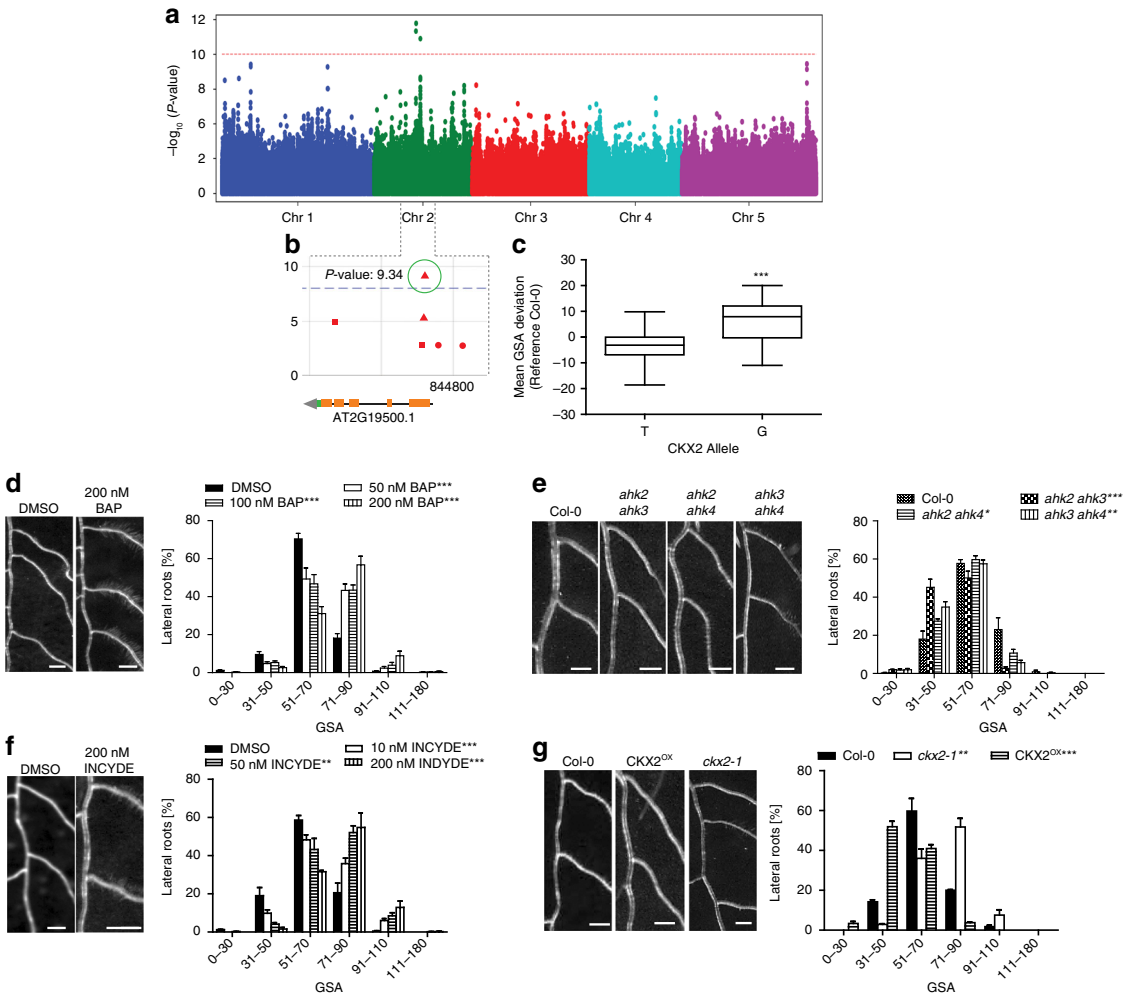

Fig. 2 Genome-wide association study (GWAS) on gravitropic set point angle (GSA). **a** Manhattan plot of GWAS results. The dotted horizontal line indicates a significance level of 0.1 after Bonferroni correction for multiple testing. **b** Magnification of the peak region on chromosome 2. A highly significant SNP was located at position 8,447,233 in the coding region of *CKX2*. **c** Mean GSA of T and G alleles of CKX2. Horizontal lines show the medians; box limits indicate the 25th and 75th percentiles; whiskers extend to the min and max values. Student's *t*-test *P*-value: ***$P < 0.001$. **d**–**g** Representative images and GSA distributions of untreated and 6-Benzylaminopurin (BAP)-treated Col-0 wild type **d**, Col-0 wild type, *ahk2 ahk3*, *ahk2 ahk4* and *ahk3 ahk4* **e**, untreated and INCYDE-treated *Col-0* wild type **f**, Col-0 wild type, *ckx2-1* and $CKX2^{OX}$ seedlings **g**. Kolmogorov–Smirnov test *P*-values: *$P < 0.05$, **$P < 0.01$, ***$P < 0.001$ (compared to DMSO solvent or Col-0 wild type control). Mean ± SEM, $n = 5$ plates (16 seedlings with 65–160 LRs per plate). Scale bars, 2 mm. **d**–**g** Experiments were repeated at least three times

mutants to medium supplemented with CK, we observed partial resistance to CK in both lines (Supplementary Fig. 4i, Supplementary Data 2). This set of data confirms that cytokinin signaling, utilizing transcription factors, such as CRF2 and CRF3, regulates angular growth of LRs.

Cytokinin integrates environmental cues into angular growth of LRs. Our data supports a role for cytokinin signaling in modulating angular growth of LRs. To investigate whether cytokinin modulates angular LR growth in response to environmental cues, we examined whether the primary GSA of *Arabidopsis* accessions is linked to geographic origins. Intriguingly, accessions with the largest GSA values predominantly originated in Nordic (above 58°N) regions (Fig. 4a). In addition, the above described minor G allele of *CKX2*, phenocopying the *ckx2-1* loss of function (in *Col-0*), was notably the most prevalent allele in the north of Sweden (Fig. 4a, b). Previous work showed that *Arabidopsis* accessions in the north of Sweden are fully vernalized before snow fall, but would sit out winter and only flower in the next spring[26]. In fact, the respective habitat in the north of Sweden is most of the year covered with snow (Supplementary Fig. 5a), indicating that these fully-grown leaf rosettes and root systems withstand long-term snow coverage. Snowpack insulation capacity can protect these plants from extreme temperatures, but may also restrict soil–atmosphere gas exchange, eventually leading to hypoxia in the soil[27]. Additionally, rapid snowmelt in spring can lead to temporary soil flooding, which depletes soil oxygen and may restrict the amount of oxygen reaching the root tissues. Intriguingly, endogenous hypoxia in roots may repress lateral root primordia development[28] and hypoxic conditions induce an organ-bending response in the primary root as a possible adaptive avoidance response[29]. Therefore, we asked whether hypoxia conditions also modulate the bending of LRs. In contrast to the primary root response, we observed that hypoxic stress reduced bending in emerged LRs (Fig. 4c, Supplementary Data 2), demonstrating distinct pathways to regulate root bending in primary and secondary roots. Interestingly, hypoxia stress for 4 h was sufficient to increase GSA of subsequently emerged LRs in *Col-0* (Fig. 4c, Supplementary Data 2), mimicking the *ckx2-1*

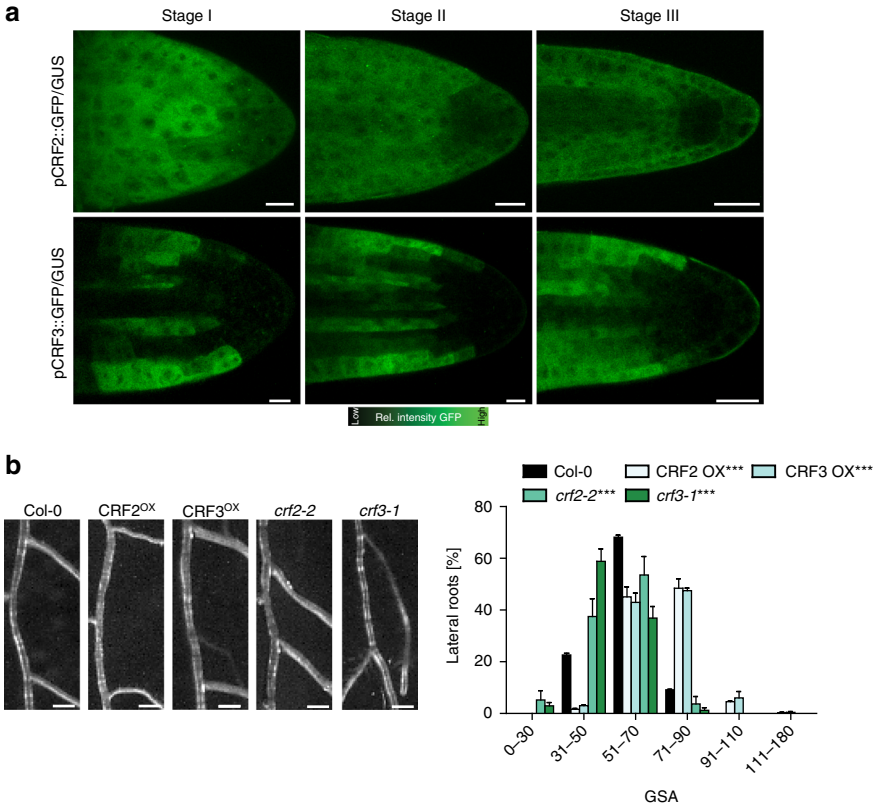

Fig. 3 Characterization of cytokinin response factors (CRFs) in lateral roots. **a** Representative images of pCRF2::GFP/GUS and pCRF3::GFP/GUS in stage I–III LRs. Scale bar, 25 µm. **b** Representative images and GSA distribution of *Col-0* wild type, *crf* mutants, and CRF^{OX} lines. Kolmogorov–Smirnov test *P*-values: ***$P < 0.001$ (compared to DMSO or *Col-0*). Mean ± SEM, $n = 5$ plates (16 seedlings with 50–120 LRs per plate). Scale bars, 2 mm. **a**, **b** Experiments were repeated at least three times

loss of function phenotype. Furthermore, hypoxic stress did not further increase GSA in the *ckx2-1* mutant (Fig. 4c, Supplementary Data 2), proposing that CK metabolism could mediate hypoxia-dependent repression of LR bending. Furthermore, the LRs of *ahk2 ahk4* CK receptor mutants were insensitive to the hypoxia-induced repression of LR bending (Fig. 4d, Supplementary Data 2). Accordingly, we conclude that CK signaling integrates environmental signals, such as hypoxia, into GSA establishment of emerged LRs.

Single base-pair variation in *CKX2* impacts on its in planta activity. Our data proposes that variation in *CKX2* is linked to the control of radial root system expansion in natural *Arabidopsis* accessions. The previously mentioned G allele of *CKX2* is associated with higher GSA values (Fig. 2c), which phenocopies the loss of *CKX2* function or increase in CK levels in the reference accession *Col-0* (Fig. 2d, g, Supplementary Data 2). Accordingly, we next assessed whether the identified SNP affects the activity of CKX2. The underlying T to G mutation alters the first amino acid in the mature enzyme from an isoleucine (I) to a methionine (M). This mutation is situated just after the predicted cleavage site of a signal peptide (SP). The SP allows CKX2 to be inserted into the endoplasmic reticulum and to be subsequently secreted into the extracellular space (apoplast)[17]. To assess potential trafficking or processing defects caused by the amino acid change[30], we generated a ratiometric CKX2 reporter by fusing the green fluorescent protein (GFP) and mScarlet to the N-terminal and C-terminal ends of CKX2, respectively. Fluorescent mScarlet signal of the non-mutated $CKX2^{I}$ readily accumulated in the apoplast, suggesting that the fluorescent tags do not abolish processing and/or secretion of CKX2-mScarlet (Fig. 5a and Supplementary Fig. 5b). Ratiometric imaging of GFP and mScarlet revealed a higher degree of co-localization for mutated version $CKX2^{M}$, suggesting reduced processing and/or secretion of $CKX2^{M}$ when compared to $CKX2^{I}$ (Fig. 5b). To visualize the effect of the T to G mutation on SP cleavage, we N-terminally tagged CKX2 with GFP and subsequently expressed $GFP^{SP}CKX2^{I}$ and its respective mutated version $GFP^{SP}CKX2^{M}$ in tobacco. Western blot analysis revealed a decreased cleavage of $GFP^{SP}CKX2^{M}$ when compared to $GFP^{SP}CKX2^{I}$ (Fig. 5c). Even though we cannot eliminate the possibility that N-terminal GFP may interfere with normal SP-processing rates, the relative differences between the two assessed alleles suggests that the identified SNP reduces the SP cleavage in CKX2.

The SP processing is an important determinant of the mature protein and, hence, we examined the enzymatic CKX2 activity in the presence and absence of the signal peptide. We expressed full length $^{SP}CKX2^{I}$ and $^{SP}CKX2^{M}$ as well as the SP-lacking counterparts $^{-SP}CKX2^{I}$ and $^{-SP}CKX2^{M}$ in *Escherichia coli* and measured their ability to oxidize CKs. Both SP-lacking forms $^{-SP}CKX2^{I}$ and $^{-SP}CKX2^{M}$ showed a 10-fold higher activity compared to the SP containing versions (Fig. 5d). This in vitro data suggests that SP processing is required to ensure full enzymatic activity of CKX2.

Next, to assess whether the T to G mutation also affects CKX2 activity in planta, we expressed full length *pCKX2::CKX2*^{I} and *pCKX2::CKX2*^{M} encoding versions in the *ckx2-1* mutant background. As expected, the wild-type (Col-0) *CKX2*^{I} was able to fully complement the *ckx2-1* mutant phenotype (Fig. 5e, Supplementary Fig. 5c, Supplementary Data 2). In contrast,

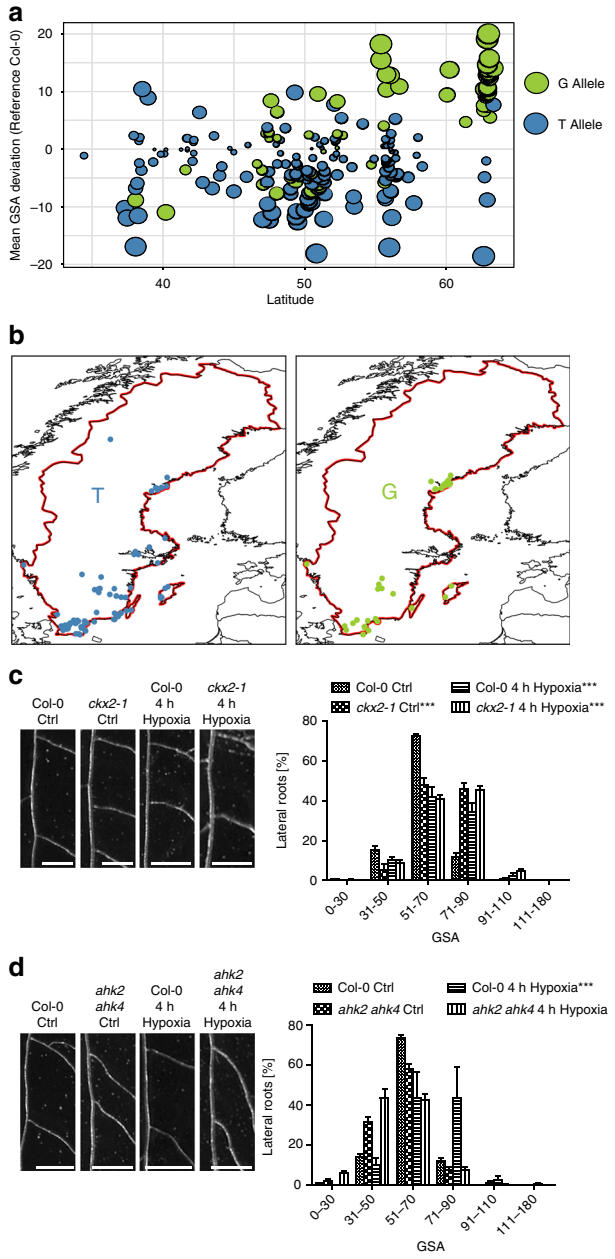

Fig. 4 Cytokinin signaling integrates environmental signals into angular lateral root growth. **a** Comparison of the mean GSA distribution and its geographical (latitude) distribution of the phenotyped accessions. T and G allele of CKX2 are depicted in blue and green, respectively. **b** Relative geographical distribution of the T and G allele of CKX2 in all sequenced Swedish *Arabidopsis* accessions. The distribution of accessions is visualized by R package "rworldmap". **c**, **d** Representative images and GSA distributions of **c** *Col-0* wild-type and *ckx2-1* or **d** *Col-0* wild type and *ahk2 ahk4* with and without hypoxia treatment for 4 h. Scale bars, 2 mm. Kolmogorov–Smirnov test *P*-values: ***$P < 0.001$ (compared to DMSO solvent or *Col-0* wild type control). Mean ± SEM, $n = 4$ plates (10 seedlings with 60–120 LRs per plate). Experiments were repeated at least three times

the mutated $CKX2^M$ version was not able to reverse the reduced LR bending of *ckx2-1* mutants (Fig. 5e and Supplementary Fig. 5c). Overall, our data suggests that the T to G mutation found in natural accessions renders *CKX2* to be largely non-functional in planta by disrupting its secretion and/or SP processing.

Thus, we conclude that variation in SP processing of CKX2 contributes to the natural variation of CK-dependent angular LR growth in *Arabidopsis*.

CKX2 does not detectably interfere with auxin signaling in emerged LRs. Next, we investigated the cellular mechanism by which CKX2 activity modulates the primary GSA of LRs. We first inspected the spatial expression of *CKX2* to identify cells in which *CKX2* may directly regulate angular growth in LRs. pCKX2::CKX2-mTurquoise was weakly expressed in the tip of stage I LRs but showed increased expression in stage II and III LRs (Fig. 6a). We confirmed that endogenous *CKX2* transcripts are strongly up-regulated in stage II and III LRs by examining expression in excised LR tissue using qPCR (Fig. 6b). Notably, *pCKX2::CKX2-mTurquoise* was not readily detectable in the primary root tip (Fig. 6b and Supplementary Fig. 6a), proposing that CKX2 might preferentially act in secondary root organs. In agreement, gravitropic response of *ckx2-1* mutant main roots were largely not distinguishable from wild type roots (Supplementary Fig. 6b).

We next aimed to investigate how deviations in CKX2-dependent modulation of CK in LRs may modulate their directional growth. CKs signaling impairs PIN-dependent auxin transport in main roots as well as in LR primordia[31]. We therefore assessed whether CKX2 activity regulates auxin transport in emerged LRs. Because PIN3 is the main regulator of asymmetric auxin redistribution in columella cells of emerged LR[7], we initially assessed whether the *ckx2-1* mutant shows defective abundance or localization of functional pPIN3::PIN3-GFP in columella cells. At the time of GSA establishment (stage II LRs), PIN3-GFP abundance and asymmetry were not detectably altered in *ckx2-1* mutants when compared to wild type (Fig. 6c and Supplementary Fig. 6c). Next, we used the auxin responsive promoter DR5 fused to GFP and assessed whether auxin signaling is affected in *ckx2-1* mutant LRs. In accordance with proper PIN3 localization, DR5 signal intensity in columella cells, and asymmetric signal in the flanks was similar in *ckx2-1* mutant and wild type stage II LRs (Fig. 6d and Supplementary Fig. 6d).

Overall, this set of data illustrates that auxin responses in gravitropic LR are not detectably altered by CKX2, suggesting that CKX2 modulates angular growth by an alternative, CK-dependent mechanism in emerged LRs.

Emerged LR display asymmetric cytokinin signaling. Our data indicates that CK regulates angular LR growth. To further assess the mechanism by which CK modulates GSA establishment in developing LRs, we visualized the spatial distribution of CK signaling, using the two-component signaling sensor (TCSn) transcriptionally fused to GFP (TCSn::GFP)[32]. We observed increased CK signaling on the upper side of stage II LRs, coinciding with gravitropic bending (Fig. 6e). This asymmetry declined in stage III LRs, which maintain the previously established GSA (Fig. 6e and Supplementary Fig. 6e). In agreement with the anticipated reduction in CK degradation, the magnitude of asymmetric CK signaling was increased in *cxk2-1* mutant LRs (Fig. 6f and Supplementary Fig. 6e). Conversely, asymmetric CK signaling was reduced in the CK receptor double mutant *ahk2 ahk4* (Fig. 6g and Supplementary Fig. 6f). These data propose that the increased magnitude of asymmetry in CK signaling across the root tip correlates with reduced LR bending towards gravity.

To determine whether asymmetric CK signaling regulates bending specifically in LRs, we examined the distribution of CK signaling in primary roots responding to gravity. Importantly, we did not observe asymmetric CK signaling in unstimulated or gravity-stimulated primary roots (Supplementary Fig. 6g–h).

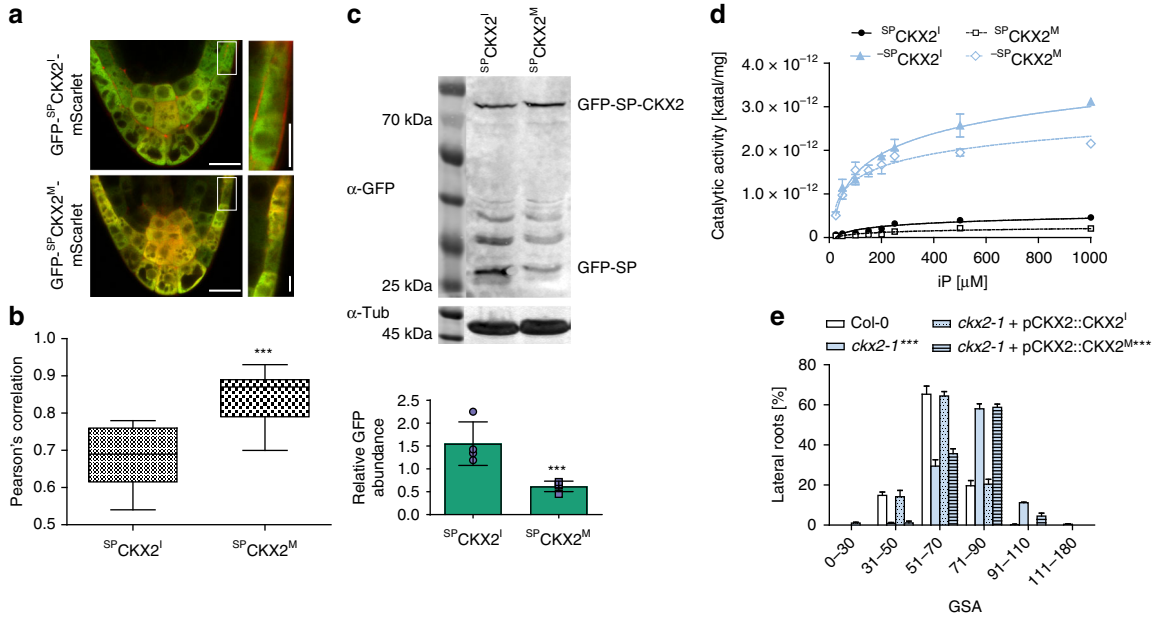

Fig. 5 Signal peptide processing is required for CKX2 activity. **a** Localization of GFP-^{SP}CKX2^{I}-mScarlet and GFP-^{SP}CKX2^{M}-mScarlet in stage II LRs. Scale bar, 25 and 10 µm, respectively. **b** Quantification of the co-localization of GFP and mScarlet signal using Pearson's correlation. Horizontal lines show the medians; box limits indicate the 25th and 75th percentiles; whiskers extend to the min and max values. Student's *t*-test *P*-Value: ***$P < 0.001$, $n = 10$–12 individual LRs. **c** Immunoblot analysis and quantification of ^{SP}CKX2^{I} and ^{SP}CKX2^{M} expressed in *N. benthamiana* leaves using anti-GFP antibody. Anti-tubulin antibody was used as loading control. The signal of GFP-SP was quantified and normalized to tubulin. Student's *t*-test *P*-Value: ***$P < 0.001$. Mean ± SEM, $n = 4$ biological replicates. **d** Saturation curves of isopentenyladenine (iP) degradation by CKX2. Reactions were performed at pH 7.4 in McIlvaine buffer with 0.5 mM DCIP as electron acceptor (black filled circle ^{SP}CKX2^{I}, white square ^{SP}CKX2^{M}, black filled triangle ^{SP}CKX2^{I}, white diamond $^{-SP}$CKX2^{M}). Mean ± SEM, $n = 8$. **e** GSA distributions of *ckx2-1* was complemented by pCKX2::CKX2I, but not by pCKX2::CKX2M. Representative lines are shown. Kolmogorov–Smirnov test *P*-value: ***$P < 0.001$ (compared to *Col-0*). Mean ± SEM, $n = 5$ plates (16 seedlings with 65–160 LRs per plate). **a**–**e** Experiments were repeated at least three times

Accordingly, we conclude that TCSn-based asymmetric CK signaling is specific to LRs and thus contributes to the distinct establishment of primary GSA in LRs. Previous work proposed a hypothetical gravitropic offset component at the upper flank of LRs. This envisioned component was presumably sensitive to the inhibition of auxin transport[14]. To assess if auxin transport similarly modulates the asymmetry of CK signaling in emerged LRs, we treated seedlings with the auxin transport inhibitor 1-N-naphthylphthalamic acid (NPA). Pharmacological interference with auxin transport indeed markedly decreased asymmetric CK signaling in stage II LRs, when compared to the DMSO solvent control (Fig. 6h and Supplementary Fig. 6i), suggesting that auxin transport indeed impacts asymmetric CK signaling in emerged LRs.

In summary, our data suggests that asymmetric CK signaling at the upper flank of LRs functions as an anti-gravitropic component in emerged LRs to promote radial root growth.

CKX2 activity determines cellular elongation in emerged LRs. Light sheet-based live cell imaging showed that cells on the upper and lower flanks of emerged LRs show differential elongation for about 8–9 h[7]. During this developmental stage II, the cellular elongation rates at the upper epidermal layers is three-fold-increased compared to the lower flank (15 µm/h versus 5 µm/h)[7]. To test if this difference can account for the primary GSA establishment, we used these quantitative growth parameters to construct a dynamic computational model of LR bending (Fig. 7a–d and Supplementary Fig. 7a–f). This model incorporates cellular mechanics to simulate cell elongation using stretchable strings as a manifestation of the cell wall elasticity and internal turgor pressure in the cell (see the "Methods" section). The anisotropic growth is simulated by extending the resting length of the string to account for three-fold differences in the growth rates between upper and lower flanks. The resulting model predicts that the incorporation of measured elongation rates on the upper LR flank is able to realistically recapitulate LR bending angle of wild type plants, reaching an angle of about 62–63° within 8–9 h (Fig. 7b, Supplementary Fig. 7a, b).

Next, we experimentally assessed whether the loss of *CKX2* or CK application interferes with cell elongation in stage II LRs. Wild type seedlings showed asymmetric elongation (longer cell length at the upper compared to the lower flank) in stage II LRs (Supplementary Fig. 8a, b). In agreement with reduced LR bending, the *ckx2-1* loss-of-function mutant, as well as wild type plants treated with BAP showed abolished asymmetry in cellular elongation (Supplementary Fig. 8a, b). Our previous work revealed that differential elongation is a major factor controlling LR bending[7]. However, the loss of *CKX2* reduced cell elongation at the upper root flank in average only by 10% (Fig. 7e). To evaluate whether the measured reduction in cell length can realize the observed quantitative changes in LR bending, we reduced cellular elongation similarly by 10% in our computational LR model. The model predicted that CKX2-dependent impact on cellular elongation mildly increases the predicted GSA of LRs (Fig. 7c, d). Thus, we raise some suspicion that the impact of CKX2 on cellular elongation fully explains the observed reduction of LR bending in *ckx2-1* mutants.

Cytokinin alters cell division rates and defines angular growth of LRs. In primary roots, CK reduces not only cellular

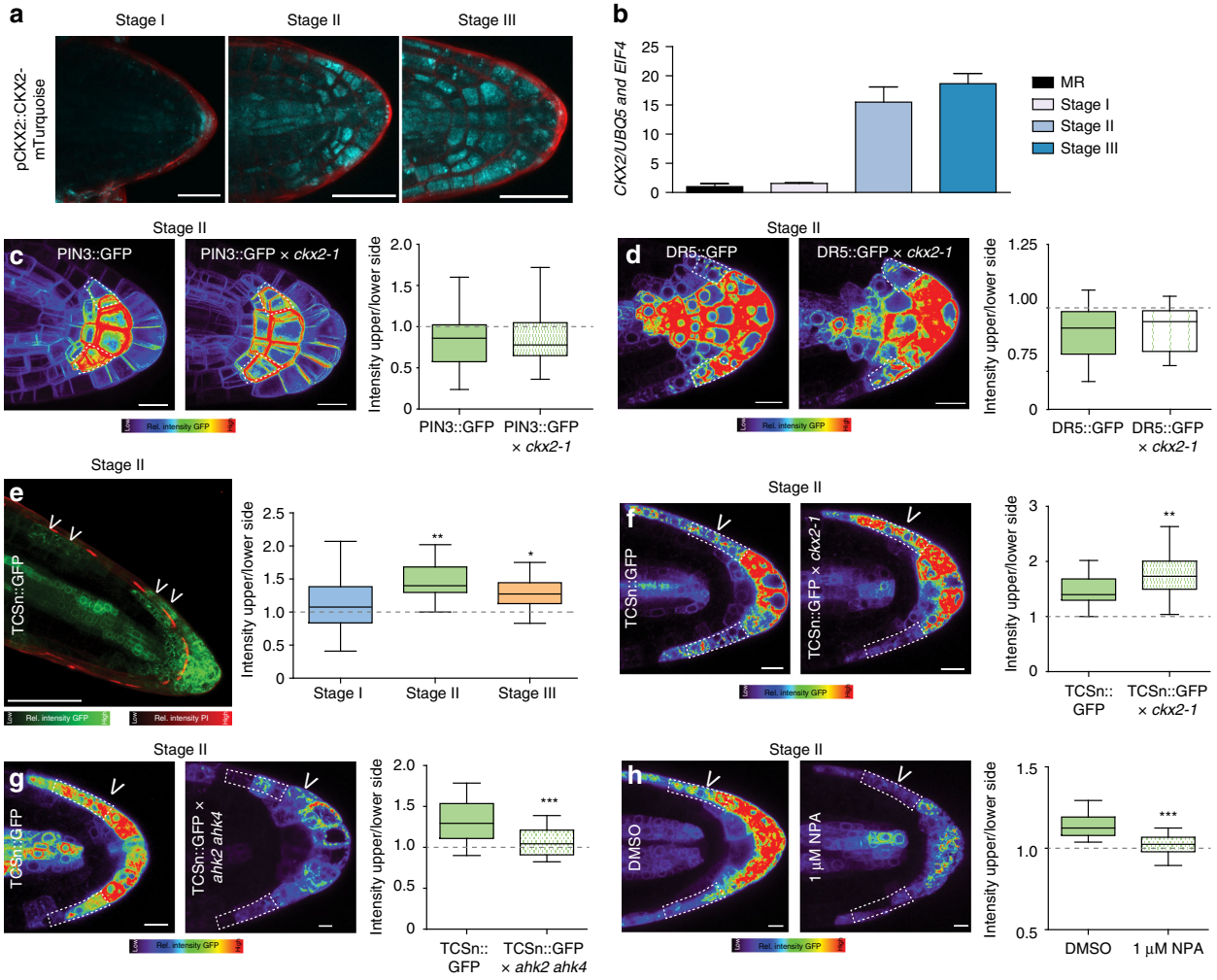

Fig. 6 CKX2 modulates asymmetric cytokinin signaling in emerged lateral roots. **a** Representative images of pCKX2::CKX2-mTurquoise in stages I–III LRs. Propidium Iodide (PI) was used for counterstaining. Scale bar, 25 µm. **b** qPCR analysis detecting the levels of *CKX2* transcript in the root tip and LRs stages I–III normalized against *UBQ5* and *EIF4*. Bars represent means ± SD, $n = 3$. **c**, **d** Representative images and signal quantification of stage II LRs of **c** pPIN3::PIN3-GFP, and **d** DR5::GFP in *Col-0* wild type and *ckx2-1* mutant background. Horizontal lines show the medians; box limits indicate the 25th and 75th percentiles; whiskers extend to the min and max values, $n = 10$–15 individual LRs. Scale bars, 10 µm. **e** Representative image (stage II) and quantification of TCSn::GFP in stages I–III LRs. PI was used for counterstaining. Scale bar, 50 µm. **f**–**h** Representative images and quantification of stage II LRs of **f** TCSn::GFP in wild type and *ckx2-1*, **g** TCSn::GFP in wild type and *ahk2 ahk4* or **h** after treatment with DMSO or 1 µM NPA for 24 h. Scale bars, 10 µm. **e**–**h** One-way ANOVA *P*-values: $^{*}P < 0.05$, $^{**}P < 0.01$, $^{***}P < 0.001$. Horizontal lines show the medians; box limits indicate the 25th and 75th percentiles; whiskers extend to the min and max values, $n = 15$–30 individual LRs. **a**–**h** Experiments were repeated at least three times. White dotted lines outline lateral root cap cells (facing the columella cells) for quantification

elongation, but also cell proliferation by distinct mechanisms[33,34]. Moreover, our computational model predicts that the rate of LR bending could be restricted by the number of cells (Supplementary Fig. 7a, b). Thus, we tested if CK might also affect the meristem of LRs and used cell division marker *pCycB1;1::GUS* to assess the spatial impact of CK on cell proliferation. BAP and INCYDE treatment reduced the abundance of p*CycB1;1::GUS* at the upper flank of stage II LRs (Supplementary Fig. 8c, d). In agreement, *ckx2-1* mutants displayed a more pronounced and statistically significant asymmetry in meristematic cell numbers when compared to wild type stage II LRs, revealing slightly less and more cell divisions at the upper and lower LR flanks, respectively (Fig. 7f). This set of data suggests that CK signaling not only restricts cellular elongation, but also induces a slight asymmetry in cell proliferation in emerged LRs.

Notably, *CDKB1;1* and other cell cycle promoting genes are down-regulated in the *crf1,3,5,6* quadruple mutant[23]. Hence, we assumed that CRF-dependent control of the cell cycle may contribute to the CK-mediated establishment of GSA in emerged LRs. To reduce cell cycle progression, we used the dominant negative (DN) allele of CDKB1;1 and the *cdkb1;1 cdkb1;2* double mutant (Fig. 7g, Supplementary Data 2), as well as the cell cycle inhibitor Roscovitine (Supplementary Fig. 8e, Supplementary Data 2). Both genetic and pharmacological interference with the cell cycle interfered with the LR bending (Fig. 7g, Supplementary Data 2, Supplementary Fig. 8e), phenocopying *ckx2-1* mutants. Intriguingly, CDKB1;1^{DN} as well as *cdkb1;1 cdkb1;2* showed a meristematic asymmetry, displaying a higher number of meristematic cells in the lower flank as compared to the upper flank (Fig. 7h). This is somewhat reminiscent to the *ckx2-1* mutant phenotype and we

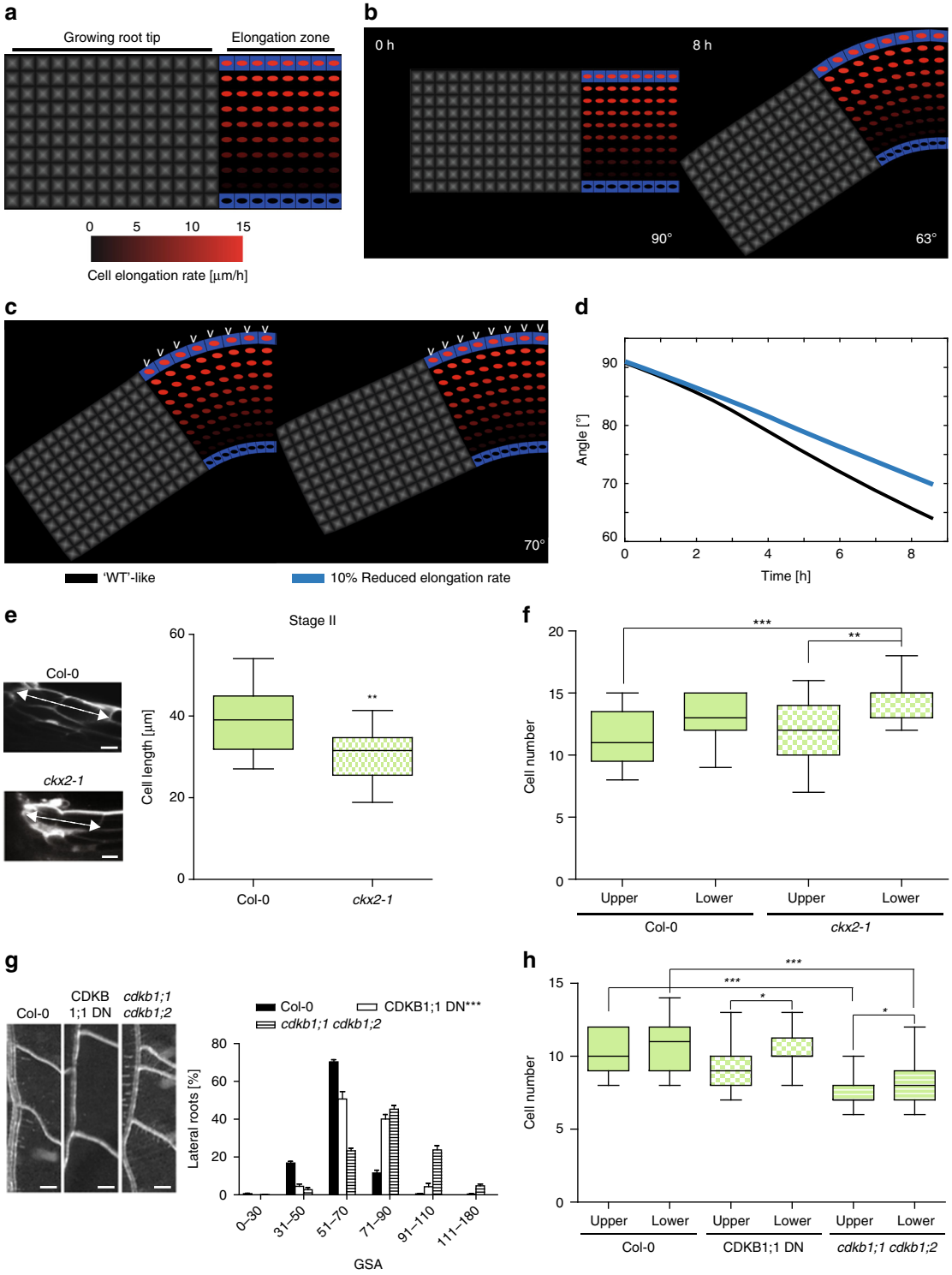

Fig. 7 Cytokinin affects cell elongation and number in lateral roots. **a** Sketch shows a simplified geometry of a lateral root (LR). LR model consists of tip and elongation zones. The cell elongation rate (visualized as red spot inside the cell) linearly increases from lower flank towards the upper flank of the LR (up to three-fold) based on estimates derived from previous work[7]. Bottom panel, color coding bar for cell elongation rates. **b** Time-lapse model simulations (screenshots) which lead to the in vivo observed LR bending (63°) after ~8 h. **c** Left panel corresponds to **b**. Right panel, 10% decrease in elongation rate only on the upper root flank (white arrow heads). Each simulation represents LR status after 9 h of dynamic elongation. **d** Time evolution of set-point angle corresponding to different scenarios in **c**. **e** Representative image and quantification of first two elongated cells of lateral roots in stage II. **f** Quantification of the cell number in the upper and lower meristem of *Col-0* and *ckx2-1*. **g** Representative images and GSA distributions of *Col-0* wild-type, CDKB1;1 DN (dominant negative) and *cdkb1;1 cdkb1;2*. Kolmogorov–Smirnov test *P*-values: ***$P < 0.001$ (compared to *Col-0*). Mean ± SEM, $n = 5$ plates (16 seedlings with 100–180 LRs per plate). Scale bars, 2 mm. **h** Quantification of the cell number in the upper and lower meristem of *Col-0*, CDKB1;1 DN and *cdkb1;1 ckdb1;2*. **e**, **f**, **h** One-way ANOVA *P*-values: *$P < 0.05$, **$P < 0.01$, ***$P < 0.001$. Horizontal lines show the medians; box limits indicate the 25th and 75th percentiles; whiskers extend to the min and max values, $n = 10$–20 individual LRs. Scale bar, 10 µm. **e**–**h** Experiments were repeated at least three times

assume that the CK-dependent, asymmetric interference with the cell cycle is amplified in these cell cycle mutants when compared to wild type. In agreement with such a scenario, the gravity response kinetics of primary roots, which lack asymmetric TCSn-based CK signaling, were not affected by the CDKB1;1^{DN} as well as *cdkb1;1 cdkb1;2* mutations (Supplementary Fig. 8f, g). This suggests that not only cellular elongation[7], but also the negative impact of CK on the cell cycle in stage II LRs is a particular determinant of directional LR growth.

Overall, this set of data suggests that CK modulates both differential cell elongation and cell proliferation to interfere with growth at the upper flank of LR, ultimately regulating angular LR growth and radial expansion of the root system.

Discussion

Because root systems are hidden beneath the soil, the study and directed improvement of root architectural traits in crop breeding programs have been delayed. There is growing interest to alleviate the harmful effects of drought stress by modulating the primary GSA of LRs[1]. Despite the apparent importance of the root system depth, the molecular mechanisms regulating the direction of LR growth are poorly understood. Thus, understanding the molecular mechanisms establishing the primary angular growth in LRs could guide future engineering of plants to suit certain habitats. Anticipating that natural variation could provide valuable insights on how to sustainably engineer root systems, we focused on the primary growth direction of LR in natural *Arabidopsis* accessions.

We reveal that the primary growth direction of LR varies substantially within a population of natural *Arabidopsis* accessions. Primary LR angles of hypo-responsive or hyper-responsive accessions followed a similar trend regardless of whether they were grown in soil, two-dimensional or three-dimensional in vitro systems. We thus conclude that this approach is suitable to assess the genetic control of angular LR growth. Using a GWAS approach, we show that angular growth of LR is controlled by CKX2-dependent metabolism of the phytohormone CK. CKX2 contains a SP to enter the secretory pathway, which could be crucial for its impact on CK perception. However, the precise site of CK receptor activity (plasma membrane and/or endoplasmic reticulum) is still under debate[35]. We conclude that variation in an amino acid substitution after the predicted cleavage site impacts on SP processing of CKX2, which consequently obstructs CKX2 activity in planta. Our data suggest that the lack of SP processing abolishes the secretion and enzymatic activity of CKX2, thereby contributing to CK-dependent GSA trait variation in natural *Arabidopsis* accessions.

Nordic accessions preferentially express an inactive *CKX2* variant, which prompted us to investigate whether environmental cues further define the root system in a CK-dependent manner. We revealed that hypoxic conditions induce more horizontal LR growth through CK signaling. The increased frequency of an inactive *CKX2* allele in Nordic accessions suggests that the allele may have been selected for in these populations, promoting more horizontal root growth. It is an intriguing possibility that more horizontal, near surface roots may rectify gas exchange under hypoxia conditions, potentially alleviating the harmful effects of hypoxic stress in these Nordic, snow covered habitats. This assumption, however, awaits further experimental validation.

Our analysis suggests that primary and secondary roots have distinct responses to CK. While CK signaling abolishes PIN-dependent transport in main roots[31], we show that CKX2-dependent interference with endogenous CK levels does not affect PIN3 and auxin signaling in emerged LRs. Moreover, CK signaling is asymmetric in emerged lateral, but not primary roots, proposing a unique role of CK in regulating asymmetric growth responses in LRs. Also abscisic acid signaling displays distinct activities in main and lateral root organs, presumably allowing distinct organ growth rates in response to environmental stresses[36]. Thus, we propose that hormone signaling might be generally co-opted in primary and secondary roots to facilitate diverged growth responses to the environment.

The increase and decrease of CK levels slightly accelerate the rate of gravitropic bending in primary root, but the developmental importance of this effect remains uncertain[37]. In contrast, we show here that CK signaling plays a developmental role in establishing the primary GSA of LRs. Moreover, an increase and decrease of CK signaling correlate with reduced and enhanced down-ward bending of LRs, respectively. Mechanistically, we showed that CK signaling interferes with cellular elongation and proliferation in emerged LR to reduce LR organ bending towards gravity. These stage II LRs undergo a de novo formation of the elongation zone[7]. During this short developmental time window, the CK-dependent reduction in cell proliferation could have hence caused an immediate influence on the number of elongating cells. We detected only a mild asymmetry in cell numbers at the LR organ flanks of *ckx2* mutants, proposing that these LRs display only few cells less at the upper compared to the lower root flanks. Such a small impact could nevertheless compromise angular LR growth, because our computational model predicted that an asymmetric reduction in cell number at the upper root flank (Supplementary Fig. 7c–f) or gradually along the LR organ (Supplementary Fig. 9a–c) would induce some constraints, additionally limiting organ bending. However, this aspect awaits experimental validation, requiring detailed live cell imaging and possibly mechanical constraint measurements in LRs.

We illustrate that CKX2 contributes to the rate of asymmetric CK signaling, but *CKX2* expression did not show a pronounced asymmetry. Similarly, the CK response factors CRF2 and CRF3 are not asymmetrically expressed in emerged LR. We, hence, conclude that additional so far unknown factors play decisive roles in establishing asymmetric CK signaling across the LR tip. Our work proposes that an auxin transport mechanism promotes the asymmetry of CK signaling. Accordingly, auxin could generate an anti-gravitropic signal to interfere with its own gravitropic impact in LRs. Unlike auxin, the mechanisms of intercellular CK transport are poorly characterized[38]. One intriguing possibility is however that the asymmetric auxin signal could favor CK relocation towards the upper side of LRs, inducing differential CK signaling and growth repression on this side. However, it is also possible that differential CK signaling occurs at the level of signal integration and might be independent of differential distribution of CK. Future work will examine these possibilities to uncover the mechanism by which CKX2 is linked to differential CK activity across a stage II LR.

At the transition to stage III, *PIN3* expression in columella cells transiently decreases[7,11]. This temporal absence of PIN proteins in gravity sensing columella cells correlates with the onset of non-differential auxin redistribution and symmetric (non-gravitropic) LR organ growth[7]. In agreement, also the asymmetry in CK signaling declines at the onset of stage III LR, proposing that gravity-induced, differential growth at upper and lower organ flanks is generally switched off at this stage. Subsequent de-repression of *PIN3* and *PIN4* expressions in columella cells of stage III LRs does not induce alterations in GSA of LR[8], suggesting that the gravitropic machinery is similarly inactive in

these older stage III LRs. On the other hand, the onset of expression and subsequent polarization of PIN7 coincide with the stage III–IV transition, which is marked by further gravitropic bending of the respective LRs[8]. It needs to be seen how gravitropic perception and/or response is reactivated in these LRs and if CK signaling also plays a role in the incremental gravitropic responses during the stage III–IV transition of LRs.

In conclusion, our genetic screen uncovered that directional LR growth depends on opposing gravitropic and anti-gravitropic phytohormonal cues (Supplementary Fig. 8h). We conclude that CK signaling reduces growth at the upper organ side, which counteracts the gravity induced, auxin-dependent reduction in cell expansion at the lower root flank. In this way, a CK-dependent mechanism allows the root system to override the gravitropic response and radially explore its surroundings. Genetic interference with CK signaling cannot only be used to define the primary growth direction of LRs, but moreover may refract certain environmental input to root architecture. Overall, these results propose that directed interference with CK responses in LRs could be used to engineer root system depth to better suit certain habitats.

Methods

Plant material and growth conditions. Seeds of *Arabidopsis thaliana* accessions were kindly provided by Magnus Nordborg and Wolfgang Busch. The following lines and constructs have been described previously: *ahk2-7* (*ahk2*), *ahk3-7* (*ahk3*)[39], *cre1-12* (*ahk4*)[40], *ahk2 ahk3*, *ahk2 ahk4*, *ahk3 ahk4*[39], *arr3*, *arr4*, *arr10-5*, *arr12-1* pARR3::GUS, pARR4::GUS, pARR10::GUS, pARR12::GUS[41], CDKB1;1 DN[42], *cdkb1;1 cdkb1;2*[43], 35S::CKX2[44], *ckx2-1*[45], *crf2-1*, *crf2-2*, *crf3-1*, *crf3-2*, RPS5a::CRF2, 35S::CRF3[24], pCRF2::GFP/GUS, pCRF3::GFP/GUS[46], pCYCB1::GUS[47], pDR5::GFP[6], pPIN3::PIN3-GFP[48], TCSn::GFP[32], TCSn::GFP *ahk2 ahk4*[49], pUBQ10::LUC2o[15]. Seeds of *Brassica napus* L. were kindly provided by Saatzucht Donau. Seeds were surface sterilized, stratified at 4 °C for 2 days in the dark. Seedlings were grown vertically on half Murashige and Skoog medium (1/2 MS salts (Duchefa), pH 5.9, 1% sucrose, and 0.8% agar). Plants were grown under long-day (16 h light/8 h dark) conditions at 20–22 °C.

Chemicals and treatments. 1-N-naphthylphthalamic acid (NPA) (Sigma), 6-Benzylaminopurin (BAP) (Sigma), *trans*-Zeatin (tZ) (OlChemim), N^6-(2-Isopentenyl)Adenine (iP) (OlChemim) were all dissolved in DMSO (Duchefa). 2-chloro-6-(3-methoxyphenyl)aminopurine (INCYDE) was synthesized and kindly donated by the Laboratory of Growth Regulators, Palacký University & Institute of Experimental Botany AS CR (Olomouc, Czech Republic) as previously described[19] and dissolved in DMSO. Treatments with NPA BAP, tZ, iP and INCYDE were all performed on 7-day-old seedlings (transferred to supplemented media).

GUS stainings were performed after 24 h and initial GSA measurements 7 days after transfer.

Genome-wide association studies (GWAS). To identify the genetic basis of the for the GSA of LRs we carried out a GWAS using an accelerated mixed model (AMM)[16]. The GWAS results can be viewed interactively online: https://gwas.gmi.oeaw.ac.at/#/analysis/12722/overview.

Rhizotrons. The basic rhizotron design was as described in ref. [15]. To adapt the rhizotrons for use in an automated rhizotron handling system (designed by Modular Science, San Francisco), several modifications were implemented. The top edge of each rhizotron sheet was beveled using a belt sander to facilitate automated watering. Two 1/16" thin aluminum hooks used for automatic handling of the rhizotron were attached on each side of the rhizotron. To reduce light exposure of the root system during growth, a 1/8" thin black acrylic rhizotron top shield was installed.

Box and holders for rhizotrons. Black 12" $W \times 18$" $L \times 12$" H boxes (Plastic-Mart) were used to grow plants in 12 rhizotrons at a time. The arrangement of 1/8"-thin black acrylic sheets of different shapes and sizes formed 12 light-proof chambers to make sure that the roots of every rhizotron were shielded from light even when one rhizotron was removed for imaging.

Rhizotron preparation was as described in ref. [15] with slight modifications required by the new rhizotron design.

Plant growth in rhizotrons. Two transfer pipettes (each ~2 ml) of quick-releasing fertilizer (Peter's 20–20–20) were added to each rhizotron after assembly. Assembled rhizotrons were placed into a box with water and allowed to absorb water overnight from the bottom side. Seeds containing the pUBQ10::LUC2o transgene[15] were stratified for 2 days at 4 °C in distilled water and three seeds were sown in the center of each rhizotron. Each rhizotron was equipped with a unique barcode. All rhizotrons were sprayed down with water and sealed with a transparent lid and packing tape. Plants were grown at 22/18 °C (day/night) under long-day conditions (16 h light, 8 h dark) using LED lights (Vayola, C-Series, N12 spectrum) with a light intensity of about 130 µmol m^{-2} s^{-1}. After 2 days, the transparent lid was unsealed, rhizotrons were watered with two transferring pipettes of water, and the lid left loose for an additional day. After removing the lid, rhizotrons were watered twice per day with two transferring pipettes of water each time until 9 days after sowing.

Plant imaging in rhizotrons. 20 days after sowing, the automated rhizotron handling system (designed by Modular Science, San Francisco) added 50 ml of 300 µM D-luciferin (Biosynth) at the top of each rhizotron and loaded the rhizotron into a fixed stage that was controlled by a Lambda 10-3 optical filter changer (Sutter Instruments, Novato, CA) in the GLO1 imaging system[15]. 5-min exposures were taken per rhizotron side.

A shoot image was taken right after the four root images using an ids UI-359xLE-C camera with a Fujinon C-Mount 8–80 mm Varifocal lens that was installed in GLO1. Three LED strips on each side of the camera were switched on before a shoot image was taken.

Image preparation of rhizotrons pictures. Image preparation was similar to that in ref. [15]: four individual root images were collected: top front, bottom front, top back, and bottom back. Using an automated ImageJ macro, a composite image was generated as follows: (1) images were rotated and translated to control for small misalignments between the two cameras; (2) the top and bottom images of each side were merged; (3) the back image was flipped horizontally; (4) the front and back images were combined using the maximum values. The final images produced were 16-bit in depth and 4096 × 2048 pixels. The scale of the images was 138.6 pixels per cm.

Hypoxia treatment. All following treatments were performed in air-tight glass desiccators in which seedlings grown on vertical agar plates were carefully placed with the lids removed. Seedlings were exposed to a hypoxia treatment by flushing the desiccators with humidified 100% N_2 gas (2 l/min) for 4 h (13.00–17.00 h) in the dark to limit photosynthesis-derived oxygen production. For the controls, desiccators were flushed with humidified air. Flow rates were controlled by mass flow controllers (MASS-VIEW, Bronkhorst). At the end of the hypoxia treatment, plates were carefully removed from the desiccators, closed, and transferred back to the climate chamber. The plates remained in the climate chambers under control growth conditions for 5 days after the treatment after which they were scanned using an EPSON Scanner V300.

DNA constructs. The promoter region and full-length $CKX2^1$ or coding DNA sequence (CDS) were amplified by PCR (Supplementary Data 3) from genomic DNA or cDNA using Q5 high-fidelity DNA polymerase (NEB) and cloned either alone or under of the 35S promoter together with GFP and mScarlet-i into pPLV03 or pGEX5×3 using Gibson Assembly Master Mix (NEB). Subsequently, this plasmid were used for in vitro mutagenesis (Supplementary Data 3) to obtain $CKX2^M$. The resulting constructs were transformed into Col-0 and *ckx2-1* plants using the floral dipping method[50] or for transient transformation in tobacco plants.

Activity measurement of recombinant proteins. Recombinant proteins were expressed as GST fusion proteins and in *Escherichia coli* BL21 codon plus strain. Proteins were purified using the Sepharose beads affinity method (Glutathione Sepharose 4B; GE Healthcare).

The activity was measured using a modified end-point method previously described[51]. In brief, the samples were incubated in a reaction mixture (total volume of 600 µl) that consisted of 200 mM McIlvaine buffer (100 mM citric acid and 200 mM Na_2HPO_4) pH 7.4, 500 µM 2,6-dichlorophenol indophenol (DCPIP; Sigma) as electron acceptor and different concentrations of N^6-(2-isopentenyl) adenine (iP; Sigma) as substrate. The volume of the enzyme sample used for the assay was adjusted based on the enzyme activity. The incubation time at 37 °C was 1 h. The enzymatic reaction was stopped after incubation by adding 300 µl of 40% trichloroacetic acid (TCA), then 200 µl 2% 4-aminophenol (Sigma) (in 6% TCA) was added and the sample was centrifuged at 20,000 × g for 5 min to remove protein precipitate. 200 µl supernatant was used to measure the absorption spectrum from 352 to 500 nm to determine the concentration of produced Schiff base with $\varepsilon 352 = 15.2$ mM^{-1} cm^{-1} using a plate reader.

Microscopy. Confocal microscopy was performed using a Leica SP5 (Leica). Fluorescence signals for GFP (excitation 488 nm, emission peak 509 nm), mScarlet-i (excitation 561 nm, emission peak 607 nm), mTurquoise (excitation 434 nm, emission peak 474 nm) and propidium iodide (PI) staining (20 µl ml^{-1}) (excitation 569 nm, emission peak 593 nm) were detected with a ×40 or ×63 (water immersion) objective. The fluorescence signal intensity (mean gray value) of the presented

markers was quantified using the maximum projections obtained from a Z-stack series that were taken and analyzed using the Leica software LAS AF 3.1. The same region of interest (ROI) was defined for each individual seedling.

To determine meristematic cell numbers and cell size in stage II LRs, 8-day-old seedlings ($n = 10–15$) were stained with PI and microscopy was performed using confocal microscope (see above). The first two epidermal cells (adjacent to the main root) were considered for cell size measurements in stage II LR. Epidermal cell numbers were counted between the quiescent center and the first elongating cell (twice as long as wide) at the upper and lower flank of stage II LRs.

Graphpad Prism software was used to evaluate the statistical significance of the differences observed between control and genotype/treatments (one-way ANOVA).

Gravitropic set-point angle measurements. Plates with 14-day-old seedlings were scanned and the initial gravitropic set-point angle (iGSA) of individual LRs was measured with reference to the gravity vector[7] using Image J software. All available LR from each seedling were measured. Individual GSA values were then sorted into eight categories: 0–30°, 31–50°, 51–70°, 71–90°, 91–110°, 111–180°. Percentages of incidence were calculated for each category and graphs of GSA distribution were generated. The test of Kolmogorov–Smirnov (KS-test) was used online (http://www.physics.csbsju.edu/stats/KS-test.n.plot_form.html) to statistically evaluate the GSA data sets generated from mutants and treated seedlings in comparison to wild type and untreated controls, respectively.

Histochemical GUS staining. GUS histochemical staining of acetone-fixed 7-day-old seedlings containing pCycB1::GUS fusion constructs followed a previously described method[52] using 5-Bromo-4-chloro-1*H*-indol-3-yl β-D-glucopyranosiduronic acid (X-Gluc, Carl Roth) as substrate. In brief: seedlings were fixed in 90% aceton for 30 min. After washing with 0.1 M Na-phosphate buffer (pH 7) seedlings were incubated for 2 h at 37 °C in the GUS staining solution (2 mM x-Gluc (dissolved in DMSO), 0.1% Trition X-100, 10 mM EDTA, 0.5 mM potassium ferrocyanide, 0.5 mM ferrycyanide, 0.1 M Na-phosphate buffer pH 7). Examination of stained seedlings and image acquisition were performed with a light microscope (Zeiss Observer D1) equipped with a DFC 300 FX camera (Zeiss). The intensity of the staining was quantified as described ref. [53] in a region of interest (ROI), which was kept constant. Graphpad Prism software was used to evaluate the statistical significance of the differences observed between control and treated groups (One-way ANOVA).

Transient transformation and western analysis. The *Agrobacterium tumefaciens* strain GV3101 was transformed with the respective construct and grown for 2 days at 28 °C in 5 ml Luria-Bertani (LB). The preculture was used to inoculate 25 ml LB and incubated for 4 h at 28 °C. Cells were pelleted and resuspended in 30 ml LB supplemented with 100 µM acetosyringone. After 2 h, cells were resuspended in 30 ml of 5% sucrose and infiltrated in tobacco (*Nicotiana tabacum*) leaves. Subcellular localization was examined 3 days after transformation by confocal laser scanning microscopy (see above) or leaves were ground to fine powder in liquid nitrogen and solubilized with extraction buffer (25 mM Tris, pH 7.5, 10 mM $MgCl_2$, 15 mM EGTA, 75 mM NaCl, 1 mM DTT, 0.1% Tween 20, with freshly added proteinase inhibitor cocktail (Roche)). Protein concentration was assessed using the Bradford method. Membranes were probed with a 1:5000 dilution of GFP antibody (#ab290, abcam) or 1:20,000 of tubulin antibody (T6074-200UL, Sigma). Goat IRDye 800CW anti-mouse (926-32210, LI-COR) or goat IRDye 800 CW anti-rabbit (926-32211, LI-COR) was used (1:20,000) as secondary. The signals were detected and quantified using the Odyssey Imagine System (LI-COR).

RNA extraction, cDNA synthesis and quantitative PCR. RNA extraction was done as described previously[54]. In brief: a pool of 10 LR or root tips were collected in 30 µl of 100% RNAlater (Thermo Fisher) and 500 µl of TRIzol (Sigma) was added followed by brief vortexing (2× for 2 s each) and incubating at 60 °C for 30 min. 100 µl of chloroform was added, and then, samples were vortexed briefly (2× for 2 s each) and incubated at room temperature for 3 min. After centrifugation at 12,000 × *g* for 15 min at 4 °C, the aqueous phase was transferred to a new tube. To precipitate the RNA, an equal volume of isopropanol and 1.5 µl of GlycoBlue (Thermo Fisher) were added followed by a −20 °C incubation for 15–18 h and centrifugation at >20,000 × *g* for 60 min at 4 °C. After removal of the supernatant, the pellet was washed by adding 500 µl of 75% ethanol, vortexing briefly and then centrifuged at >20,000 × *g* for 15 min at 4 °C. The 75% ethanol wash step was repeated 1×. As much ethanol as possible was removed followed by the drying of the pellet by letting the Eppendorf tube sit on ice with lid open for 10 min. Precipitated RNA was then resuspended with 5–12 µl of nuclease-free water, stored at −80 °C. cDNA synthesis was performed using SuperScript II (Thermo Fisher) and qPCR using 2x Takyon for SYBR Assay—no ROX (Eurogentec) following the manufacturer's instructions on a CFX96 Touch Real-Time PCR Detection System (Bio-Rad). Expression values were normalized to the expression of ubiquitin 5 (UBQ5) and translation initiation factor EIF4A.

Cytokinin measurements. Quantification of cytokinin metabolites was performed according to the method described by Svačinov et al. [55], including modifications described in ref. [56]. Briefly, root samples (20 mg FW) were extracted in 1 ml of modified Bieleski buffer[57] together with a cocktail of stable isotope-labeled internal standards used as a reference (0.25 pmol of CK bases, ribosides, N-glucosides, and 0.5 pmol of CK O-glucosides, nucleotides per sample added). The extracts were purified using the Oasis MCX column (30 mg/1 ml, Waters) and cytokinin levels were determined using the LC–MS/MS system consisting of an ACQUITY UPLC System and a Xevo TQ-S triple quadrupole mass spectrometer (Waters). Results are presented as the average of five biological replicates ± standard deviation in pmol/g FW. Statistical examinations were made between Col-0 wild type and *ckx2-1* roots using one-way ANOVA analysis.

Assessment of gravitropic main root growth. We used infrared-based time lapse of gravitropic main roots (90° tilted plates) in the dark. Growth rate normalization was performed as described in ref. [58].

Maps. The maps were created in R using the package "rworldmap"[59].

Description of the computer model of LR. For the sake of simplicity, our model is composed of rectangular grid in which each box represents a single cell—a basic space discretization unit in the model. Cell walls are modeled as a linear elastic spring (connecting two adjacent vertices) that can expand and contract in order to minimize forces acting on each spring. The magnitude of force exerted by this spring is $k_x \cdot (L_{u,v} - |p_u - p_v|)$ and is positive for spring compression. The k_x characterizes the stiffness of the spring and was set to 0.9 in all simulations. This force is in the direction of the spring $\frac{p_u - p_v}{|p_u - p_v|}$. p_u is the position of vertex **u**, and p_v is the position of neighboring vertex **v**. The total force exerted on vertex **u** located at position p_u by all such springs can be written as

$$F^u_{\text{linear}} = \sum_{u \in N_u} k_x \cdot (L_{u,v} - |p_u - p_v|) \cdot \frac{p_u - p_v}{|p_u - p_v|}$$

where $\mathbf{N_u}$ is the set of vertices adjacent to vertex **u**. The norm symbol indicates the Euclidean distance between the points.

In addition to the forces acting on a vertex due to springs, a force due to the turgor pressure inside the cell ($p_{\text{const}} = 0.05$) acts in the direction normal to each wall ($\boldsymbol{n}$):

$$F^u_{\text{pressure}} = p_{\text{const}} \cdot \hat{n} \cdot |p_u - p_v|$$

This cell turgor pressure helps to maintain cell shape protecting from artificial deformations[60].

Combining the individual force components, the total force acting on a vertex **u** is the sum of forces acting on each cell wall and internal pressure inside the cells.

According to the second Newton's Law of dynamics we calculated the velocity (Vel_u) and position (p_u) of vertex **u** over time for point mass $m_u = 1$ with the following formulas:

$$\frac{d\text{Vel}_u}{dt} = \frac{F^u_{\text{total}}}{m_u} - \beta \cdot \text{Vel}_u, \frac{dp_u}{dt} = \text{Vel}_u$$

where $\beta = 0.2$ is a damping constant.

Other details of a model setup and methodology as well as its successful applicability for resolving the organ bending simulations can be found in ref. [60]. The LR root model is spatially divided into two zones (root tip and cell elongation zones) along *x*-axis based on the threshold parameter that defines distance between individual cell center and right-most cell centers. The right-most boundary vertices were fixed in *x*-direction to mimic connection to the main root axis (outermost right) such that growth occurs only from the main root axis as observed experimentally. We use thresholds that controls either the length of whole elongation zone or simply the number of elongating cells only on the upper root flank or progressively from the top to the bottom to mimic the input of an asymmetric meristem in our simulations (Supplementary Figs. 7 and 9). Along *y*-axis cells elongate at different rates based on the linear interpolation between the minimal measured elongation rate at the bottom part of the LR (5 µm h^{-1}) to the maximal elongation rate at the top flank of the LR (15 µm h^{-1})[7]. Furthermore, we found that linear interpolation gave the best fit to the experimental observations in terms of >2-fold change in cell size between upper and lower LR root flanks. To simulate reduced elongation, we consequently reduced the maximal rate of cell elongation on upper root flank by 10%. Cell elongation is simulated by expanding the resting length of linear springs at each growth time step (0.003). The growth time step occurs after mass-spring system reaches the transient equilibrium such that the slower growth and faster mechanics steps follow consecutive iterations[60].

$$\frac{dL_{u,v}}{dt} = L_{u,v} \cdot r(d)$$

where $r(d)$ is an linearly interpolated growth rate and d is the relative distance from the bottom part of the LR such that $r_{\min}(0) = 5$ µm h^{-1} and $r_{\max}(1) = 15$ µm h^{-1}.

The geometry of the model was created using a version of the VV simulator[61,62] embedded in the modeling software L-studio[63] (http://algorithmicbotany.org/lstudio). Cell mechanics and growth steps was solved using the forward Euler method. All simulations were terminated after 9 h of growth to match the experimental observations.

Reporting summary. Further information on research design is available in the Nature Research Reporting Summary linked to this article.

Data availability

All data generated or analyzed during this study are included in this article and its supplementary information files. Seeds and plasmids are available from the corresponding author upon request. The GWAS data set has been deposited at https://gwas.gmi.oeaw.ac.at/#/analysis/12722/overview.

Code availability

All information for building the model is indicated in the manuscript. Further information is available from the corresponding author upon request.

Received: 7 March 2019 Accepted: 16 July 2019
Published online: 06 August 2019

References

1. Uga, Y. et al. Control of root system architecture by DEEPER ROOTING 1 increases rice yield under drought conditions. *Nat. Publ. Group* **45**, 1097–1102 (2013).
2. Su, S.-H., Gibbs, N. M., Jancewicz, A. L. & Masson, P. H. Molecular mechanisms of root gravitropism. *Curr. Biol.* **27**, R964–R972 (2017).
3. Leitz, G., Kang, B. H., Schoenwaelder, M. E. A. & Staehelin, L. A. Statolith sedimentation kinetics and force transduction to the cortical endoplasmic reticulum in gravity-sensing *Arabidopsis* columella cells. *Plant Cell Online* **21**, 843–860 (2009).
4. Kleine-Vehn, J. et al. Gravity-induced PIN transcytosis for polarization of auxin fluxes in gravity-sensing root cells. *Proc. Natl Acad. Sci. USA* **107**, 22344–22349 (2010).
5. Friml, J., Wiśniewska, J., Benková, E., Mendgen, K. & Palme, K. Lateral relocation of auxin efflux regulator PIN3 mediates tropism in *Arabidopsis*. *Nature* **415**, 806–809 (2002).
6. Friml, J. et al. Efflux-dependent auxin gradients establish the apical–basal axis of *Arabidopsis*. *Nature* **426**, 147–153 (2003).
7. Rosquete, M. R. et al. An auxin transport mechanism restricts positive orthogravitropism in lateral roots. *Curr. Biol.* **23**, 817–822 (2013).
8. Ruiz Rosquete, M., Waidmann, S. & Kleine-Vehn, J. PIN7 auxin carrier has a preferential role in terminating radial root expansion in *Arabidopsis thaliana*. *Int. J. Mol. Sci.* **19**, 1238, (2018).
9. Digby, J. & Firn, R. D. The gravitropic set-point angle (GSA): the identification of an important developmentally controlled variable governing plant architecture. *Plant Cell Environ.* **18**, 1434–1440 (1995).
10. Wang, H.-Z. et al. Transcriptional regulation of PIN genes by FOUR LIPS and MYB88 during *Arabidopsis* root gravitropism. *Nat. Commun.* **6**, 1–9 (2015).
11. Guyomarc'h, S. et al. Early development and gravitropic response of lateral roots in *Arabidopsis thaliana*. *Philos. Trans. R. Soc. B* **367**, 1509–1516 (2012).
12. Schöller, M., Kleine-Vehn, J. & Feraru, E. Cortical cell length analysis during gravitropic root growth. *Methods Mol. Biol.* **1761**, 191–197 (2018).
13. Mullen, J. L. & Hangarter, R. P. Genetic analysis of the gravitropic set-point angle in lateral roots of *Arabidopsis*. *Adv. Space Res* **31**, 2229–2236 (2003).
14. Roychoudhry, S., Del Bianco, M., Kieffer, M. & Kepinski, S. Auxin controls gravitropic setpoint angle in higher plant lateral branches. *Curr. Biol.* **23**, 1497–1504 (2013).
15. Rellán-Álvarez, R. et al. GLO-Roots: an imaging platform enabling multidimensional characterization of soil-grown root systems. *Elife* **4**, e07597, (2015).
16. Seren, Ü. et al. GWAPP: a web application for genome-wide association mapping in *Arabidopsis*. *Plant Cell* **24**, 4793–4805 (2012).
17. Schmülling, T., Werner, T., Riefler, M., Krupková, E. & Bartrina y Manns, I. Structure and function of cytokinin oxidase/dehydrogenase genes of maize, rice, *Arabidopsis* and other species. *J. Plant Res.* **116**, 241–252 (2003).
18. Galuszka, P. et al. Biochemical characterization of cytokinin oxidases/dehydrogenases from *Arabidopsis thaliana* expressed in *Nicotiana tabacum* L. *J. Plant Growth Regul.* **26**, 255–267 (2007).
19. Zatloukal, M. et al. Novel potent inhibitors of *A. thaliana* cytokinin oxidase/dehydrogenase. *Bioorg. Med. Chem.* **16**, 9268–9275 (2008).
20. Rashotte, A. M. et al. A subset of *Arabidopsis* AP2 transcription factors mediates cytokinin responses in concert with a two-component pathway. *Proc. Natl Acad. Sci. USA* **103**, 11081–11085 (2006).
21. Jeon, J., Cho, C., Lee, M. R., Van Binh, N. & Kim, J. CYTOKININ RESPONSE FACTOR2(CRF2) and CRF3 regulate lateral root development in response to cold stress in *Arabidopsis*. *Plant Cell Online* **28**, 1828–1843 (2016).
22. Skylar, A., Hong, F., Chory, J., Weigel, D. & Wu, X. STIMPY mediates cytokinin signaling during shoot meristem establishment in *Arabidopsis* seedlings. *Development* **137**, 541–549 (2010).
23. Raines, T. et al. The cytokinin response factors modulate root and shoot growth and promote leaf senescence in *Arabidopsis*. *Plant J.* **85**, 134–147 (2015).
24. Šimášková, M. et al. Cytokinin response factors regulate PIN-FORMED auxin transporters. *Nat. Commun.* **6**, 8717 (2015).
25. Brady, S. M. et al. A high-resolution root spatiotemporal map reveals dominant expression patterns. *Science* **318**, 801–806 (2007).
26. Duncan, S. et al. Seasonal shift in timing of vernalization as an adaptation to extreme winter. *Elife* **4**, 11632 (2015).
27. Martz, F., Vuosku, J., Ovaskainen, A., Stark, S. & Rautio, P. The snow must go on: ground ice encasement, snow compaction and absence of snow differently cause soil hypoxia, CO_2 accumulation and tree seedling damage in boreal forest. *PLoS One* **11**, e0156620–18 (2016).
28. Shukla, V. et al. Endogenous hypoxia in lateral root primordia controls root architecture by antagonizing auxin signaling in *Arabidopsis*. *Mol. Plant* 1–55, (2019). https://doi.org/10.1016/j.molp.2019.01.007.
29. Eysholdt-Derzsó, E. & Sauter, M. Root bending is antagonistically affected by hypoxia and ERF-mediated transcription via auxin signaling. *Plant Physiol.* **175**, 412–423 (2017).
30. Samalova, M., Fricker, M. & Moore, I. Ratiometric fluorescence-imaging assays of plant membrane traffic using polyproteins. *Traffic* **7**, 1701–1723 (2006).
31. Marhavý, P. et al. Cytokinin modulates endocytic trafficking of PIN1 auxin efflux carrier to control plant organogenesis. *Dev. Cell* **21**, 796–804 (2011).
32. Liu, J. & Müller, B. Imaging TCSn::GFP, a synthetic cytokinin reporter, in *Arabidopsis thaliana*. *Methods Mol. Biol.* **1497**, 81–90 (2017).
33. Ruzicka, K. et al. Ethylene regulates root growth through effects on auxin biosynthesis and transport-dependent auxin distribution. *Plant Cell Online* **19**, 2197–2212 (2007).
34. Street, I. H. et al. Ethylene inhibits cell proliferation of the *Arabidopsis* root meristem. *Plant P*hysiology **169**, 338–350 (2015).
35. Romanov, G. A., Lomin, S. N. & Schmülling, T. Cytokinin signaling: from the ER or from the PM? That is the question! *New Phytol.* **218**, 41–53 (2018).
36. Ding, Z. & De Smet, I. Localised ABA signalling mediates root growth plasticity. *Trends Plant Sci.* **18**, 533–535 (2013).
37. Pernisova, M. et al. Cytokinins influence root gravitropism via differential regulation of auxin transporter expression and localization in *Arabidopsis*. *New Phytol.* **212**, 497–509 (2016).
38. Kang, J., Lee, Y., Sakakibara, H. & Martinoia, E. Cytokinin transporters: GO and STOP in signaling. *Trends Plant Sci.* **22**, 455–461 (2017).
39. Riefler, M. Arabidopsis cytokinin receptor mutants reveal functions in shoot growth, leaf senescence, seed size, germination, root development, and cytokinin metabolism. *Plant Cell Online* **18**, 40–54 (2006).
40. Inoue, T. et al. Identification of CRE1 as a cytokinin receptor from *Arabidopsis*. *Nature* **409**, 1060–1063 (2001).
41. To, J. P. C. Type-A *Arabidopsis* response regulators are partially redundant negative regulators of cytokinin signaling. *Plant Cell Online* **16**, 658–671 (2004).
42. Boudolf, V. The plant-specific cyclin-dependent kinase CDKB1;1 and transcription factor E2Fa-DPa control the balance of mitotically dividing and endoreduplicating cells in *Arabidopsis*. *Plant Cell Online* **16**, 2683–2692 (2004).
43. Xie, Z. et al. Regulation of cell proliferation in the stomatal lineage by the *Arabidopsis* MYB FOUR LIPS via direct targeting of core cell cycle genes. *Plant Cell Online* **22**, 2306–2321 (2010).
44. Werner, T. Cytokinin-deficient transgenic *Arabidopsis* plants show multiple developmental alterations indicating opposite functions of cytokinins in the regulation of shoot and root meristem activity. *Plant Cell* **15**, 2532–2550 (2003).
45. Bartrina, I., Otto, E., Strnad, M., Werner, T. & Schmülling, T. Cytokinin regulates the activity of reproductive meristems, flower organ size, ovule formation, and thus seed yield in *Arabidopsis thaliana*. *Plant Cell* **23**, 69–80 (2011).
46. Jeon, J. et al. A subset of cytokinin two-component signaling system plays a role in cold temperature stress response in *Arabidopsis*. *J. Biol. Chem.* **285**, 23371–23386 (2010).
47. Ferreira, P. C. et al. Developmental expression of the arabidopsis cyclin gene cyc1At. *Plant Cell Online* **6**, 1763–1774 (1994).
48. Zadnikova, P. et al. Role of PIN-mediated auxin efflux in apical hook development of *Arabidopsis thaliana*. *Development* **137**, 607–617 (2010).
49. Pernisova, M. et al. Cytokinin signalling regulates organ identity via the AHK4 receptor in *Arabidopsis*. *Development* **145**, dev163907–48 (2018).
50. Clough, S. J. & Bent, A. F. Floral dip: a simplified method for Agrobacterium-mediated transformation of *Arabidopsis thaliana*. *Plant J.* **16**, 735–743 (1998).
51. Frébort, I. et al. Cytokinin oxidase/cytokinin dehydrogenase assay: optimized procedures and applications. *Anal. Biochem.* **306**, 1–7 (2002).

52. Crone, D., Rueda, J., Martin, K. L., Hamilton, D. A. & Mascarenhas, J. P. The differential expression of a heat shock promoter in floral and reproductive tissues. *Plant Cell Environ.* **24**, 869–874 (2001).
53. Béziat, C., Kleine-Vehn, J. & Feraru, E. Histochemical staining of β-glucuronidase and its spatial quantification. *Methods Mol. Biol.* **1497**, 73–80 (2017).
54. Hofmann, F., Schon, M. A. & Nodine, M. D. The embryonic transcriptome of *Arabidopsis thaliana*. *Plant Reprod.* 1–15, (2019). https://doi.org/10.1007/s00497-018-00357-2.
55. Svačinová, J. et al. A new approach for cytokinin isolation from *Arabidopsis* tissues using miniaturized purification: pipette tip solid-phase extraction. *Plant Methods* **8**, 17 (2012).
56. Antoniadi, I. et al. Cell-type-specific cytokinin distribution within the *Arabidopsis* primary root apex. *Plant Cell* **27**, 1955–1967 (2015).
57. Hoyerová, K. et al. Efficiency of different methods of extraction and purification of cytokinins. *Phytochemistry* **67**, 1151–1159 (2006).
58. Schöller, M., Sarkel, E., Kleine-Vehn, J. & Feraru, E. Growth rate normalization method to assess gravitropic root growth. *Methods Mol. Biol.* **1761**, 199–208 (2018).
59. South, A. rworldmap: a new R package for mapping global data. *R J.* **3**, 35–43 (2011).
60. Žádníková, P. et al. A model of differential growth-guided apical hook formation in plants. *Plant Cell Online* **28**, 2464–2477 (2016).
61. Smith, R. S. et al. A plausible model of phyllotaxis. *Proc. Natl Acad. Sci. USA* **103**, 1301–1306 (2006).
62. Smith, C., Prusinkiewicz, P. & Samavati, F. in *Applications of Graph Transformations with Industrial Relevance*.Editors: John L. Pfaltz, Manfred Nagl and Boris Böhlen, Vol. 3062, 313–327 (Springer, Berlin, Heidelberg, 2003).
63. Karwowski, R. and Przemyslaw, P. The L-system-based plant-modeling environment L-studio 4.0. In *Proc. 4th International Workshop on Functional–Structural Plant Models*. Abstracts of papers and posters, 7-11 June 2004, Montpellier, France. Editors: Christophe Godin, Jim Hanan, Winfried Kurth, André Lacointe, Akio Takenaka, Przemyslaw Prusinkiewicz, Thedore M. Dejong, Christine Beveridge. CIRAD-AMIS-UMR AMAP. Montpellier: CIRAD-AMAP, 403–406.

Acknowledgements

We are grateful to Bruno Müller, Thomas Schmülling, Magnus Nordborg, Wolfgang Busch, Ben Scheres, Jiri Friml, Dirk Inze, Jungmook Kim, Tomas Werner, Marketa Pernisova, Eva Benkova, Joseph Kieber, and Lieven De Veylder for sharing published material; Marget Sauter, Ilka Reichardt-Gomez, Ümit Seren and Envel Kerdaffrec for helpful discussions; Jit Thacker for help with preparing the manuscript; Hana Martínková for help with phytohormone analyses; and the BOKU-VIBT Imaging Centre for access and expertize. This work was supported by the Austrian Academy of Sciences (ÖAW) (DOC fellowship to K.D.), Fulbright-Austria Marshall Plan student grant (to E.S.), Vienna Research Group (VRG) program of the Vienna Science and Technology Fund (WWTF) (to J.K-V.), the Austrian Science Fund (FWF) (P29754) (to J.K-V.), the European Research Council (ERC) (Starting Grant 639478-AuxinER) (to J.K-V.), Deutsche Forschungsgesellschaft fellowship (LI 2776/1-1) (to H.L.); and work was funded by the Ministry of Education, Youth and Sports of the Czech Republic (National Program for Sustainability I, grant no. LO1204) (to O.N.), and Programa de Atracción de Talento 2017 (Comunidad de Madrid, 2017-T1/BIO-5654 to K.W.).

Author contributions

S.W. performed most experiments. M.R.R. initiated the project. M.S., E.S. and K.D. performed confocal microscopy. H.L., T.L.R. and J.R.D. contributed GLO-Roots data. I.P. and O.N. conducted quantification of endogenous cytokinins. S.M. and R.S. performed hypoxia experiments K.W. designed and described the dynamic computer model simulation. J.K.-V. devised and coordinated the project. S.W. and J.K.-V. wrote the manuscript. All authors saw and commented on the manuscript.

Additional information

Supplementary Information accompanies this paper at https://doi.org/10.1038/s41467-019-11483-4.

Competing interests: The authors declare no competing interests.

Reprints and permission information is available online at http://npg.nature.com/reprintsandpermissions/

Peer review information: *Nature Communications* thanks Jie Le, Kirsten H.W.J. ten Tusscher, Yusaku Uga and other anonymous reviewer(s) for their contribution to the peer review of this work. Peer reviewer reports are available.

Publisher's note: Springer Nature remains neutral with regard to jurisdictional claims in published maps and institutional affiliations.

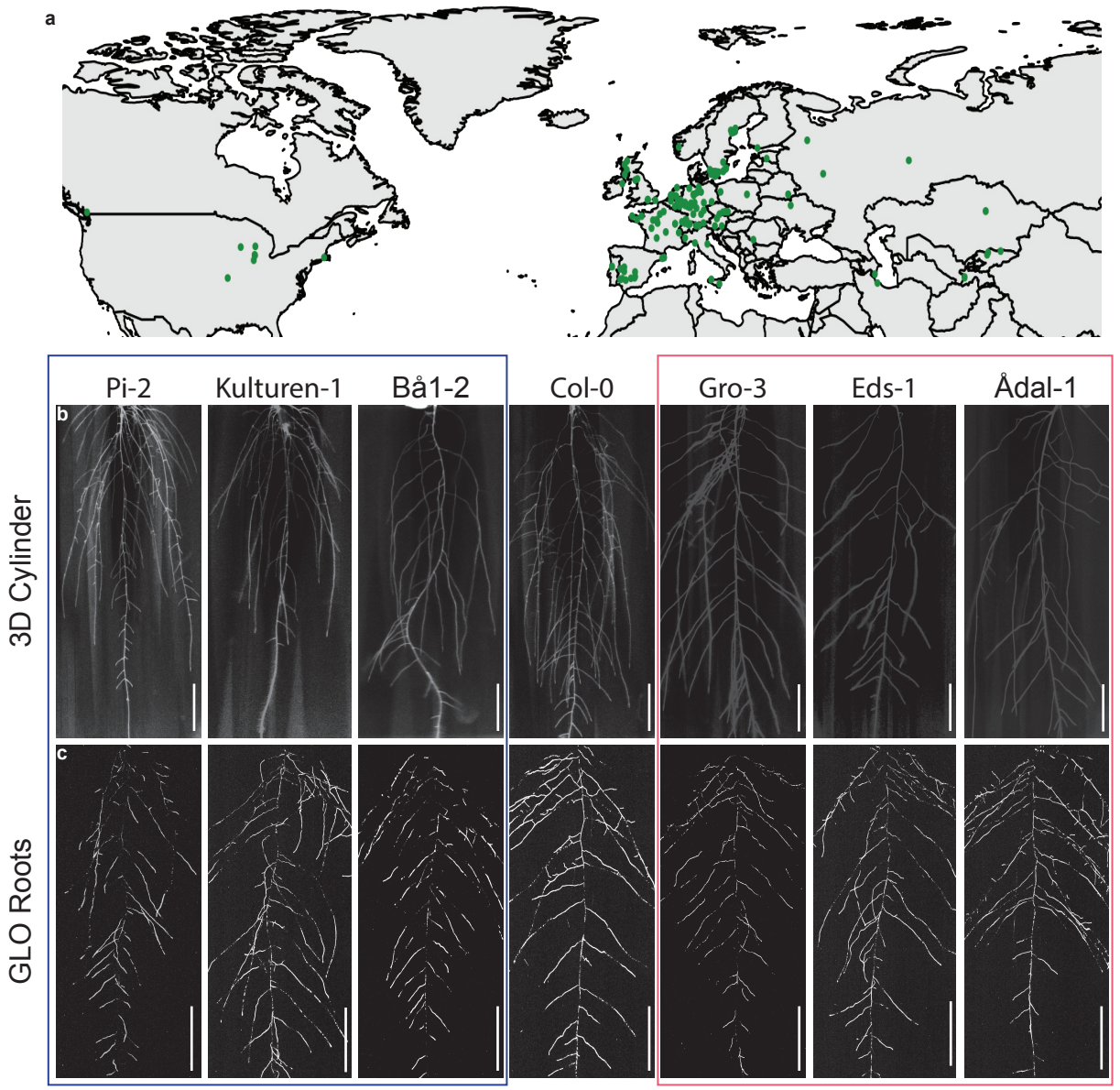

Supplementary Fig. 1. Accessions used in this study and representative root system images of selected accessions.
(a) Geographical distribution of natural Arabidopsis thaliana accessions used in this study. The distribution of accessions is visualized by R package “rworldmap”.
(b) 10-day old accessions grown in 3D agar cylinders. Scale bars, 1 cm.
(c) 20-day old accessions grown in soil. Scale bars, 5 cm.
(b)-(c) Representative images are shown. Experiments were repeated at least three times.

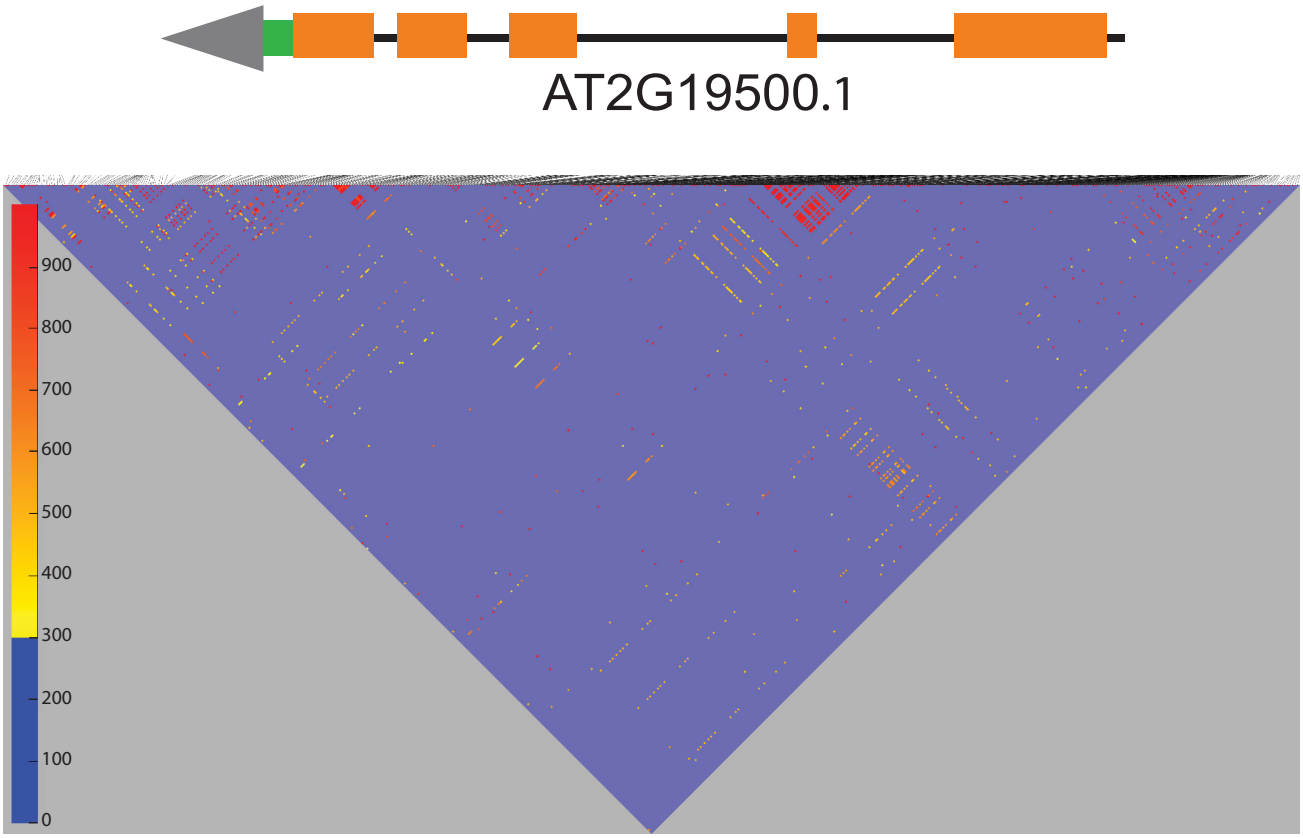

Supplementary Fig. 2. Calculation of linkage disequilibrium by pairwise comparison of 500 SNPs.
r2 value is scaled and color-coded (blue to red) from 0 to 1 (low to high association). Underlying code can be found at github https://github.com/timeu/PyGWAS/blob/master/pygwas/core/genotype.py#L59).

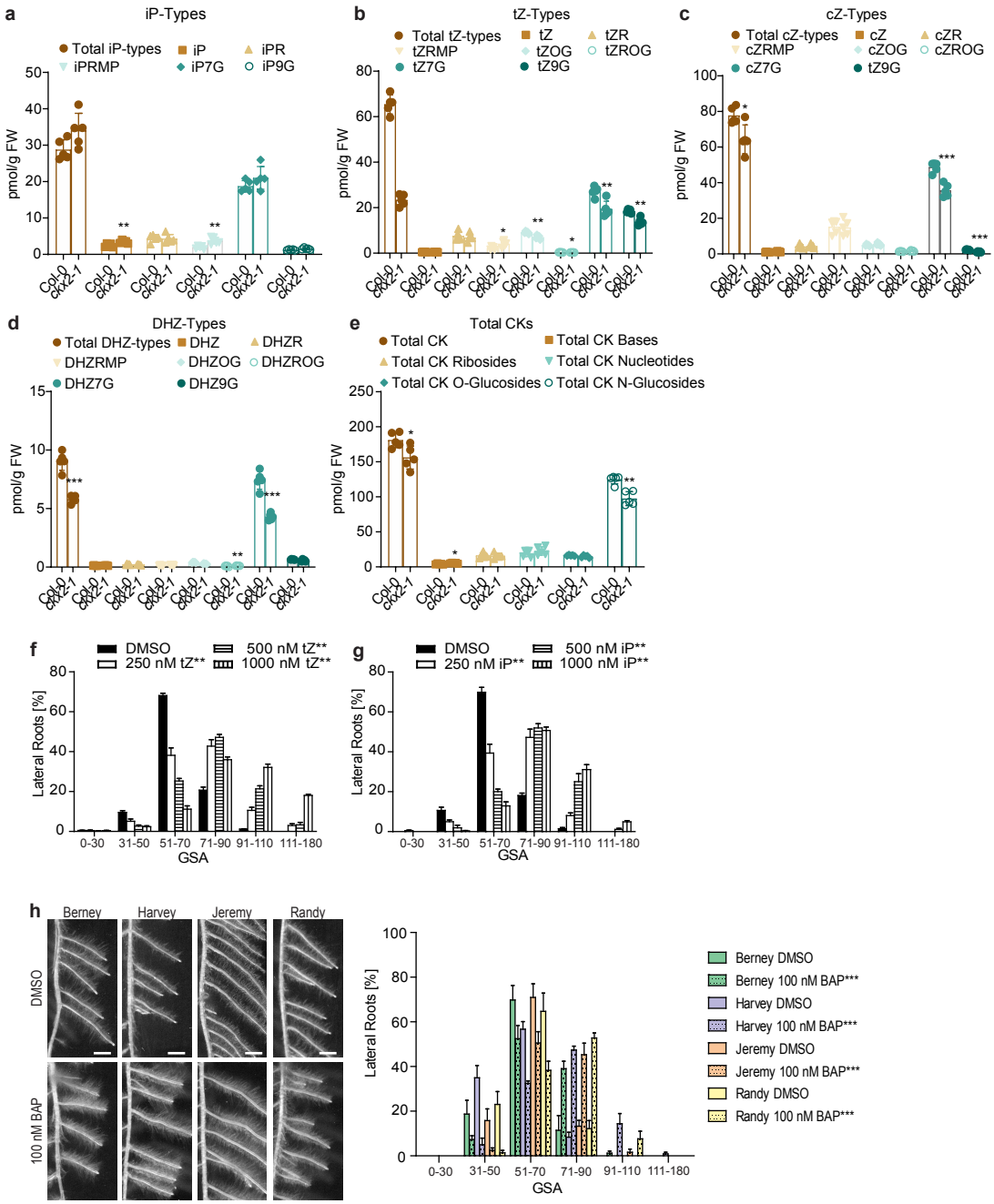

Supplementary Fig. 3. Influence of cytokinin on GSA of lateral roots.

(a)-(e) Quantification of different CK forms (nucleotides (precursors), ribosides (transported forms), free bases (active forms), and O-/N-glucosides (reversible/irreversible inactivated storage forms) in *Col-0* wild type and *ckx2-1* mutant roots. (a) iP-Types, (b) tZ-Types, (c) cZ-Types, (d) DHZ-Types, (e) Total CKs.

(f)-(g), GSA distributions of DMSO and (f) trans-zeatin (tZ)-treated or (g) isopentenyladenine (iP)-treated *Col-0* wild type seedlings.

(h) Representative images and GSA distributions of four different untreated and BA-treated winter oilseed rape (*Brasica napus* L.) genotypes.

(a)-(e) One-way ANOVA analysis P-values: * P < 0.05, ** P < 0.01, *** P < 0.001. Mean ± SD, n = 5 extractions.

(f)-(h) Kolmogorov-Smirnov test P-values: * P < 0.05, ** P < 0.01, *** P > 0.001 (compared to DMSO or *Col-0*, respectively). Mean ± SEM, for *A. thaliana*: n = 5 plates (16 seedlings with 80-160 LRs per plate), for oilseed rape: n = 3 seedlings with 25-50 LRs per seedling). Experiments were repeated at least three times.

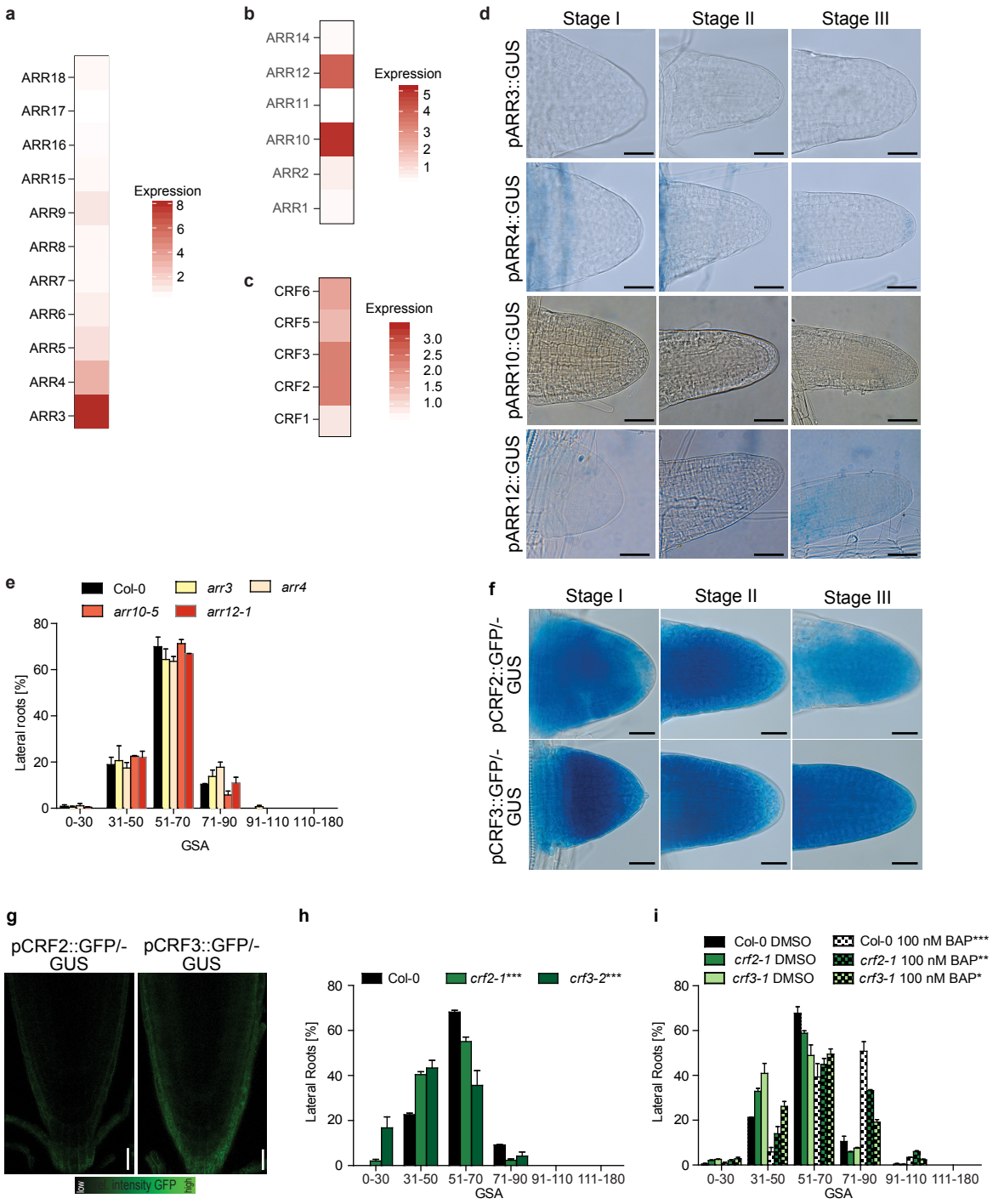
a
ARR18
ARR17
ARR16
ARR15
ARR9
ARR8
ARR7
ARR6
ARR5
ARR4
ARR3
Expression
8
6
4
2
b
ARR14
ARR12
ARR11
ARR10
ARR2
ARR1
Expression
5
4
3
2
1
c
CRF6
CRF5
CRF3
CRF2
CRF1
Expression
3.0
2.5
2.0
1.5
1.0
d
Stage I
Stage II
Stage III
pARR3::GUS
pARR4::GUS
pARR10::GUS
pARR12::GUS
e
Col-0
arr3
arr4
arr10-5
arr12-1
Lateral roots [%]
80
60
40
20
0
0-30
31-50
51-70
71-90
91-110
110-180
GSA
f
Stage I
Stage II
Stage III
pCRF2::GFP/-GUS
pCRF3::GFP/-GUS
g
pCRF2::GFP/-GUS
pCRF3::GFP/-GUS
low
Intensity GFP
high
h
Col-0
crf2-1***
crf3-2***
Lateral Roots [%]
80
60
40
20
0
0-30
31-50
51-70
71-90
91-110
111-180
GSA
i
Col-0 DMSO
crf2-1 DMSO
crf3-1 DMSO
Col-0 100 nM BAP***
crf2-1 100 nM BAP**
crf3-1 100 nM BAP*
Lateral Roots [%]
80
60
40
20
0
0-30
31-50
51-70
71-90
91-110
111-180
GSA

Supplementary Fig. 4. Role of Arabidopsis response regulators (ARRs) and cytokinin response factors (CRFs) in the GSA establishment in LRs.
(a) Expression of type-A ARRs in lateral roots. Data from[25].
(b) Expression of type-B ARRs in lateral roots. Data from[25].
(c) Expression of CRFs in lateral roots. Data from[25].
(d) GUS staining of pARR3::GUS, pARR4::GUS, pARR10::GUS and pARR12::GUS. Scale bars, 25 μm.
(e) GSA distribution of *Col-0* wild-type, *arr3*, *arr4*, *arr10-5* and *arr12-1* mutants. Kolmogorov-Smirnov test. Mean ± SEM, n = 5 plates (16 seedlings with 25-120 LRs per plate).
(f) Representative images after GUS staining of pCRF2::GFP-GUS and pCRF3::GFP-GUS in stage I-III LRs. Scale bars, 10 μm.
(g) Representative images of pCRF2::GFP-GUS and pCRF3::GFP-GUS in the main root tip. Scale bars, 25 μm.
(h) GSA distribution of *Col-0* wild type and crf single mutants.
(i) GSA distribution of DMSO and BAP treated *Col-0* wild type, *crf2-1* and *crf3-1* single mutants.
(h) – (i) Kolmogorov-Smirnov test P-values: * $P < 0.05$, ** $P < 0.01$, *** $P > 0.001$ (compared to DMSO or *Col-0*). Mean ± SEM, n = 5 plates (16 seedlings with 20-180 LRs per plate).
(d)-(i) Experiments were repeated three times.

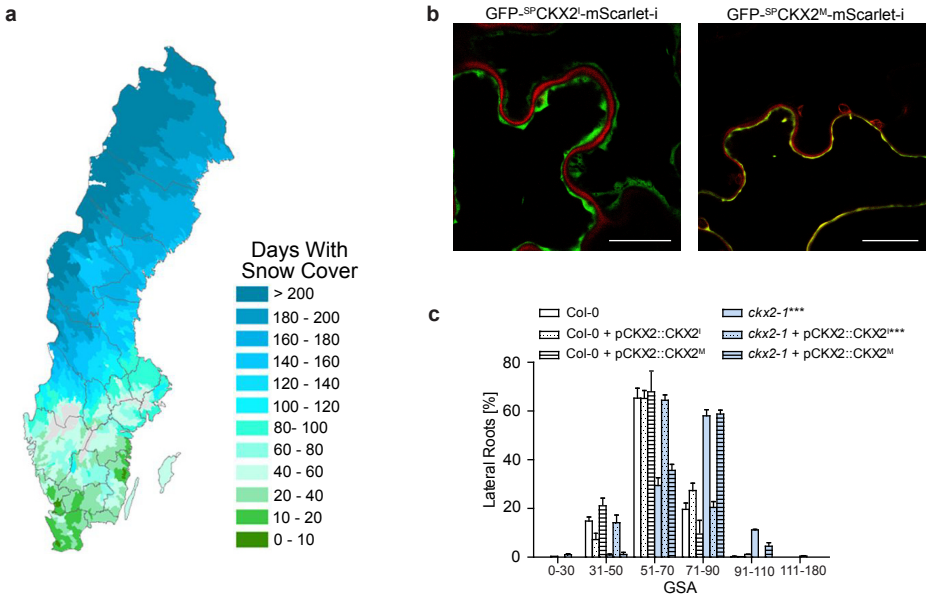

Supplementary Figure 5. Snow cover in Sweden and characterization of CKX2^{I} and CKX2^{M}.

Supplementary Fig. 5. Snow cover in Sweden and characterization of CKX2I and CKX2M.

(a) Average number of days with snow cover in Sweden between 1961-1990. Source: https://bit.ly/2UmLAeT

(b) Localization of GFP-^{SP}CKX2^{I}-mScarlet and GFP-^{SP}CKX2^{M}-mScarlet. Tobacco leaves were infiltrated with Agrobacterium tumefaciens containing constructs and the expression of CKX2 fluorescent protein was visualized by confocal laser scanning microscopy three days after infiltration. Scale bar, 25 μm. Representative images are shown.

(c) GSA distributions of *Col-0* and *ckx2-1* as well as CKX2^{I} and CKX2^{M} expressing lines in both backgrounds. Kolmogorov-Smirnov test P-value: *** P < 0.001 (compared to Col-0). Mean ± SEM, n = 5 plates (16 seedlings with 80-160 LRs per plate).

(b)-(c) Experiments were repeated at least three times.

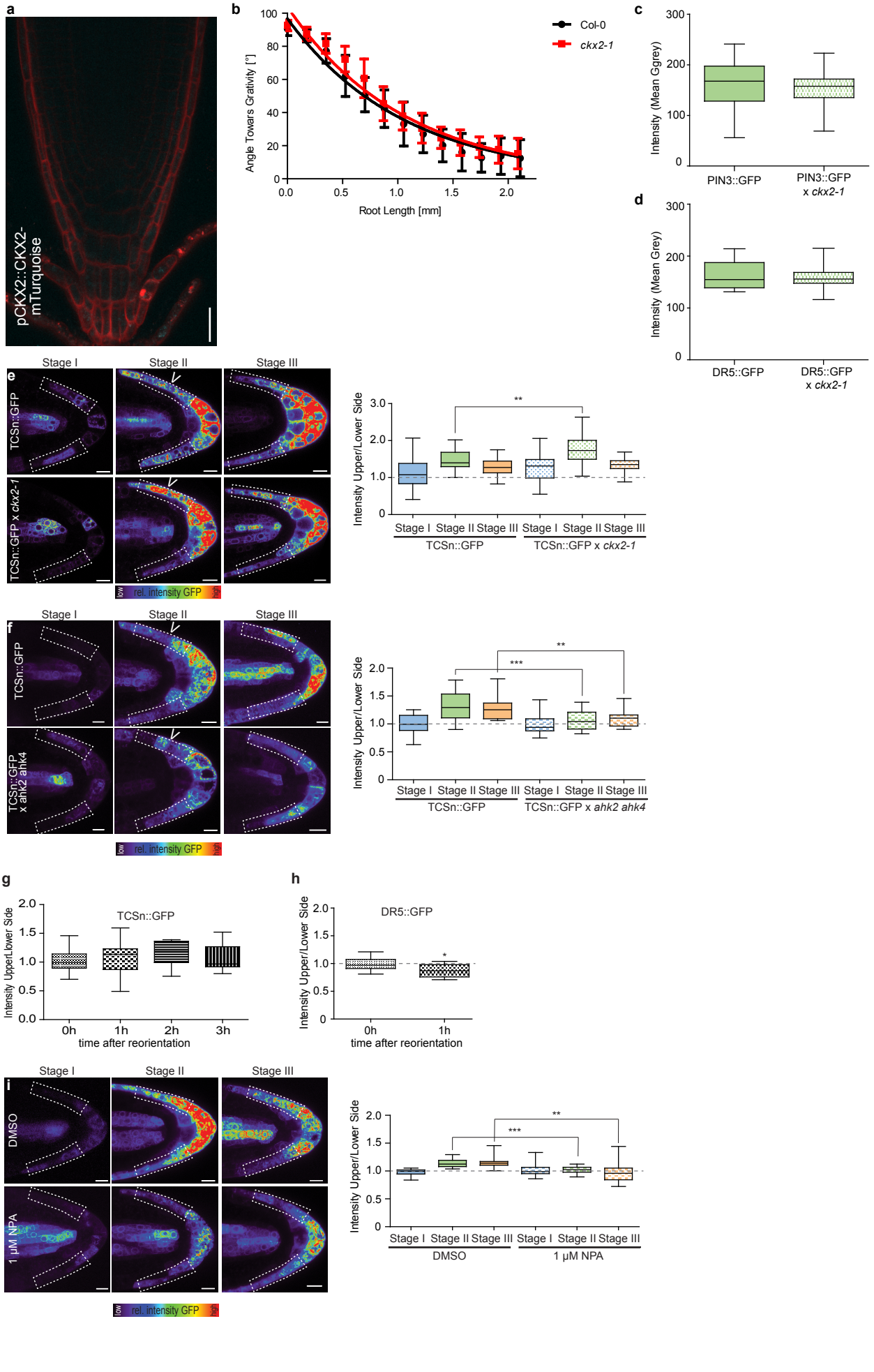
a
pCKX2::CKX2-mTurquoise
b
Col-0
ckx2-1
Angle Towars Gravitity [°]
Root Length [mm]
c
Intensity (Mean Ggrey)
PIN3::GFP
PIN3::GFP x ckx2-1
d
Intensity (Mean Grey)
DR5::GFP
DR5::GFP x ckx2-1
e
Stage I
Stage II
Stage III
TCSn::GFP
TCSn::GFP x ckx2-1
low
rel. intensity GFP
high
Intensity Upper/Lower Side
TCSn::GFP
TCSn::GFP x ckx2-1
f
TCSn::GFP x ahk2 ahk4
TCSn::GFP x ahk2 ahk4
g
TCSn::GFP
Intensity Upper/Lower Side
time after reorientation
h
DR5::GFP
Intensity Upper/Lower Side
time after reorientation
i
DMSO
1 µM NPA
Intensity Upper/Lower Side

Supplementary Fig. 6. Localization of CKX2 in the main root tip and characterization of cytokinin responses in *ckx2-1* mutants.
(a) Representative images of pCKX2::CKX2-mTurquoise in the main root. Propidium Iodide (PI) was used for counterstaining. Scale bar, 25 µm.
(b) Gravitropic response of dark grown *Col-0* and *ckx2-1*. Mean ± SD, n = 10-15 individual roots.
(c)-(d) Signal quantification of (b) pPIN3::PIN3-GFP and (c) DR5::GFP in stage II LRs.
(e)-(f) Representative images and quantifications of (a) TCSn::GFP in *Col-0* wild type and *ckx2-1*, (b) TCSn::GFP in *Col-0* wild type and *ahk2 ahk4* in stage I – III LRs. Scale bar, 10 µm.
(g) Signal quantification of TCSn::GFP in the main root after gravity stimulation.
(h) Signal quantification of DR5::GFP in the main root after gravity stimulation (positive control for (g).
(i) Representative images and quantifications of TCSn::GFP in *Col-0* wild type after treatment with DMSO or 1 µM NPA for 24h in stage I – III LRs. Scale bar, 10 µm.
(c)-(d), (e)-(i) One-way ANOVA P-values: * $P < 0.05$, ** $P < 0.01$, *** $P < 0.001$. Horizontal lines show the medians; box limits indicate the 25th and 75th percentiles; whiskers extend to the min and max values. n = 10-40 individual LRs or main roots.
(a)-(i)Experiments were repeated at least three times.

a
63°
70°
76°
Size of Elongation Zone
c
63°
70°
78°
Number of Elongating Cells (Only Upper Flank)
e
63°
70°
75°
'WT'-like
10% Reduced Elongation Rate
10% Reduced Elongation Rate Less Elongationg Cells (Upper Flank)
b
d
f
Angle [°]
Time [h]
Cell Area [µm²]
Upper Flank
Lower Flank
Angle [°]

Supplementary Figure 7. Simulations of dynamic computer model of lateral root predict an inverse relation between set-point angle and the number of cells in elongation zone or the size of elongation zone.

(a)-(b) A positive impact of the size of elongation zone on the GSA angle. The longer the elongation zone (white arrow heads) the larger the GSA angle is.

(c)-(d) The number of cells on the upper flank has strong negative effect on the GSA angle. Also, model predicts that the fold difference between the size of elongating cell on the upper versus lower LR root flanks may decreases with strongly reduced number of cells, largely due to mechanical constrains present on the upper root flank.

(e)-(f) Upper panel, corresponds Fig. 7b. Middle panel, 10% decrease in elongation rate only on the upper root flank (white arrow heads). Lower panel, combination of 10% decrease in elongation rate and number of cells (shorter meristem) only on the upper root flank. Each simulation represents LR status after 9h of dynamic elongation.

(b), (d, (f) Upper panel: Time evolution of set-point angle corresponding to respective scenarios. Lower panel: Predicted GSA angle plotted against the predicted cell size.

Colours at the left side (a), (c), (e) matches simulations in (b), (d), (f). Simulations represent LR status after 8h of dynamic elongation. Other symbols are as in Figure 7.

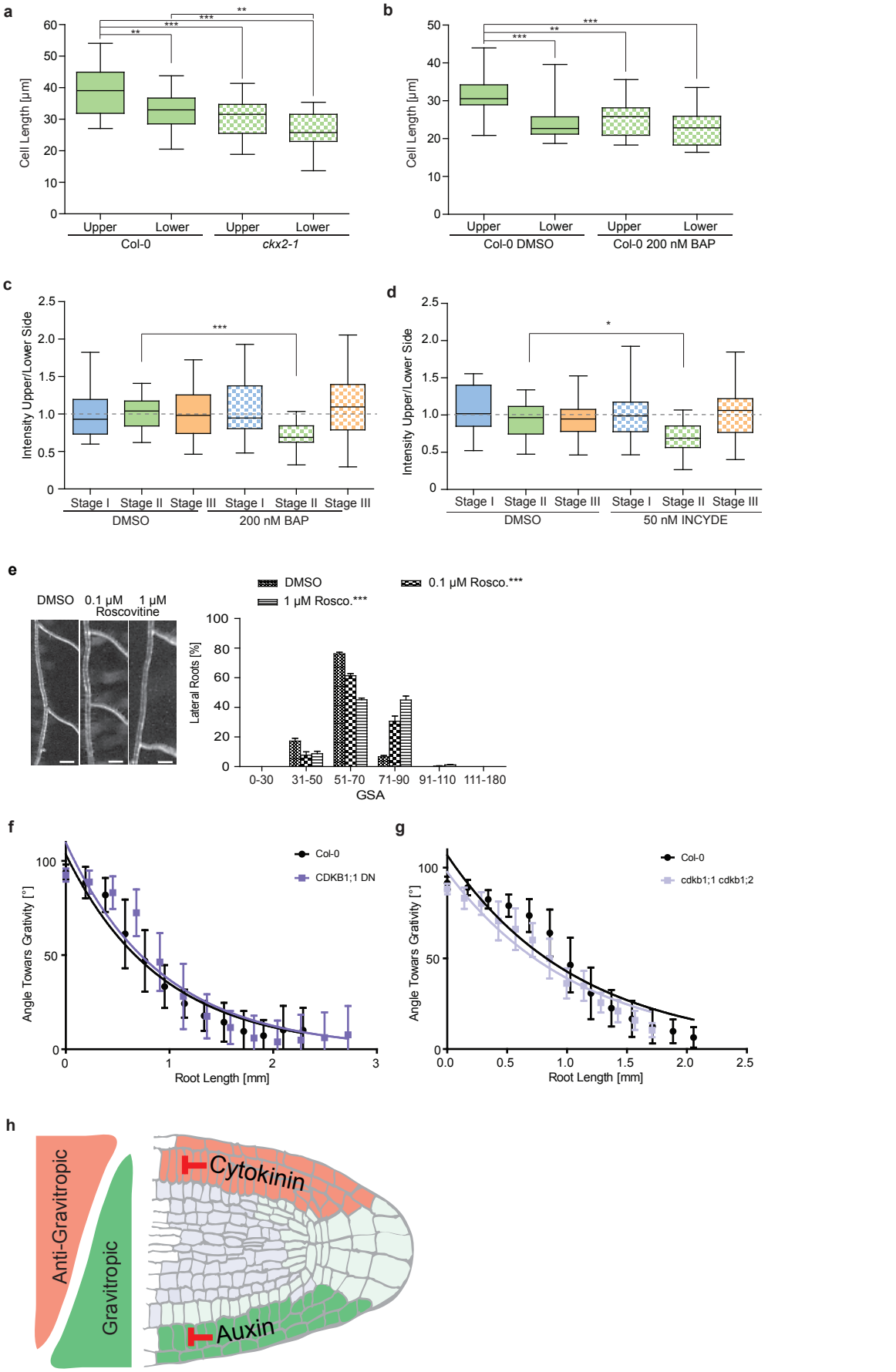
a
Cell Length [µm]
Upper
Lower
Upper
Lower
Col-0
ckx2-1
b
Cell Length [µm]
Upper
Lower
Upper
Lower
Col-0 DMSO
Col-0 200 nM BAP
c
Intensity Upper/Lower Side
Stage I
Stage II
Stage III
Stage I
Stage II
Stage III
DMSO
200 nM BAP
d
Intensity Upper/Lower Side
Stage I
Stage II
Stage III
Stage I
Stage II
Stage III
DMSO
50 nM INCYDE
e
DMSO
0.1 µM Roscovitine
1 µM
DMSO
0.1 µM Rosco.***
1 µM Rosco.***
Lateral Roots [%]
0-30
31-50
51-70
71-90
91-110
111-180
GSA
f
Angle Towars Gravity [°]
Col-0
CDKB1;1 DN
Root Length [mm]
g
Angle Towars Gravity [°]
Col-0
cdkb1;1 cdkb1;2
Root Length [mm]
h
Anti-Gravitropic
Gravitropic
Cytokinin
Auxin

Supplementary Figure 8. Cytokinin-dependent interference with cell elongation and division rates defines angular growth of lateral roots.

(a)-(b) Quantification of first two elongated cells in the upper and lower flank of stage II lateral roots of (a) *Col-0* and *ckx2-1* and (b) after treatment with DMSO or 200 nM BAP for 24h.

(c)-(d) Quantification of pCycB1;1::GUS after treatment with (c) DMSO or 200 nM BAP or (d) DMSO or 50 nM INCYDE for 24h.

(a)-(d) One-way ANOVA P-values: * $P < 0.05$, *** $P < 0.001$. Horizontal lines show the medians; box limits indicate the 25th and 75th percentiles; whiskers extend to the min and max values. (a)-(b) n = 10-15 individual LRs, (c)-(d) n= 15-40 individual LRs.

(e) Representative images and GSA distributions of Roscovitine treated Col-0 wild-type seedlings. Kolmogorov-Smirnov test P-values: *** $P < 0.001$ (compared to DMSO solvent control). Mean ± SEM, n = 5 plates (16 seedlings with 90-130 LRs per plate). Scale bars, 2 mm.

(f)-(g) Gravitropic growth rates to quantitatively asses gravitropic response of dark grown (f) *Col-0* and *CDKB1;1 DN* as well as (g) *Col-0* and *cdkb1;1 ckdb1;2*. Mean ± SD, n = 10-15 individual roots.

(a)-(g) Experiments were repeated at least three times.

(h) Schematic model depicts spatially defined gravitropic and anti-gravitropic hormonal cues at opposing organ flanks. Cytokinin signalling functions as an anti-gravitropic growth regulator at the upper side and thereby counterbalances auxin-dependent gravitropic growth of lateral roots.

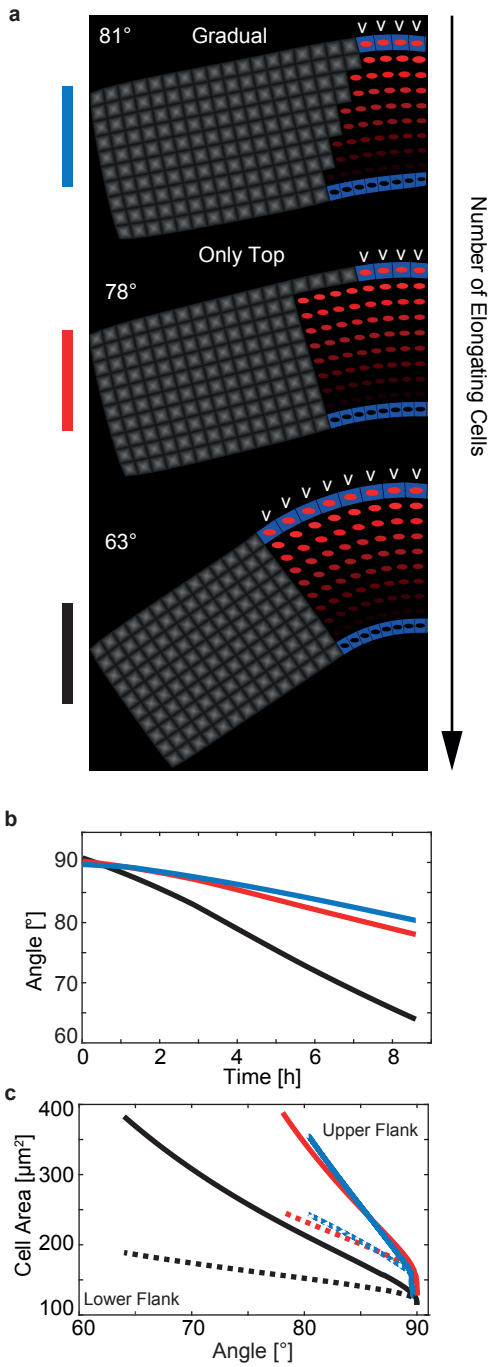

Supplementary Figure 9. Simulations of dynamic computer model addressing the gradual decrease of cell numbers along a lateral root organ.

(a) Simulated reduction of elongating cells, which are either restricted to the upper part (red) or gradually extent from the bottom towards the top (blue), induce reduced curvature compared to the control scenario (black).

(b) Time evolution of set-point angle corresponding to respective scenarios.

(c) Predicted GSA angle plotted against the predicted cell size. Dashed and filled lines depict lower and upper root flank, respectively. Colours in (b) and (c) correspond to (a). Simulations represent LR status after 8h of dynamic elongation.

PALACKÝ UNIVERSITY IN OLOMOUC
FACULTY OF SCIENCE
Laboratory of Growth Regulators

Ivan Petřík

Determination of the bioactive compounds using modern LC-MS methods

P1527 Biology
1501V019 Experimental Biology

Summary of the Ph.D. thesis

Supervisor: Prof. Mgr. Ondřej Novák, Ph.D.
Consultant: Prof. Karin Ljung, Ph.D.

Olomouc
2024

This Ph.D. thesis was realised in the Laboratory of Growth Regulators within the framework of internal Ph.D. study of Experimental Biology, guaranteed by the Laboratory of Growth Regulators, Faculty of Science, Palacký University in Olomouc, in the period 2017-2024.

Ph.D. candidate: **Mgr. Ivan Petřík**

Supervisor: **prof. Mgr. Ondřej Novák, Ph.D.**
Laboratory of Growth Regulators, Faculty of Science, Palacký University & Institute of Experimental Botany of the Czech Academy of Sciences, Olomouc, Czech Republic

Consultant: **Prof. Karin Ljung, Ph.D.**
Department of Forest Genetics and Plant Physiology, Umeå Plant, Science Centre (UPSC), Swedish University of Agricultural Sciences, Umeå SE-901 83, Sweden

Opponents: **doc. RNDr. Radomíra Vaňková, Ph.D.**
Laboratory of Hormonal Regulations in Plants, Institute of Experimental Botany of the Czech Academy of Sciences, Prague, Czech Republic

prof. PharmDr. Lucie Nováková, Ph.D.
Department of Analytical Chemistry, Faculty of Pharmacy, Charles University, Hradec Králové, Czech Republic

The evaluation of this Ph.D. thesis was written by **prof. Ing. Miroslav Strnad, CSc. DSc.**, Laboratory of Growth Regulators, Faculty of Science, Palacký University & Institute of Experimental Botany of the Czech Academy of Sciences in Olomouc.

The oral defence will take place on 20. 6. 2024 in the front of Commission for the Ph.D. thesis of the Study Program Experimental Biology, **Seminary Room, Building No. 52**, Šlechtitelů 241/27, 779 00 Olomouc – Holice.

The Ph.D. thesis and expert reviews will be available 14 days before the defence in the Study Department of Faculty of Science (Mgr. Martina Karásková), Palacký University, 17. listopadu 1192/12, Olomouc.

After the defence, the Ph.D. thesis will be stored in the Library of the Biological Departments of Faculty of Science, Palacký University, Šlechtitelů 241/27, 779 00 Olomouc – Holice.

prof. Ing. Miroslav Strnad, CSc. DSc.
Chairman of the Commission for the Ph.D. thesis,
Study Program Experimental Biology,
Faculty of Science, Palacký University in Olomouc

Content

1 Introduction

It has been nearly a century since the elucidation of evidence for plant growth regulation. Auxin, one of the most extensively studied phytohormones to date, was identified as the first substance responsible for proliferation in meristematic tissues in grain crops (Went, 1926). Subsequent and continuous research efforts have led to the discovery of numerous signalling molecules with diverse chemical structures, natural occurrences, and biological activities. Despite their chemical and functional variability, three common features have been attributed to all of them: (i) low concentration in plant tissues, (ii) engagement in specific signalling pathways within cells, and (iii) a shared nomenclature - plant hormone or phytohormone.

The revolution in plant hormone research was catalysed by advances in technologies during the 20th century. First, the application of antibodies in immunoassays, such as radioimmunoassay or enzyme-linked immunosorbent assay, enabled the determination and quantification of naturally occurring plant hormones (Pengelly and Meins, 1976; Hofman et al., 1986; Geier et al., 1990). This breakthrough provided new insights into plant physiology in the 1970s and 1980s. Second, the development of liquid chromatography (LC) coupled with mass spectrometry (MS) systems toward the end of the millennium introduced new tools with improved separation performance and reduced detection limits. State-of-the-art ultra-high performance liquid chromatography (UHPLC) coupled with tandem mass spectrometry (MS/MS) systems with attomolar sensitivity and high scan speed, has facilitated the monitoring of multiple plant hormones at trace amounts (Tarkowská et al., 2014).

Over the past decade, various methods for determining plant hormones in plant tissues based on UHPLC-MS/MS have emerged. These methods span a spectrum from deeply focused approaches targeting single or multiple compounds to targeted metabolomics of plant hormones. Most of these methods involve sample preparation procedures that aim to reduce sample complexity and simplify analysis. Modern analytical methods for plant hormones tend to emphasize miniaturization and high-throughput, utilizing minute amounts of plant samples to facilitate studies at the tissue, cellular or subcellular levels (Novák et al., 2017).

Plant hormonomics, in conjunction with reversed genetics and complementary omics approaches such as genomics, transcriptomics, proteomics or phenomics, has become an integral part of modern plant physiology research.

2 Aims and scopes

The aim of this doctoral thesis was to develop innovative methods for determining plant hormones, aligning with the current trend toward miniaturization and high-throughput. The thesis encompasses an exploration of the physiological roles, biosynthesis, metabolism and homeostasis of selected groups of plant hormones together with the methodologies employed for their determination in biological samples. This comprehensive approach promises valuable insights into plant hormone dynamics and their impact on plant physiology.

The main objectives of the doctoral thesis were outlined as follows:

1. Conduct an extensive literature review covering the physiology, biosynthesis and metabolism of cytokinins (CKs) and acidic phytohormones. Next, review methodologies utilizing UHPLC-MS/MS to quantify these hormones in plants.
2. Develop a pioneering method for preparing CK samples employing Parallel Artificial Liquid Membrane Extraction (PALME).
3. Innovate the isolation method of CKs, auxins, and abscisic acid (ABA) using miniaturized dispersive solid-phase extraction (SPE).
4. Introduce a ground-breaking analytical technique based on supercritical fluid chromatography (SFC) coupled with MS/MS.
5. Utilize advanced methodologies based on UHPLC-MS/MS to explore the roles of CKs, salicylic acid (SA), and jasmonates (JAs) in regulating plant growth, development and stress responses.

3 Material and methods

3.1 Chemicals

The plant hormone chemical standards and their stable isotope-labelled analogues were obtained from Olchemim Ltd. or Palacký University in Olomouc, Faculty of Science (both Olomouc, Czech Republic). Stable isotope-labelled standards of CK N^7- and N^9-glucosides were synthetized at the Department of Organic Chemistry, Faculty of Science, Palacký University in Olomouc (Czech Republic). The organic solvents methanol, acetonitrile and 2-propanol, all in LC-MS purity, were purchased from Merck (Darmstadt, Germany). Ammonia hydroxide solution 25% (v/v) and formic acid 99% (v/v), both for LC-MS, were obtained from Honeywell Fluka™ (Bucharest, Romania). Ultrapure deionized water was produced in-house using Millipore Direct-Q® 3 UV system (Millipore, Bedford, MA, USA).

3.2 Plant material

Arabidopsis thaliana (ecotype *Col-0*) seeds were planted on half Murashige & Skoog medium. The whole seedlings, grown under long-day conditions, were harvested 10 or 21 days after germination. Hybrid aspen clone T89 (*Populus tremula* × *tremuloides*) was obtained from the transformation facility at the Umeå Plant Science Centre (Umeå, Sweden). The leaves of 3-month-old treelings, cultivated under long-day conditions, were harvested 3 hours after dawn. *Triticum aestivum* (winter type, variety Turandot) was grown in the Laboratory of Growth Regulators in vermiculite irrigated with Hoagland's nutrient solution (Arnon and Hoagland, 1940), and 7-day-old leaves were harvested. The treelings of Norway spruce (*Pinea abies*) were obtained from the Umeå Plant Science Centre (Umeå, Sweden). Spruce cotyledons were harvested 14 days after sowing and growing under long-day conditions (Brunoni et al., 2020). The harvested samples of *Arabidopsis*, poplar, wheat and spruce were homogenized into fine powder using liquid nitrogen and stored in -70 °C for subsequent weighing of fresh weight (FW). The liverwort *Merchantia polymorpha* strain Tak1 were obtained from the Centre for Research in Agricultural Genomics (Barcelona, Spain). Gametophytes of this liverwort were harvested from 3-week-old individuals planted on half Gamborg's B5 media under long-day conditions. The cyanobacterium *Nostoc sp.* CCAP 1453/38 was obtained from the Institute of Microbiology, Czech Academy of Sciences (Třeboň, Czech Republic) and grown according to previously described protocol (Chmelík et al., 2019). The samples of *Merchantia* and *Nostoc* were lyophilized and used subsequently as a dry weight.

3.3 Instrumentation

UHPLC-MS/MS experiments were performed with an Acquity UPLC® I-Class (Waters, Milford, USA) coupled to a Xevo TQ-XS triple quadrupole equipped with an electrospray ionisation (ESI) source (Waters, Manchester, UK). All CK profiles were determined by the previously described methodology in Svačinová et al. (2012). Auxin analysis followed the method published in Pěnčík et al. (2018). Stress related compounds were analysed according to Floková et al. (2014). The full phytohormone profiles were obtained by plant hormonomics method (Šimura et al., 2018). All methods worked with reverse-phase chromatography acquiring data in multiple reaction monitoring mode. Data were processed using MassLynx v4.2 (Waters, Manchester, UK). Concentrations of the targeted compounds were calculated by the isotope dilution method (Rittenberg and Foster, 1940).

The SFC-MS/MS method was developed using an Agilent 1260 Infinity II LC/SFC hybrid system coupled with an Agilent 6495B Triple Quadrupole equipped with Jet Stream and Dual Ion Funnel systems. During the development, four different chromatographic columns were tested: Zorbax Eclipse Plus C18 3×50 mm, 1.8 μm (Agilent Technologies, Santa Clara, CA USA) (C18); Torus DIOL 3×100 mm, 1.7 μm (Waters, Milford, CT, USA) (DIOL); Zorbax RX-SIL 4.6×150 mm, 5.0 μm (Agilent Technologies, Santa Clara, CA USA) (RX-SIL); Torus 2-PIC 3×100 mm, 1.7 μm (Waters, Milford, CT, USA) (2-PIC).

3.4 Sample preparation

3.4.1 Extraction of CKs and acidic plant hormones

10 mg FW of homogenized plant material was weighed into 2 ml microtube and extracted with 1 ml 5% formic acid in 10% methanol (both v/v). Stable isotope-labelled IS were added to the sample as follows: 0.2 pmol for CK bases, CK ribosides and *N*-glucosides, 0.5 pmol for CK nucleotides and *O*-glucosides, 5 pmol for ABA, indole-3-acetic acid (IAA), 2-oxoindole-3-acetic acid (oxIAA), IAA amino acid conjugates and glucosyl esters. Three zirconium oxide 2.0 mm extraction beads (Next Advance, Troy, NY, USA) were added and the sample was crushed using a Retsch MM400 bead mill (Retsch, Haan, Germany) at 27 Hz for 5 min. The extract was sonicated for 3 min, incubated in a refrigerator for 30 min with mild shaking and then centrifuged for 15 min at 20,000 rpm and 4 °C (Allegra 64R benchtop centrifuge, Beckman Coulter, USA). The resulting supernatant was collected.

3.4.2 Purification of phytohormones with dispersive SPE on micro-spin filter (DisperSpin SPE)

Here, 100 mg of bulk Oasis® MCX sorbent 30 μm (Waters, Milford, CT, USA) was weighed into a 2 ml microtube. The sorbent was moistened with 1 ml methanol, vortexed and centrifuged at 10,000 rpm for 2 min (Allegra 64R benchtop centrifuge, Beckman Coulter, USA). The supernatant was removed by pipetting and exchanged for 1 ml of 1 mol/l formic acid in water. The suspension of bulk sorbent was mixed thoroughly and 20-300 μl (2-30 mg) of suspension was pipetted onto a MicroSpin centrifuge nylon filter with 0.2 μm pores (Chromservis Ltd., Czech Republic). The crude plant extracts were loaded onto the sorbent aliquot on the filter and centrifuged at 2000 rpm for 5 min. The filtrate was discarded, sorbent on the filter was washed with 0.4 ml of 1 mol/l formic acid in water and centrifuged. The following solvents were applied in the same way: 0.4 ml of 80% aqueous methanol (v/v) for ABA and auxin elution, 0.4 ml of 0.35 mol/l of aqueous ammonia for polar CKs elution and 0.4 ml of 0.35 mol/l ammonia in 60% aqueous methanol (v/v) for semi-polar CKs elution. The eluates were evaporated, dissolved in 40 μl of 10% methanol (v/v) and transferred into a glass insert placed in an LC vial (Chromservis Ltd., Czech Republic).

3.4.3 Extraction of CK standards with PALME procedure

A CK mixture of non-labelled standards (at a concentration 1 pmol) was diluted into 250 μl of sodium phosphate buffer pH 7.5 and then transferred into a 96-well plate. The membrane container, either polypropylene (PP) or polyvinylidene fluoride (PVDF), was activated using one of the following organic solvents: 1-hexanol, 1-octanol, 2-octanone, 2-nonanone, dihexyl ether, dodecyl acetate, dihexyl ether modified with 15% bis(2-ethylhexyl)phosphinic acid (DEHP) and dodecyl acetate modified with 15% DEHP. The container with the activated liquid membrane was inserted onto the sample in the well and covered with 40 μl of acceptor containing an aqueous solution of formic acid at different concentrations (0.01, 0.05, 0.1 or 0.2 mol/l). The plate was covered with a lid and shaken on VWR® Standard 3500 Orbital Shaker (VWR, USA) operated at 900 rpm for 30 min. The acceptor solution was transferred into a LC vial equipped with a glass insert.

3.4.4 Extraction and purification of JAs and SA from plant material

The protocol followed the previously published procedure by Floková et al. (2014). Briefly, 10 mg FW of homogenized plant material was weighed into 2 ml microtubes, 1 ml of

10% aqueous methanol and three zirconium extraction beads were added. Stable isotope-labelled internal standards were pipetted into the extracts. Similar to Extraction of CKs, auxins and ABA, sample was extracted on a bead mill at 27 Hz for 5 min, sonicated for 3 min and incubated for 30 min in a refrigerator. The samples were finally centrifuged at 20,000 rpm and 4 °C for 15 min and supernatants were collected. The supernatants were purified using the reverse-phase SPE extraction cartridges Oasis® HLB 30 mg/1 cc (Waters, Milford, CT, USA). The samples were reconstituted in 15% acetonitrile (v/v) and transferred into an LC vial with a glass insert.

3.5 Multivariate data analysis and statistics

3.5.1 Estimation of PALME parameters effect on the extraction efficiency

PALME related data were processed using R studio. The percentage yields of the total CK bases were calculated as a ratio of the molar amount determined in the acceptor and the theoretical molar amount added into the donor. All missing values were replaced by ⅔ of mean detection limit. Data were fitted by a linear model predicting the percentage yield based on the membrane type, organic solvent type, concentration of DEHP and concentration of formic acid in the acceptor. The model was cross-validated using leave one out training method to assess goodness of fit ($R^2 = 0.72$) and goodness of prediction ($Q^2 = 0.57$), both suggesting moderate correlation. The model coefficients were visualized in the bar chart with error bars represented the 95% confidence interval of an estimated effect.

3.5.2 Estimation of DisperSpin SPE parameters effect on the extraction efficiency

For the initial screening, four parameters of DisperSpin SPE were selected to assess their effect on percentage extraction yield. This study was conducted using a full factorial design of experiment for four factors (Box and Hunter, 1957). The percentage yield of each individual compound was calculated as a ratio between the molar amount determined in the purified extract and the molar amount added before the extraction. Data were analysed using Simca® 17 software (Sartorius Stedim Data Analytics AB, Umeå, Sweden). First, principal component analysis was performed to assess the data structure and detect potential outliers. The data were then fitted by partial least square regression calculating the covariance between method parameters and extraction yield (Wold et al., 2001). The resultant loadings of the two most important principal components were plotted against each other to visualize the relative effects

of the factors on compound yield. The resultant model was cross-validated using leave one out method to assess its predictability. The multiple linear model predicting the extraction yield of three representative phytohormones based on the DisperSpin SPE parameters was calculated using Modde® 11 software (Sartorius Stedim Data Analytics AB, Umeå, Sweden). The predicted yield was visualized in the contour plots.

3.5.3 Optimization of DisperSpin SPE parameters

The amount of Oasis® MCX bulk sorbent (2-30 mg) and the amount of Arabidopsis seedlings or poplar leaves (2-20 mg FW) were selected to find the optimal setpoint determining an MS response of endogenous concentration of plant hormones. The optimization was performed using response surface methodology and D-Optimal design of experiment, both calculated by Modde® 11 software (Sartorius Stedim Data Analytics AB, Umeå, Sweden). The signal-to-noise ratio was determined by a peak-to-peak algorithm in MassLynx v4.2 software (Waters, Manchester, UK). Data were fitted by multiple regression including interaction and quadratic terms. The estimation of signal to noise ratio values was visualized as the contour plots.

4 Survey of results

First, during the Ph.D. study, a review was prepared on the topic "Spatio-temporal plant hormonomics: From tissue to subcellular resolution", which summarizes the current state of plant hormone analysis, their determination and visualization in the living organisms (Petřík et al., submitted after revisions in Journal of Experimental Botany).

4.1 Results and discussion

4.1.1 Method development of CKs purification based on PALME

The initial batch of experiments aimed to examine the extraction yield using pure CK chemical standards. The standards diluted in a weak alkaline sodium-phosphate buffer as a donor solvent were extracted through the liquid membrane consisting of PP moistened in dodecyl acetate into a solution of formic acid as an acceptor. Surprisingly, this experimental setup facilitated the extraction of only CK bases and CK ribosides. Other metabolites, including CK glucosides and CK nucleotides, were not detected. Moreover, the extraction efficiency of CK bases and ribosides was low, accounting for an average of 0.5% for CK ribosides and 16.8% for CK bases. Consequently, dodecyl acetate was replaced with less hydrophobic water-immiscible solvents such as 1-hexanol, 1-octanol, 2-octanone and 2-nonanone. However, liquid membranes consisting of these solvents suffered from poor reproducibility. Depending on the boiling point and partial miscibility with water, the thin layer of these organic solvents was corrupted during the PALME procedure, resulting in the loss of the acceptor. This effect was observed particularly for all organic solvents, except dodecyl acetate and dihexyl ether.

A previous study focused on the UHPLC-MS/MS analysis of the pharmaceutically significant compound hydralazine in human plasma employed PALME for sample preparation (Pilařová et al., 2017). Similar to CKs, hydralazine is a heterocyclic nitrogen-rich low molecular compound. In that study, the mean recovery of hydralazine was 16% with dodecyl acetate, dihexyl ether, or 2-nonanone, and 76% with 1-octanol. This finding was consistent with our observations regarding the impact of the liquid membrane on the extraction of CK bases. However, it is important to note certain limitations in making this comparison. First, in the case of hydralazine, all organic solvents were modified with 15% DEHP. Second, although the poor stability of the liquid membrane was not reported, a high variability in recovery was observed instead.

To solve problems related to unstable liquid membrane and high variability in yield, the relatively efficient 1-octanol was excluded from the study. Instead, it was replaced with dodecyl acetate modified with 15% DEHP, a compound previously shown to facilitate the transfer of analytes through the liquid membrane (Pilařová et al., 2017). This modification resulted in an increase in the mean yield to 3.8% for CK ribosides and 22.6% for CK bases in our study.

Subsequently, our attention turned to optimizing the acceptor phase. Previous studies have highlighted the significance of acceptor phase composition in affecting the extraction yield (Lorenzo-Parodi et al., 2023; Ahmed et al., 2024). Consequently, we varied the concentration of formic acid in the acceptor phase to identify the optimal conditions. Interestingly, while concentrations of 10 mmol/l, 50 mmol/l, and 100 mmol/l yielded comparable extraction efficiencies, a concentration of 200 mmol/l resulted in a significant increase in yield.

The optimal concentration of formic acid, as reported in a study focusing on the extraction of repaglinide, a medication for diabetic patients, was found to be the same as in our investigation (Ahmed et al., 2024). Interestingly, the optimal concentration of formic acid for hydralazine extraction was five times higher (Pilařová et al., 2017). Recent studies have recommended the use of PP membrane instead of commercially available PVDF to prevent nonspecific binding with basic analytes (Lorenzo-Parodi et al., 2023; Ahmed et al., 2024). Surprisingly PVDF in our study exhibited similar behaviour to PP, showing no significant change in the extraction yield of weakly basic CKs. Nevertheless, PP membranes were preferred due to their in-house production. Despite the improvements in the PALME protocol described in this Ph.D. thesis, the extraction efficiency remained far from those achieved in SPE-based sample purification protocols (Dobrev and Kamínek, 2002; Svačinová et al., 2012).

Thus, we further examined the extraction capacity of dodecyl acetate modified with 15% DEHP by comparing it with ethyl acetate in a traditional liquid-liquid extraction (LLE) setup. Ethyl acetate, recognized as the most polar organic water-immiscible solvent, was previously utilized for LLE of CKs (Hahn, 1975). Our test results indicated that modified dodecyl acetate in the LLE setting provided similar extraction efficiency as ethyl acetate for most of the compounds, resulting in significantly higher yields (up to 70% on average) compared to PALME (Krnáčová, 2021). However, compare to dodecyl acetate, extraction with ethyl acetate was effective only for CK bases and CK ribosides. No enhancement was observed for CK nucleotides and CK glucosides, which were found below the detection limit. Consequently, it was concluded that PALME has limited applicability and does not allow for the determination of the entire CK profile compared to SPE. Hence, further efforts have been directed towards

the development of a purification method derived from SPE, which promises better extraction efficiency and applicability for a wider range of analyte polarities (Dobrev and Kamínek, 2002).

4.1.2 Method development of phytohormones purification based on DisperSpin SPE

Current methods for plant hormone sample preparation rely mostly on SPE in extraction cartridges using mix-mode sorbents (Dobrev and Kamínek, 2002). This approach has obvious benefits. The extraction cartridges are commercially available, robust and easy-to-use with a wide range of applications. However, dispersive SPE also known as QuEChERs (Quick, Easy, Cheap, Effective, Rugged, and Safe) extraction was adopted for plant hormones purification (Petřík et al., in preparation). Unlike the cartridge setup, dispersive SPE facilitates the contact of solvents with a large sorbent surface area, potentially suggesting higher extraction efficiency. This Ph.D. thesis was aimed on the development of miniaturized dispersive SPE method based on commercially available sorbents typically used in cartridge SPE, such as Oasis® MCX 30 µm (Waters, Milford, CT, USA).

The experimental setup was designed employing MicroSpin centrifuge nylon filters with 0.2 µm pores (Chromservis Ltd., Czech Republic), from which the name "DisperSpin SPE" was derived. This modification resulted in improved reproducibility and extraction efficiency comparable to the cartridge SPE (Dobrev and Kamínek, 2002). It has been shown that balance between the sorbent amount and the elution volume determines the extraction efficiency. CK nucleotides and CK *O*-glucosides benefited from the high amount of sorbent used (30 mg), whereas CK bases, CK ribosides and IAA achieved higher efficiency at low amount of sorbent (2 mg). Importantly, ABA, oxIAA and IAA amino acid conjugates were sensitive to changes in parameters related to elution (number of elution cycles and elution volume). All of them benefited from high number of cycles and/or high volume. This means that one elution cycle with 0.4 ml elution solvent provided sufficient extraction yields for all compounds. The optimal amount of plant tissue corresponded to the capacity of SPE sorbent. The optimal setpoint was calculated for the combination of 10 mg FW of plant extract with 10 mg of Oasis® MCX bulk sorbent. The optimized method was validated based on Food and Drug Administration guidelines. The method reported 9% mean accuracy, 7% mean precision, 47% mean extraction efficiency and 21% mean relative matrix effect, all indicating good reliability of the proposed method. Finally, the validated method was applied for profiling of CKs, auxins and ABA in various types of plant material – *Arabidopsis thaliana* seedlings, *Populus sp.* leaves (both representatives of dicots), *Triticum aestivum* leaves (monocots), *Picea*

abies seedlings (conifer), *Marchantia polymorpha* thallus (liverwort) and *Nostoc* colony (algae).

In summary, the presented DisperSpin SPE method offers a reliable tool for purification of selected CKs, auxins and ABA. The extraction efficiency and related MS response mostly depends on the capacity of Oasis® MCX bulk sorbent. The users focussing mainly on CK bases, CK ribosides and IAA should use a small amount of sorbent (2 mg), whereas researchers aiming on CK nucleotides and CK *O*-glucosides should increase the sorbent amount to 30 mg to achieve the optimal MS response. However, the DisperSpin SPE has not been applied yet for the purification of other classes of plant hormones, such as JAs, SA or brassinosteroids. Since these classes of compounds are weak acids or relatively non-polar compounds, the utilization of reverse-phase or anion-exchange bulk sorbents are proposed to explore the further possibilities of DisperSpin SPE.

4.1.3 Method development of CKs analysis based on SFC-MS/MS

The next goal of the Ph.D. thesis was the development of an analytical method for the CK quantification based on SFC-MS/MS. Importantly, SFC utilizes carbon dioxide in supercritical conditions ($scCO_2$) as the major component of the mobile phase and a miscible organic solvent such as methanol, as a modifier. The addition of a modifier to the mobile phase enables control of the physico-chemical properties of the mobile phase and consequently allows the elution of relatively polar compounds. However, unlike LC, the modification of SFC mobile phase is limited with emphasis on the restricted use of water. Therefore, the separation of polar and semi-polar CK isomers was the most challenging part of the work. Four types of stationary phases (C18, bare silica, DIOL and 2-PIC) were tested for the separation of CK isomers.

C18 has been proven to be not efficient for the retention of CKs combined with $scCO_2$/methanolic mobile phase. Sufficient retention of CKs was achieved using a Torus DIOL column (Waters, Milford, CT, USA). Importantly, zeatin glucoside has been shown to consist of six isomers, namely *trans*-zeatin O-glucoside (*t*ZOG), *cis*-zeatin O-glucoside (*c*ZOG), *trans*-zeatin N^7-glucoside (*t*Z7G), *cis*-zeatin N^7-glucoside (*c*Z7G), *trans*-zeatin N^9-glucoside (*t*Z9G) and *cis*-zeatin N^9-glucoside (*c*Z9G) was the most critical group of compounds to separate. The mobile phase consisted of $scCO_2$ modified by methanol with the addition of ammonium formate, which was prepared by titration of ammonia into formic acid. The ratio between ammonia and formic acid determined the separation of CK *O*- and N^9-glucosides, whereas column temperature affected the selectivity of N^7- and N^9-glucosides. Interestingly, the baseline

separation was not achieved with any combination ammonium formate and column temperature. While *c*ZOG and *c*Z9G were separated at low concentration of ammonia (5 mmol/l), *t*ZOG and *t*Z9G coeluted in one chromatographic peak. Conversely, at a high concentration of ammonia (50 mmol/l), satisfactory separation was observed for *t*ZOG and *t*Z9G but not for *cis*- isoforms.

Another effort was dedicated to the separation of zeatin glucosides with Zorbax RX-SIL column (Agilent Technologies, Santa Clara, CA USA), which possess similar retention mechanisms like DIOL column. A gradient elution of $scCO_2$ modified by pure methanol was used to elute CKs from RX-SIL column. Column temperature and back pressure regulation has a significant effect on density of mobile phase, which was critical for the selectivity of zeatin glucoside isomers. The baseline separation was achieved by a combination of high temperature (60 °C) and high back pressure regulation (300 bar). However, the combination of silica-based column and $scCO_2$/methanol mobile phase resulted in poor inter-day repeatability of the method manifested by peak broadening and retention time instability. This effect may be related with absence of the water in the mobile phase leading to the methylation of silanol groups on stationary phase and the loss of its retention properties (Plachká et al., 2021). The addition of 5% water into the modifier led to a significant change of the selectivity and baseline separation of zeatin glucosides. Nonetheless, the presence of water also resulted in the loss of the selectivity of DHZ glucosides. Therefore, silica-based chromatographic column was discarded from the study and replaced with Torus 2-PIC column (Waters, Milford, CT, USA), which showed sufficient selectivity and chromatographic resolution for all targeted CK metabolites. The final SFC-MS/MS method used linear gradient elution with $scCO_2$ modified with 5 mmol/l ammonia in methanol starting at 5% and ending at 40% in 7 min with a constant flow rate of 1.5 ml/min. Furthermore, methanol was employed as a make-up solvent to improve the ionization efficiency of subsequent MS-based detection. The new SFC-MS/MS method was validated based on the guidelines recommended by the Food and Drug Administration and used to determine the CK profile in *Arabidopsis thaliana* seedlings. It was shown that both the novel SFC-MS/MS and previously published UHPLC-MS/MS method provided similar results, emphasising the major representation of *N*-glucosides in the CK profile of *Arabidopsis* seedling.

4.1.4 Application of modern UHPLC-MS/MS methods for determination of phytohormones in plants

Determination of free SA in Arabidopsis roots to reveal its role in pathogen infection

The concentration levels of free SA were quantified in the roots of Arabidopsis seedlings in two developmental stages (5 and 10 days after germination). Three genotypes of Arabidopsis were involved in the study. The mutant *sid2* was deficient in SA biosynthesis, the mutant *crp6* was altered to overproduce the SA, and *Col-0* was a standard line with no alteration. The research question was whether the concentration of free SA depends on genotype and/or developmental stage. The samples were prepared according to the previously described protocol (Floková et al., 2014). Whereas the mutant line *sid2* showed no significant change compared to *Col-0*, *crp6* reported twice higher concentration. This effect was observed in both developmental stages. Combined with the results from morphology analysis of lateral roots, protein immunoblotting, phosphorylation assays and gene expression the following conclusion of the study was conducted. When plant is infected by a pathogen, the cross-talk between SA and auxin is recruited to induce the defence response. A high concentration of SA in the cytosol blocks the enzymatic activity of phosphatase 2A responsible for dephosphorylation of auxin transporter PIN2. This leads to hyperphosphorylation of PIN2 and efflux of auxin from the nucleus. Hence, the auxin response is attenuated and root development is inhibited.

Quantification of CKs in Arabidopsis roots to reveal the nitrogen signalling response

This study addressed the question of what is the role of CKs in long-distance root-to-shoot signalling in response to nitrate heterogeneity. The study was performed with hydroponically grown Arabidopsis seedlings. Nitrogen heterogeneity was simulated by splitting the root system. Half of the root system was grown in a potassium nitrate solution simulating a nitrogen-rich environment, and the second half in a potassium chloride solution with no nitrogen source. The plants growing only in potassium nitrate and potassium chloride were involved into the study as controls. The samples of roots and shoots were prepared by extraction into modified Bieleski buffer followed by purification using mix-mode SPE. Finally, CK content was determined using UHPLC-MS/MS as described previously (Svačinová et al., 2012). Two mutant lines were employed in the study to elucidate the CK role in nitrogen heterogeneity. Triple mutant *ipt3,5,7* was deficient in CK biosynthesis and *abcg14* mutant line was altered in CK transport. Depending on mutant line and growth conditions, the total CK

content varied from 50 to 300 pmol/g FW. The concentration of *trans*-zeatin (*t*Z) in roots was shown to be significantly decreased in the *ipt3,5,7* mutant, whereas both mutants *ipt3,5,7* and *abcg14* reported significant concentration drop in shoots. In conclusion, biosynthesis of CK *t*Z-types in the root depends on the availability of exogenous nitrogen. The translocation of *t*Z into the shoot induces short- and long-term responses by regulating of nitrogen-responsive genes, and regulating nitrate transport and root development. It has also been suggested that nitrogen distribution is mediated by glutamate and glutamine metabolism, which is putatively regulated by *t*Z signalling after root-to-shoot translocation.

Determination of JAs in Pinguicula carnivorous plant

Carnivorous plants represent a special group within the plant kingdom that have developed evolutionarily alternative strategies for nutrient uptake. These strategies reacted on nutrient deficiency in the soil by the transformation of leaves into traps for capturing a prey. Several orders of carnivorous plants with different trapping mechanisms have been described (Albert et al., 1992). One of them is Lamiales order involving *Pinguicula sp.*, also known as butterwort, which is typical by its flowering and rosette of oval shaped leaves. The leaves are covered by the glands producing the sticky and digestive fluids to capture and digest the prey. The aim of this study was to answer the question whether the butterwort utilizes stress-related compounds in the signalling pathway inducing enzyme activity in response to prey capture similarly to Venus flytrap (*Dionaea muscipula*) from Caryophyllales order (Pavlovič et al., 2017). Leaves of the horticultural hybrid of *Pinguicula* × *Tina* were wounded mechanically or fed by *Drosophyla melanogaster* prey and collected in time-points 0 h, 2 h and 24 h after feeding/wounding. The wounding experiment was performed to obtain information about positive stress response. The samples were processed for determination of stress-related compounds using SPE sample clean-up and UHPLC-MS/MS analysis by Floková et al. (2014). Upregulation of (+)-7-iso-jasmonic acid (JA), its biosynthetic precursor cis-(+)-12-oxo-phytodienoic acid (*cis*-OPDA) and bioactive (+)-7-iso-jasmonoyl-L-isoleucine (JA-Ile) were shown to be triggered only in response for wounding but not for feeding. In combination with the results of membrane potential measurement of wounded/fed leaves and proteomics analysis of digestive fluid composition, the following conclusion was made: while both *Pinguicula* and *Dionaea* have similar composition of digestive enzymes, *Pinguicula*, unlike *Dionaea*, do not co-opt JAs in response to prey capture. Hence, the *Dionaea* digestion signalling remains elusive.

Elucidation of JAs role in prey digestion of aquatic carnivorous plants

As already indicated in the previous paragraph, several carnivorous plants, such as *Dionaea muscipula* from Caryophyllales order, have co-opted the JA signalling in the digestion of the captured prey. However, this strategy was not observed in the carnivorous plant *Pinguicula* from Lamiales order, whose digestion signalling is not yet fully explained (*Supplement VI*). In this study, two aquatic carnivorous plant species, *Aldrovanda vesiculosa* from Caryophyllales and *Utricularia reflexa* from Lamiales, were investigated in terms of JA accumulation after feeding. Interestingly, the traps of *Aldrovanda* utilize a similar mechanism of capture like terrestrial *Dionea*, as both are based on an electric action potential. On the other hand, the traps of *Utricularia* are passive flexible hollow bladders with the sealing. The plant continuously pumps the water out of the trap, maintaining a negative pressure inside the trap and driving the prey to be captured. This mechanistical difference raised the question of how the JA signalling defence pathway is incorporated in prey digestion in aquatic carnivorous plants. The traps of *Aldrovanda* and *Utricularia* containing prey were collected 2 h and 24 h after feeding and lyophilised, resulting in 2.5 mg of dry weight per sample. Dry trap samples were processed according to the protocol published by Floková et al. (2014) based on extraction in 10% methanol, subsequent purification using Oasis HLB cartridges and then UHPLC-MS/MS analysis. Results from plant hormone profiling were integrated with proteomics analysis of digestive enzymes and data from induced trap closing time span. Interestingly, feeding of *Aldrovanda* induced the accumulation of JA, JA-Ile, *cis*-OPDA, SA and IAA, but *Utricularia* fed traps showed no significant change compared to empty traps. Whereas both species used the same digestion enzymes, the mechanism of trapping/digesting action is closely related to the order. Representatives of Caryophyllales, *Aldrovanda* and *Dionaea* have reported co-optation of JA signalling from plant defence, suggesting that both species are derived from a common terrestrial ancestor. On the other hand, *Utricularia* and *Pinguicula* (studied in *Supplement VI*) both co-opted a different signalling mechanism that is not yet fully understood (Pavlovič et al., 2024).

Elucidation of anti-gravitropic mechanism mediated by CKs

The gravitropism is the main force of the root growth mediated by auxin signalling. However, as revealed in this work, CKs play a crucial role in Arabidopsis lateral root development. The CK content was determined in the roots of the standard genotype *Col-0* and the double mutant *ckx2-1*, which is deficient in CK metabolism by knock-out of the CKX isoforms. The method

used for CK determination was adopted from Svačinová et al. (2012). Results from CK profiling showed an increased level of iP-types in *ckx2-1* mutant line. This is consistent with previous findings that iP-types are preferred substrate for CKX degradation (Galuszka et al., 2007). On the other hand, other CK types were downregulated in *ckx2-1* mutant line, suggesting a compensation mechanism. Taken together with a genome-wide association study, the data showed that the naturally varied angular growth of lateral root is regulated by CK response factors. Enzymatic activity of CKX2 has a significant impact of lateral root development. The CK activity is tightly connected to cellular elongation and cell division in lateral roots determining its angular growth.

5 Conclusion and perspectives

Plant physiology research has evolved into an interdisciplinary field, encompassing proteomics, genomics, transcriptomics, genetics, phenomics, and notably, plant hormonomics. Integrating data from these diverse fields drives modern plant science forward. As interest in plant physiology narrows from organs to organelles, there is a need for novel tools capable of detecting plant hormones in minute samples. This Ph.D. thesis focuses on developing methods to address current analytical limitations, particularly in downscaling, enhancing throughput and ensuring robustness. Key findings are outlined below:

- A novel analytical method based on SFC-MS/MS was successfully developed and validated for the determination of CKs in plants. This method introduced an innovative chromatographic approach for plant hormone analysis.
- The PALME method was effective for sample preparation of less polar CKs. However, its applicability for broader phytohormonal profiling has been limited.
- A new method for the purification of CKs, auxins and ABA using DisperSpin SPE has demonstrated the protocol robustness and the extraction efficiency. Due to its practicality and easy-to-use, it has become firmly established as a routine procedure in the Laboratory of Growth Regulators.
- State-of-the-art analytical methods based on UHPLC-MS/MS have contributed to the elucidation of the role of CK in nutrient signalling and lateral root development, the involvement of SA in plant defence mechanisms, and the function of JA in botanical carnivory.

The findings highlight the increasing complexity of plant hormonomics data, especially when integrated with other omics fields. To navigate through large datasets effectively, researchers require advanced multivariate statistical approaches that can convert vast amounts of data into understandable results. While DoE represents a well-established advanced statistical method in industry, its application in integrated plant sciences remains limited. Plants as living organisms are inherently more complex compared to industrial processes, exhibiting higher random variability and non-linear dependencies that must be addressed. Therefore, adopting of DoE in plant hormone research is quite a challenging task. However, its successful implementation can significantly help to answer the questions of plant physiology research in a much shorter time with much less financial resources than so far.

6 References

Ahmed SA, Abdallah NA, Almaghrabi M, Alahmadi YM. 2024. Parallel artificial liquid membrane extraction coupled with UPLC-ESI-MS/MS method for high-throughput quantitation of repaglinide in diabetic patients. Talanta 269, 125498.

Albert VA, Williams SE, Chase MW. 1992. Carnivorous plants: phylogeny and structural evolution. Science 257, 1491–1495

Arnon DI, Hoagland DR. 1940. Crop production in artificial culture solutions and in soils with special reference to factors influencing yields and absorption of inorganic nutrients. Soil Science 50, 463–485.

Brunoni F, Collani S, Casanova-Sáez R, Šimura J, Karady M, Schmid M, Ljung K, Bellini C. 2020. Conifers exhibit a characteristic inactivation of auxin to maintain tissue homeostasis. New Phytol 226(6), 1753–1765.

Chmelík D, Hrouzek P, Fedorko J, Vu DL, Urajová P, Mareš J, Červený J. 2019. Accumulation of cyanobacterial oxadiazine nocuolin A is enhanced by temperature shift during cultivation and is promoted by bacterial co-habitants in the culture. Algal Research 44, 101673.

Dobrev PI, Kamínek M. 2002. Fast and efficient separation of cytokinins from auxin and abscisic acid and their purification using mixed-mode solid-phase extraction. J Chromatogr A 950, 21–29.

Floková K, Tarkowská D, Miersch O, Strnad M, Wasternack C, Novák O. 2014. UHPLC-MS/MS based target profiling of stress-induced phytohormones. Phytochemistry 105, 147–57.

Galuszka P, Popelková H, Werner T, Frébortová J, Pospíšilová H, Mik V, Köllmer I, Schmülling T, Frébort I. 2007. Biochemical characterization of cytokinin oxidases/dehydrogenases from Arabidopsis thaliana expressed in Nicotiana tabacum L. J Plant Growth Regul 26, 255–267.

Geier U, Werner O, Bopp M. 1990. Indole-3-acetic acid uptake in isolated protoplasts of the moss Funaria hygrometrica. Physiol Plant. 80(4), 584–592.

Hofman PJ, Featonby-Smith BC, VanStaden J. 1986. The Development of ELISA and IRA for Cytokinin Estimation and their Application to a Study of Lunar Periodicity in Ecklonia maxima (Osbeck) Papenf. J Plant Phys 122(5), 455–466.

Krnáčová A. 2021. Izolace fytohormonů s využitím paralelní extrakce pomocí umělých kapalných membrán. Bakalářská práce. Olomouc: Univerzita Palackého v Olomouci, Přírodovědecká fakulta.

Lorenzo-Parodi N, Kaziur-Cegla W, Gjelstad A, Schmidt TC. 2023. Liquid-phase microextraction of aromatic amines: hollow fiber–liquid-phase microextraction and parallel artificial liquid membrane extraction comparison, Anal Bioanal Chem 415, 1765–1776.

Novák O, Napier R, Ljung K. 2017. Zooming In on Plant Hormone Analysis: Tissue- and Cell-Specific Approaches. Annu Rev Plant Biol 68, 323–348.

Pavlovič A, Jakšová J, Novák O. 2017. Triggering a false alarm: wounding mimics prey capture in the carnivorous Venus flytrap (Dionaea muscipula). New Phytologist 216, 927–938.

Pavlovič A, Koller J, Vrobel O, Chamrád I, Lenobel R, Tarkowski P. 2024. Is the co-option of jasmonate signalling for botanical carnivory a universal trait for all carnivorous plants? J Exp Bot 75, 334–349.

Pěnčík A, Casanova-Sáez R, Pilařová V, Žukauskaite A, Pinto R, Micol JL, Ljung K, Novák O. 2018. Ultra-rapid auxin metabolite profiling for high-throughput mutant screening in Arabidopsis. J Exp Bot 69(10), 2569–2579.

Pilařová V, Sultani M, Ask KS, Nováková L, Pedersen-Bjergaard S, Gjelstad A. 2017. One-step extraction of polar drugs from plasma by parallel artificial liquid membrane extraction. J Chromatogr B 1043, 25–32.

Plachká K, Střítecký J, Švec F, Nováková L. 2021. The effect of column history in supercritical fluid chromatography: Practical implications. J Chromatogr A 1651, 462272.

Svačinová J, Novák O, Plačková L, Lenobel R, Holík J, Strnad M, Doležal K. 2021. A new approach for cytokinin isolation from Arabidopsis tissues using miniaturized purification: pipette tip solid-phase extraction. Plant Methods 8(1), 17.

Pengelly W, Meins F. 1976. Radioimmunoassay for indole-3-acetic acid. Plant Physiol 57(5), 30–30.

Rittenberg D, Foster GL. 1940. A new procedure for quantitative analysis by isotope dilution, with application to the determination of amino acids and fatty acids. J Biol Chem 133, 727–744.

Šimura J, Antoniadi I, Široká J, Tarkowská D, Strnad M, Ljung K, Novák O. 2018. Plant Hormonomics: Multiple Phytohormone Profiling by Targeted Metabolomics. Plant Physiol 177, 476–489.

Tarkowská D, Novák O, Floková K, Tarkowski P, Turečková V, Grúz J, Rolčík J, Strnad M. 2014. Quo vadis plant hormone analysis? Planta 240, 55–76.

Wold S, Sjostrom M, Eriksson L. 2001. PLS-regression: a basic tool of chemometrics. Chemom Intell Lab Syst 58, 109–130.

7 List of author's publications

7.1 First author papers published in scientific journals

Petřík I, Pěnčík A, Stýskala J, Tranová L, Amakorová P, Strnad M, Novák O. Rapid profiling of cytokinins using supercritical fluid chromatography coupled with tandem mass spectrometry. Analytica Chimica Acta 2024, 1285, 342010.

Petřík I, Hladík P, Zhang C, Pěnčík A, Novák O. Spatio-temporal plant hormonomics: From tissue to subcellular resolution. J Exp B [Submitted after revisions]

Petřík I, Valníčková A, Stýskala J, Strnad M, Ljung K, Novák O. DisperSpin solid phase micro-extraction: next generation micro-purification method for UHPLC MS/MS determination of naturally occurring phytohormones. [In preparation]

7.2 Co-author papers published in scientific journals

Amirbekov A, Vrchovecka S, Riha J, **Petrik I**, Friedecky D, Novak O, Cernik M, Hrabak P, Sevcu A. 2024. Assessing HCH isomer uptake in Alnus glutinosa: implications for phytoremediation and microbial response. Scientific Reports 14(1), 4187.

Castander-Olarieta A, Moncaleán P, Pereira C, Pěnčík A, **Petřík I**, Pavlović I, Novák O, Strnad M, Goicoa T, Ugarte MD, Montalbán IA. 2021. Cytokinins are involved in drought tolerance of Pinus radiata plants originating from embryonal masses induced at high temperatures. Tree Physiology 41(6), 912–926.

Castander-Olarieta A, Pereira C, Montalbán IA, Pěnčík A, **Petřík I**, Pavlović I, Novák O, Strnad M, Moncaleán P. 2021. Quantification of endogenous aromatic cytokinins in Pinus radiata embryonal masses after application of heat stress during initiation of somatic embryogenesis. Trees: Structure and Function 35, 1075–1080.

Grant JE, Ninan A, Cripps-Guazzone N, Shaw M, Song J, **Petřík I**, Novák OE, Tegeder M, Jameson PE. 2021. Concurrent overexpression of amino acid permease AAP1(3a) and SUT1 sucrose transporter in pea resulted in increased seed number and changed cytokinin and protein levels. Functional Plant Biology 48(9), 889–904.

Hladík P, **Petřík I**, Žukauskaitė A, Novák O, Pěnčík A. 2023. Metabolic profiles of 2-oxindole-3-acetyl-amino acid conjugates differ in various plant species. Frontiers in Plant Science 14, 1217421.

Jakšová J, Libiaková M, Bokor B, **Petřík I**, Novák O, Pavlovič A. 2020. Taste for protein: Chemical signal from prey stimulates enzyme secretion through jasmonate signalling in the carnivorous plant Venus flytrap. Plant Physiology and Biochemistry 146, 90–97.

Jakšová J, Adamec L, **Petřík I**, Novák O, Šebela M, Pavlovič A. 2021. Contrasting effect of prey capture on jasmonate accumulation in two genera of aquatic carnivorous plants (Aldrovanda, Utricularia). Plant Physiology and Biochemistry 166, 459–465.

Jakšová J, Rác M, Bokor B, **Petřík I**, Novák O, Reichelt M, Mithöfer A, Pavlovič A. 2021. Anaesthetic diethyl ether impairs long-distance electrical and jasmonate signaling in Arabidopsis thaliana. Plant Physiology and Biochemistry 169, 311–321.

Kloth KJ, Abreu IN, Delhomme N, **Petřík I**, Villard C, Ström C, Amini F, Novák O, Moritz T, Albrectsen BR. 2019. PECTIN ACETYLESTERASE9 Affects the Transcriptome and Metabolome and Delays Aphid Feeding. Plant Physiology 181(4), 1704–1720.

Kocáb O, Jakšová J, Novák O, **Petřík I**, Lenobel R, Chamrád I, Pavlovič A. 2020. Jasmonate-independent regulation of digestive enzyme activity in the carnivorous butterwort Pinguicula × Tina. Journal of Experimental Botany 71(12), 3749–3758.

Masondo NA, Aremu OA, Kulkarni MG, **Petřík I**, Plačková L, Šubrtová M, Novák O, Grúz J, Doležal K, Strnad M, Finnie JF, Van Staden J. 2019. How Do Different Watering Regimes Affect the Growth, Chlorophyll Fluorescence, Phytohormone, and Phenolic Acid Content of Greenhouse-Grown Ceratotheca triloba? Journal of Plant Growth Regulation 38, 385–399.

Masondo NA, Aremu OA, Kulkarni MG, **Petřík I**, Plačková L, Šubrtová M, Novák O, Grúz J, Doležal K, Strnad M, Finnie JF, Van Staden J. 2019. Elucidating the role of Kelpak® on the growth, phytohormone composition, and phenolic acids in macronutrient-stressed Ceratotheca triloba. Journal of Applied Phycology 31, 2687–2697.

Mi J, Vallarino JG, **Petřík I**, Novák O, Correa SM, Chodasiewicz M, Havaux M, Rodriguez-Concepcion M, Al-Babili S, Fernie AR, Skirycz A, Moreno JC. 2022. A manipulation of carotenoid metabolism influence biomass partitioning and fitness in tomato. Metabolic Engineering 70, 166–180.

Pavlović I, **Petřík I**, Tarkowská D, Lepeduš H, Vujčić Bok V, Radić Brkanac S, Novák O, Salopek-Sondi B. 2018. Correlations between Phytohormones and Drought Tolerance in Selected Brassica Crops: Chinese Cabbage, White Cabbage and Kale. International Journal of Molecular Sciences 19(10), 2866.

Pavlovič A, Libiaková M, Bokor B, Jakšová J, **Petřík I**, Novák O, Baluška F. 2020. Anaesthesia with diethyl ether impairs jasmonate signalling in the carnivorous plant Venus flytrap (Dionaea muscipula). Annals of Botany 125(1), 173–183.

Pereira C, Castander-Olarieta A, Montalbán IA, Pěnčík A, **Petřík I**, Pavlović I, Oliveira ED, Fraga HPD, Guerra MP, Novák O, Strnad M, Canhoto J, Moncaleán P. 2020. Embryonal Masses Induced at High Temperatures in Aleppo Pine: Cytokinin Profile and Cytological Characterization. Forests 11, 807.

Poitout A, Crabos A, **Petřík I**, Novák O, Krouk G, Lacombe B, Ruffel S. 2018. Responses to Systemic Nitrogen Signaling in Arabidopsis Roots Involve trans-Zeatin in Shoots. Plant Cell 30(6), 1243–1257.

Prerostova S, Zupkova B, **Petrik I**, Simura J, Nasinec I, Kopecky D, Knirsch V, Gaudinova A, Novak O, Vankova R. 2021. Hormonal responses associated with acclimation to freezing stress in Lolium perenne. Environmental and Experimental Botany 182, 104295.

Ptošková K, Szecówka M, Jaworek P, Tarkowská D, **Petřík I**, Pavlović I, Novák O, Thomas SG, Phillips AL, Hedden P. 2022. Changes in the concentrations and transcripts for

gibberellins and other hormones in a growing leaf and roots of wheat seedlings in response to water restriction. BMC Plant Biology 22(1), 284.

Smolikova G, Krylova E, **Petřík I**, Vilis P, Vikhorev A, Strygina K, Strnad M, Frolov A, Khlestkina E, Medvedev S. 2024. Involvement of Abscisic Acid in Transition of Pea (Pisum sativum L.) Seeds from Germination to Post-Germination Stages. Plants (Basel) 13(2), 206.

Tan S, Abas M, Verstraeten I, Glanc M, Molnár G, Hajný J, Lasák P, **Petřík I**, Russinova E, Petrášek J, Novák O, Pospíšil J, Friml J. 2020. Salicylic Acid Targets Protein Phosphatase 2A to Attenuate Growth in Plants. Curr Biol. 30(3), 381–395.

Waidmann S, Ruiz Rosquete M, Schöller M, Sarkel E, Lindner H, LaRue T, **Petřík I**, Dünser K, Martopawiro S, Sasidharan R, Novak O, Wabnik K, Dinneny JR, Kleine-Vehn J. 2019. Cytokinin functions as an asymmetric and anti-gravitropic signal in lateral roots. Nature Communications 10(1), 3540.

Yang B, Minne M., Brunoni F, Plackova L, **Petrik I**, Sun YB, Nolf J, Smet W, Verstaen K, Wendrich JR, Eekhout T, Hoyerova K, Van Isterdael G, Haustraete J, Bishopp A, Farcot E, Novak O, Saeys Y, De Rybel B. 2021. Non-cell autonomous and spatiotemporal signalling from a tissue organizer orchestrates root vascular development. Nature Plants 7, 1485–1494.

Zhang C, Žukauskaite A, **Petřík I**, Pěnčík A, Hönig M, Grúz J, Široká J, Novák O, Doležal K. 2021. In situ characterisation of phytohormones from wounded Arabidopsis leaves using desorption electrospray ionisation mass spectrometry imaging. Analyst 146(8), 2653–2663.

Žukauskaitė A, Saiz-Fernández I, Bieleszová K, Iškauskienė M, Zhang C, Smýkalová I, Dzedulionytė K, Kubeš MF, Sedlářová M, Pařízková B, Pavlović I, Vain T, **Petřík I**, Malinauskienė V, Šačkus A, Strnad M, Robert S, Napier R, Novák O, Doležal K. 2023. New PEO-IAA-Inspired Anti-Auxins: Synthesis, Biological Activity, and Possible Application in Hemp (Cannabis Sativa L.) Micropropagation. Journal of Plant Growth Regulation 42, 7547–7563.

7.3 Published abstracts

Petřík I, Valníčková A, Strnad M, Novák O. Dispersive solid phase extraction as a new tool for purification of phytohormones. *Auxins and Cytokinins in Plant Development (ACPD)*, Prague, Czech Republic, poster presentation (2018).

Petřík I, Valníčková A, Ljung K, Strnad M, Novák O. Innovative, effective, robust, fast and cheap purification of phytohormones using dispersive solid phase extraction. *Chemistry and Biology of Phytohormones and Related Substances (CBPRS)*, Luhačovice, Czech Republic, oral presentation (2019).

Petřík I, Valníčková A, Ljung K, Strnad M, Novák O. The new approaches for phytohormone isolation from plant tissues. *15th Student Days of Plant Experimental Biology (CSEBR)*, České Budějovice, Czech Republic, oral presentation (2019).

Petřík I, Valníčková A, Ljung K, Strnad M, Novák O. Innovative, effective, robust, fast and cheap purification of phytohormones using dispersive solid phase extraction. *Green for Good V (G4G)*, Olomouc, Czech Republic, poster presentation (2019).

Petřík I, Pěnčík A, Amakorová P, Strnad M, Novák O. On the Edge of the Limits. *3th STARSS Conference on Separation Science*, Hradec Králové, Czech Republic, oral presentation (2019).

Petřík I, Valníčková A, Novák O., Ljung K, Strnad M. Dispersive extraction purification – innovative, effective, robust, fast and cheap method to purify phytohormones. *23th Conference of International Plant Growth Substances Association (IPGSA)*, Paris, France, poster presentation (2019).

Petřík I, Valníčková A, Stýskala J, Strnad M, Ljung K, Novák O. Modern trends in phytohormone analysis: DisperSpin solid phase extraction. *Chemistry and Biology of Phytohormones and Related Substances (CBPRS)*, Bystřice nad Pernštejnem, Czech Republic, oral presentation (2022).

Petřík I, Valníčková A, Stýskala J, Strnad M, Ljung K, Novák O. DisperSpin solid phase micro-extraction as a novel tool of phytohormonal analysis. *Advances in Chromatography and Electrophoresis & Chiranal*, Olomouc, Czech Republic, oral presentation (2022).

Petřík I, Pěnčík A, Stýskala J, Tranová L, Amakorová P, Strnad M, Novák O. Analysis of cytokinins with supercritical fluid chromatography coupled with tandem mass spectrometry. *Chemistry and Biology of Phytohormones and Related Substances (CBPRS)*, Velké Losiny, Czech Republic, oral presentation (2023).

Petřík I, Pěnčík A, Stýskala J, Tranová L, Amakorová P, Strnad M, Novák O. Rapid screening of cytokinins in Arabidopsis plants using UHPSFC-MS/MS. *24th Conference of International Plant Growth Substances Association (IPGSA)*, Gyeongju, Republic of Korea, poster presentation (2023).

8 Souhrn (Summary, in Czech)

V posledním desetiletí se rostlinná fyziologie stala multidisciplinárním oborem zahrnujícím proteomiku, transkriptomiku, genetiku, fenomiku, a co je důležité, i rostlinnou hormonomiku. Metody výzkumu v současnosti kladou důraz na miniaturizaci a vysokou propustnost, protože oblast zájmu se zaměřuje na stále menší části rostlinného organismu. Tato dizertační práce se věnuje vývoji nových miniaturizovaných a vysoko-propustných metod stanovení bioaktivních rostlinných hormonů, jejich metabolitů a prekurzorů v nepatrném vzorku rostlin. Její cíle byly vytyčeny takto:

- Vypracovat literární rešerši zabývající se fyziologií, biosyntézou a metabolismem cytokininů a kyselých fytohormonů, a metodami jejich stanovení pomocí ultra-vysokoúčinné kapalinové chromatografie s tandemovou hmotnostní detekcí (UHPLC-MS/MS).
- Prozkoumat metodu přípravy vzorku cytokininů (CK) s využitím extrakce pomocí umělých kapalných membrán (PALME).
- Vyvinout metodu přípravy vzorků CK, auxinů a kyseliny abscisové založenou na disperzivní extrakci tuhou fází.
- Zavést novou analytickou metodu stanovení CK na bázi superkritické fluidní chromatografie a tandemové hmotnostní detekce (SFC-MS/MS).
- S využitím nejmodernějších technik a ve spolupráci s příbuznými obory rostlinné fyziologie odhalit dosud neznámé role CK, kyseliny salicylové a jasmonátů v regulaci růstu rostlin a odpovědi na okolní prostředí.

Ukázalo se, že PALME metodika je vhodná spíše pro extrakci nepolárních CK bází, což omezuje její využití v profilování více fytohormonů současně. V tomto ohledu se jako výkonná metoda ukázala být disperzivní SPE, která byla pro svou účinnost, jednoduchost a praktičnost zavedena jako rutinní postup přípravy rostlinného vzorku v Laboratoři růstových regulátorů. Kromě toho nově vyvinutá metoda analýzy CK založená na SFC-MS/MS nabízí jednak rychlé kvantitativní stanovení, a pak ukazuje nový směr chromatografického řešení pro separaci rostlinných hormonů. S využitím UHPLC-MS/MS byla objasněna role jasmonátů při trávení kořisti masožravými rostlinami, role kyseliny salicylové v obraně proti patogenům, a role CK v adaptaci na heterogenní přísun dusíku v půdě a růst laterálních kořenů. Dizertační práce ukázala, že výzkum na rostlinných hormonech generuje čím dál rozsáhlejší a komplexnější data. To naznačuje, že pokročilé statistické metody budou pro rostlinnou fyziologii stále více esenciální.